



**US Army Corps
of Engineers**
Waterways Experiment
Station

AD-A269 947



Miscellaneous Paper GL-93-13
August 1993

2

Site-Specific Earthquake Response Analysis for Portsmouth Gaseous Diffusion Plant, Portsmouth, Ohio

*by David W. Sykora, Jennifer J. Davis
Geotechnical Laboratory*

DTIC
ELECTE
OCT 01 1993
S A D

Approved For Public Release; Distribution Is Unlimited

93-22815



DISCLAIMER

This report was prepared as an account of work sponsored by the United States Government. Neither the United States nor the United States Department of Energy, nor any of their employees, makes any warranty, express or implied, or assumes any legal liability or responsibility for the accuracy, completeness, or usefulness of any information, apparatus, product, or process disclosed, or represents that its use would not infringe privately owned rights. Reference herein to any specific commercial product, process, or service by trade name, mark, manufacturer, or otherwise, does not necessarily constitute or imply its endorsement, recommendation, or favoring by the United States Government or any agency thereof. The views and opinions of authors expressed herein do not necessarily state or reflect those of the United States Government or any agency thereof.



PRINTED ON RECYCLED PAPER

Site-Specific Earthquake Response Analysis for Portsmouth Gaseous Diffusion Plant, Portsmouth, Ohio

by David W. Sykora, Jennifer J. Davis
Geotechnical Laboratory

U.S. Army Corps of Engineers
Waterways Experiment Station
3909 Halls Ferry Road
Vicksburg, MS 39180-6199

Accession For	
NTIS	GRAM
DTIC	DTIC
Unlimited	Unlimited
Justification	
By	
Distribution	
Availability Codes	
Dist	Availability for Special
A-1	

Final report

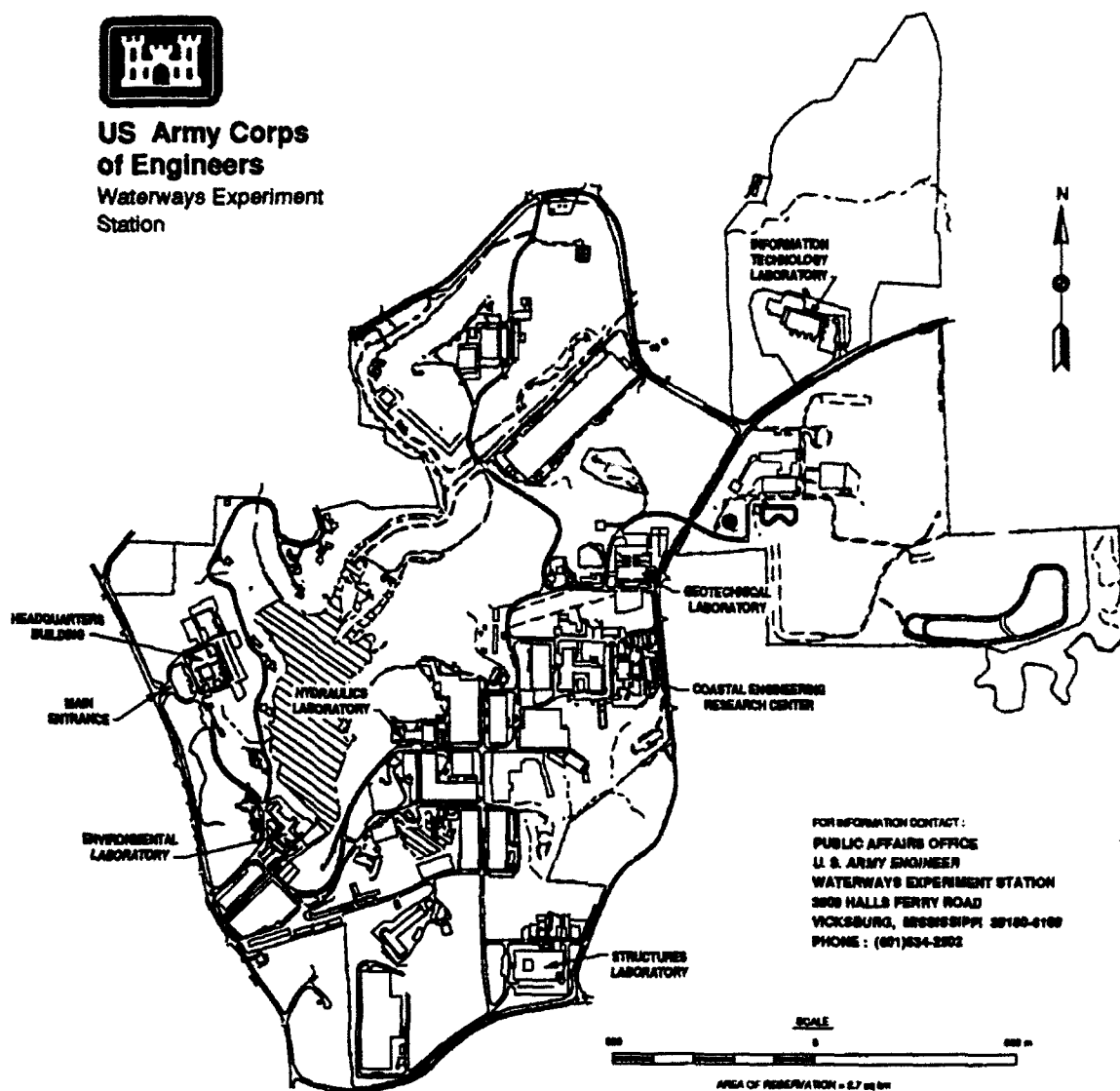
Approved for public release; distribution is unlimited

DTIC QUALITY INSPECTED 1

Prepared for U.S. Department of Energy
Oak Ridge Operations
Oak Ridge, Tennessee 37381-8650



**US Army Corps
of Engineers**
Waterways Experiment
Station



Waterways Experiment Station Cataloging-In-Publication Data

Sykora, David W.

Site-specific earthquake response analysis for Portsmouth Gaseous Diffusion Plant, Portsmouth, Ohio / by David W. Sykora, Jennifer J. Davis; prepared for U.S. Dept. of Energy, Oak Ridge Operations.

402 p.: ill.; 28 cm. -- (Miscellaneous paper; GL-93-13)

Includes bibliographical references.

1. Earthquake hazard analysis -- Ohio -- Portsmouth. 2. Gaseous diffusion plants -- Ohio -- Portsmouth. 3. Nuclear facilities -- Ohio -- Portsmouth. I. Davis, Jennifer J. II. United States. Dept. of Energy. Oak Ridge Operations Office. III. U.S. Army Engineer Waterways Experiment Station. IV. Title. V. Series: Miscellaneous paper (U.S. Army Engineer Waterways Experiment Station); GL-93-13.

TA7 W34m no.GL-93-13

EXECUTIVE SUMMARY

A site-specific earthquake response study was conducted for the U.S. Department of Energy (DOE) Portsmouth Gaseous Diffusion Plant (PORTS), located near Portsmouth, Ohio, to provide guidance for the seismic safety analysis and future design of structures and facilities there. The methods used for this study generally follow widely-accepted and validated practices of the geotechnical earthquake engineering profession as documented in professional literature.

Three earthquake events developed using probabilistic methodologies were considered. Two horizontal components of rock outcrop motion in terms of acceleration versus time were used independently (uncoupled). The peak horizontal accelerations at rock outcrop are 0.04, 0.07 and 0.13 g for the 500-year, 1000-year, and 5000-year events, respectively.

Input parameters describing soil column idealization, geotechnical engineering properties, and seismic velocities for fifteen individual soil columns were obtained from reports summarizing two previous major site investigations for the proposed Gaseous Diffusion Add-On Plant and proposed Gas Centrifuge Enrichment Plant, both published in 1978. Soils at PORTS generally consist of Pleistocene-age lacustrine deposits overlying alluvium then shale or sandstone. Idealized soil column heights range from 20 to 61 ft. The computer program *SHAKE* was used to calculate the site response corresponding to each of the fifteen sites.

The predominant site period for horizontal response is about 0.1 sec. Other site periods were also calculated corresponding to sites with a thicker soil deposit or higher shear wave velocity (stiffness). The motions calculated at the ground surface of free field (soil over rock) were amplified over rock outcrop motions for all cases at almost all periods. The peak horizontal accelerations at (free field) ground surface were calculated to be 0.12, 0.17 and 0.36 g for the 500-year, 1000-year, and 5000-year events, respectively. Peak spectral velocities of 4, 7, and 9 in./sec were calculated for the 500-year, 1000-year, and 5000-year events, respectively.

A sensitivity study was conducted using an average soil column and the 1000-year earthquake event. Calculations of site response were found to be most sensitive to the maximum shear modulus and the height of the column.

PREFACE

This report documents the site response evaluations performed for the U.S. Department of Energy (DOE) Portsmouth Gaseous Diffusion Plant (PORTS) located north of Portsmouth, Ohio. The U.S. Army Engineer Waterways Experiment Station (WES) was authorized to conduct this study from FY91 to FY93 by the DOE, Oak Ridge Operations (ORO), Oak Ridge, Tennessee, through Inter-Agency Agreement (IAG) No. DE-AI05-91OR21971. The study was conducted under the Gaseous Diffusion Plant Safety Analysis Report (GDP SAR) Program. Dr. Ronald O. Hultgren and Mr. James A. Reafsnnyder, ORO, were the DOE Program Officers.

The IAG was managed for Martin Marietta Energy Systems, Inc., by Ms. Karen E. Shaffer, Uranium Enrichment, Martin Marietta Energy Systems, Inc., Oak Ridge, Tennessee. Mr. William R. Brock, Deputy Engineering GDP SAR Manager, Technical Operations, and Mr. R. Joe Hunt, Center for Natural Phenomena Engineering, Uranium Enrichment, provided technical requirements and oversight for the study. The overall project manager was Mr. Anthony Angelelli, GDP SAR Manager, Technical Operations. A similar study was conducted for the DOE Paducah Gaseous Diffusion Plant (PGDP), located near Paducah, Kentucky, under the same IAG and is reported under separate cover.

An attempt was made at the initiation of this study to obtain geotechnical information from investigations conducted by the U.S. Army Corps of Engineers in the 1950's at PORTS for original construction of the plant. Despite considerable effort, this information was not found.

The WES Principal Investigator was Mr. David W. Sykora, Earthquake Engineering and Seismology Branch (EESB), Earthquake Engineering and Geosciences Division (EEGD), Geotechnical Laboratory (GL), WES. Ms. Jennifer J. Davis, a co-op student from Mississippi State University, assisted Mr. Sykora. Mr. Gregory D. Comes, EESB, provided additional engineering assistance and Messrs. William M. McGeehee, Daniel M. Habeeb, and Bennie L. Washington, EEGD, helped to prepare report figures. Dr. Mary Ellen Hynes was the Chief, EESB, during this study.

Overall direction at WES was provided by Dr. A. G. Franklin, Chief, EEGD, and Dr. William F. Marcuson III, Director, GL.

At the time of publication of this report, Director of WES was Dr. Robert W. Whalin. Commander was COL Bruce K. Howard, EN.

CONTENTS

	<u>Page</u>
EXECUTIVE SUMMARY.....	1
PREFACE.....	2
LIST OF TABLES.....	5
LIST OF FIGURES.....	5
CONVERSION FACTORS, NON-SI to SI METRIC UNITS OF MEASUREMENT.....	8
PART I: INTRODUCTION.....	9
Purpose.....	9
Procedure of Site Response Analysis.....	12
Special Considerations for Study at PORTS.....	13
Report Organization.....	14
PART II: DESIGN EARTHQUAKES.....	15
500-Year Event.....	16
1000-Year Event.....	20
5000-Year Event.....	24
PART III: SITE DESCRIPTION AND SOIL COLUMNS.....	28
Site Geology.....	28
Individual Soil Columns.....	37
Average Soil Column.....	56
PART IV: SITE RESPONSE CALCULATIONS.....	58
Method of Response Calculations.....	58
Application of Free-Field Results.....	62
Presentation of Output.....	63
PART V: RESULTS FROM COLLECTION OF INDIVIDUAL SITES.....	72
500-Year Event.....	72
1000-Year Event.....	77
5000-Year Event.....	86
Combined Events.....	91
PART VI: SENSITIVITY ANALYSIS USING AVERAGE COLUMN.....	97
Impedance Ratio.....	99
Depth to Bedrock.....	99
Assignment of Modulus Relationships.....	102
Assignment of Damping Ratio Relationships.....	102
Maximum Shear Modulus.....	105

Conclusions.....	108
PART VII: SUMMARY AND CONCLUSIONS.....	109
REFERENCES.....	111
APPENDIX A: LOCATIONS OF BORINGS USED FOR SOIL COLUMNS.....	A1
APPENDIX B: ACCELERATION-TIME RECORDS FOR 500-YEAR EVENT.....	B1
APPENDIX C: SHEAR STRAINS FOR 500-YEAR EVENT.....	C1
APPENDIX D: TRIPARTITE RESPONSE SPECTRA FOR 500-YEAR EVENT.....	D1
APPENDIX E: ACCELERATION SPECTRA FOR 500-YEAR EVENT.....	E1
APPENDIX F: RATIO OF ACCELERATION SPECTRA FOR 500-YEAR EVENT.....	F1
APPENDIX G: AMPLIFICATION RATIOS FOR 500-YEAR EVENT.....	G1
APPENDIX H: ACCELERATION-TIME RECORDS FOR 1000-YEAR EVENT.....	H1
APPENDIX I: SHEAR STRAINS FOR 1000-YEAR EVENT.....	I1
APPENDIX J: TRIPARTITE RESPONSE SPECTRA FOR 1000-YEAR EVENT.....	J1
APPENDIX K: ACCELERATION SPECTRA FOR 1000-YEAR EVENT.....	K1
APPENDIX L: RATIO OF ACCELERATION SPECTRA FOR 1000-YEAR EVENT.....	L1
APPENDIX M: AMPLIFICATION RATIOS FOR 1000-YEAR EVENT.....	M1
APPENDIX N: ACCELERATION-TIME RECORDS FOR 5000-YEAR EVENT.....	N1
APPENDIX O: SHEAR STRAINS FOR 5000-YEAR EVENT.....	O1
APPENDIX P: TRIPARTITE RESPONSE SPECTRA FOR 5000-YEAR EVENT.....	P1
APPENDIX Q: ACCELERATION SPECTRA FOR 5000-YEAR EVENT.....	Q1
APPENDIX R: RATIO OF ACCELERATION SPECTRA FOR 5000-YEAR EVENT.....	R1
APPENDIX S: AMPLIFICATION RATIOS FOR 5000-YEAR EVENT.....	S1

LIST OF TABLES

<u>No.</u>		<u>Page</u>
1	Characteristics of 500-Year Event Outcrop Motions.....	16
2	Characteristics of 1000-Year Event Outcrop Motions.....	20
3	Characteristics of 5000-Year Event Outcrop Motions.....	24
4	Normalized Modulus and Damping Ratio Relationships.....	45
5	Assignment of Shear Modulus Relationships.....	52
6	Miscellaneous Parameters in <i>SHAKE</i> Used for This Study.....	62
7	Calculated Peak Ground Accelerations.....	73
8	Calculated Maximum Effective Shear Strains.....	75

LIST OF FIGURES

<u>No.</u>		<u>Page</u>
1	Aerial photograph of Portsmouth Gaseous Diffusion Plant looking southwest.....	10
2	Overhead aerial photograph of Portsmouth Gaseous Diffusion Plant.....	11
3	Three primary control points for a site response analysis.....	12
4	Horizontal components of acceleration versus time for the 500-year design earthquake event (Risk Engineering, Inc. 1992).....	17
5	Variation of acceleration, velocity, and displacement for 500-year design earthquake event.....	18
6	Acceleration (outcrop) response spectra for the 500-year design earthquake event.....	19
7	Horizontal components of acceleration versus time for the 1000-year design earthquake event (Risk Engineering, Inc. 1992).....	21
8	Variation of acceleration, velocity, and displacement for 1000-year design earthquake event.....	22
9	Acceleration (outcrop) response spectra for the 1000-year design earthquake event.....	23
10	Horizontal components of acceleration versus time for the 5000-year design earthquake event (Risk Engineering, Inc. 1992).....	25
11	Variation of acceleration, velocity, and displacement for 5000-year design earthquake event.....	26
12	Acceleration (outcrop) response spectra for the 5000-year design earthquake event.....	27
13	General location map of PORTS showing existing plant and proposed additions amongst geologic setting (modified from Law Engineering Testing Company 1978 and Taylor et al. 1977).....	29
14	General geologic section through PORTS and Scioto River Valley looking north (from Law Engineering Testing Company 1978 and Taylor et al. 1977).....	30

LIST OF FIGURES (Continued)

<u>No.</u>		<u>Page</u>
15	Site plan of PORTS showing locations of previous studies, locations of profile lines, and geophysical measurements.....	31
16	General stratigraphic profiles A-A and B-B looking north (ERCE 1990).....	32
17	General stratigraphic profiles C-C looking north (ERCE 1990).....	33
18	General stratigraphic profiles D-D and E-E looking west (ERCE 1990).....	34
19	Contours representing thickness of fill in GCEP area (Law Engineering Testing Company 1978).....	36
20	Contours representing top-of-rock elevations in GCEP area (Law Engineering Testing Company 1978).....	38
21	Site plan showing locations of soil columns with respect to locations of profile lines.....	39
22	Soil columns PT-1 through PT-6 corresponding to site investigations conducted for GCEP.....	41
23	Soil columns PT-7 through PT-9 corresponding to site investigations conducted for GDAP.....	42
24	Soil columns PT-10 through PT-12 corresponding to site investigations conducted for GDAP.....	43
25	Soil columns PT-13 through PT-15 corresponding to site investigations conducted for GDAP.....	44
26	Results of laboratory tests showing relationship between shear modulus and damping versus shear strain for CL lacustrine soils.....	46
27	Results of laboratory tests showing relationship between shear modulus and damping versus shear strain for ML & ML-CL lacustrine soils.....	47
28	Standardized relationships between shear modulus and damping ratio for cohesionless soils (Seed and Idriss 1970 and Seed et al. 1986).....	49
29	Standardized relationships between shear modulus and damping ratio for cohesive soils (Sun, Golesorkhi, and Seed 1988).....	50
30	Relationships between shear modulus and damping ratio versus shear strain used for this study.....	51
31	Shear wave velocity profiles.....	53
32	Combined profiles of soil stiffness.....	55
33	Average soil column.....	57
34	Comparison of general cyclic behavior of soil and equivalent linear model with iterative scheme.....	61
35	Example figure showing a profile of the variation of acceleration with time.....	65
36	Example figure showing a profile of the variation of effective shear strain with time.....	66
37	Example figure showing pseudo-velocity response spectra in tripartite format (5 percent damping).....	68
38	Example figure showing the absolute acceleration response spectra for rock outcrop and free-field motions.....	69

LIST OF FIGURES (cont'd)

<u>No.</u>		<u>Page</u>
39	Example figure showing the ratio of absolute acceleration response spectra for free field to rock outcrop motions.....	70
40	Example figure showing the amplification ratios (absolute acceleration response spectra normalized to peak horizontal acceleration) for rock outcrop and free-field motions.....	71
41	Pseudo-velocity response spectra for 500-year event.....	76
42	Absolute response acceleration spectra for 500-year event.....	78
43	Ratio of free field to rock outcrop absolute acceleration response spectra for 500-year event.....	79
44	Amplification ratio for 500-year event.....	80
45	Pseudo-velocity response spectra for 1000-year event.....	83
46	Absolute response acceleration spectra for 1000-year event.....	84
47	Ratio of free field to rock outcrop absolute acceleration response spectra for 1000-year event.....	85
48	Amplification ratio for 1000-year event.....	87
49	Pseudo-velocity response spectra for 5000-year event.....	89
50	Absolute response acceleration spectra for 5000-year event.....	90
51	Ratio of free field to rock outcrop absolute acceleration response spectra for 5000-year event.....	92
52	Amplification ratio for 5000-year event.....	93
53	Ratio of free field to rock outcrop absolute acceleration response spectra for all events.....	94
54	Amplification ratio for all events.....	96
55	Comparison of results for average column and range produced from individual sites.....	98
56	Pseudo-velocity response spectra showing sensitivity of results to impedance contrast.....	100
57	Pseudo-velocity response spectra showing sensitivity of results to depth to bedrock.....	101
58	Pseudo-velocity response spectra showing sensitivity of results to modulus curves.....	103
59	Pseudo-velocity response spectra showing sensitivity of results to damping ratio.....	104
60	Range of stiffnesses used to evaluate sensitivity of results to maximum shear modulus.....	106
61	Pseudo-velocity response spectra showing sensitivity of results to maximum shear modulus.....	107

CONVERSION FACTORS, NON-SI to SI (METRIC)
UNITS OF MEASUREMENT

Non-SI units of measurement used in this report can be converted to SI (metric) units as follows:

<u>Multiply</u>	<u>Abbreviation</u>	<u>By</u>	<u>To Obtain</u>
acres	-	0.4047	square kilometers
feet	ft	0.3048	meters
inches	in.	2.54	centimeters
miles (US statute)	mis.	1.609	kilometers
pounds (mass) per cubic foot	pcf	16.01846	kilograms per cubic meter
pounds (mass) per square foot	psf	4.882428	kilograms per square meter
pounds (force) per inch	psi	6.894757	kilopascals

SITE-SPECIFIC EARTHQUAKE RESPONSE ANALYSIS FOR
PORTSMOUTH GASEOUS DIFFUSION PLANT
PORTSMOUTH, OHIO

PART I: INTRODUCTION

1. The Portsmouth Gaseous Diffusion Plant (PORTS), owned by the U.S. Department of Energy (DOE) and operated under contract by Martin Marietta Energy Systems, Inc., is located north of Portsmouth, Ohio. Photographs of the plant are shown in Figures 1 and 2. This plant was constructed in the 1950's and is one of only two gaseous diffusion plants in operation in the United States; the other is located near Paducah, Kentucky.

2. The facilities at PORTS are currently being evaluated for safety in response to natural seismic hazards. Design and evaluation guidelines to evaluate the effects of earthquakes and other natural hazards on DOE facilities follow probabilistic hazard models as have been outlined by Kennedy et al. (1990). Criteria also established by Kennedy et al. (1990) classify diffusion plants as "moderate hazard" facilities.

3. The U.S. Army Engineer Waterways Experiment Station (WES) was tasked to calculate the site response using site-specific design earthquake records developed by others and the results of previous geotechnical investigations for the proposed Gas Centrifuge Enrichment Plant (GCEP) and Gaseous Diffusion Add-On Plant (GDAP) as inputs. In all, six earthquake records at three hazard levels and fifteen individual and one average soil columns were used.

Purpose

4. The purpose of this study was to calculate a reasonable range of expected site-specific, free-field earthquake response at PORTS to three hazard-level earthquakes, a 500-year, 1000-year and a 5000-year design event, using geotechnical and geophysical information collected at the site during previous investigations for proposed major additions to the facility. The response was calculated independently for two components of horizontal motion at each hazard level. The emphasis of the evaluation was on the 1000-year event which represents the Design Basis Earthquake (DBE) for design and seismic evaluation studies at moderate hazard DOE facilities. Calculated



Figure 1. Aerial photograph of Portsmouth Gaseous Diffusion Plant looking southwest



Figure 2. Overhead aerial photograph of Portsmouth Gaseous Diffusion Plant

field response will be used to select spectra to be used for seismic safety evaluations and the future design of structures.

Procedure of Site Response Analysis

5. A site response analysis, sometimes referred to as a soil amplification analysis, involves the determination of components of ground motion for design or seismic evaluation. Typically, as in this study, that determination is made for a "free-field" response—the response at the ground surface of an ideal soil deposit (horizontal layers extending to infinity) to a spatially-uniform, horizontal motion applied at the base. The conceptual relationship between free-field response with respect to two other primary control points—rock outcrop and base rock—in a site response analysis is shown in Figure 3. The motions at these three points, as well as any other point in the vertical profile, are unique. Design earthquake motions are most often specified as corresponding to rock outcrop. Mathematical expressions (transfer functions) are then used to find the equivalent motion for the baserock and then the seismic waves are propagated through the soil column to determine the free-field motion at the surface.

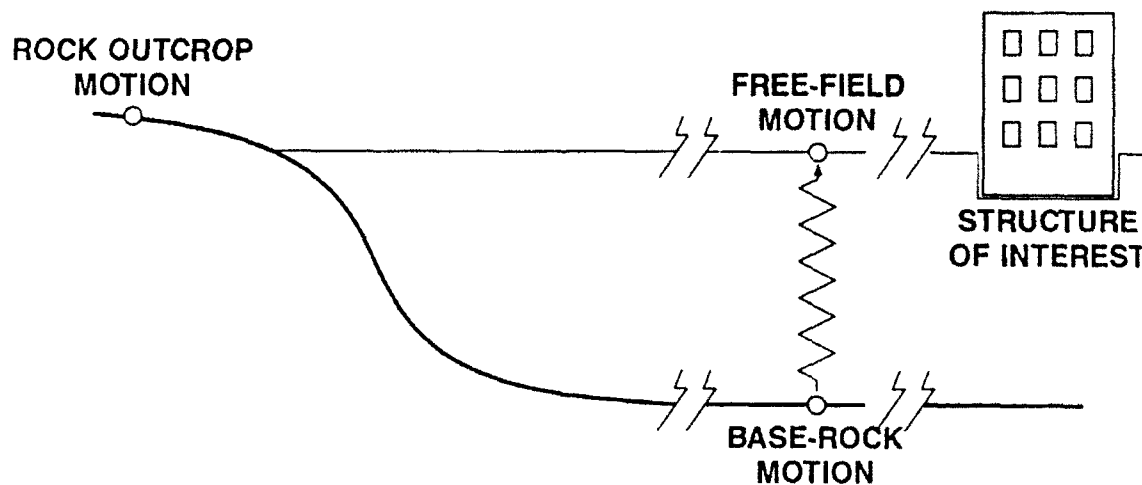


Figure 3. Three primary control points for a site response analyses

6. The determination of site-specific earthquake response of soil deposits generally involves three basic steps:

- a. Determination of earthquake hazard and the selection or derivation of design motions.
- b. Idealization of stratigraphy and selection of material properties.
- c. Calculation and evaluation of site response.

For this study, step (a) and part of step (b), listed above, were conducted by others and submitted to WES by Martin Marietta Energy Systems, Inc. The idealizations reported by Law Engineering Testing Company (1978) based on geotechnical and geophysical investigations for GCEP were used directly (six soil columns). WES obtained additional data from site investigations conducted by WES (Curro and Marcuson 1978) for GDAP to create an additional nine soil columns. WES was wholly responsible for the calculation and evaluation of site-specific earthquake response (step (c) listed above).

7. At the direction of Martin Marietta Energy Systems, Inc., the computer program *SHAKE* (Schnabel, Lysmer, and Seed 1972) was used to calculate site response for purposes of this study. *SHAKE* is a one-dimensional, total stress code that solves the wave equation in the frequency domain (complex response technique). The soil profile is represented with an idealized soil column of homogeneous, visco-elastic layers of infinite extent.

8. *SHAKE* is widely used by the geotechnical earthquake engineering profession for the calculation of site response for horizontal motions. Several investigators have reported close comparisons between the results using *SHAKE* and the measured horizontal response from strong-motion instruments triggered during earthquakes at periods less than 2 sec (e.g., Seed et al. 1987 and Seed, Dickenson, and Idriss 1991). The experience of these investigators suggest that for periods greater than 4 sec, motions are likely to be significantly affected by two-dimensional effects and surface wave energy and are not well represented with *SHAKE*.*

Special Considerations for Study at PORTS

9. Two conditions specific to PORTS should be considered when evaluating the site response—the stratigraphy of the valley and the

* Personal communication, Prof. Raymond Seed, University of California at Berkeley, 23 September 1991.

distribution of soil columns. The geometry of the bedrock and valley fill in the vicinity of PORTS suggest that two-dimensional effects of wave propagation may be important, particularly at locations close to the margins of the valley. The evaluation of these effects was beyond the scope of this study. The locations of the borings used to construct the soil columns for this study are not well distributed among the existing plant structures as will be described in Part III. Since evaluation of the site response is especially desired in the vicinity of key facilities, some judgement may be required to interpret appropriate site response in particular areas of interest.

10. A comprehensive sensitivity analysis of inputs was performed to account for reasonable uncertainties in measured shear wave velocities, estimated relationships between shear modulus and damping ratio versus shear strain, and modulus curves. The range of results were also compared with a range produced for an average site column using the recommendations of the Nuclear Regulatory Commission (1989).

Report Organization

11. The presentation of information henceforth generally will follow the order of site response analysis listed earlier. First, the synthetic records used in the analysis are presented in Part II. Then, stratigraphic and material property information is presented in Part III. Detailed descriptions of calculations and methods of presentation are given in Part IV. The results of calculations for the 500-year, 1000-year, and 5000-year events are presented in Part V. The sensitivity analysis was conducted using an average column intended to represent all fifteen sites and the 1000-year event and is summarized in Part VI. A summary and conclusions sections completes the report. Figures representing many of the computations conducted for the study are contained in the appendices for reference.

PART II: DESIGN EARTHQUAKE EVENTS

12. The determination of earthquake hazard and the selection or derivation of appropriate design records represent the first step of a site response analysis. Based on DOE Standard 1024-92 (Department of Energy 1992) and the moderate hazard classification assigned to PORTS, probabilistic methods of hazard analysis were used to derive parameters defining the design events and to develop corresponding synthetic records.

13. The probabilistic assessment of seismic hazard was conducted by Risk Engineering, Inc. (1993) using a recent methodology developed by the Electric Power Research Institute (EPRI) and funded by the Seismic Owners Group (SOG). Results using the EPRI/SOG methodology (Electric Power Research Institute 1988) were then combined with the results by Davis and Savy (1990) who used the Lawrence Livermore National Laboratory (LLNL) method funded by the U.S. Nuclear Regulatory Commission (NRC). The DOE standard provides a method for determining the dominant earthquake magnitudes and epicentral distances for the 500-year, 1000-year, and 5000-year events and developing site-specific uniform hazard response spectra at these three levels of hazard. The dominant magnitudes and epicentral distance are: 5.6 at 140 km for the 500-year event, 5.7 at 130 km for the 1000-year event, and 5.9 at 130 km for the 5000-year event.

14. Three sets of synthetic earthquake records were developed for this study corresponding to three median levels of hazard (500-year, 1000-year, and 5000-year events) and represent rock outcrop motions. Synthetic earthquake records were developed by Risk Engineering, Inc., (1992) to completely envelop the uniform hazard spectra. Two components of horizontal motion were provided for each earthquake event. A time step of 0.01 sec (i.e., 100 samples per second) was used which corresponds to a Nyquist frequency of about 50 Hz, a value well above the free-field natural frequency at the site. Records of the variation of acceleration, velocity, and displacement with time and absolute acceleration response spectra are presented below for the three design events using a constant vertical plot scale for consistency. The acceleration and velocity records were integrated exactly by WES to allow inspection of the variations of velocity and displacement, respectively, with time.

500-Year Event

15. The three components of the synthetic 500-year design earthquake event for rock outcrop are shown in Figure 4 and particular characteristics are summarized in Table 1. The peak horizontal ground acceleration is 0.04 g for both components. Neither record contains any strong motion (as defined by peak accelerations ≥ 0.05 g). The variation of acceleration, velocity, and displacement for the two horizontal components of the 500-year event are shown in Figure 5.

Table 1
Characteristics of 500-Year Event Outcrop Motions

Component	Peak Acceleration (cm/sec ²)	Peak Velocity (cm/sec)	Peak Displacement (cm)	Duration Strong Motion (sec)
Horizontal 1	37	1.5	0.8	0
Horizontal 2	38	2.6	2.0	0

16. The variation of velocity and displacement for the two horizontal components differ noticeably both in the peak amplitude and the number of times that it crosses the zero amplitude line. The Horizontal 2 component has a peak velocity and displacement on the order of twice the Horizontal 1 component with about half the number of crossover points. Therefore, the computed ground response is expected to be greater for the Horizontal 2 component. The displacement for the Horizontal 2 component also does not entirely converge to zero at the end of the acceleration record (in fact the displacement diverges rapidly beyond 18 sec).

17. The absolute acceleration response spectra at six levels of system damping for the 500-year event are shown for both components of rock outcrop motion in Figure 6. The two spectra are relatively uniform over the period range of 0.02 to 0.3 sec with several peak spectral accelerations between 0.08 and 0.10 g for 5 percent damping. The Horizontal 2 component shows a slight tendency to have more energy at very low periods (less than 0.03 sec).

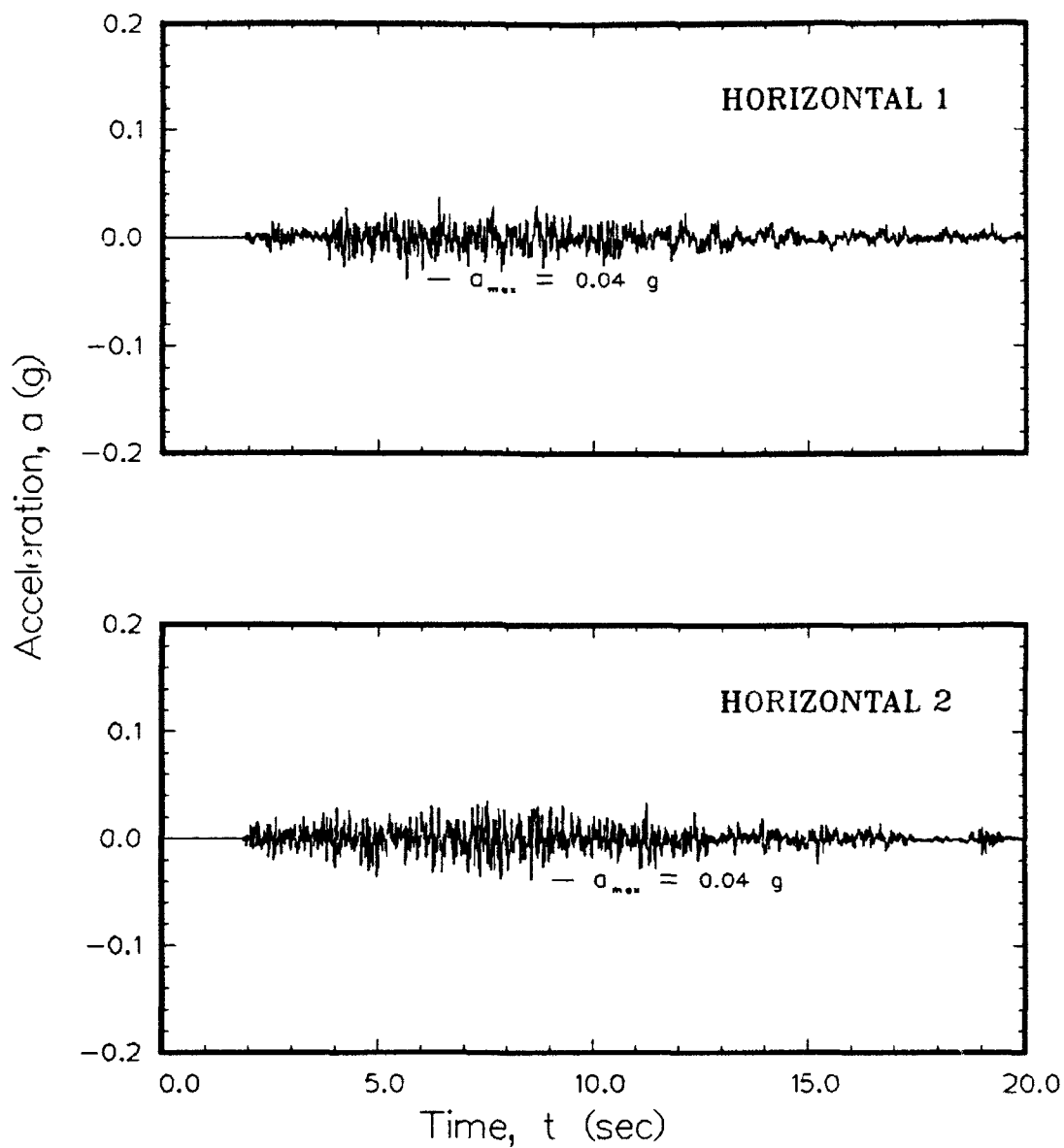
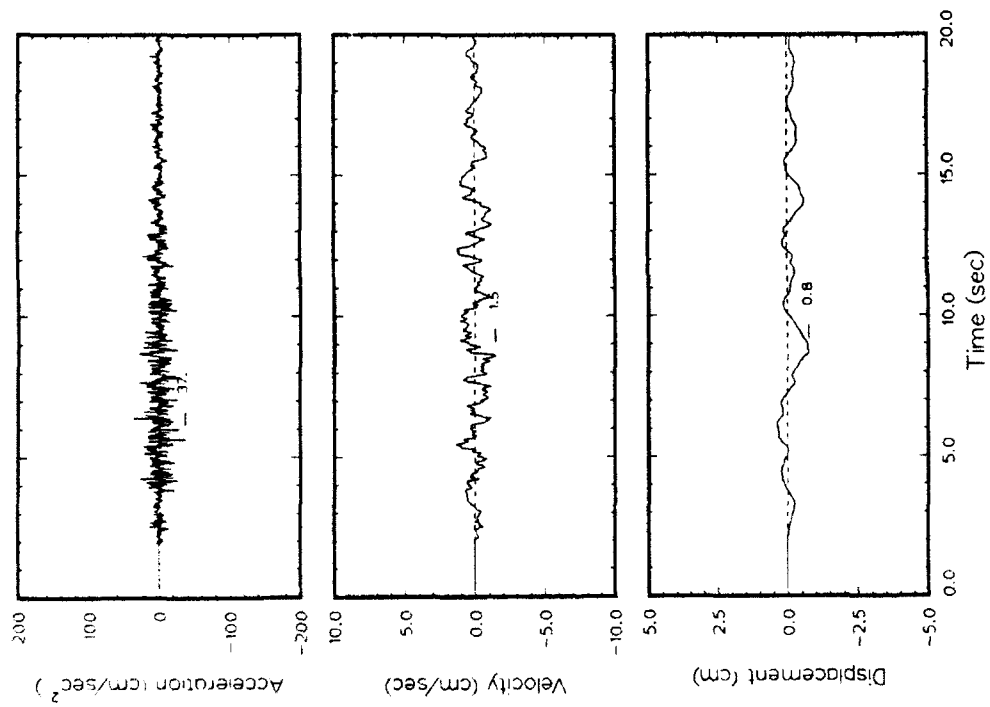
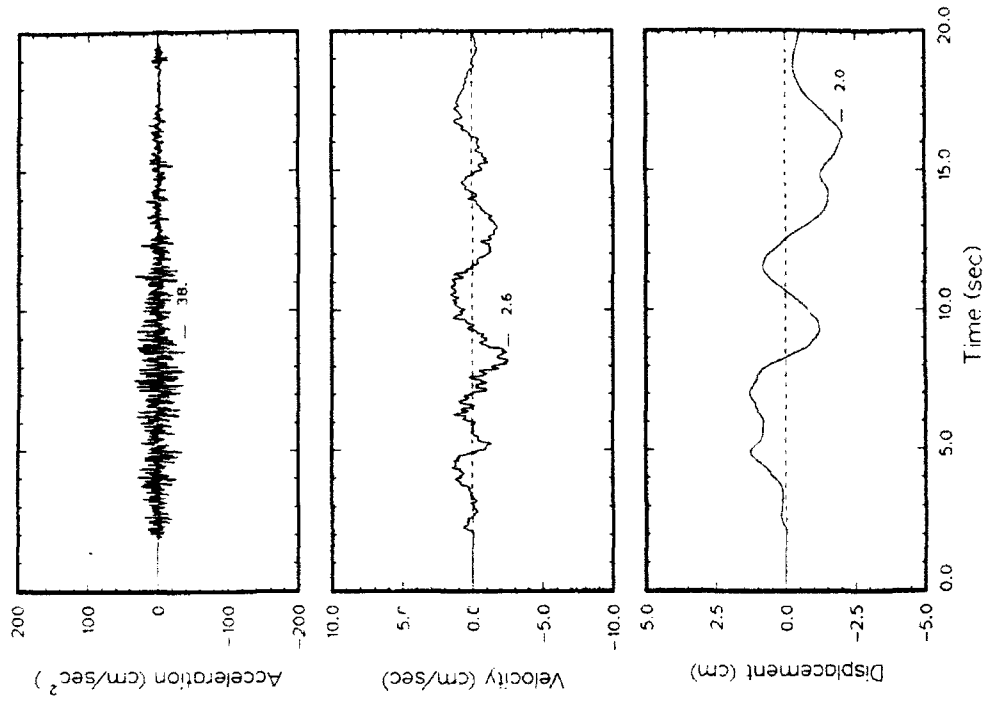


Figure 4. Horizontal components of acceleration versus time
for the 500-year design earthquake event
(Risk Engineering, Inc. 1992)



a. Horizontal 1 component



b. Horizontal 2 component

Figure 5. Variations of acceleration, velocity, and displacement for 500-year design earthquake event

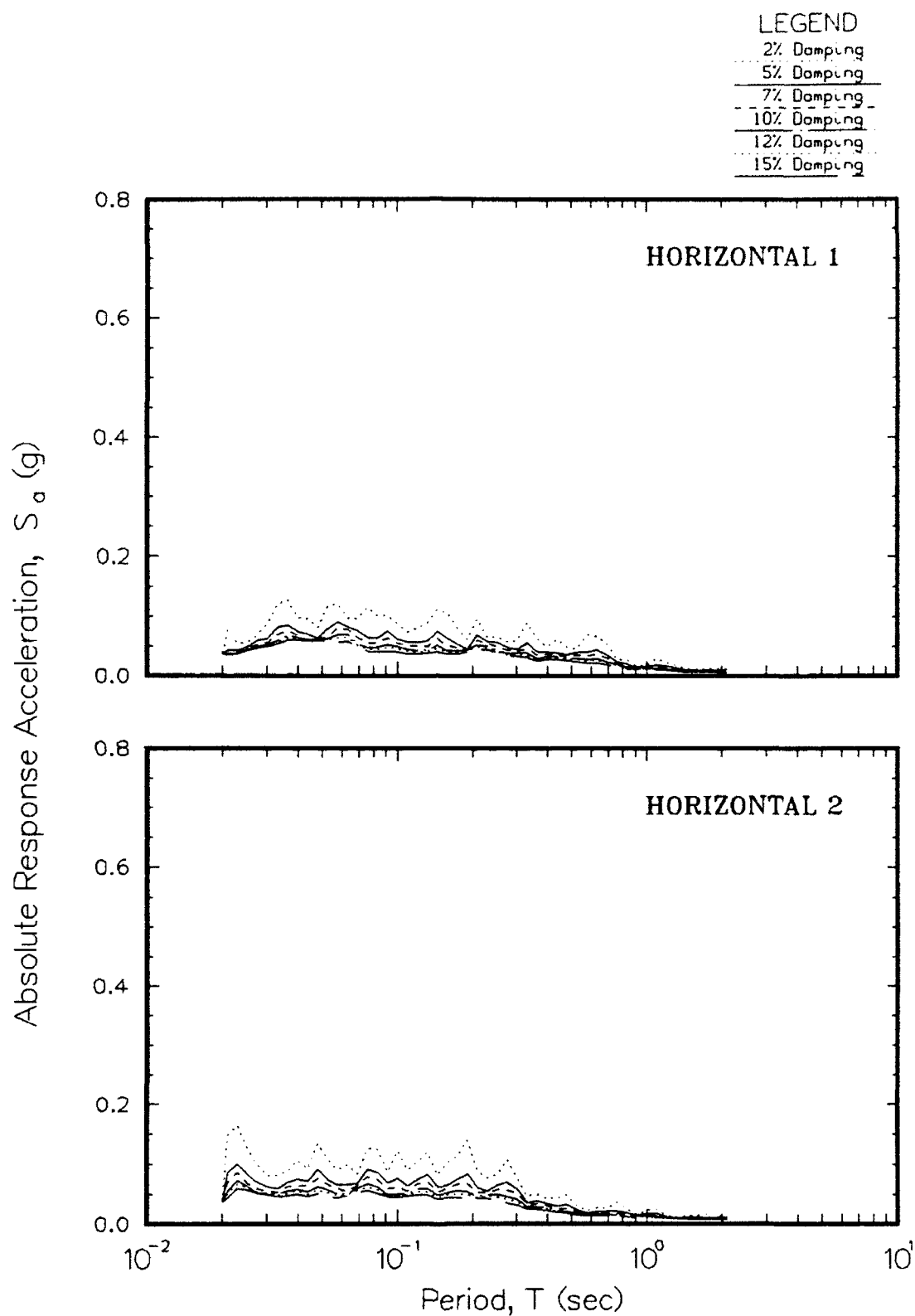


Figure 6. Acceleration (outcrop) response spectra for the 500-year design earthquake event

1000-Year Event

18. The three components of the synthetic 1000-year design earthquake event for rock outcrop are shown in Figure 7 and particular characteristics are summarized in Table 2. The peak horizontal ground acceleration is 0.07 g for both components and the durations of strong motion (accelerations \geq 0.05 g) are 1 and 5 seconds. The variation of acceleration, velocity, and displacement for the two horizontal components of the 1000-year event are shown in Figure 8.

Table 2
Characteristics of 1000-Year Event Outcrop Motions

Component	Peak Acceleration (cm/sec ²)	Peak Velocity (cm/sec)	Peak Displacement (cm)	Duration Strong Motion (sec)
Horizontal 1	66	3.3	3.2	1
Horizontal 2	71	3.2	4.4	5

19. The variation of velocity and displacement for the two horizontal components differ noticeably in the number of cycles that cross the zero amplitude line; the amplitudes are comparable. The Horizontal 2 component again has a fewer number of crossover points. The variation of displacement for both components show a strong preference to one (negative) direction. These relative values and difference in duration suggest that the Horizontal 2 component may tend to produce greater ground response.

20. The absolute acceleration response spectra at six levels of system damping for the 1000-year event are shown for both components of rock outcrop motion in Figure 9. The two spectra are again relatively uniform over the period range of 0.02 to 0.3 sec with several peak spectral accelerations between 0.10 and 0.15 g for 5 percent damping. The Horizontal 2 component shows a slight tendency to have more energy at mid-range periods (between 0.07 and 0.2 sec) than the Horizontal 1 component.

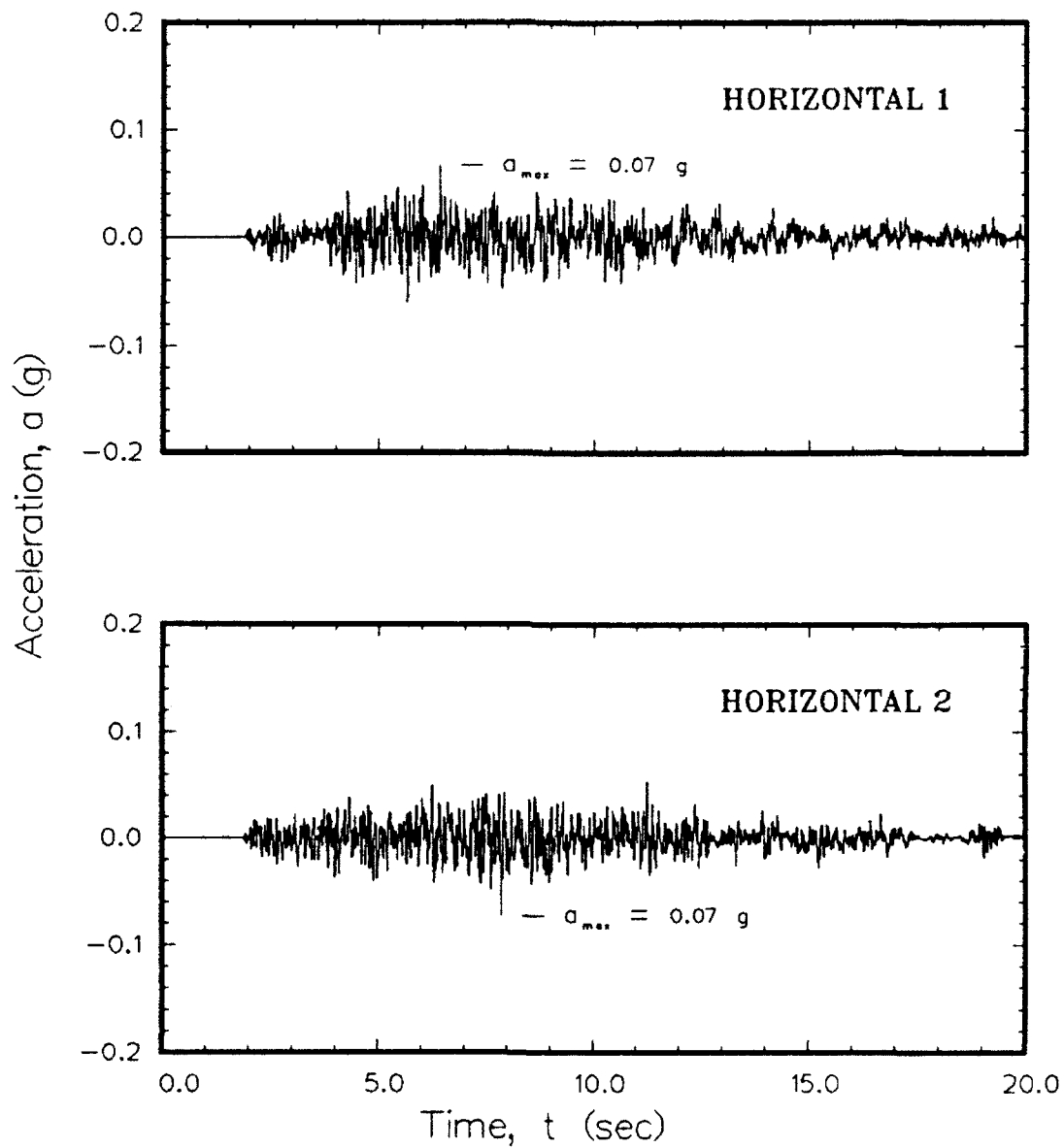
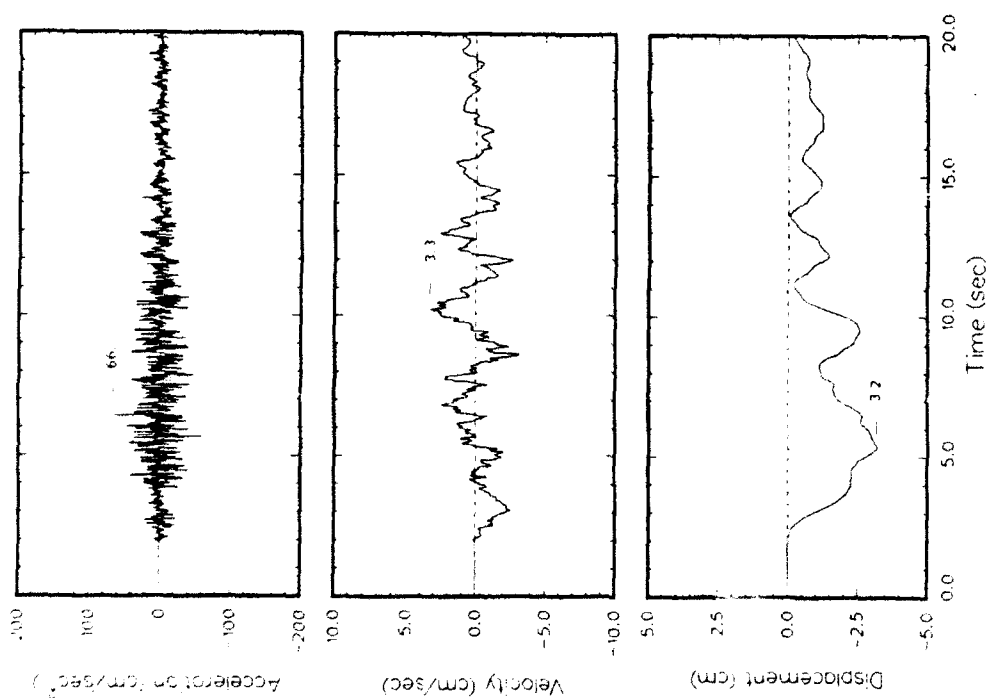
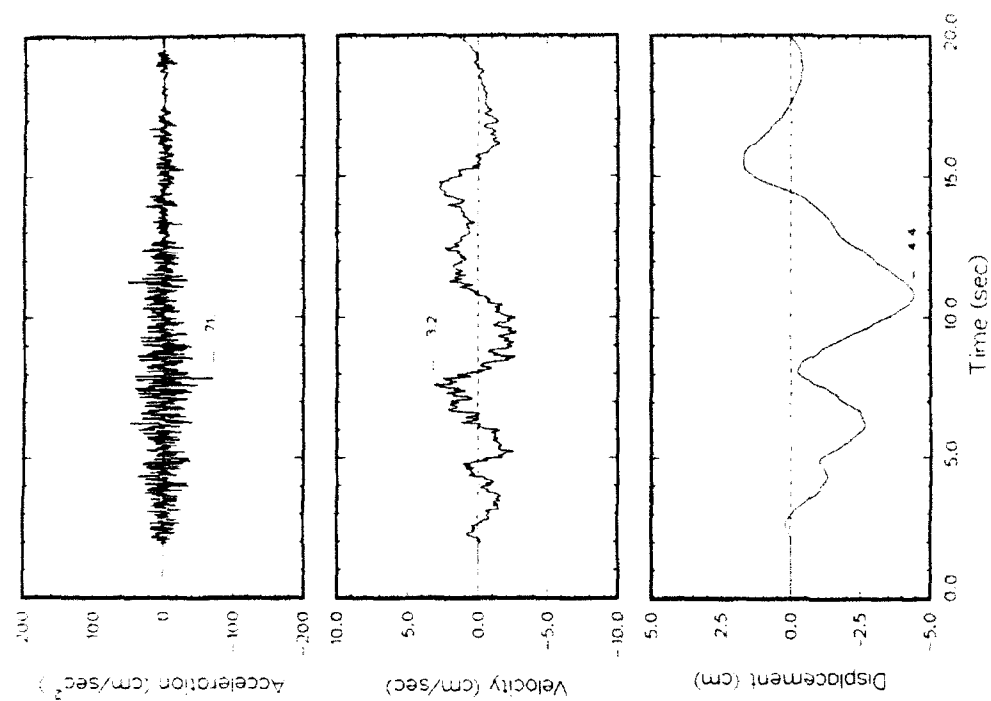


Figure 7. Horizontal components of acceleration versus time
for the 1000-year design earthquake event
(Risk Engineering, Inc. 1992)



a. Horizontal 1 component



b. Horizontal 2 component

Figure 8. Variations of acceleration, velocity, and displacement for 1000-year design earthquake event

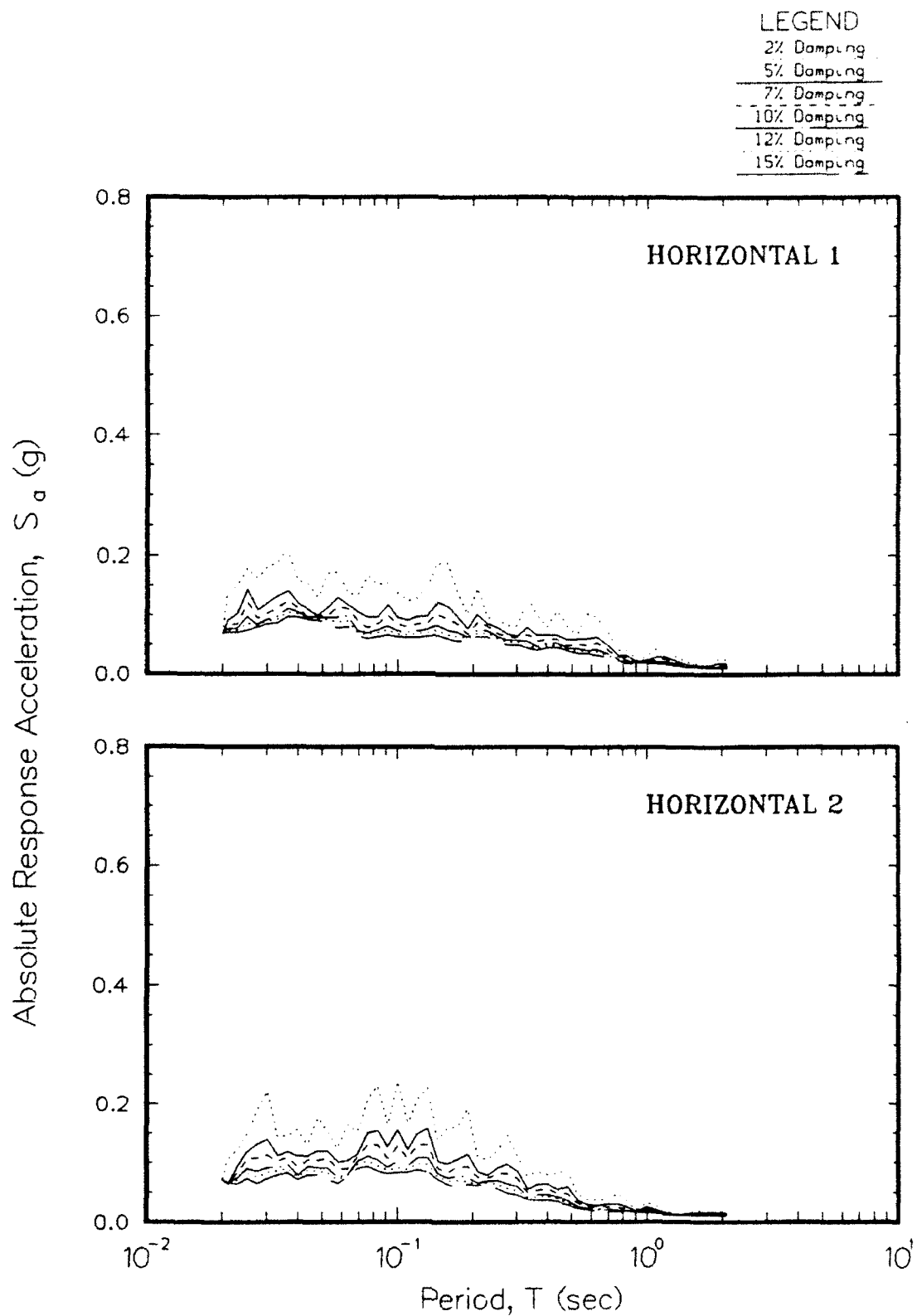


Figure 9. Acceleration (outcrop) response spectra for the 1000-year design earthquake event

5000-Year Event

21. The three components of the synthetic 5000-year design earthquake event for rock outcrop are shown in Figure 10 and particular characteristics are summarized in Table 3. The peak horizontal ground acceleration is 0.13 g for both components and the durations of strong motion (accelerations \geq 0.05 g) are 13 and 15 sec. The variation of acceleration, velocity, and displacement for the two horizontal components of the 5000-year event are shown in Figure 11.

Table 3
Characteristics of 5000-Year Event Outcrop Motions

Component	Peak Acceleration (cm/sec ²)	Peak Velocity (cm/sec)	Peak Displacement (cm)	Duration Strong Motion (sec)
Horizontal 1	123	5.4	3.4	13
Horizontal 2	132	5.5	3.7	15

22. The variation of velocity and displacement for the two horizontal components are comparable, much more so than the other two design earthquakes. The similarity between components suggests that there will be little preference for stronger ground response between the two components.

23. The absolute acceleration response spectra at six levels of system damping for the 1000-year event are shown for both components of rock outcrop motion in Figure 12. The two spectra have peak spectral accelerations occurring at low periods (0.035 to 0.04 sec) and then a relatively gradual decrease in spectral acceleration as period increases. The Horizontal 2 component has a more predominant peak at 5 percent damping (0.5 g at 0.035 sec) whereas the Horizontal 1 component is smoother (peak of 0.35 g at a period of 0.4 sec).

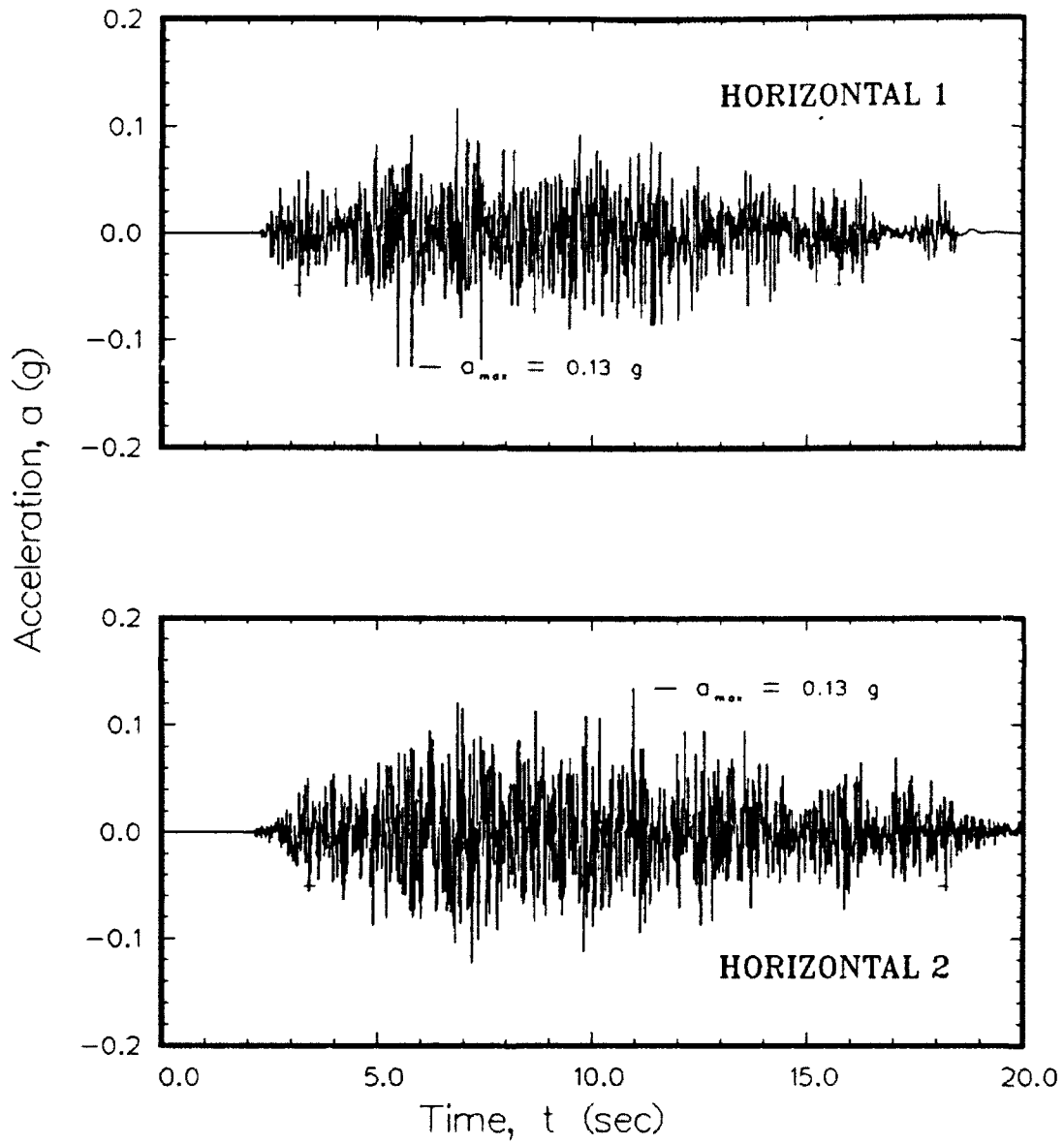
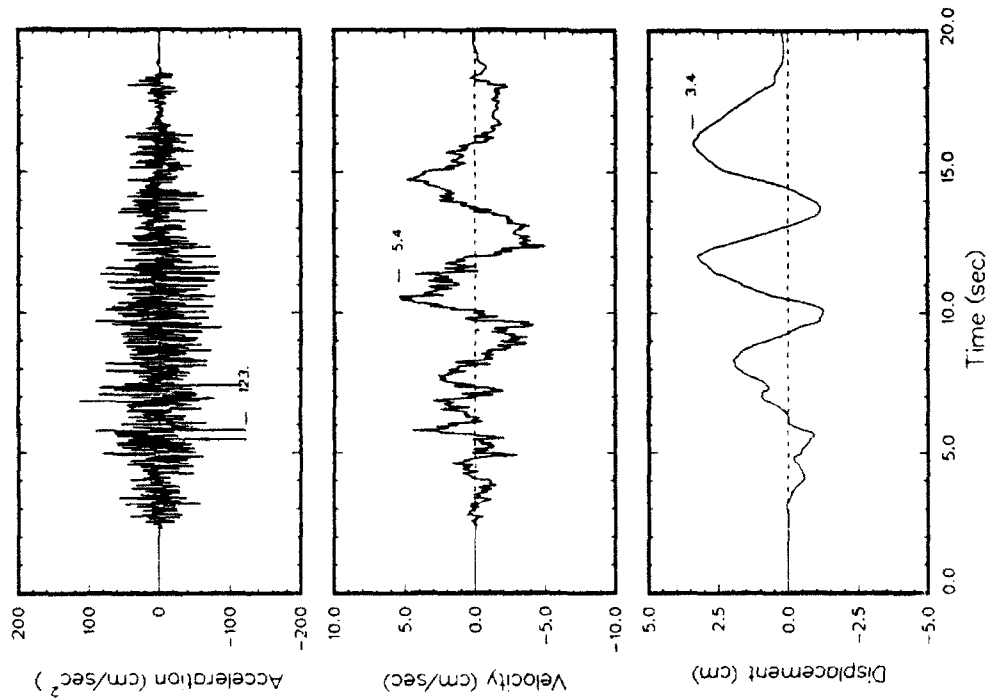
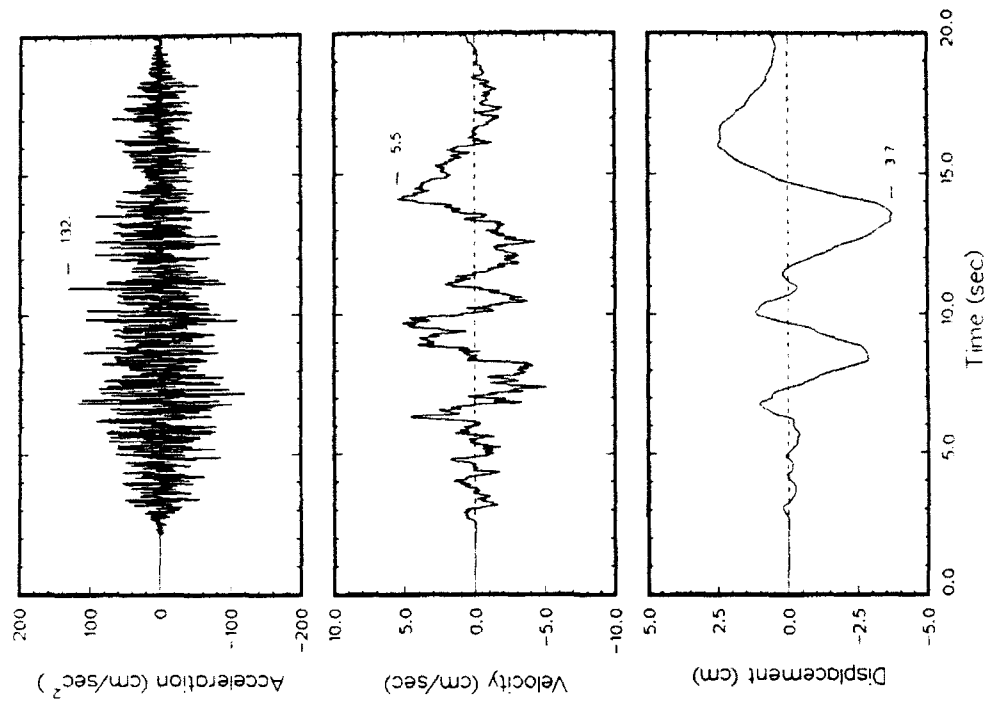


Figure 10. Horizontal components of acceleration versus time for the 5000-year design earthquake event (Risk Engineering, Inc. 1992)



a. Horizontal 1 component



b. Horizontal 2 component

Figure 11. Variations of acceleration, velocity, and displacement for 5000-year design earthquake event

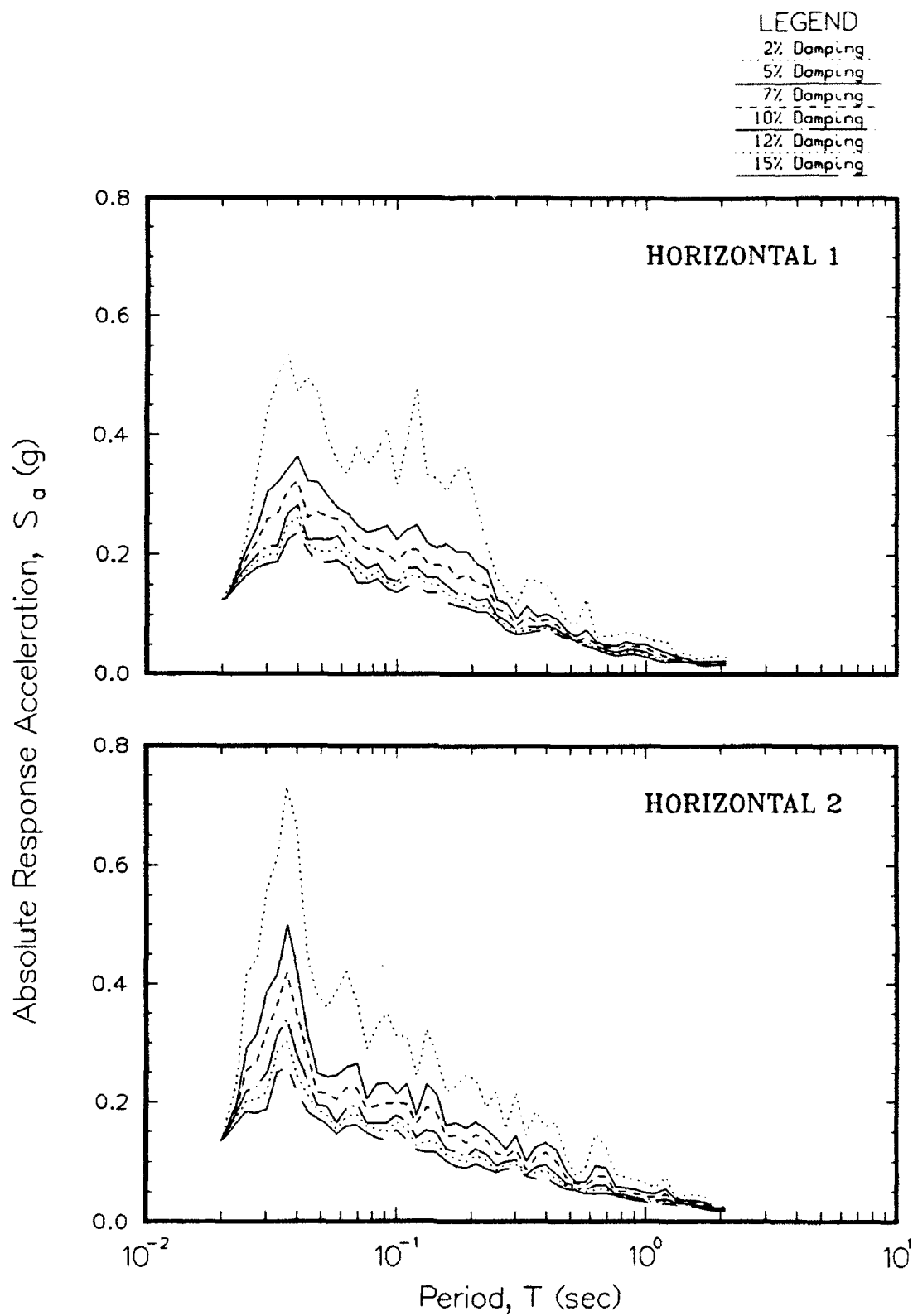


Figure 12. Acceleration (outcrop) response spectra for the 5000-year design earthquake event

PART III: SITE DESCRIPTION AND SOIL COLUMNS

24. PORTS is located about 20 miles** north of Portsmouth, in east central Pike County, Ohio, about 2 to 3 miles east of the Scioto River. The site is located in the Appalachian Plateau Province, within the boundary of the pre-glacial Portsmouth River Valley. This valley is about 1 mile wide (in a east-west direction) at PORTS with an average surface elevation of about 670 ft and topographic relief generally less than 10 ft. The valley is generally well drained, with overall drainage to the south.

Site Geology

25. The surface geology in the vicinity of the plant area is shown in Figure 13. The pre-glacial Portsmouth River valley is a tributary to the pre-glacial Teays River immediately to the north of PORTS. A general section of the geology along a line (section AA) perpendicular to the Scioto River Valley and through the plant area is shown in Figure 14. The elevation of the Scioto River floodplain is about 540 ft, while older terraces are at an elevation of about 580 ft. (Taylor et al. 1977) The plant area is underlain by Sunbury Shale or Berea Sandstone, or both, overlying Bedford and Ohio Shales.

26. Soils in the ancient Portsmouth River Valley at PORTS consist primarily of Pleistocene-age lacustrine (lake bed) deposits of silt and clay and are sometimes underlain by Pleistocene-age alluvial deposits of the Portsmouth River. Holocene-age alluvium exist in remnant stream channels. In addition, fill exists at several locations in the plant area.

27. General stratigraphic profiles through the plant area were constructed by ERCE (1990) using available subsurface information. A map of the plant layout showing the locations of some of these profiles and corresponding borings are shown in Figure 15. The five profiles are shown in Figures 16 through 18.+ Also shown are the general proximity of previous geotechnical studies and the number of respective borings. Over 600 borings

** A table of factors for converting US customary units of measurement to metric (SI) units is presented on page 8.

+ The actual profiles reported by ERCE (1990) are reproduced even though some discrepancies exist in elevations of soil units at the intersections between profiles.

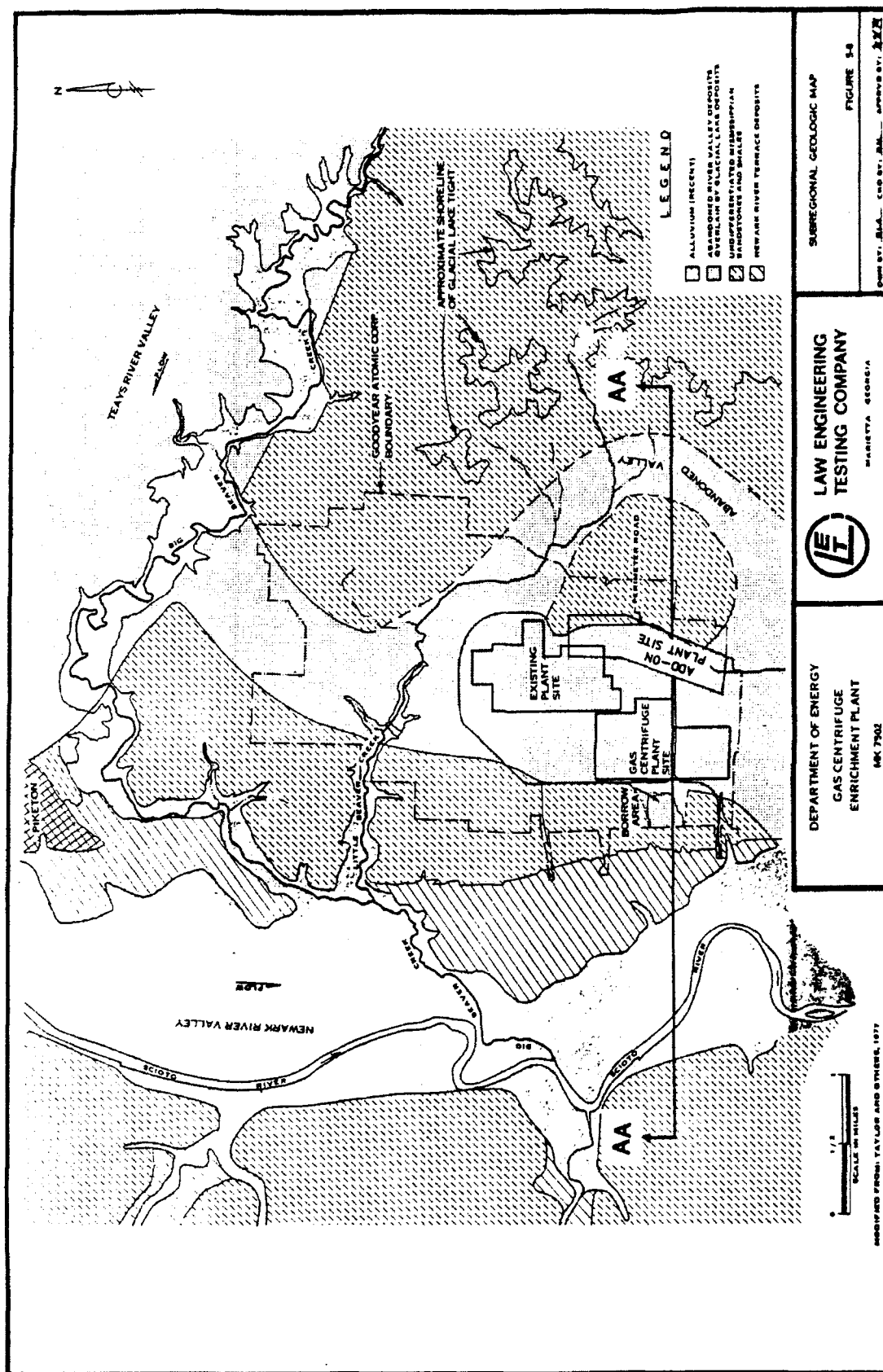


Figure 13. General location map of PORTS showing existing plant and proposed additions amongst geologic setting (modified from Law Engineering Testing Company 1978 and Taylor et al. 1977)

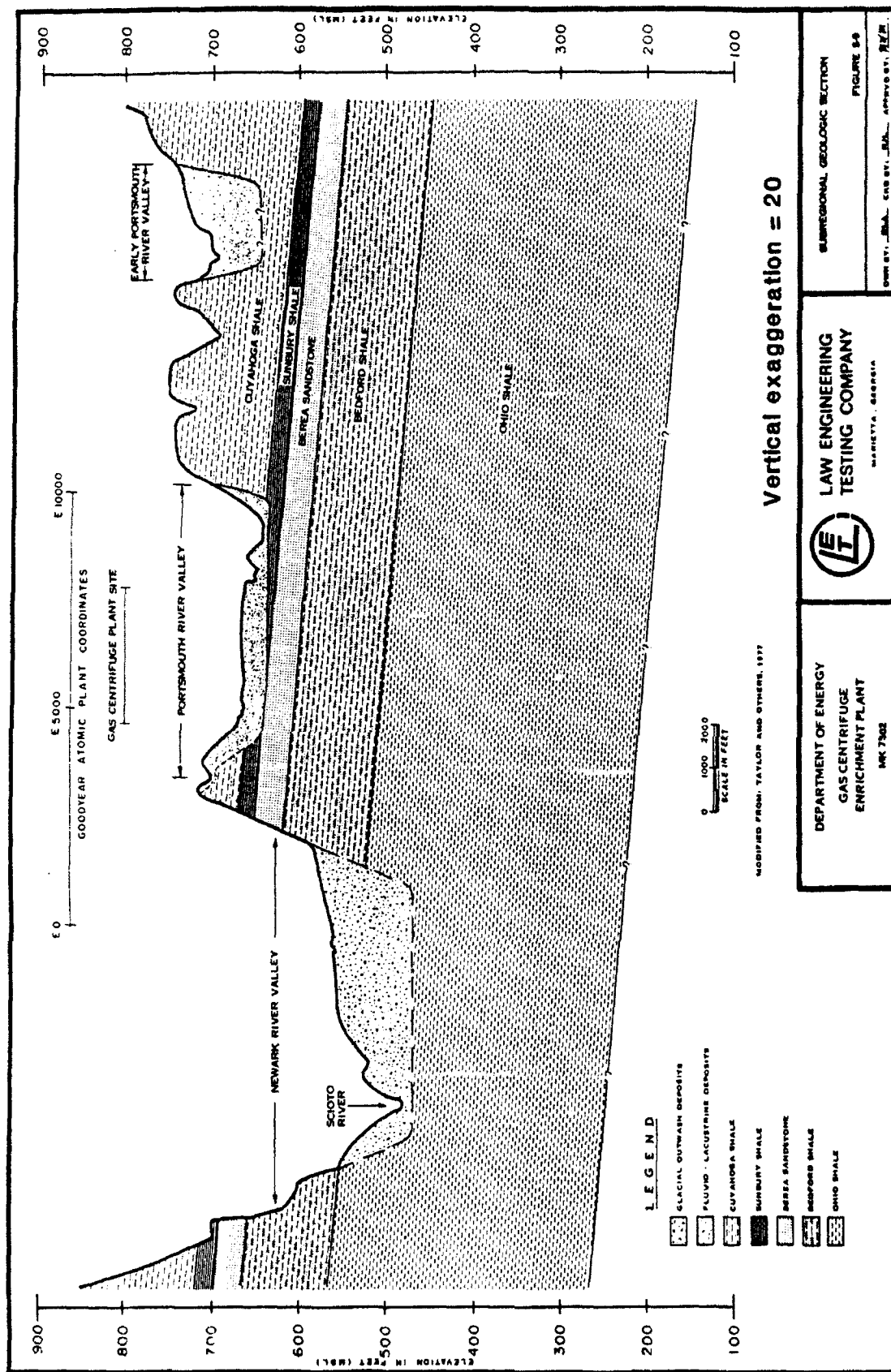


Figure 14. General geologic section through PORTS and Scioto River Valley looking north (from Law Engineering Company 1978 and Taylor et al. 1977)

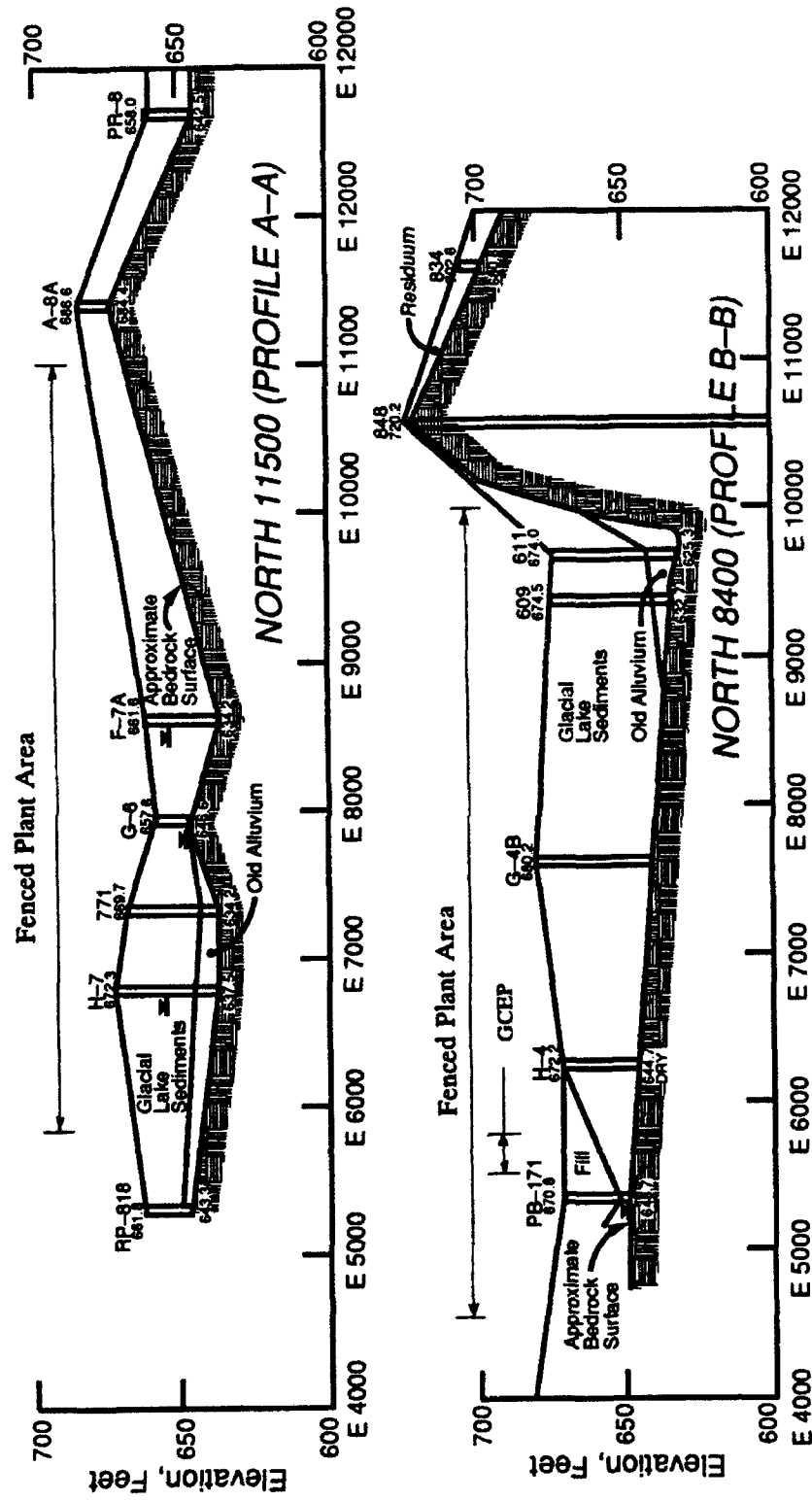


Figure 16. General stratigraphic profiles A-A and B-B looking north (ERCE 1990)

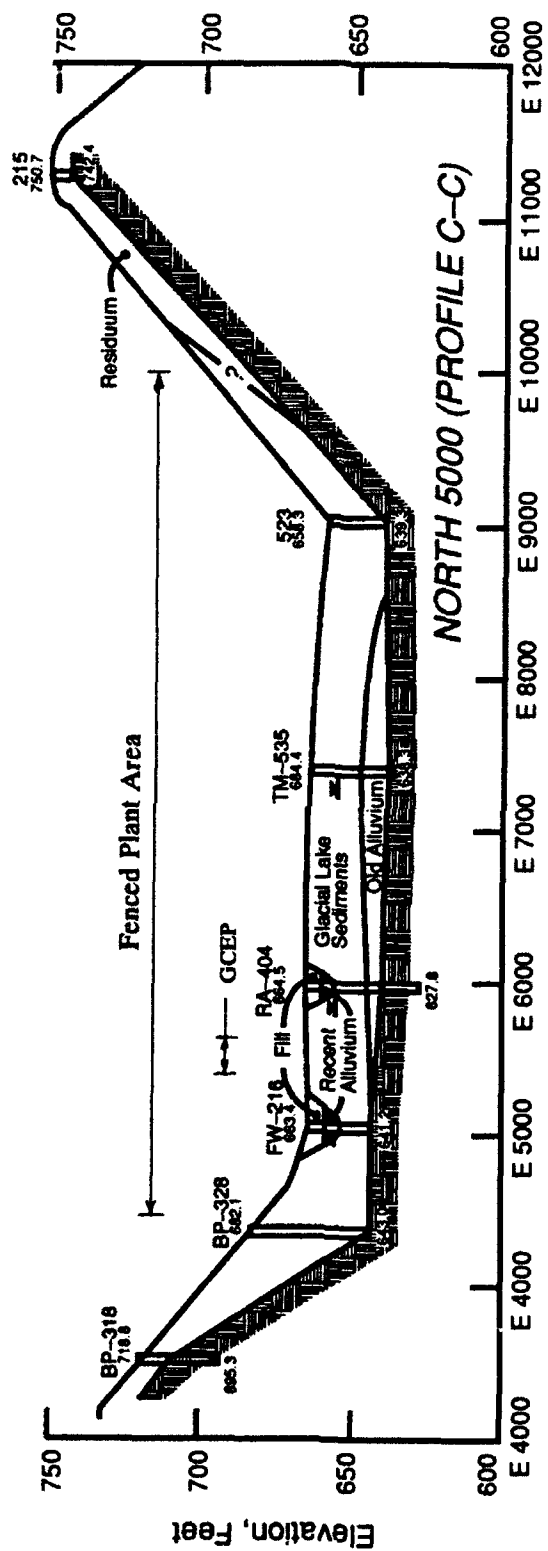


Figure 17. General stratigraphic profile C-C looking north (ERCE 1990)

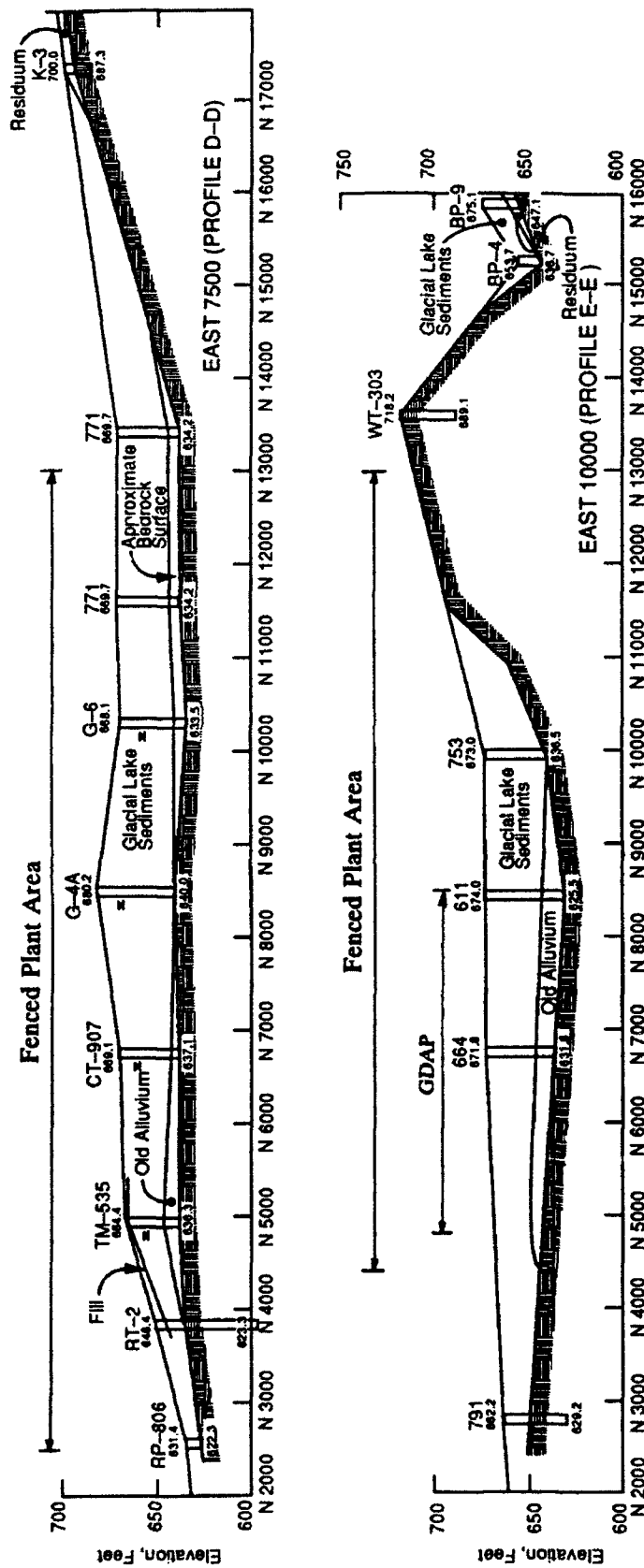


Figure 18. General stratigraphic profiles D-D and E-E looking west (ERCE 1990)

have been made at this site but the records for most of the 1950's work could not be found. The general locations of recent geophysical measurements in the profiles for the two additions are also shown in these figures.

28. These profiles show that the lacustrine deposits are generally much thicker than the alluvium and that the total thickness of soil within the fenced plant area varies between 0 and 45 ft. The soil-bedrock contact is relatively horizontal except near the east and northeast margins (at edge of valley). Recent alluvium and fill are generally confined to stream channels. It is believed that up to 60 ft of overburden has been removed by natural processes at the site during Holocene time (Taylor et al. 1977). Therefore, the older Pleistocene-age soils are expected to be moderately over-consolidated. Brief descriptions of the soil units and upper bedrock units are presented below.

29. Fill. Fill is the consequence of site grading using cut-and-fill procedures used during construction in the 1950's. The maximum thickness of fill is estimated to be about 20 ft and consists of silty clay of lacustrine origin. Records of fill placement and construction specifications were not available for this study. Contours of the thickness of fill in the GCEP area are shown in Figure 19 as an example of the potential range of thickness and distribution of fill.

30. Holocene-age alluvium. Holocene alluvium is present in very small quantities, being confined to narrow stream channels that have been buried with fill during construction (refer to section C-C in Figure 17). These deposits were not encountered in the two geotechnical studies nor given special consideration for the site response analysis. Their small extent is not likely to impact the overall response.

31. Lacustrine deposits. Lacustrine deposits constitute the majority of materials at PORTS. These Pleistocene-age deposits are the consequence of damming the ancient Teays and Portsmouth Rivers by glaciers during the last glacial period. These deposits are predominantly silts and clays with USCS classifications of ML, ML-CL, CL, and CH and can be categorized as being firm to very stiff. Plastic (fat) clays (CH's) were encountered near the ground surface in seven of the borings used to idealize soil columns.

32. Pleistocene-age deposits. Pleistocene-age alluvium (channel deposits of sand and gravel and floodplain deposits of silt and clay) of the ancient Portsmouth River underlie various parts of the plant. Gravel deposits

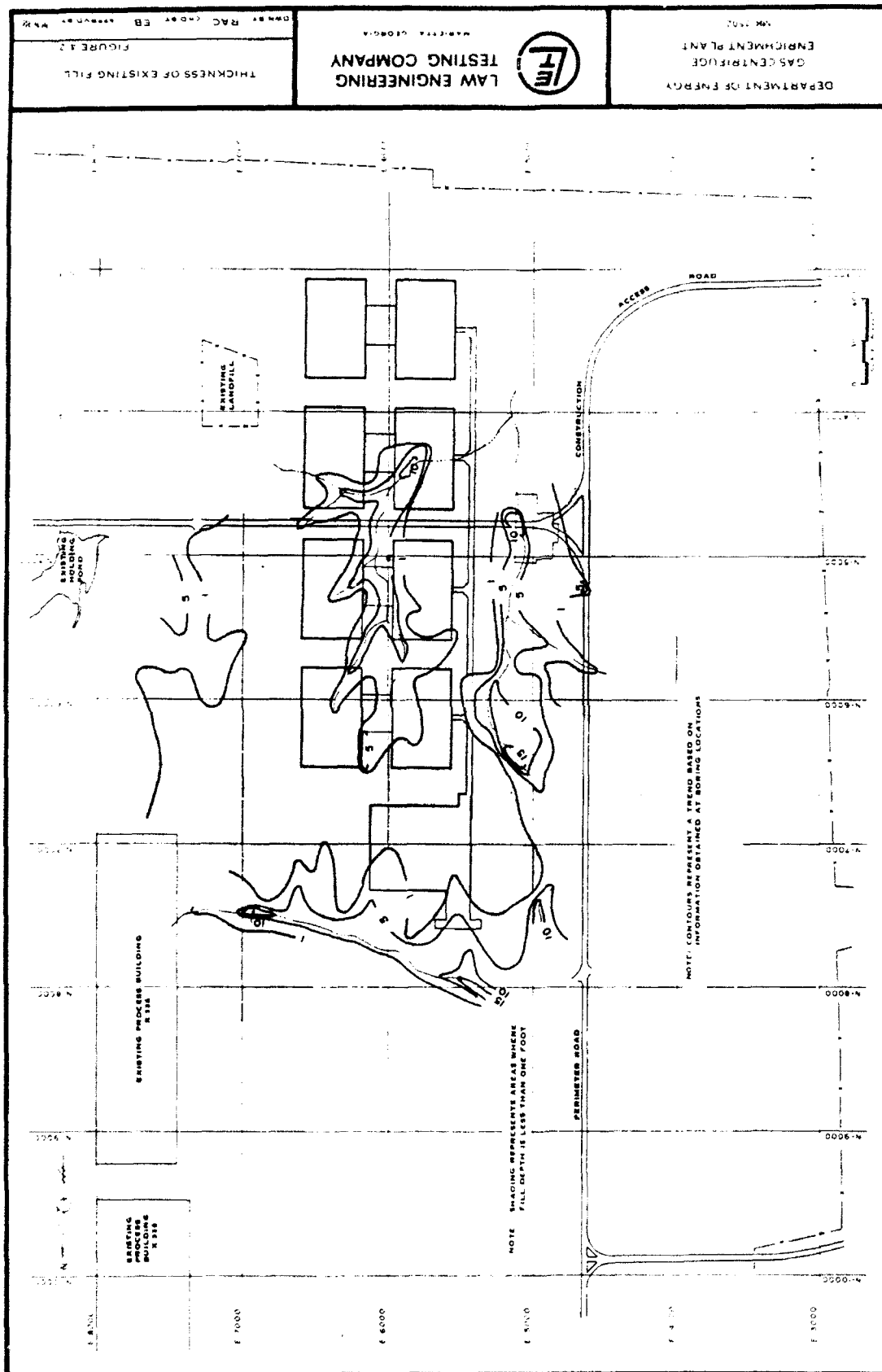


Figure 19. Contours representing thickness of fill in GCEP area
(Law Engineering Testing Company 1978)

range from "sandstone gravel" to clayey gravel. The maximum thicknesses of these deposits are 10 ft for gravels and 7 ft for clays.

33. Bedrock. Bedrock at PORTS is the Berea Sandstone. Sunbury shale exists above the sandstone in the eastern valley (corresponding to GDAP) and pinches out near the center of the valley along the east-west profile shown in Figure 14. Contours of bedrock shown in Figure 20 suggest that the soil-bedrock contact is relatively smooth and level in the central portion of the ancient Portsmouth River Valley and slopes significantly at the eastern valley margin. Either sandstone or shale was used as base rock (refer to Figure 3) for site response calculations.

Individual Soil Columns

34. A "soil column" is a one-dimensional idealization of a layered soil deposit. This representation assumes that the soil layers and surface of the deposit are horizontal and that the material properties do not vary over the thickness of any one layer. The primary components of a soil column are: geometry (number of layers and thickness of each layer), geotechnical engineering data, and seismic geophysical data. General descriptions of each of these categories are provided in the following sections.

35. Fifteen individual soil columns were available or derived from previous geotechnical engineering investigations at PORTS. Six columns were obtained directly from a study for GCEP; nine columns were derived from independent locations from investigations performed for GDAP. The general locations of these areas are shown in Figure 15. The locations of borings used to derive these columns are shown in Figure 21. The locations of profile lines are shown for reference. The relative locations of these sites are also provided in the soil profiles shown previously in Figures 16, 17, and 18. Tabulated coordinates and surface elevations are presented in Appendix A.

36. The locations of the fifteen soil columns are not well distributed about the complete plant area. Specifically, measurement of seismic velocities have been not been made in the near vicinity of Buildings X333 and X330. The northern edge of these two buildings is about 3000 ft north of the furthest northern extent of seismic measurements. However, the previous presentation of stratigraphic sections and bedrock contours provides evidence

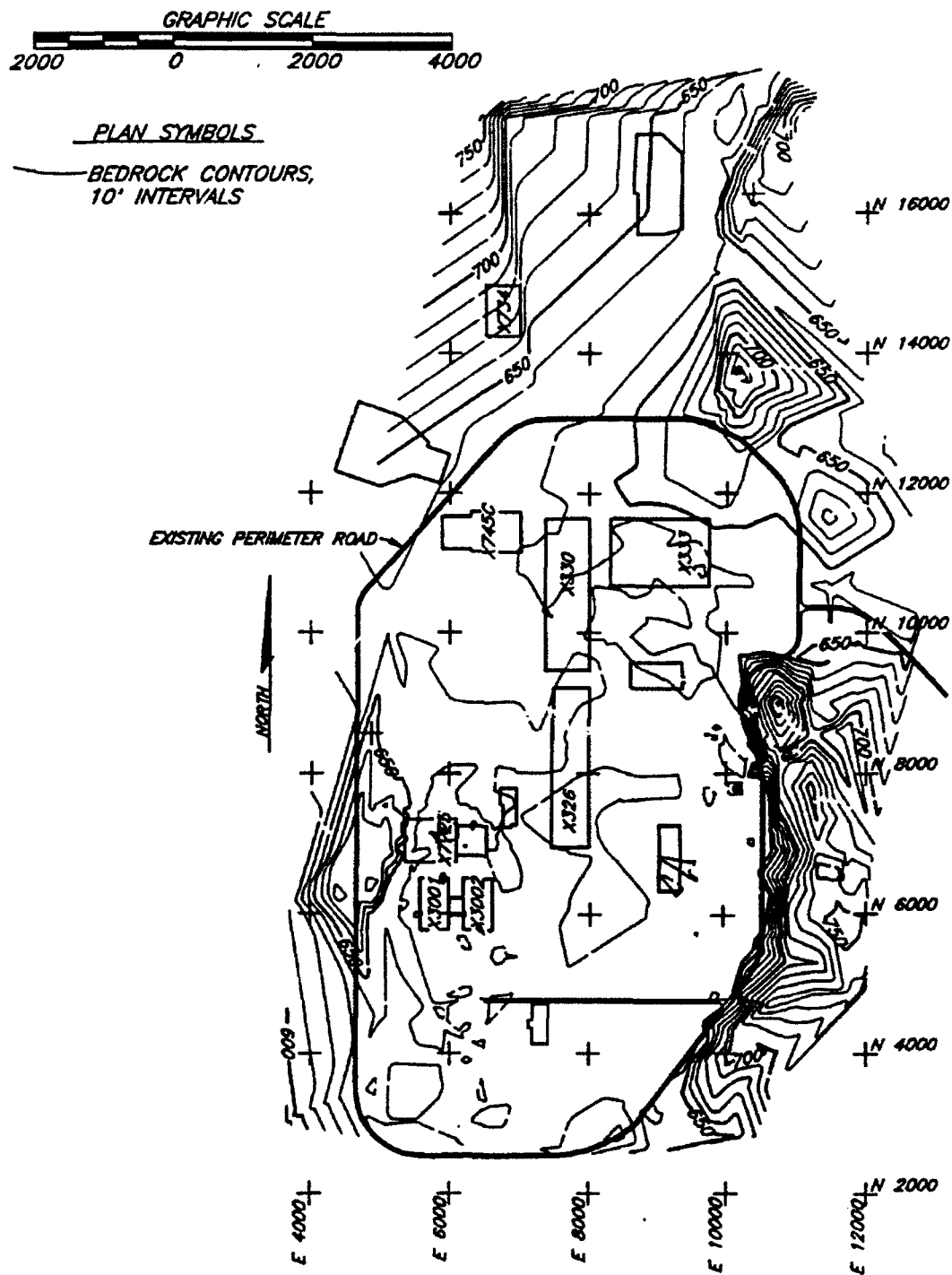


Figure 20. Contours representing top-of-rock elevations (ERCE 1990)

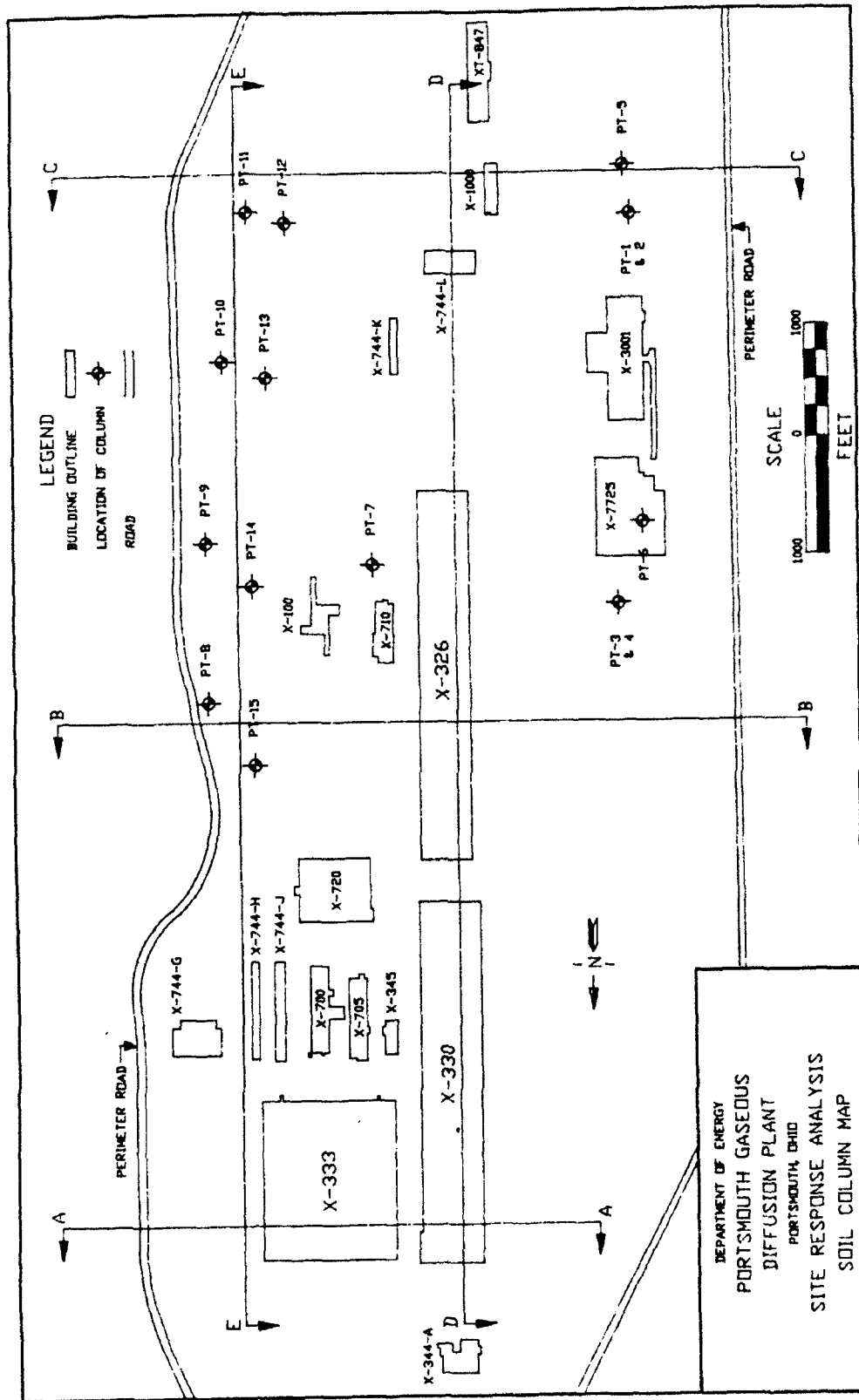


Figure 21. Site plan showing locations of soil columns

that the extent of possible conditions in terms of height of column and individual material types may be adequately addressed with existing columns.

37. The fifteen idealized soil columns are shown in Figures 22 through 25. Changes in material types shown on these figures are designated with solid horizontal line segments across the column whereas changes in parameters for the same material type are designated with a dashed horizontal line segment. Specifics about each component are described below.

Geometry

38. The basic geometric components of a soil column are values defining the thickness of soil layers and depth to bedrock. The range of column heights is 20 to 61 ft with an average overall height being 35 ft with an average soil layer thickness of about 6.5 ft. The cross sections indicated a range of soil heights between 0 and 45 ft. The general idealizations representing the GCEP and GDAP areas are significantly different.

39. At the GCEP area, the six columns correspond to six sets of geophysical measurements made at four sets of borings. (At two locations, RA-413 and PB-75, two sets of measurements were taken.) In general, the height of these columns is uniform, ranging from 24 to 33 ft. The number of soil layers in each column is between four and six. Pleistocene-age deposits were encountered in borings representing three of the six columns for this area (PT-1, PT-2, and PT-5). Fill was also reported at PT-5.

40. The heights of columns at the GDAP area vary considerably more, ranging from 20 to 47 ft with one column extending to 61 ft (PT-8). This much taller column is expected to produce a noticeably different response than the other sites. The number of soil layers for these nine sites range between three and seven and Pleistocene-age deposits were encountered in all borings except those representing column PT-10. (The geometry of PT-10 is most like sites at GCEP.)

Geotechnical engineering data

41. Geotechnical engineering data refer to gradation and plasticity index (PI), unit weights (densities), and the variations of shear modulus and damping ratio with shear strain. The (maximum) magnitude of shear modulus and the variations of density with depth were derived from seismic geophysical measurements described in the next section. The depth of the phreatic (groundwater) surface is also noted but was not necessary for this study. The

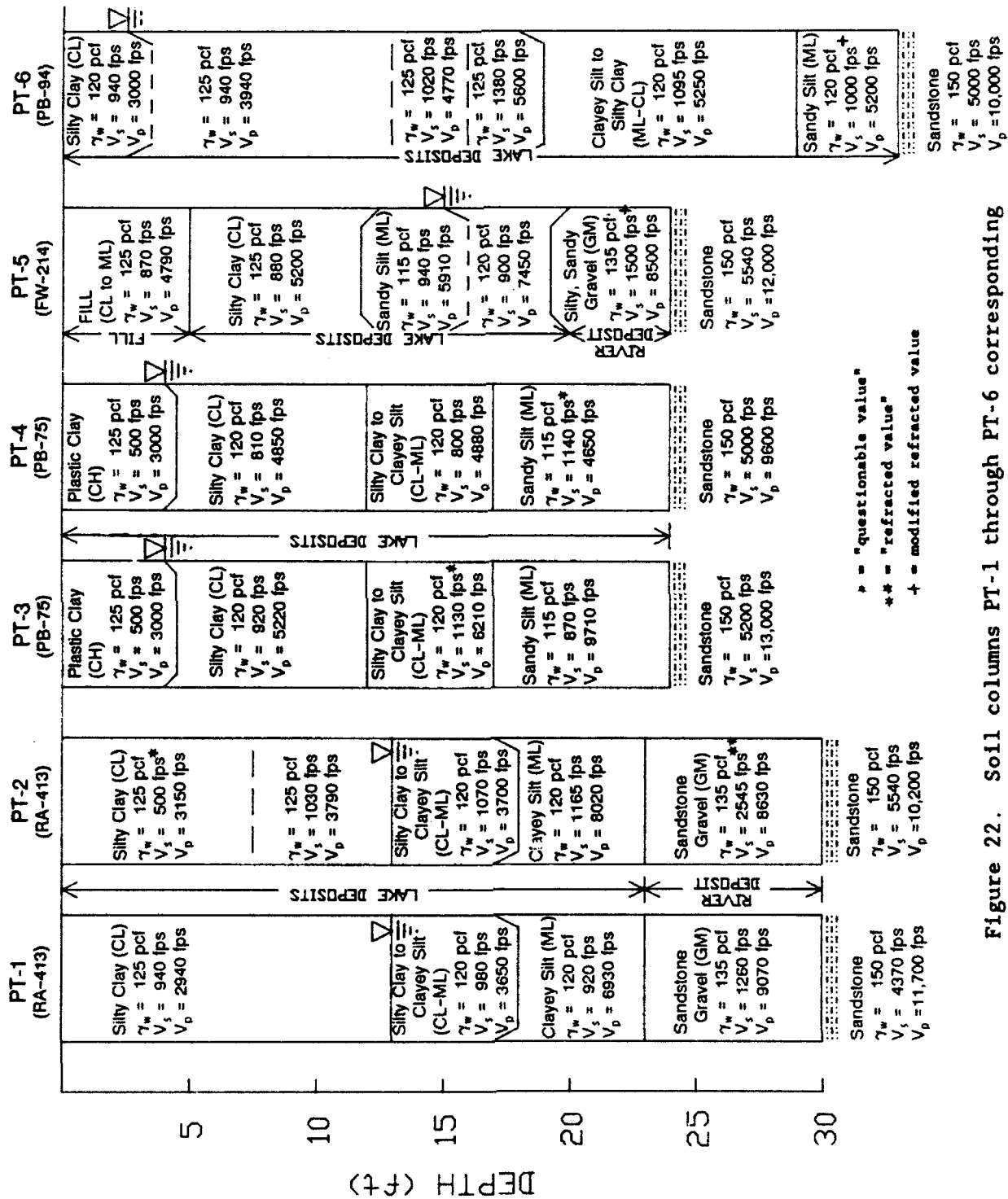


Figure 22. Soil columns PT-1 through PT-6 corresponding to site investigations conducted for GCEP

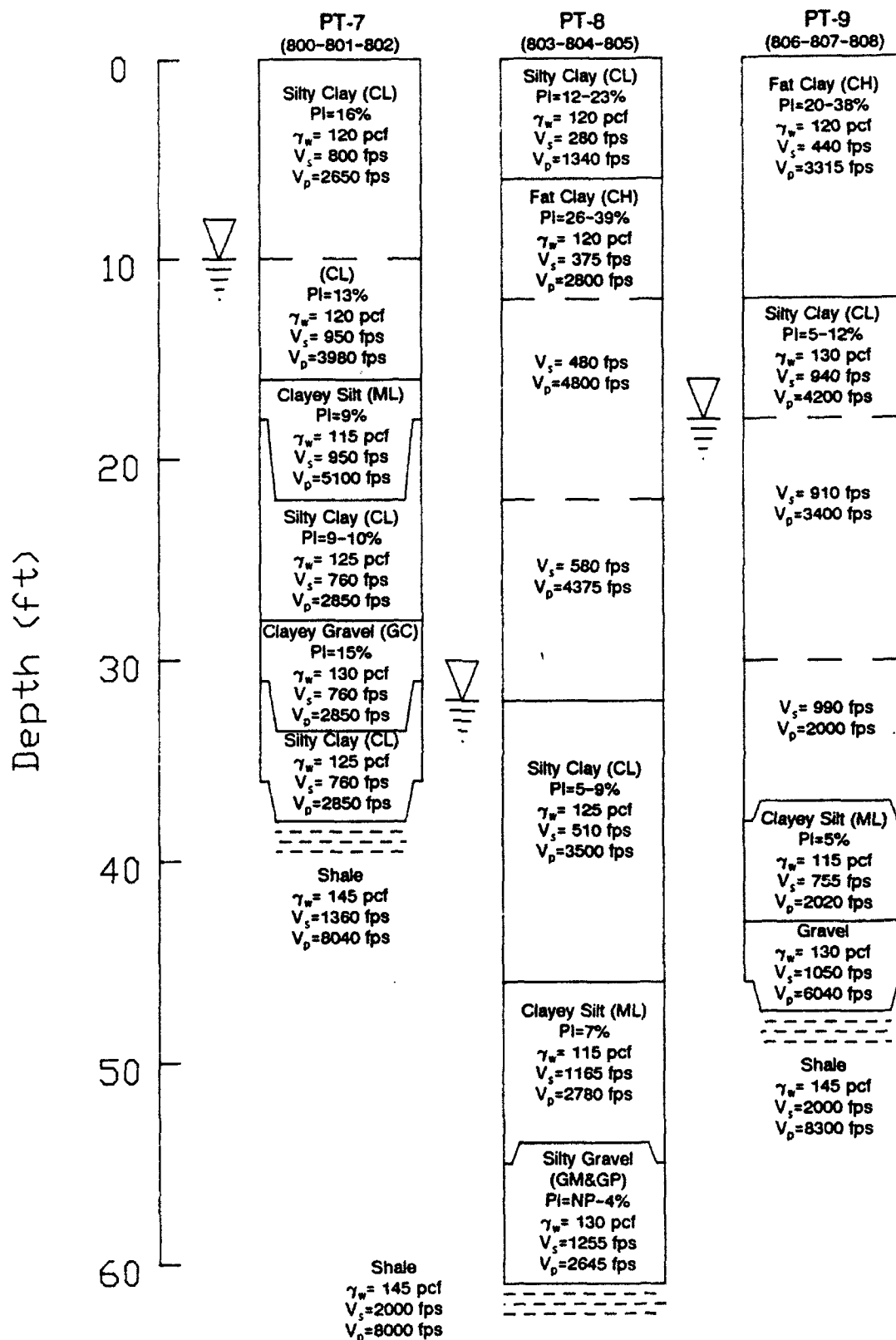


Figure 23. Soil columns PT-7 through PT-9 corresponding to site investigations conducted for GDAP

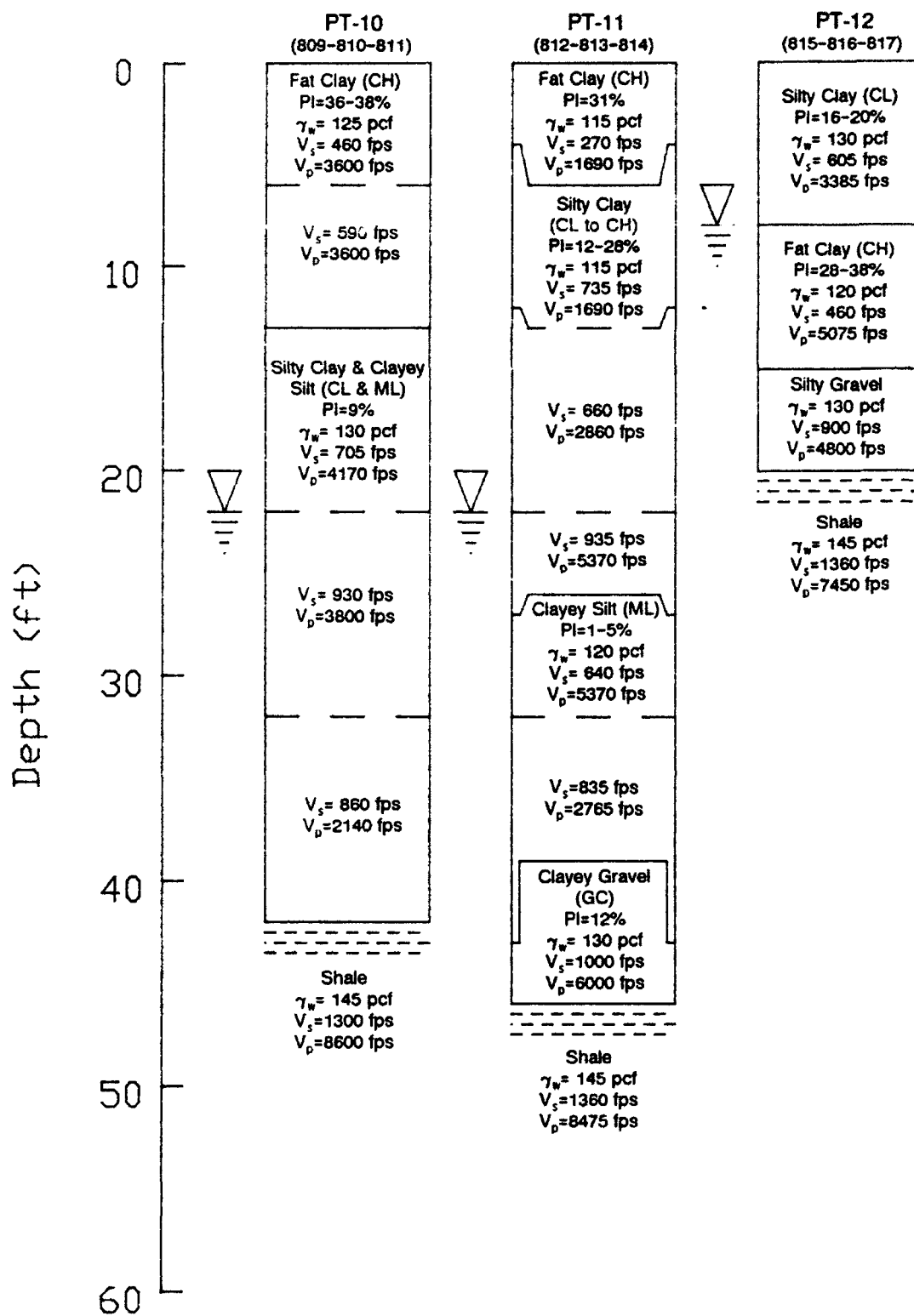


Figure 24. Soil columns PT-10 through PT-12 corresponding to site investigations conducted for GDAP

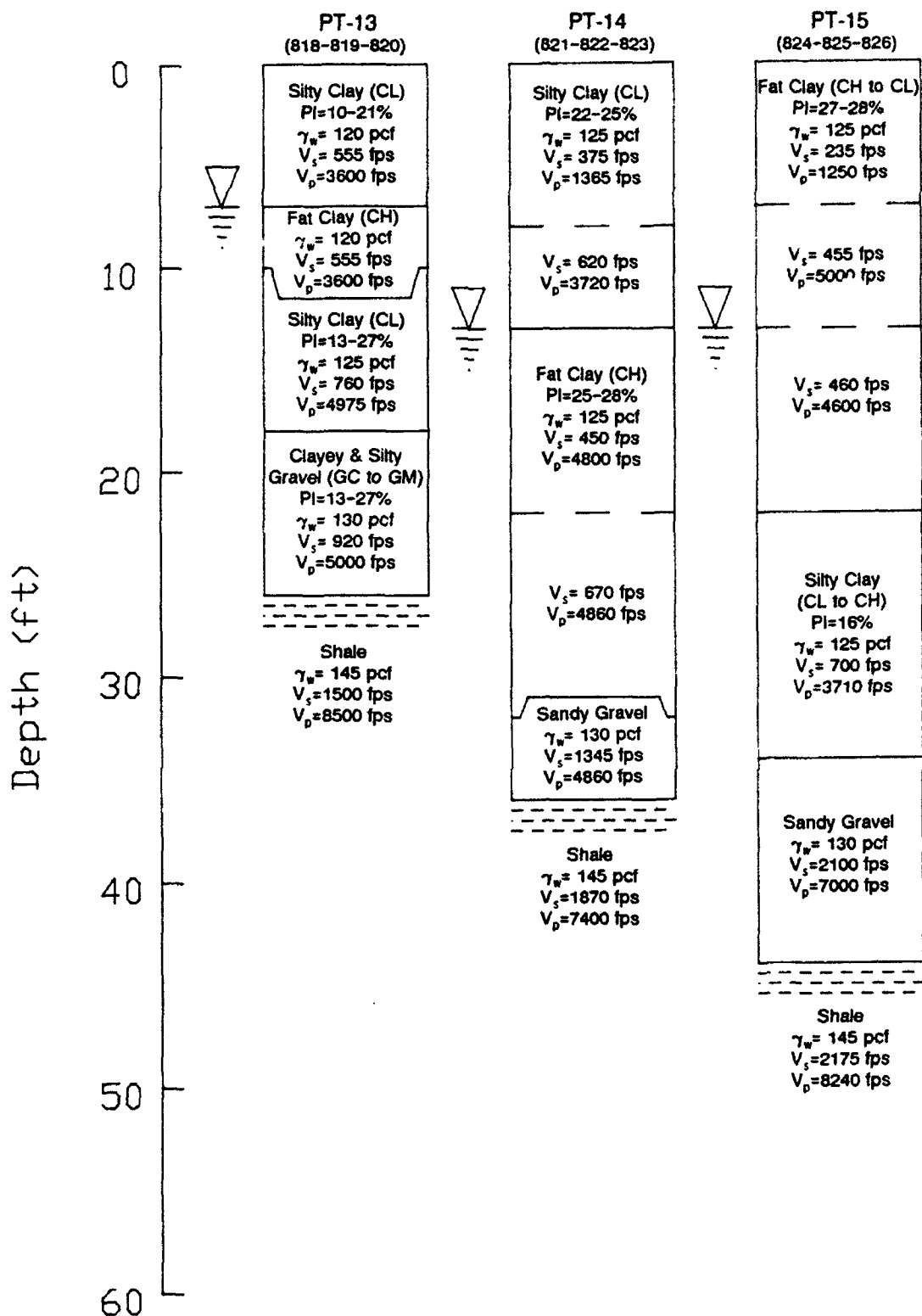


Figure 25. Soil columns PT-13 through PT-15 corresponding to site investigations conducted for GDAP

values of unit weight for the various soils range from 115 to 135 pcf and are based on laboratory measurements reported by others.

42. Site-specific relationships defining the variations in shear modulus and damping ratio with shear strain for lacustrine clays and silt were measured in the laboratory for GCEP using 41 resonant column samples. The collection of results are shown in Figures 26 and 27. The shear moduli for these tests are shown normalized to a shear strain of 10^{-2} rather than the maximum shear modulus more common for present reporting. Only minor differences exist between the best-fit relationships for modulus and damping ratio for the ML-CL and the CL lacustrine soils with the latter generally having greater values of modulus and damping ratio at any given shear strain.

43. Standard relationships defining the variation of shear modulus and damping with shear strain published by others were used for other soils at PORTS. These relationships represent a best-fit for the compilation of results from numerous sites throughout the U.S. In the absence of site-specific data, these relationships have proven to work well in most applications for site response analyses. Upper-bound and lower-bound relationships are also considered for some applications, as with this study. The sources for the relationships are summarized in Table 4.

Table 4
Normalized Modulus and Damping Ratio Relationships

Material Type	Reference	
	Modulus	Damping
Rock	Schnabel (1973)	Schnabel (1973)
Gravel	Seed et al (1986)	Seed & Idriss (1970)
Sand	Seed & Idriss (1970)	Seed & Idriss (1970)
Alluvial clay:	Sun, Golesorkhi, and Seed (1988)	Seed & Idriss (1970)
Lacustrine ML & ML-CL	Law Engineering Testing Company (1978)	Law Engineering Testing Company (1978)
Lacustrine CL	"	"

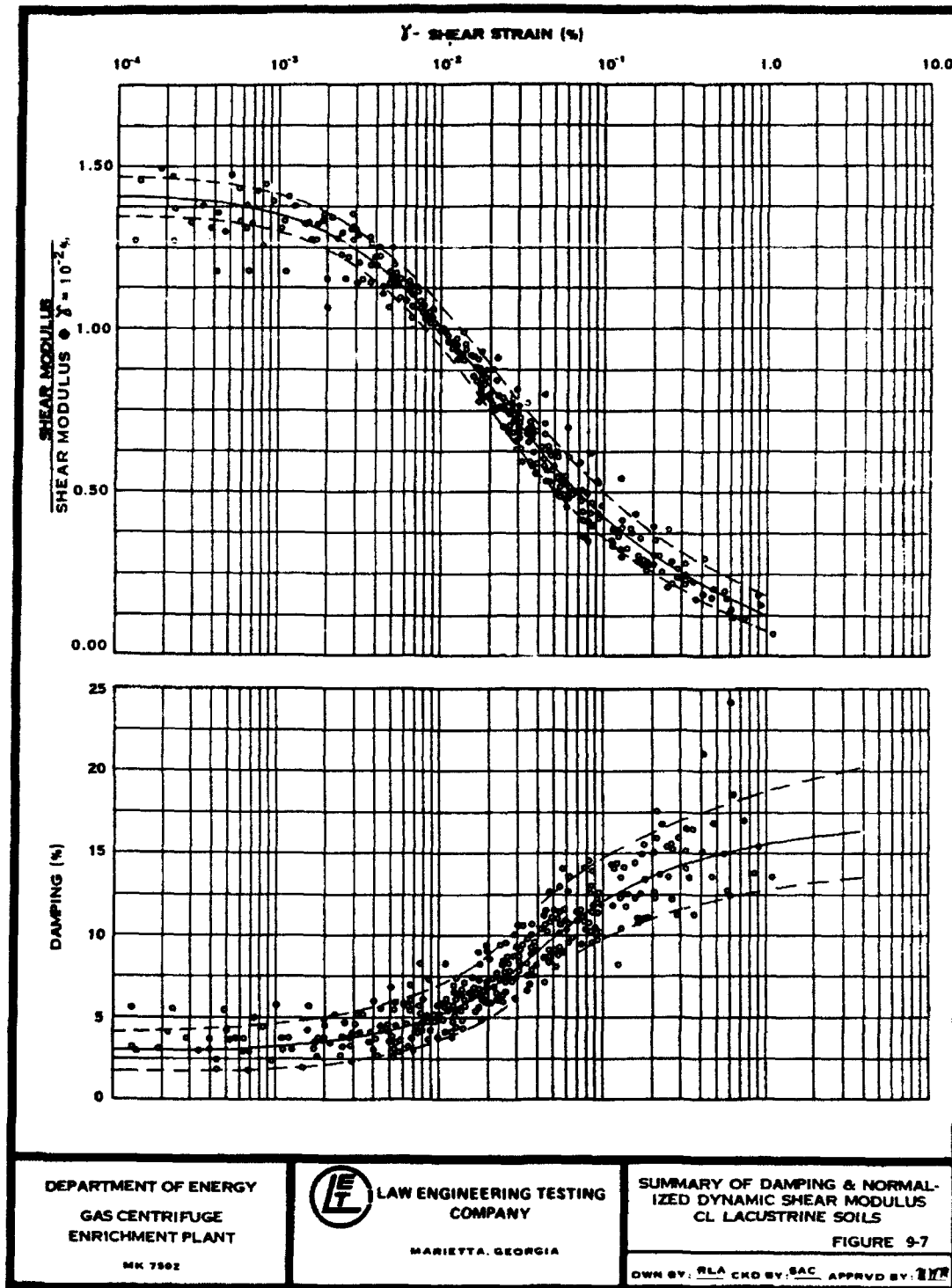


Figure 26. Results of laboratory tests showing relationship between shear modulus and damping versus shear strain for CL lacustrine soils

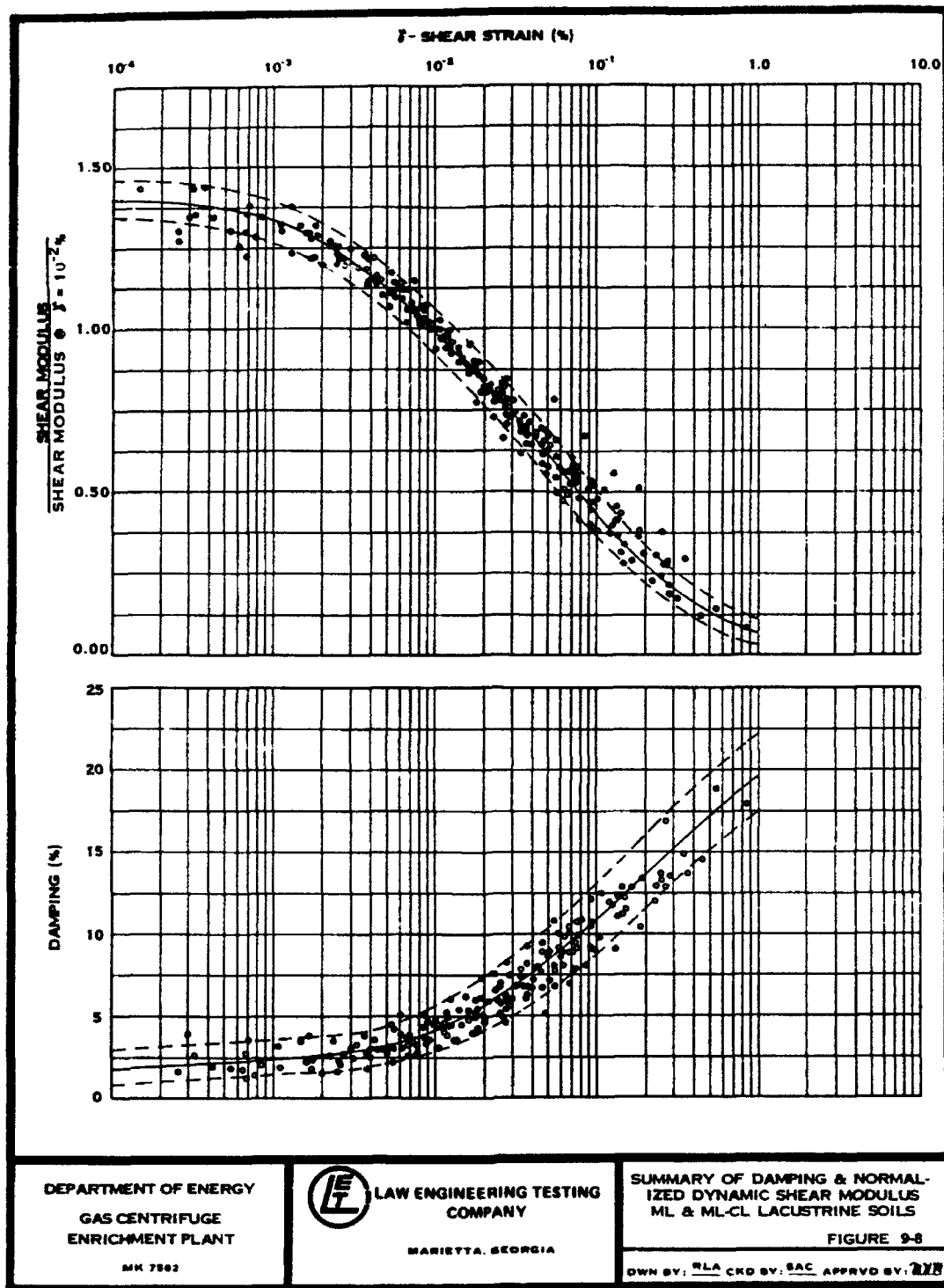


Figure 27. Results of laboratory tests showing relationship between shear modulus and damping versus shear strain for ML & ML-CL lacustrine soils

44. For cohesionless soils, relations representing an average of the data originally published by Hardin and Drnevich (1972) and Seed and Idriss (1970) and later confirmed with additional data by Seed et al. (1986) were used. These relationships and the range of data and best-fit relationships are shown in Figure 28. For Pleistocene-age clays and plastic (fat) clays, relationships proposed by Sun, Golesorkhi, and Seed (1988) as a function of PI were used. These relationships are shown in Figure 29.

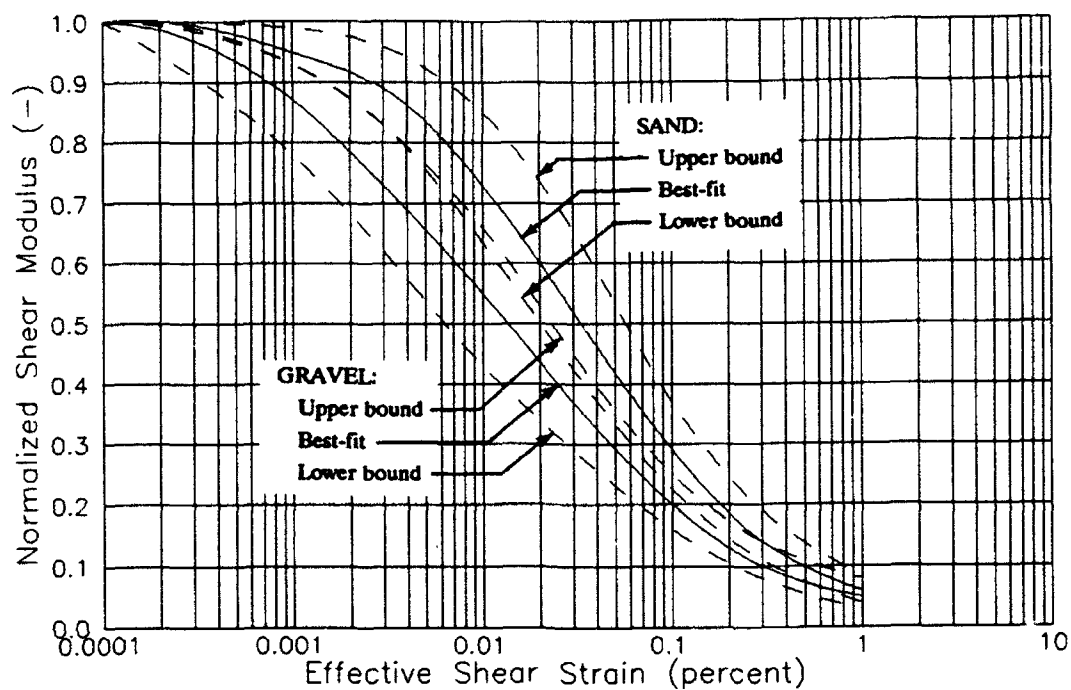
45. Relationships for rock were developed by Schnabel (1973) and have been used consistently and successfully by the profession. The influence of the relationships for rock generally are not noticeable because of the small overall changes as shear strain increases. Shear strains were generally small making the modulus reduction and damping ratio increases small.

46. The combined set of relationships used are shown in Figure 30. Four of the modulus relationships are very similar—sand, lacustrine soils, and the standardized curves for low plasticity soils. The recommended cap of 15 percent damping (Nuclear Regulatory Commission 1989) was used as shown. Assignments of appropriate modulus and damping relationships are shown in Table 5. No adjustments were made to account for the effective confining stress since the highest overburden stress is under 3 tsf.

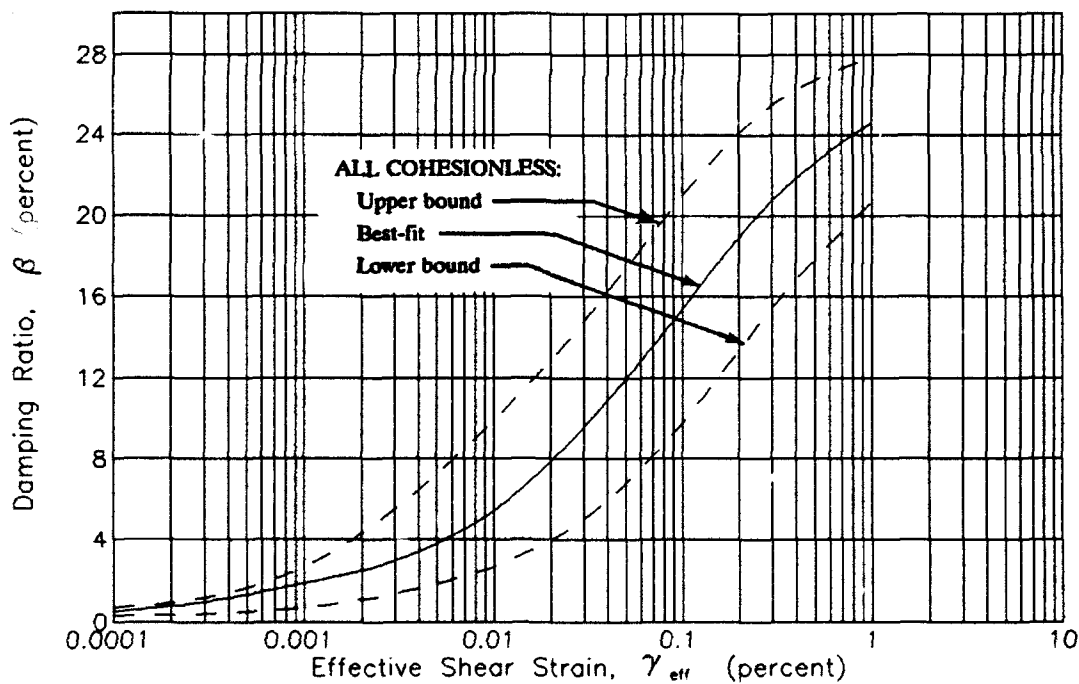
Seismic geophysical data

47. Compression and shear wave velocities of materials were measured in situ using three different geophysical techniques—seismic crosshole, downhole, and surface refraction. Compression wave velocities were not of interest and are, therefore, not discussed further. Idealized values of shear wave velocity representing each layer were shown previously in Figures 22 to 25.

48. GCEP Site. Law Engineering Testing Company (1978) report that crosshole techniques were used exclusively for investigations at the GCEP site. It is not apparent how or why two sets of velocities were obtained from each of the arrays at borings RA-413 and PG-75. Some velocities were reported to be "questionable" or "refracted." Five of the six columns have one of these uncertain values and most velocities are believed to err on the high side (with the 500 fps layer the exception). The use of velocities greater than in-situ values tends to produce lower natural site periods and stronger surface motions. Four of the uncertain values were used as shown in Figure 22 because of the absence of additional information. Two others velocities were adjusted to reflect more realistic values (also shown in Figure 22).

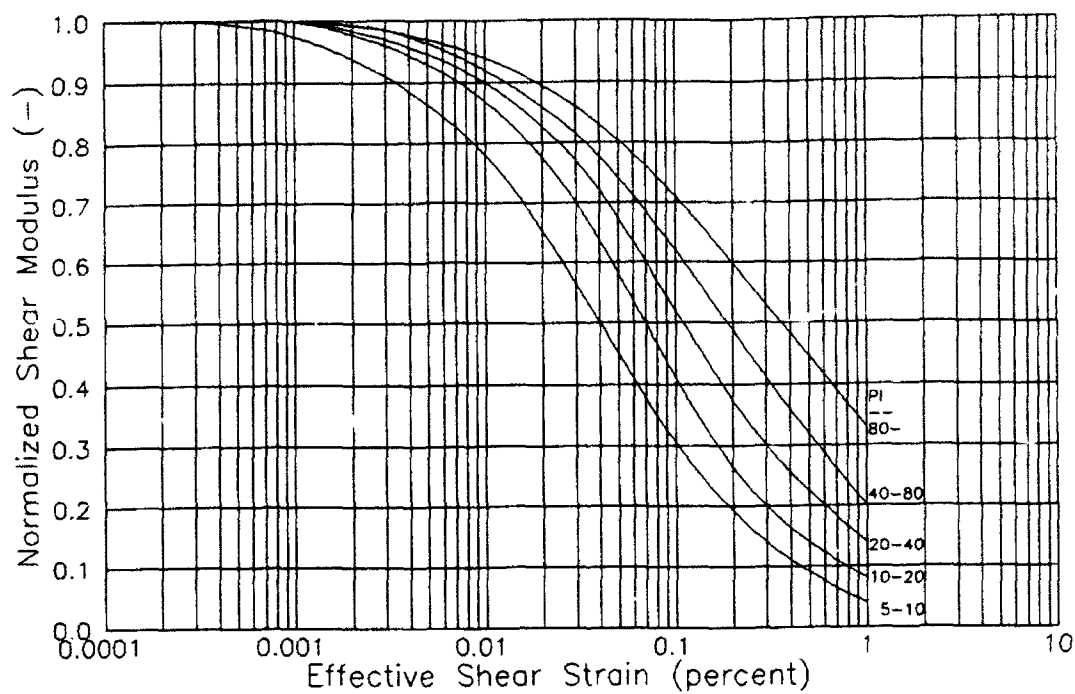


a. Shear modulus

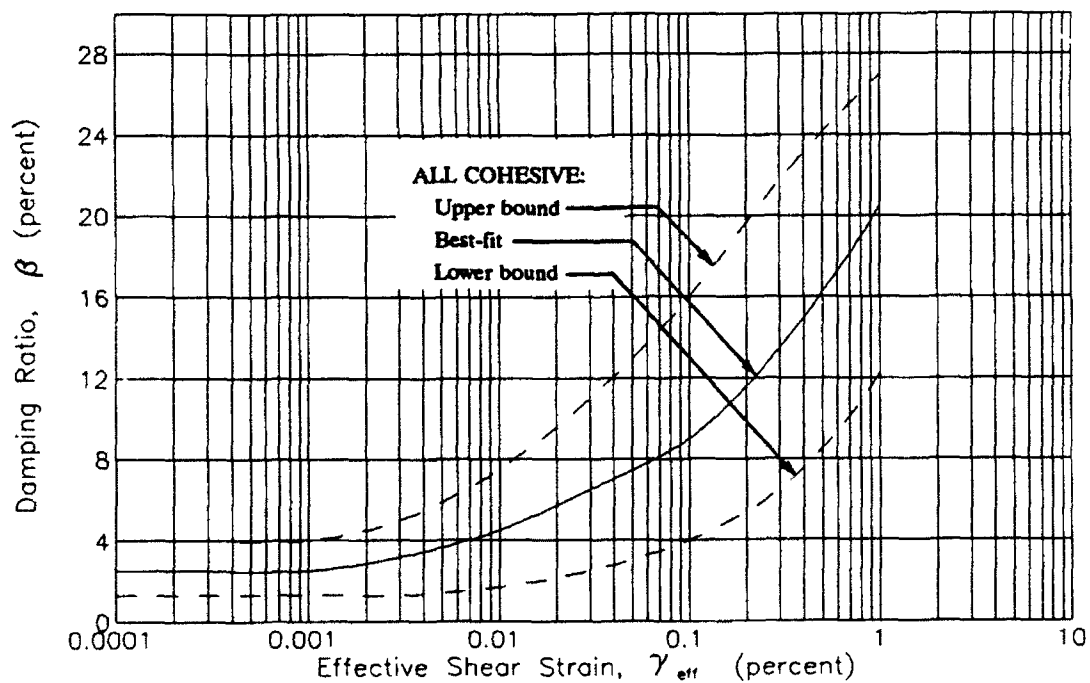


b. Damping ratio

Figure 28. Standardized relationships between shear modulus and damping ratio for cohesionless soils (Seed and Idriss 1970 and Seed et al. 1986)

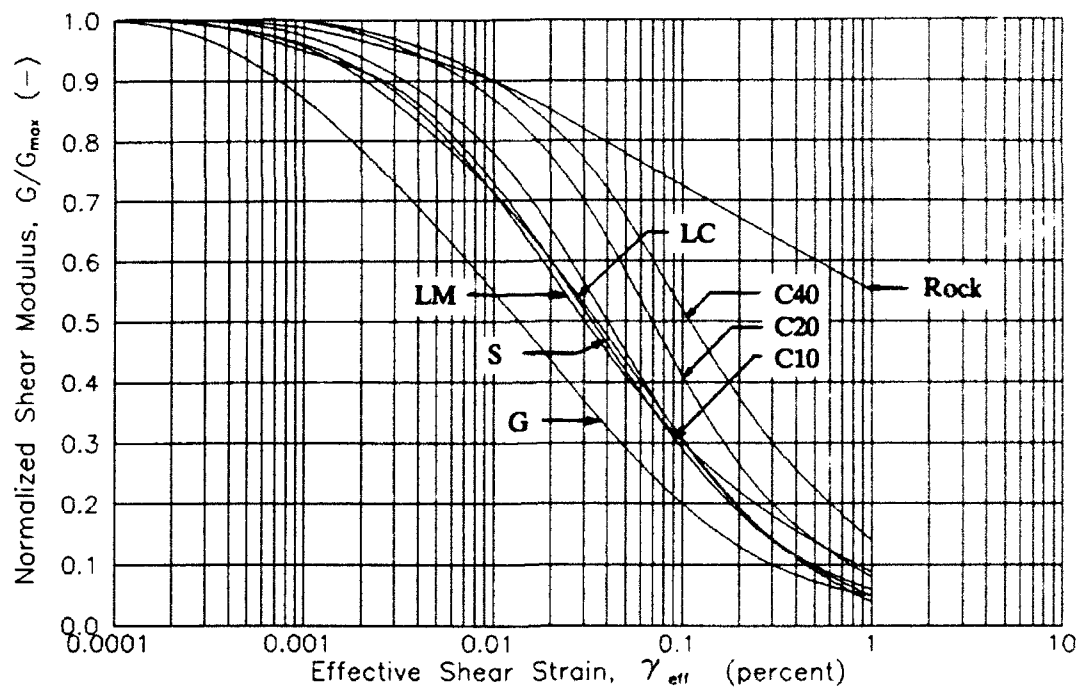


a. Shear modulus

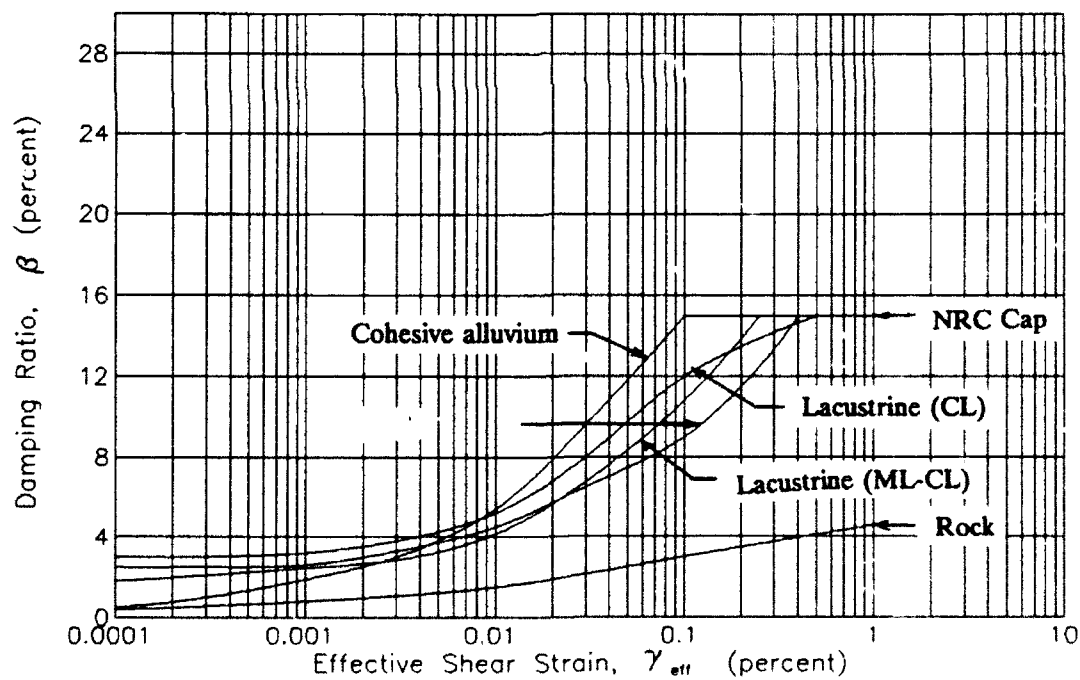


b. Damping ratio

Figure 29. Standardized relationships between shear modulus and damping ratio for cohesive soils (Sun, Golesorkhi, and Seed 1988)



a. Shear modulus



b Damping ratio

Figure 30. Relationships between shear modulus and damping ratio versus shear strain used for this study

Table 5
Assignment of Shear Modulus Relationships

Layer	Site														
	1	2	3	4	5	6	7	8	9	10	11	12	13	14	15
1	LC	LC	C40	C40	C20	LC	LC	LC	C40	C40	C40	LC	LC	LC	C40
2	LM	LC	LC	LC	LC	LC	LC	C40	LC	C40	LC	C40	C40	LC	C40
3	LM	LM	LM	LM	LM	LC	LM	C40	LC	LC	LC	G	LC	C40	C40
4	G	LM	LM	LM	LM	LC	LC	C40	LC	LM	LC	-	G	C40	C20
5	-	G	-	-	G	LM	G	LC	LM	LC	LM	-	-	G	G
6	-	-	-	-	-	LM	C20	LM	G	-	LM	-	-	-	-
7	-	-	-	-	-	-	-	G	-	-	G	-	-	-	-
						GCEP	GDAP								

LM - lacustrine silts
LC - lacustrine clays
C10 - standard cohesive soil ($5 \leq PI \leq 10$)
C20 - standard cohesive soil ($10 \leq PI \leq 20$)
C40 - standard cohesive soil ($20 \leq PI \leq 40$)
G - gravel
S - sand

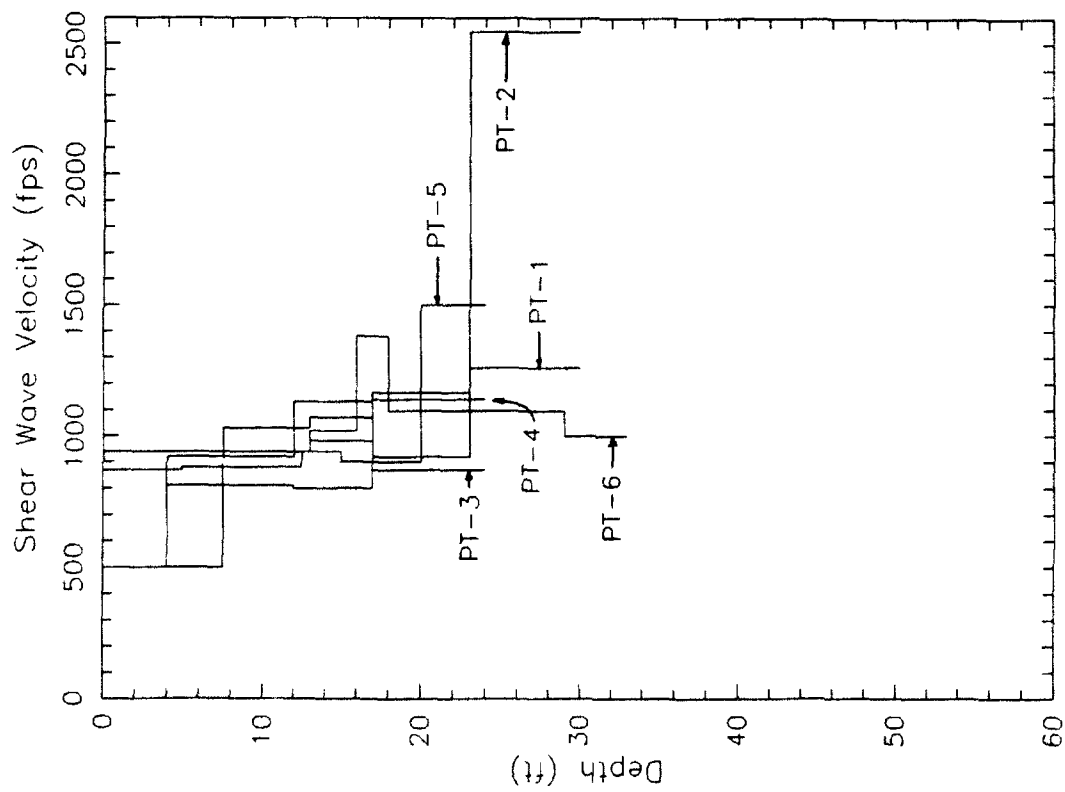
49. The shear wave velocities measured at GCEP (PT-1 through PT-6) are shown in Figure 31a. In general, shear wave velocity increases with depth and with reasonable variability except near the bedrock contact (where most of the uncertain velocities were noted). The velocities range from 500 fps for surficial deposits to 1,380 fps for lacustrine clays at depth. The shear wave velocity of fill was measured at PT-5 to be 870 fps. The Pleistocene-age deposits have velocities between 1,260 and 1,500 fps with one profile (PT-2) having a velocity of 2,545 fps. This profile may be unrealistic but it pushes the collective range of response to be conservative. The shear wave velocity for the sandstone bedrock is significantly higher, ranging between 4,370 and 5,540 fps.

50. GDAP Site. Curro and Marcuson (1978) used all three geophysical techniques at the GDAP site to provide redundancy, thereby increasing the reliability of measured values. In general, the seismic velocities measured using different methods were in good agreement and the results of crosshole tests were used to develop these nine soil columns.

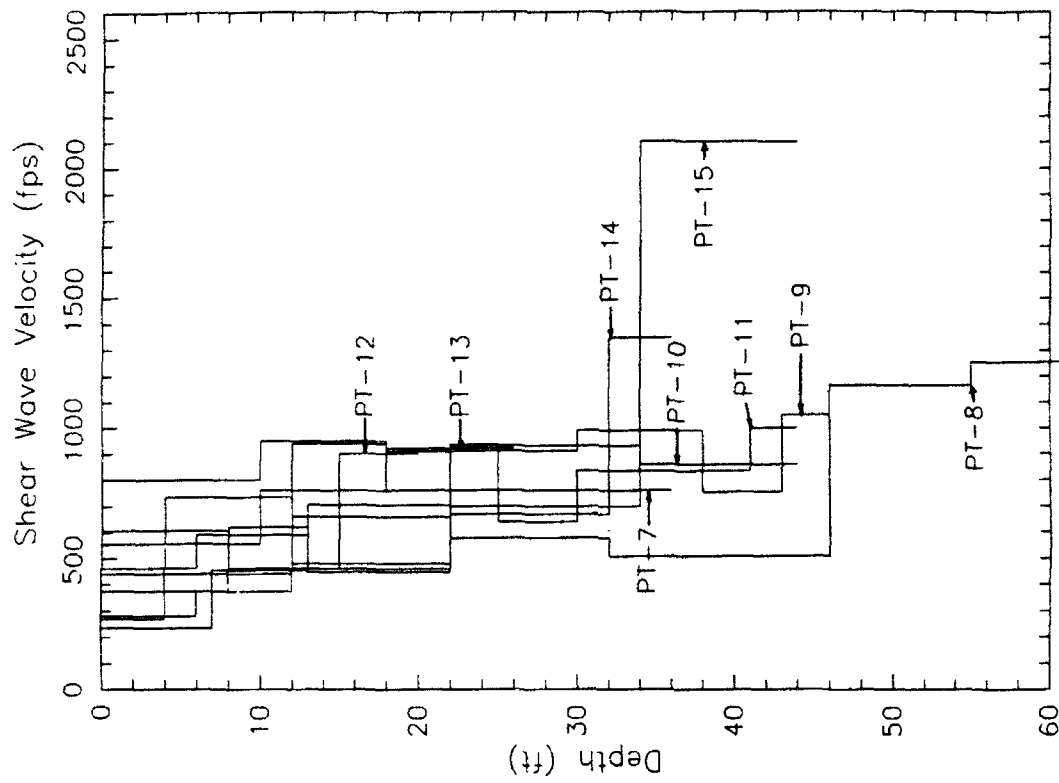
51. The shear wave velocities in soil columns PT-7 through PT-15 are shown in Figure 31b. These velocities also increase with depth and seem to have about the same magnitude of variability (500 fps) down to depths of 30 ft. At a depth of 34 ft, the velocity for PT-15 deviates considerably. Notice, too, that the profile for PT-8 is much deeper making the natural period higher. For lacustrine deposits of silt and clay, the velocities range from 280 fps for surficial deposits to 1,165 fps for clay at depth. The alluvial deposits have velocities between 760 and 1,000 fps with one profile (PT-15) having a velocity of 2,100 fps. In general, the upper bounds of these two ranges are relatively high. The shear wave velocities measured in the soft shale bedrock are fairly low, ranging between 1,360 and 2,175 fps.

52. A comparison between shear wave velocity profiles shown in Figures 31a and 31b suggests that the velocities from the GDAP area are generally less than those measured in the GCEP area, respective of depth. Typically only two or three of the velocity profiles from GDAP are within the range defined for GCEP. The velocities at GCEP seem to increase with depth at a higher rate, too.

53. Combined stiffness profiles. The profiles of shear wave velocity shown in Figures 31a and 31b were combined and are shown in Figure 32a. The corresponding profiles of shear modulus are shown in Figure 32b. (Values of

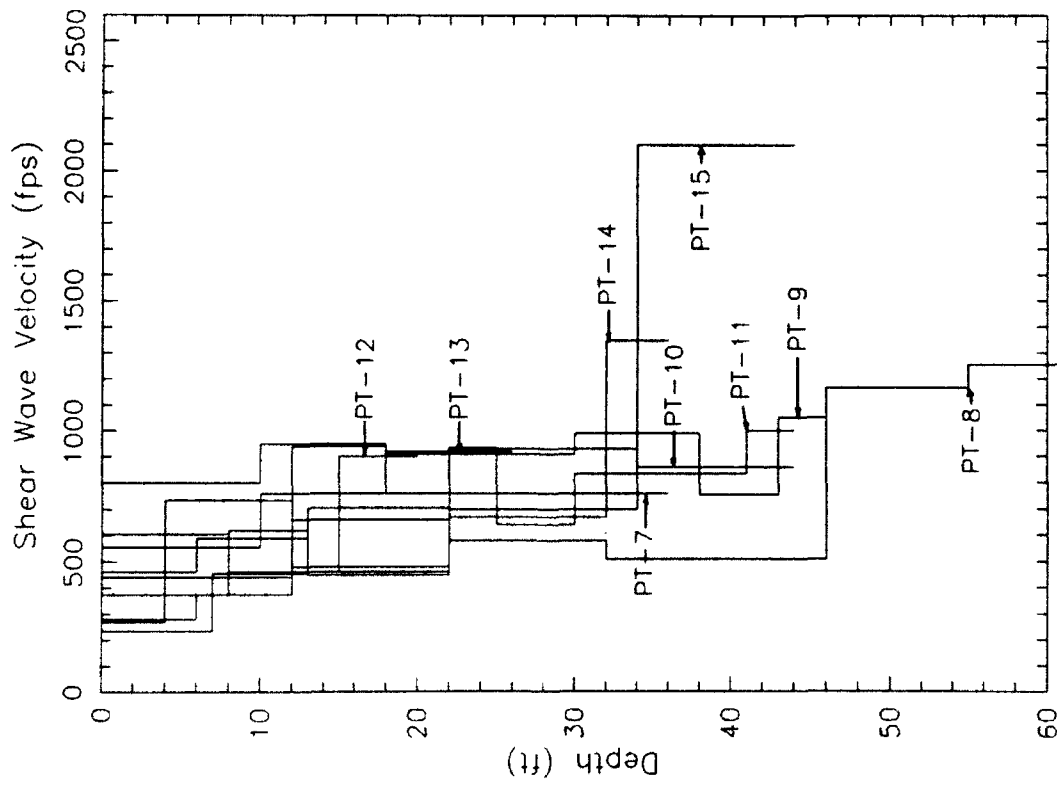


a. GCEP area

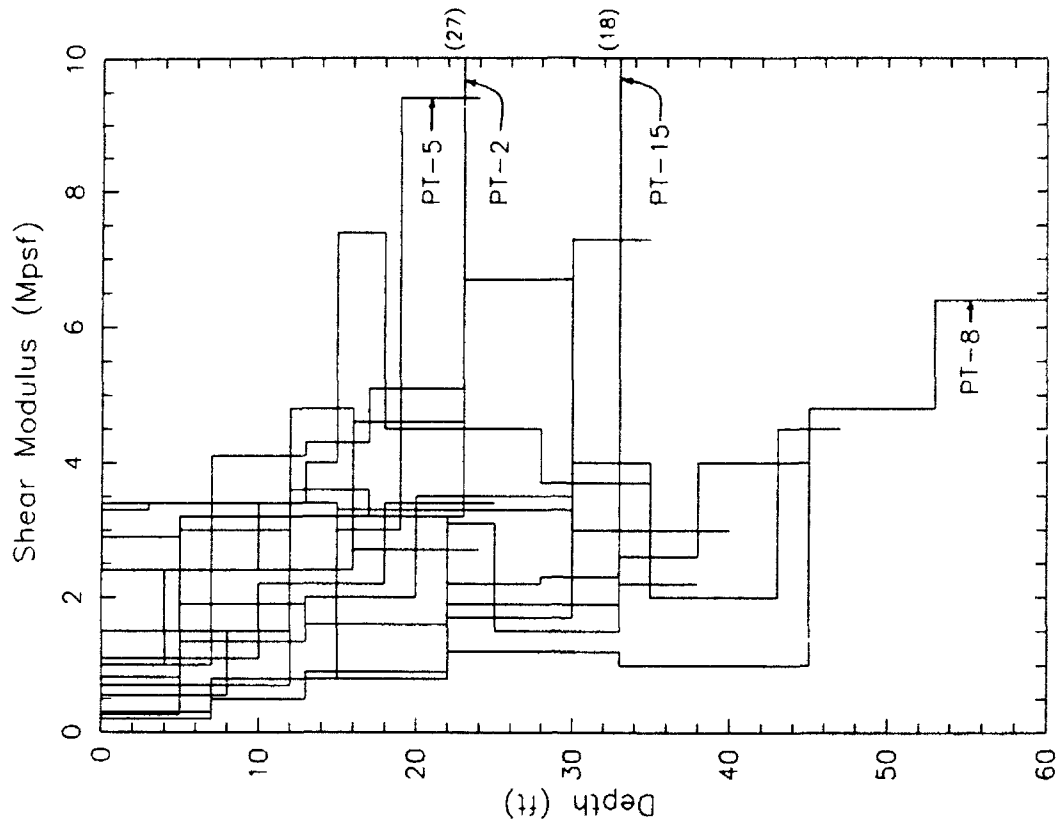


b. GDAP area

Figure 31. Shear wave velocity profiles



a. Shear wave velocity



b. Shear modulus

Figure 32. Combined profiles of soil stiffness

modulus exceeding the limits of the plot are shown in parentheses.) These figures show that a great deal of variability exists in the shear wave velocities (and moduli) measured at PORTS. The profiles that significantly extend beyond the general range of data are: PT-2 and PT-5 (uncertain velocities), PT-8 (deep site), and PT-15 (may be refracted velocity) as shown in Figures 32a and 32b. The calculated response for these four sites is expected to be noticeably different than that for the other 11 sites with stronger response parameters and greater natural periods of motion.

Average Soil Column

54. An average column is intended to represent the overall site and was created to conduct sensitivity studies described in Part VI. This column is shown in Figure 33. This means of representation is usually lacking for cases such as PORTS where the velocities and depths to bedrock vary considerably. However, an average column can be useful to evaluate the sensitivity of the analysis to various inputs.

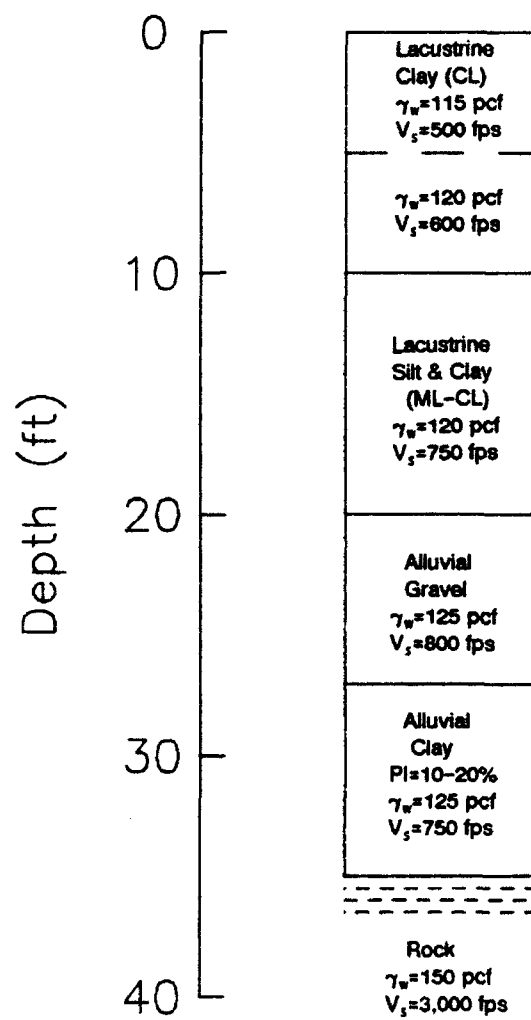


Figure 33. Average soil column

PART IV: SITE RESPONSE CALCULATIONS

55. Site response calculations and analysis of the results comprise the third step of a site-specific earthquake response analysis. Site response calculations are presented below; the presentation of results and analysis is made in later parts of this report. Different mathematical formulations can be used to calculate site response including the solution of the wave equation and use of a shear beam analogy (both continuous solutions) and lumped mass (discrete). Initial formulations for site specific calculations were reported in the U.S. by Roesset and Whitman (1969) and Roesset (1970) and have been enhanced since. A number of computer programs are presently available to calculate site response analyses including two- and three-dimensional formulations.

Method of Response Calculations

56. The computer program *SHAKE* was used to calculate site-specific response caused by the synthetic earthquakes. *SHAKE* was developed at the University of California at Berkeley (Schnabel, Lysmer, and Seed 1972) and written in FORTRAN IV to run on a CDC 6400 computer. WES has developed pre- and post-processing routines and made enhancements to the program on two platforms—the personal IBM-compatible computer (Sykora, Wahl, and Wallace 1992) and the U.S. Army CRAY Y-MP at WES by Sykora. The latter platform was used for purposes of this study to take advantage of computational speed and massive file storage capabilities. The time necessary to iterate to the proper solution was about 1 sec.

Background

57. *SHAKE* was developed to calculate the horizontal response caused by an earthquake at any depth of a soil profile. The methodology and algorithms incorporated in the program are fairly simple and straight-forward and quite adequate for the purpose intended as clearly evident through the prolific publication of results and favorable comparisons with measured response (e.g., Seed et al. 1987 and Seed, Dickenson, and Idriss 1991). The simplicity associated with *SHAKE* is attributed to some basic assumptions regarding the cyclic behavior of materials and geometry of the problem. The basic assumptions of importance to this study are:

- a. Soil layers are horizontal and extend to "infinity";
- b. Ground surface is level;
- c. Each soil layer is completely defined by the shear modulus and damping ratio as a function of strain, the thickness, and unit weight;
- d. The cyclic behavior of each soil (and base rock) is represented by the equivalent-linear constitutive model; and
- e. The incident earthquake motions are uniform, horizontally-polarized shear waves propagating vertically.

In general, assumptions (a), (b), and (c) are consistent with site conditions at PORTS. The equivalent-linear constitutive model, assumption (d), described further into this section, is widely accepted by the geotechnical earthquake engineering profession as a simple but effective model for the dynamic response of soils. The last assumption, (e) above, narrows the focus to a simple class of problems, but, is a common assumption for this type of problem.

58. The computer program *SHAKE* has been in common use for almost 20 years. In that time, more knowledge has become available with regard to specification of inputs to the program and significant advances have been made in computer technology. As these findings have been made available, WES has updated and refined the program and method of data input. One of the most striking differences in the versions available at WES is the option to specify shear wave velocity for each soil layer as opposed to using the modulus coefficient, K_2 , or undrained shear strength, S_u . WES has also continually updated a library of soil modulus and damping relationships. Important input parameters to *SHAKE* for this study are described below.

Solution algorithm

59. The one-dimensional wave equation model (Kanai 1951) was used to develop *SHAKE*. This model has proven to be effective despite the simplicity and number of assumptions involved. The solution algorithm involves the complex response technique and the Fast Fourier Transform (Cooley and Tukey 1965). The general formulation of the wave equation is not unique to horizontally-polarized shear wave motion; the equation can also be solved for the vertical propagation of compression waves.

Constitutive model

60. In general, soil is a non-linear material that exhibits hysteretic behavior under cyclic loading. An example of the stress-strain behavior is shown in Figure 34a. Soil is difficult to model accurately for cyclic

response; exact representations are unavailable. The constitutive model incorporated into SHAKE is linear with simulated nonlinear effects to account for dependency of moduli on shear strain. This model, called the equivalent-linear method, was proposed by Seed and Idriss (1970) and is widely used in geotechnical earthquake engineering studies.

61. The basic components of the equivalent-linear method are the maximum shear modulus, G_{max} , moist unit weight, and ratio of critical damping, β . G_{max} , which corresponds to the linear-elastic, continuum material property (Lamé 1852), can be calculated from low-strain seismic shear wave velocity using:

$$G_{max} = \rho V_s^2 \quad (1)$$

where

ρ = mass density (moist unit weight / gravitational constant)
 V_s = shear wave velocity

or from the maximum (low-strain) shear modulus coefficient, $(K_2)_{max}$, which is defined by Seed and Idriss (1970):

$$G_{max} = 1000 (K_2)_{max} (\sigma'_m)^{0.5} \quad (2)$$

where

σ'_m = mean effective stress, in psf
 G_{max} is in psf

Shear wave velocities (using equation 1) were used exclusively for this study.

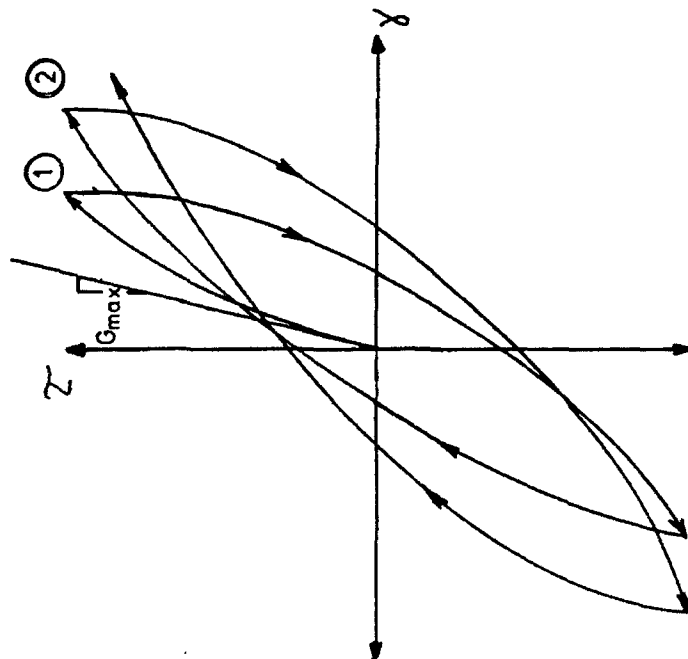
62. At a certain threshold of shear strain, generally accepted to be about 10^{-4} percent or less, the stiffness decreases to some value less than G_{max} . The equivalent-linear model uses secant shear moduli that are adjusted during each iteration to account for this. Damping is input by using complex moduli, G^* , and hysteretic damping (which is independent of frequency):

$$G^* = G (1 - 2\beta^2 + 2i\beta\sqrt{1 - \beta^2}) \quad (3)$$

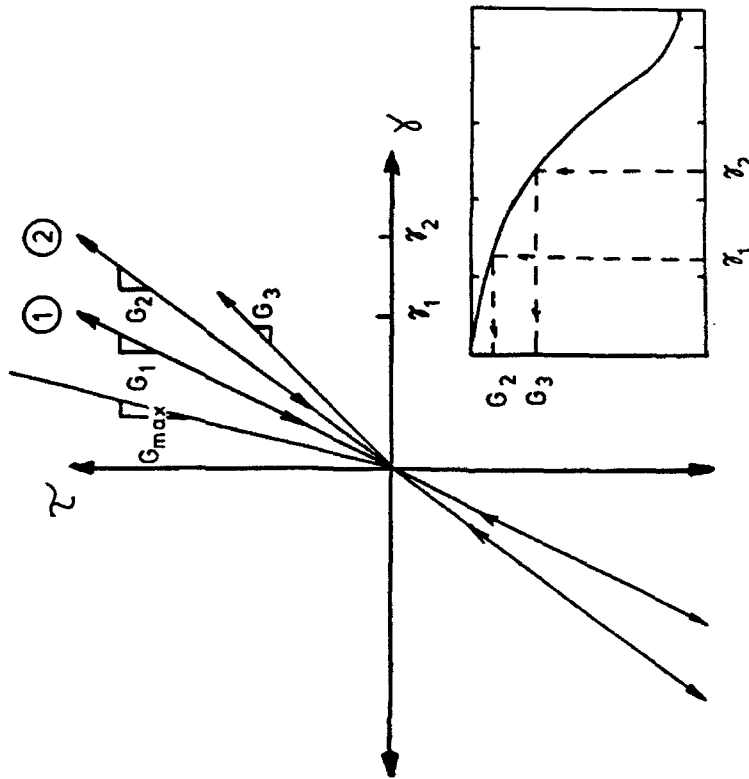
where

$$i = \sqrt{-1}$$

Damping increases as shear strain increases. The character of these functions of strain was first addressed in studies by Hardin and Drnevich (1972), Seed and Idriss (1970), and Schnabel (1973). Later studies include: Zen and Higuchi (1984), Seed et al. (1986), Sun, Golesorkhi, and Seed (1988), and



a. Ideal soil behavior



b. Equivalent linear model

Figure 34. Comparison of general cyclic behavior of soil and equivalent linear model with iterative scheme

Vucetic and Dobry (1991). A presentation of the relationships used for this study was made in Part III.

Iteration scheme

63. An example of the iterative procedure for the equivalent-linear model is shown in Figure 34b and described below. Assuming shear wave propagation, the model is initiated with an assumed value of shear modulus, G_1 , typically chosen to be slightly less than, or equal to, G_{max} . For the first cycle of loading, the stress-strain relation is linear between $\pm \tau_1$ with a slope of G_1 . The ordered pair (G_1, τ_1) comes from the appropriate modulus degradation curve as discussed in Part III of this report and shown schematically in Figure 34b. Maximum shear strains are obtained from the solution of the wave equation. Effective shear strain, PRMUL, is some fraction of the maximum shear strain and is used to obtain a new value of shear modulus, G_2 , from the appropriate modulus curve. A new value of β is also obtained. This process is repetitive until the moduli and damping for two successive iterations are within a prescribed tolerance, ERR. A summary of system input parameters is presented in Table 6.

Table 6
Miscellaneous Parameters in SHAKE Used for This Study

Parameter	Description	Value
MAMAX	Maximum number of points in the Fast Fourier Transform	4096
SKO*	Lateral coefficient of earth at rest	0.45
ITMAX	Maximum number of iterations	100
ERR	Maximum acceptable difference for modulus and damping	1 %
PRMUL	Effective shear strain factor	0.65

* Did not affect the calculations for this study since G was calculated using V_s , not K_2 .

Application of Free-Field Results

64. It may not be appropriate to directly apply the free-field response to the base of the structure for a number of reasons, including:

- a. The depths of the footings most likely are not at the ground surface and motions will vary with depth.
- b. The weight of the structure acting on the footings will affect the motions beneath the footings.
- c. The friction acting on the sides of the footing will affect the motions acting on the footing.
- d. The impedance contrast between the soil and foundation is normally quite large.

The application of ground motions to the base of structures, i.e., the consideration of points such as those listed, is commonly referred to as dynamic soil-structure interaction (DSSI).

65. Basic design approaches for dynamic soil-structure interaction have recently been documented by Johnson (1980) and Veletsos, Prasad, and Tang (1988). Evaluation of simple foundation systems in the latter study suggests the following rule of thumb: at lower periods, DSSI will have no effect on the response; at higher periods, DSSI will reduce the maximum response; for intermediate periods, DSSI might increase or decrease the maximum response.

Presentation of Output

66. Although a number of output options are available using *SHAKE*, the primary focus of this study was to calculate the pseudo velocity response spectra and present the results using the tripartite representation. It was specified in the scope of work for this study that damping ratios of 2, 5, 7, 10, 12, and 15 percent be used. Other forms of data were also used to evaluate and present the results including the ratio of acceleration response spectra between free field and rock outcrop motions and the variation of ground acceleration with time as a function of depth.

67. *SHAKE* may be used to calculate spectral ordinates at periods up to 10 sec. The experience of investigators who have compared calculated free-field response using *SHAKE* with measured response from major earthquakes suggest that *SHAKE* works well at periods less than 2 sec. At periods greater than 4 sec, motions are likely to be significantly affected by two-dimensional effects and surface wave energy and are not well represented with *SHAKE* (reference in Part I). Between 2 and 3 sec, the two responses typically begin to diverge. For purposes of this study, data was presented only for periods less than 2 sec. In many cases, the response did not drop significantly enough within this range of periods to conclude unequivocally that the peak

response had been predicted. The use of other computer models may be necessary to define peak response values.

68. Six different figures and various tables are used to present different aspects of the results for each case considered. The use of different forms of results is described in the sections below and examples are presented. Each of these types of data presentation are included in appendices for each case analyzed. Care was taken to keep scales of plots consistent with respect to the earthquake event to facilitate comparisons between figures. Additional aspects of the computer code, including options not presented, are described in the program documentation. For this reason, further discussion is not included herein.

Acceleration-time records

69. The variation of particle acceleration with time was considered for this study primarily to provide insight as to the effects of various layers on wave propagation and to detect any potential anomalies. An example of the presentation of this data is shown in Figure 35. An acceleration record is plotted for each layer in the soil column, corresponding to the top of the labeled layer. The peak accelerations are also identified and labeled and are generally summarized in tables.

Shear strains

70. Shear strains corresponding to the mid-height of layers are used to update shear modulus and damping ratio from normalized relationships. The actual value used for this purpose is called the effective shear strain, γ_{eff} , which is calculated from the maximum value of shear strain, γ , as:

$$\gamma_{eff} = PRMUL * \gamma \quad (4)$$

where

PRMUL = 0.65 for this study

The variation of effective shear strain with time at different layer contacts are shown using a format similar to that for accelerations as shown in Figure 36. The top and bottom of the column are excluded since the shear strains are always zero.

Pseudo-velocity response spectrum

71. Pseudo-velocity spectrum is the response, in terms of velocity, of an equivalent damped single-degree-of-freedom (SDOF) system to the free-field motion. This spectrum is used for design and analysis by structural

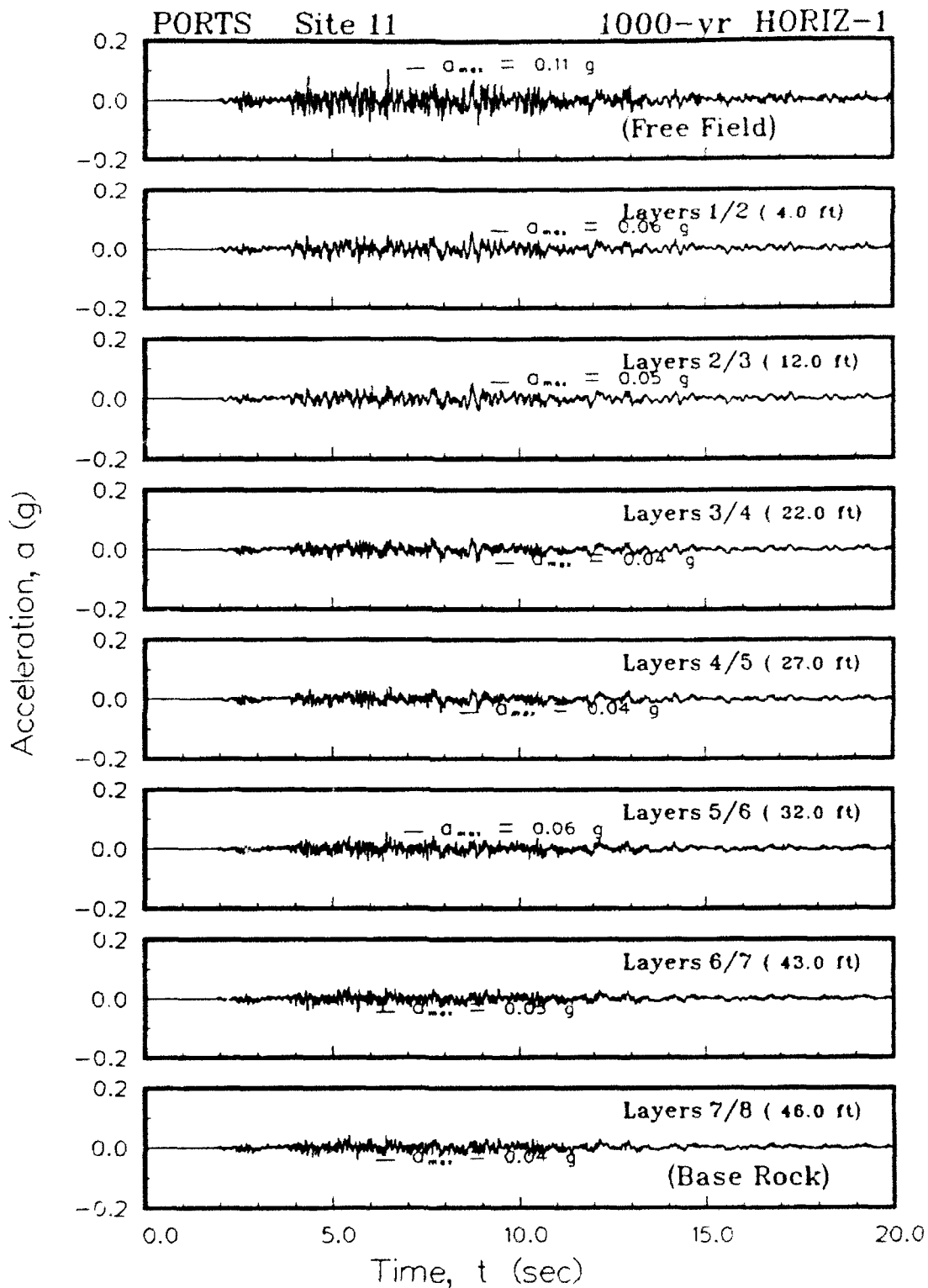


Figure 35. Example figure showing a profile of the variation of acceleration with time

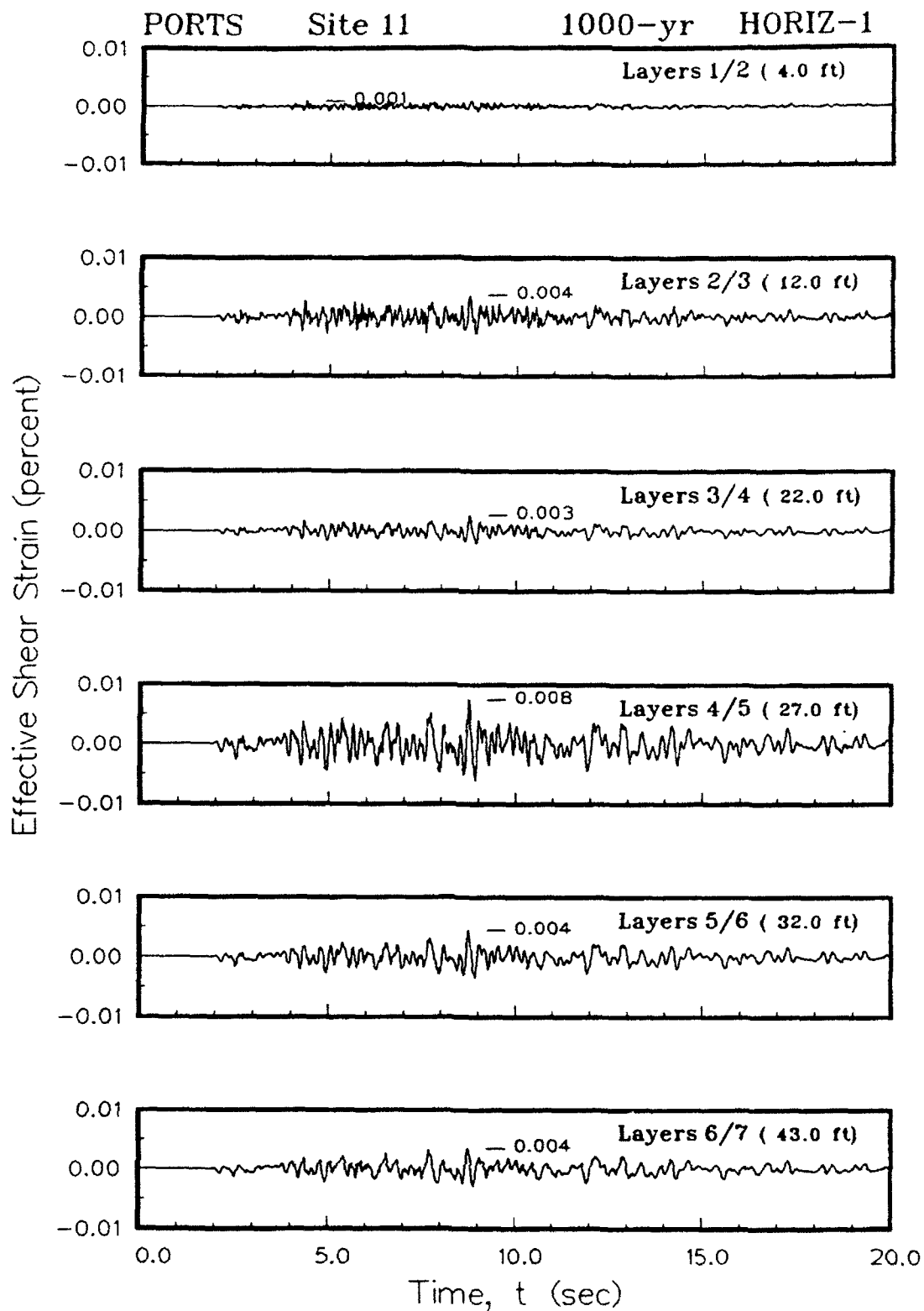


Figure 36. Example figure showing a profile of the variation of effective shear strain with time

engineers. An example of the presentation of this pseudo-velocity response spectrum at the free field (ground surface) in tripartite form for the six levels of system damping is shown in Figure 37.

Absolute acceleration response spectrum

72. An absolute psuedo-acceleration response spectrum is the response, in terms of acceleration, of an equivalent damped single-degree-of-freedom (SDOF) system to the free-field motion. Absolute rather than relative accelerations were used for this study as recommended by Wiegel (1970). An example of the presentation of the absolute acceleration response spectrum for rock outcrop and free-field motions is shown in Figure 38. The spectrum for rock outcrop is reproduced in a separate subplot using the same format for easy comparison. The peak accelerations denoted in acceleration-time records for this study generally correspond to response spectral accelerations at very low periods.

Ratios of acceleration spectra

73. The ratio of free-field ground surface acceleration spectrum to rock outcrop acceleration spectrum at each period was calculated to evaluate the periods at which motions are amplified the most and to determine the site period. The variation of this ratio with period at six levels of system damping will be used for design and seismic stability evaluations. An example of the presentation of this ratio is shown in Figure 39.

Dynamic amplification

74. Some studies of site response (e.g., Seed, Ugas, and Lysmer 1974) and design manuals (e.g., Department of the Army 1986 and Uniform Building Code (International Conference of Building Officials 1991)) use a "normalized spectra" that is calculated by dividing the acceleration response spectra by the peak horizontal acceleration. This is sometimes referred to as the dynamic amplification factor. An example figure is shown in Figure 40. Recall that absolute response accelerations are used (not pseudo response accelerations).

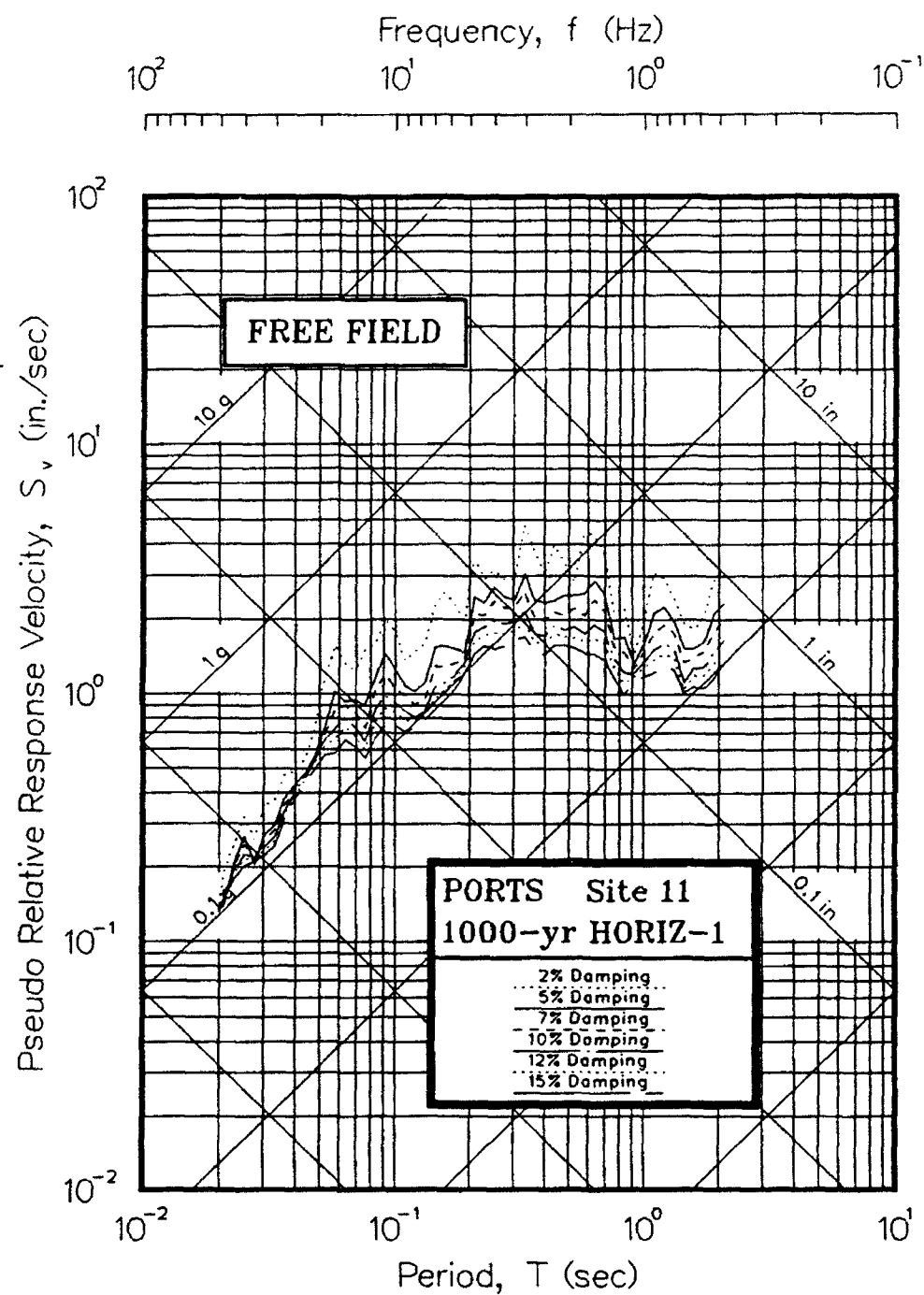


Figure 37. Example figure showing pseudo-velocity response spectra in tripartite format (5 percent damping)

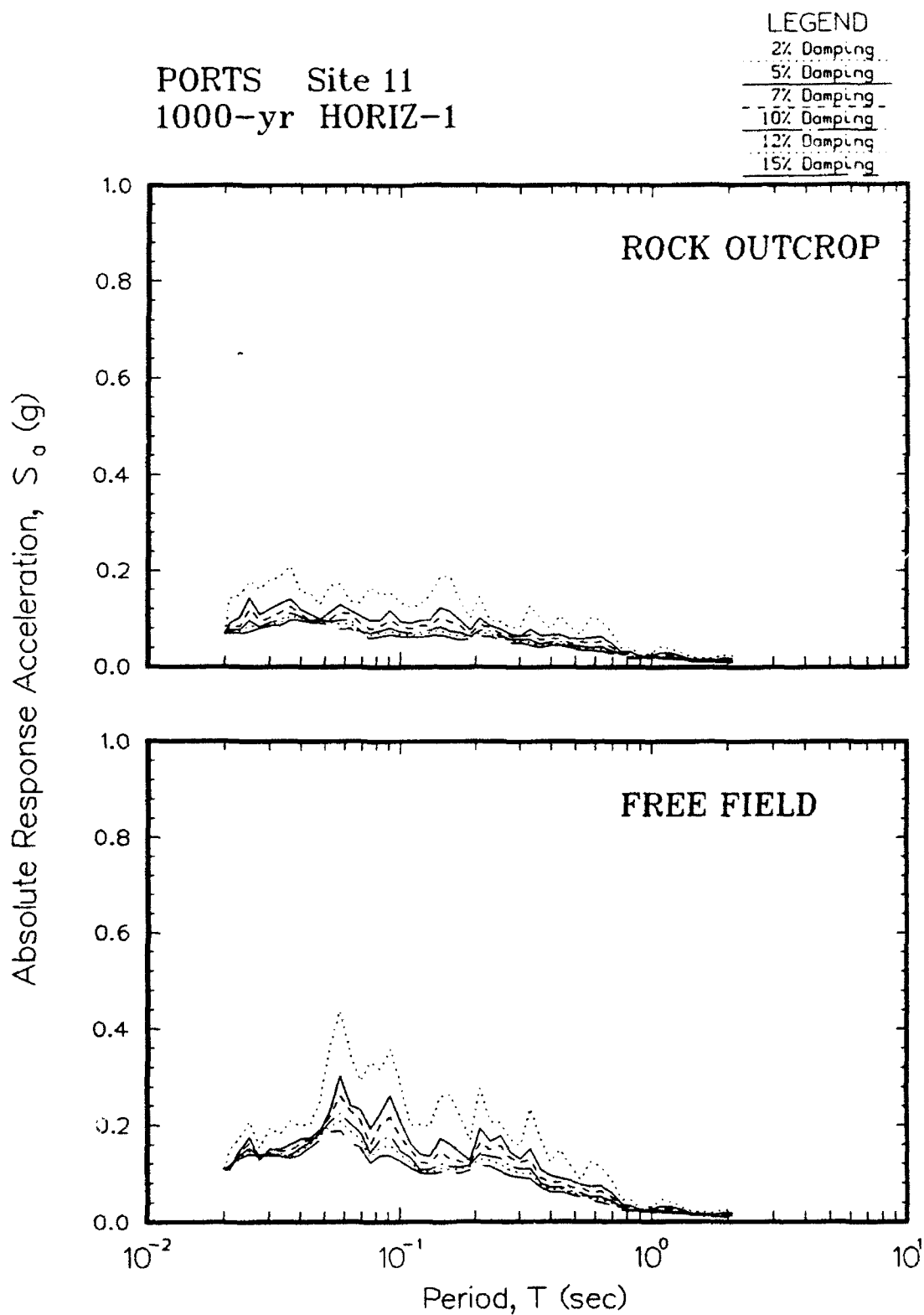


Figure 38. Example figure showing the absolute acceleration response spectra for rock outcrop and free-field motions

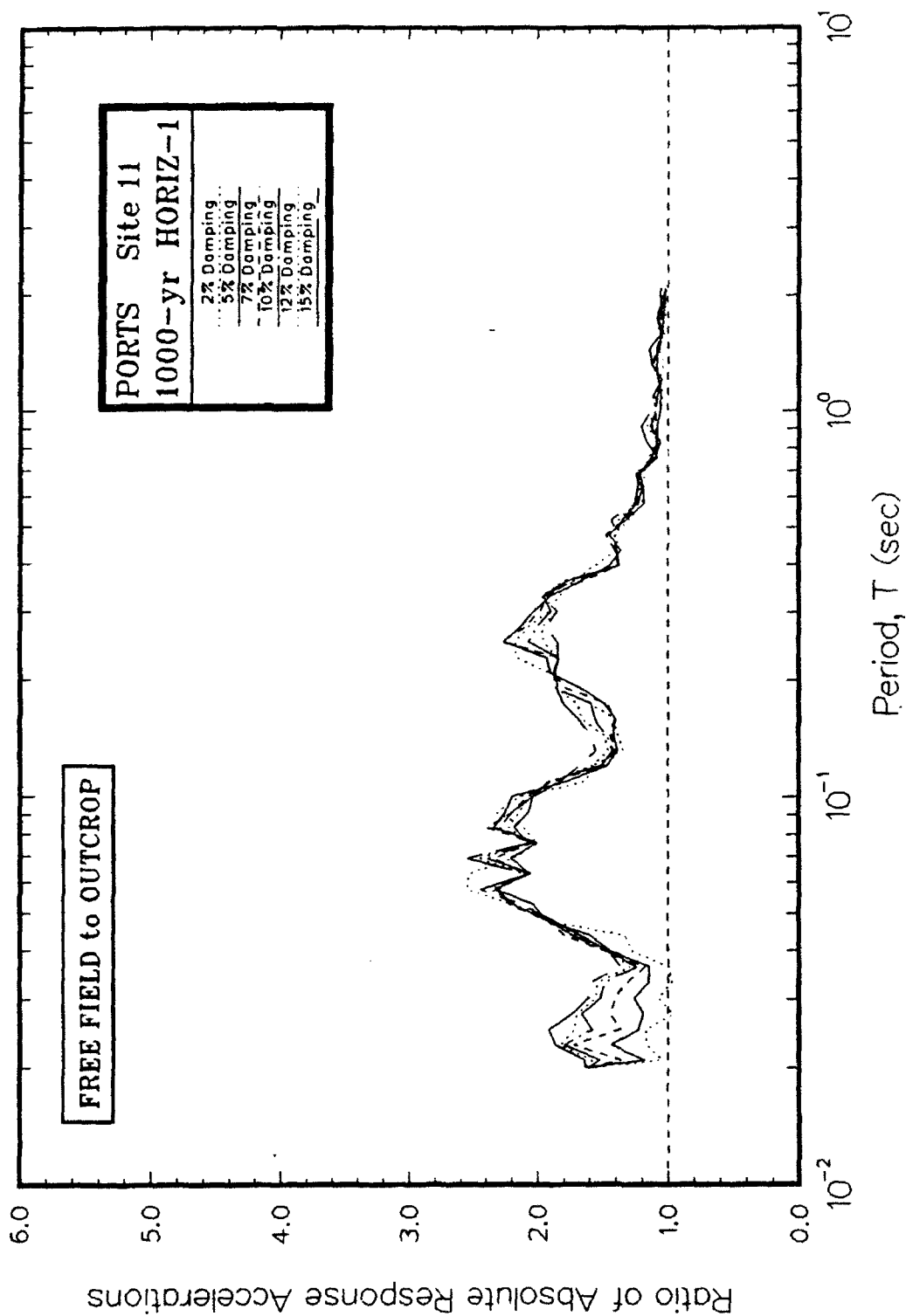


Figure 39. Example figure showing the ratio of absolute acceleration response spectra for free field to rock outcrop motions

PORTSMOUTH
Site 11

1000-yr Event
Horizontal 1

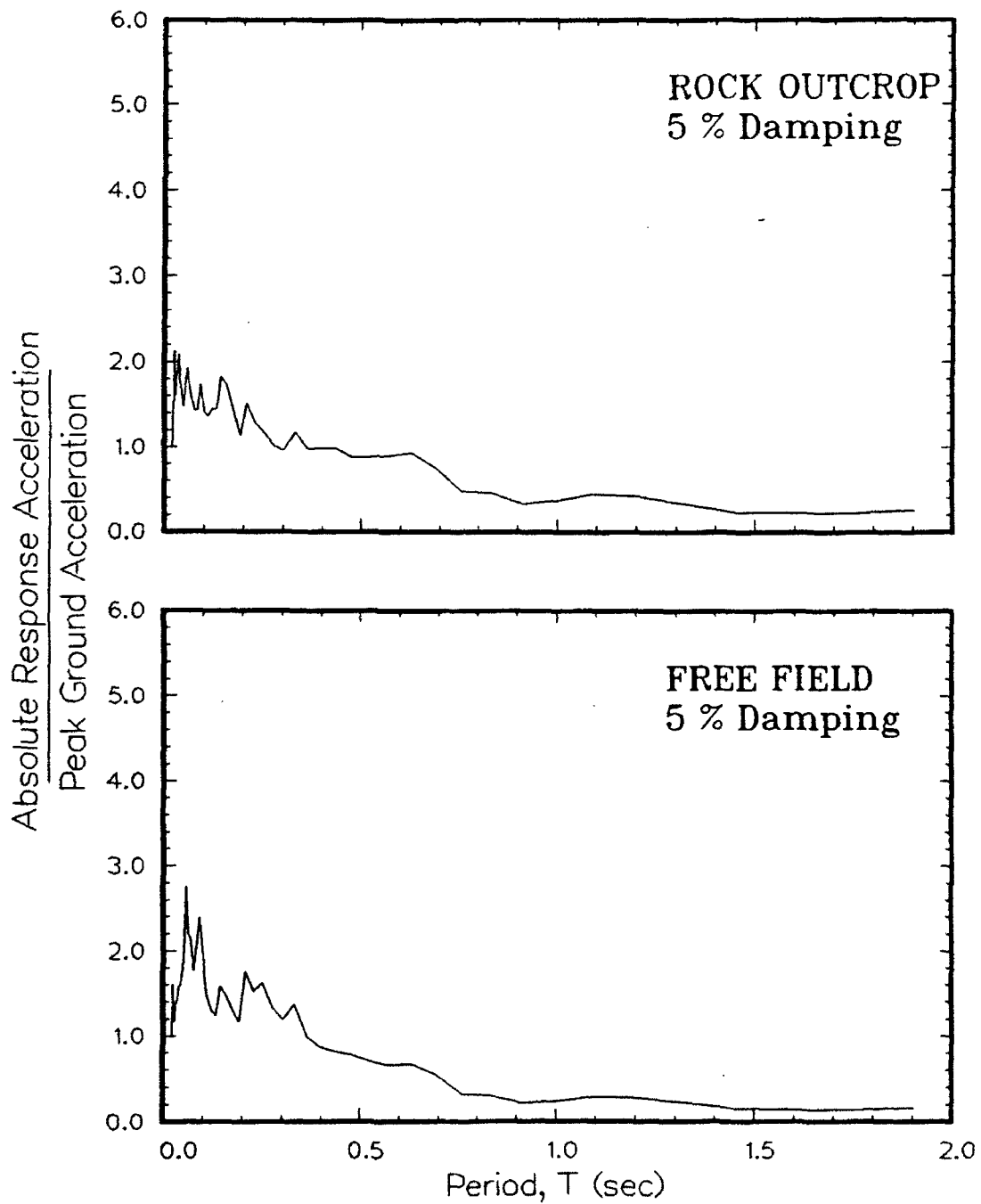


Figure 40. Example figure showing the amplification ratios (absolute acceleration response spectra normalized to peak horizontal acceleration) for rock outcrop and free field motions

PART V: RESULTS FROM COLLECTION OF INDIVIDUAL SITES

75. The results of site response calculations for individual sites are presented below respective of the three design events. Results at 5 percent system damping are shown using the formats described in Part IV. The plot scales were kept consistent, except for shear strains and spectral accelerations for the 5000-year event, to aid in comparing values among the three events. The sensitivity of calculated response to soil column inputs using the average column is presented in Part VI.

76. In general, the calculated horizontal responses at the six GCEP sites (PT-1 through PT-6) were significantly different from the nine GDAP sites (PT-7 through PT-15). This is attributed to general differences in the total thickness of soil overlying rock (generally deeper at GDAP sites) and shear wave velocities (generally lower at GDAP) and impedance contrast at the base of the columns (generally higher at GCEP). The first two differences suggest that the natural site periods for GDAP are greater. The difference in impedance ratio is expected to affect the peak effective shear strains and the peak horizontal accelerations. The presentation of data below oftentimes includes differentiation between calculated response for sites at GCEP versus GDAP because of these differences.

500-Year Event

77. The calculated response for the 500-year event at the fifteen sites indicates that small peak accelerations and shear straining can be expected for this event. Amplification of motions is expected at all periods between 0.02 and 2.0 sec. The range of response spectra is fairly wide reflecting the wide range of column heights and velocity profiles. Discussion of the data is presented below.

Acceleration versus time

78. The calculated motions for the top of each layer for the fifteen sites and two horizontal input motions are presented in Appendix B. A comparison of peak accelerations is made in Table 7. The propagation of shear waves through the fifteen soil columns with two different horizontal earthquake components always produced amplification in terms of peak acceleration. The peak horizontal acceleration at base rock is 0.04 g

Table 7
Calculated Peak Ground Acceleration

Site	Peak Acceleration (g's)					
	500-Year Event		1000-Year Event		5000-Year Event	
	Horizontal 1	Horizontal 2	Horizontal 1	Horizontal 2	Horizontal 1	Horizontal 2
PT-1	0.08	0.09	0.12	0.15	0.22	0.23
PT-2	0.09	0.12	0.17	0.16	0.33	0.34
PT-3	0.09	0.11	0.13	0.16	0.30	0.28
PT-4	0.10	0.11	0.16	0.17	0.31	0.32
PT-5	0.09	0.11	0.13	0.13	0.24	0.36
PT-6	0.08	0.09	0.12	0.14	0.21	0.22
PT-7	0.05	0.06	0.08	0.08	0.14	0.15
PT-8	0.07	0.06	0.09	0.09	0.17	0.16
PT-9	0.06	0.08	0.09	0.12	0.19	0.23
PT-10	0.05	0.07	0.08	0.09	0.18	0.17
PT-11	0.07	0.08	0.11	0.10	0.21	0.18
PT-12	0.06	0.07	0.09	0.09	0.15	0.16
PT-13	0.06	0.06	0.11	0.11	0.20	0.22
PT-14	0.06	0.08	0.10	0.12	0.20	0.21
PT-15	0.08	0.10	0.12	0.16	0.25	0.23

for both horizontal components. The peak horizontal accelerations at ground surface range from 0.05 (PT-7 and PT-10) to 0.12 g (PT-2). The Horizontal 2 component nearly always produced a greater peak ground acceleration. The peak accelerations for the GCEP area are generally greater than those for the GDAP area.

79. Observations of the acceleration records in Appendix B indicate that, in general, the amplitude of acceleration decreases and higher frequencies are filtered as waves propagate upwards through each layer. In only a few cases were peak accelerations reduced as waves passed through a layer. Most amplification occurred in the upper 10 ft of the column.

Shear strains versus time

80. The calculated effective shear strains at each contact between soil layers for fifteen sites and two horizontal components are presented in Appendix C. The peak (effective) shear strains for each column are listed in Table 8. (Note that the shear strains in Table 8 represent values calculated at the mid-height of layers whereas shear strains presented in Appendix C were calculated at layer interfaces.) In most cases, the maximum strains occur in the lower half of each column and at the same depth for both horizontal components. At the GCEP sites, the peak effective shear strains do not exceed 0.003 percent. The largest strains occur at PT-8 and PT-15.

81. In general, the peak effective shear strains correspond to a small amount of straining. The range in shear modulus for soils corresponding to these strains is about 92 to 69 percent of the small-strain (maximum) modulus. The range in damping ratio is between 2 and 6 percent for soil layers.

82. A good correlation appears to exist between the maximum effective shear strain and the total height of the soil column respective of plant area. The median value for the ratio of effective shear strain to column height is 9×10^{-5} (percent/ft height).

Pseudo-velocity spectra

83. The pseudo-velocity response spectra for the fifteen individual sites are presented in Appendix D. The combined spectra at five percent damping for all sites and both horizontal components is shown in Figure 41. The range produced by the 30 spectra is rather wide. The upper bound is essentially defined by the responses for PT-2, PT-8, and PT-15 with a peak spectral velocity of 4 in./sec.

Table 8

Calculated Maximum Effective Shear Strain

Site		Peak Effective Shear Strain (percent)					
		500-Year Event		1000-Year Event		5000-Year Event	
		Horizontal 1	Horizontal 2	Horizontal 1	Horizontal 2	Horizontal 1	Horizontal 2
PT-1	20	0.002	0.003	0.004	0.006	0.010	0.008
PT-2	4	0.002	0.003	0.004	0.005	0.012	0.013
PT-3	20.5	0.002	0.003	0.004	0.006	0.013	0.009
PT-4	14.5	0.002	0.003	0.004	0.006	0.011	0.008
PT-5	17.5	0.002	0.002	0.003	0.005	0.010	0.008
PT-6	31	0.002	0.003	0.004	0.006	0.012	0.010
PT-7	29.5	0.004	0.004	0.005	0.006	0.013	0.010
PT-8	39	0.010	0.007	0.018	0.013	0.030	0.027
PT-9	40.5	0.006	0.005	0.008	0.007	0.014	0.013
PT-10	39	0.003	0.003*	0.004	0.004*	0.007*	0.007
PT-11	29.5	0.005	0.004	0.007	0.006	0.013	0.013
PT-12	11.5	0.004	0.005	0.006	0.008	0.015	0.012
PT-13	8.5	0.002	0.002	0.004	0.004	0.007	0.007
PT-14	17.5	0.008	0.007	0.011	0.010	0.021	0.016
PT-15	3.5	0.007*	0.011	0.013	0.019	0.017*	0.026

* At depth of 17.5 ft

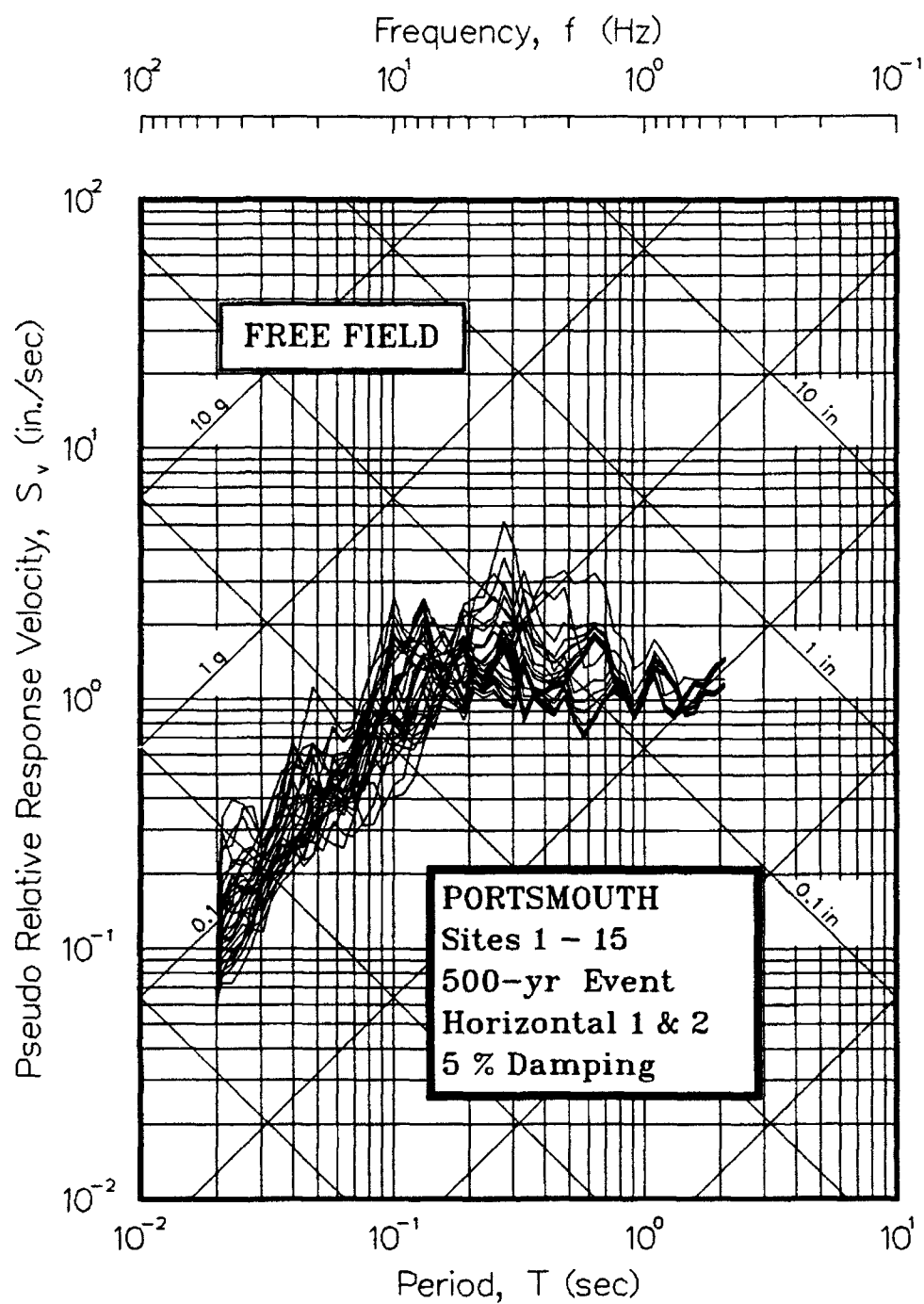


Figure 41. Pseudo-velocity response spectra for 500-year event

Absolute acceleration spectra

84. Absolute acceleration response spectra for the fifteen individual sites are presented in Appendix E. The combined spectra at five percent damping for all sites and both horizontal components are shown in Figure 42. Some curves with pronounced peaks are identified. The spectra for rock are included for comparison (refer to Figure 6). The combined free-field spectra indicate that the largest spectral acceleration is 0.41 g at 0.1 sec and was calculated for the Horizontal 2 component applied to PT-2. The spectral accelerations at periods greater than 0.5 sec are negligible.

Ratio of acceleration spectra

85. The ratios of free field to outcrop acceleration response spectra for the fifteen individual sites are presented in Appendix F. Combined spectra at all sites for both horizontal motions are shown in Figure 43. (The ratio for rock outcrop is 1.) Spectra with sharp peaks are identified. The 30 spectra produce a wide range of expected response. At any given period between 0.02 and 0.5 sec, the ratio can be between 1 and 3 and as high as 6. Some trends exist, however. For the GCEP area, the ratios typically have a well-pronounced peak between 0.1 and 0.15 sec. For the GDAP area, the spectral ratios have much-less definition. A general range of peaks seems to occur at periods between 0.06 and 0.3 sec.

Amplification ratio

86. The ratios of free-field spectral acceleration to peak horizontal acceleration for the fifteen individual sites are shown in Appendix G. Combined relationships at all sites for both horizontal motions are shown in Figure 44. The ratios for rock outcrop are also shown for comparison. The range of relationships is moderately-wide but somewhat uniform. The ratios for the GCEP area typically have a well-defined peak at periods less than 0.2 sec and then a gradual decrease. The ratios for the GDAP area have poorly-defined peaks and typically show significant values at periods greater than 0.5 sec.

1000-Year Event

87. The calculated response for the 1000-year event at the fifteen sites indicates that small peak accelerations and shear straining can be expected for this event. Amplification of motions is expected at all periods

PORTSMOUTH
Sites 1 - 15

500-yr Event
Horizontal 1 & 2

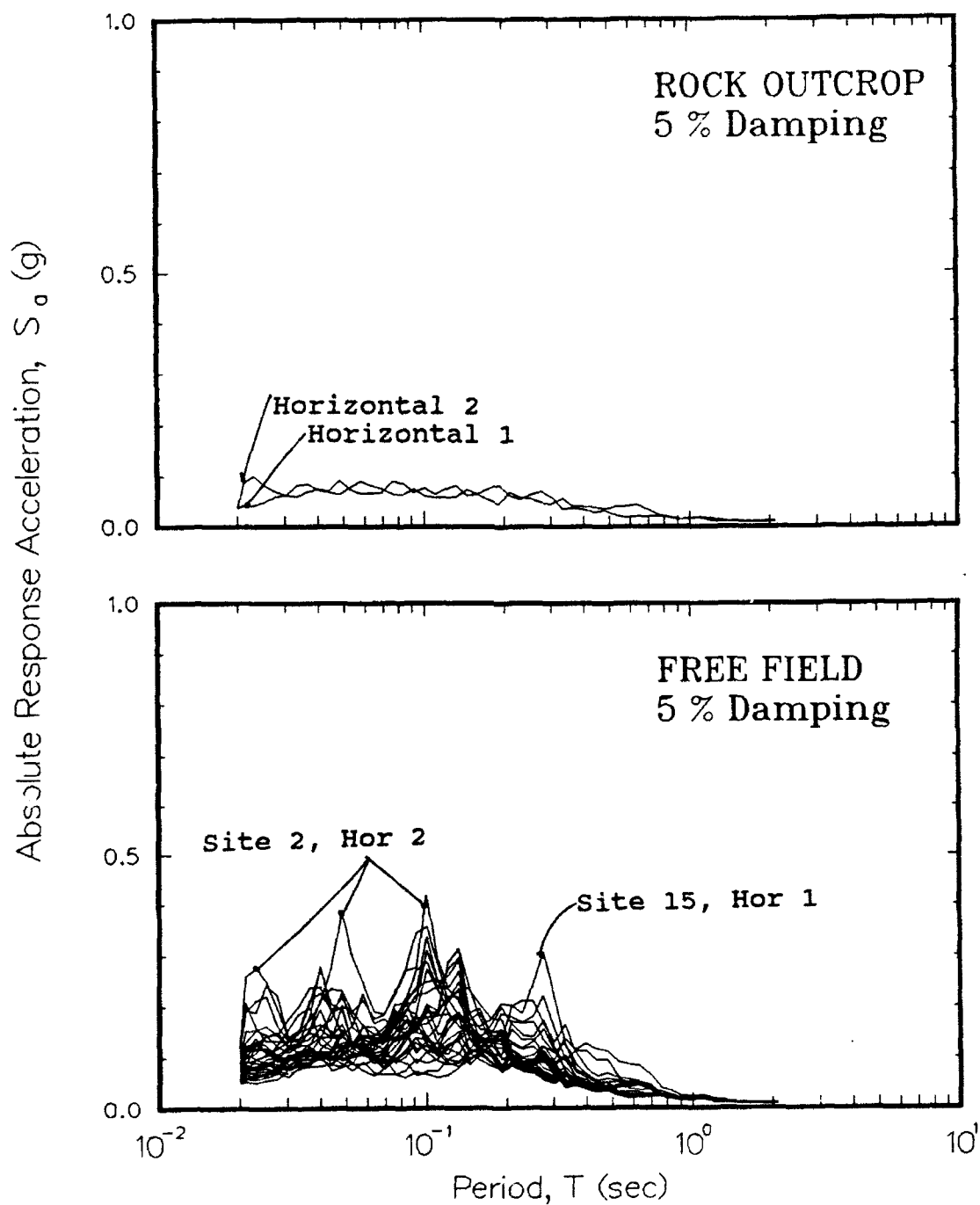


Figure 42. Absolute response acceleration spectra for 500-year event

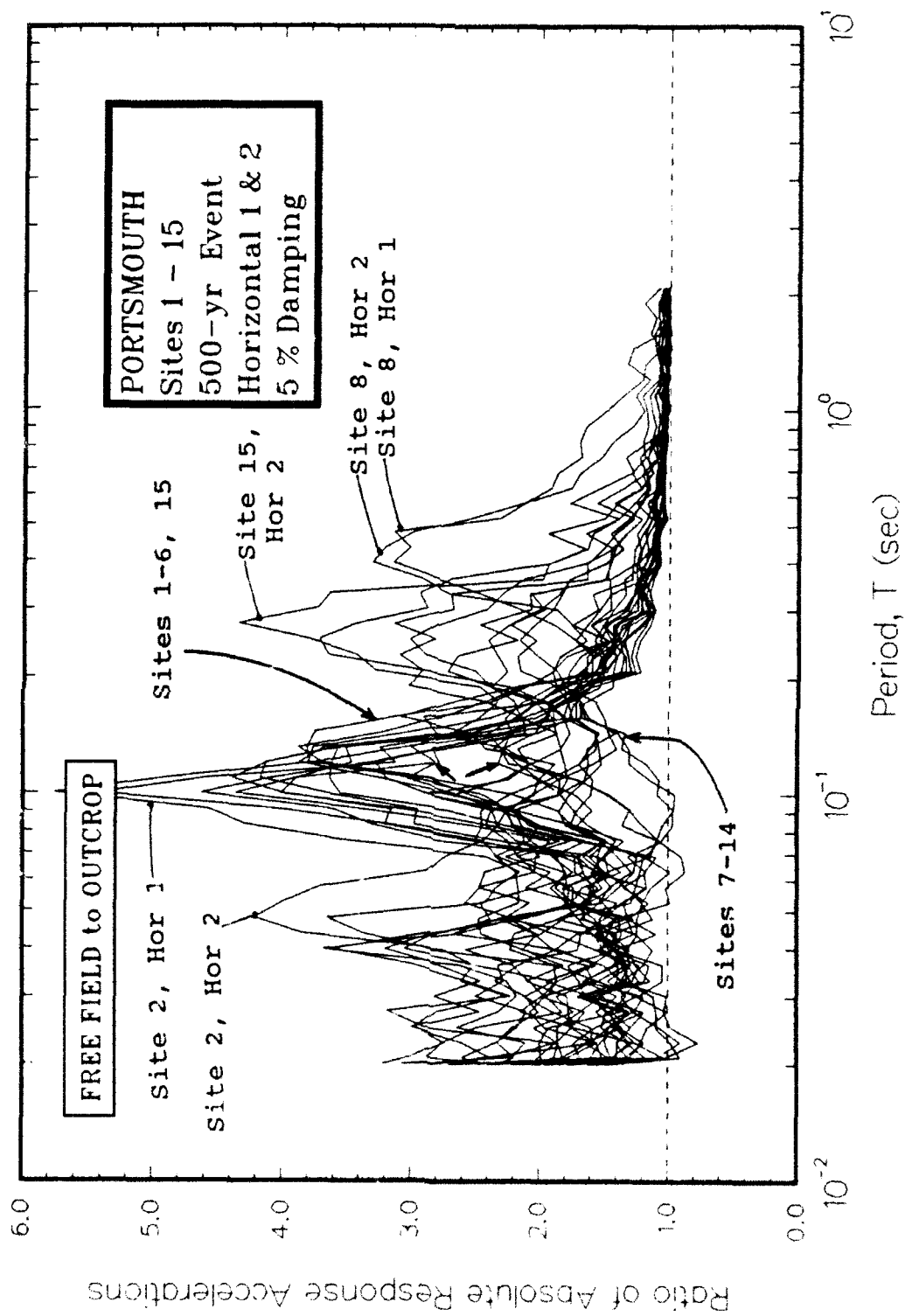


Figure 43. Ratio of free field to rock outcrop absolute acceleration response spectra for 500-year event

PORTSMOUTH
Sites 1 - 15

500-yr Event
Horizontal 1 & 2

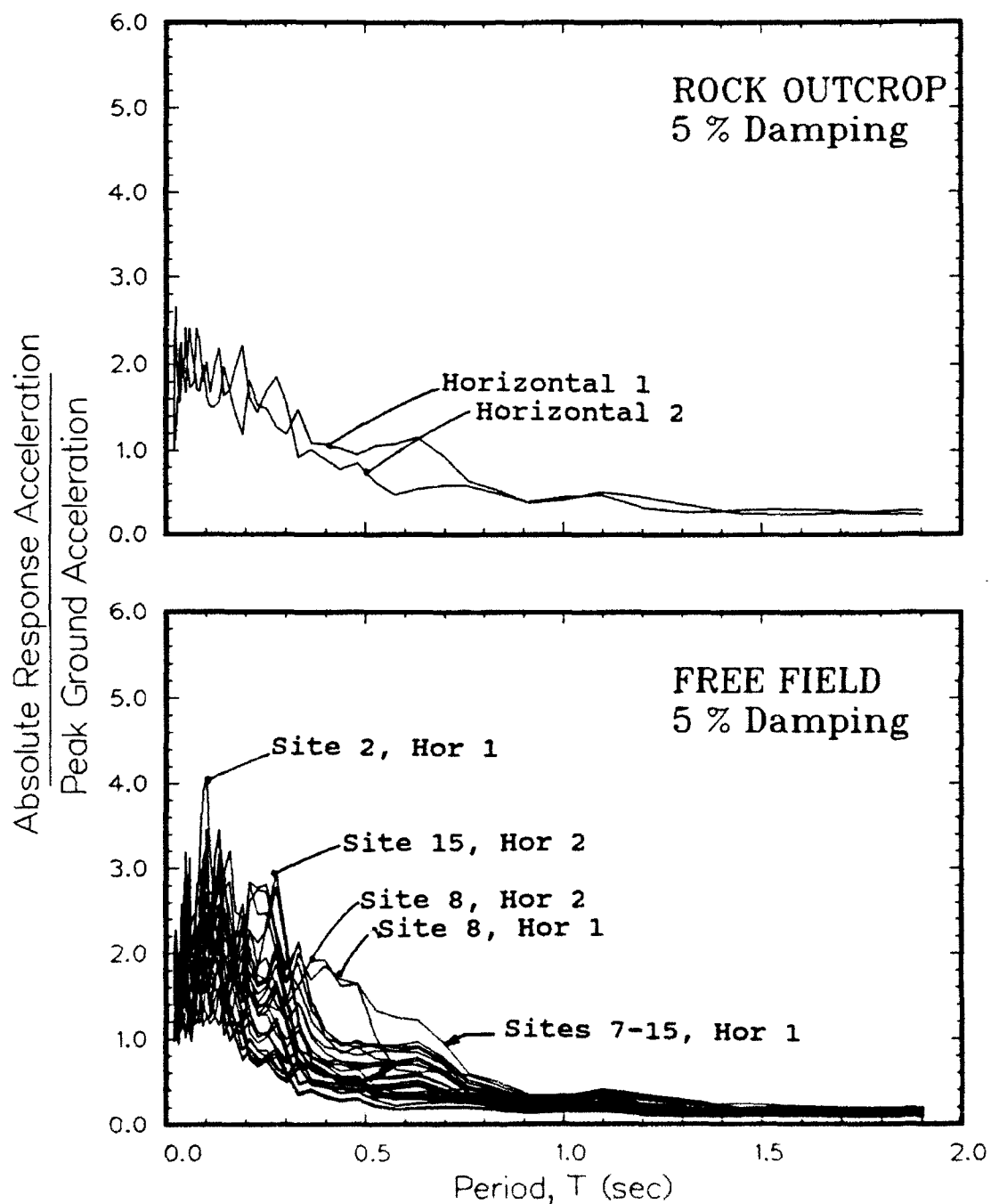


Figure 44. Amplification ratio for 500-year event

between 0.02 and 2.0 sec. The range of response spectra is fairly wide reflecting the wide range of column heights and velocity profiles. Discussion of the data is presented below.

Acceleration versus time

88. The calculated motions for the top of each layer for the fifteen sites and two horizontal input motions are presented in Appendix H. A comparison of peak accelerations is made in Table 7. The propagation of shear waves through the fifteen soil columns with two different horizontal earthquake components always produced amplification in terms of peak acceleration. The peak horizontal acceleration at base rock is 0.05 g for both horizontal components. The peak horizontal accelerations at ground surface range from 0.08 (PT-7 and PT-10) to 0.17 g (PT-4). Neither horizontal component shows a strong tendency to produce higher accelerations. However, the peak accelerations for the GCEP area are generally greater than those for the GDAP area. The peak accelerations for this event are about 50 percent greater than the accelerations for the 500-year event.

89. In general, the horizontally-polarized shear waves were amplified slightly by each layer passed. In only a few cases were peak accelerations reduced as waves passed through a layer. Most amplification occurred in the upper 10 ft of the column.

Shear strains versus time

90. The calculated effective shear strains at each contact between soil layers for fifteen sites and two horizontal components are presented in Appendix I. The peak (effective) shear strains for each column are listed in Table 8. In nearly all cases, the peak strains occur in the lower half of each column and at the same depths that peak strains occurred for the 500-year event. At nine of the sites, the peak effective shear strains are 0.006 percent or less. At the other six sites the values are greater, ranging up to 0.19 percent.

91. In general, the magnitude of calculated shear strains correspond to a small amount of straining. The range in shear modulus for soils corresponding to these strains is about 95 to 63 percent of the small-strain (maximum) moduli. The range in damping ratio is between 3 and 8 percent for soils (refer to Figure 30).

92. Again, a good correlation appears to exist between the peak effective shear strain and the total height of the soil column. The mean

ratio of effective shear strain to column height is about 17×10^{-5} (percent/ft height), almost twice that for the 500-year event.

Pseudo-velocity spectra

93. The pseudo-velocity response spectra for the fifteen individual sites are presented in Appendix J. The combined spectra at five percent damping for all sites and both horizontal components is shown in Figure 45. The peak spectral velocity is about 7 in./sec. The range and pattern produced by the 30 spectra are very consistent with the results for the 500-year event (refer to Figure 41) if the base spectral velocity for the 500-year event are shifted upwards by about 50 percent. A few peaks between 0.1 and 0.12 sec have increased slightly. Again, the upper bound is essentially defined by the collection of spectra for PT-2, PT-8, and PT-15.

Absolute acceleration spectra

94. Absolute acceleration response spectra for the fifteen individual sites are presented in Appendix K. The combined spectra at five percent damping for all sites and both horizontal components are shown in Figure 46. Some curves that are on the margins of the range are identified. The spectra for rock are included for convenience (refer to Figure 9).

95. Two strong patterns begin to develop for the 1000-year event over the 500-year event--peaks at periods of 0.025 to 0.05 and 0.1 to 0.13 sec. A lesser peak is forming at periods of about 0.26 sec. The velocity response is negligible at periods greater than 0.7 sec. The Horizontal 2 component tends to produce more spectra on the margins of the range. The peak spectral accelerations are in the range of 0.3 to 0.8 g compared to 0.2 to 0.4 g for the 500-year event (about doubled).

Ratio of acceleration spectra

96. The ratios of free field to outcrop acceleration response spectra for the fifteen individual sites are presented in Appendix L. Combined spectra at all sites for both horizontal motions are shown in Figure 47. Some curves that are on the margins of the range are identified. The 30 spectra produce a great deal of variation not unlike the plot for the 500-year event (Figure 43). At any given period between 0.02 and 0.05 sec, the ratio could possibly be between less than unity and 3.5. The trends identified for the 500-year event also exist. For the GCEP area, the ratios typically have a well-pronounced peak between 0.1 and 0.15 sec. For the GDAP area, the spectral ratios have much less definition.

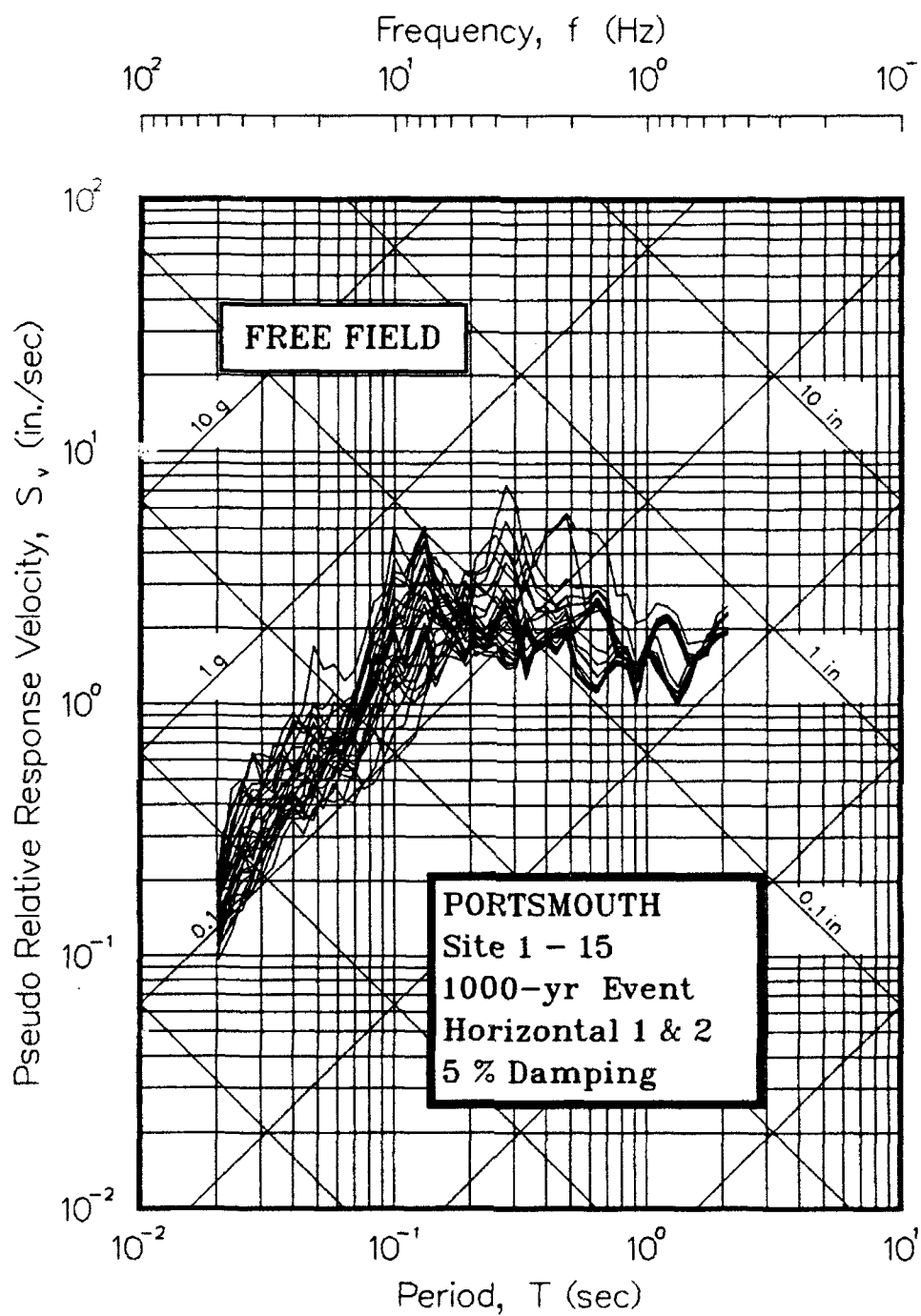


Figure 45. Pseudo-velocity response spectra for 1000-year event

PORTSMOUTH
Sites 1 - 15

1000-yr Event
Horizontal 1 & 2

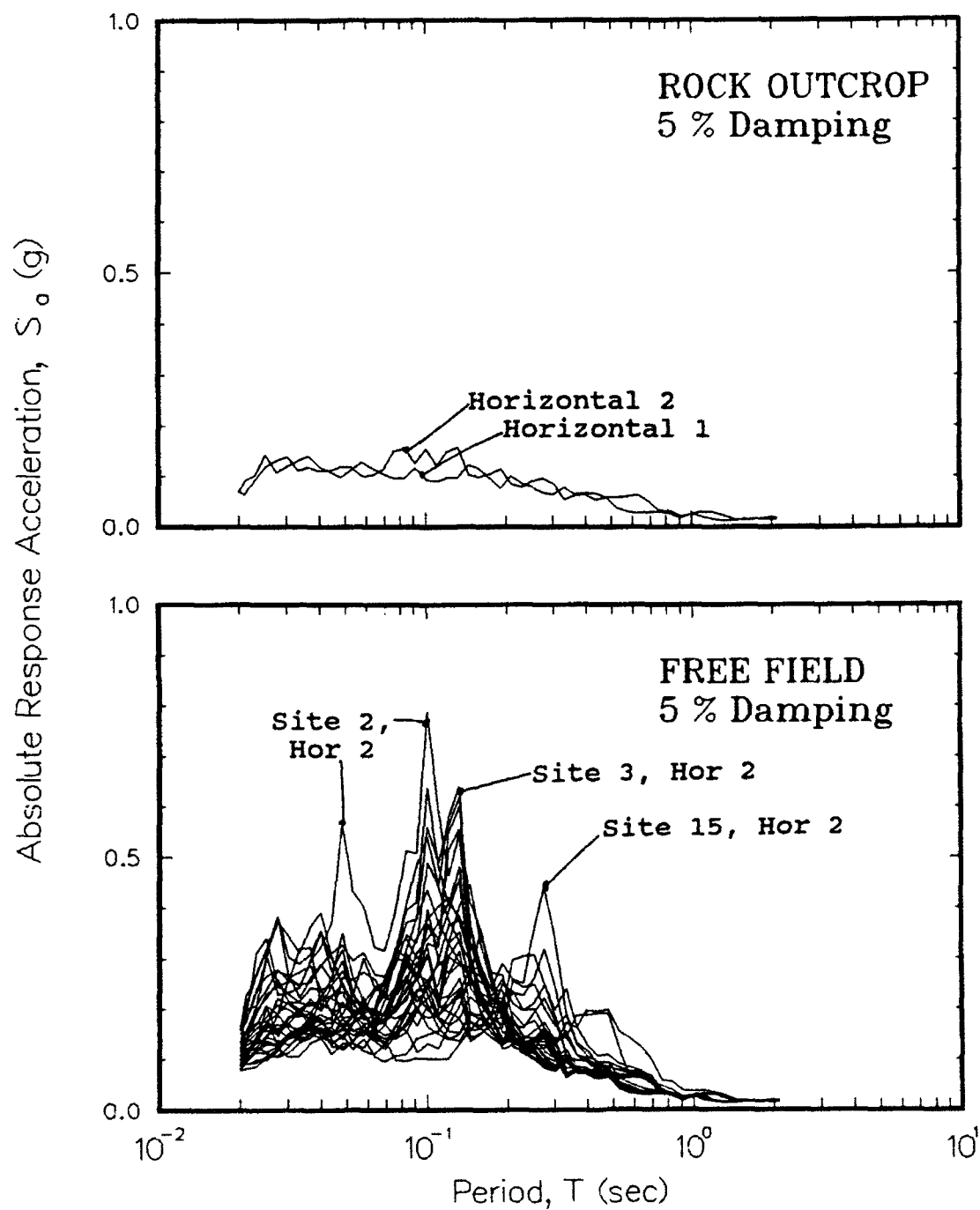


Figure 46. Absolute response acceleration spectra for 1000-year event

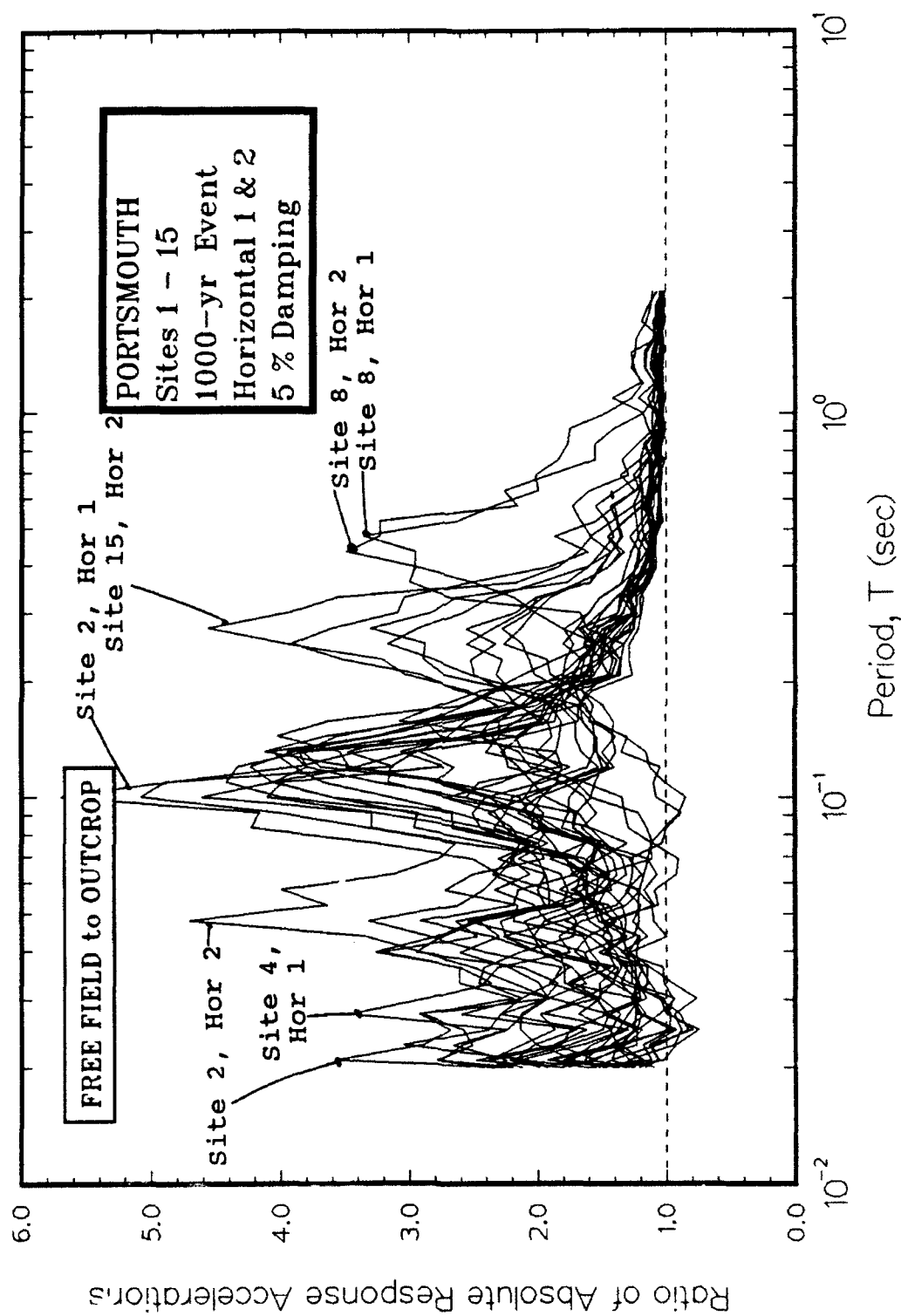


Figure 47. Ratio of free field to rock outcrop absolute acceleration response spectra for 1000-year event

Amplification ratio

97. The ratios of free-field spectral acceleration to peak horizontal acceleration for the fifteen individual sites are shown in Appendix M. Combined relationships at all sites for both horizontal motions are shown in Figure 48. The range of relationships is moderately-wide but somewhat uniform and the range and magnitudes are very similar to those calculated for the 500-year event. The ratios for the GCEP area typically have a well-defined peak at periods less than 0.2 sec and then a decrease gradually. The ratios for the GDAP area have poorly-defined peaks and typically show significant values at periods greater than 0.2 sec.

5000-Year Event

98. The calculated response for the 5000-year event at the fifteen sites indicates that small to moderate peak accelerations and shear straining can be expected for this event. Amplification of motions is expected at all periods between 0.02 and 2.0 sec. The range of response spectra is fairly wide reflecting the wide range of column heights and velocity profiles. Discussion of the data is presented below.

Acceleration versus time

99. The calculated motions for the top of each layer for the fifteen sites and two horizontal input motions are presented in Appendix N. A comparison of peak accelerations is made in Table 7. The propagation of shear waves through the fifteen soil columns with two different horizontal earthquake components always produced amplification in terms of peak acceleration. The peak horizontal acceleration at base rock is 0.13 g for both horizontal components. The peak horizontal accelerations at ground surface range from 0.14 (PT-7) to 0.36 g (PT-5). The Horizontal 2 component shows a moderate tendency to produce higher accelerations. The peak accelerations for the GCEP area are generally greater than those for the GDAP area and they are about 90 percent greater than those for the 1000-year event. In general, the horizontally-polarized shear waves were amplified slightly by each layer passed. In only a few cases were peak accelerations reduced as waves passed through a layer. Most amplification occurred in the upper 10 ft of the column.

PORTSMOUTH
Sites 1 - 15

1000-yr Event
Horizontal 1 & 2

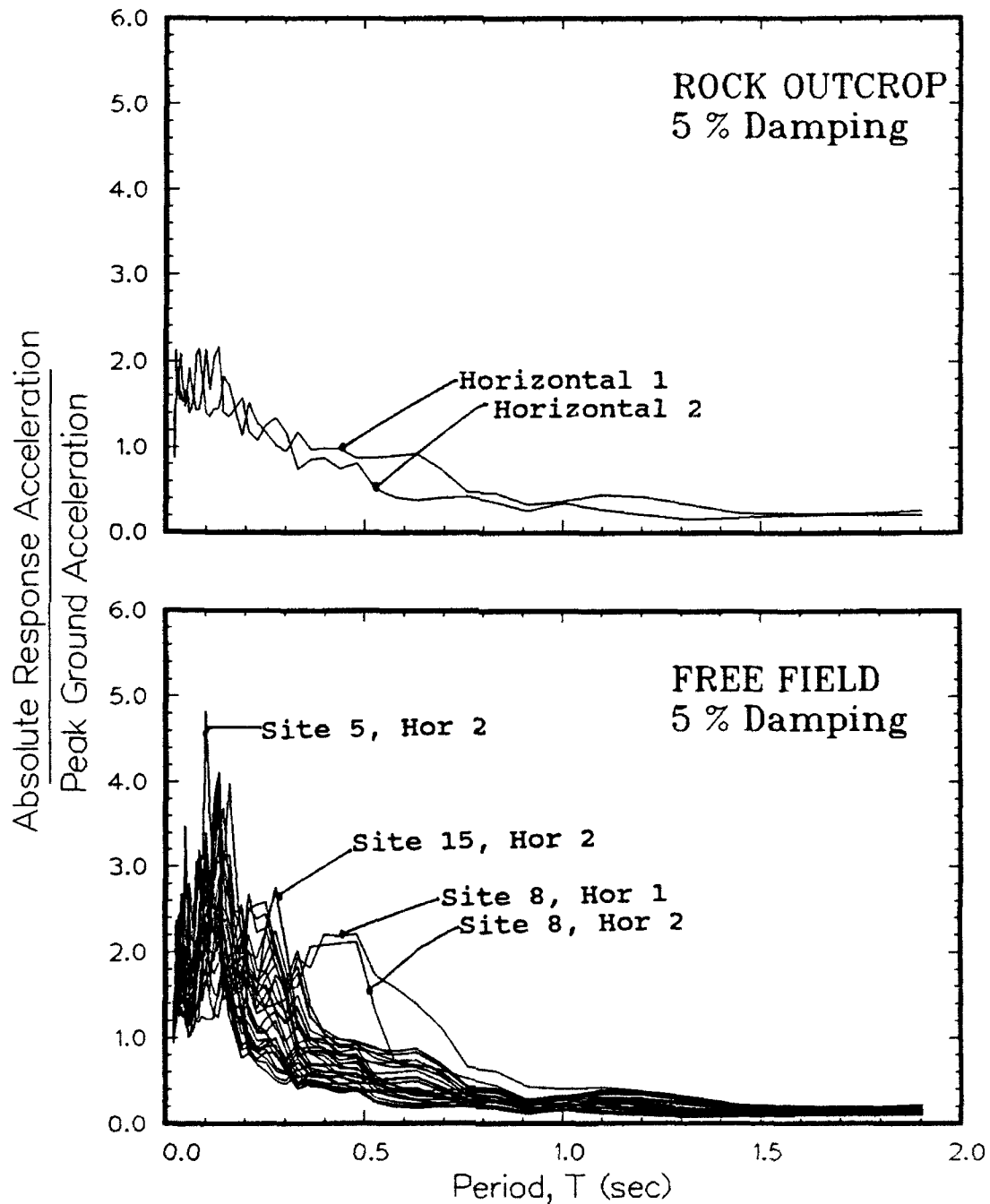


Figure 48. Amplification ratio for 1000-year event

Shear strains versus time

100. The calculated effective shear strains at each contact between soil layers for fifteen sites and two horizontal components are presented in Appendix O. The peak (effective) shear strains for each column are listed in Table 8. In most cases, the maximum strains occur in the lower half of each column. In general, the magnitude of calculated shear strains correspond to a small to moderate amount of straining. The range in shear modulus for soils corresponding to these strains is 92 to 50 percent of the maximum modulus. The range in damping ratio is between 1.5 and 7 percent for soils (refer to Figure 30).

101. A good correlation appears to exist between the maximum effective shear strain and the total height of the soil column. The mean ratio of effective shear strain to column height is about 17×10^{-5} (percent/ft height), the same as that for the 1000-year event.

Pseudo-velocity spectra

102. The pseudo-velocity response spectra for the fifteen individual sites are presented in Appendix P. The combined spectra at five percent damping for all sites and both horizontal components is shown in Figure 49. The peak spectral velocity is about 9 in./sec. The range produced by the 30 spectra are very consistent with the results for the 1000-year event (refer to Figure 45) if the base spectral velocity for the 1000-year event are shifted upwards by about 90 percent. The upper bounds of the range is defined by PT-2 at periods below 0.13 sec and by PT-8 at periods above 0.20 sec.

Absolute acceleration spectra

103. Absolute acceleration response spectra for the fifteen individual sites are presented in Appendix Q. The combined spectra at five percent damping for all sites and both horizontal components are shown in Figure 50. Some curves that are on the margins of the range are identified. The spectra for rock are included for comparison (refer to Figure 12).

104. A new peak developed for the 5000-year event at periods between 0.025 and 0.05. The peak spectral acceleration is 1.4 g compared to 0.8 g for the 1000-year event (almost doubled). The Horizontal 2 component tends to produce more spectra at the upper bound of the range.

Ratio of acceleration spectra

105. The ratios of free field to outcrop acceleration response spectra for the fifteen individual sites are presented in Appendix R. Combined

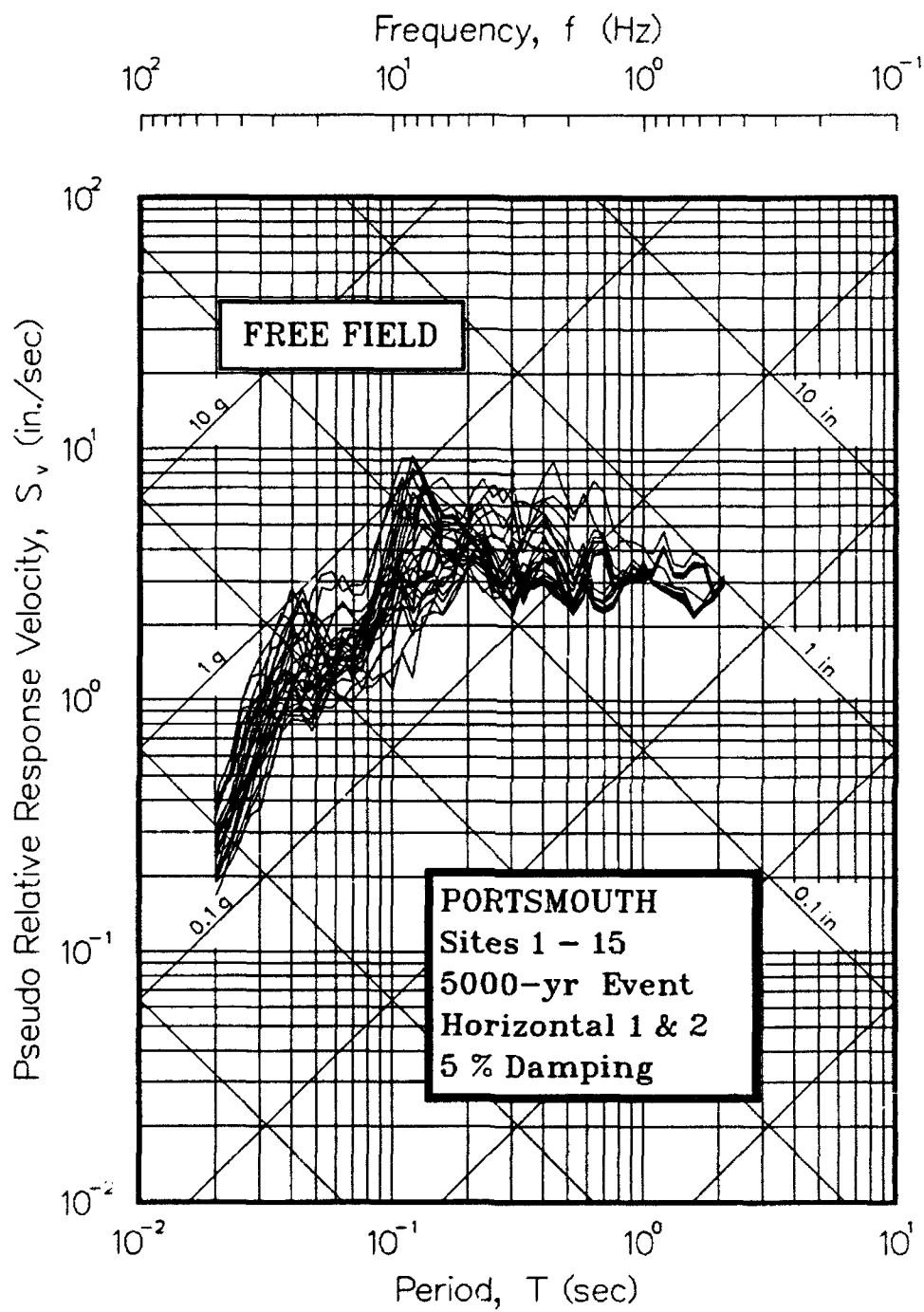


Figure 49. Pseudo-velocity response spectra for 5000-year event

PORTSMOUTH
Sites 1 - 15

5000-yr Event
Horizontal 1 & 2

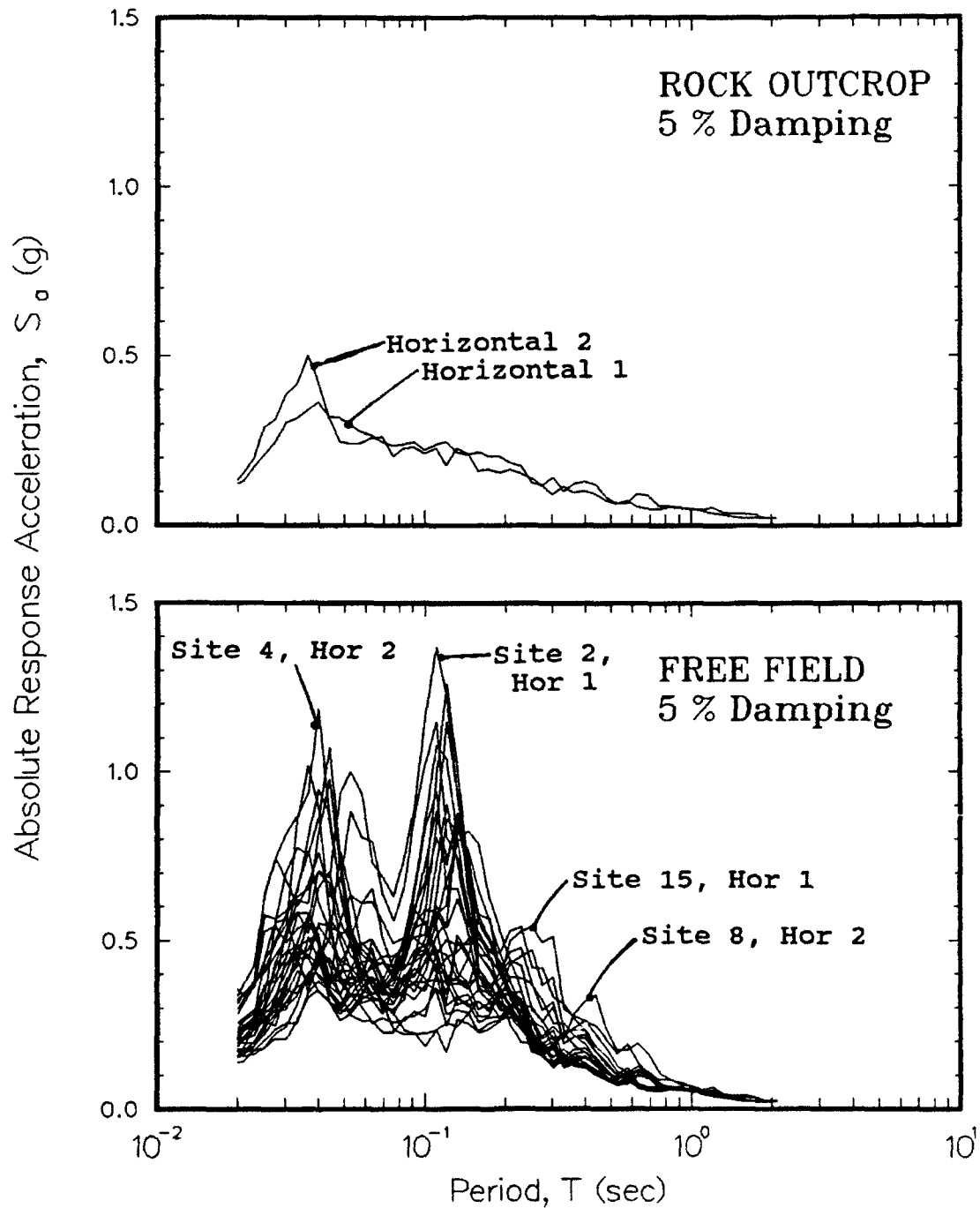


Figure 50. Absolute response acceleration spectra for 5000-year event

spectra at all sites for both horizontal motions are shown in Figure 51. Some curves that are on the margins of the range are identified.

106. The 30 curves shown in Figure 51 produce a wide range very much like the plots for the 500- and 1000-year events (Figures 43 and 47). The peak ratios at periods other than at 0.1 sec are slightly less than for the other events. The trends identified for the other two events also exist for the 500-year event. For the GCEP area, the ratios typically have a well-pronounced peak between 0.1 and 0.15 sec. For the GDAP area, the spectral ratios have much less definition.

Amplification ratio

107. The ratios of free-field spectral acceleration to peak horizontal acceleration for the fifteen individual sites are shown in Appendix S. Combined relationships at all sites for both horizontal motions are shown in Figure 52. The range of relationships is moderately-wide; the range and magnitudes are very similar to those calculated for the 500- and 1000-year events. The ratios for the GCEP area typically have a well-defined peak at periods less than 0.2 sec and then a decrease gradually. The ratios for the GDAP area have poorly-defined peaks and typically show significant values at periods greater than 0.2 sec.

Combined Events

108. The similarity of shapes and amplitudes for all three earthquake events was noted for two sets of data: the ratio of absolute acceleration response and the amplification ratio. These results for all three events were combined and are described below. Spectra that fall outside the general range of data are identified. These similarities may not exist for more severe earthquakes, however.

109. The ratio of absolute acceleration calculated at all fifteen sites for both components of three events are shown in Figure 53 representing ninety spectra. In general, the range of data at most periods is wide. However, the range for all three events is not much different from that produced for each individual event (Figures 43, 47, and 51). For each site, the spectral ratios are fairly consistent, relatively independent of the horizontal component or earthquake event.

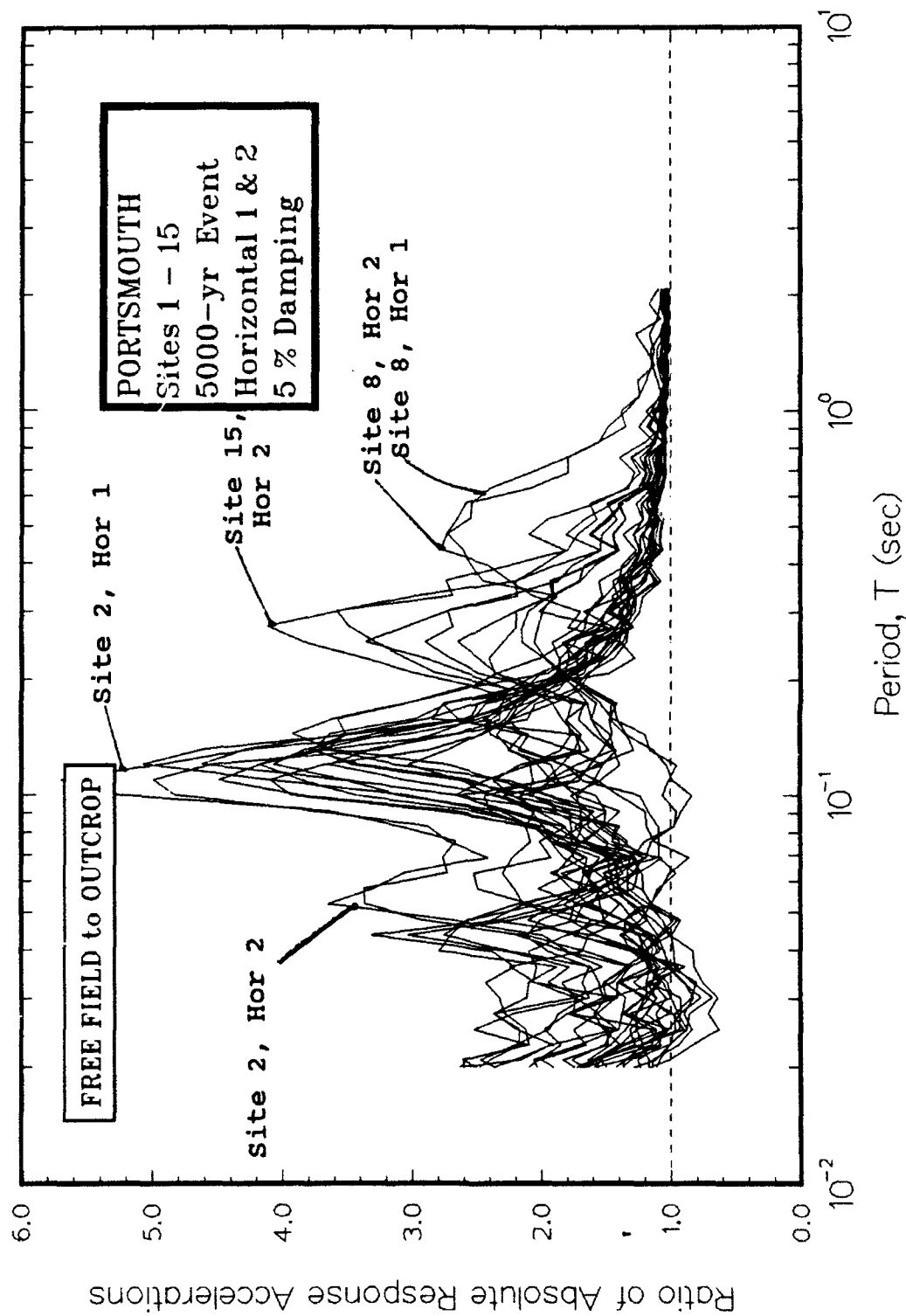


Figure 51. Ratio of free field to rock outcrop absolute acceleration response spectra for 5000-year event

PORTSMOUTH
Sites 1 - 15

5000-yr Event
Horizontal 1 & 2

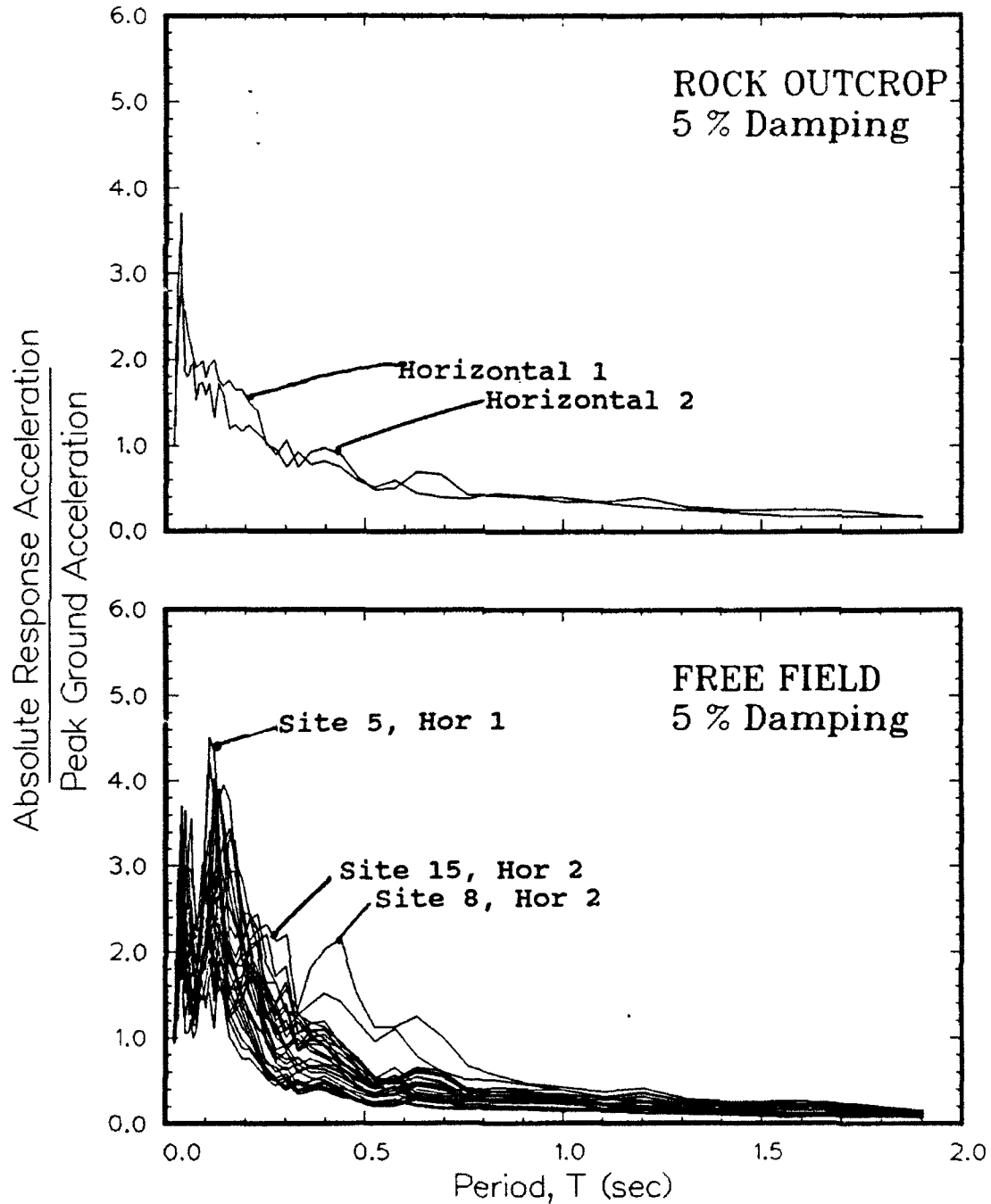


Figure 52. Amplification ratio for 5000-year event

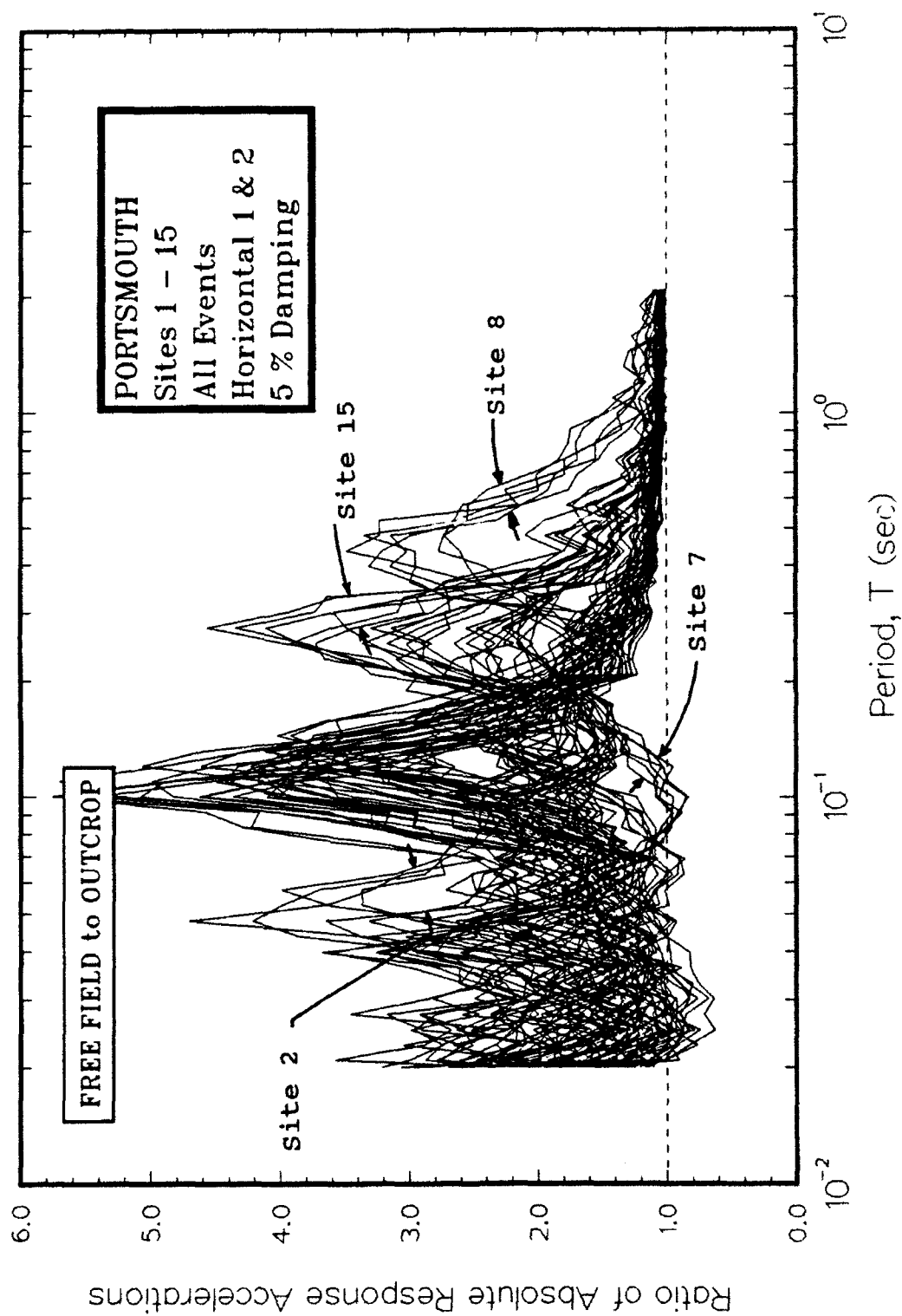


Figure 53. Ratio of free field to rock outcrop absolute acceleration response spectra for all events

110. The spectra from four sites (PT-2, PT-7, PT-8, and PT-15) that tend to deviate from the rest of the group are identified. Recall that PT-2 and PT-15 have very high velocity values and column PT-8 is the deepest. These non-uniform profiles produce a wide scattering of the response.

111. The amplification ratio calculated at all fifteen sites for both components of three events are shown in Figure 54. Six spectra represent rock outcrop and ninety spectra represent free-field soil response. The range in soil response is fairly uniform except for data from PT-8. The ratio is generally less than one at periods less than 0.4 sec and has peaks of 2 to 4.5 at periods of 0.05 to 0.3 sec.

PORTSMOUTH
Sites 1 - 15

All Events
Horizontal 1 & 2

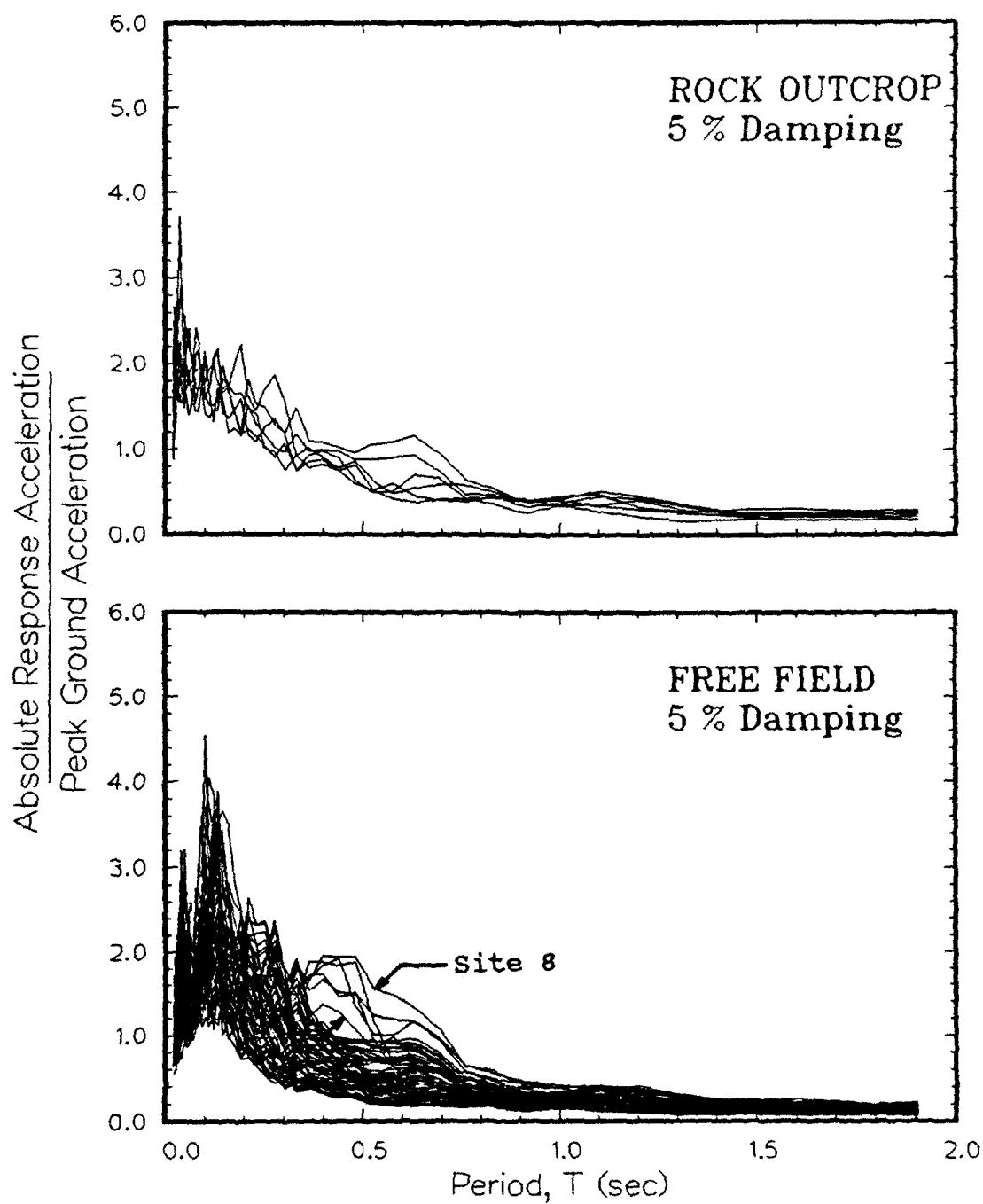


Figure 54. Amplification ratio for all events

PART VI: SENSITIVITY ANALYSIS USING AVERAGE COLUMN

112. An important aspect of any site response analysis is an evaluation of how various system and site parameters affect the calculated results. This evaluation is important because the site has been idealized—all the information for the site has been summarized in a finite number of soil columns. Soil and rock parameters were evaluated because of the variability and/or uncertainty associated with each as noted throughout this report. Soil deposits can vary significantly in geometry and properties, especially at large projects such as PORTS. The sensitivity to system parameters (e.g., those listed in Table 6) were performed for this study and found to have negligible effect. Therefore, this analysis is not reported.

113. The sensitivity analysis of site parameters for this study was conducted using the average column described in Part III (Figure 33) and the DBE (the 1000-year event). Five of the most important site parameters are: bedrock impedance ratio (ratio of density times velocity between soil and rock), depth to bedrock, shear modulus relationship used, damping ratio relationship used, and maximum shear modulus. Impedance ratio was chosen because of the variability of measured shear wave velocities in the sandstone and shale. The depth to bedrock was considered because of the variability of column heights representing the site. The assignment of shear modulus and damping ratio relationships were considered because site-specific relationships were not available for some of the soils. "Average" relationships actually represent a range of data. Maximum shear modulus was considered because of the high variability in measured data over the site. The results of the sensitivity analysis are presented using the tripartite format.

114. The response of the average column to two components of the 1000-year event is shown in Figure 55 and compared with the range of individual responses (refer to Figure 45). The two spectra fall within the band for individual sites except at periods of 0.2 sec and generally are in the middle of the band. However, at periods around 0.1 and 0.5 sec, the average column response falls toward the bottom of the range. The two average column spectra (shown as solid lines) are used as a baseline for comparison with sensitivity studies (shown as dashed lines) described below.

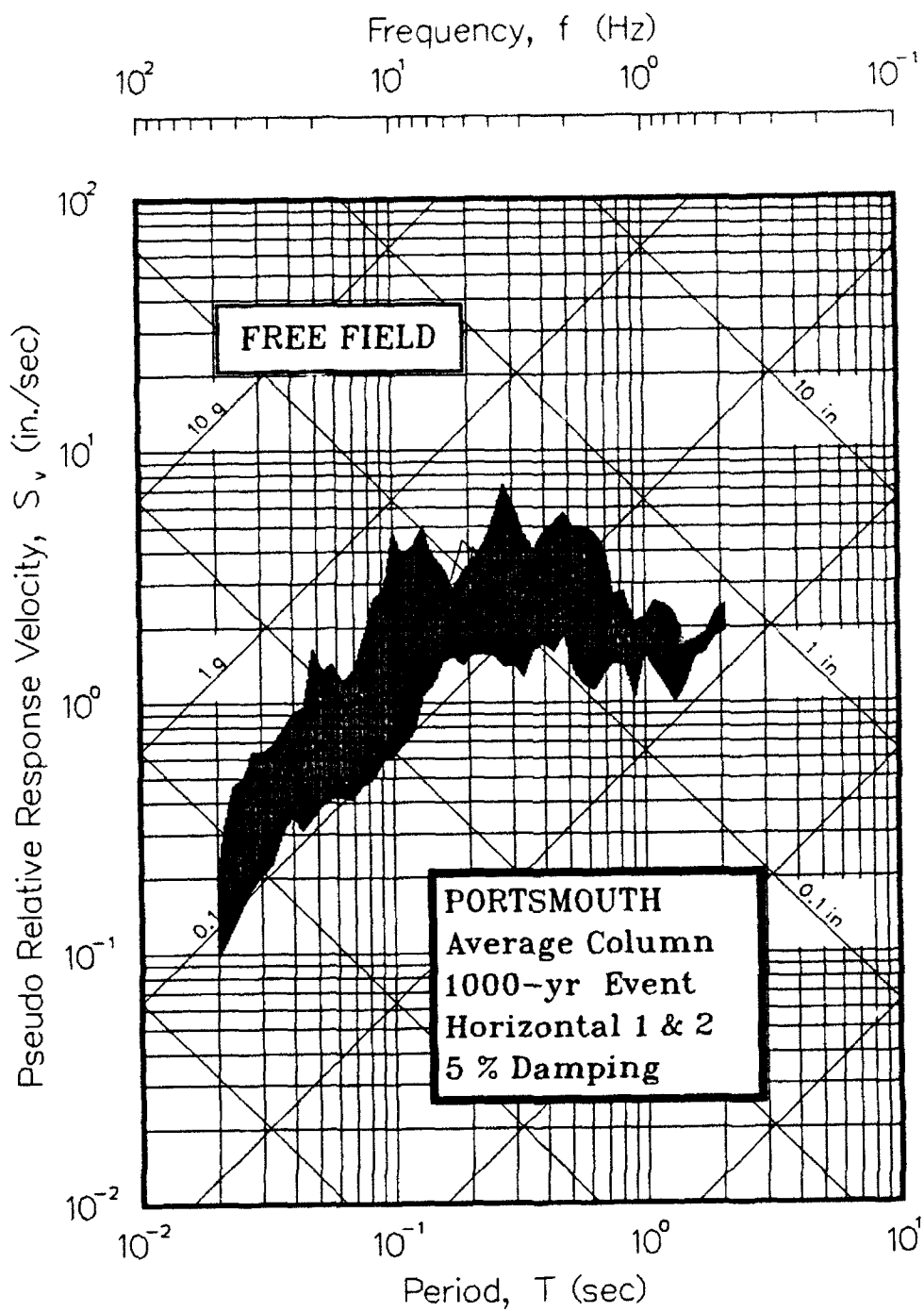


Figure 55. Comparison of results for average column and range produced from individual sites

Impedance Ratio

115. The shear wave velocity of bedrock was set at 2,000, 4,000, and 6,000 fps to evaluate the effect of impedance ratio on calculated response. Recall that the measured shear wave velocities for rock varied between 4,370 and 5,540 fps at GCEP and at 1,300 and 2,175 fps at GDAP and the average column has a rock velocity of 3,000 fps. The pseudo-velocity response spectra for each velocity and both horizontal components are shown in Figure 56.

116. The impedance ratio has an important effect on calculated response. As impedance ratio increases, the spectral ordinates increase. The results for the 2,000 fps rock are consistently below the average column whereas the results for the other two velocities are above the average column responses. The greatest effect is at periods between 0.07 and 0.1 sec and 0.15 and 0.20 sec. There is essentially no effect at periods greater than 0.5 sec and only a slight difference at all other periods. There is no significant change in the periods corresponding to these values. The wide range of measured rock velocities at the site, then, serve to create a wide range of calculated site response. The rock velocity used for the average column is appropriate to derive response in the mid-range of individual site responses.

Depth to Bedrock

117. The depth to bedrock was varied ± 5 ft from the 35-foot average height. The variation was applied by adjusting the height of the bottom-most layer. This variation is appropriate to address uncertainty for shallow sites for the average column although it does not envelop the range of individual column heights (20 to 62 ft). The results of the calculations are shown in Figure 57.

118. The depth to bedrock has a very important effect on calculated response at shallow sites like PORTS. The natural period of an ideal layer is proportional to the height. The deeper column produced a period-increasing shift in the spectra and a slight increase in spectral velocity at 0.3 sec. The shallower column produced period-decreasing shift in the spectra with a decrease in spectral velocity at 0.08 sec. There is essentially no effect at periods greater than 0.8 sec. These results represent only one-fourth of the

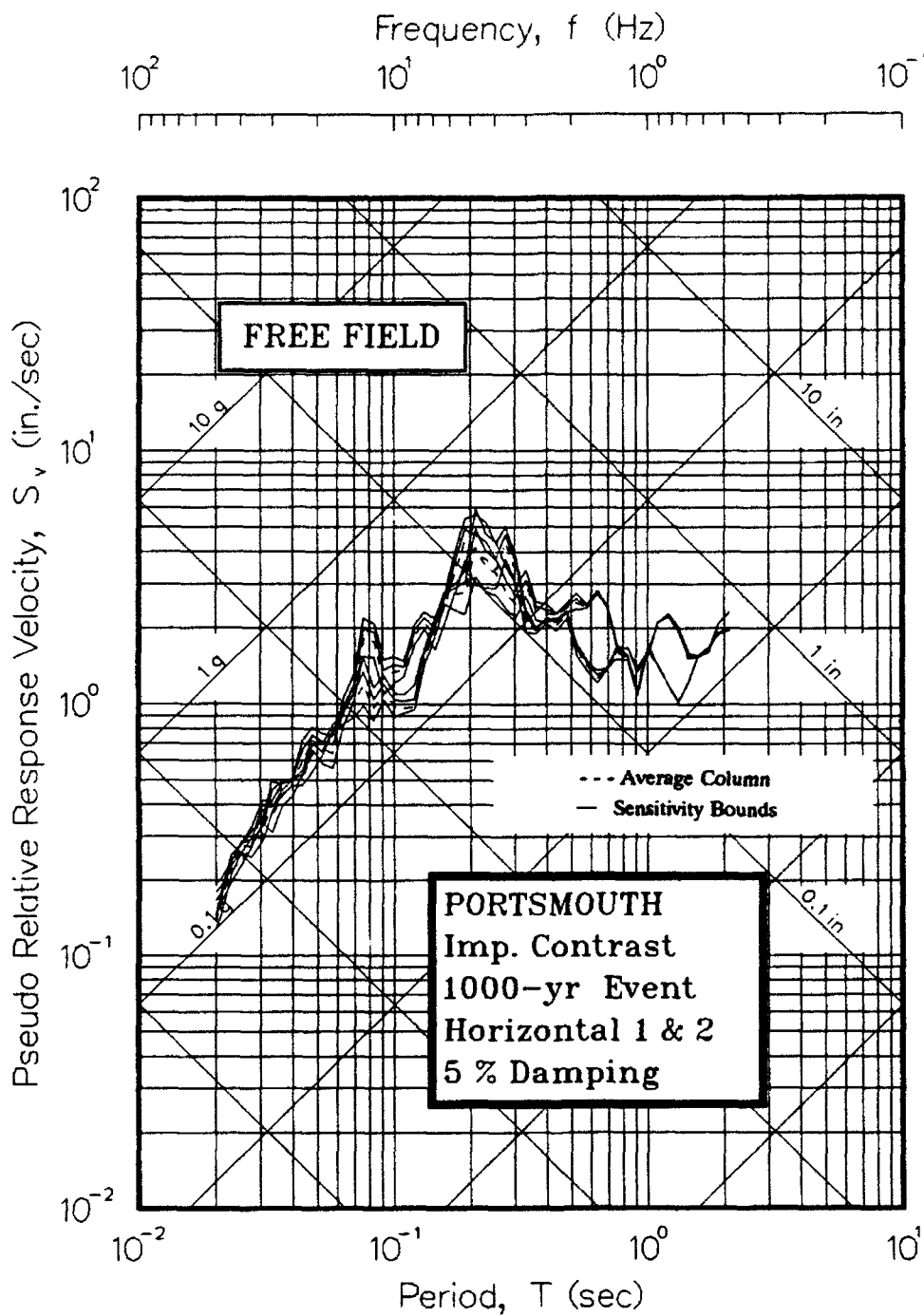


Figure 56. Pseudo-velocity response spectra showing sensitivity of results to impedance contrast

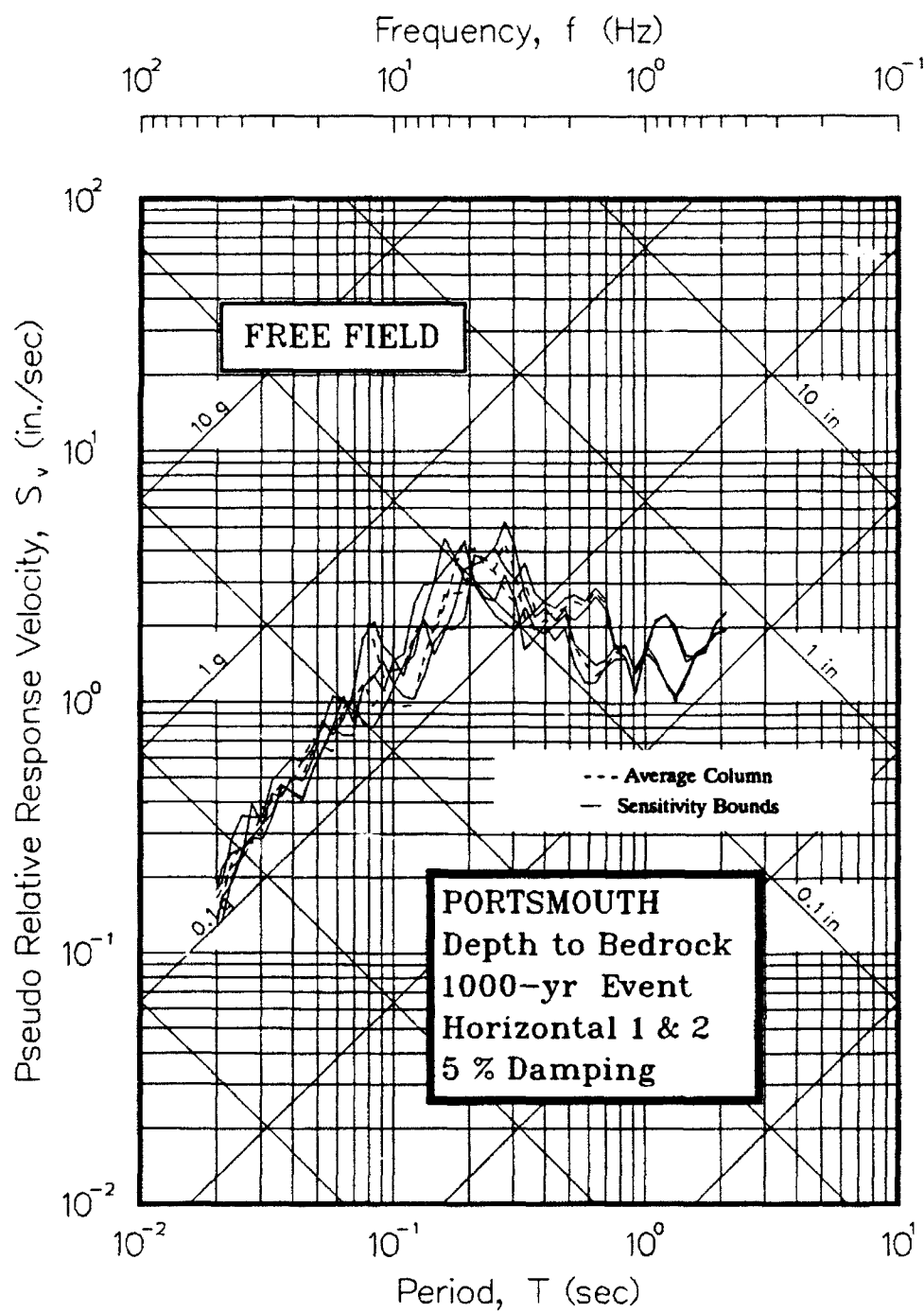


Figure 57. Pseudo-velocity response spectra showing sensitivity of results to depth to bedrock

variation measured at the individual columns. A broader representation of variation was not considered because of the implications on other parameters such as velocity and material types.

Assignment of Modulus Relationships

119. Response spectra were calculated for upper-bound and lower-bound assignments of modulus degradation for all soil layers in the average column. The upper and lower bounds for sands and gravels correspond to the limits in the range of data as shown in Figure 28. The upper and lower bounds for silts and clays were obtained by shifting one (cohesive) curve to the right or left, respectively. The results of the calculations are shown in Figure 58.

120. The assignments of shear modulus relationships have a small impact on the calculated average column response. Nearly all of the deviation from the average column responses is a consequence of using the lower bound curves. The modulus degradation for gravels, especially at the lower bound, is significant at any strain level and this relationship tends to control the response. The assignments for sands, silts, and clays are not important for PORTS, especially since the relationships are so similar (excluding the high-plasticity clay curve).

Assignment of Damping Ratio Relationships

121. Response spectra were calculated for upper-bound and lower-bound assignments of damping ratio for all soil layers in the average column. The upper and lower bounds for all soils correspond to the limits in the range of data as shown in Figure 28 (except that the 15 percent cap was applied). The results of the calculations are shown in Figure 59.

122. The assignments of damping ratio relationships have a small impact on the calculated average column response, similar to the modulus relationships. The increase in damping (upper bound) decreases spectral ordinates and vice versa. The variations for upper bound and lower bound response from the average column response are about the same. The assignments for sands, silts, and clays are not important for PORTS.

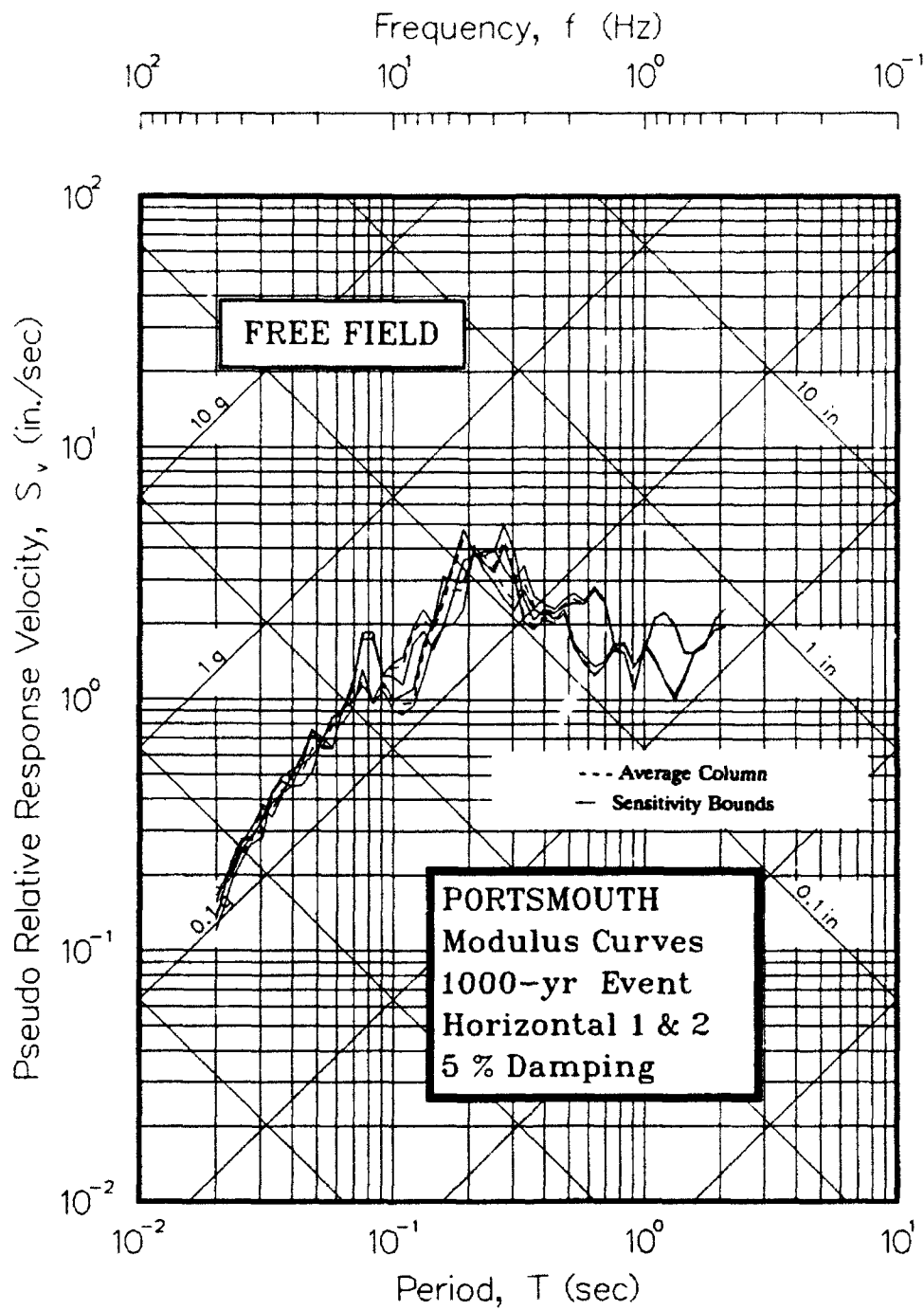


Figure 58. Pseudo-velocity response spectra showing sensitivity of results to modulus curves

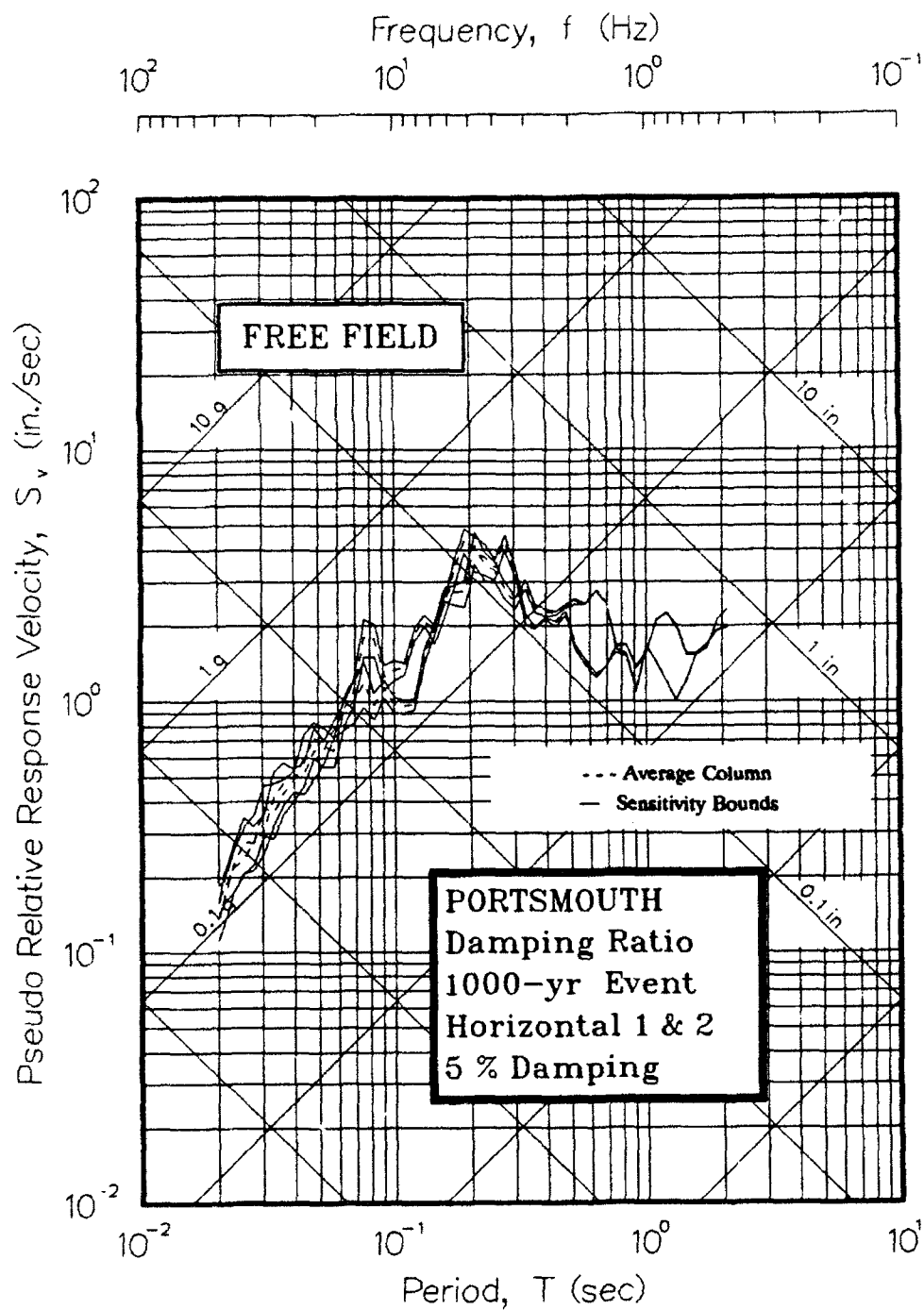


Figure 59. Pseudo-velocity response spectra showing sensitivity of results to damping ratio

Maximum Shear Modulus

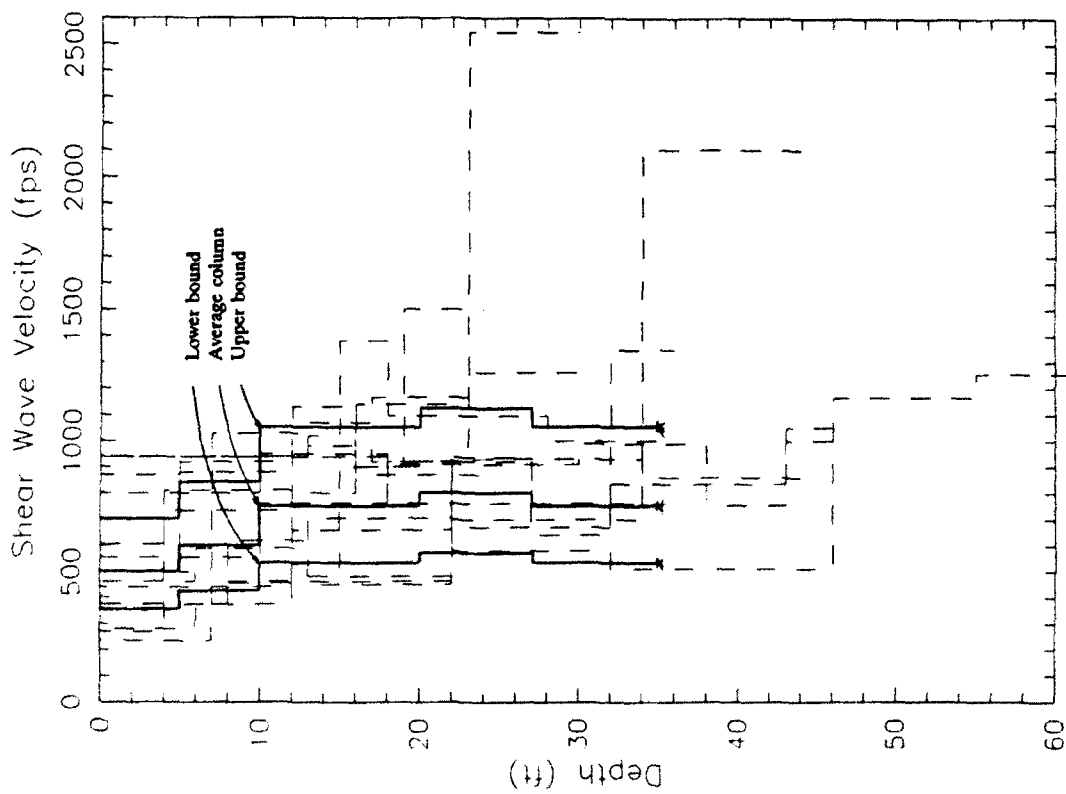
123. The NRC Standard Review Plan (Nuclear Regulatory Commission 1989) specifies upper and lower bounds of maximum shear modulus for use in seismic safety assessments. The bounds are defined by:

Lower bound:
$$(G_{\max})^{lb} = \frac{G_{\max}}{2.0} \quad (5)$$

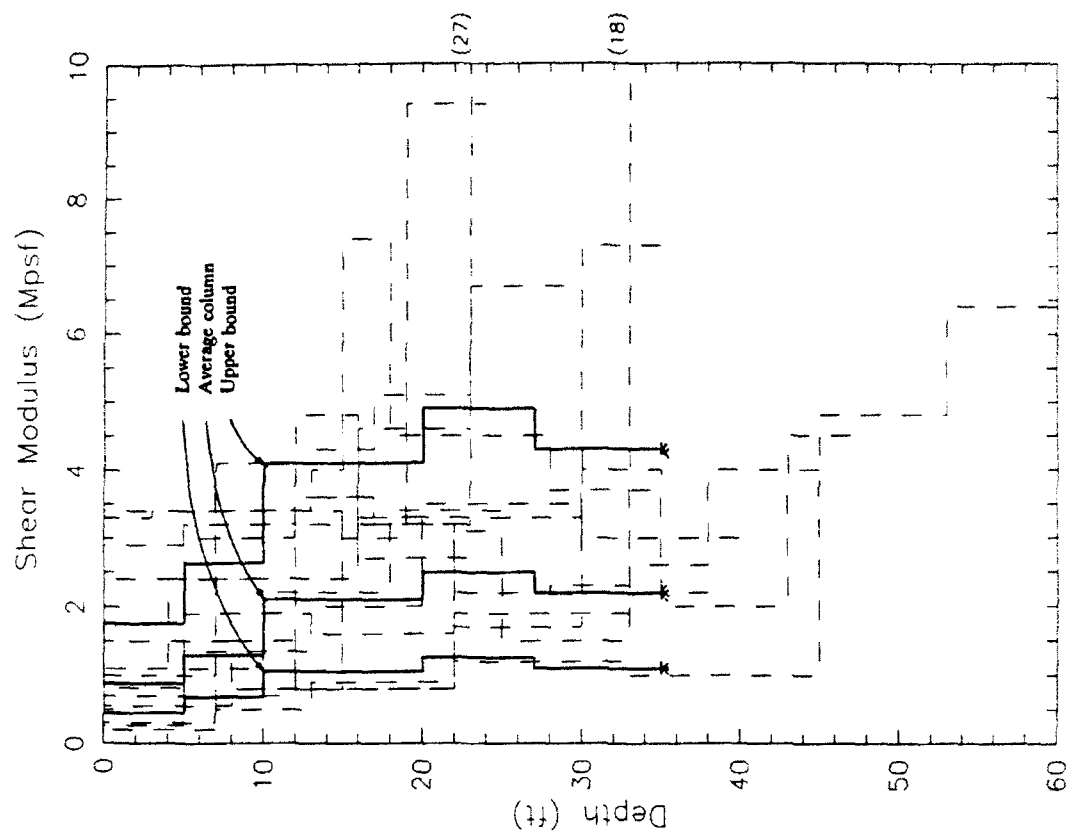
Upper bound:
$$(G_{\max})^{ub} = 2.0 \cdot G_{\max} \quad (6)$$

These bounds were used to define conservative limits to the range of shear modulus for the average column. The rock velocity was also adjusted to negate any effects of varying impedance ratio. A comparison of the shear wave velocity and shear modulus profiles for the average column and the corresponding lower and upper bounds are shown in Figure 60. The profiles for the individual columns are also shown for comparison. The upper and lower bounds for the average column defined by NRC do not envelop the combined range of individual columns. The average column and upper and lower bounds seem to be adequate to represent the range of data, however.

124. The maximum shear modulus has a very important effect on calculated response. The results for the sensitivity to shear modulus are shown in Figure 61. The natural period of an ideal layer is inversely-proportional to the shear wave velocity. The results for the lower bound modulus show spectral ordinates generally below the average column response at periods less than 0.09 sec and between periods of 0.12 and 0.24 sec; at all other periods the lower-bound response is greater. Conversely, the results for the upper bound modulus show spectral ordinates above the average column response at periods less than 0.06 sec and between 0.09 sec and 0.17 sec; at all other periods the upper-bound response is less. Much of this difference is due to a general shifting in period of the spectra—the lower bound moduli produce an increase in natural period and vice versa. The wide range of measured velocities at the site, then, serve to create a wide range of calculated site response.



a. Shear wave velocity



b. Shear modulus

Figure 60. Range of stiffnesses used to evaluate sensitivity of results to maximum shear modulus

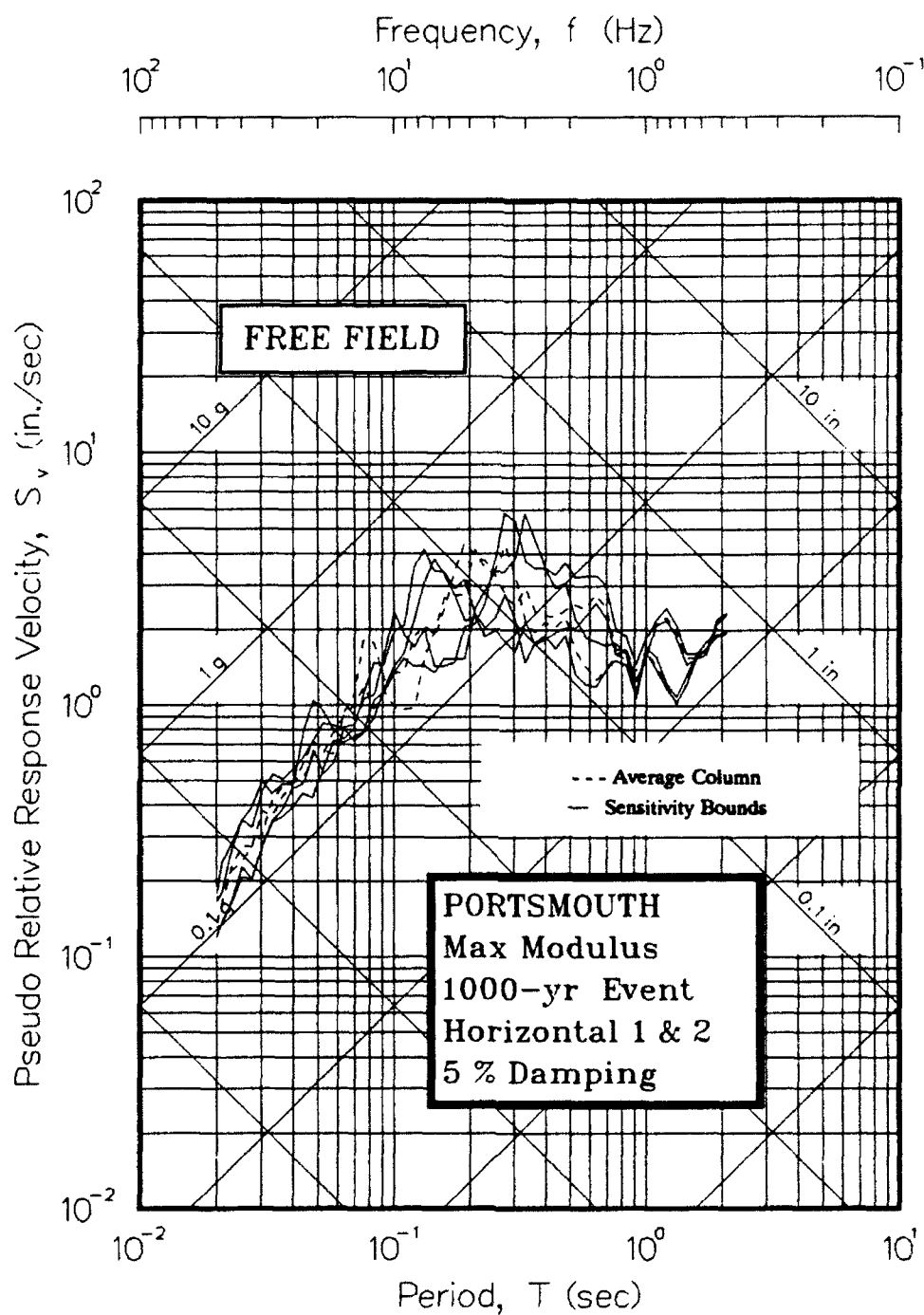


Figure 61. Pseudo-velocity response spectra showing sensitivity of results to maximum shear modulus

Conclusions

125. The sensitivity analysis indicates that the depth to bedrock and the maximum shear modulus are the most important factors affecting the site response analysis at PORTS. The impedance ratio is also important and the assignment of shear modulus and damping ratio relationships is secondary. The ranges of depth to bedrock, impedance ratio, and maximum shear modulus do not entirely reflect the measured variability at the site. The range in shear modulus recommended by NRC is well within the range of measured data. The range of variability and uncertainty were fully addressed to assess the impact of the modulus and damping ratio relationships.

PART VI: SUMMARY AND CONCLUSIONS

126. The site-specific, free-field earthquake response was calculated for fifteen, idealized, one-dimensional soil columns at the Portsmouth Gaseous Diffusion Plant. Two components of three design earthquakes—a 500-year, a 1000-year (DBE), and a 5000-year event—have been used for the analysis. The computer program *SHAKE* was used on a U.S. Army CRAY Y-MP supercomputer to perform the calculations and determine site response. *SHAKE* has been validated for horizontal response calculations at periods less than 2.0 sec on numerous occasions and consequently is widely accepted in the geotechnical earthquake engineering profession as useful tool for site response analysis.

127. Information available from two previous site-specific geotechnical investigations at the proposed GCEP and GDAP sites was used to create fifteen unique idealized soil columns for this study. A relatively wide range of site conditions in terms of overall height of soil over bedrock was found to exist. A wide range in measured shear wave velocities was also noted, but part of this difference is attributed to documented uncertainties in measurements for the GCEP project. Although the locations of borings used to create soil columns are concentrated in southern portions of the plant area, the range of potential in-situ conditions in terms of stratigraphy, depth of the phreatic surface, seismic velocities, total soil thickness, and material types seem to be adequately represented by the soil columns created.

128. The range of soil column heights used in the analysis was 20 to 61 ft. Soil profiles and bedrock elevation contours indicate that rock outcrops within the fenced plant area. Although the shortest soil column considered was 20 ft the spectra calculated for the rock input motions (which correspond to rock outcrop) can be used to represent areas with rock or shallow soil. In nearly all cases, the spectra representing rock are at the lower bound of response. Therefore, the range of site conditions modeled is considered to be adequate.

129. A wide range of free-field response was calculated using the collection of fifteen columns. This wide range is attributed to the variability of input parameters. Most importantly, the range calculated is expected to essentially bracket the actual response to the specified earthquakes because of the wide range of conditions in soil columns.

130. Natural site periods exist at 0.1 and 0.3 sec. The range of conditions at PORTS is likely to include combinations of layer heights, velocities, etc. that produce predominant periods that are also between these two periods and possibly slightly outside these bounds. Peak spectral velocities of 4, 7, and 9 in./sec for the 500-year, 1000-year, and 5000-year events, respectively, occur in this range of periods at a system damping of 5 percent. Peak spectral accelerations of 0.4, 0.8, and 1.4 g for these three events, respectively, occur at a period of 0.1 sec. The ratio of spectral accelerations at free field over rock are as large as 5.8 at the natural period and decrease with increasing severity of motion. The amplification ratio (spectral acceleration normalized to peak time-domain acceleration) are as large as 4.6 at a period of 0.1 sec.

131. In general, the motions at the base of the column are amplified at nearly every wave period between 0.2 and 2 sec. The calculated peak ground accelerations (period of 0.2 sec) at free field for the three events are: 0.12, 0.17, and 0.36 g for the 500-year, 1000-year, and 5000-year event, respectively. The ratio of spectral accelerations is generally between 1 and 3 and has peaks up to nearly 6 at a period of 0.1 sec.

132. A sensitivity analysis was conducted using an average column to represent the site and the DBE (1000-year event). The results of the sensitivity analysis suggest that the depth to bedrock and maximum shear modulus are the two most important factors for site response calculations at PORTS. The bedrock impedance ratio is also important, but to a lesser degree. The depth to bedrock contours and cross sections provide simple guidance as to the range of this parameter. The assignment of shear modulus and damping ratio relationships was found to have a small effect on the analysis, primarily because the site-specific relationships do not vary considerably and are very similar to standardized curves. The range of response calculated using the individual columns is considered to be comparable or even wider than a pseudo-range of response developed using an average column and all possible combinations of variability and uncertainty using guidelines such as that established by NRC.

REFERENCES

- Cooley, J. W. and Tukey, J. W. 1965. "An Algorithm for the Machine Calculation of Complex Fourier Series," Mathematics of Computation, Vol 19, No. 90, pp 297-301.
- Curro, J. R., Jr., and Marcuson, W. F., III 1978. "In Situ and Laboratory Determinations of Shear and Young's Moduli for the Portsmouth, Ohio, Gaseous Diffusion Add-On Site," US Army Engineer Waterways Experiment Station, Miscellaneous Report, S-78-12, Vicksburg, MS, 99 pgs.
- Davis, B. C. and Savy, J. B. 1990. "Paducah and Portsmouth Seismic Hazard Analysis," Lawrence Livermore National Laboratory, Livermore, CA, Nov.
- Department of Energy 1992. "Guidelines for Use of Probabilistic Seismic Hazard Curves at Department of Energy Sites," DOE-STD-1024-92, Washington, D.C., Dec.
- Department of the Army 1986. "Seismic Design Guidelines for Essential Buildings," Technical Manual TM 5-809-10-1, Washington, DC, 27 February.
- Electric Power Research Institute 1988. "Seismic Hazard Methodology for the Central and Eastern United States," EPRI NP-4726-A, Vol 1, pt 1 & 2, Palo Alto, CA.
- ERCE 1990. "Portsmouth Gaseous Diffusion Plant, Final Safety Analysis Report, Section 3.6: Geology and Seismicity," Draft Report to Martin Marietta Energy Systems, ERCE File No. C529, Knoxville, TN.
- Hardin, B. O. and Drnevich, V. P. 1972. "Shear Modulus and Damping in Soils: Design Equations and Curves," Journal of Soil Mechanics and Foundation Engineering, ASCE, Vol 98. No. SM7, pp 667-692.
- International Conference of Building Officials 1991. Uniform Building Code, Whittier, CA.
- Johnson, J. J. 1980. "Soil-Structure Interaction: The Status of Current Analysis Methods and Research," U.S. Nuclear Regulatory Commission, NUREG/CR-1780, Washington, D.C.
- Kanai, K. 1951. "Relation Between the Nature of Surface Layer and the Amplitude of Earthquake Motions," Bull. Tokyo Earthquake Research Institute, Tokyo, JAPAN, (in Japanese).
- Kennedy, R. P., Short, S. A., McDonald, J. R., McCann, M. W., Jr., Murray, R. C., and Hill, J. R. 1990. "Design and Evaluation Guidelines for Department of Energy Facilities Subjected to Natural Phenomena Hazards," Lawrence Livermore National Laboratory, UCRL-15910, Livermore, CA.
- Lamé 1852. "*Leçons sur la théorie mathématique de l'élasticité des corps solides*," Paris, FRANCE.

Law Engineering Testing Company 1978. "Gas Centrifuge Enrichment Plant, Geotechnical Investigation, Portsmouth, Ohio," Final Report to US Department of Energy, Vol 2, Marietta, GA, 28 April.

Nuclear Regulatory Commission 1989. "Standard Review Plan," NUREG-0800, Section 3.7.2, rev. 2, Office of Nuclear Reactor Regulation, Washington, DC.

Risk Engineering, Inc. 1992. "Pseudo-Velocity Response Spectra and Time Histories, Portsmouth Gaseous Diffusion Plant," floppy disk submitted to Martin Marietta Energy Systems, Inc., Oak Ridge, TN.

_____, 1993. "Seismic Hazard Evaluation for the Portsmouth Gaseous Diffusion Plant, Portsmouth, Ohio," Rpt. K/GDP/SAR/SUB-2, US Dept. of Energy, Oak Ridge, TN.

Roesset, J. M. 1970. "Fundamentals of Soil Amplification," Seismic Design for Nuclear Power Plants, ed. R. Hansen, MIT Press, Cambridge, MA, pp. 183-244.

Roesset, J. M. and Whitman, R. V. 1969. "Theoretical Background for Amplification Studies," Research Report No. R69-15, Soils Publication No. 231, Massachusetts Institute of Technology, Cambridge, MA.

Schnabel, P. B. 1973. "Effects of Local Geology and Distance from Source on Earthquake Ground Motions," PhD Thesis, University of California, Berkeley, CA.

Schnabel, P. B., Lysmer, J., and Seed, H. B. 1972. "SHAKE: A Computer Program for Earthquake Response Analysis of Horizontally Layered Sites," Report EERC-72/12, Earthquake Engineering Research Center, Berkeley, CA.

Seed, R. B., Dickenson, S. E., and Idriss, I. M. 1991. "Principal Geotechnical Aspects of the 1989 Loma Prieta Earthquake," Soils and Foundations, Vol 31, No. 1, pp 1-26.

Seed, H. B. and Idriss, I. M. 1970. "Soil Moduli and Damping Factors for Dynamic Response Analysis," Report EERC-70/10, Earthquake Engineering Research Center, Berkeley, CA.

Seed, H. B., Romo, M. P., Sun, J., Jaime, A., and Lysmer, J. 1987. "Relationships Between Soil Conditions and Earthquake Ground Motions in Mexico City in the Earthquake of Sept. 19, 1985," Report EERC-87/15, Earthquake Engineering Research Center, Berkeley, CA.

Seed, H. B., Ugas, C., and Lysmer, J. 1974. "Site-Dependent Spectra for Earthquake-Resistant Design," Report EERC-74/12, Earthquake Engineering Research Center, Berkeley, CA.

Seed, H. B., Wong, R., Idriss, I. M., and Tokimatsu, K. 1986. "Moduli and Damping Factors for Dynamic Analysis of Cohesionless Soils," Journal of the Geotechnical Engineering Division, Vol 112, No. 11, pp 1016-1032.

Sun, J. I., Golesorkhi, R., and Seed, H. B. 1988. "Dynamic Moduli and Damping Ratios for Cohesive Soils," Report EERC-88/15, Earthquake Engineering Research Center, Berkeley, CA.

Sykora, D. W., Wahl, R. E., and Wallace, D. C. 1992. "USACE Geotechnical Earthquake Engineering Software, Report 1: WESHAK for Personal Computers (version 1.)," Instructional Report GL IR-92-4, US Army Engineer Waterways Experiment Station, Vicksburg, MS, 215 pg.

Taylor, H. M., Jr., Bennett, R. D., Horz, R. C., Hunt, R. W., Lutton, R. J., and Mitchell, G. B., 1977. "Title I Design Foundation Investigation for Static Loading, Gaseous Diffusion Add-On Plant, Portsmouth, Ohio," US Army Engineer Waterways Experiment Station, Miscellaneous Paper, S-77-20, Vicksburg, MS.

Veletsos, A. S., Prasad, A. M., and Tang, Y. 1988. "Design Approaches for Soil-Structure Interaction," Technical Report NCEER-88-0031, National Center for Earthquake Engineering Research, Buffalo, NY, 25 pgs.

Vucetic, M. and Dobry, R. 1991. "Effect of Soil Plasticity on Cyclic Response," Journal, Geotechnical Engineering Division, Vol 117, No. 1, pp 89-107.

Wiegel, R. L. 1970. Earthquake Engineering, Prentice-Hall, Inc., Englewood Cliffs, NJ, pg 85.

Zen, K. and Higuchi, Y. 1984. "Prediction of Vibratory Shear Modulus and Damping Ratio for Cohesive Soils, Proc., Eighth Int'l Conference on Earthquake Engineering, San Francisco, CA, Vol 3, pp 23-30.

APPENDIX A: LOCATIONS OF BORINGS
USED FOR SOIL COLUMNS

Site	Boring No.*	Northing (ft)	Easting (ft)	Elevation (ft)	Date of Drilling
PT-1	RA-413**	5,250	5,700	668.0	Fall '77
PT-2	"	5,250	5,700	668.0	"
PT-3	PB-75**	7,609	5,847	661.4	Fall '77
PT-4	"	7,609	5,847	661.4	"
PT-5	FW-214	4,970	5,770	663.8	Fall '77
PT-6	PB-94	7,130	5,720	673.6	Fall '77
PT-7	800	7,490	8,497	660.6	Oct '76
PT-8	803	8,275	10,362	693.0	Nov '76
PT-9	806	7,275	10,362	678.4	Nov '76
PT-10	809	6,134	10,172	679.5	Nov '76
PT-11	812	5,168	9,914	679.0	Nov '76
PT-12	815	5,295	9,438	657.5	Oct '76
PT-13	818	6,260	9,698	659.1	Nov '76
PT-14	821	7,525	9,850	674.2	Nov '76
PT-15	824	8,650	9,850	671.1	Oct '76

* Only one of three borings used for geophysical seismic testing referenced. Typically, one boring of an array was also used to obtain geotechnical engineering parameters and this boring was used as the reference location for purposes of this table.

** Two sets of seismic geophysical measurements ("nests") were available at this location.

APPENDIX B: ACCELERATION-TIME RECORDS FOR 500-YEAR EVENT

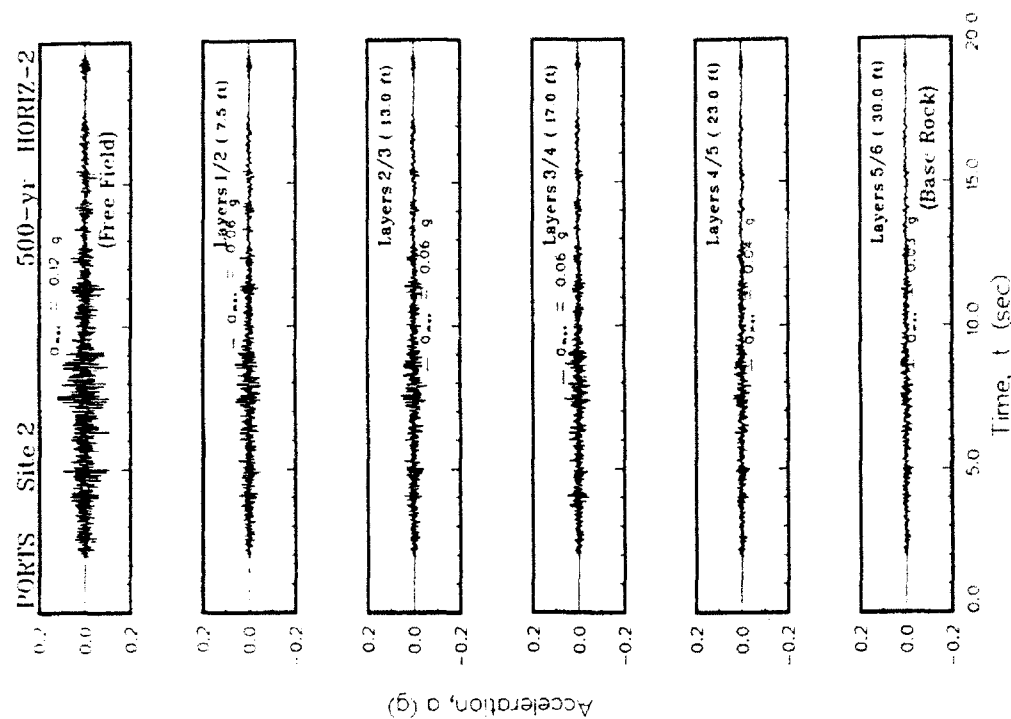
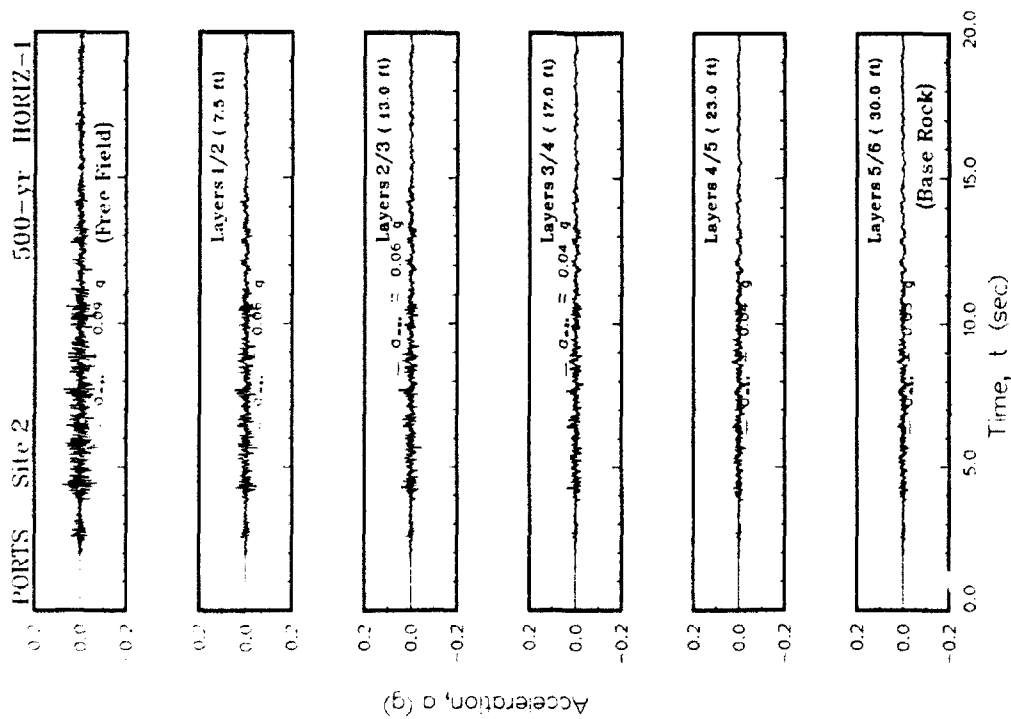


Figure B2. Variation of acceleration with time at the top of each layer for Site 2

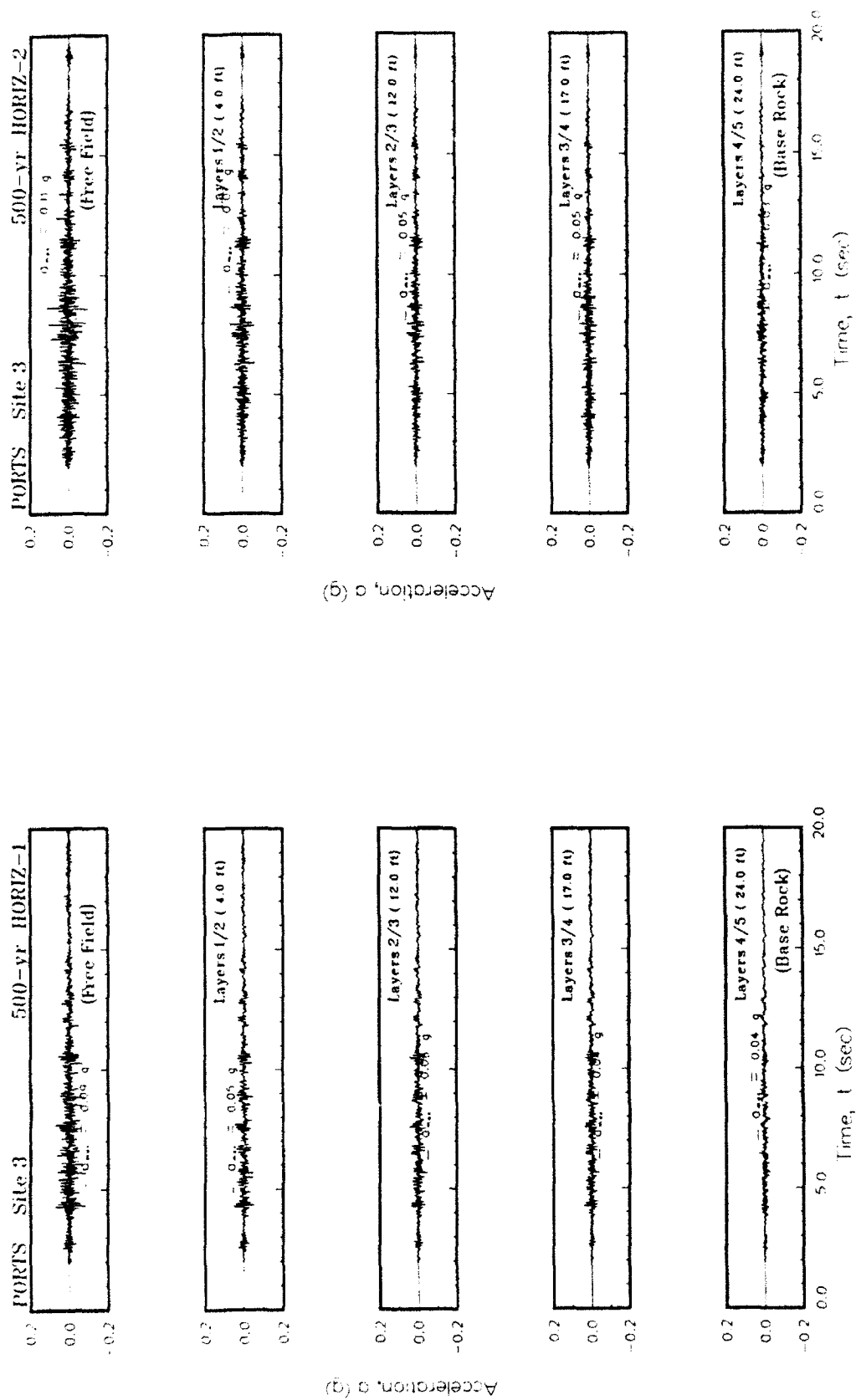


Figure B3. Variation of acceleration with time at the top of each layer for Site 3

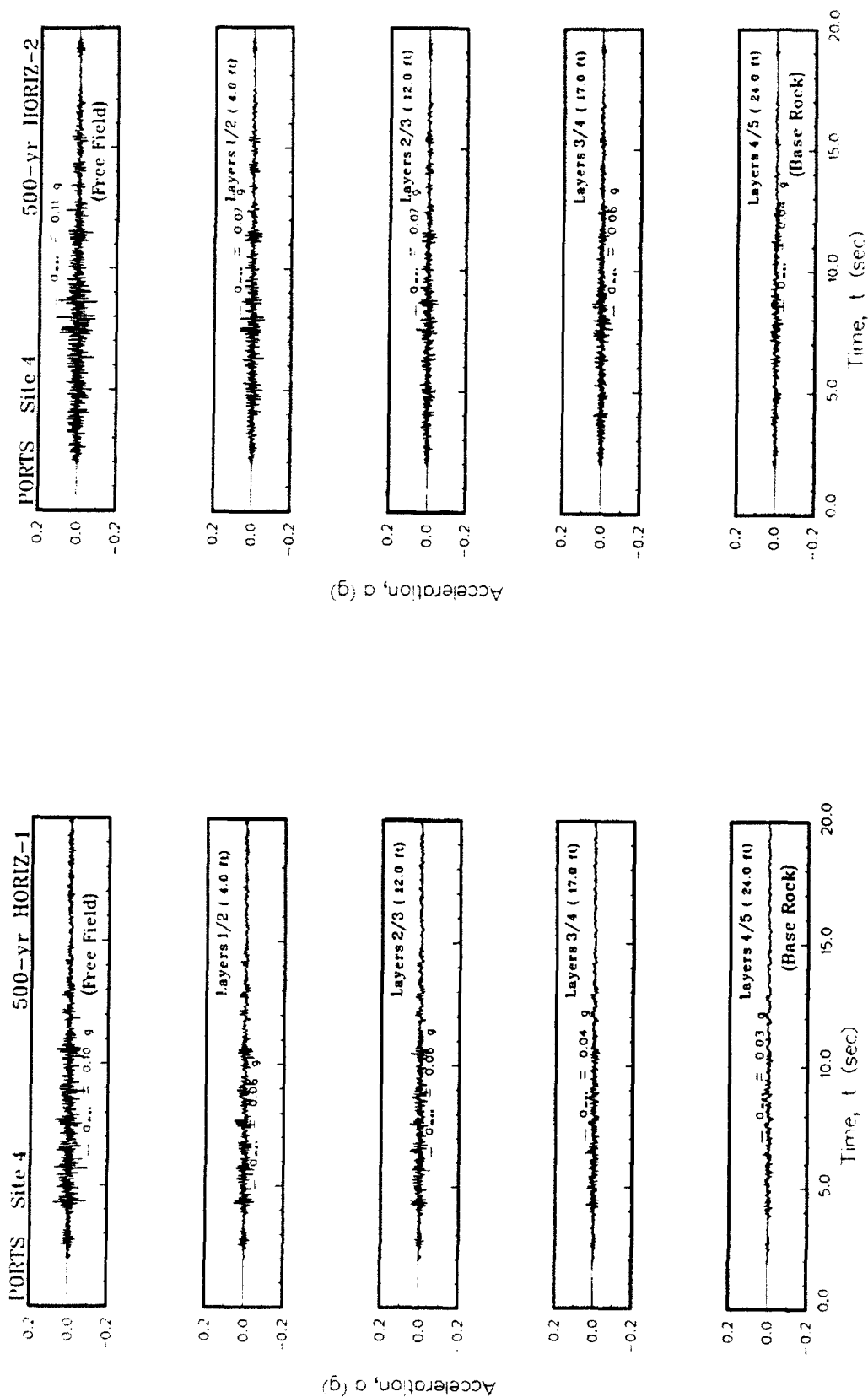


Figure B4. Variation of acceleration with time at the top of each layer for Site 4

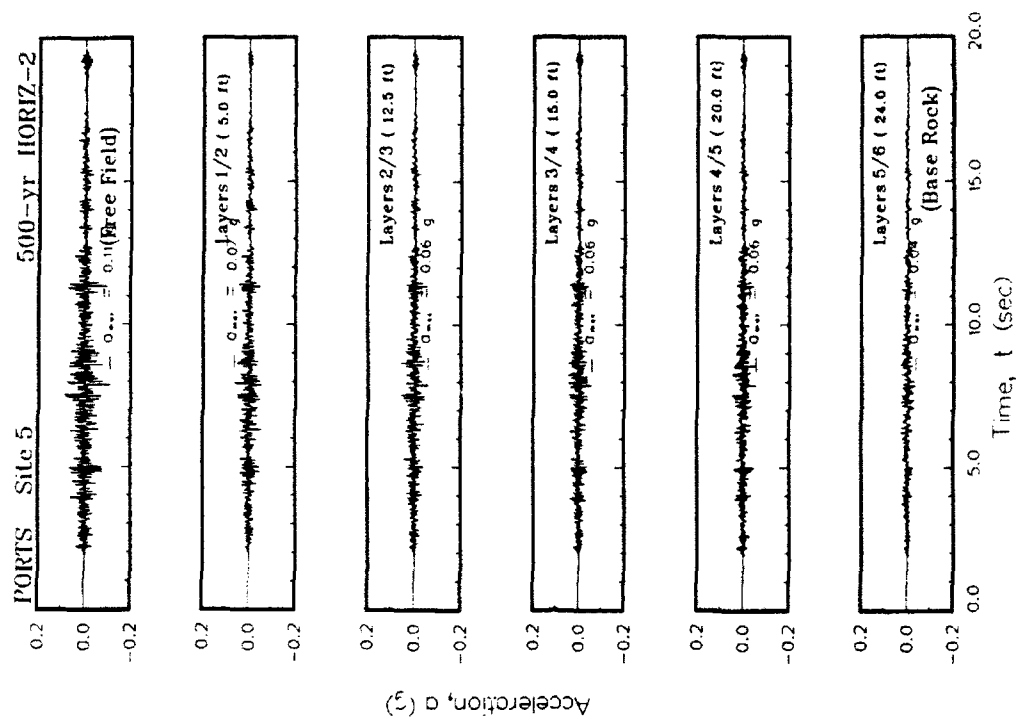
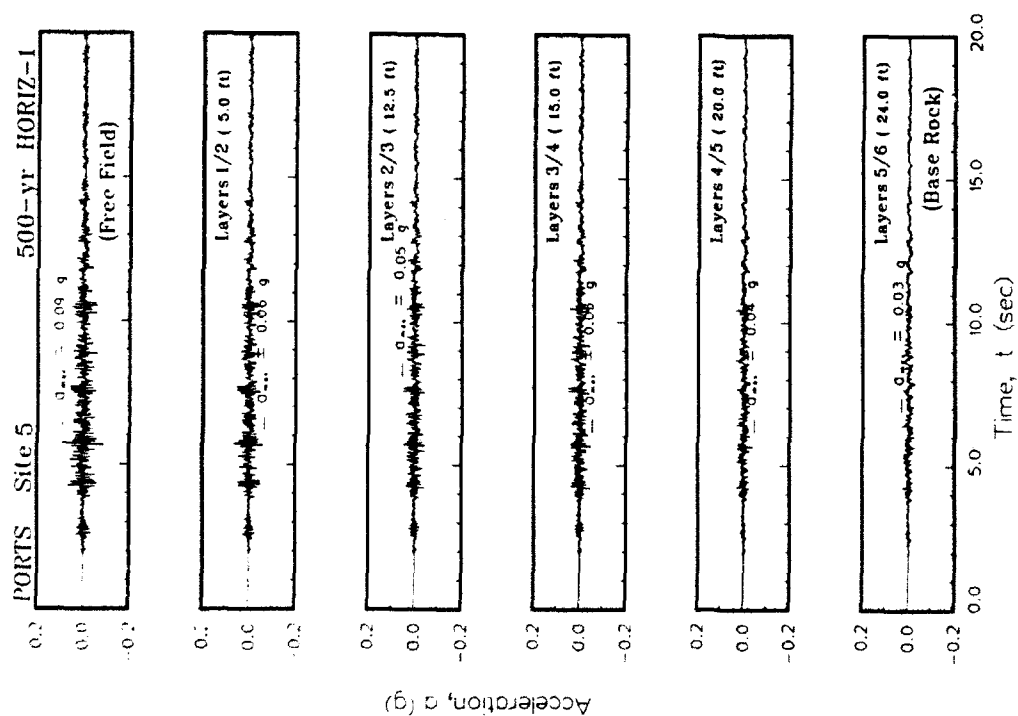


Figure B5. Variation of acceleration with time at the top of each layer for Site 5

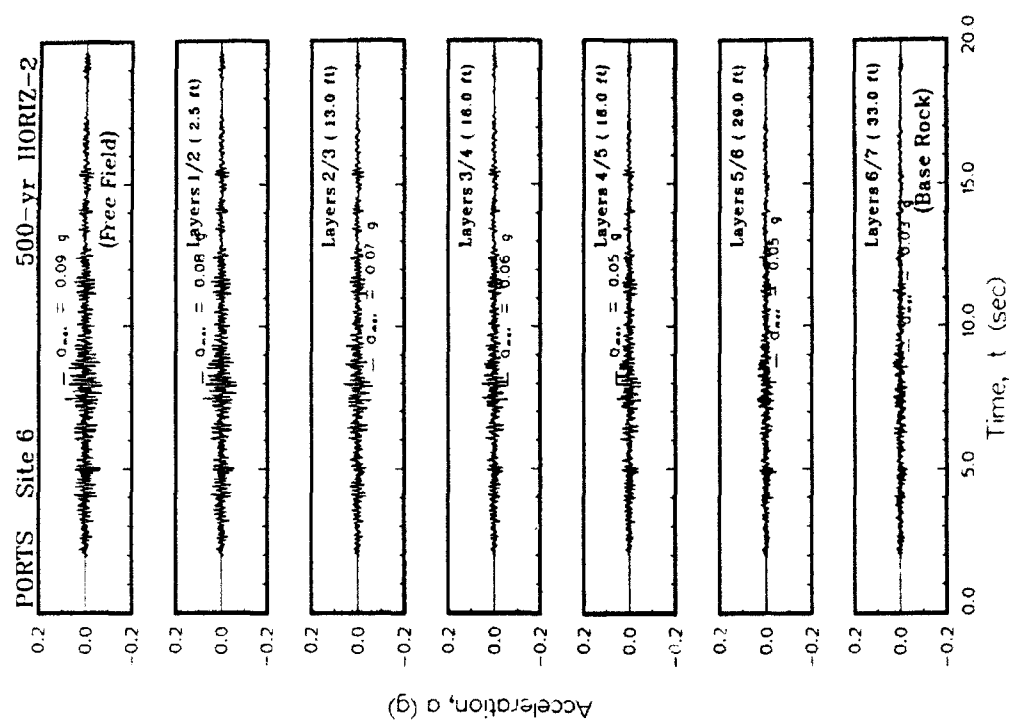
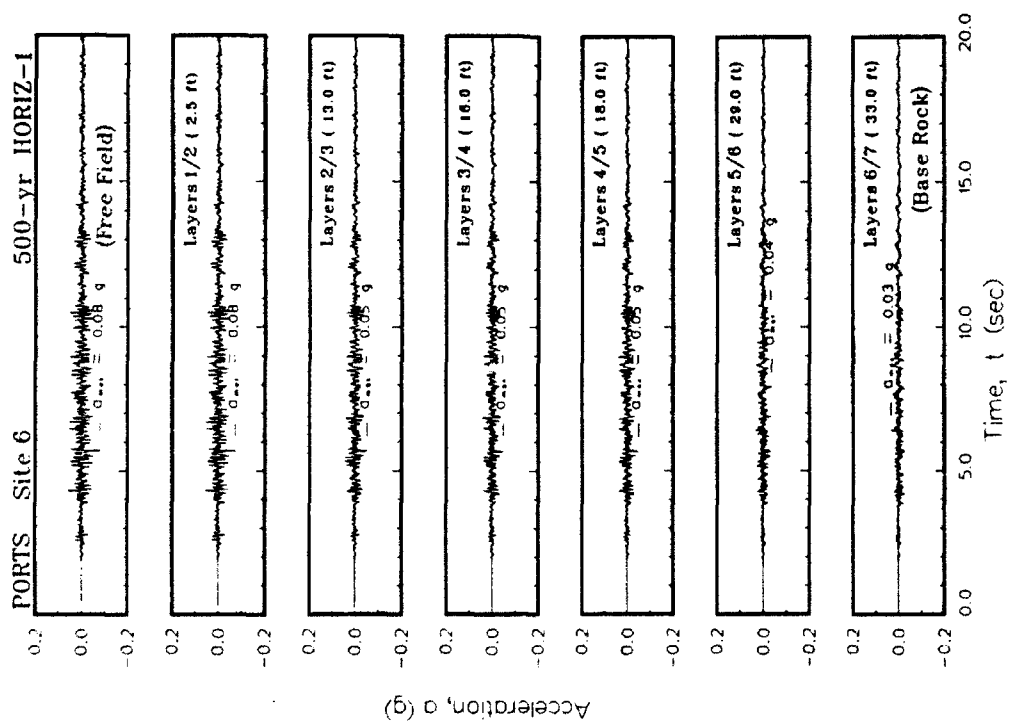


Figure B6. Variation of acceleration with time at the top of each layer for Site 6

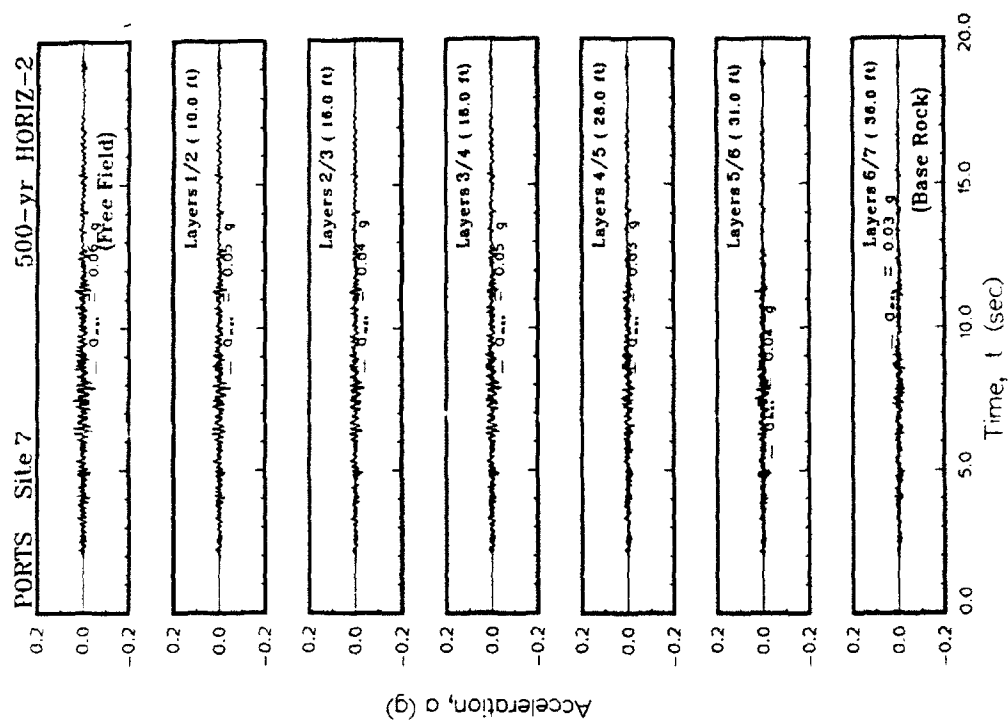
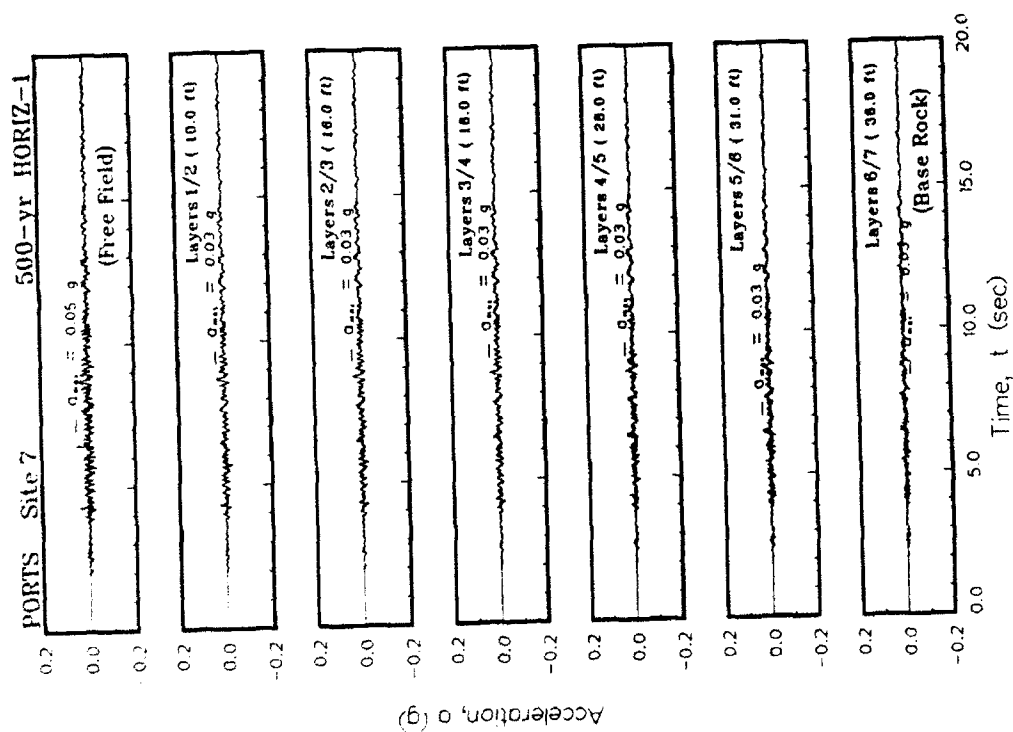


Figure B7. Variation of acceleration with time at the top of each layer for Site 7

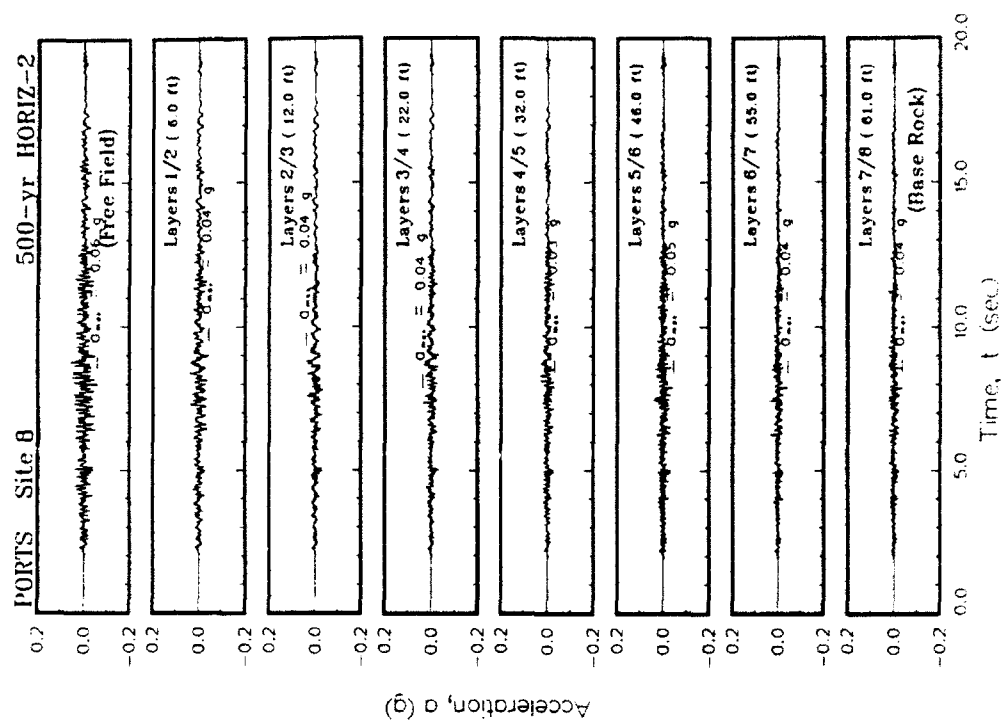
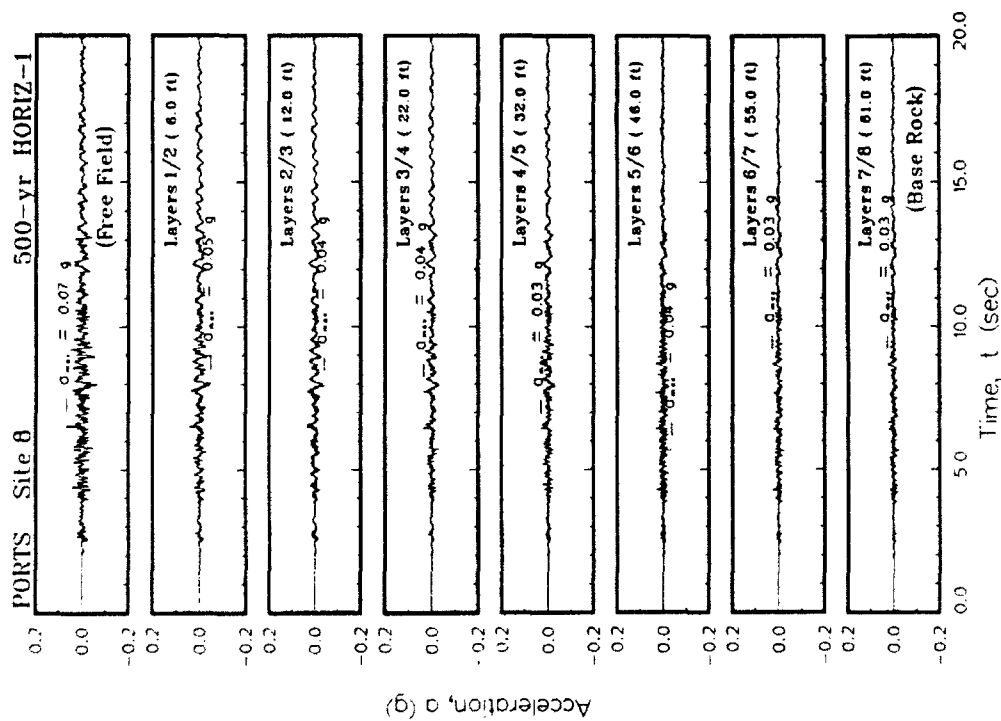


Figure B8. Variation of acceleration with time at the top of each layer for Site 8

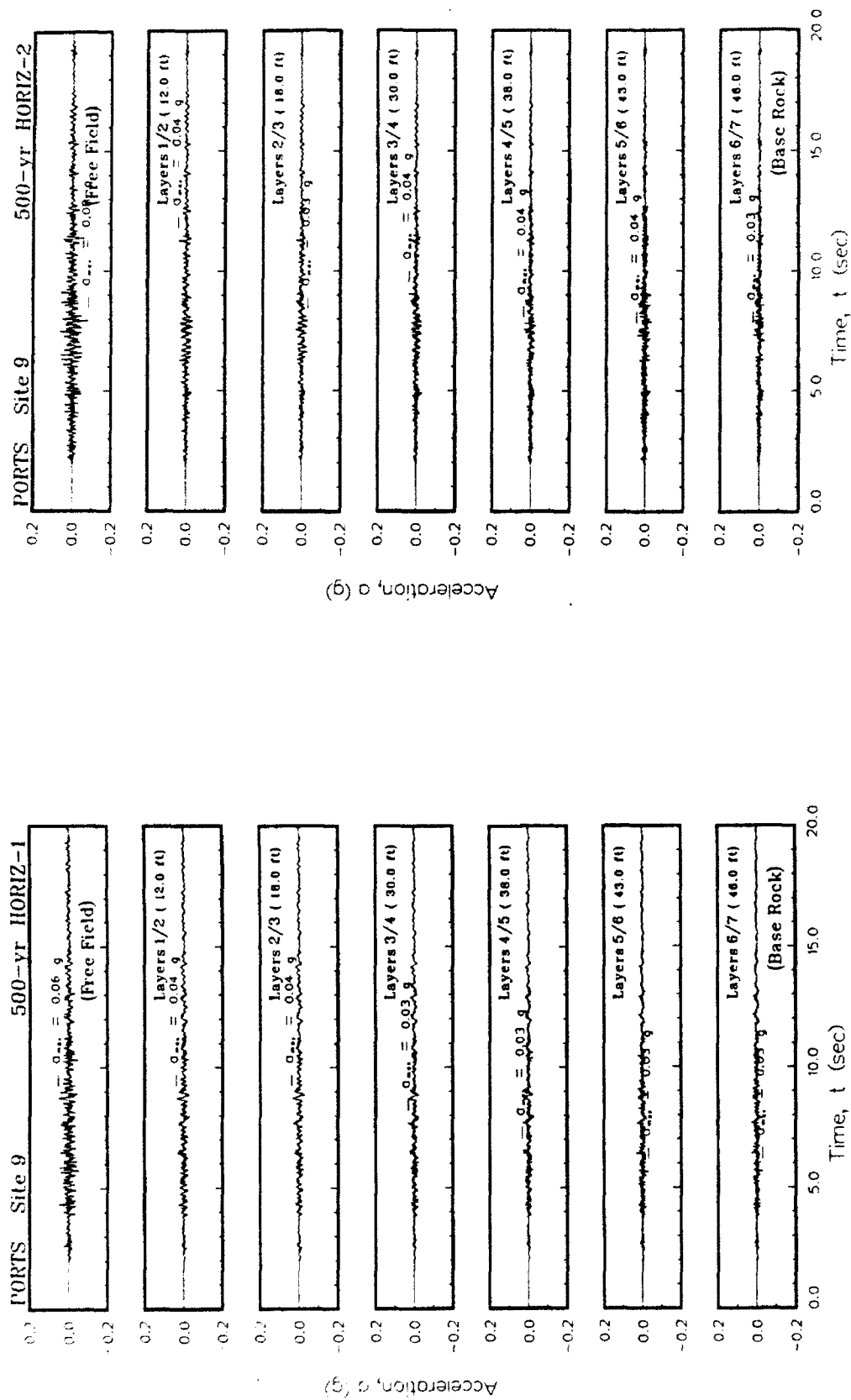


Figure B9. Variation of acceleration with time at the top of each layer for Site 9

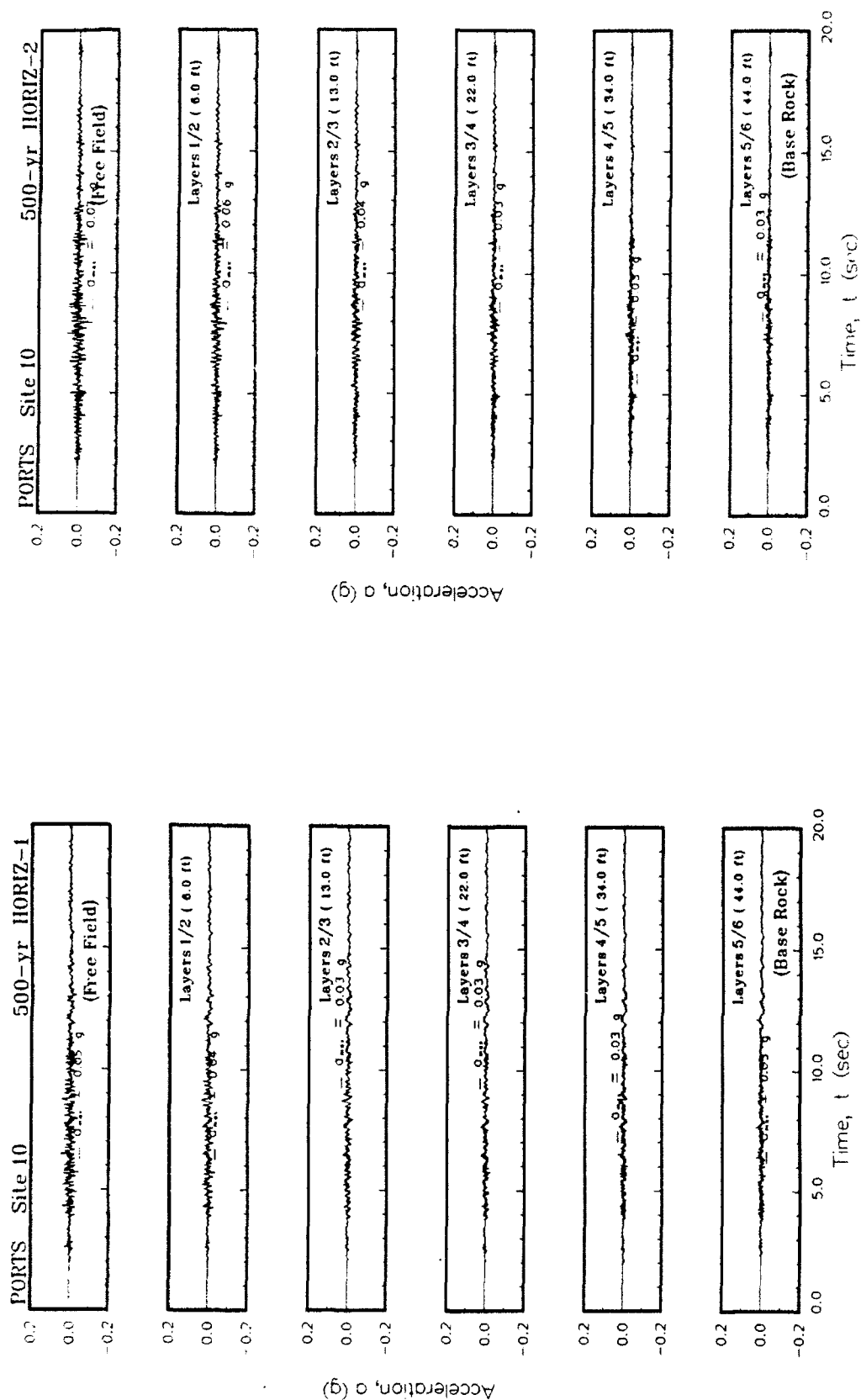


Figure B10. Variation of acceleration with time at the top of each layer for Site 10

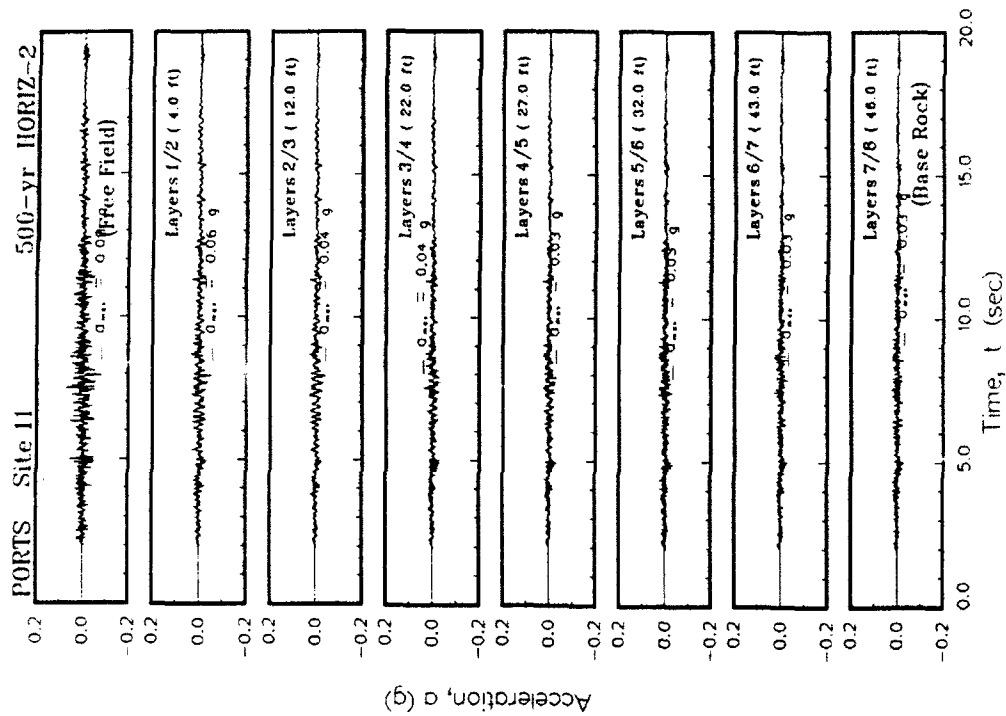
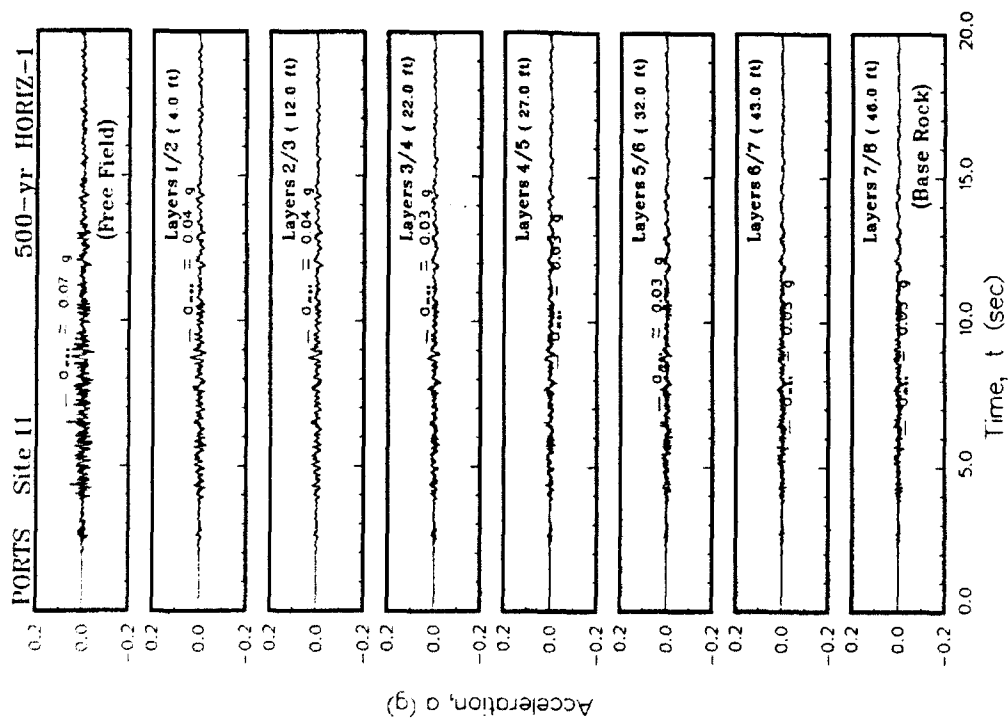


Figure B11. Variation of acceleration with time at the top of each layer for Site 11

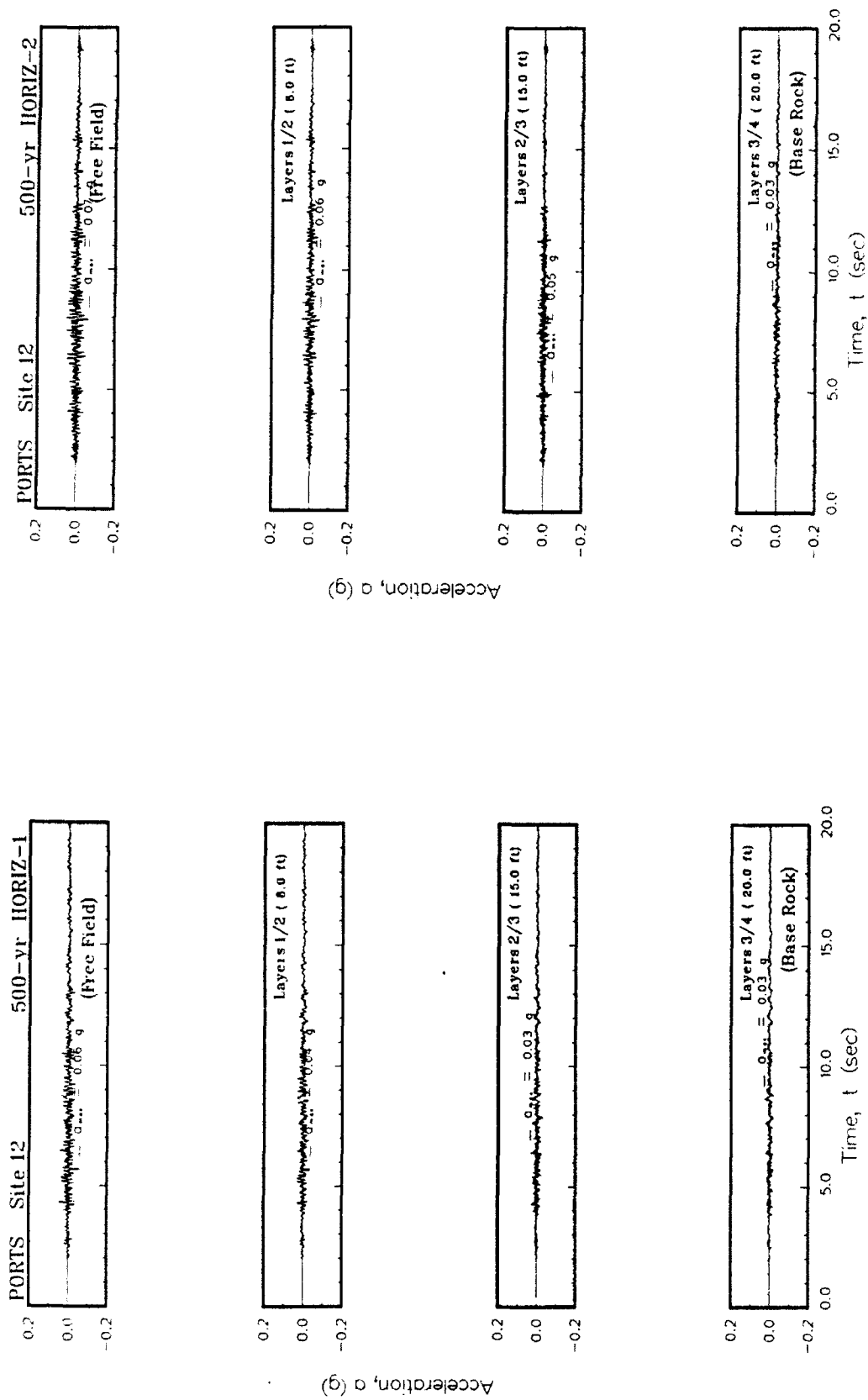
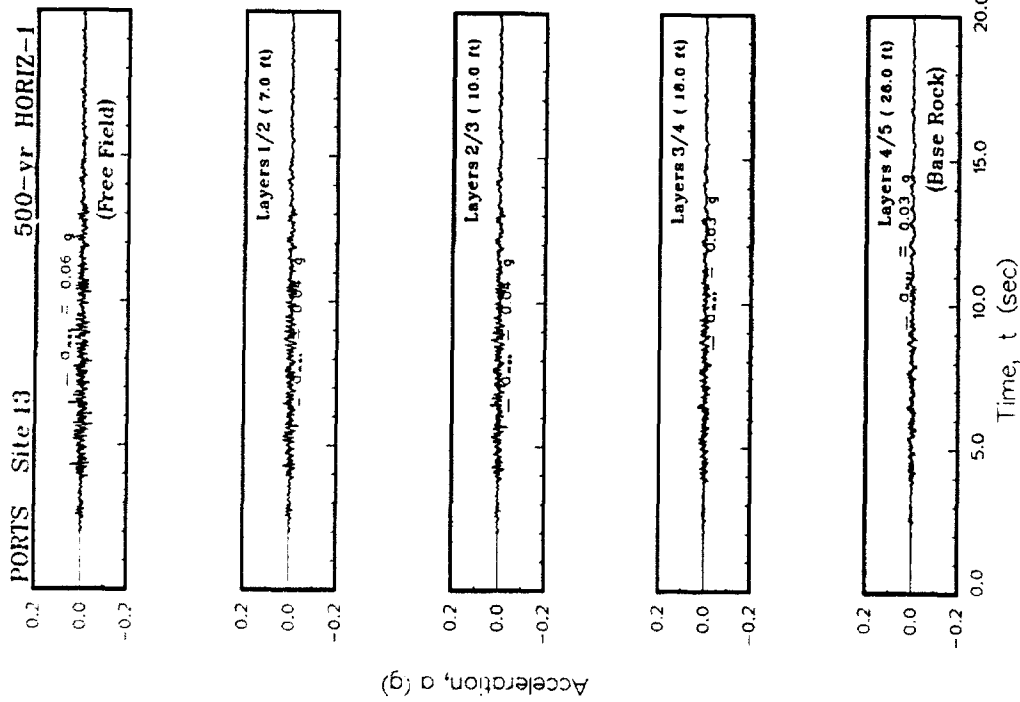
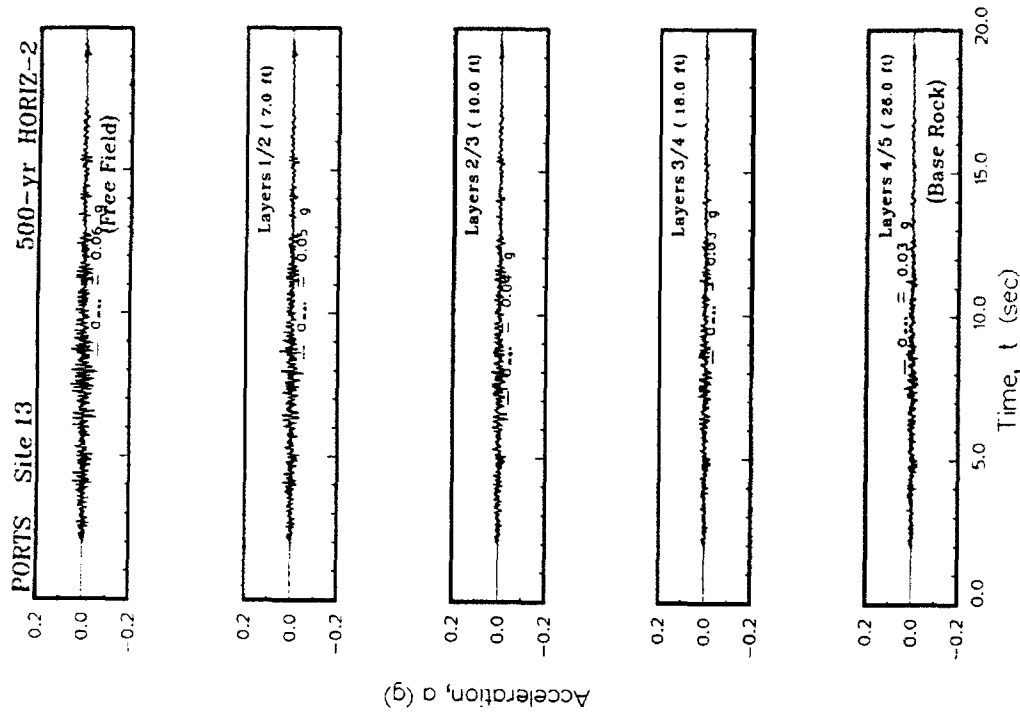


Figure B12. Variation of acceleration with time at the top of each layer for Site 12



Acceleration, a (g)



Acceleration, a (g)

Figure B13. Variation of acceleration with time at the top of each layer for Site 13

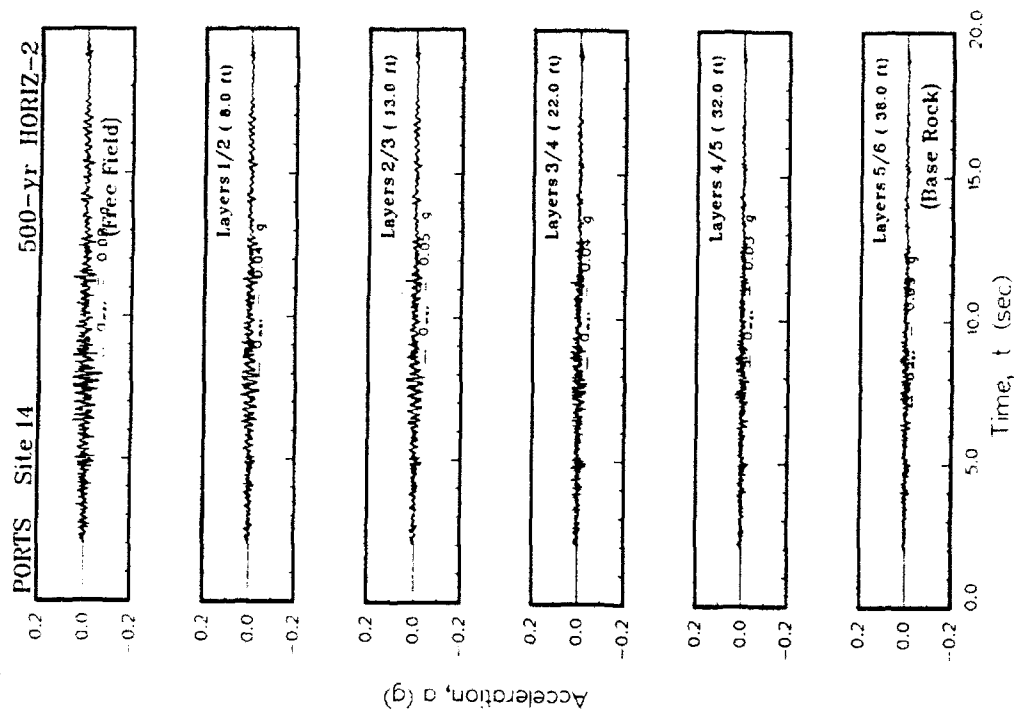
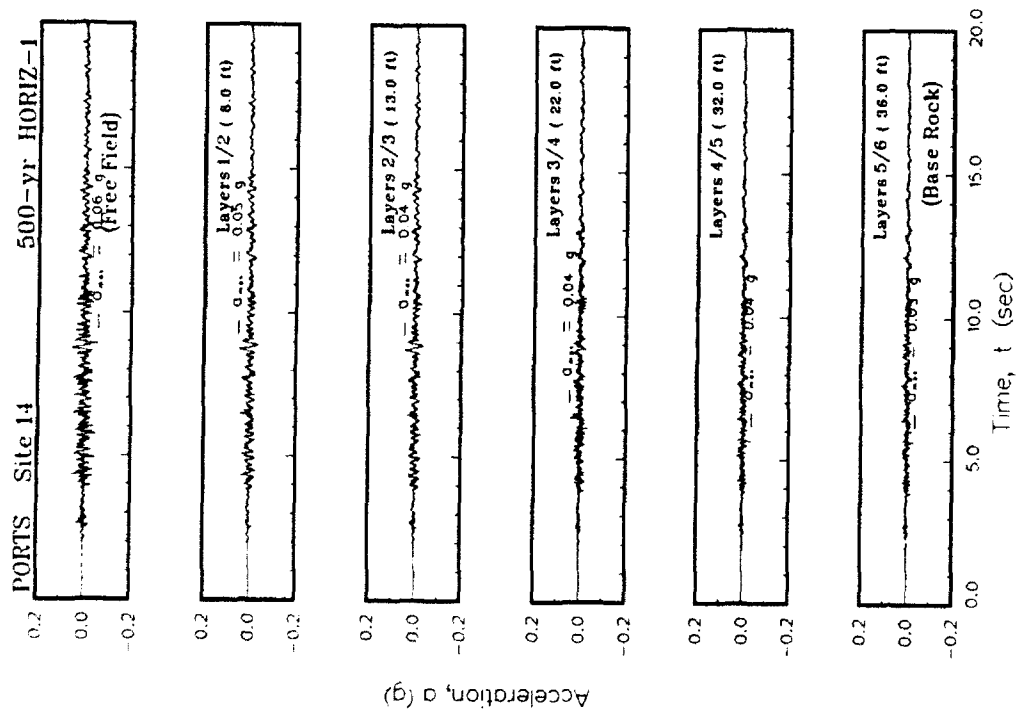


Figure B14. Variation of acceleration with time at the top of each layer for Site 14

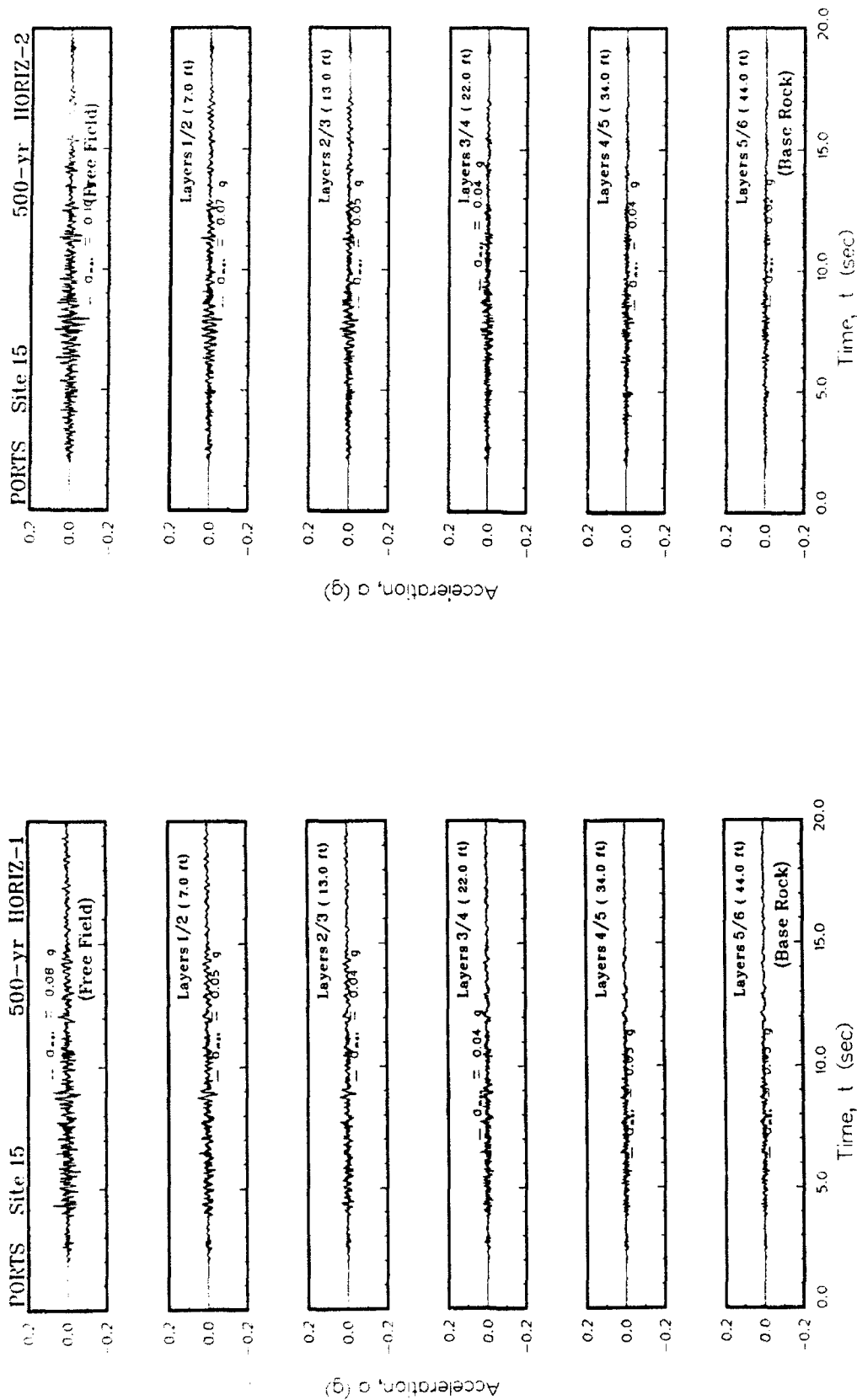


Figure B15. Variation of acceleration with time at the top of each layer for Site 15

APPENDIX C: SHEAR STRAINS FOR 500-YEAR EVENT

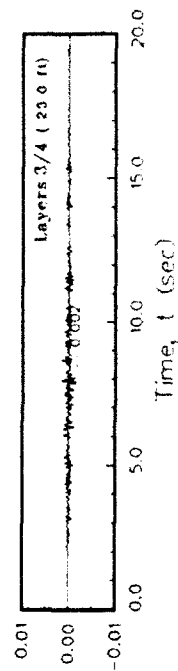
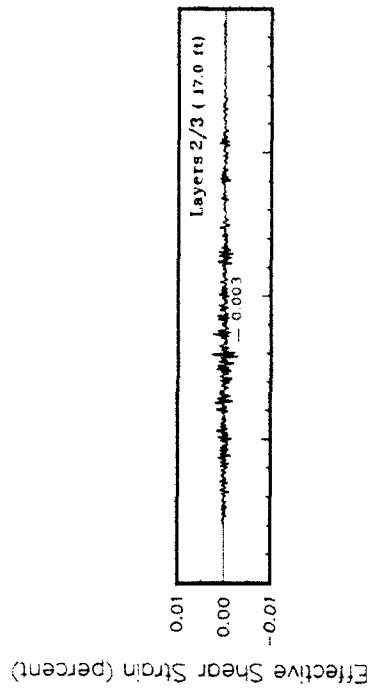
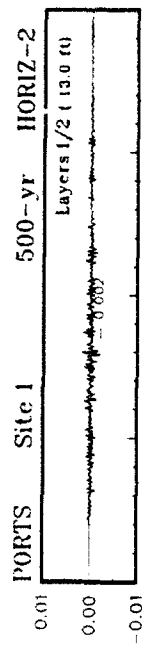
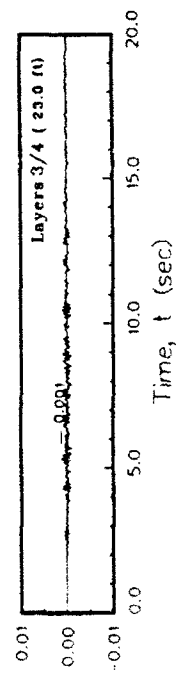
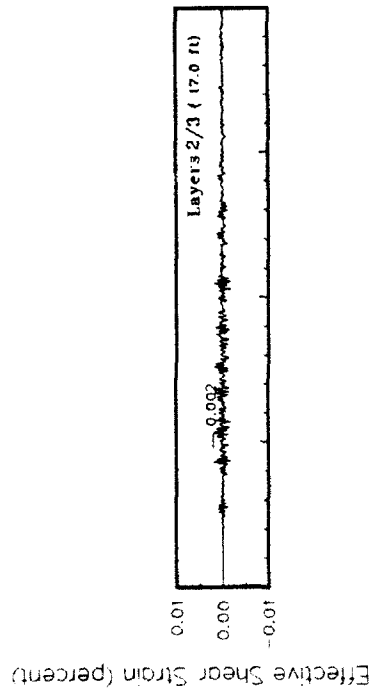
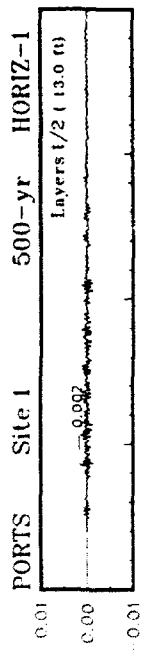


Figure C1. Variation of shear strain with time at contacts between layers for Site 1

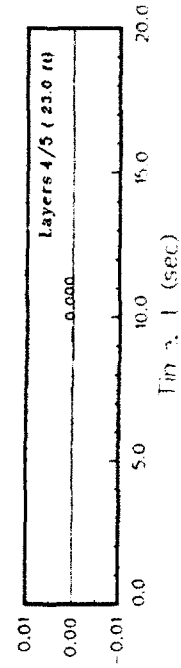
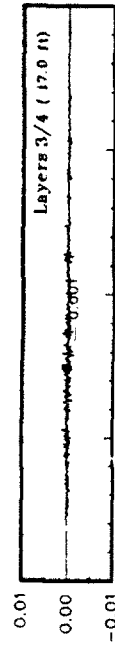
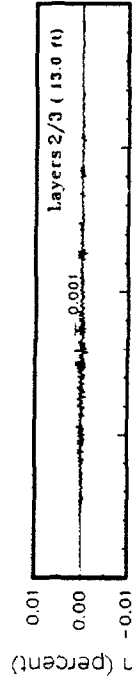
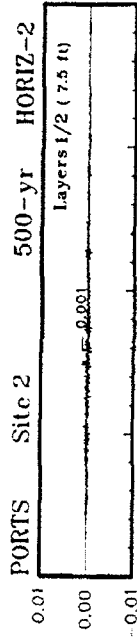
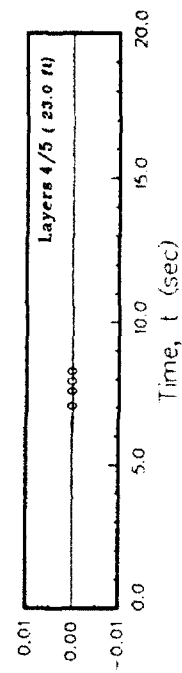
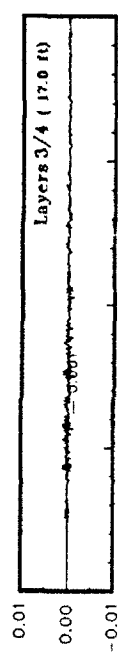
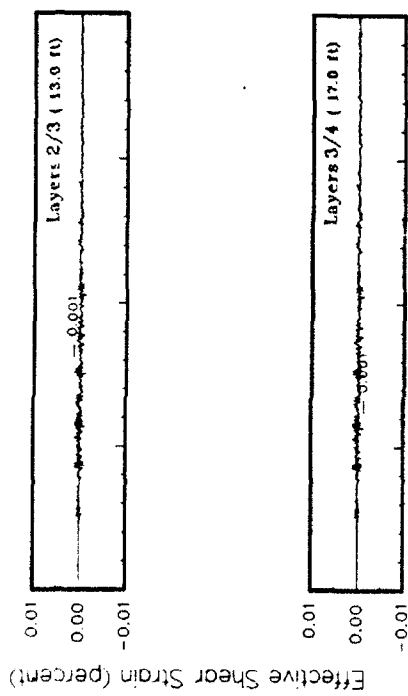
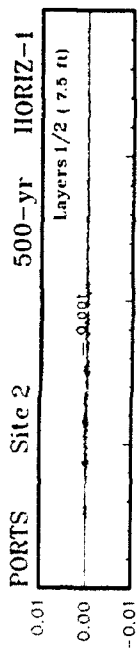
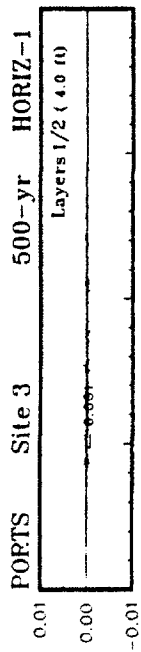
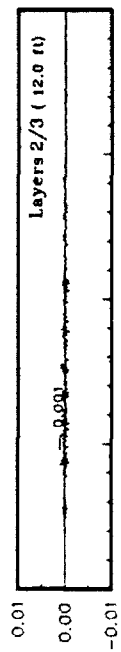


Figure C2. Variation of shear strain with time at contacts between layers for Site 2



Effective Shear Strain (percent)



Effective Shear Strain (percent)

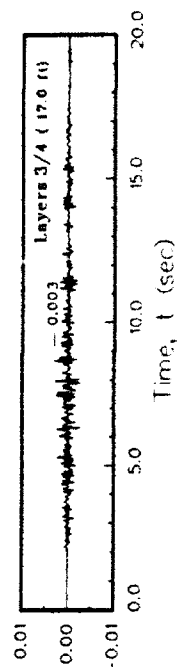
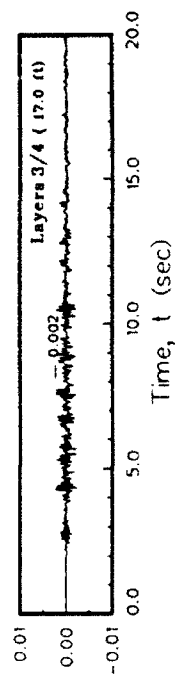
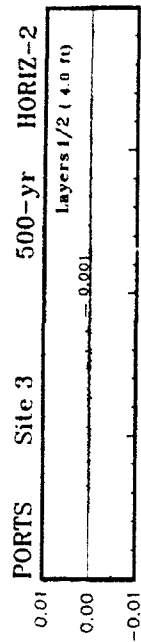
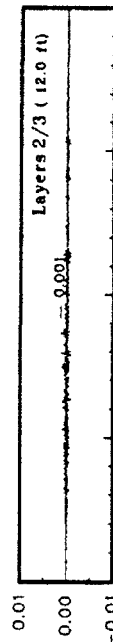
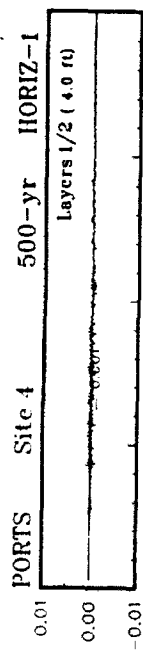
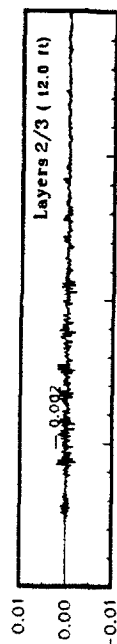


Figure C3. Variation of shear strain with time at contacts between layers for Site 3



Effective Shear Strain (percent)



Effective Shear Strain (percent)

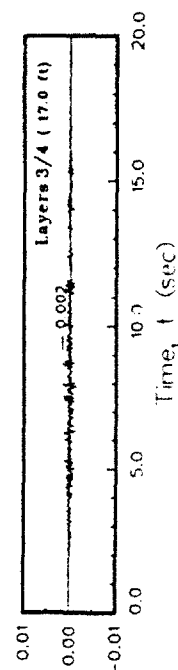
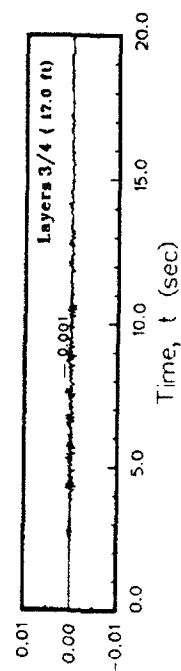
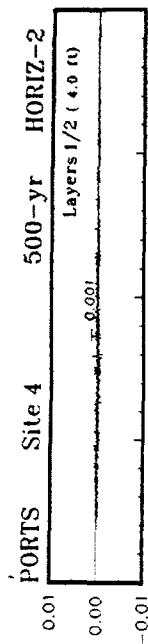


Figure C4. Variation of shear strain with time at contacts between layers for Site 4

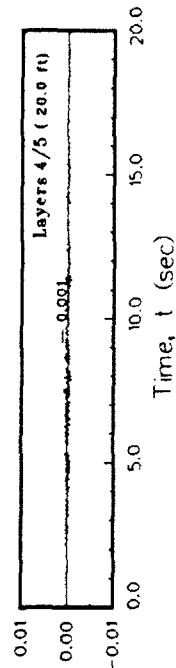
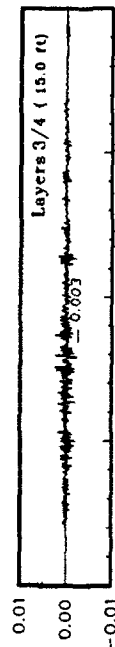
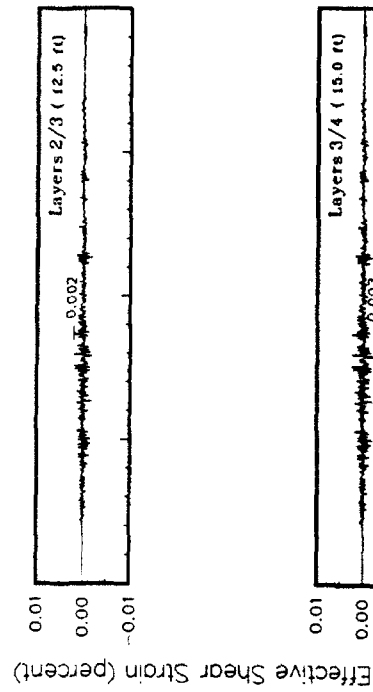
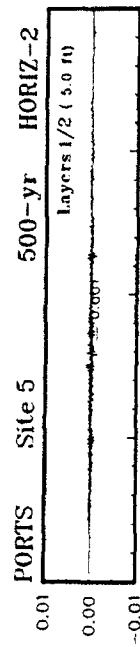
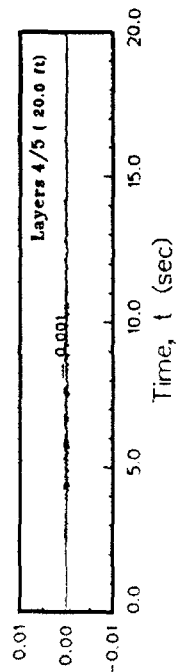
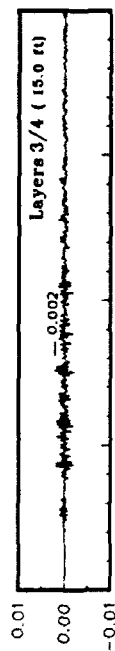
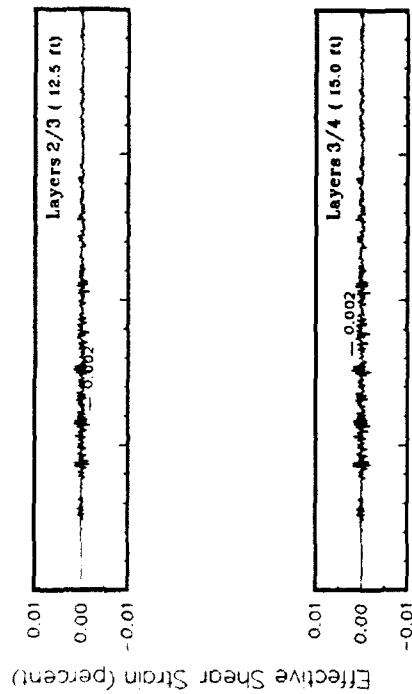
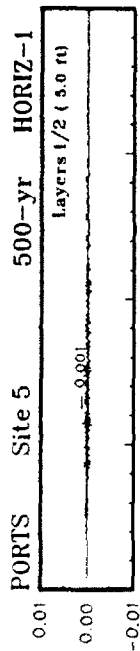


Figure C5. Variation of shear strain with time at contacts between layers for Site 5

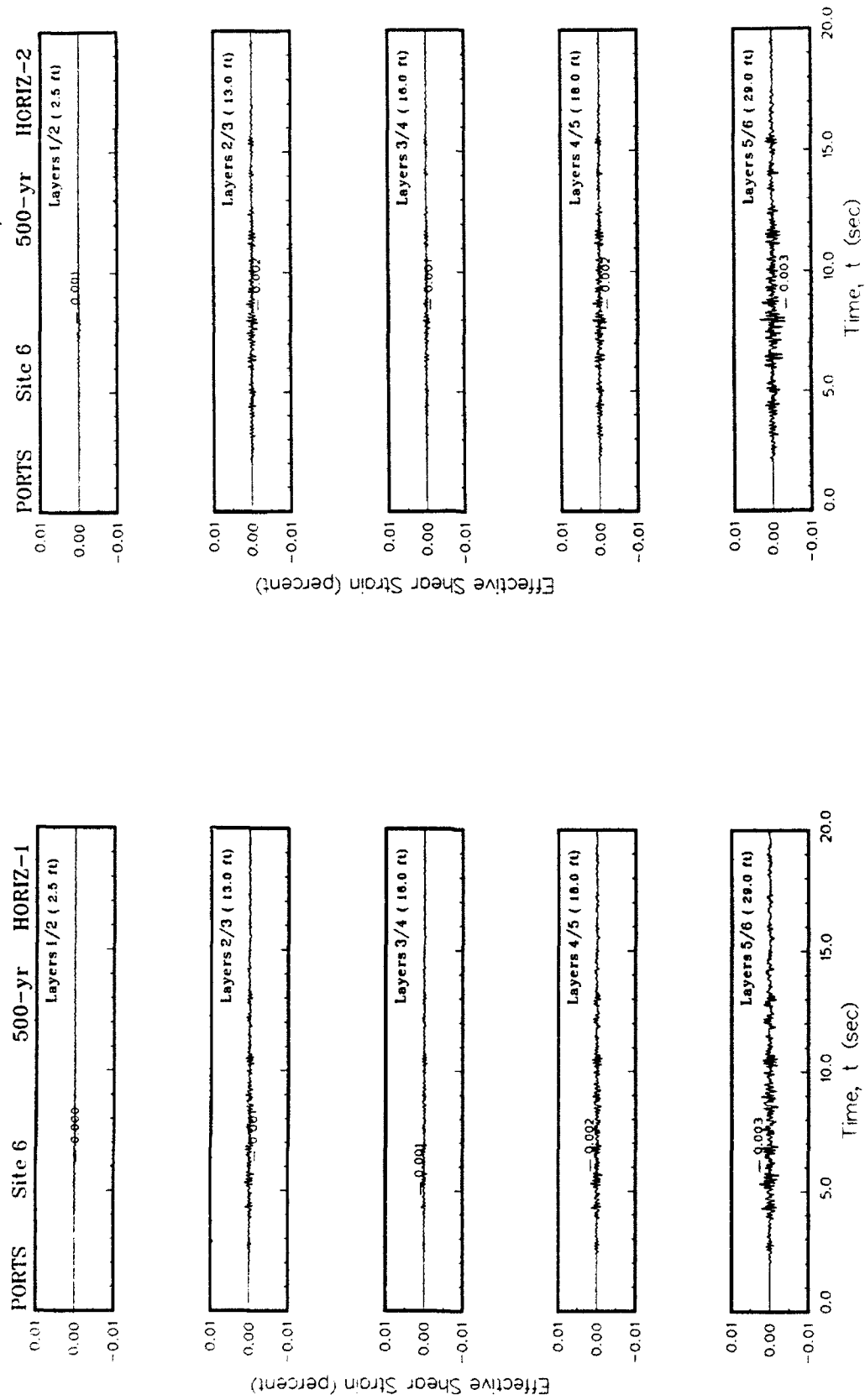


Figure C6. Variation of shear strain with time at contacts between layers for Site 6

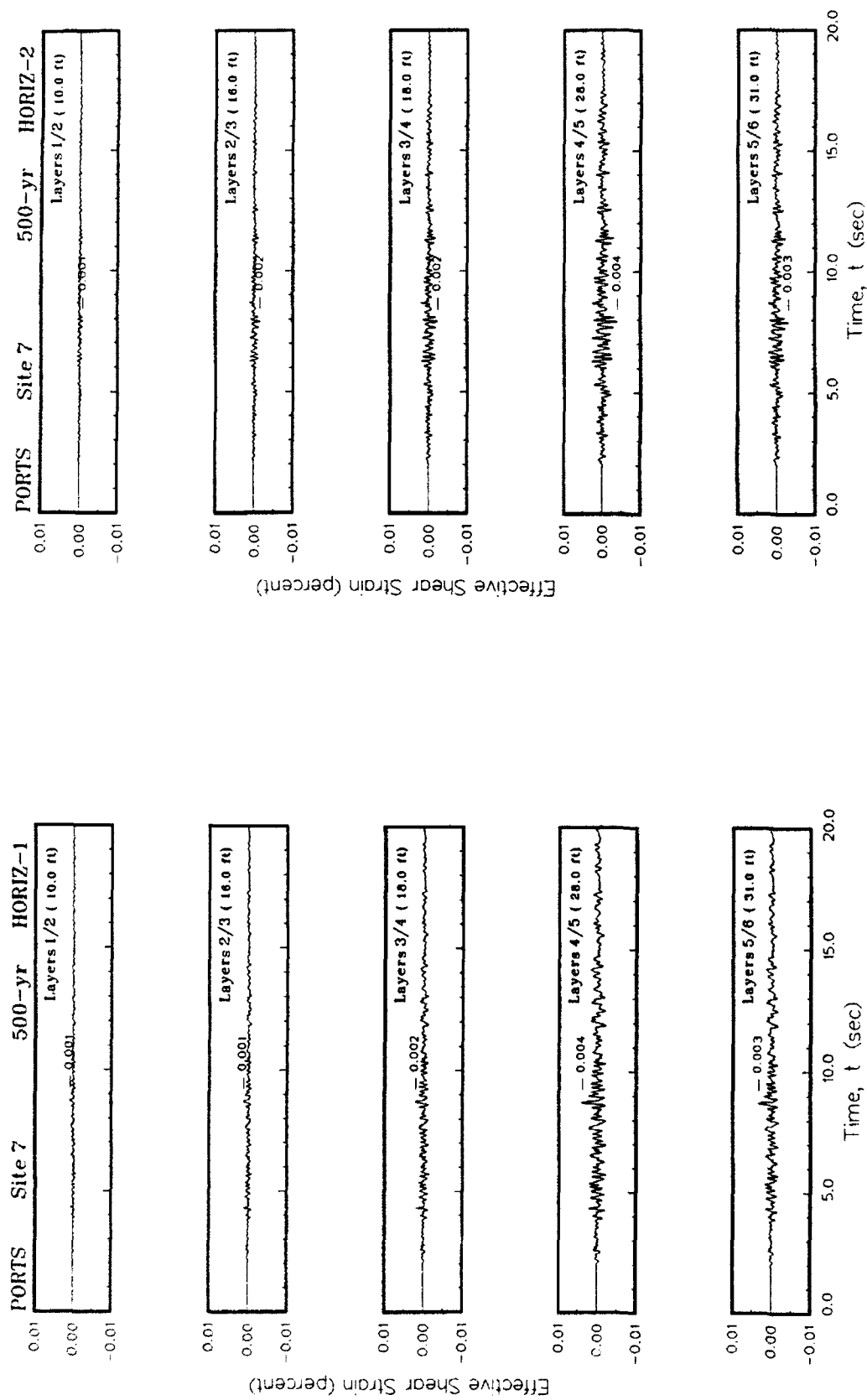


Figure C7. Variation of shear strain with time at contacts between layers for Site 7

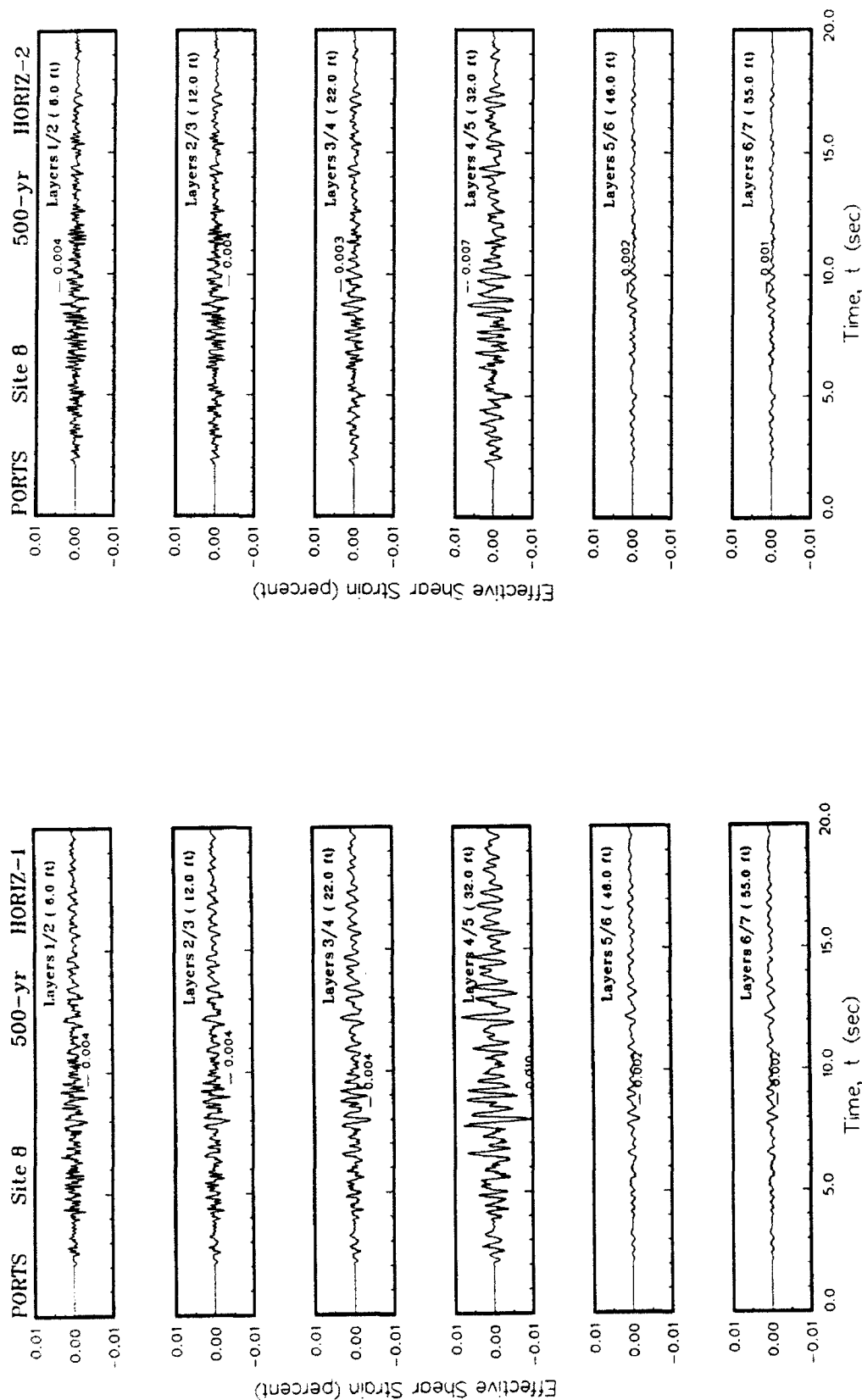


Figure C8. Variation of shear strain with time at contacts between layers for Site 8

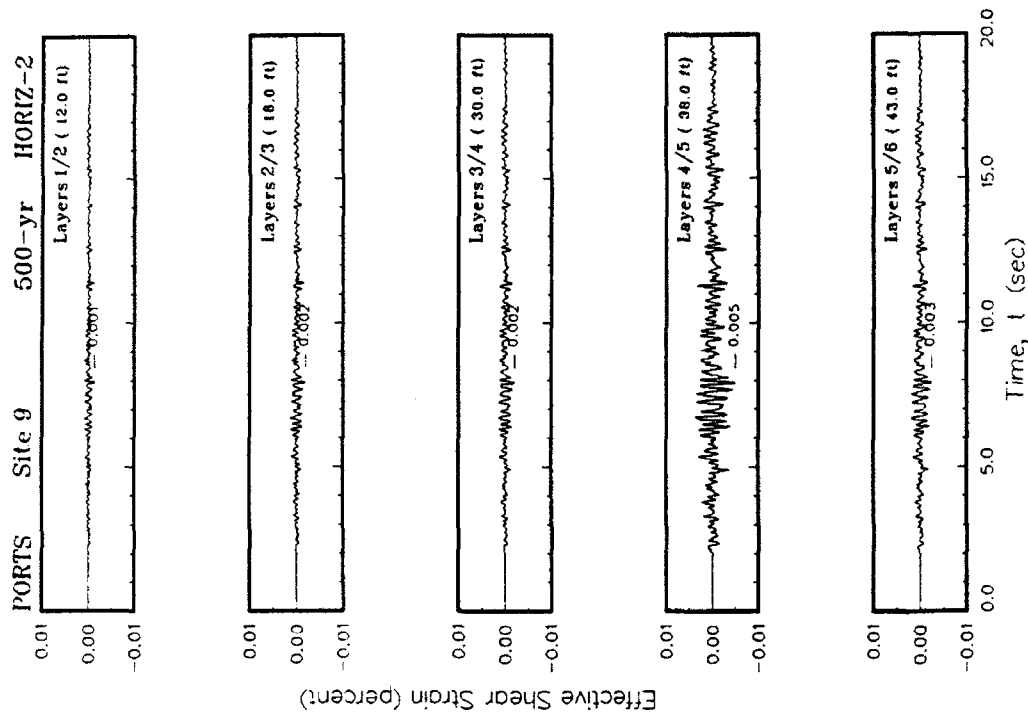
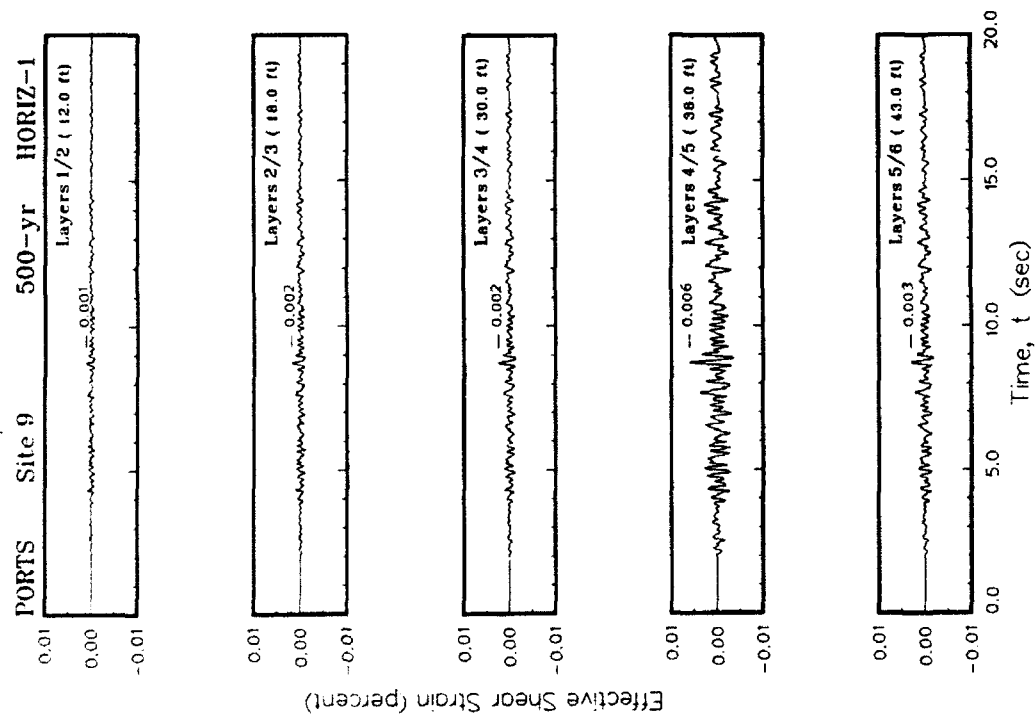


Figure C9. Variation of shear strain with time at contacts between layers for Site 9

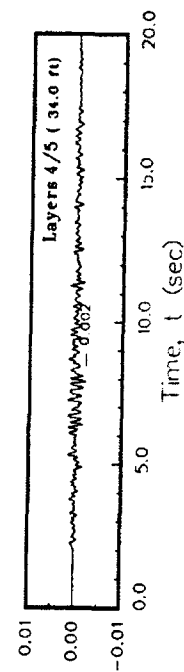
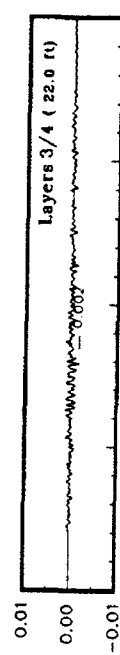
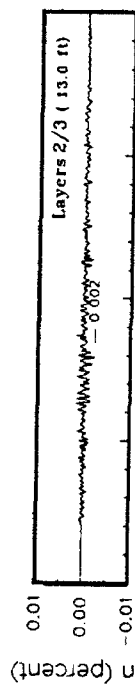
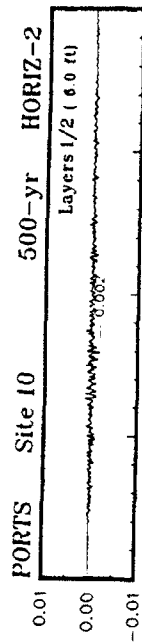
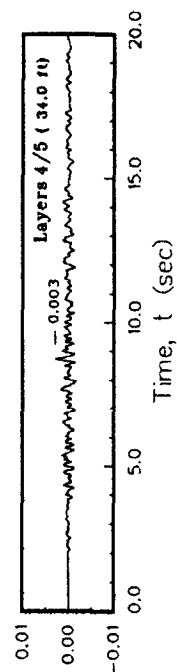
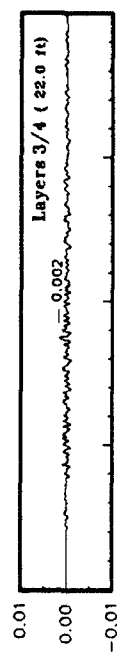
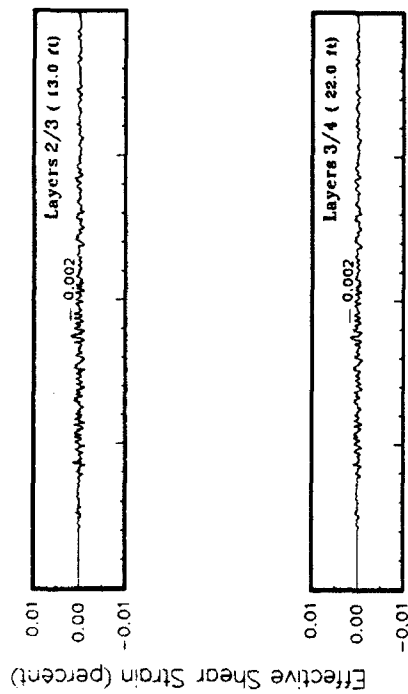
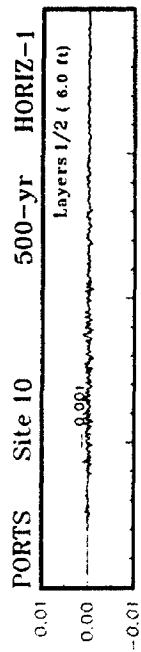


Figure C10. Variation of shear strain with time at contacts between layers for Site 10

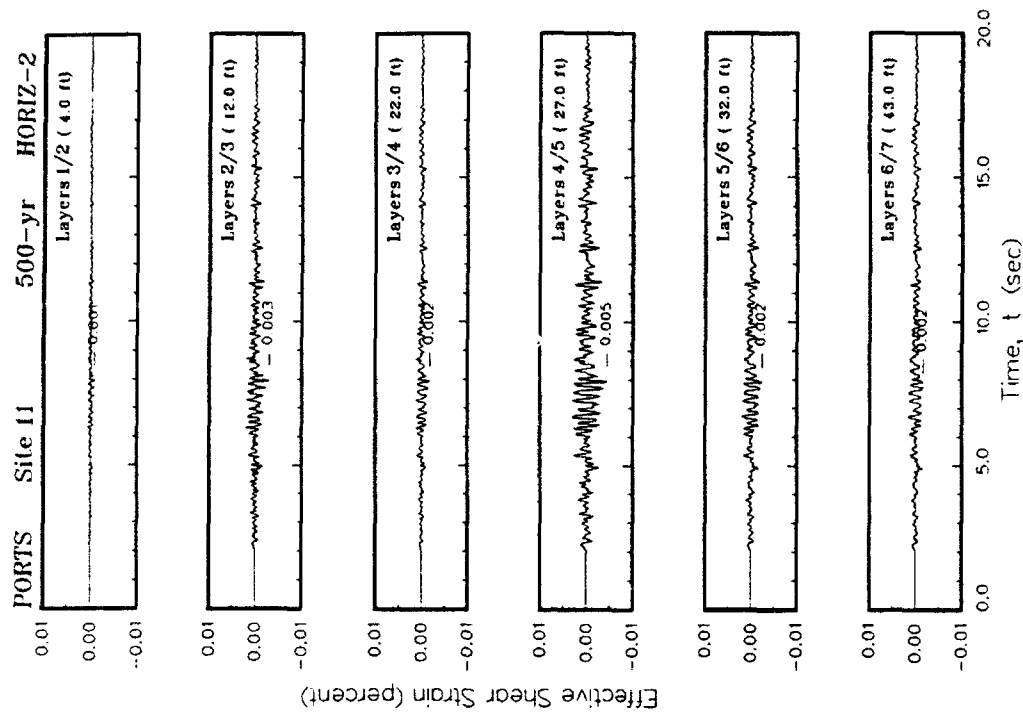
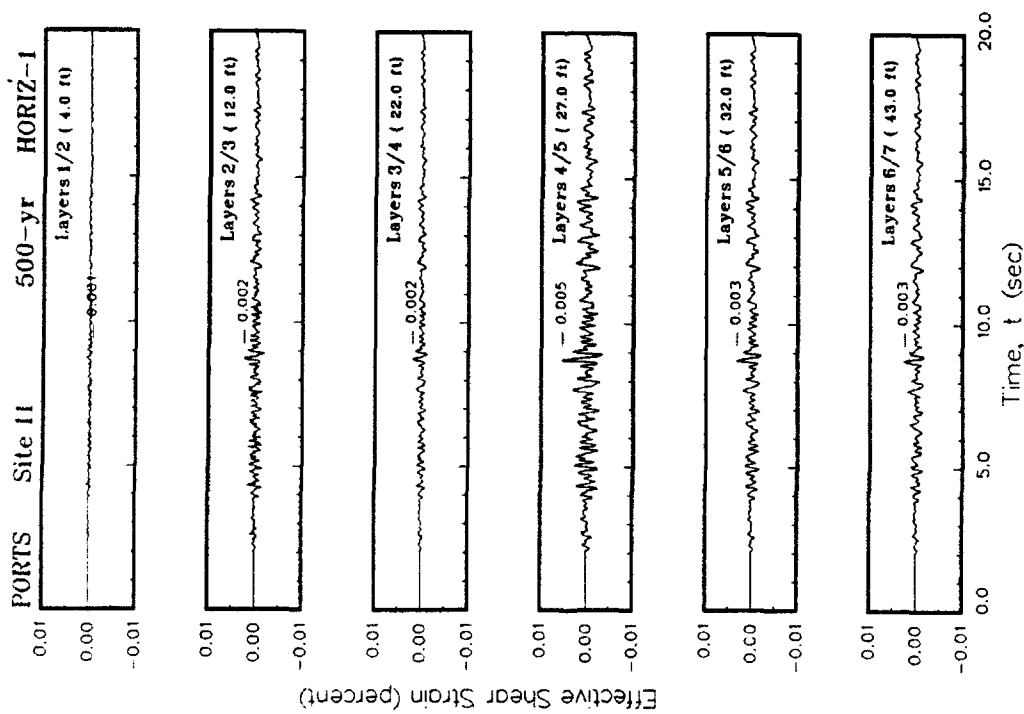
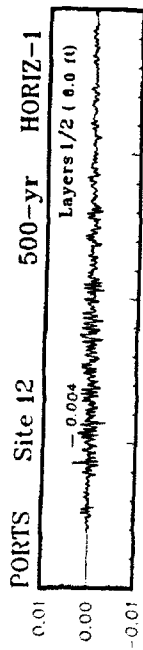
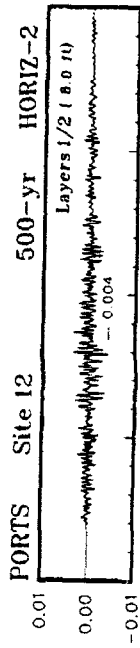


Figure C11. Variation of shear strain with time at contacts between layers for Site 11



Effective Shear Strain (percent)



Effective Shear Strain (percent)

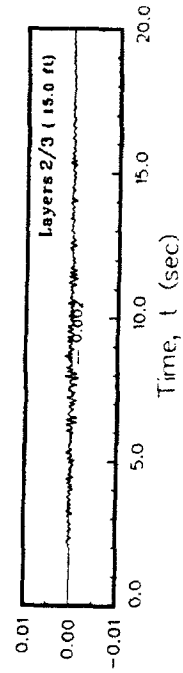
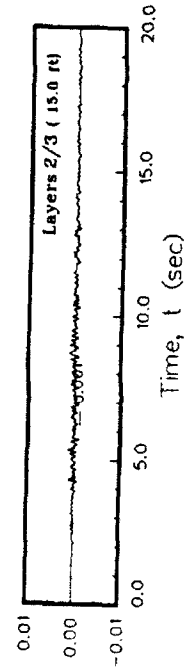


Figure C12. Variation of shear strain with time at contacts between layers for Site 12

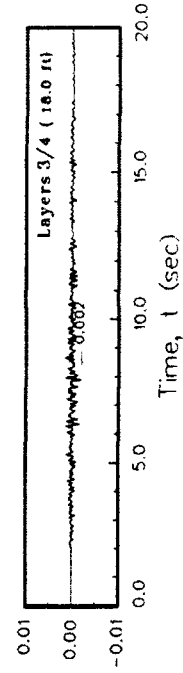
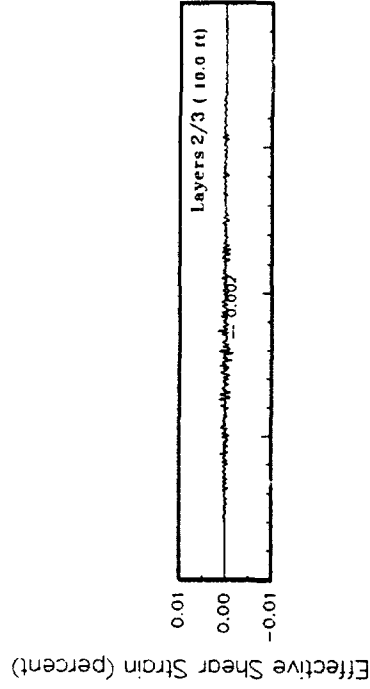
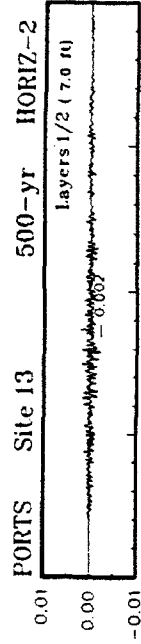
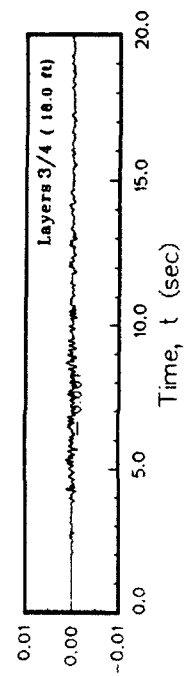
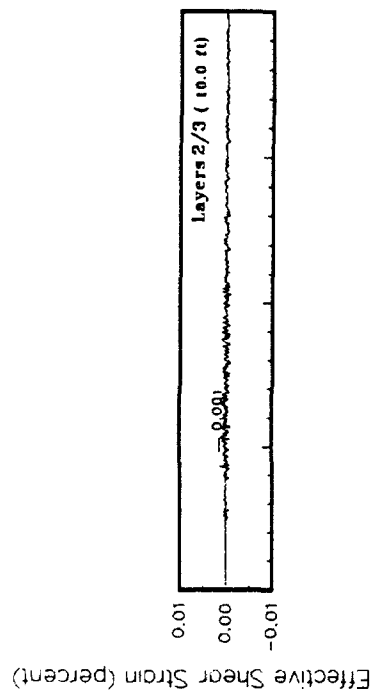
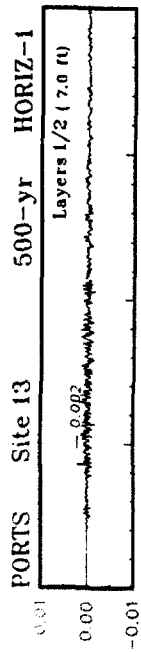


Figure C13. Variation of shear strain with time at contacts between layers for Site 13

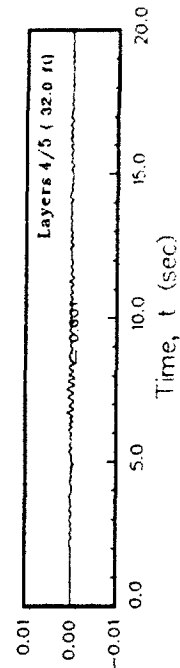
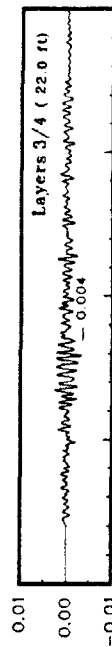
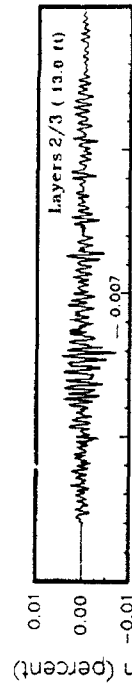
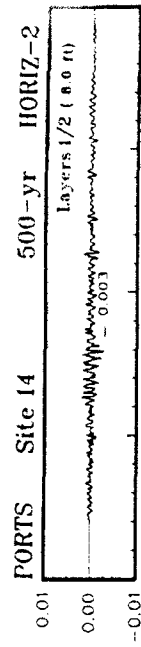
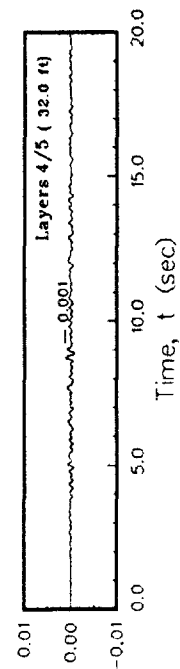
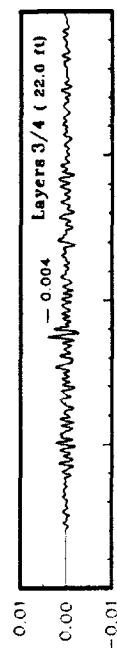
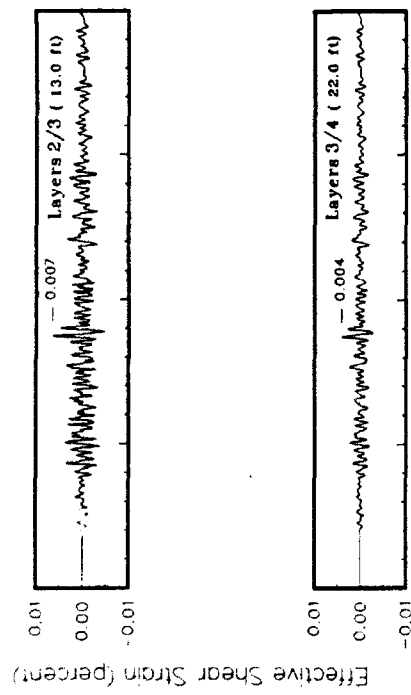
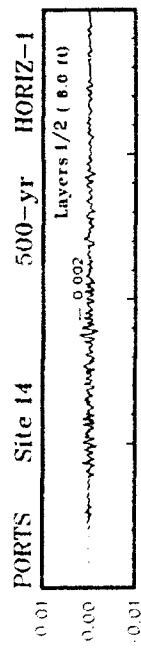


Figure C14. Variation of shear strain with time at contacts between layers for Site 14

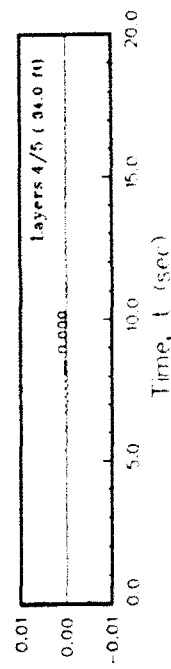
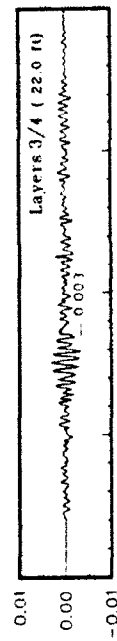
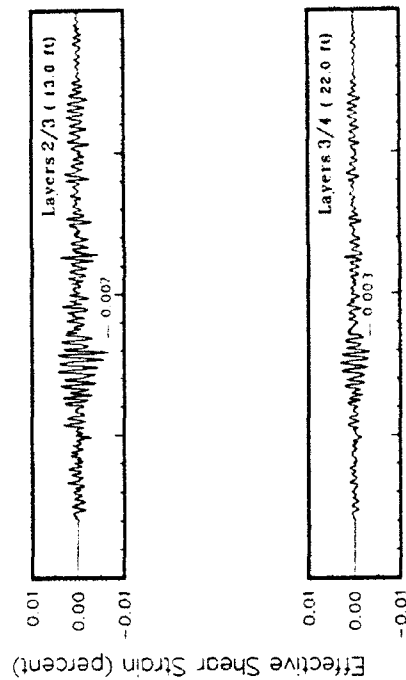
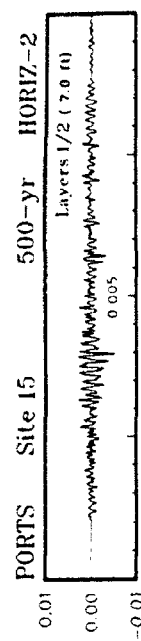
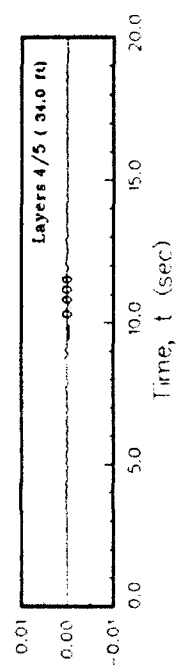
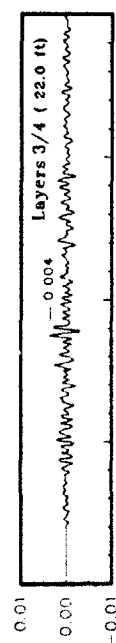
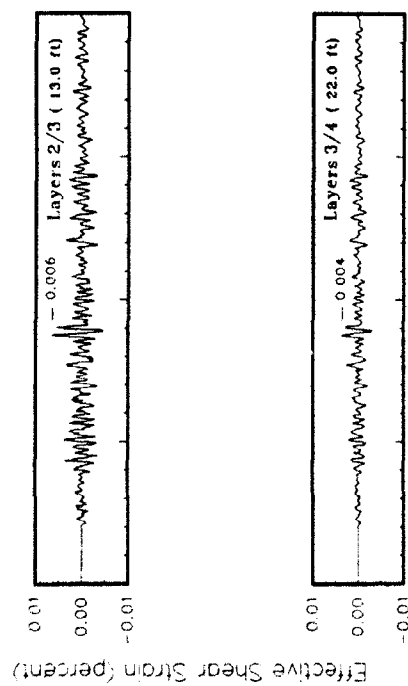
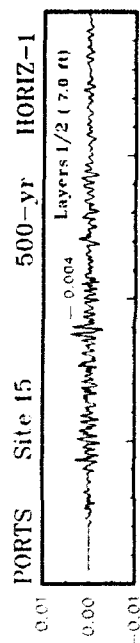


Figure C15. Variation of shear strain with time at contacts between layers for Site 15

APPENDIX D: TRIPARTITE RESPONSE SPECTRA FOR 500-YEAR EVENT

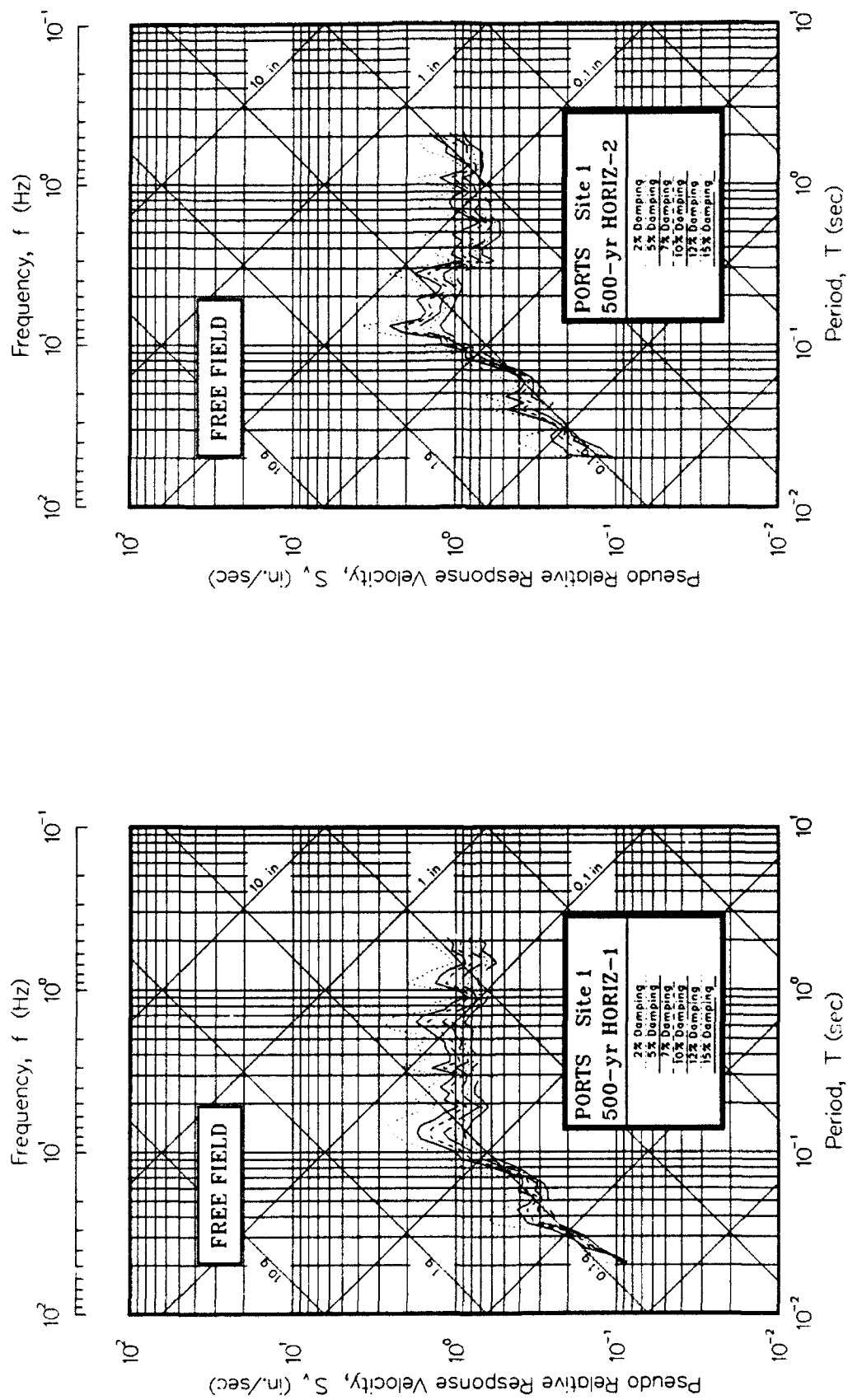


Figure D1. Psuedo-relative velocity spectra in tripartite form at free field for Site 1

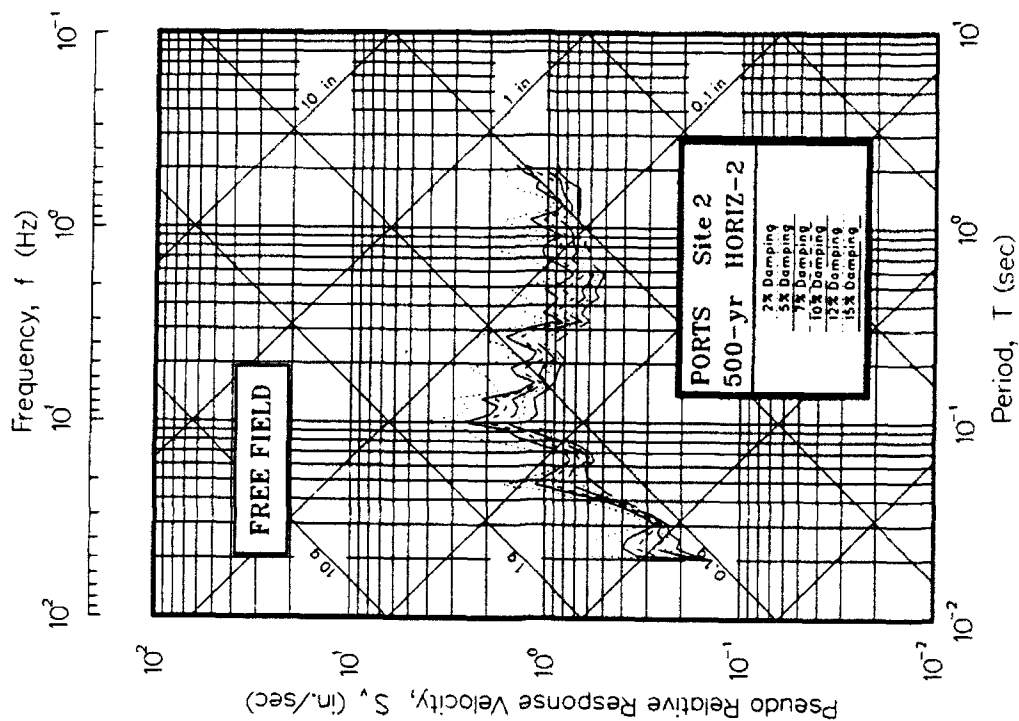
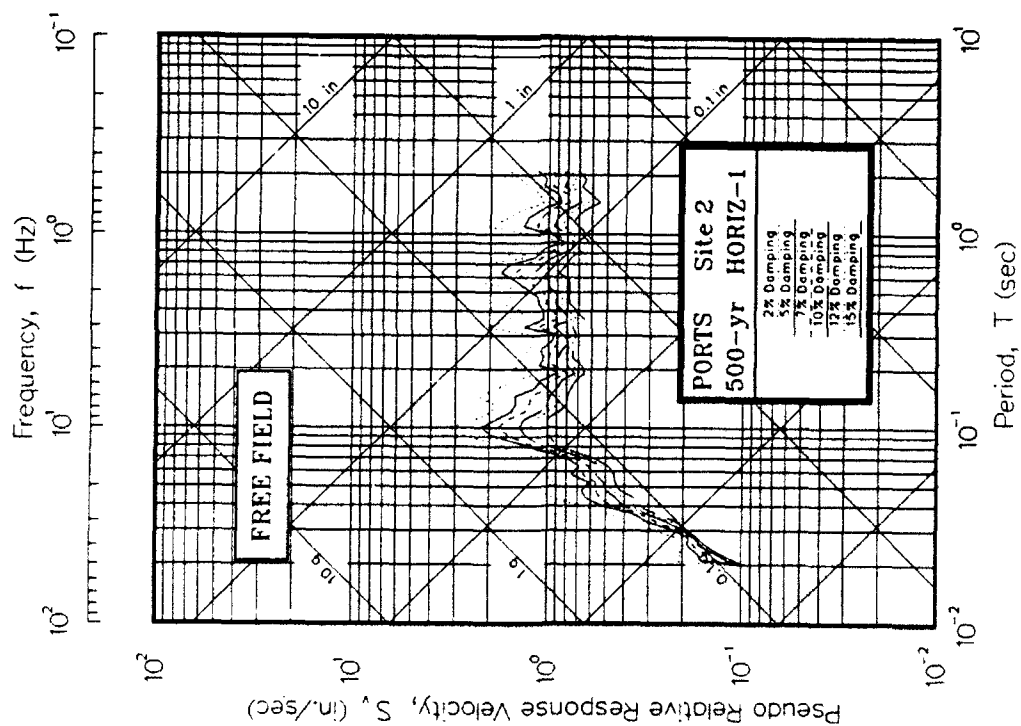


Figure D2. Psuedo-relative velocity spectra in tripartite form at free field for Site 2

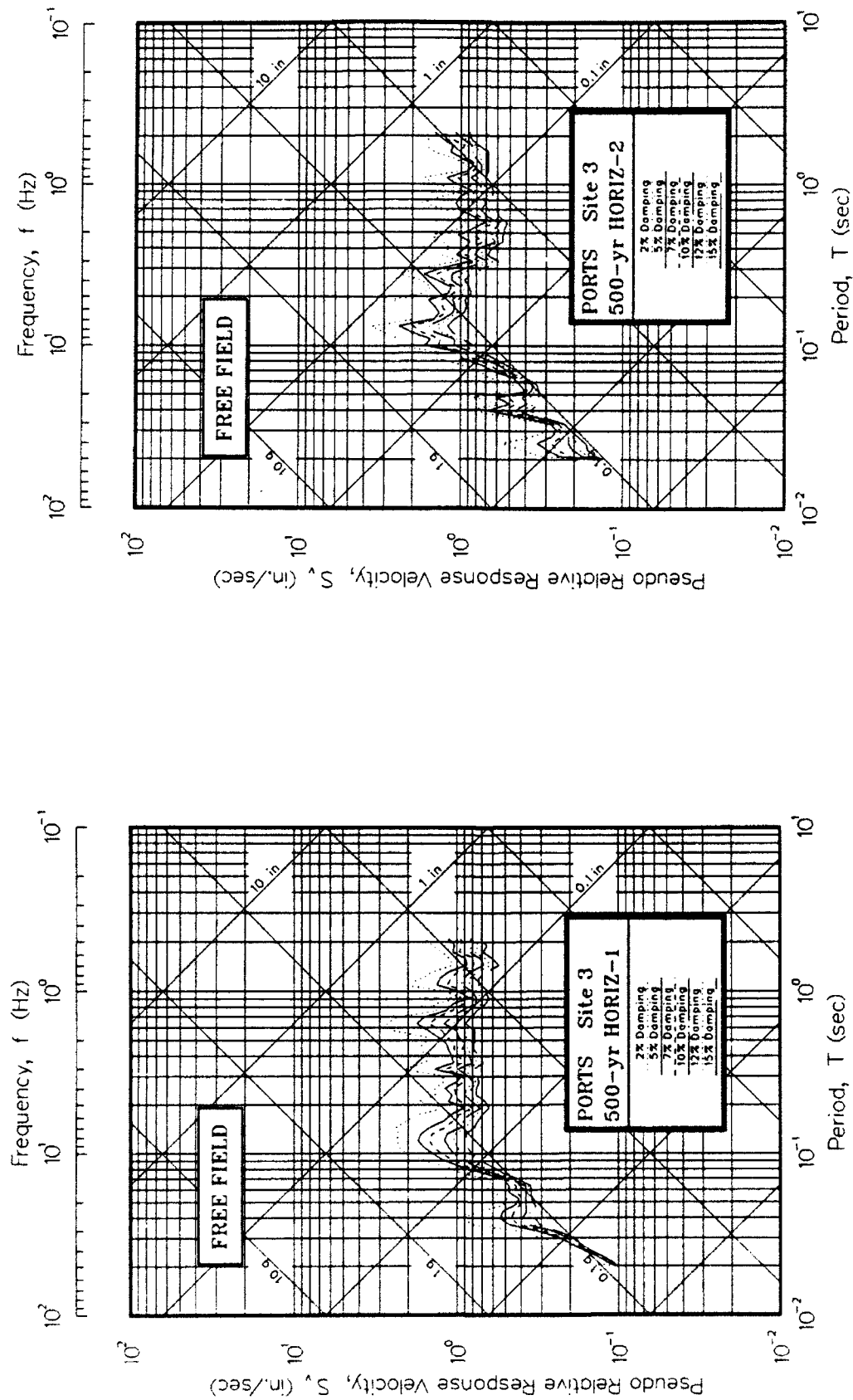


Figure D3. Psuedo-relative velocity spectra in tripartite form at free field for Site 3

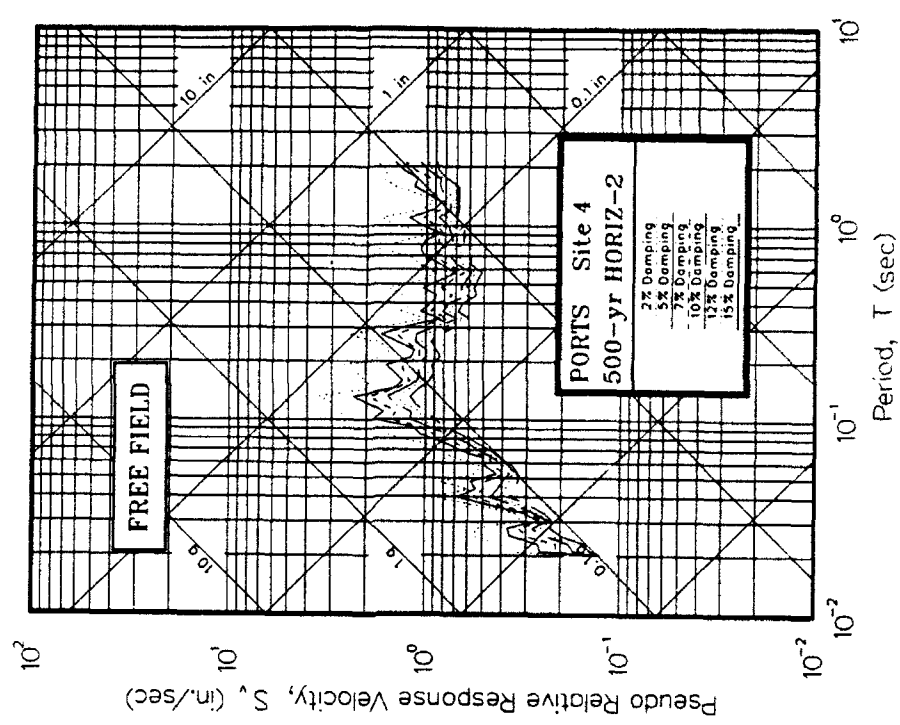
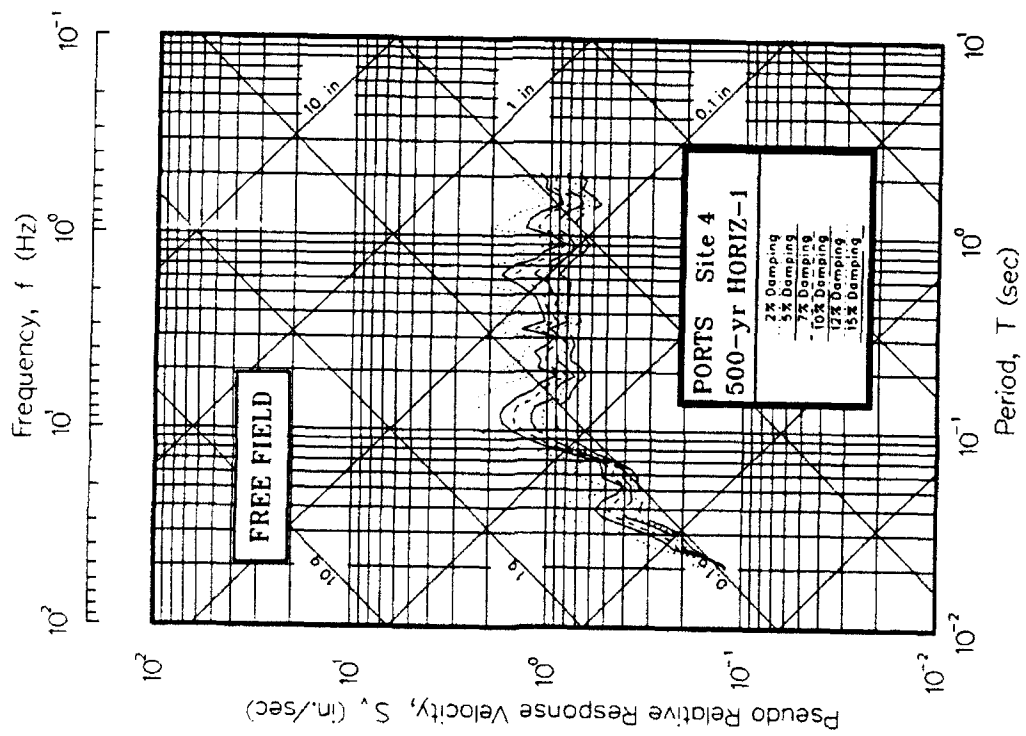
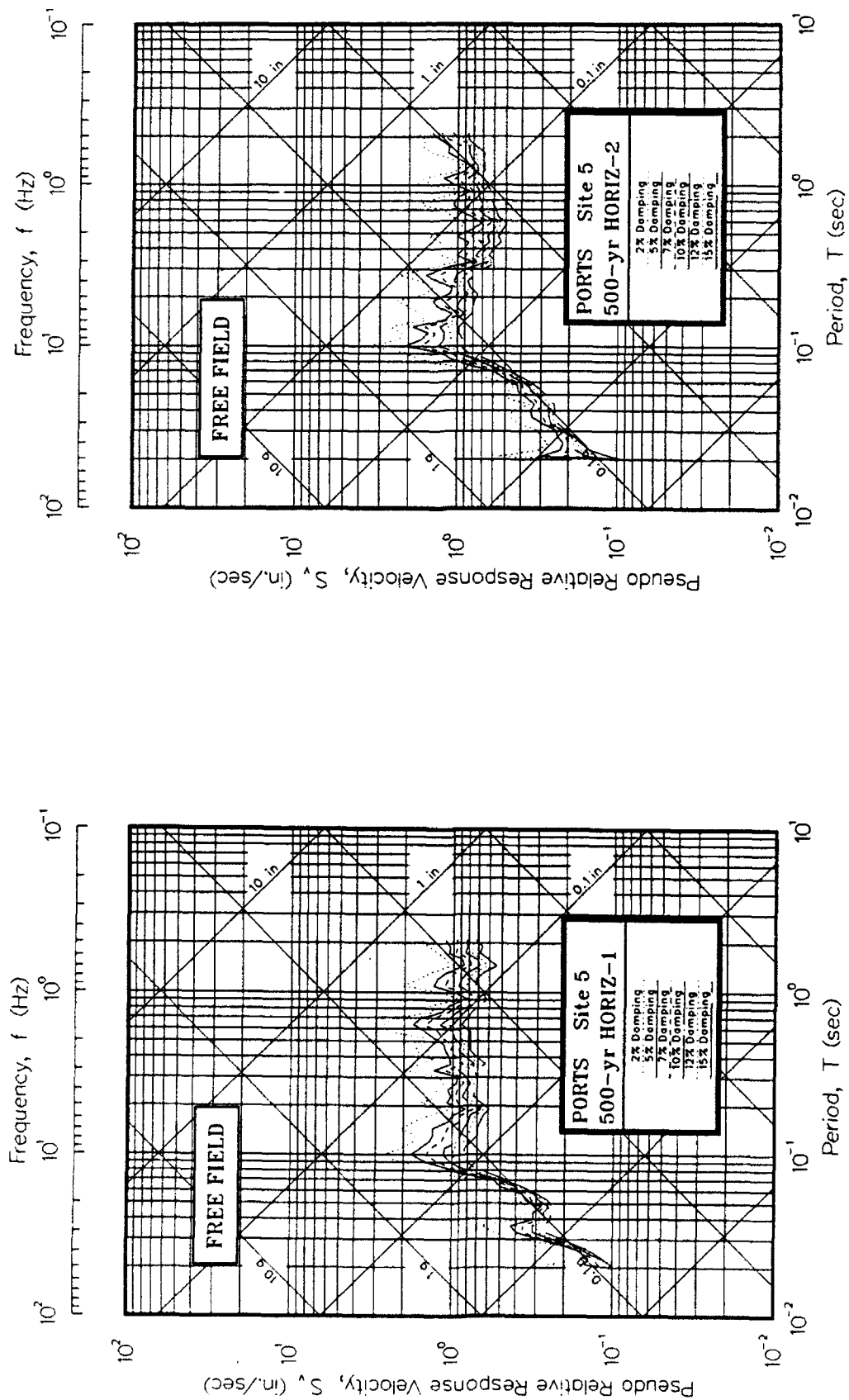


Figure D4. Pseudo-relative velocity spectra in tripartite form at free field for Site 4



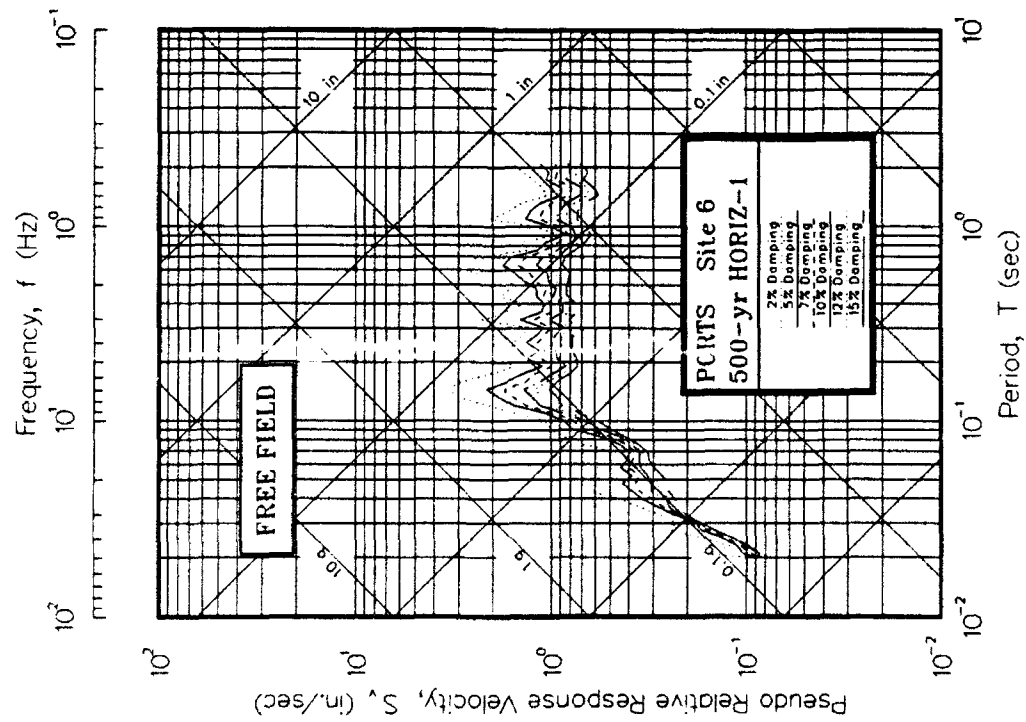
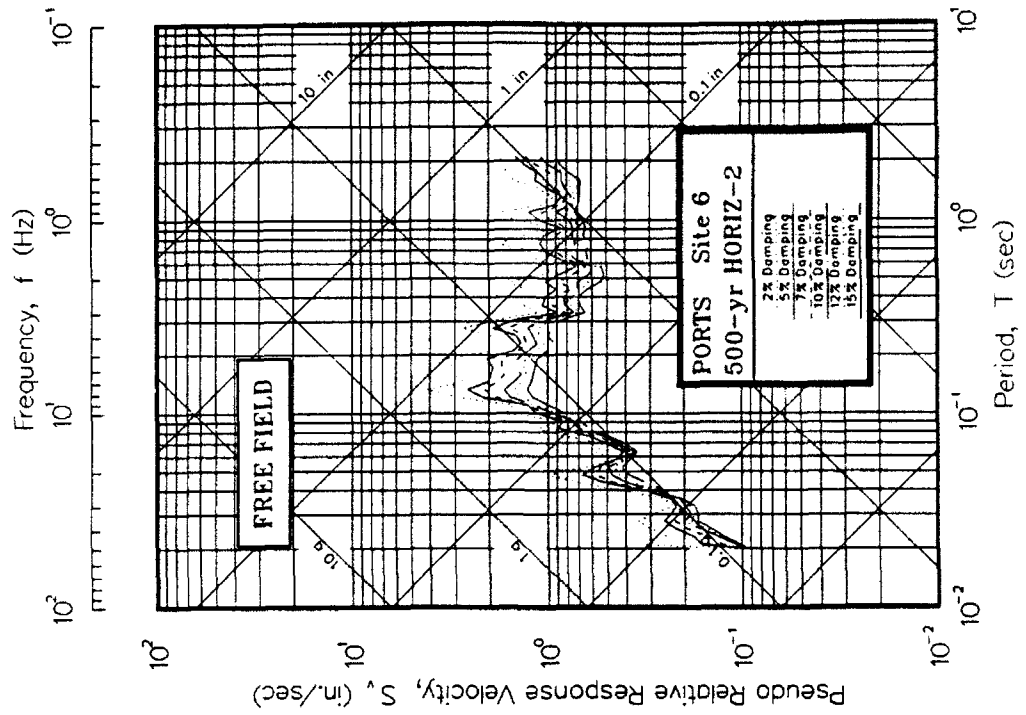


Figure D6. Psuedo-relative velocity spectra in tripartite form at free field for Site 6

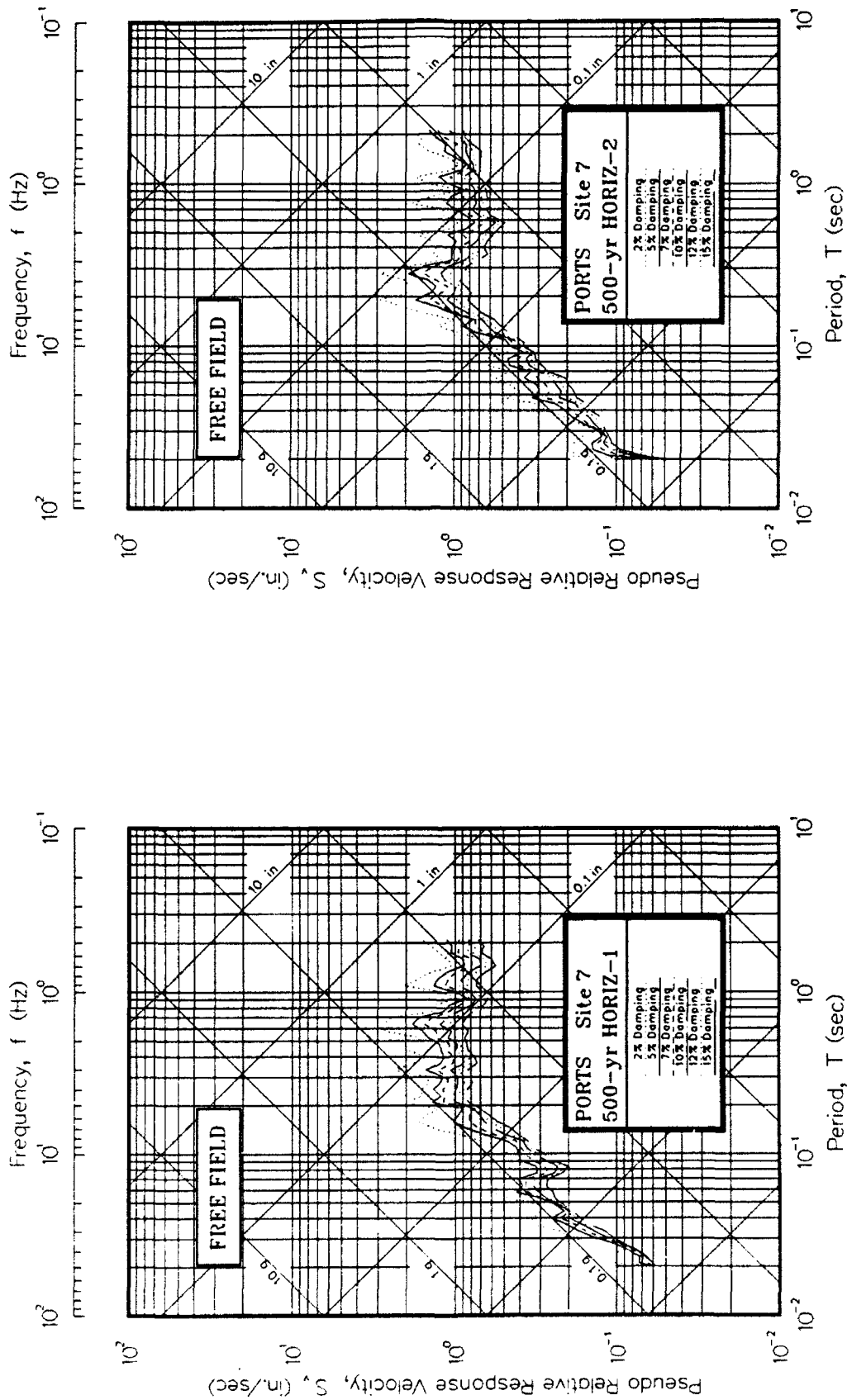


Figure D7. Psuedo-relative velocity spectra in tripartite form at free field for Site 7

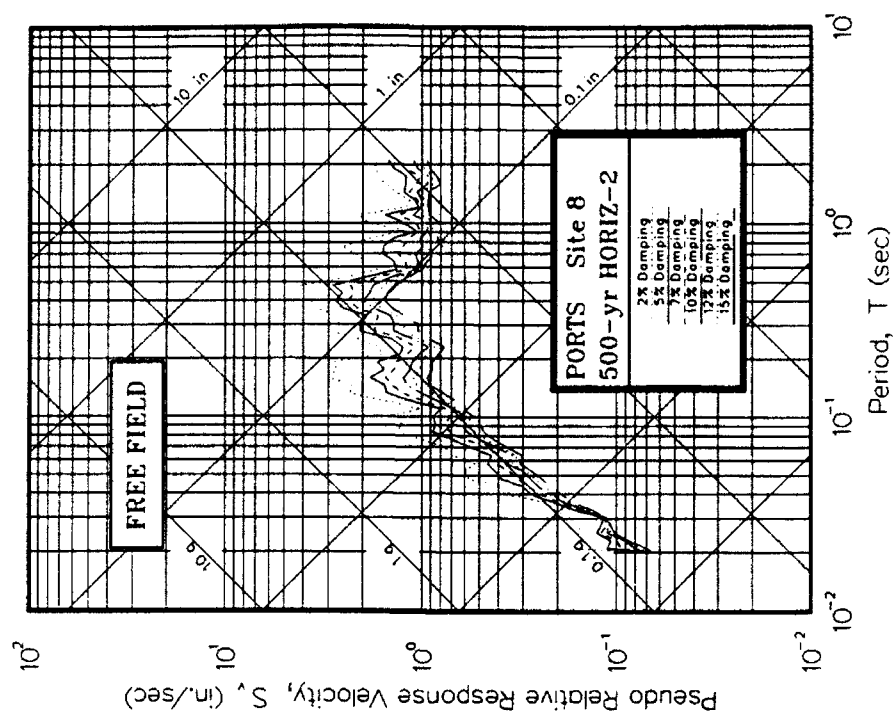
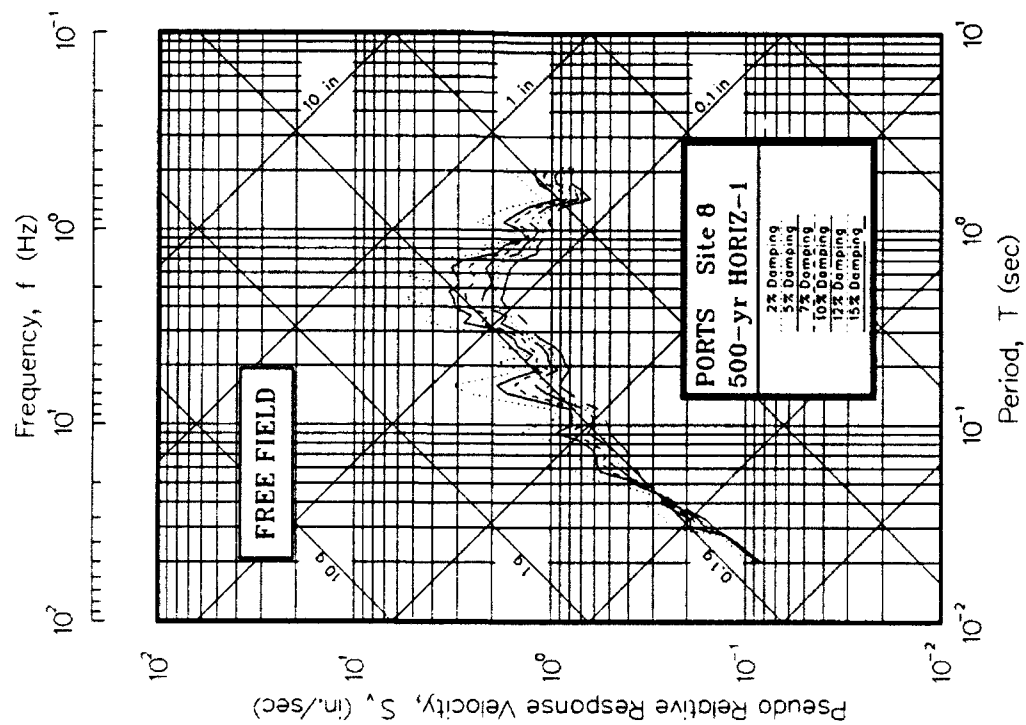


Figure D8. Psuedo-relative velocity spectra in tripartite form at free field for Site 8

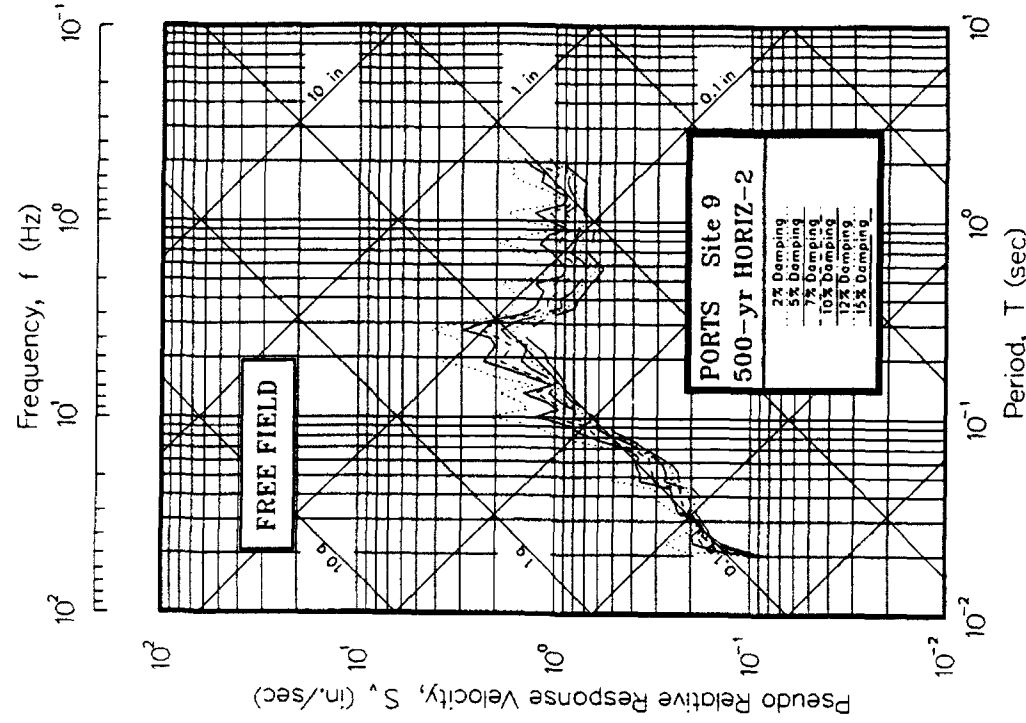
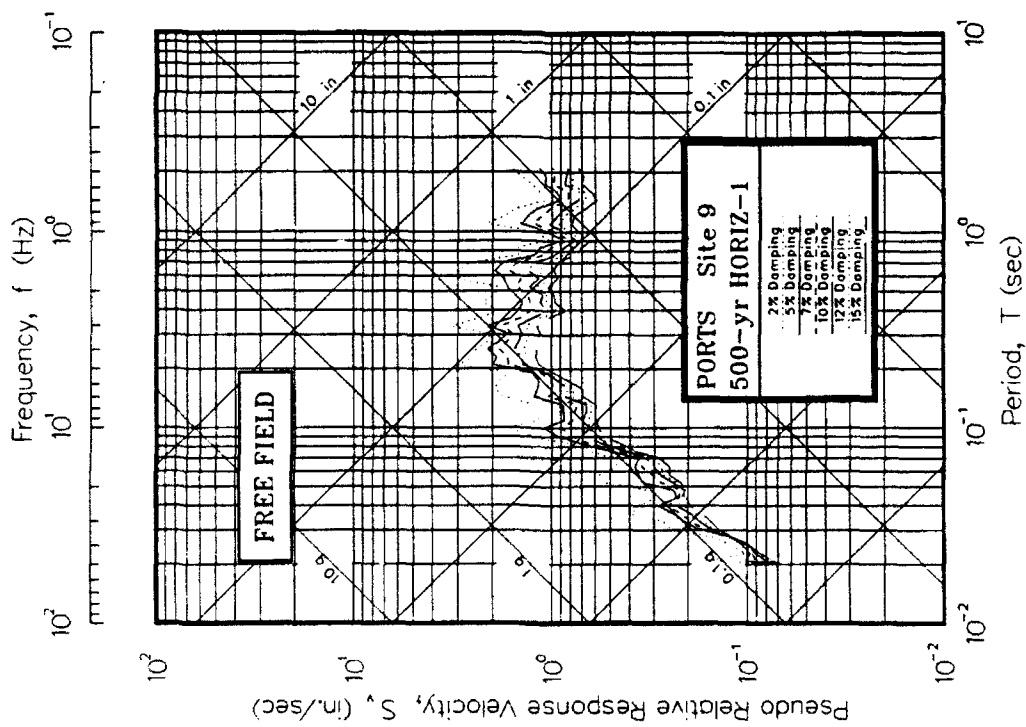


Figure D9. Psuedo-relative velocity spectra in tripartite form at free field for Site 9

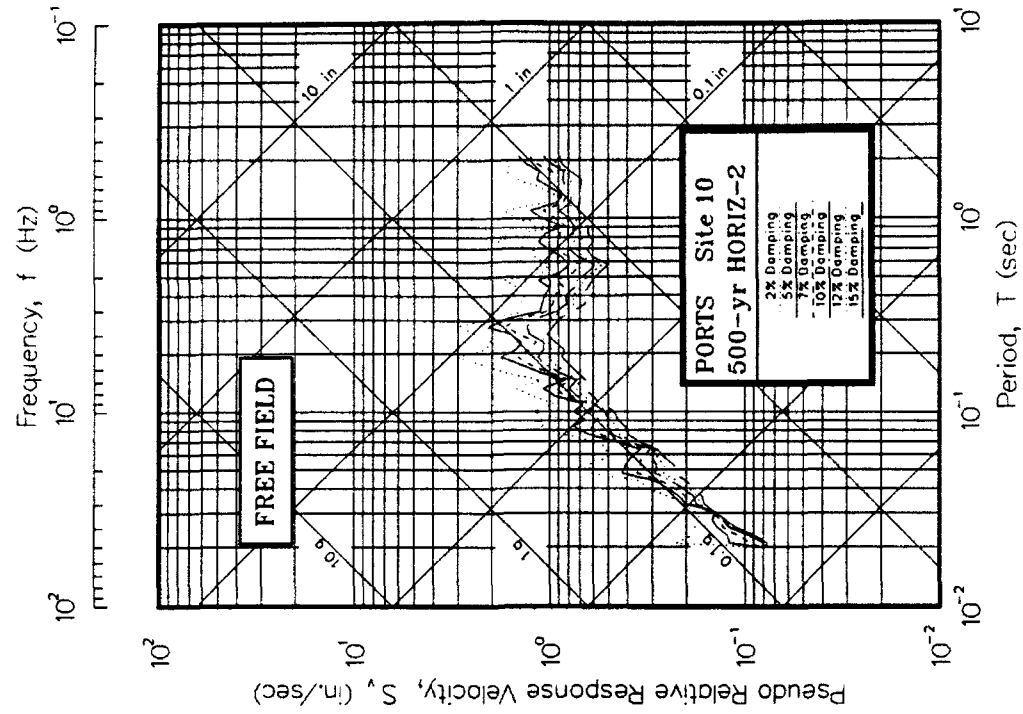
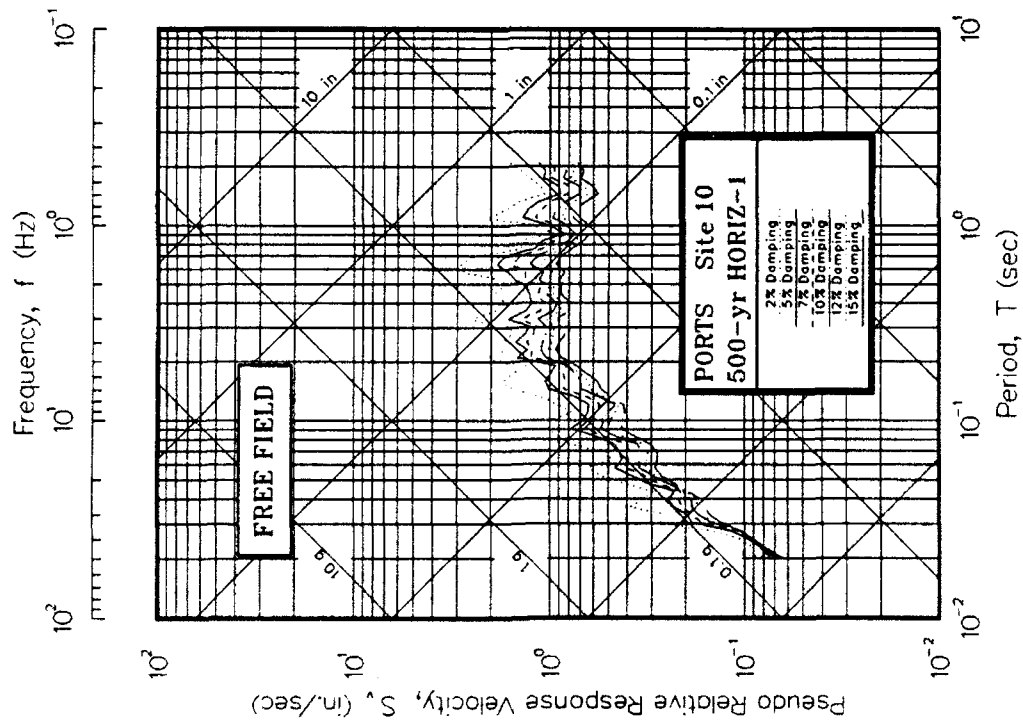


Figure D10. Psuedo-relative velocity spectra in tripartite form at free field for Site 10

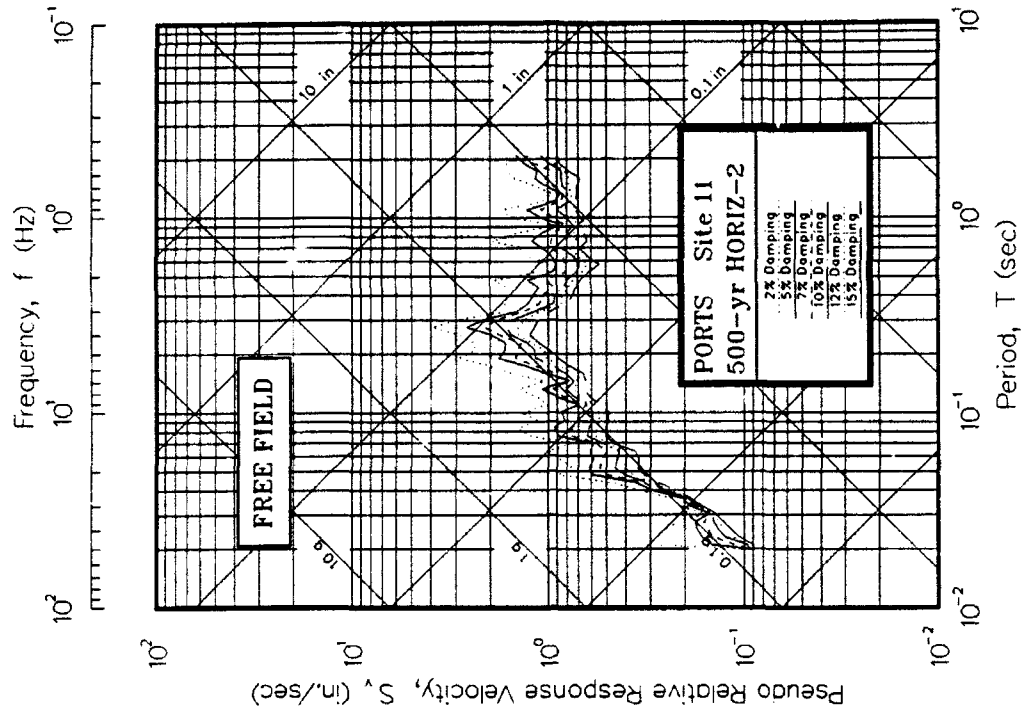
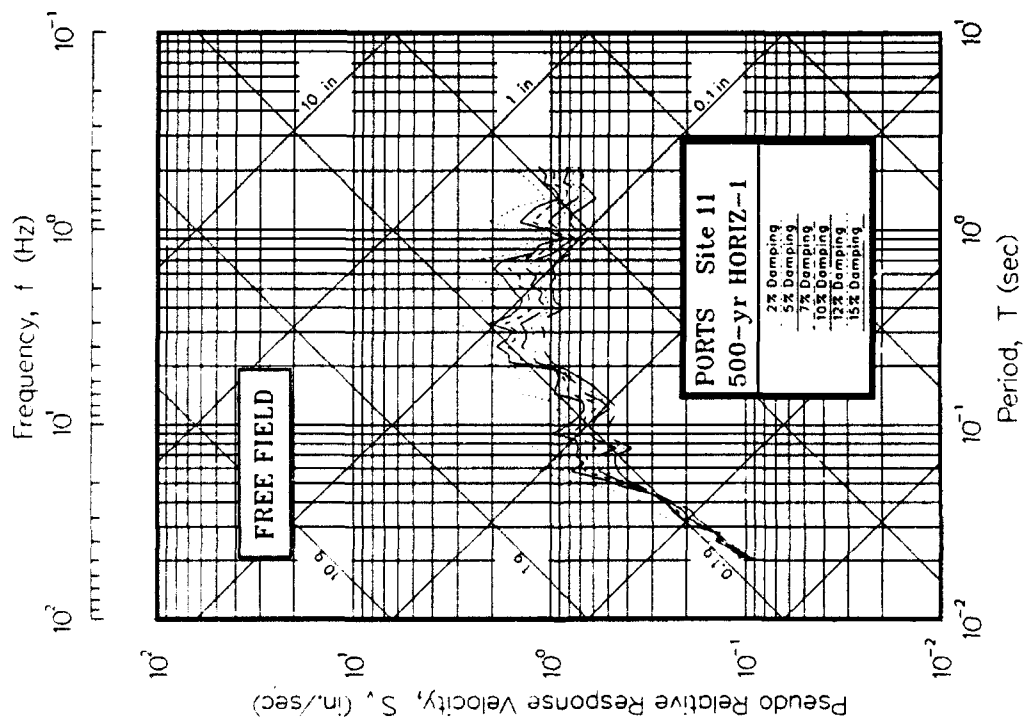


Figure D11. Psuedo-relative velocity spectra in tripartite form at free field for Site 11

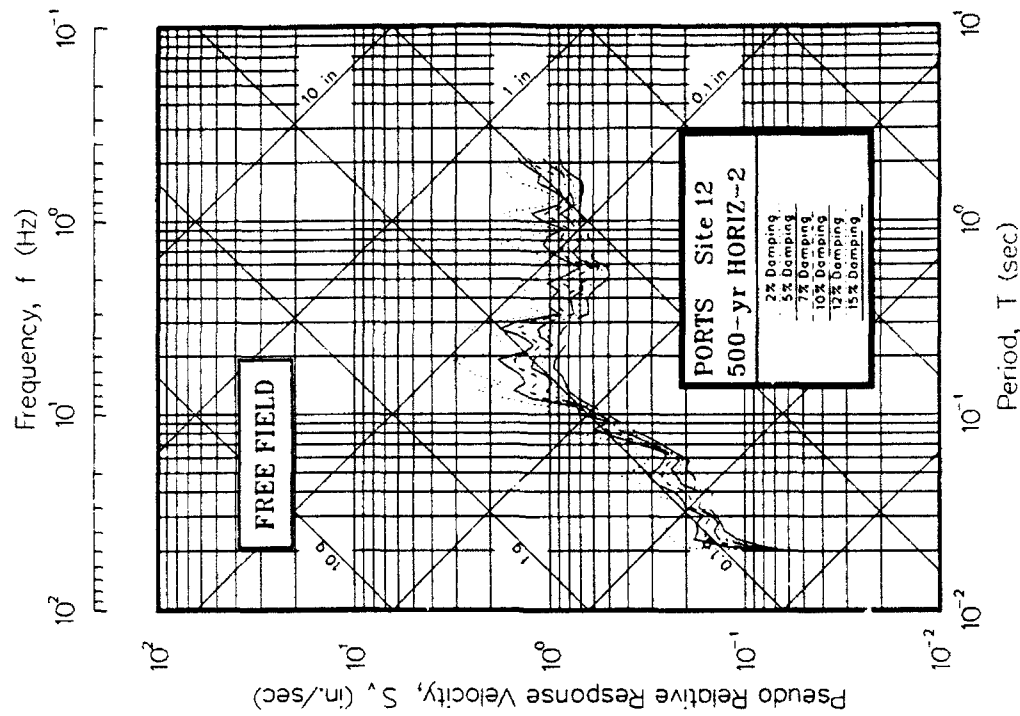
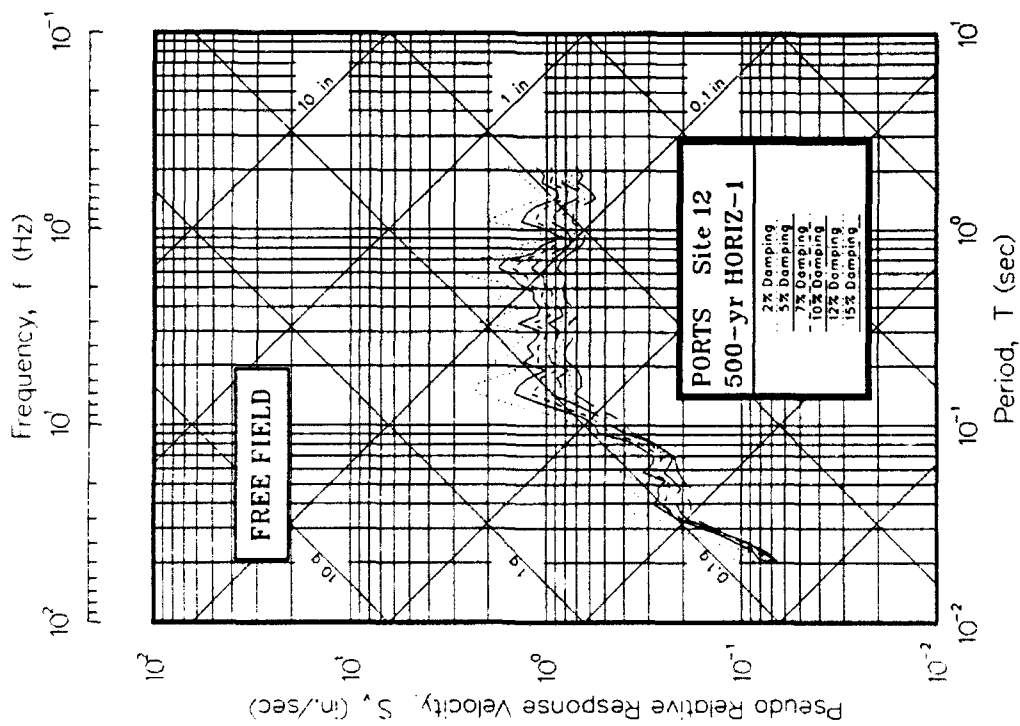


Figure D12. Psuedo-relative velocity spectra in tripartite form at free field for Site 12

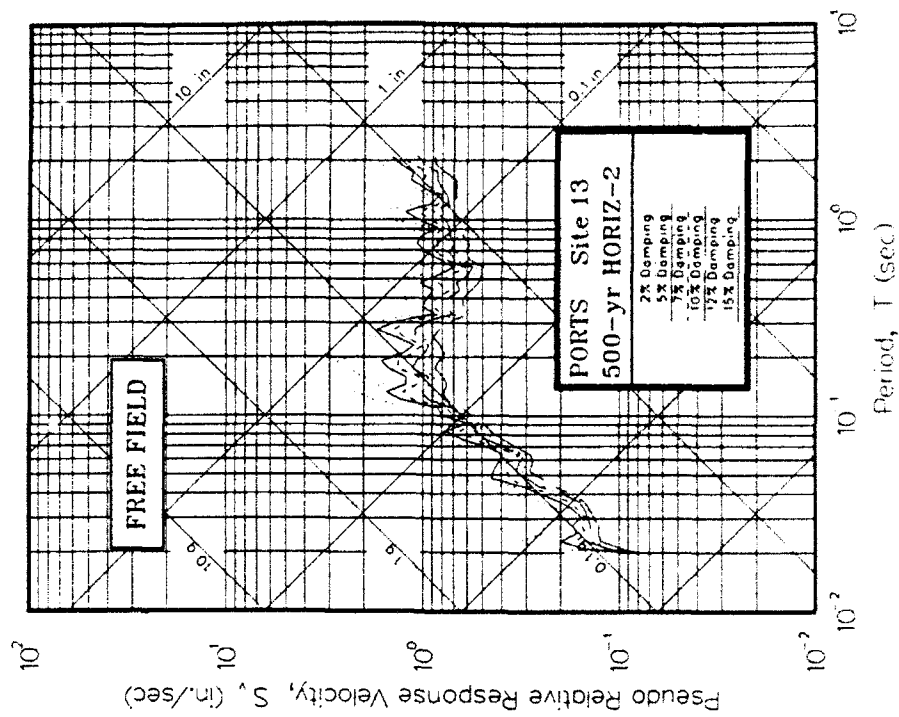
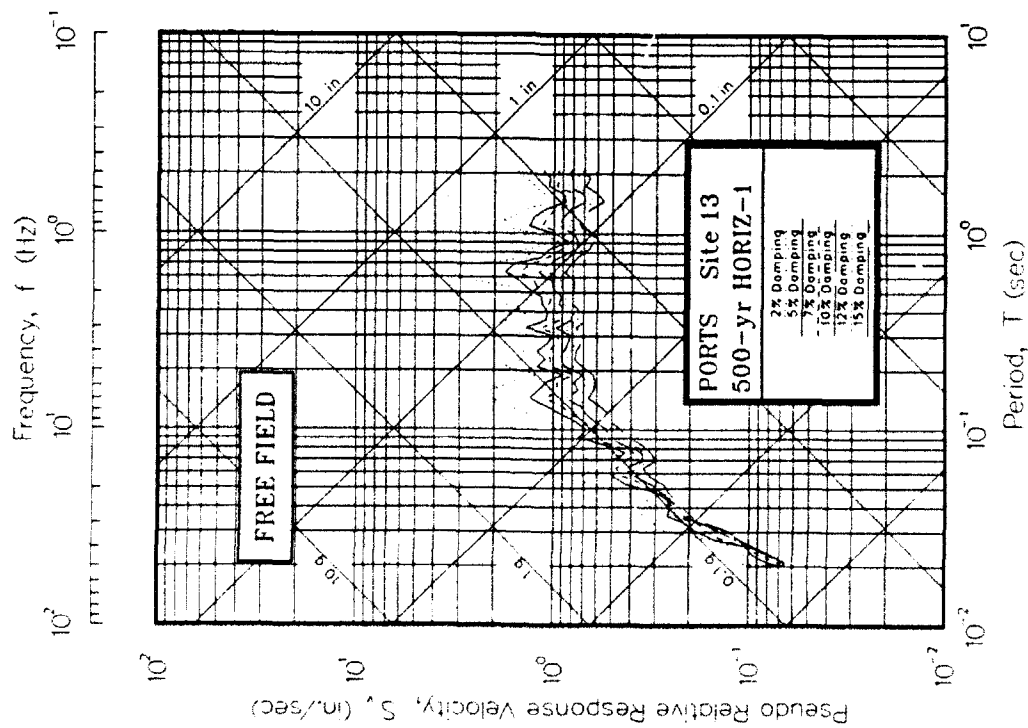


Figure D13. Psuedo-relative velocity spectra in tripartite form at free field for Site 13

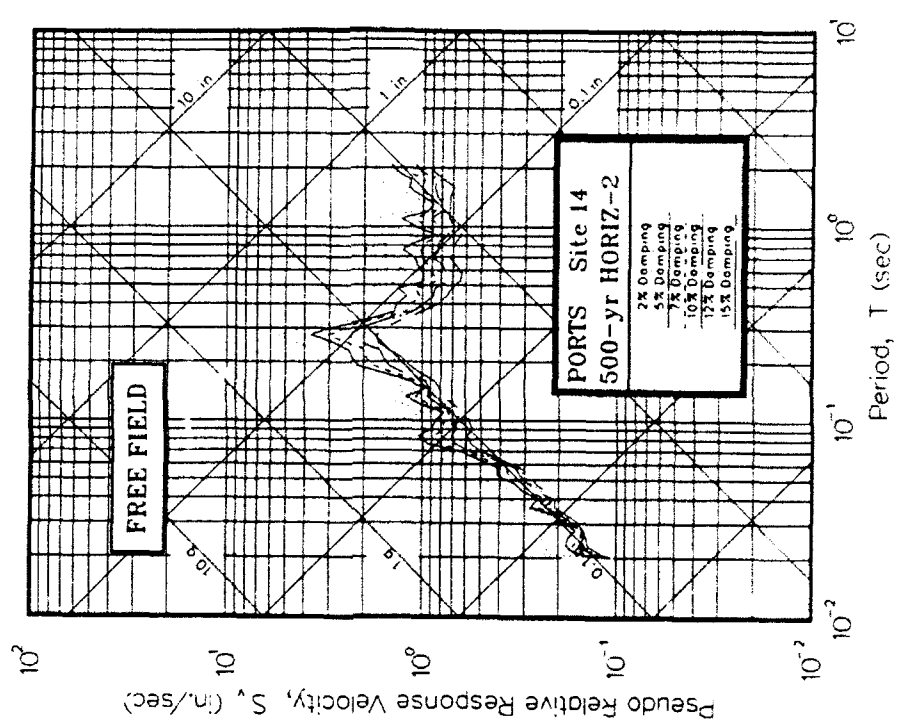
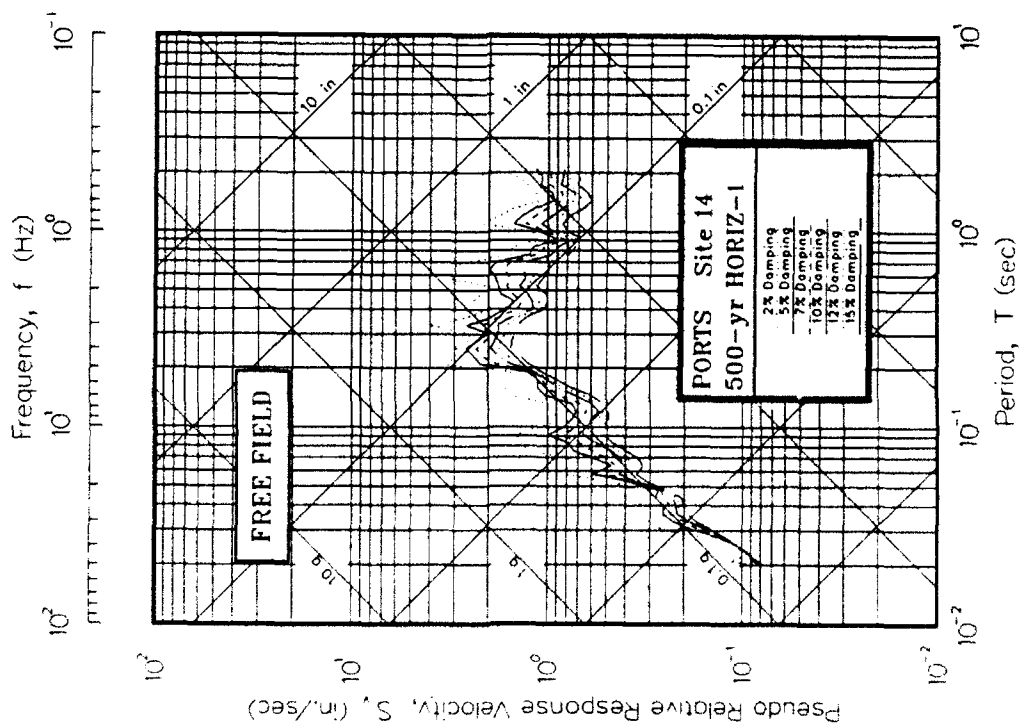


Figure D14. Pseudo-relative velocity spectra in tripartite form at free field for Site 14

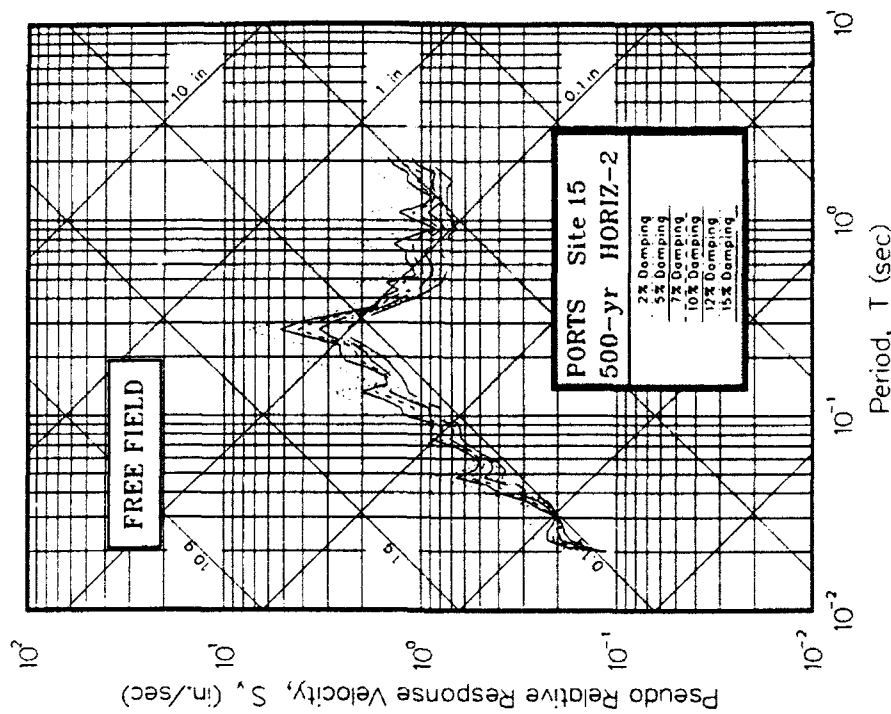
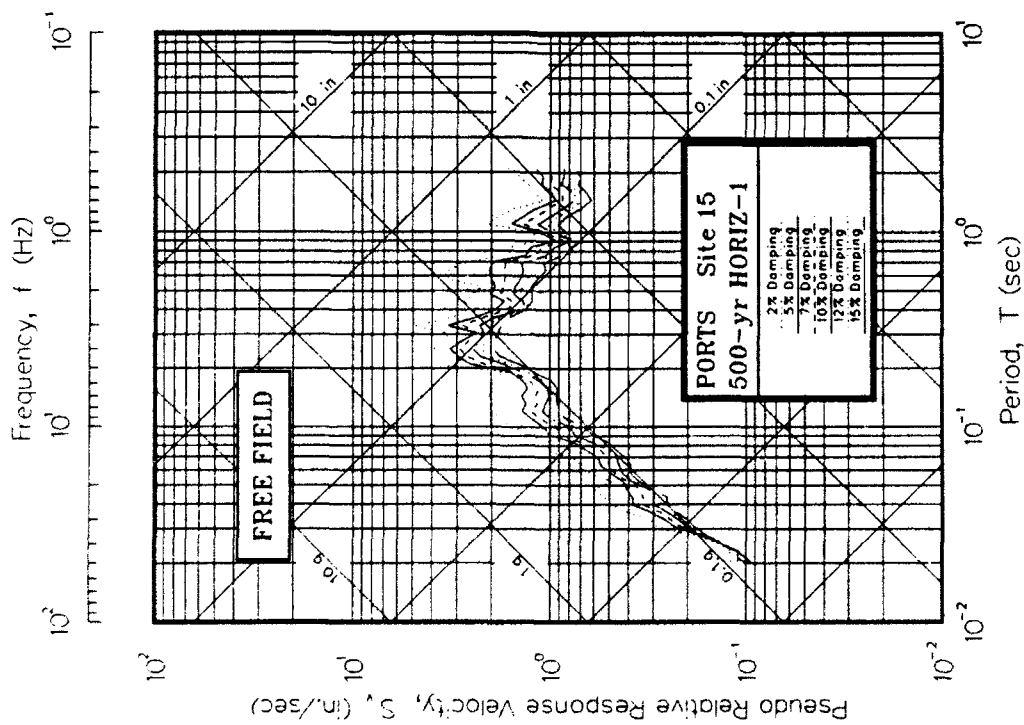


Figure D15. Psuedo-relative velocity spectra in tripartite form at free field for Site 15

APPENDIX E: ACCELERATION SPECTRA FOR 500-YEAR EVENT

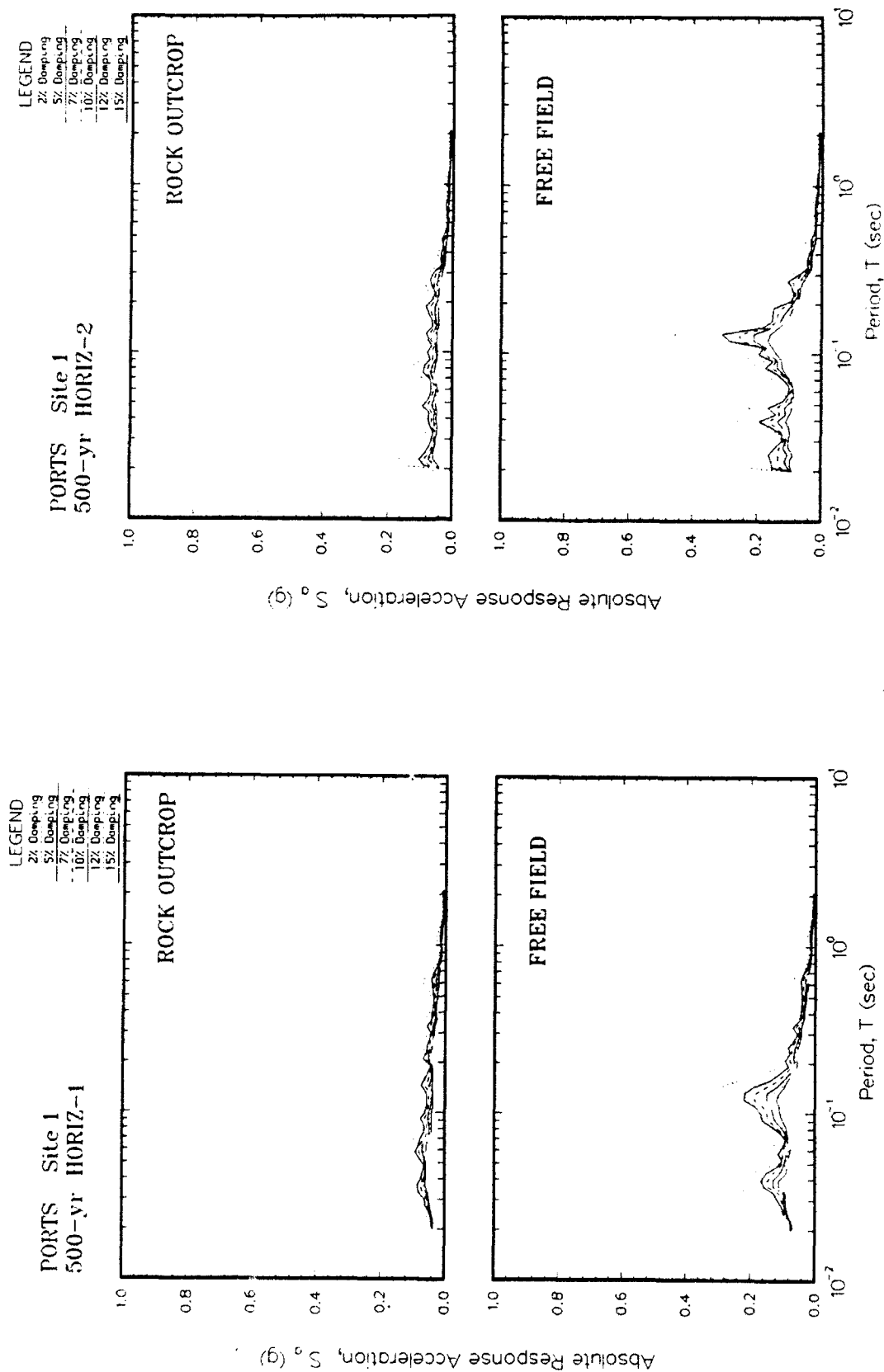


Figure E1. Absolute acceleration response spectra at free field for Site 1

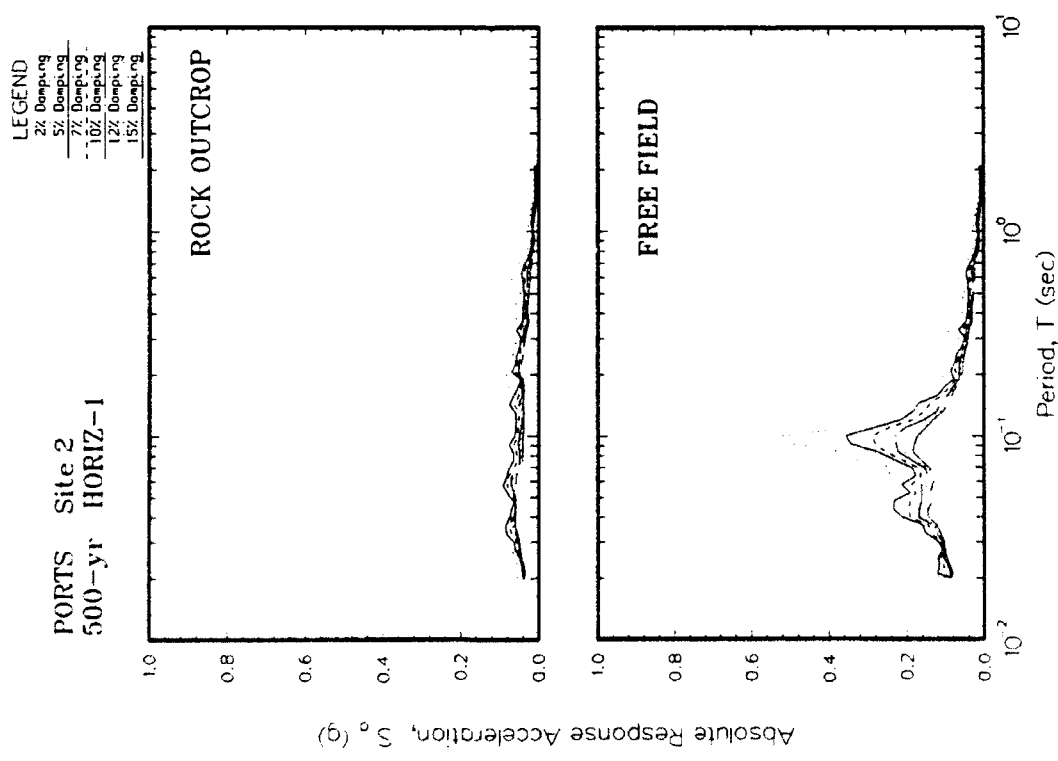
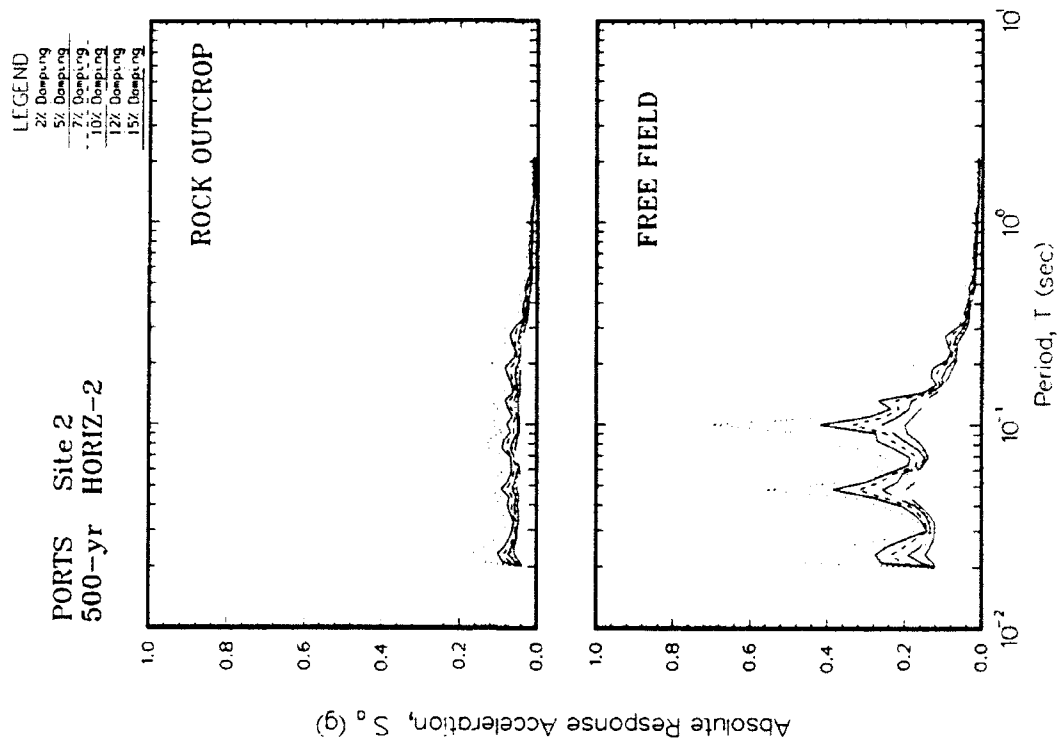


Figure E2. Absolute acceleration response spectra at free field for Site 2

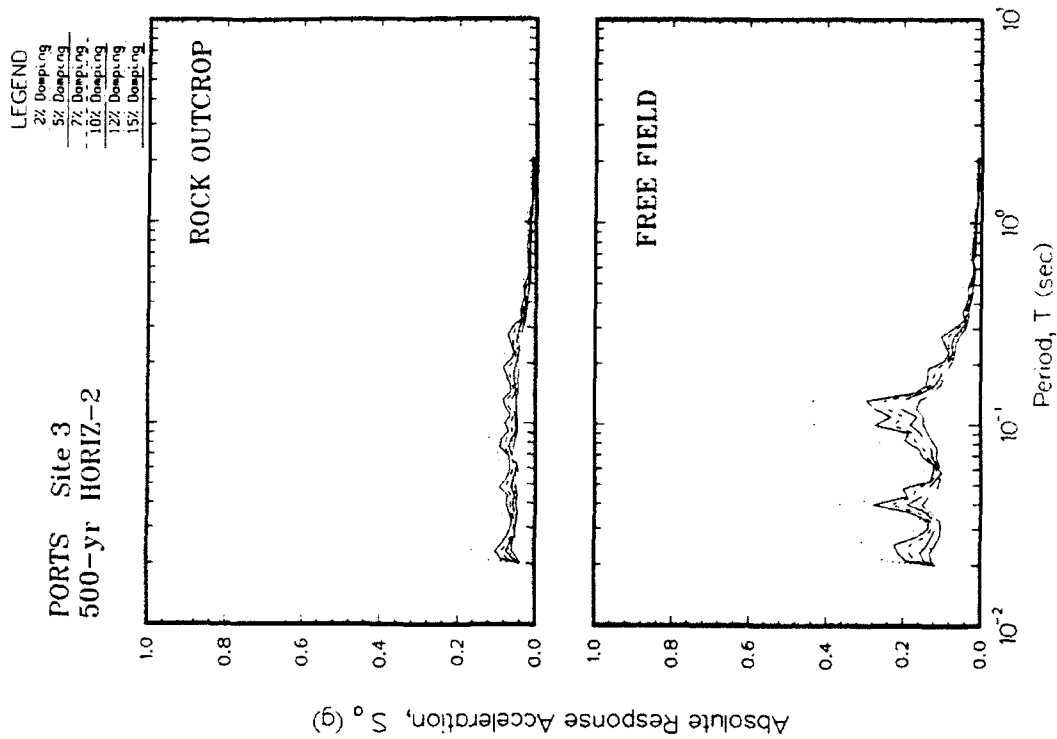
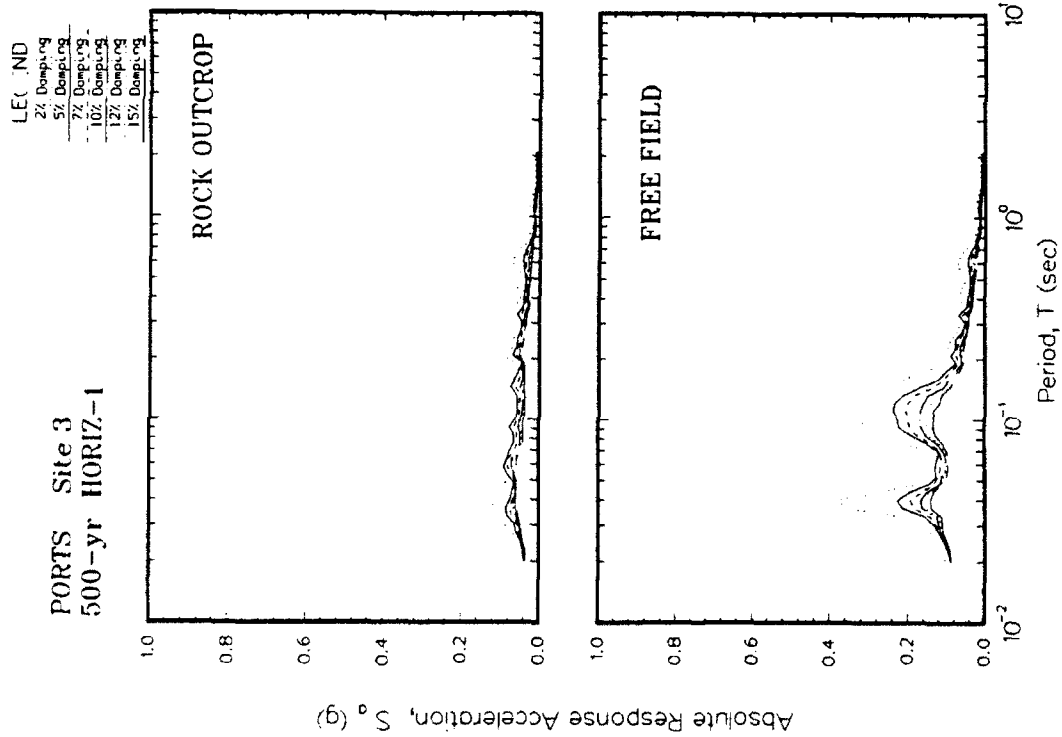


Figure E3. Absolute acceleration response spectra at free field for Site 3

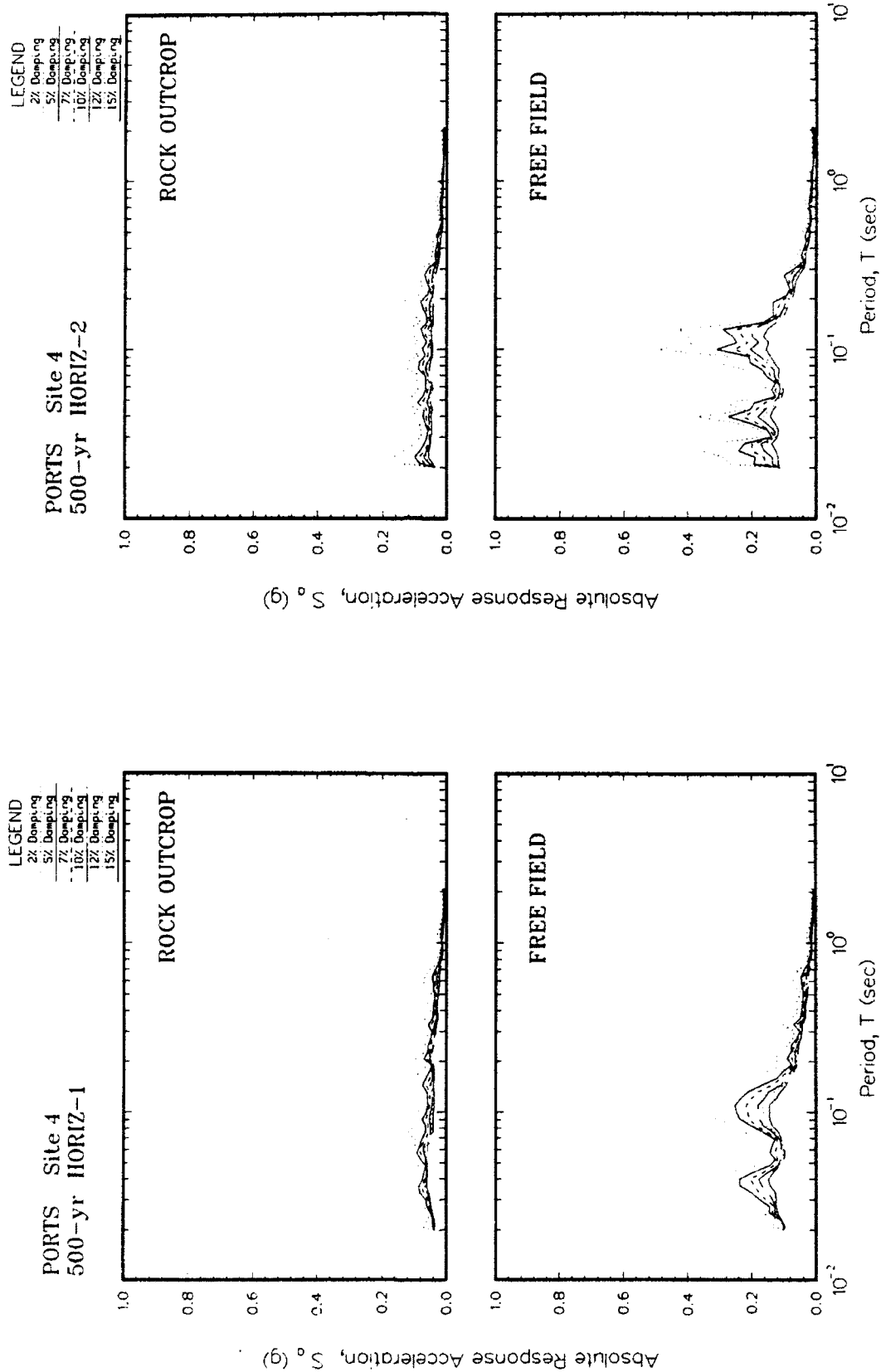


Figure E4. Absolute acceleration response spectra at free field for Site 4

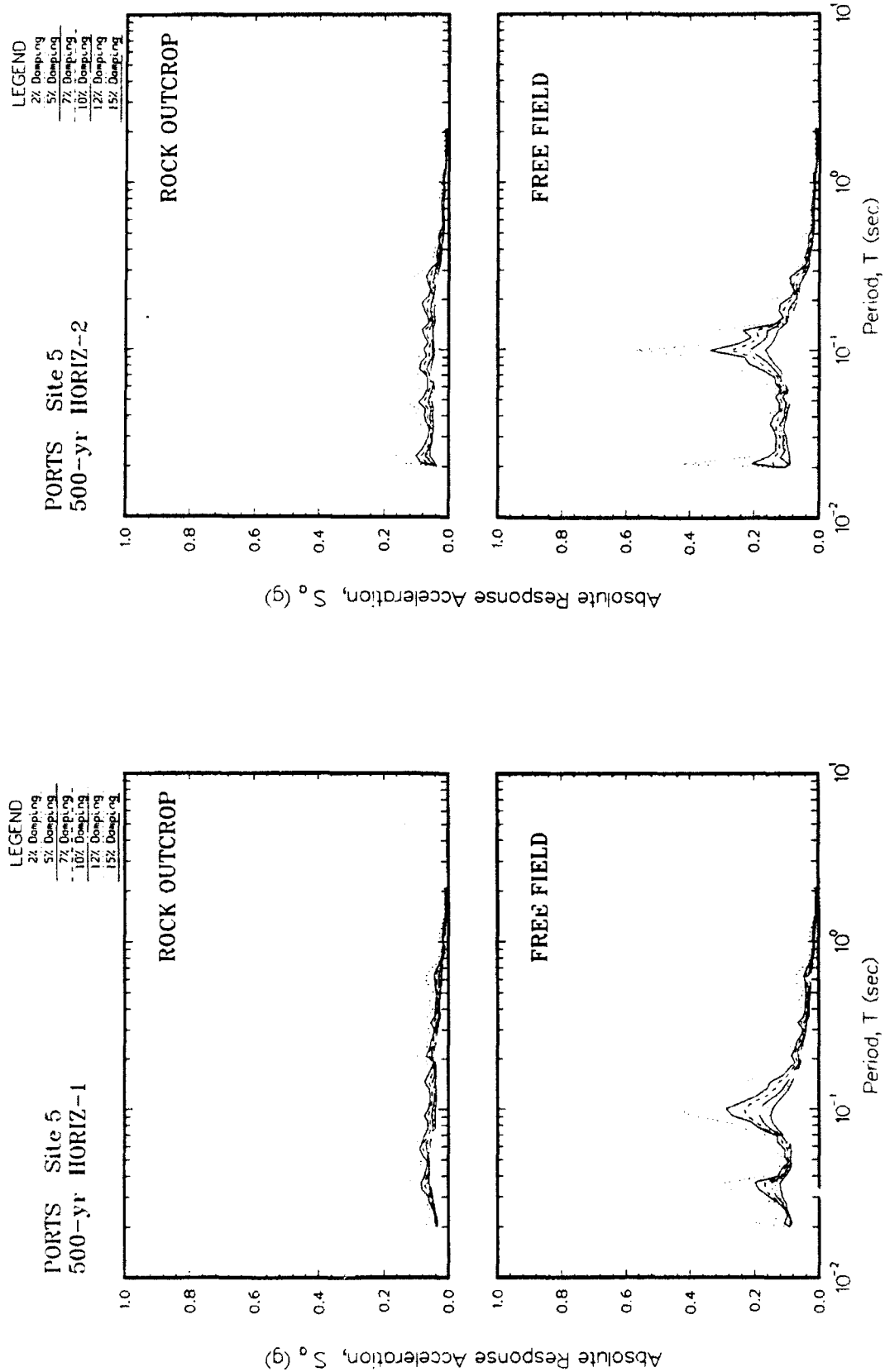


Figure E5. Absolute acceleration response spectra at free field for Site 5

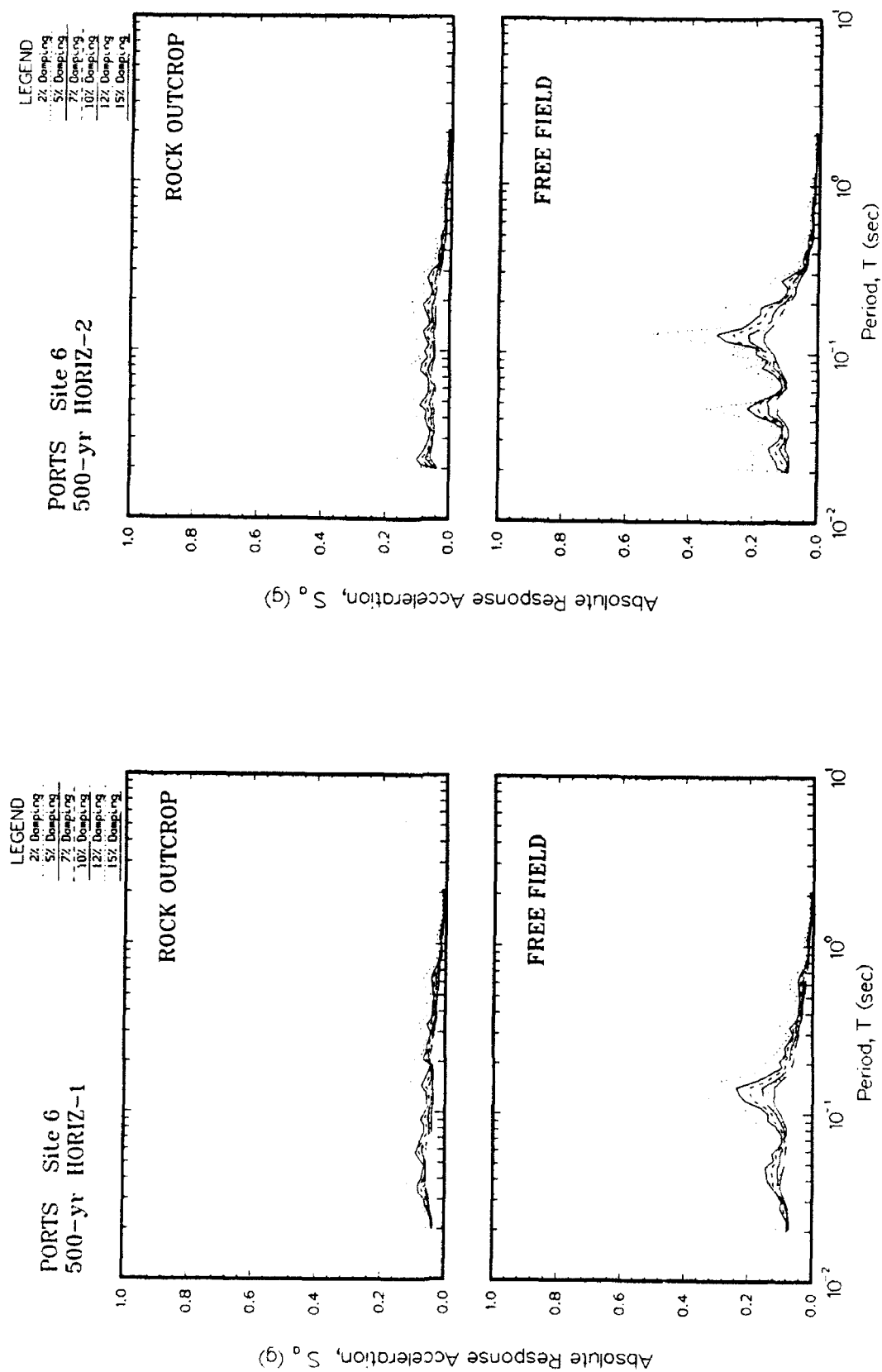


Figure E6. Absolute acceleration response spectra at free field for Site 6

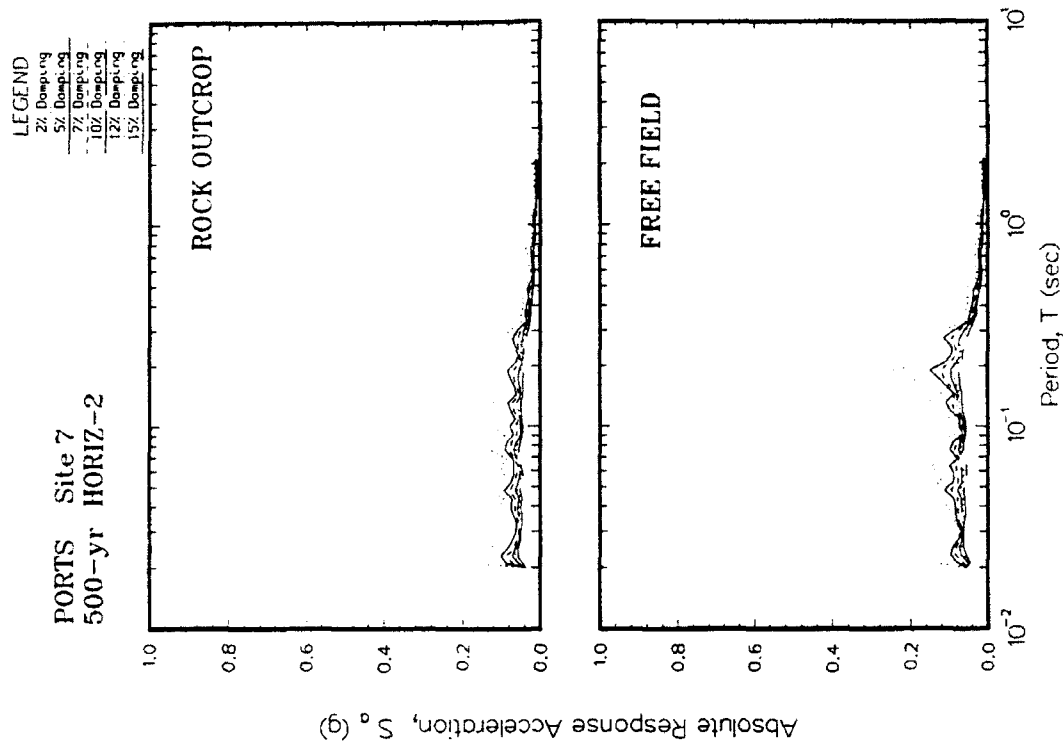
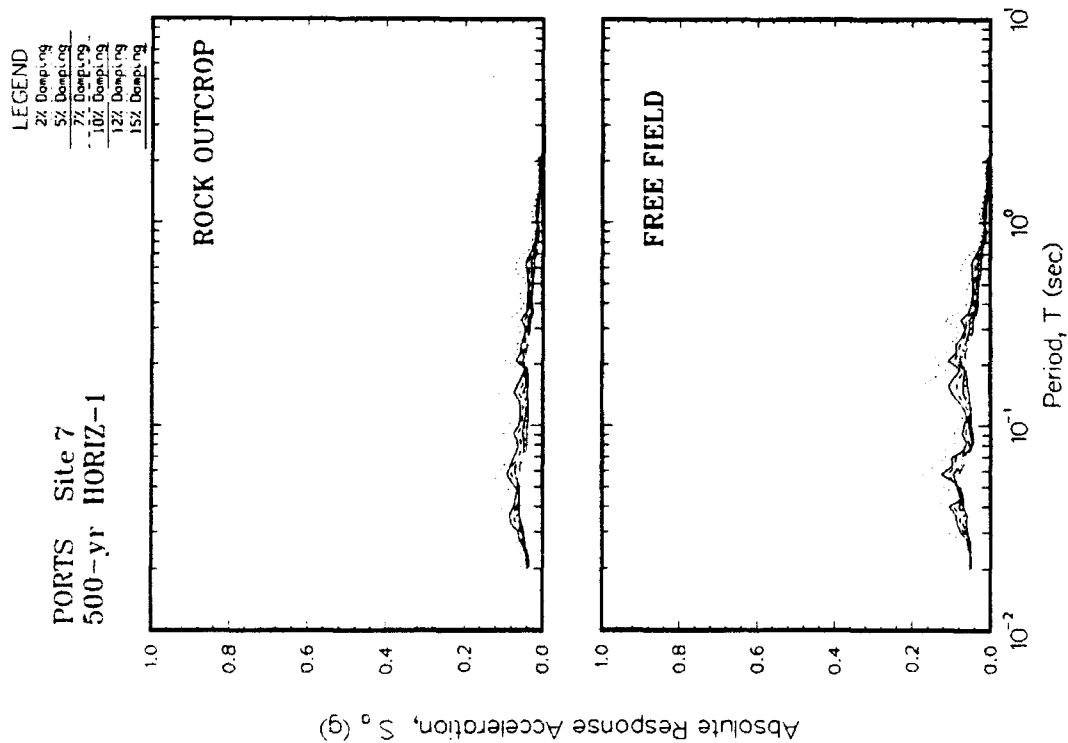


Figure E7. Absolute acceleration response spectra at free field for Site 7

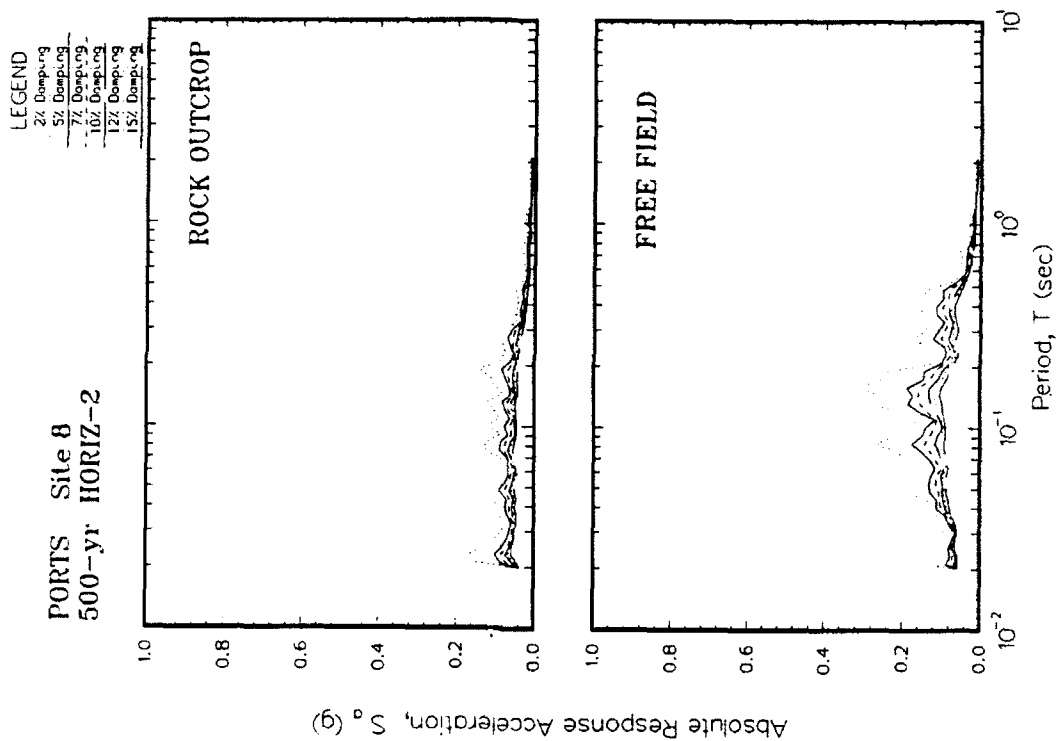
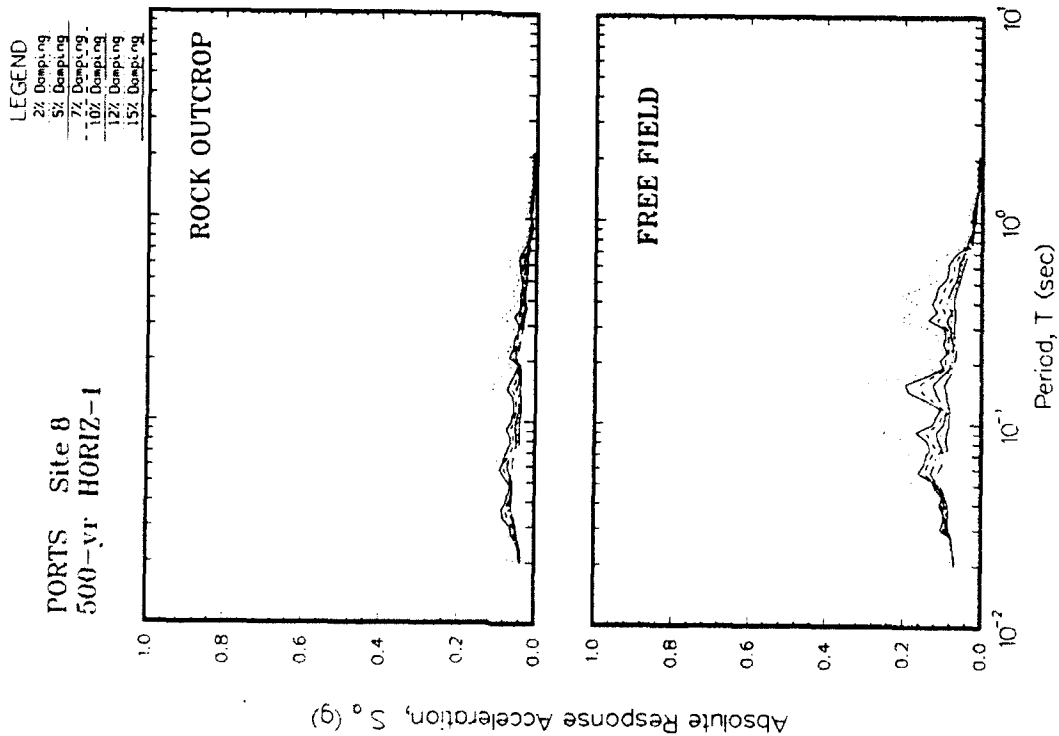


Figure E8. Absolute acceleration response spectra at free field for Site 8

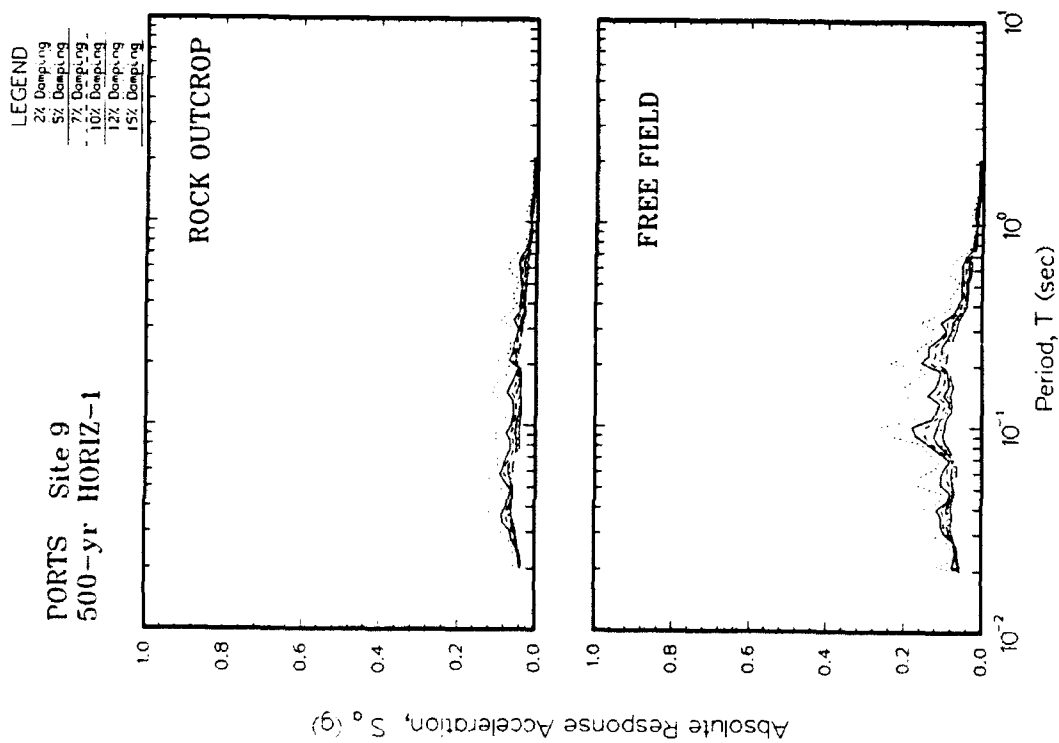
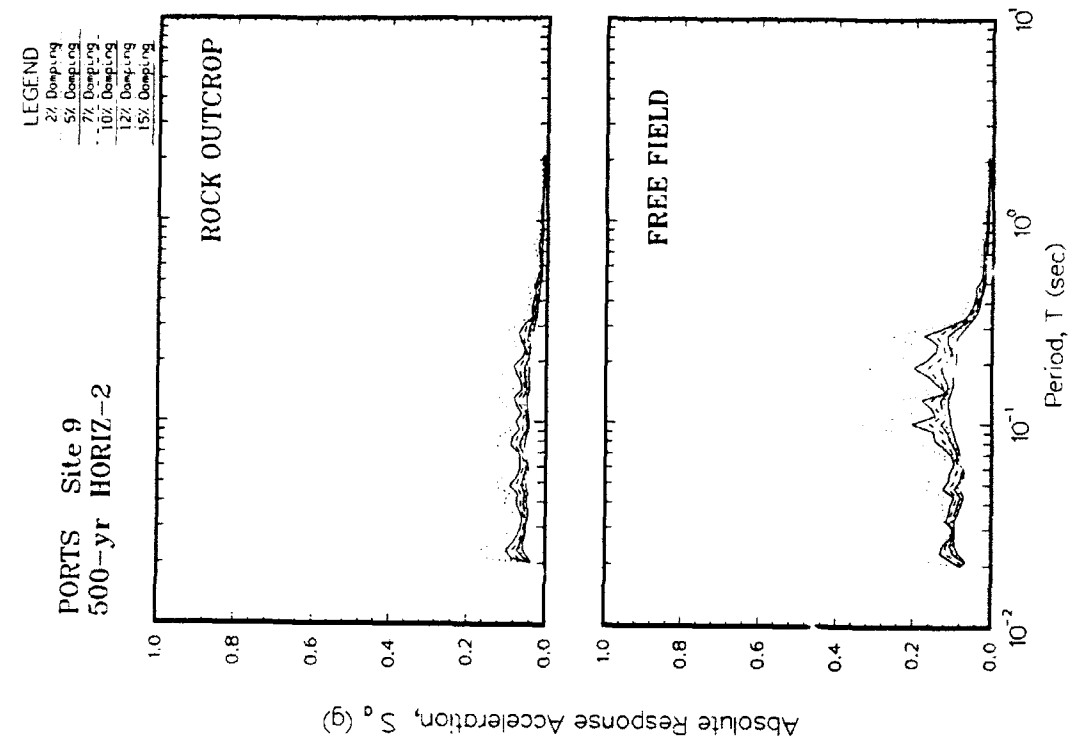


Figure E9. Absolute acceleration response spectra at free field for Site 9

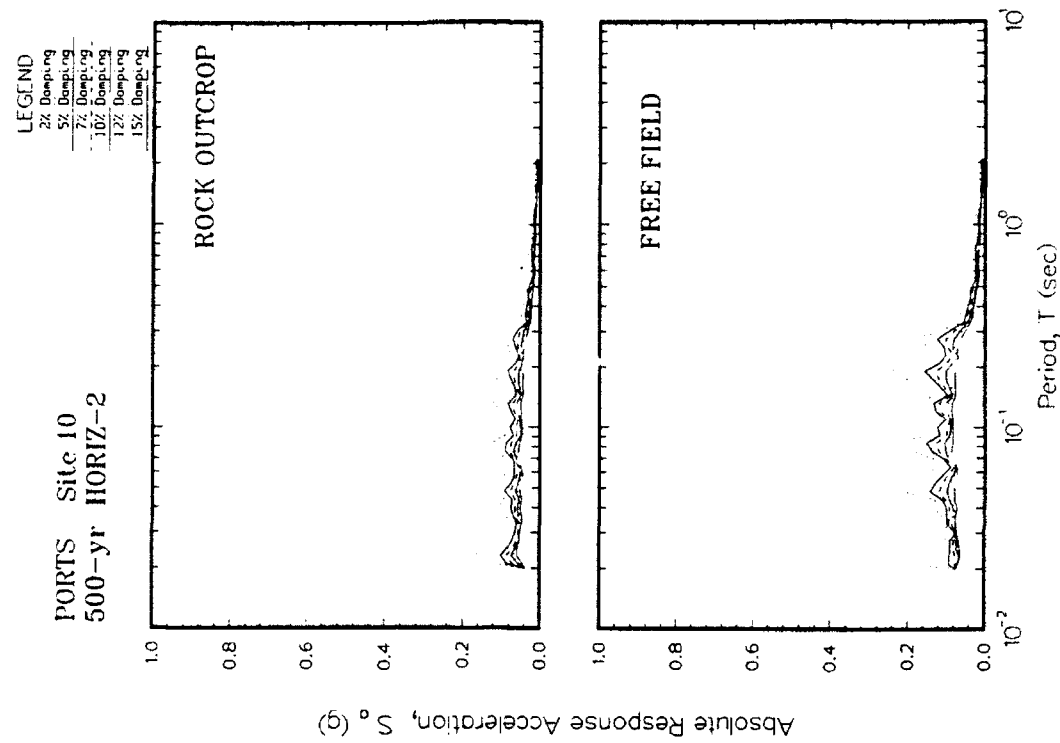
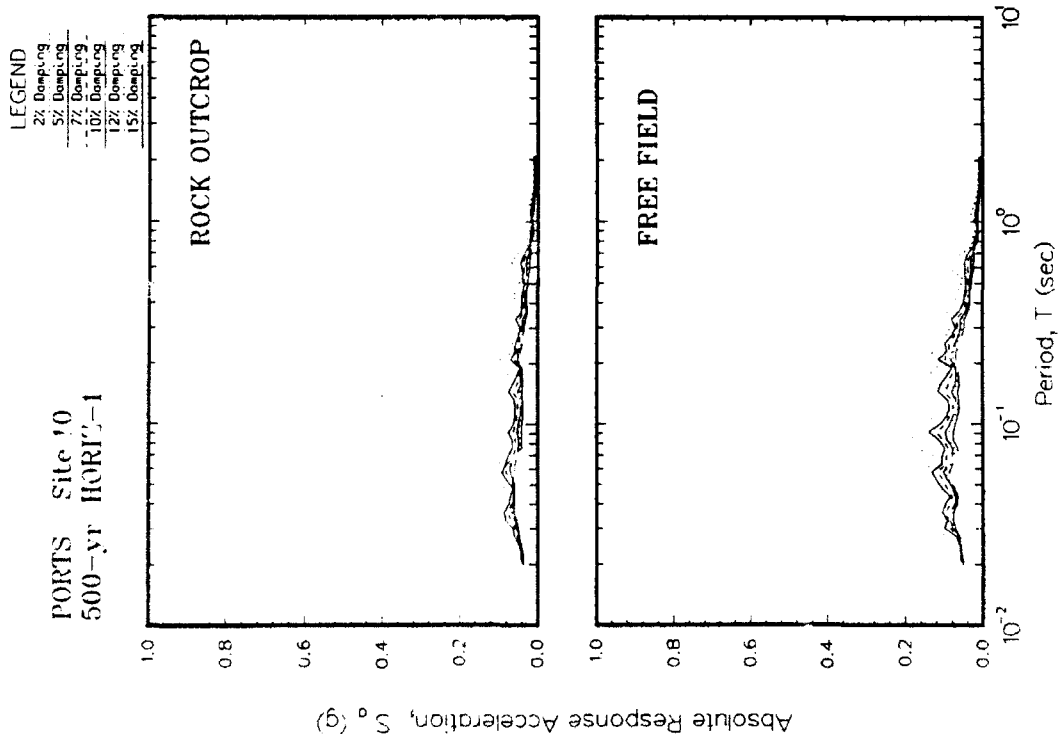


Figure E10. Absolute acceleration response spectra at free field for Site 10

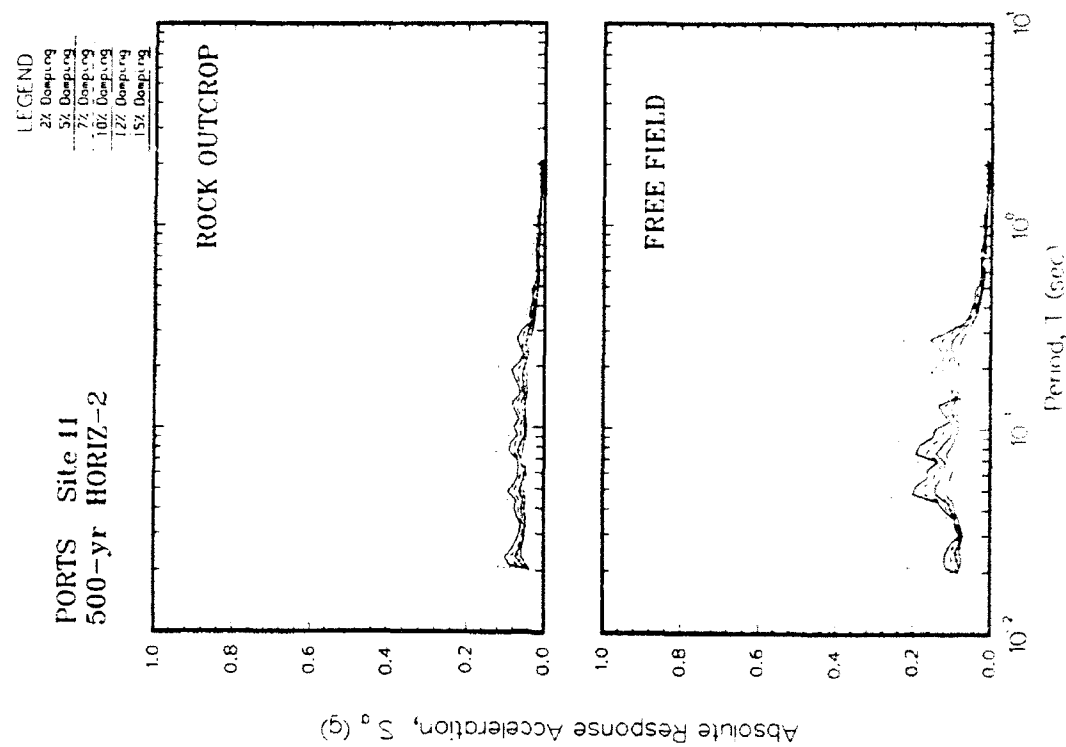
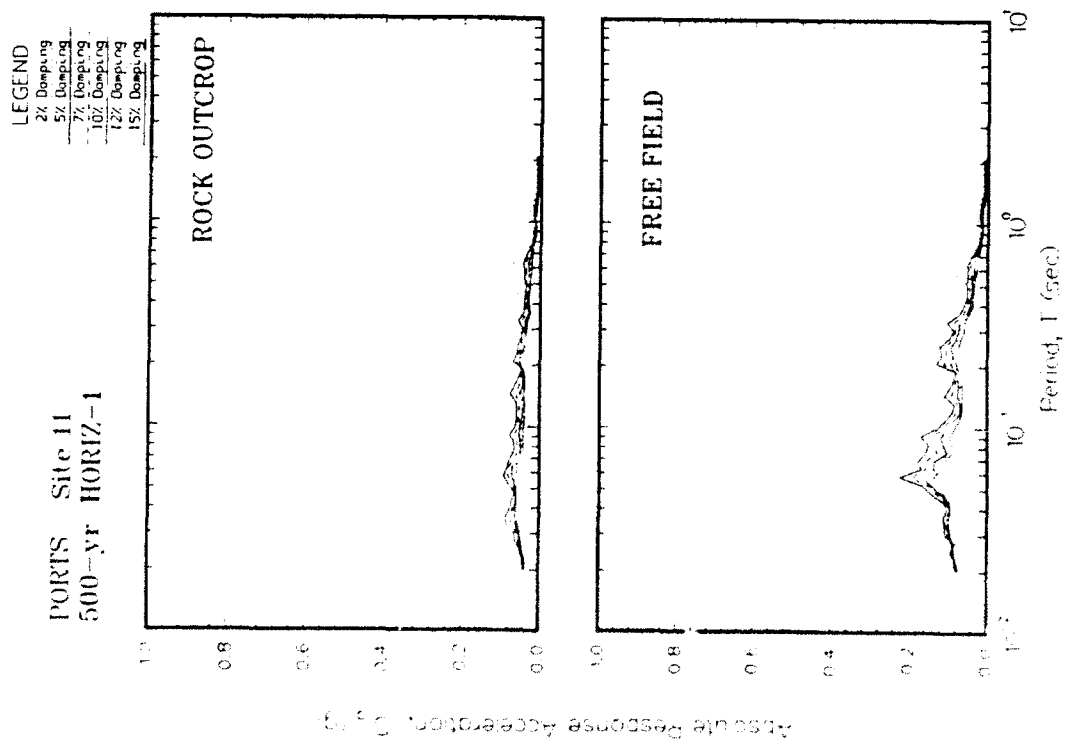


Figure E11. Absolute acceleration response spectra at free field for Site 11

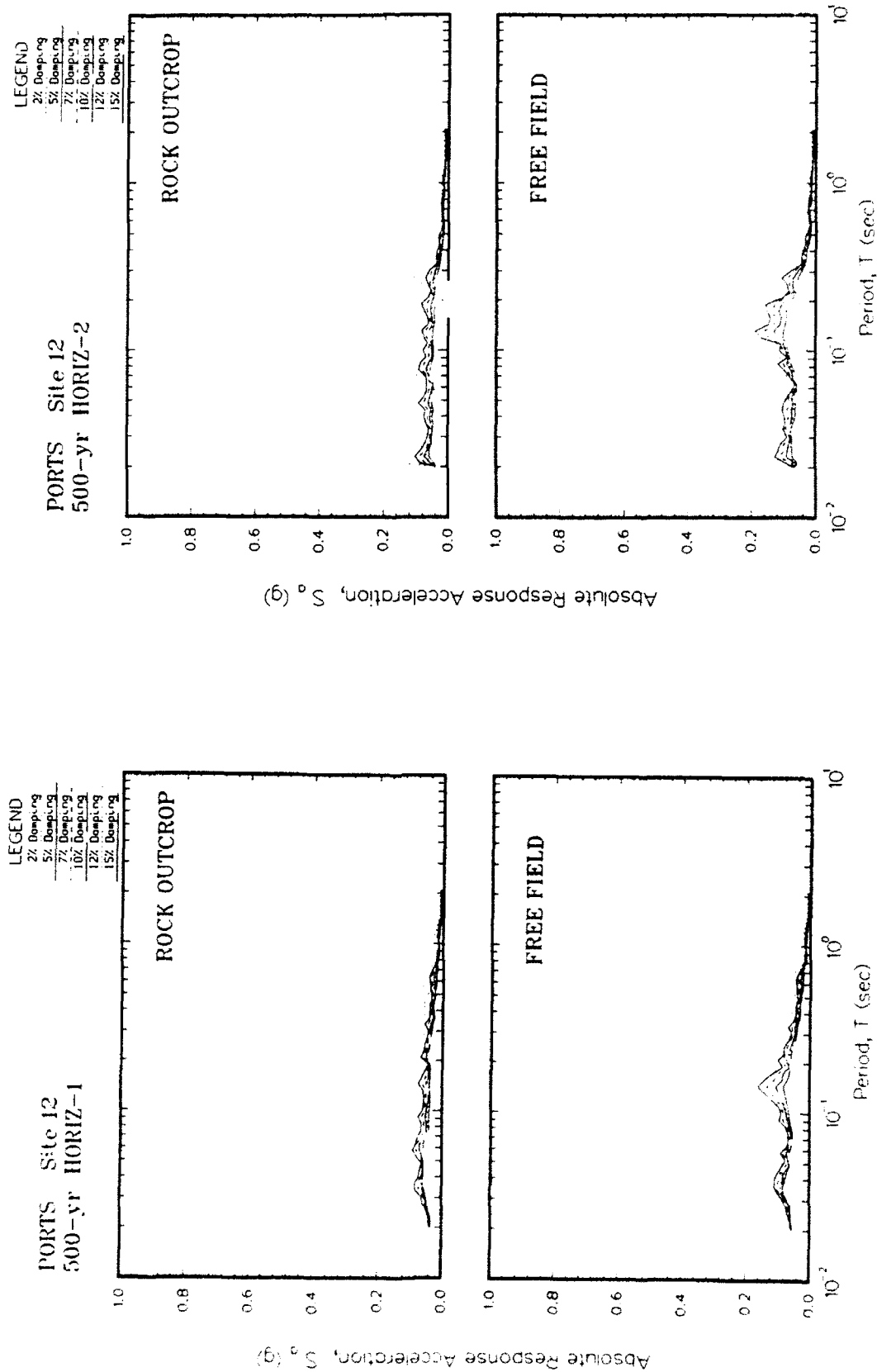


Figure E12. Absolute acceleration response spectra at free field for Site 12

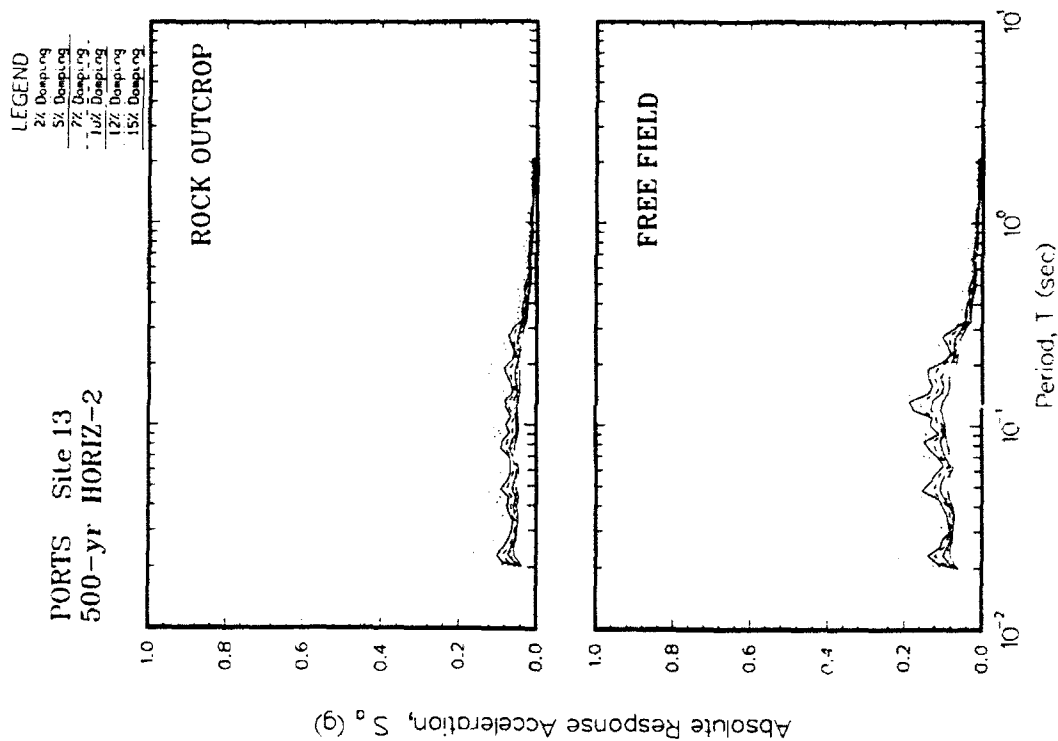
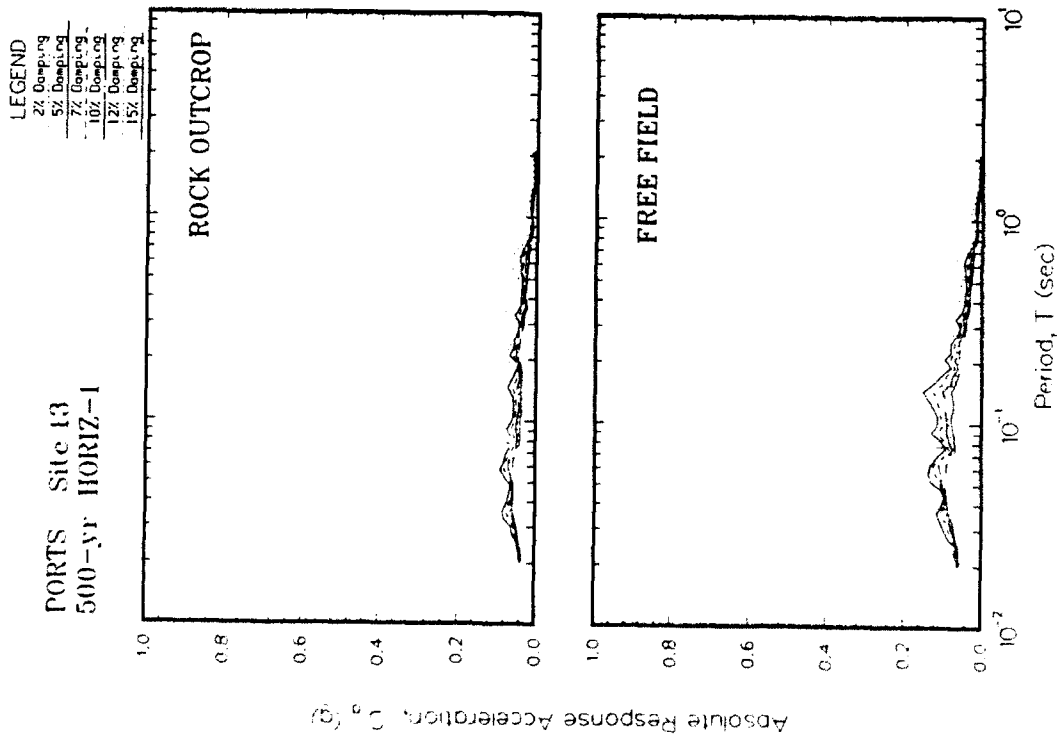


Figure E13. Absolute acceleration response spectra at free field for Site 13

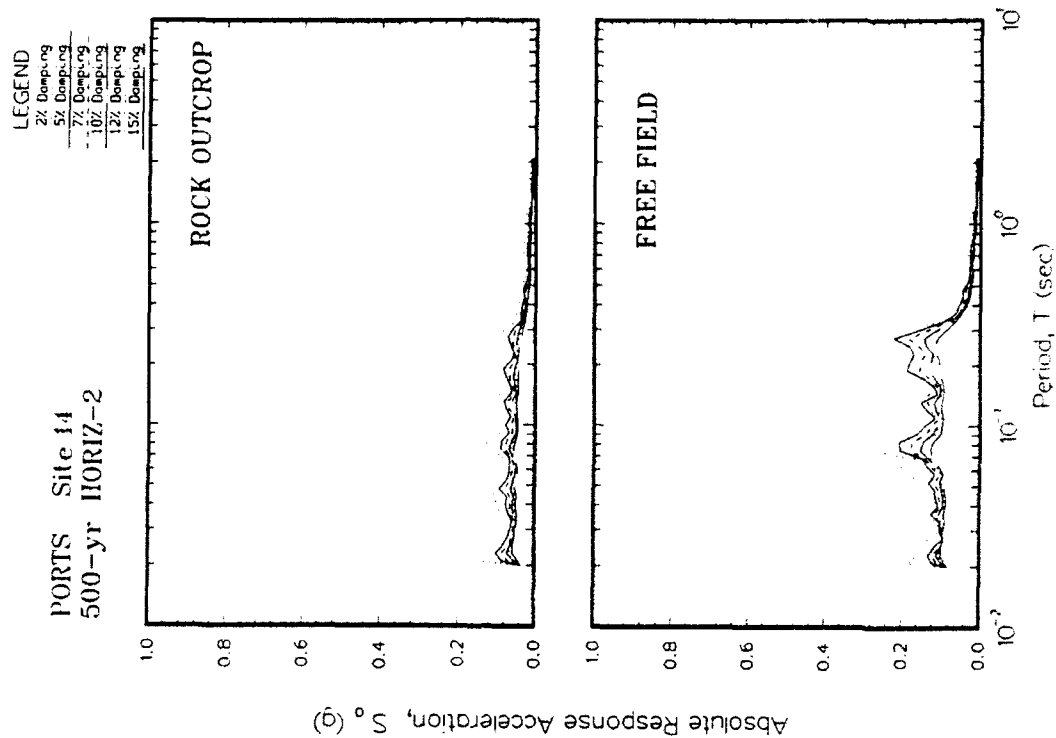
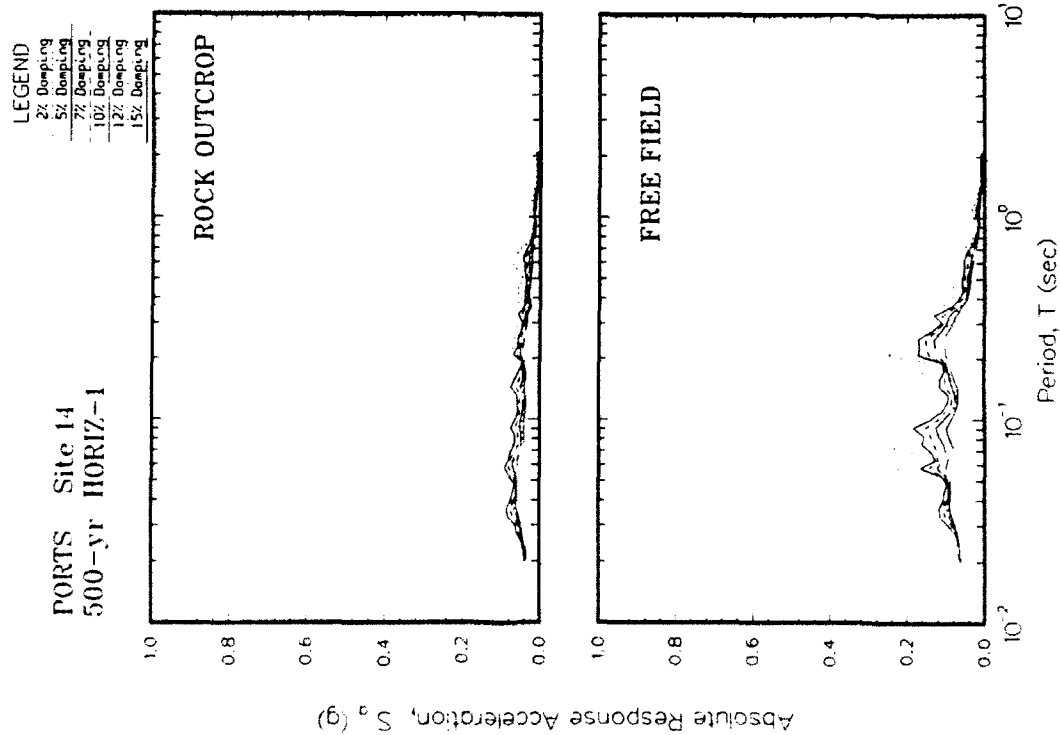


Figure E14. Absolute acceleration response spectra at free field for Site 14

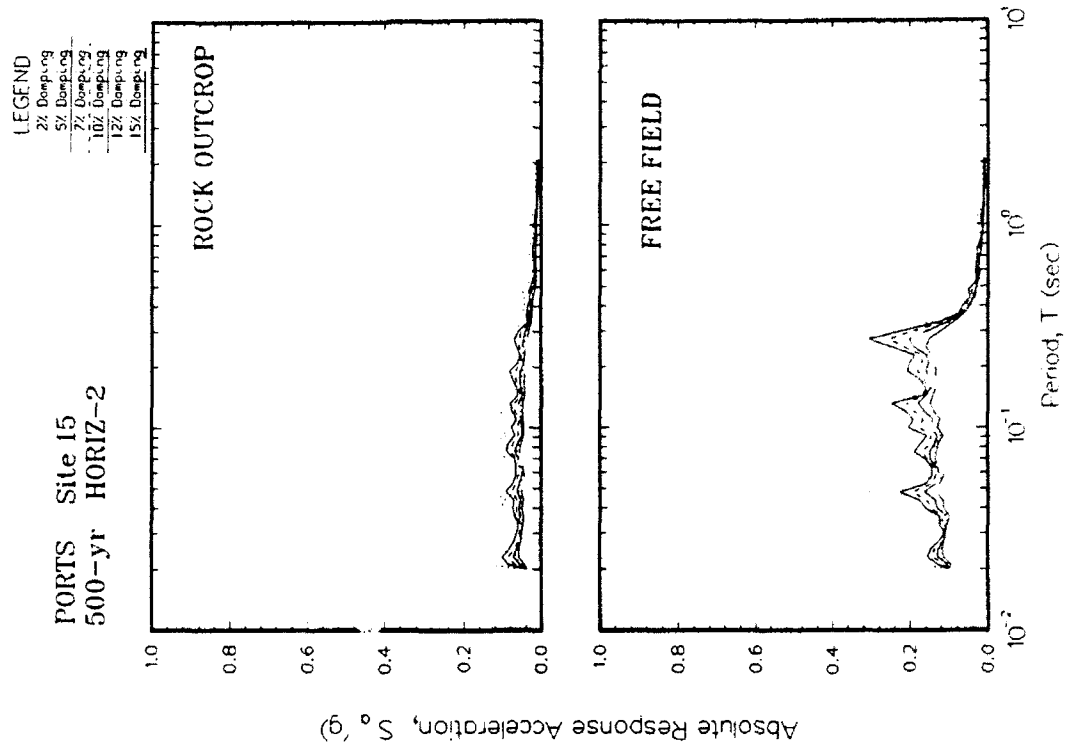
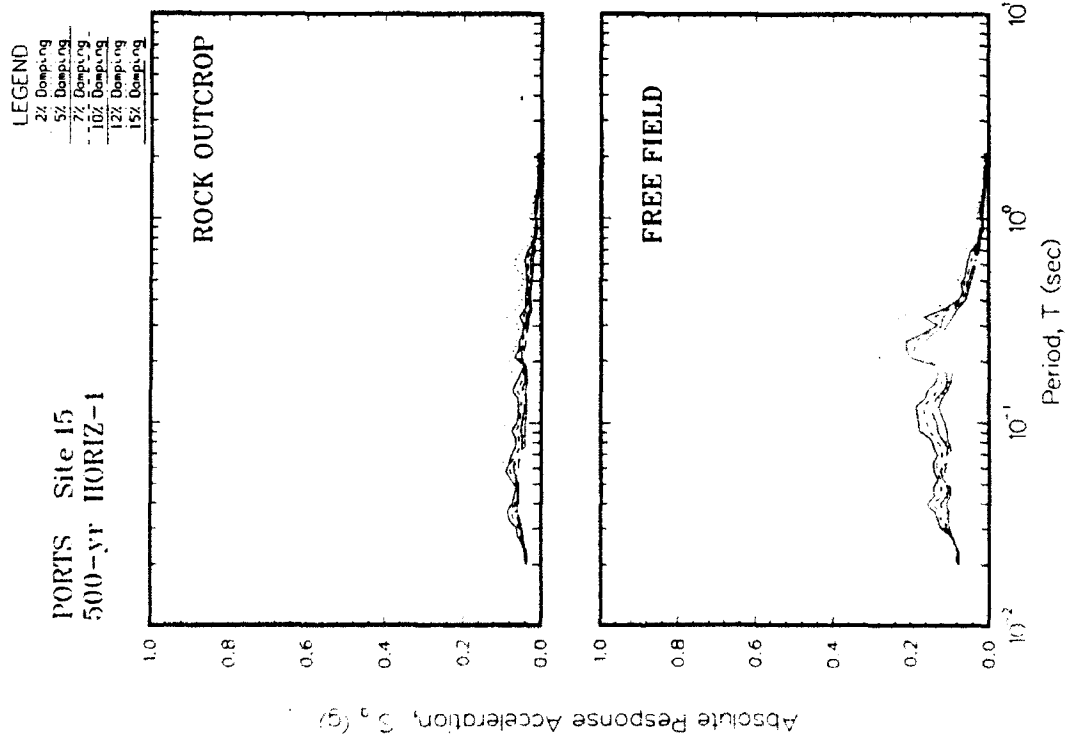


Figure E15. Absolute acceleration response spectra at free field for Site 15

APPENDIX F: RATIO OF ACCELERATION SPECTRA FOR 500-YEAR EVENT

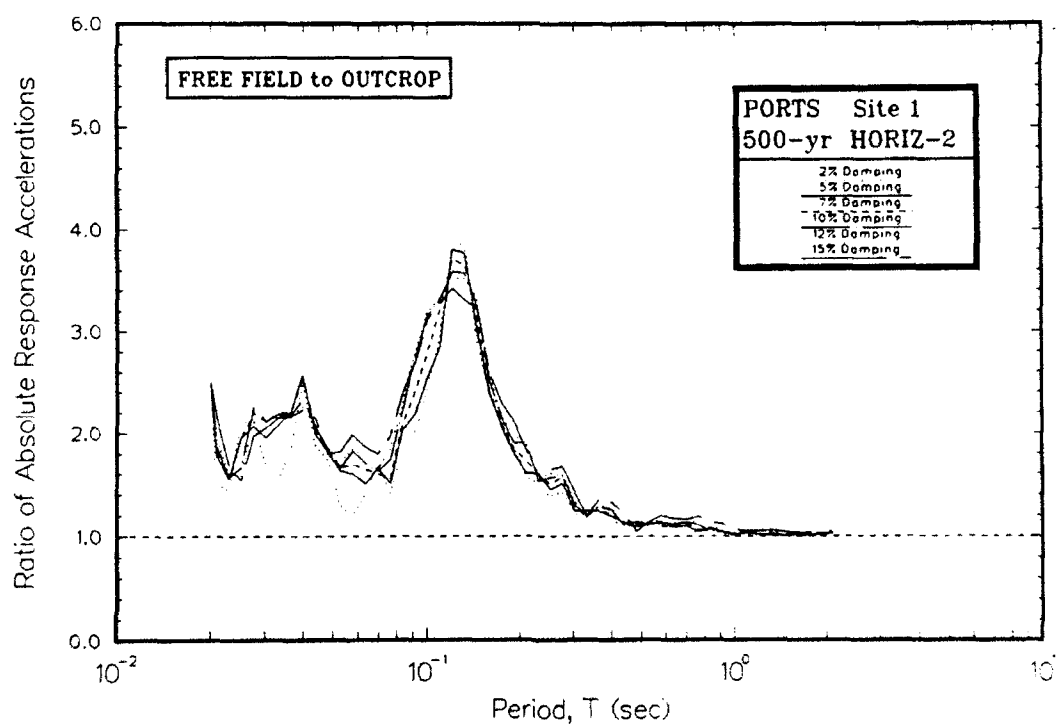
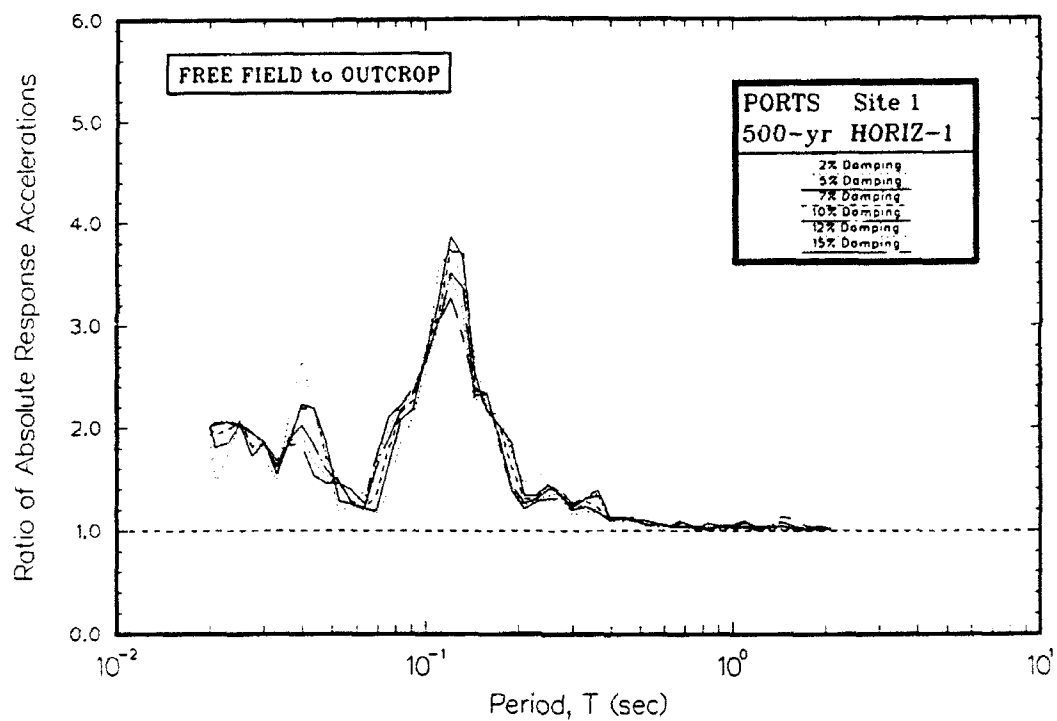


Figure F1. Ratio of absolute acceleration response spectra at free field to rock for Site 1

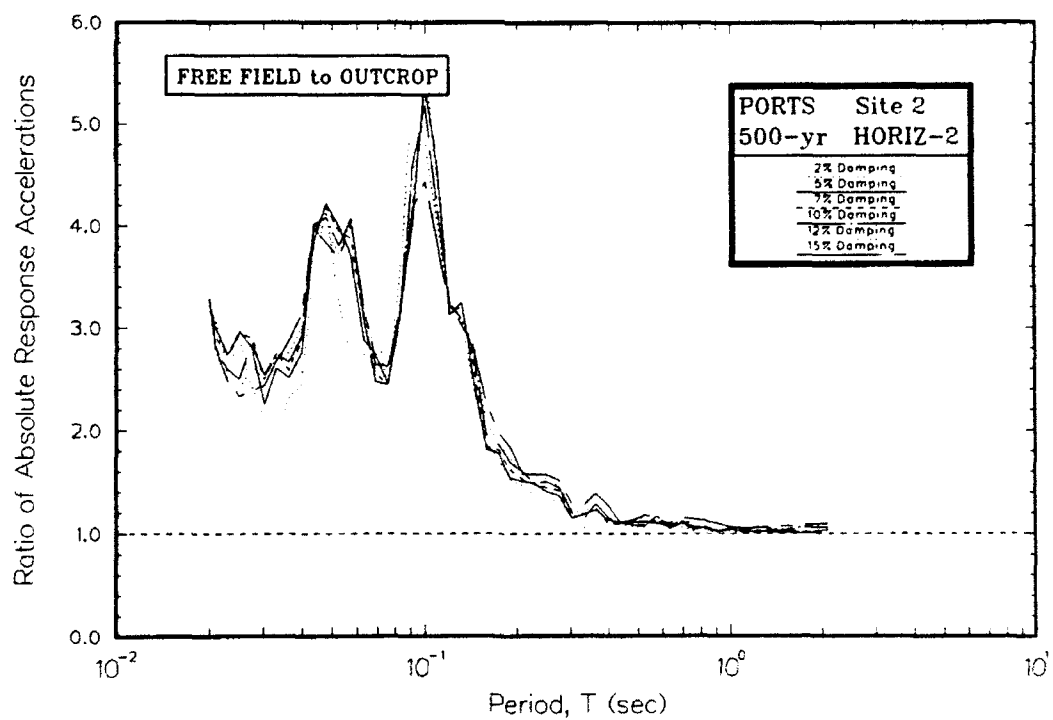
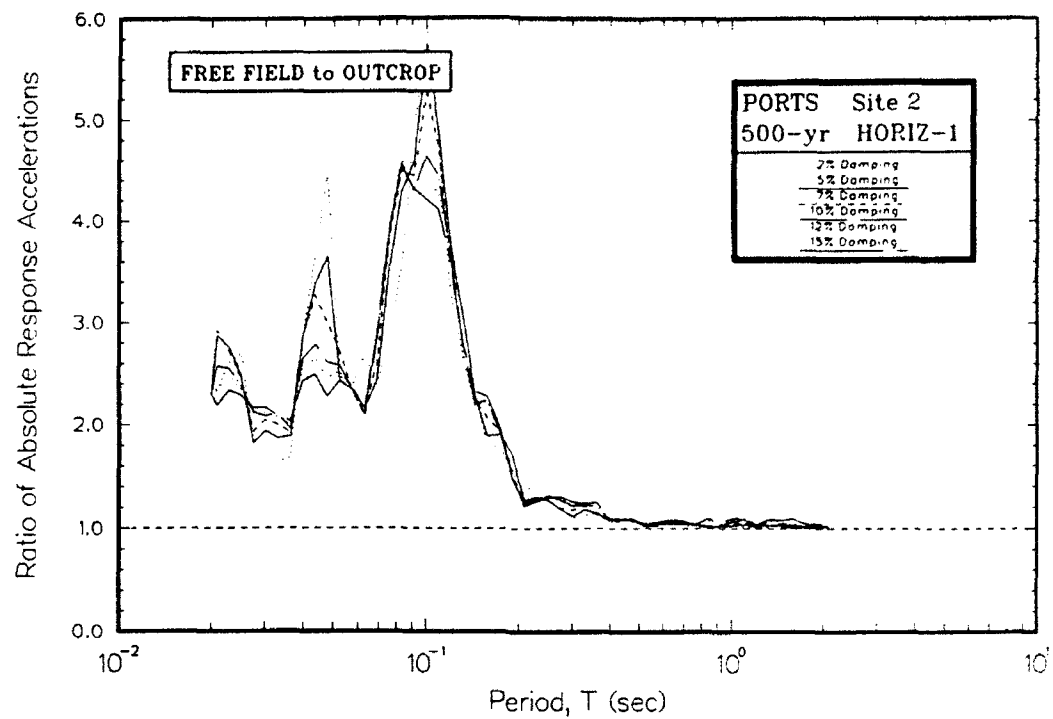


Figure F2. Ratio of absolute acceleration response spectra at free field to rock for Site 2

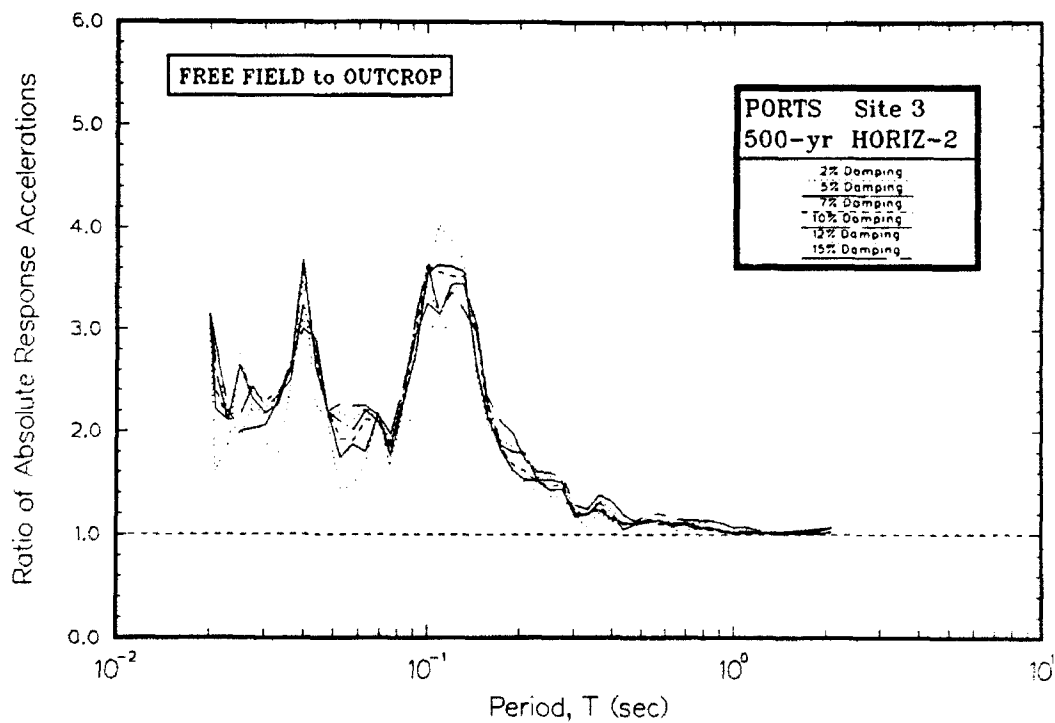
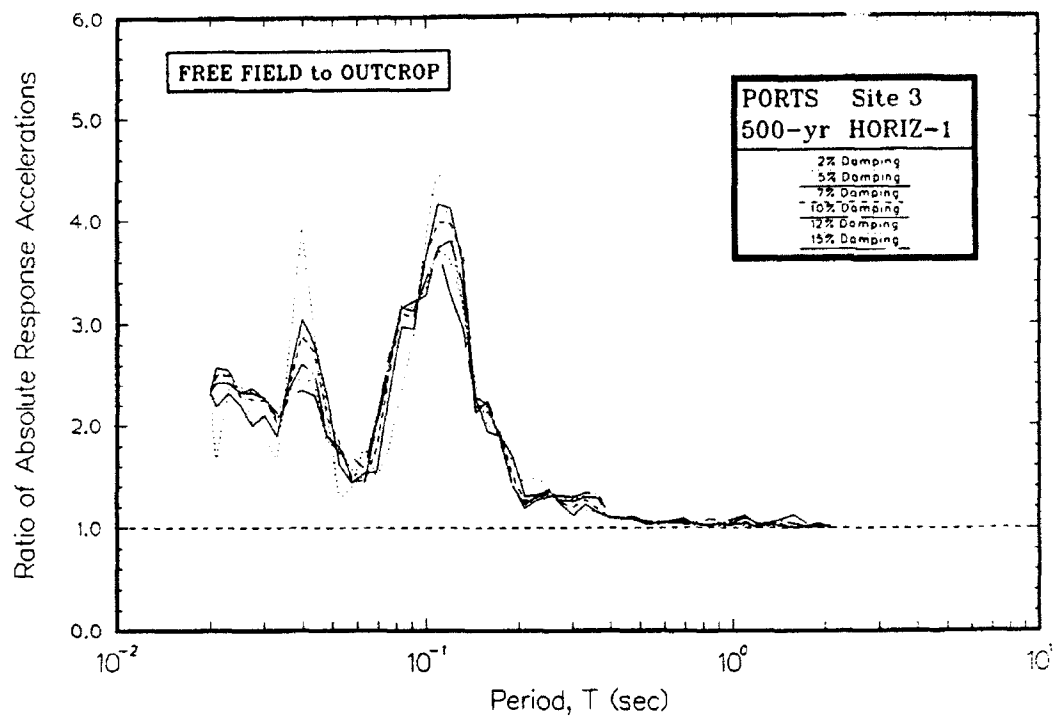


Figure F3. Ratio of absolute acceleration response spectra at free field to rock for Site 3

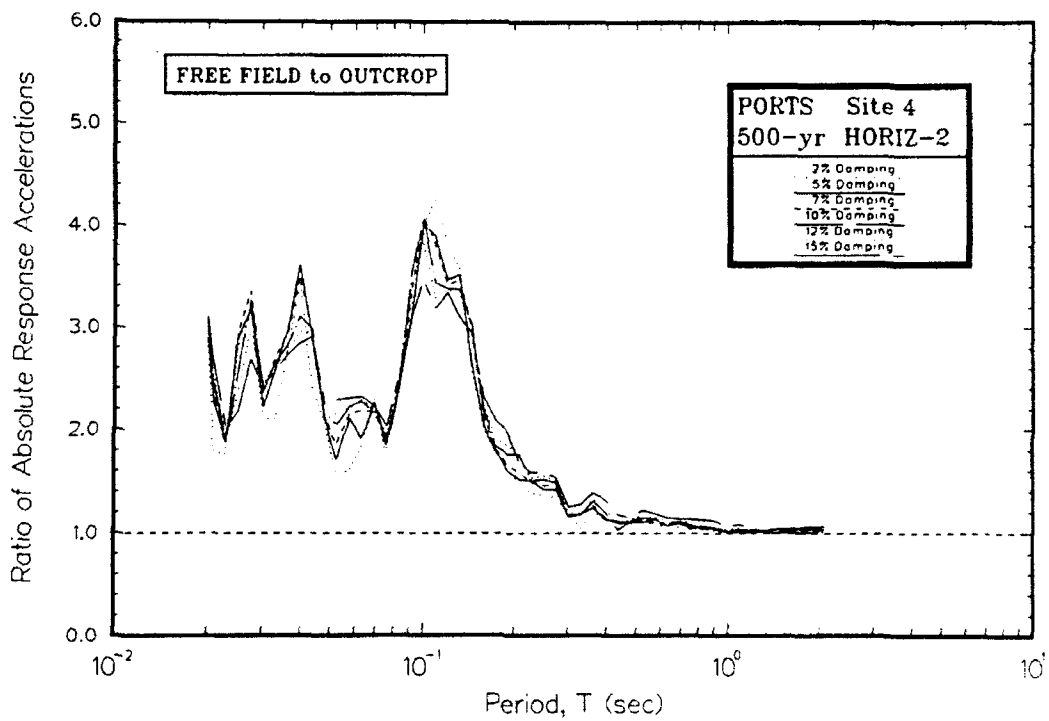
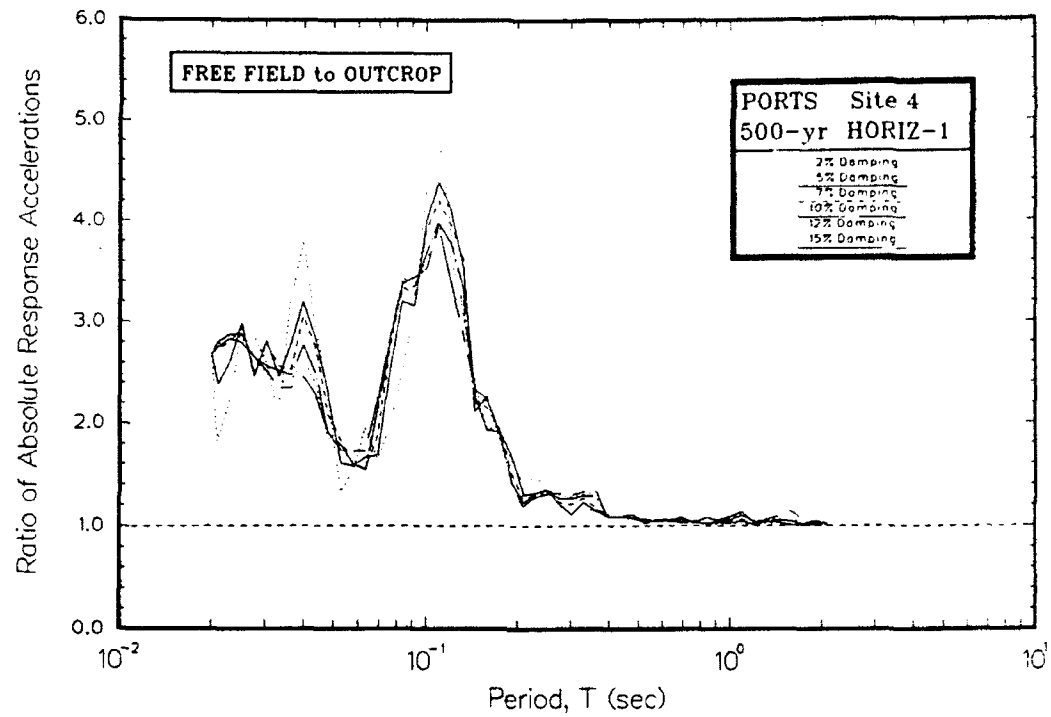


Figure F4. Ratio of absolute acceleration response spectra at free field to rock for Site 4

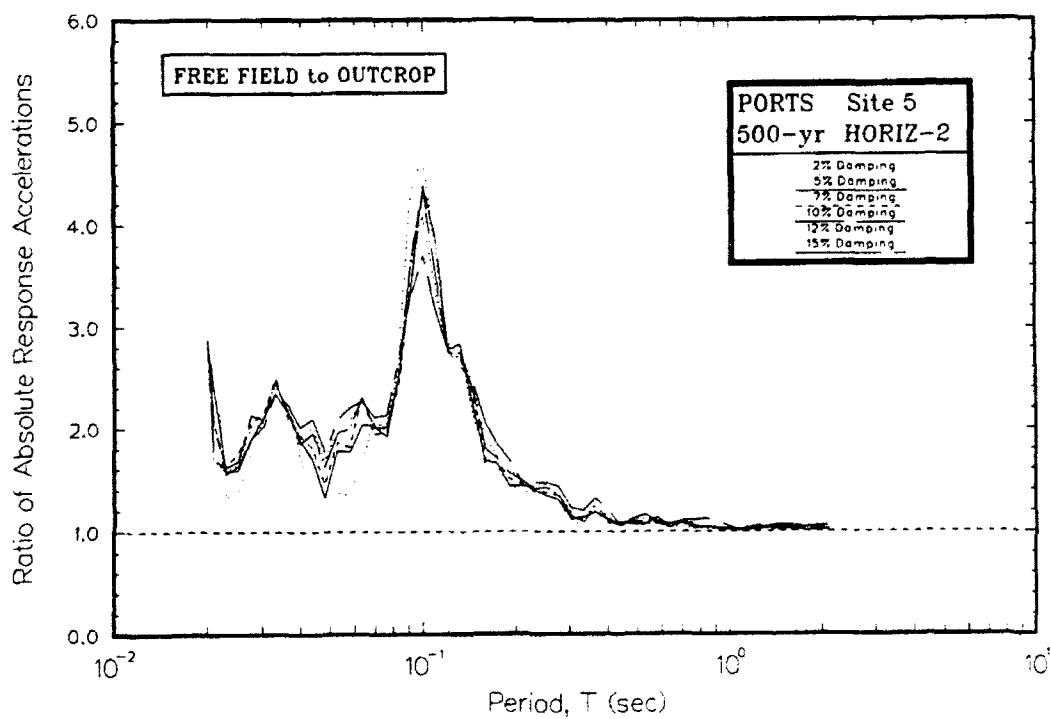
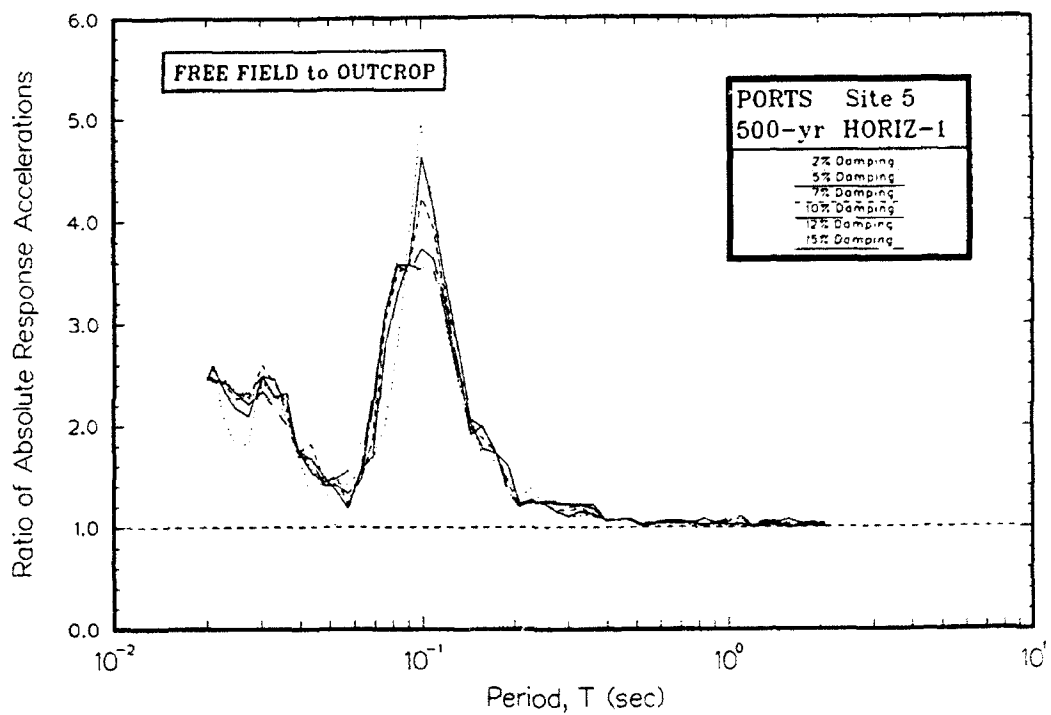


Figure F5. Ratio of absolute acceleration response spectra at free field to rock for Site 5

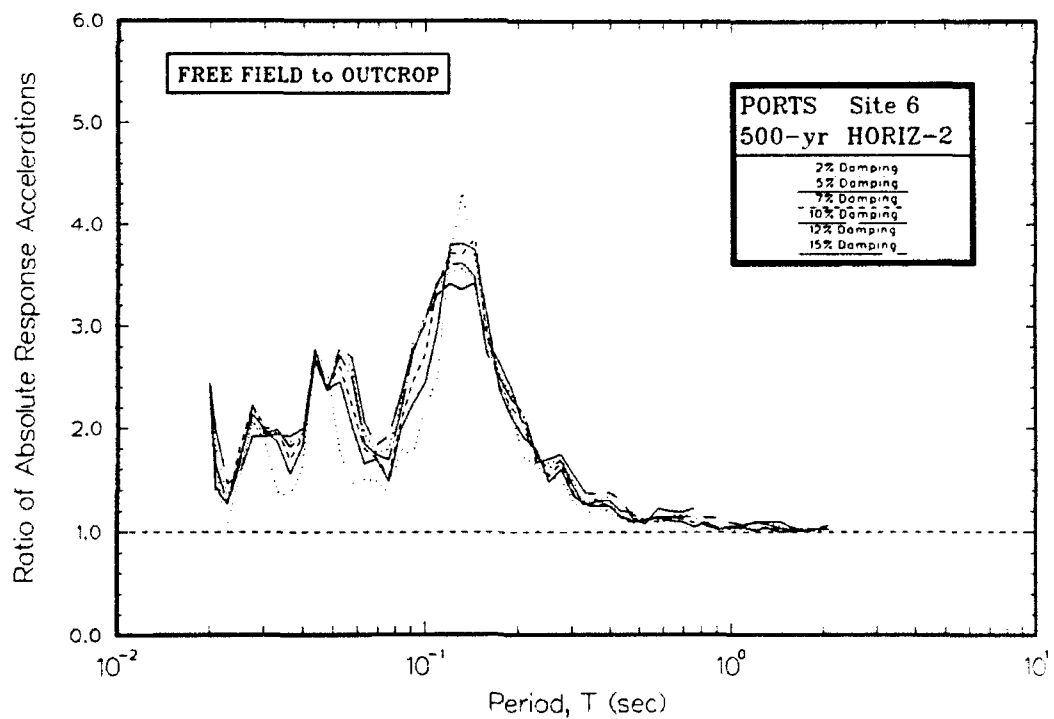
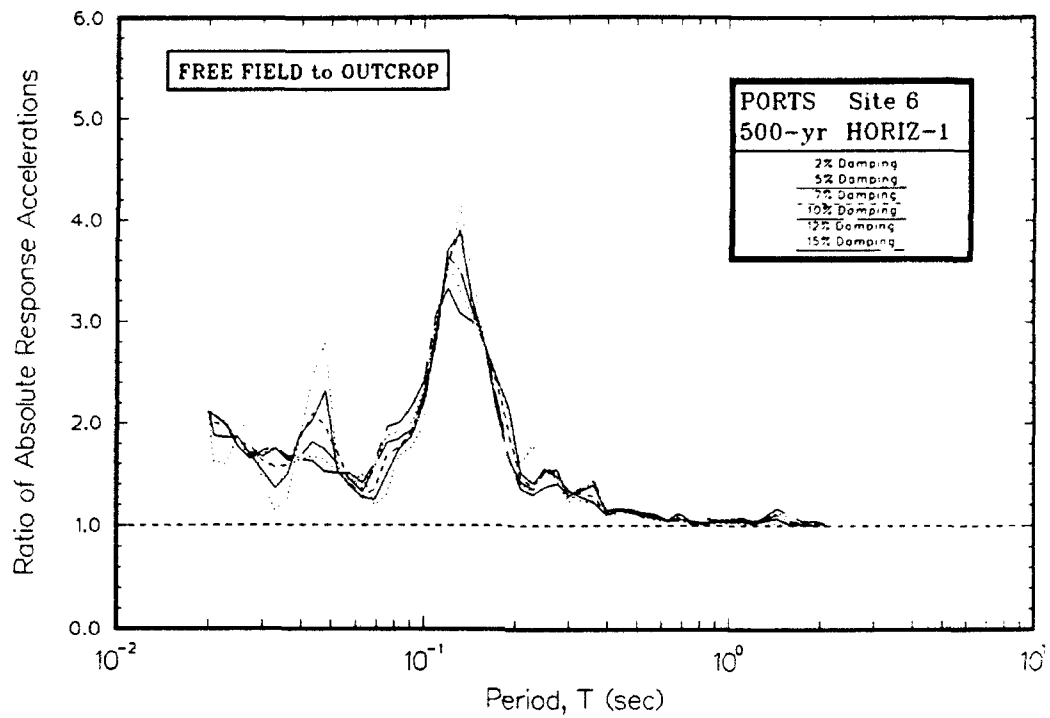


Figure F6. Ratio of absolute acceleration response spectra at free field to rock for Site 6

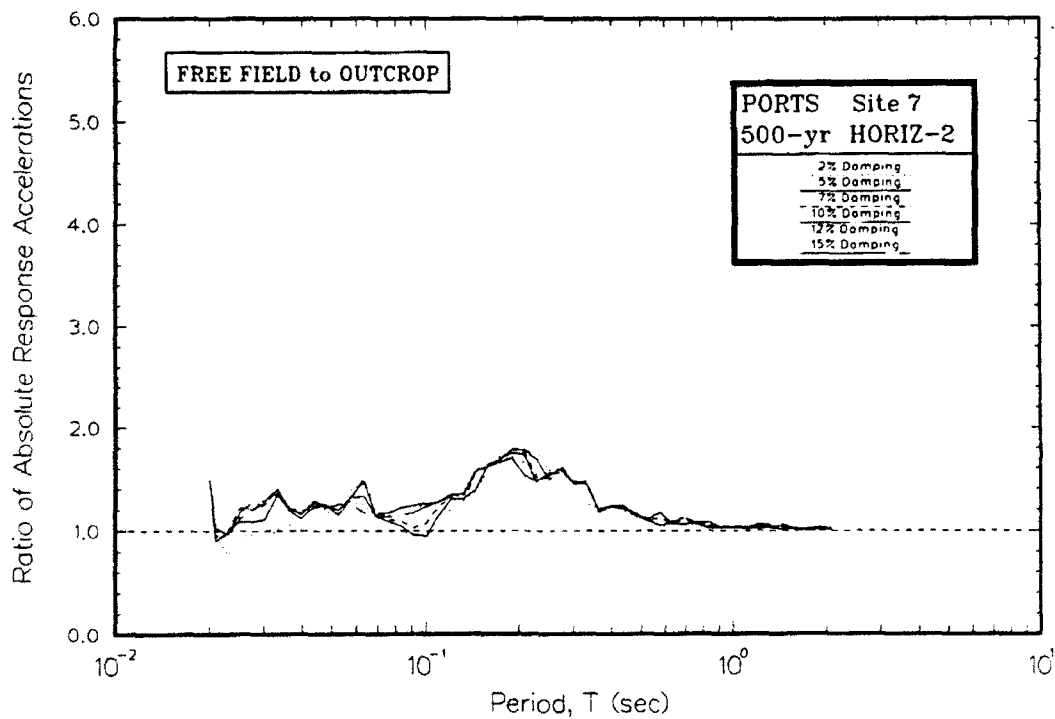
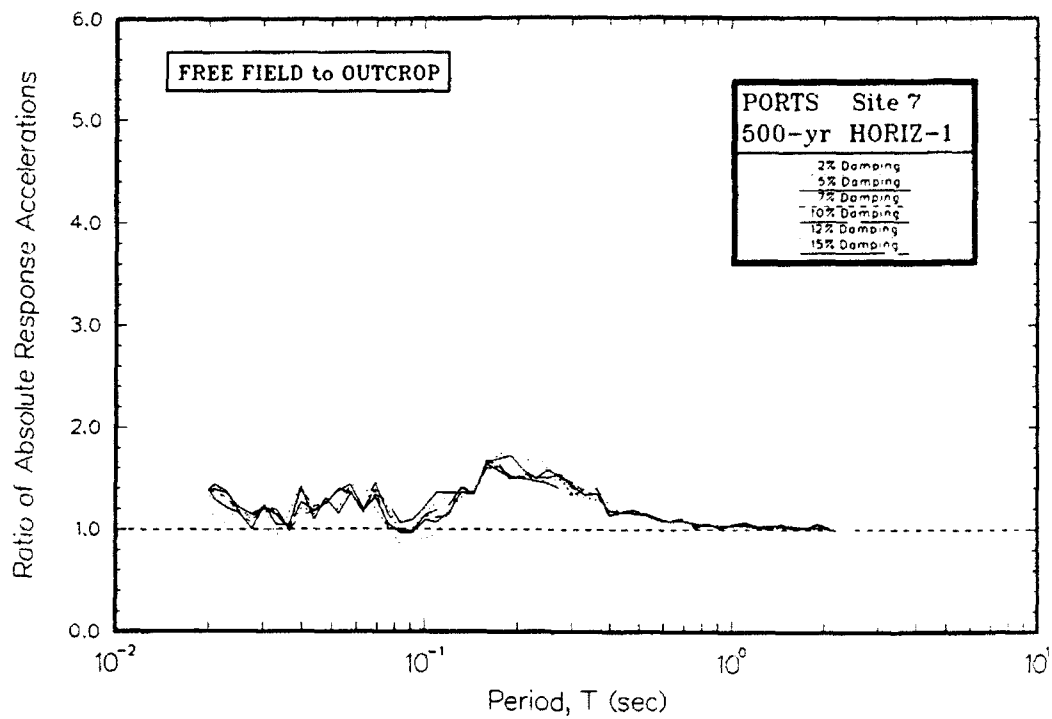


Figure F7. Ratio of absolute acceleration response spectra at free field to rock for Site 7

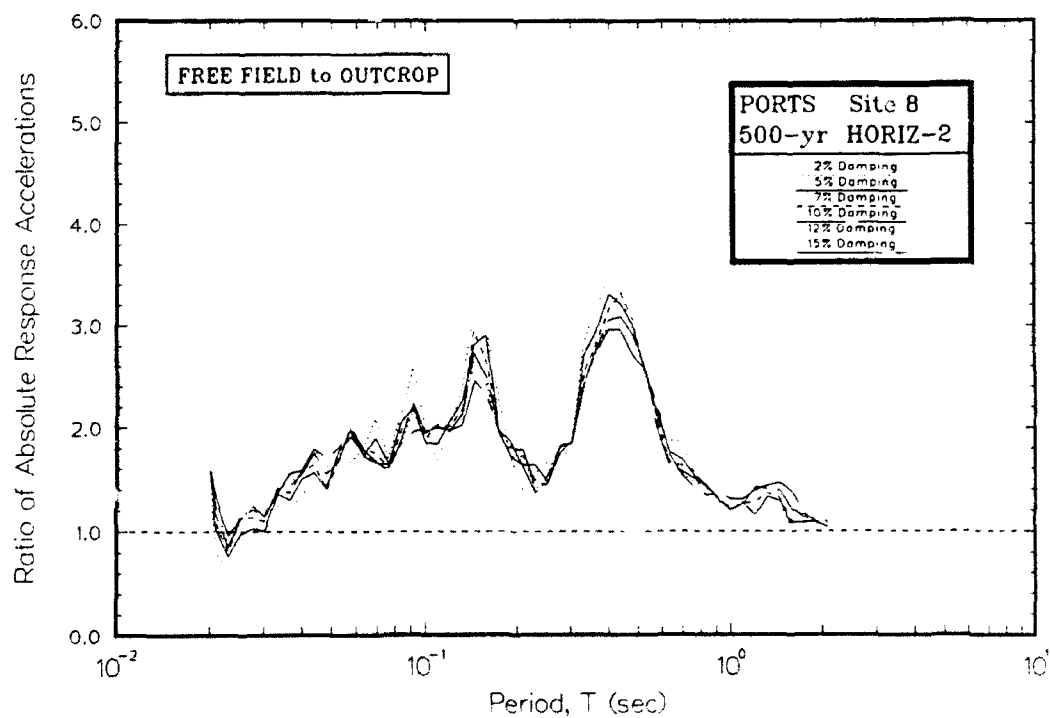
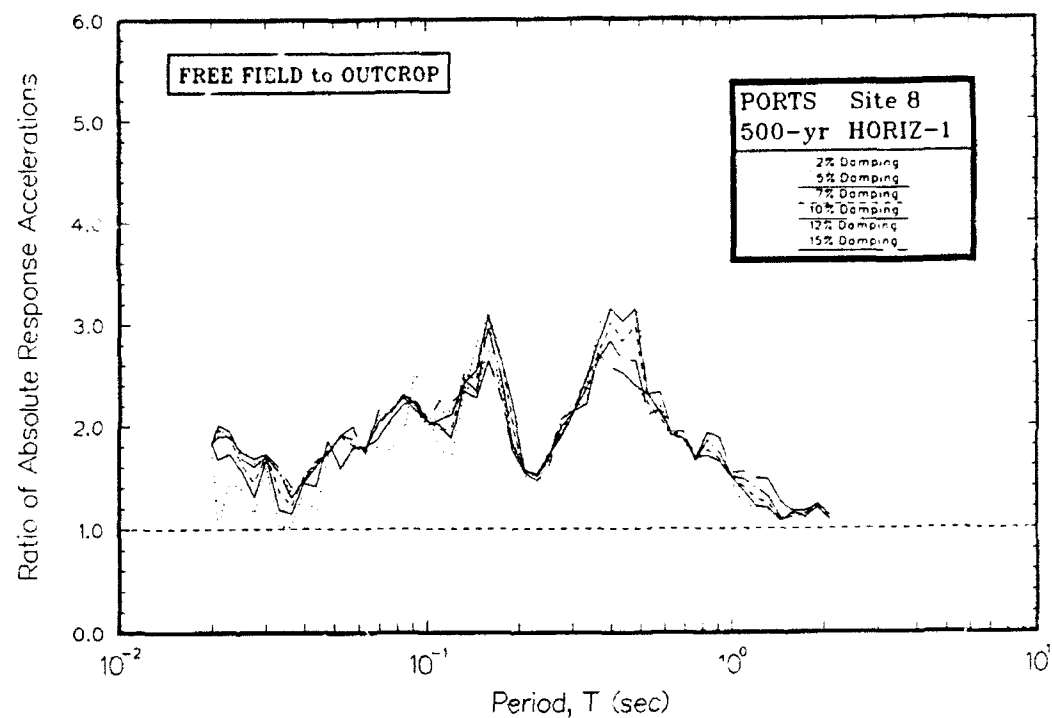


Figure F8. Ratio of absolute acceleration response spectra at free field to rock for Site 8

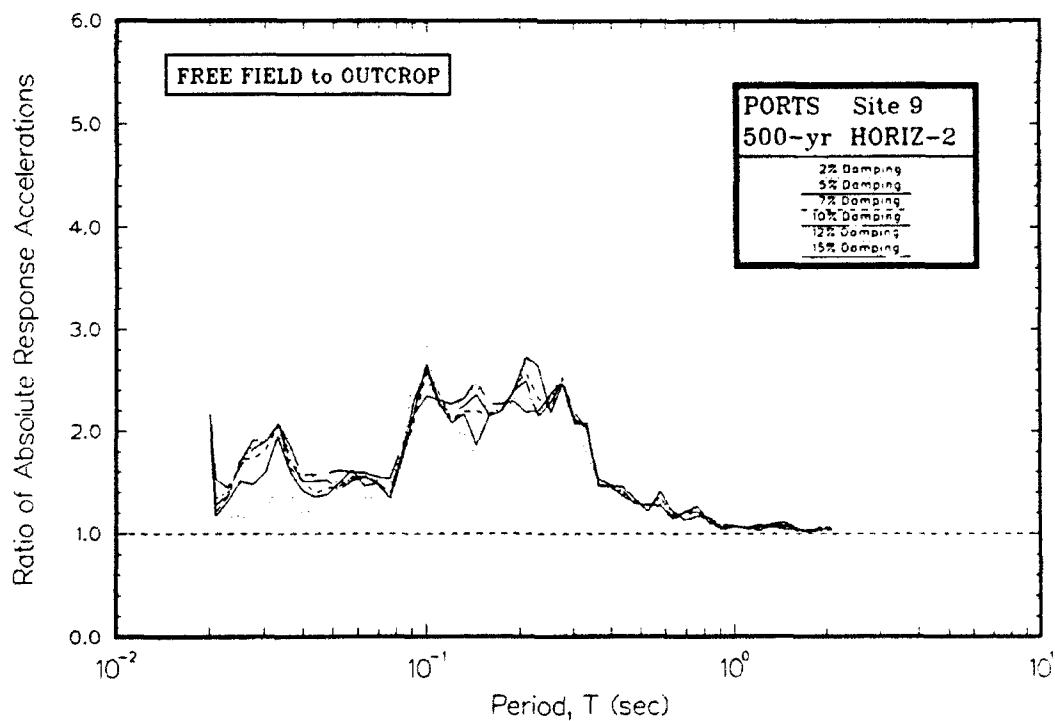
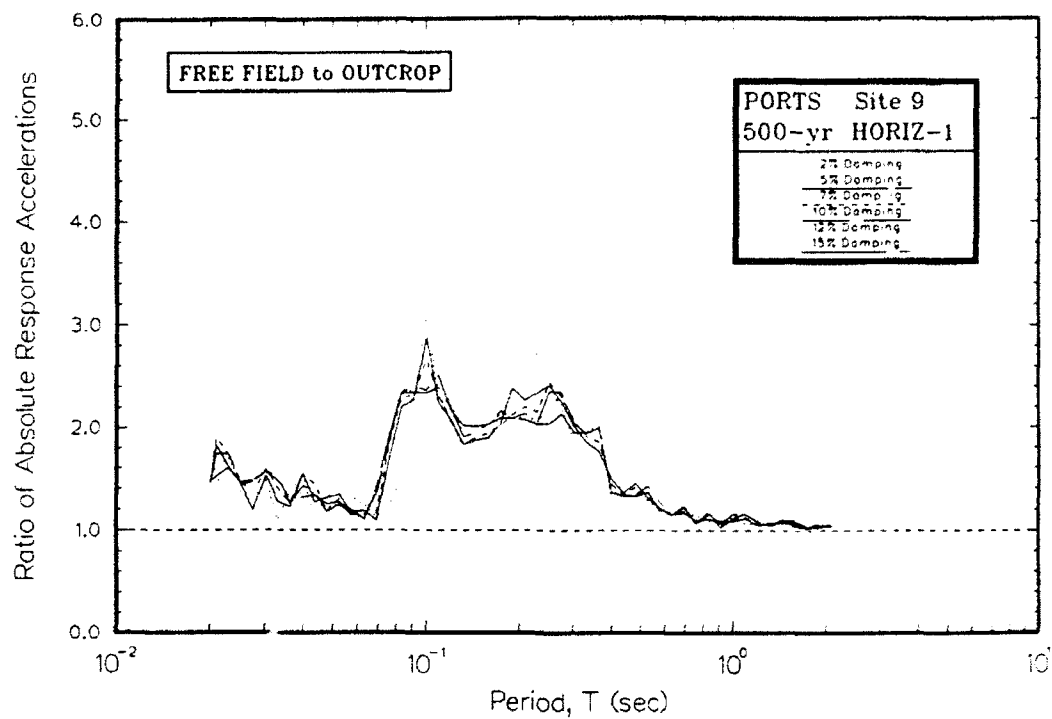


Figure F9. Ratio of absolute acceleration response spectra at free field to rock for Site 9

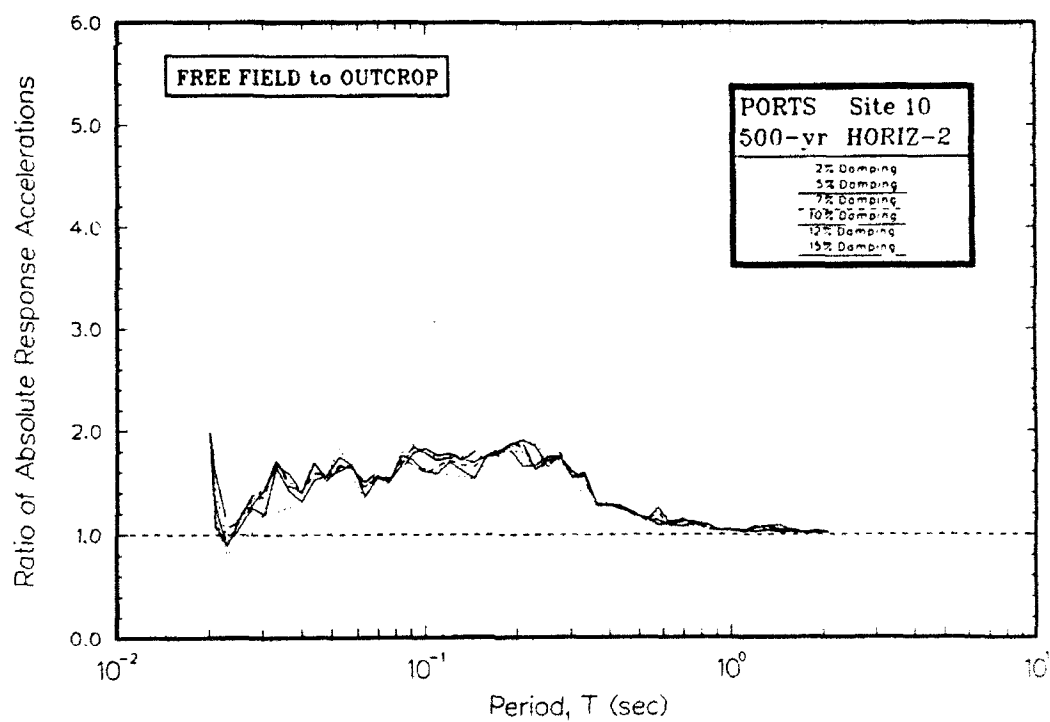
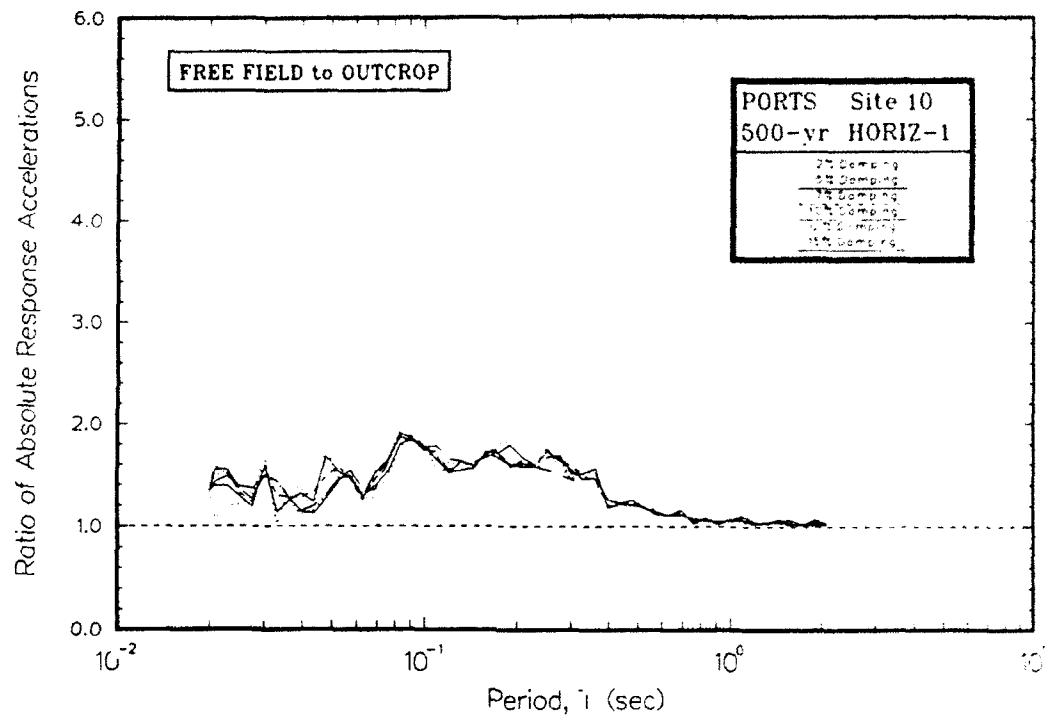


Figure F10. Ratio of absolute acceleration response spectra at free field to rock for Site 10

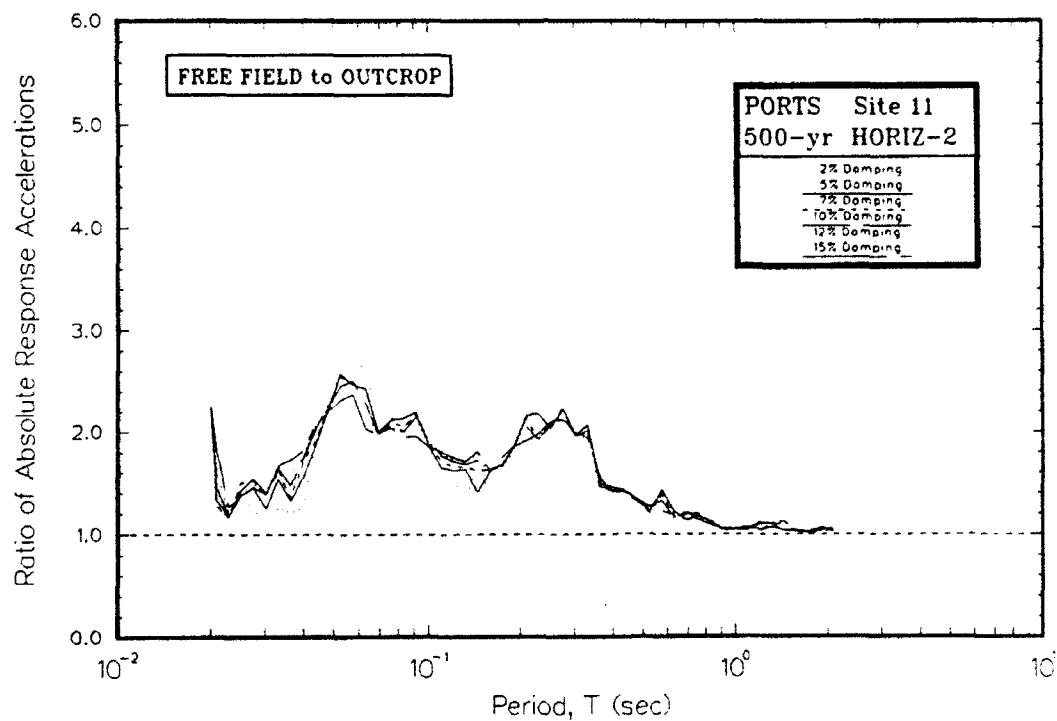
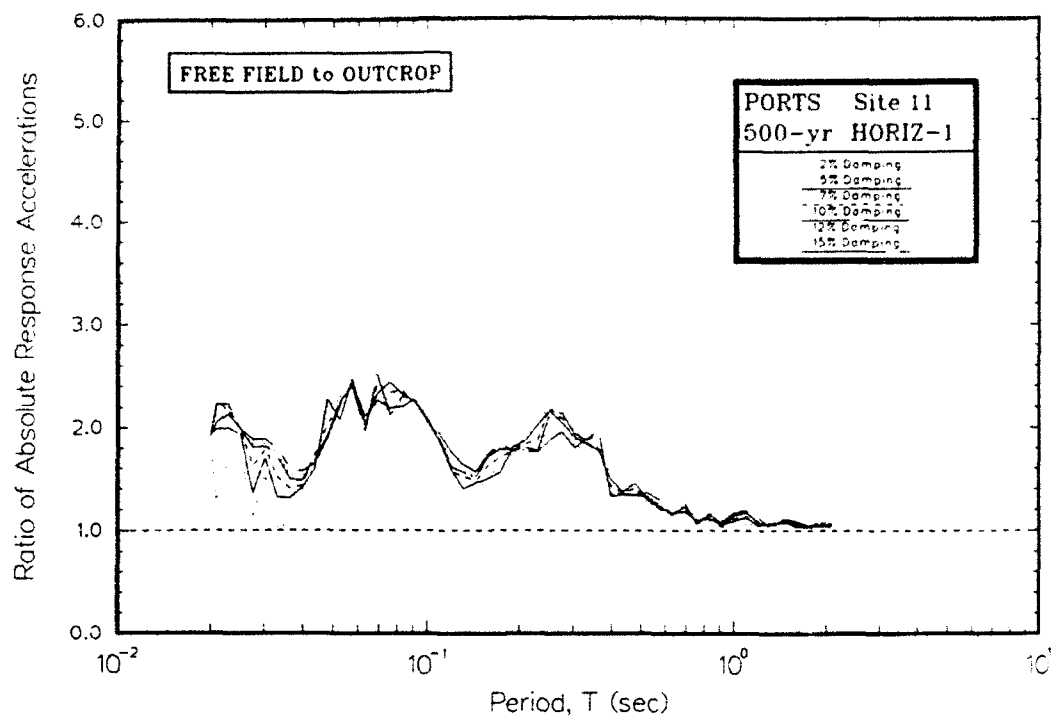


Figure F11. Ratio of absolute acceleration response spectra at free field to rock for Site 11

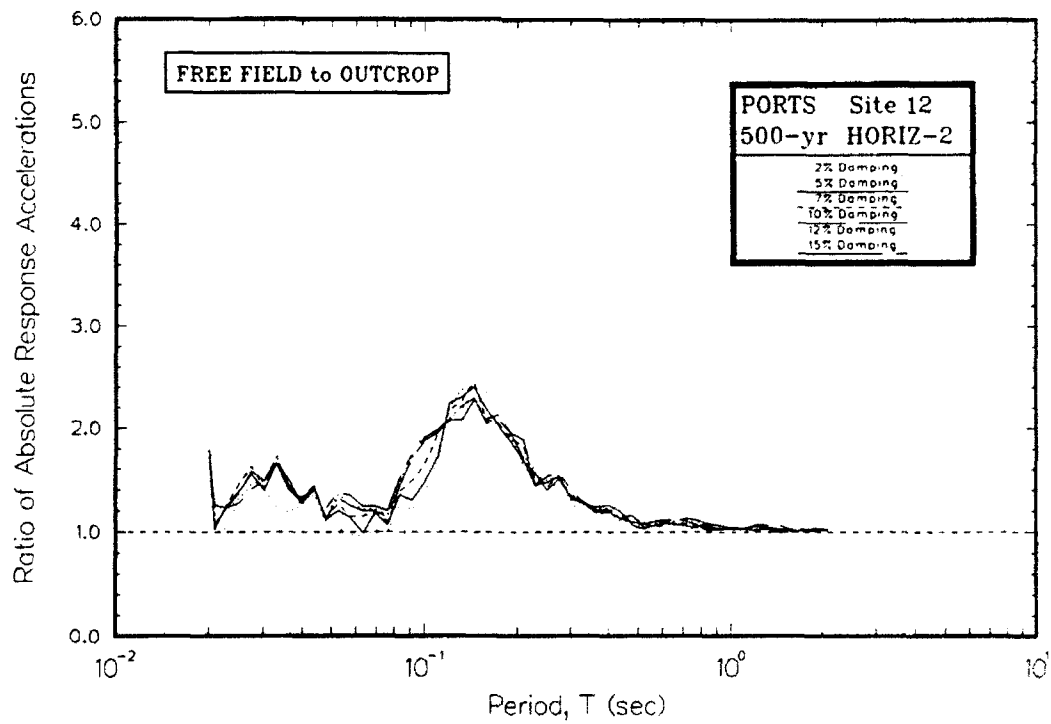
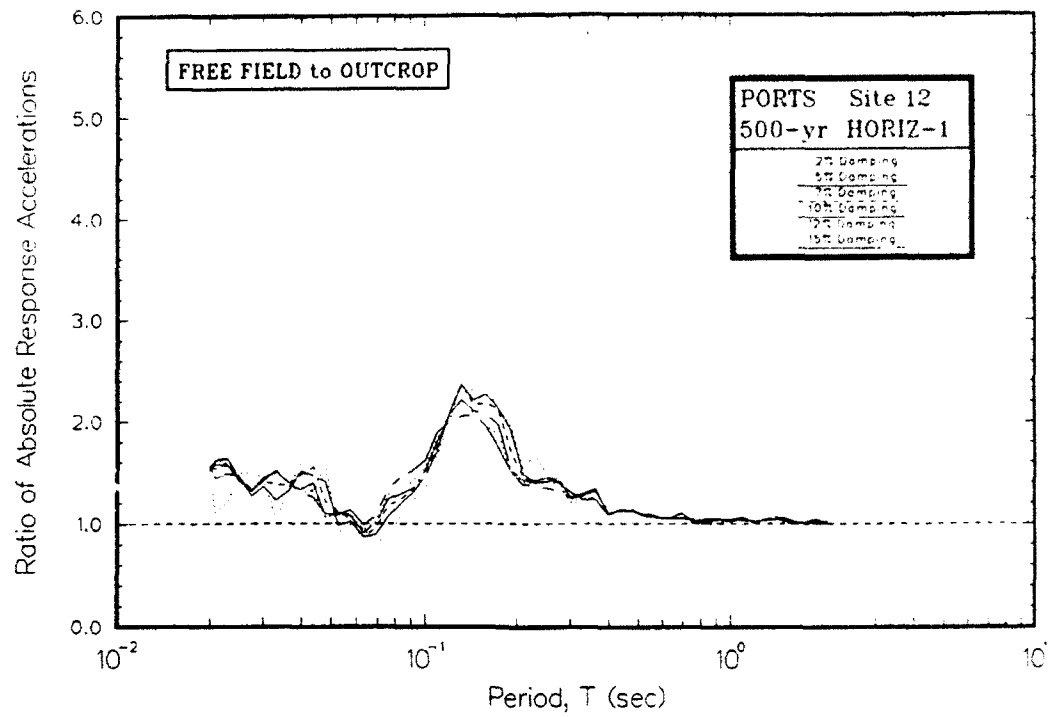


Figure F12. Ratio of absolute acceleration response spectra at free field to rock for Site 12

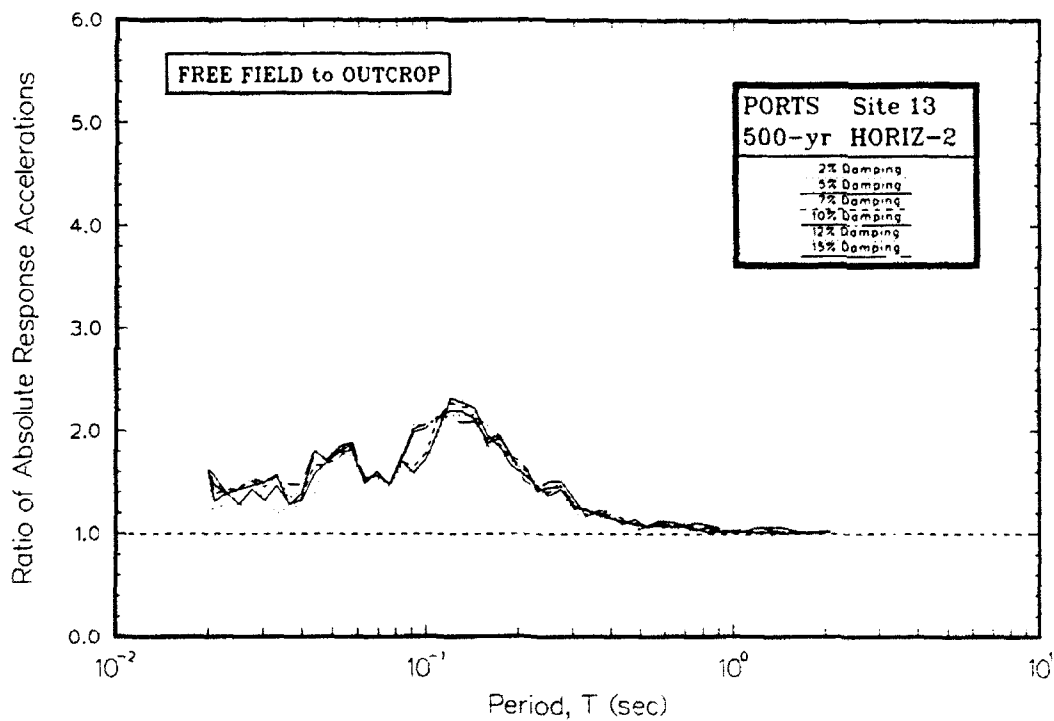
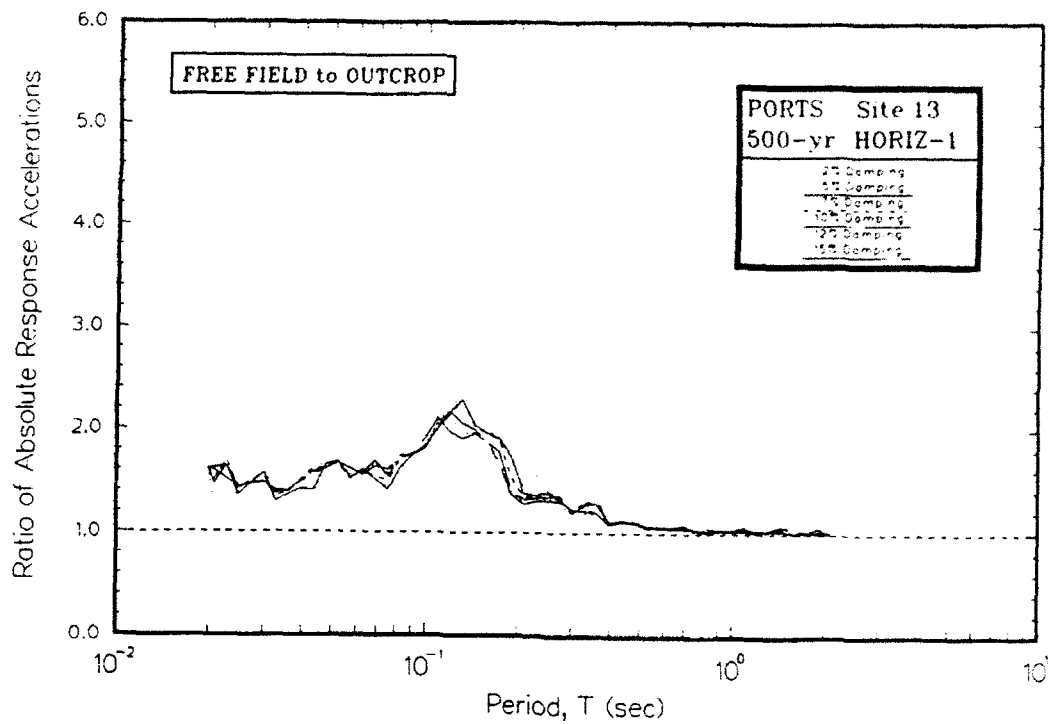


Figure F13. Ratio of absolute acceleration response spectra at free field to rock for Site 13

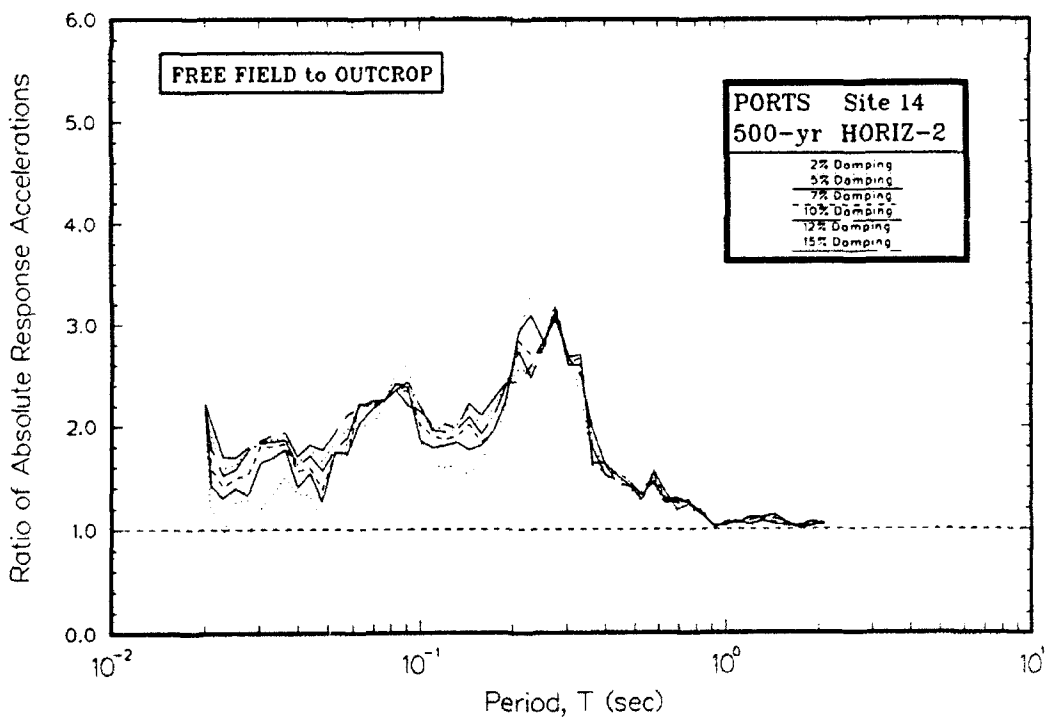
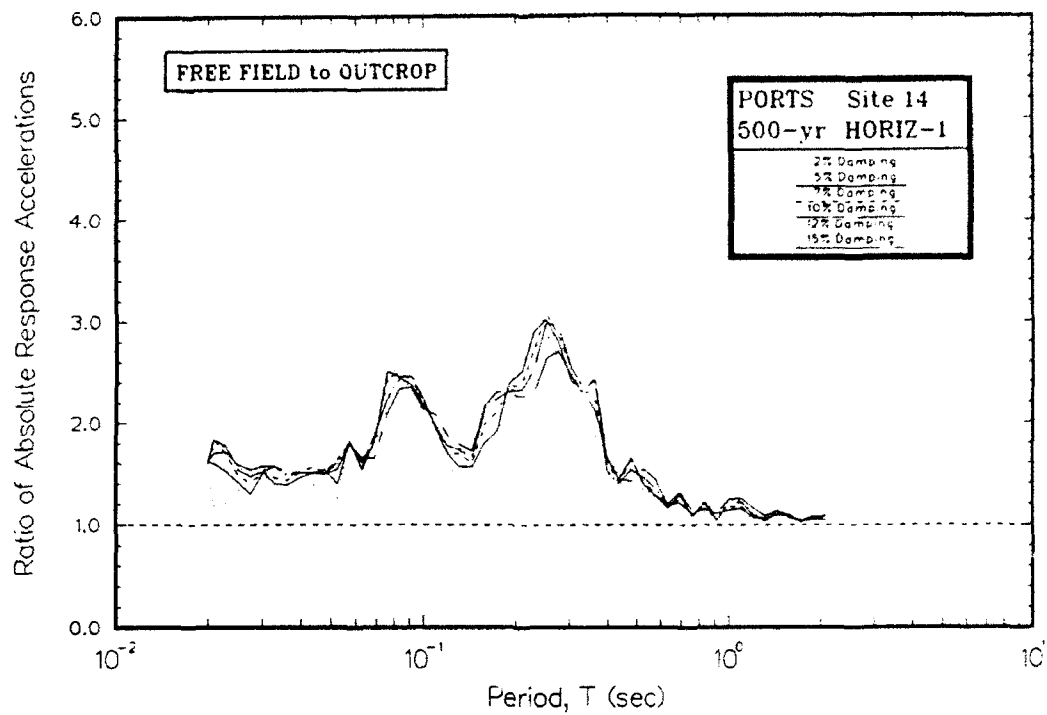


Figure F14. Ratio of absolute acceleration response spectra at free field to rock for Site 14

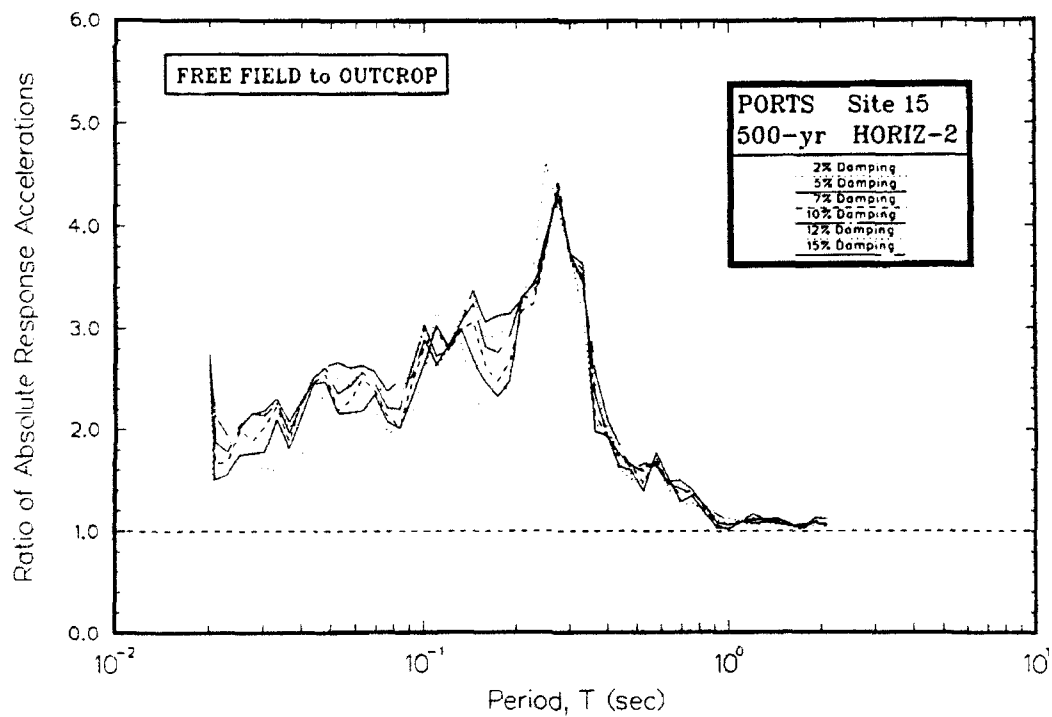
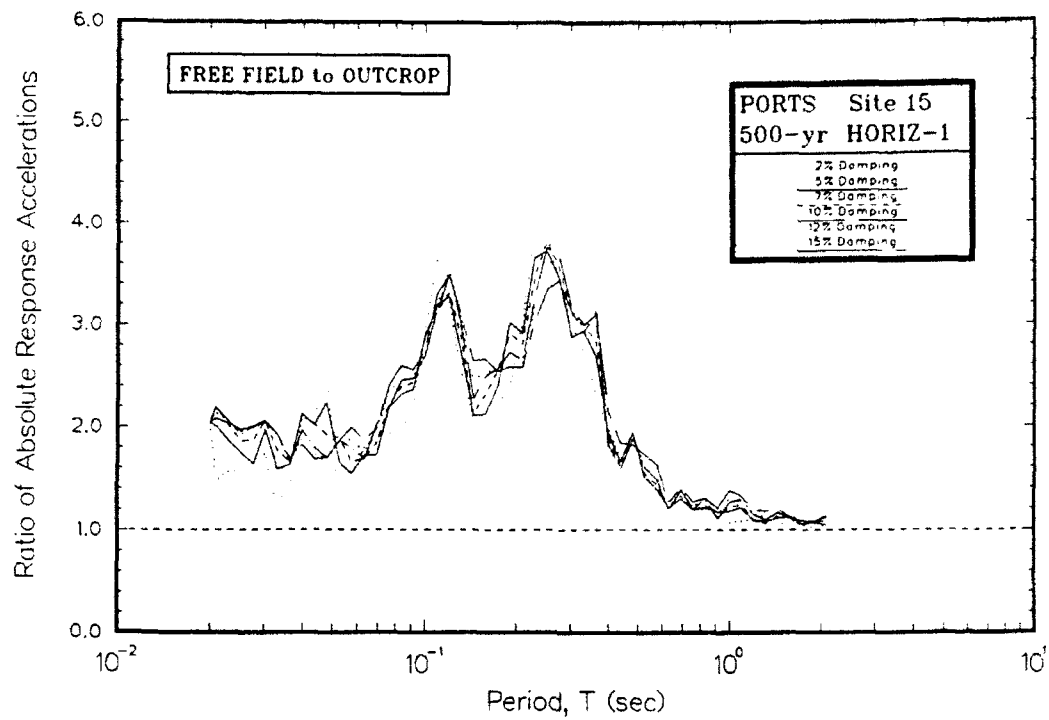


Figure F15. Ratio of absolute acceleration response spectra at free field to rock for Site 15

APPENDIX G: AMPLIFICATION RATIOS FOR 500-YEAR EVENT

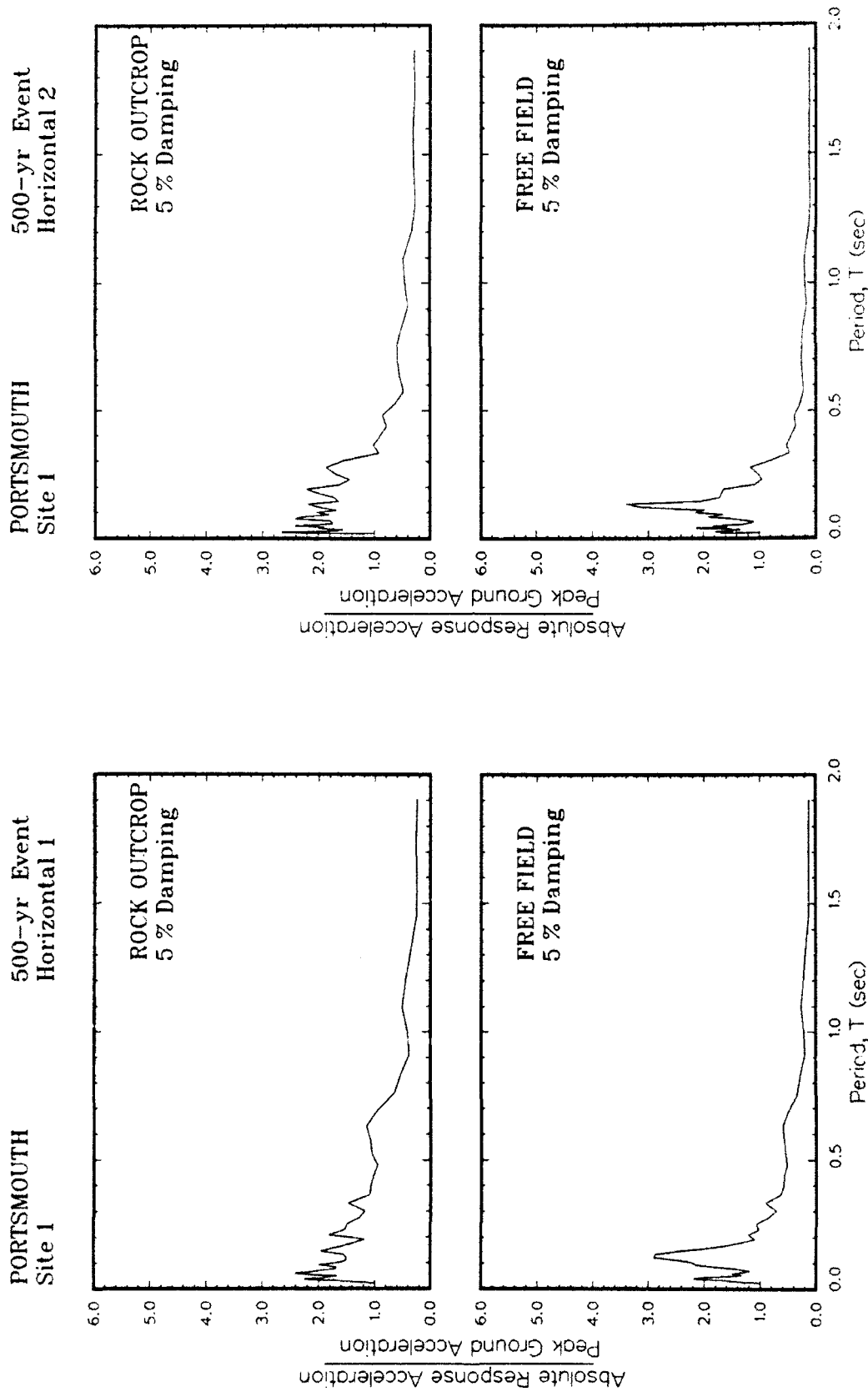


Figure G1. Ratio of amplification of absolute acceleration response spectra to peak acceleration at free field for Site 1

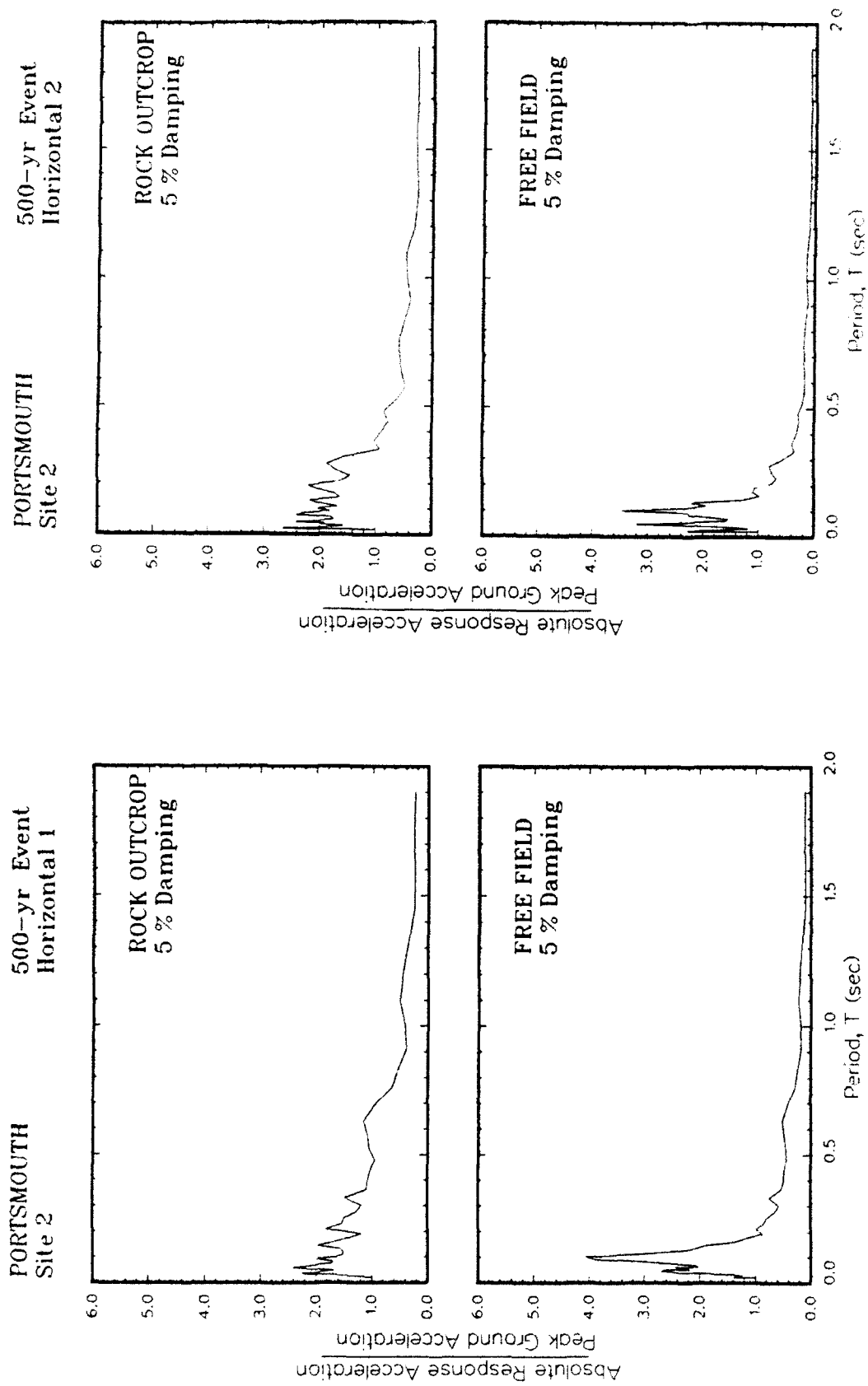


Figure G2. Ratio of amplification of absolute acceleration response spectra to peak acceleration at free field for Site 2

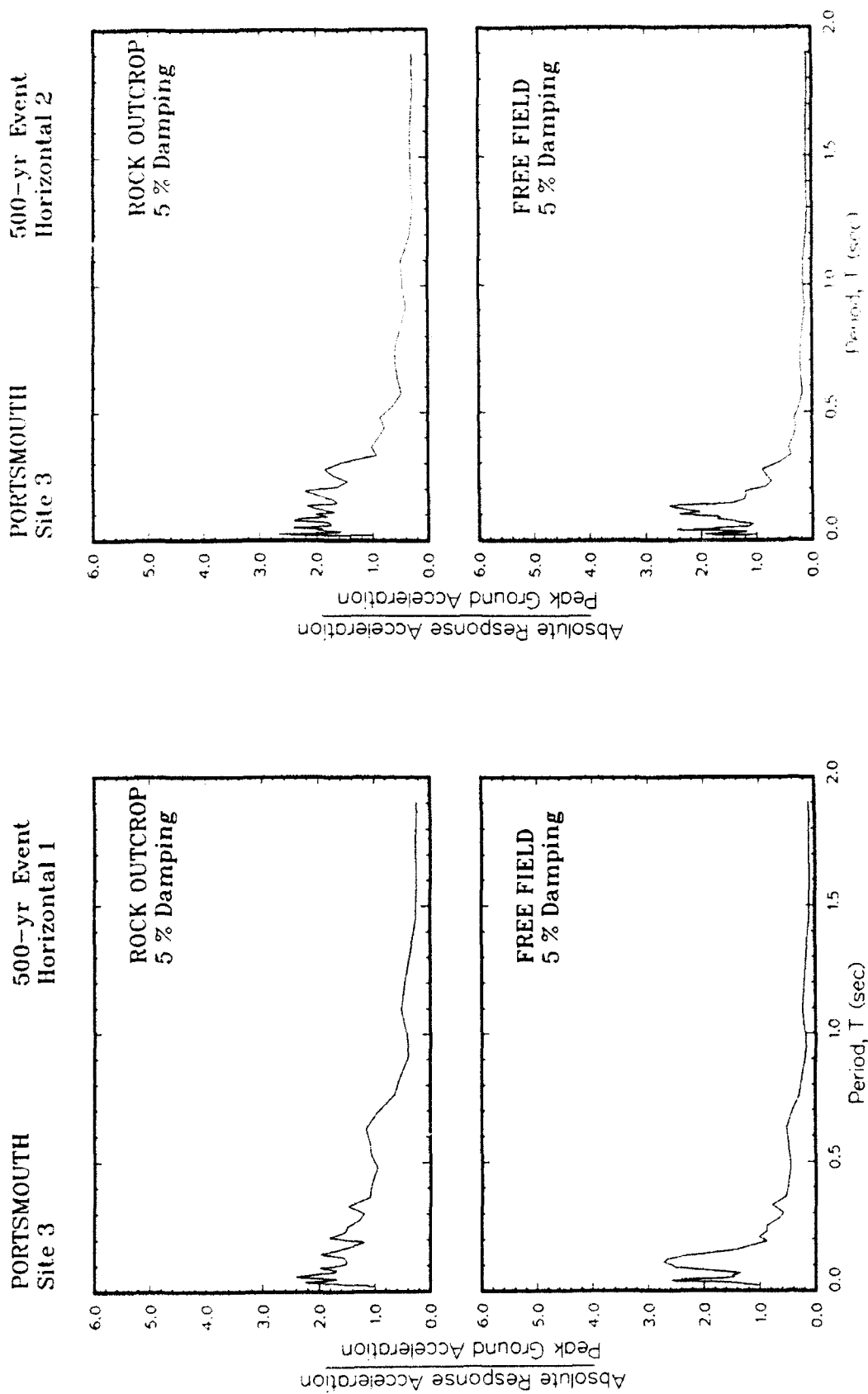


Figure G3. Ratio of amplification of absolute acceleration response spectra to peak acceleration at free field for Site 3

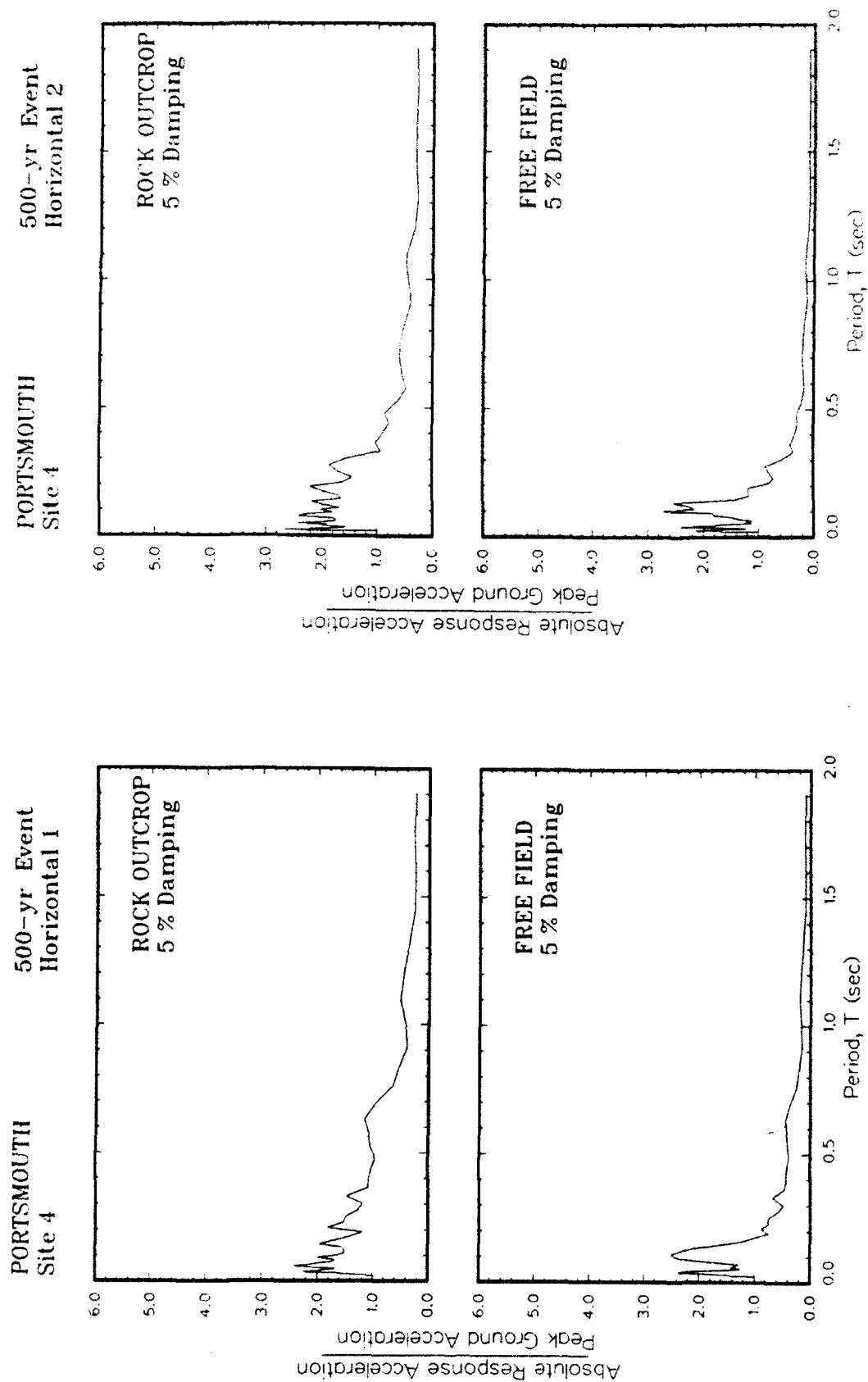


Figure G4. Ratio of amplification of absolute acceleration response spectra to peak acceleration at free field for Site 4

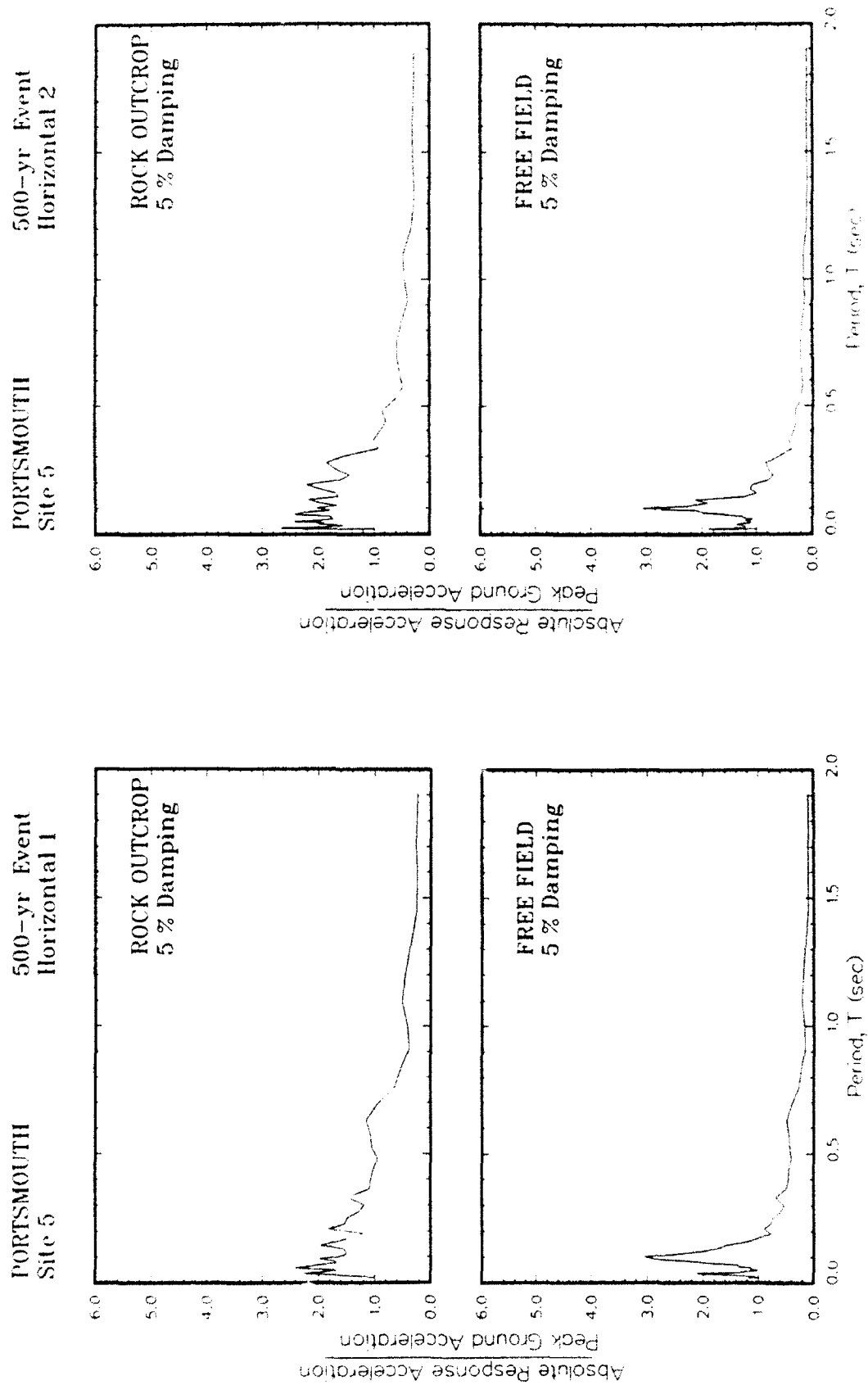


Figure G5. Ratio of amplification of absolute acceleration response spectra to peak acceleration at free field for Site 5

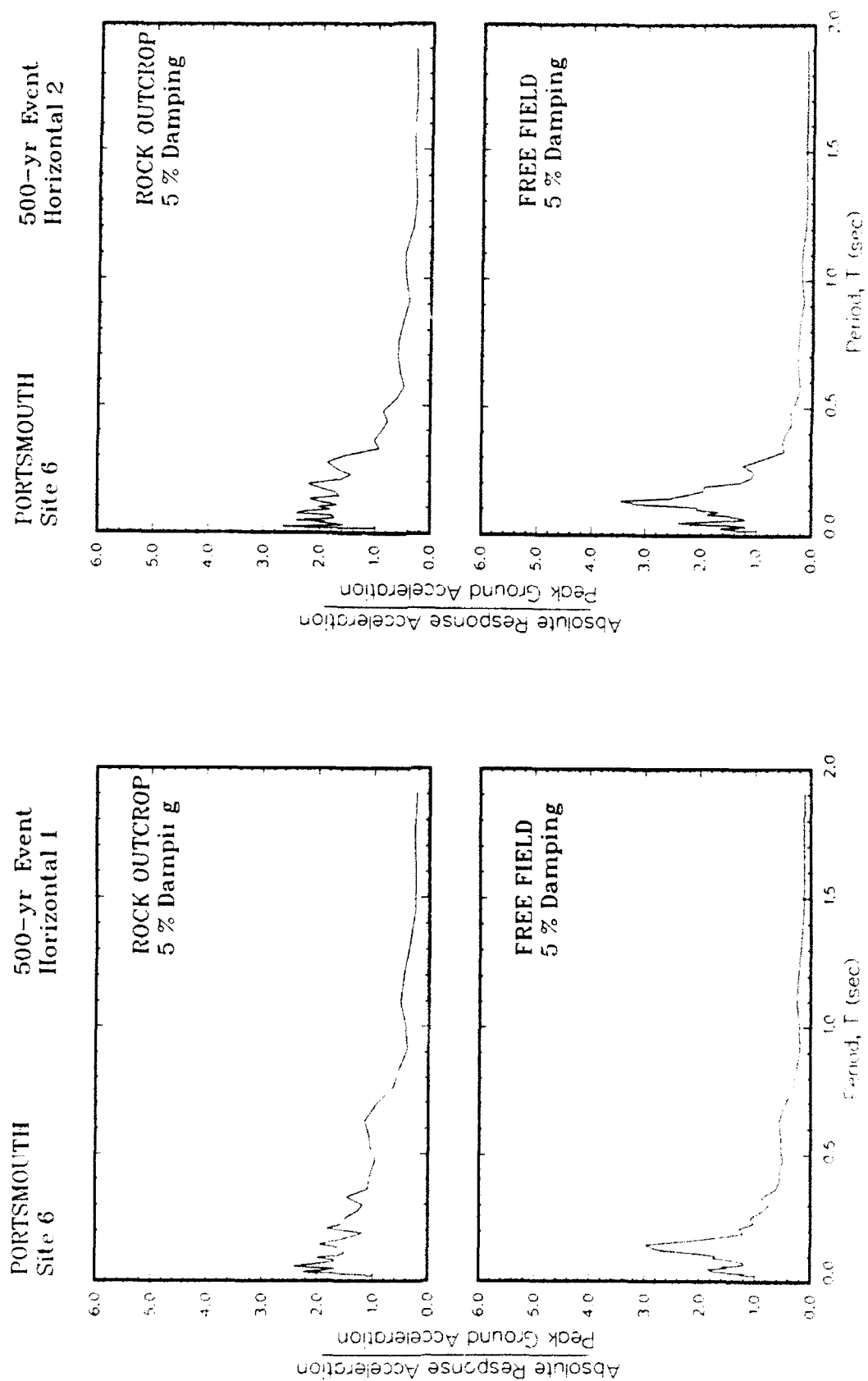


Figure G6. Ratio of amplification of absolute acceleration response spectra to peak acceleration at free field for Site 6

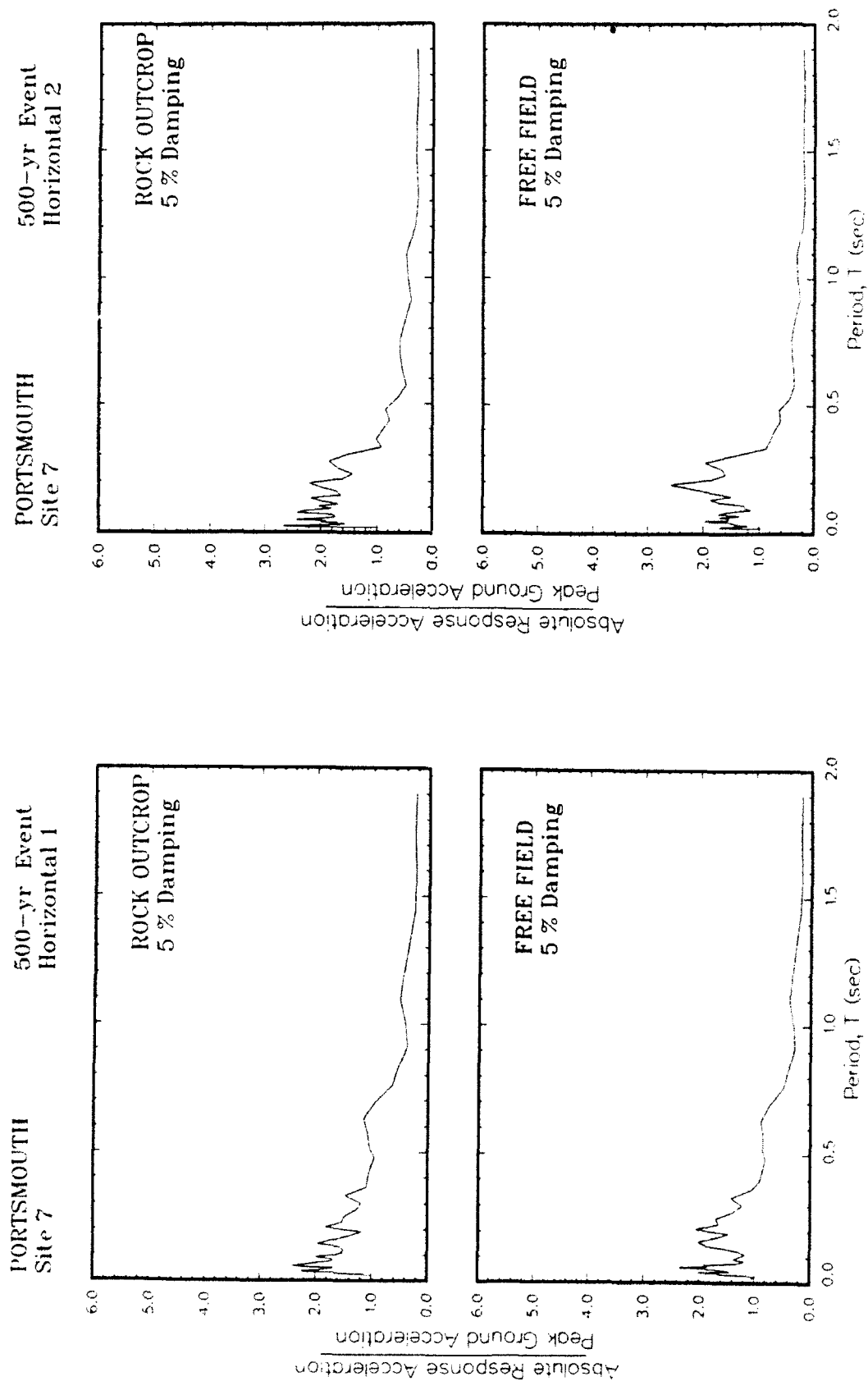


Figure G7. Ratio of amplification of absolute acceleration response spectra to peak acceleration at free field for Site 7

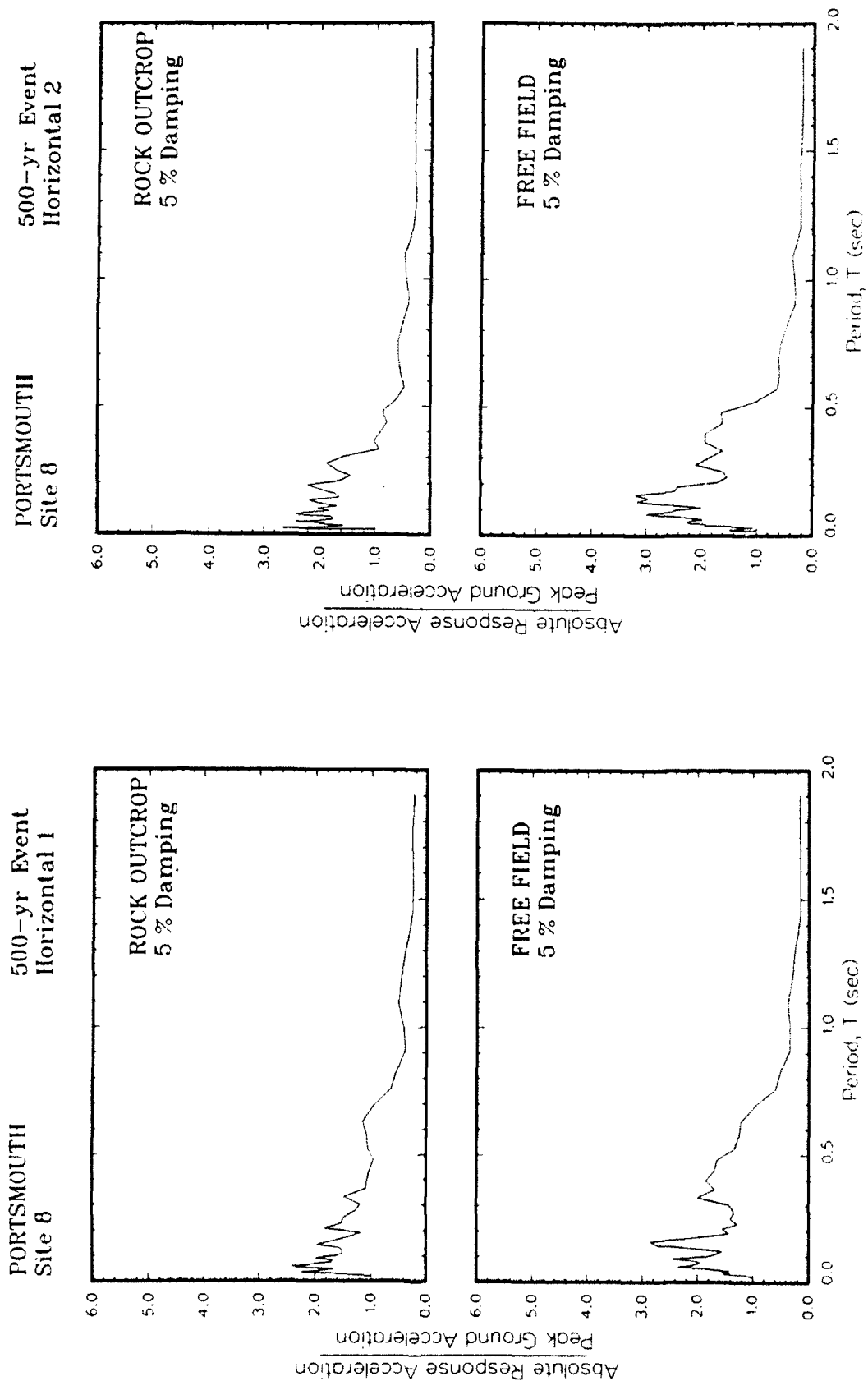


Figure G8. Ratio of amplification of absolute acceleration response spectra to peak acceleration at free field for Site 8

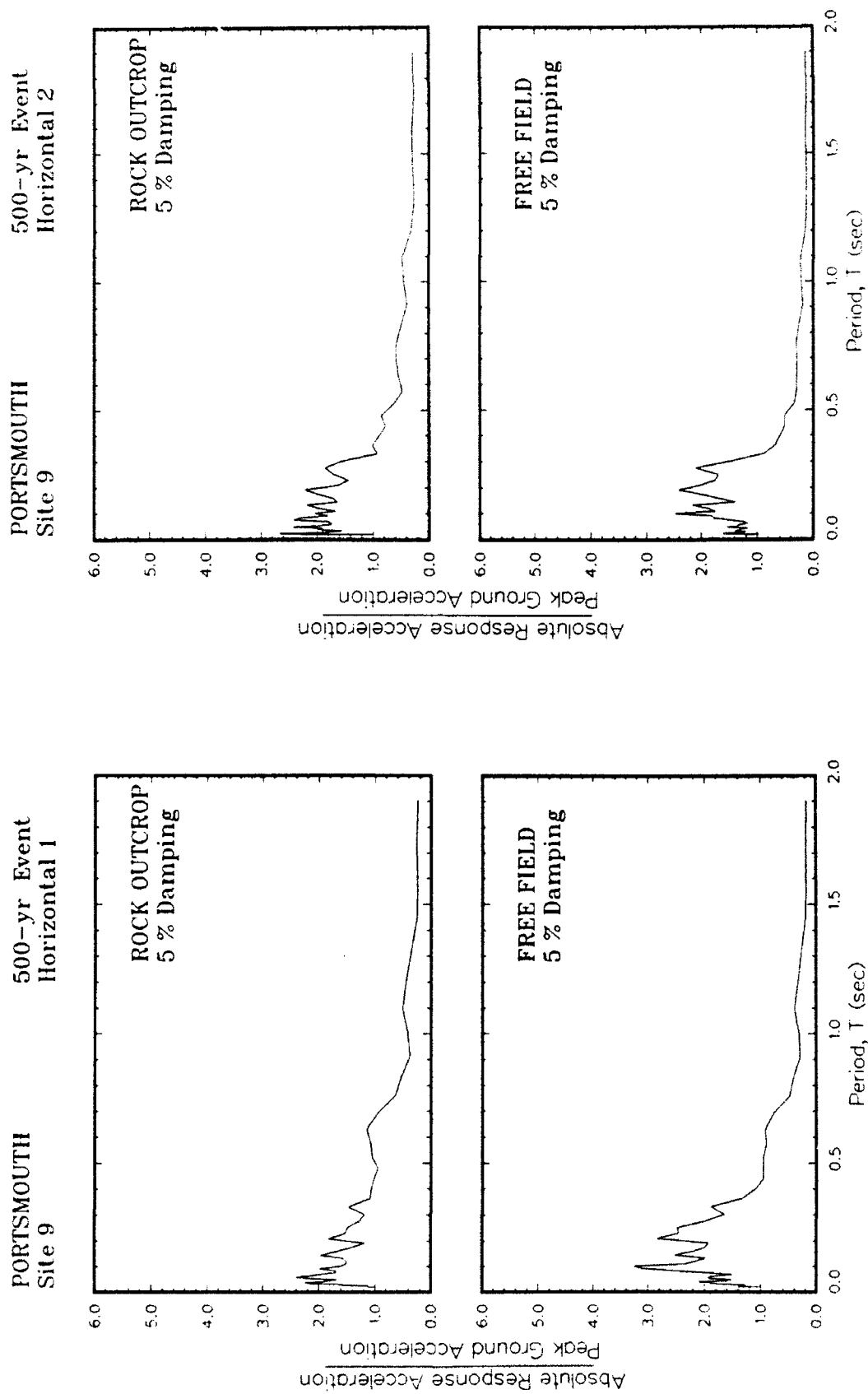


Figure G9. Ratio of amplification of absolute acceleration response spectra to peak acceleration at free field for Site 9

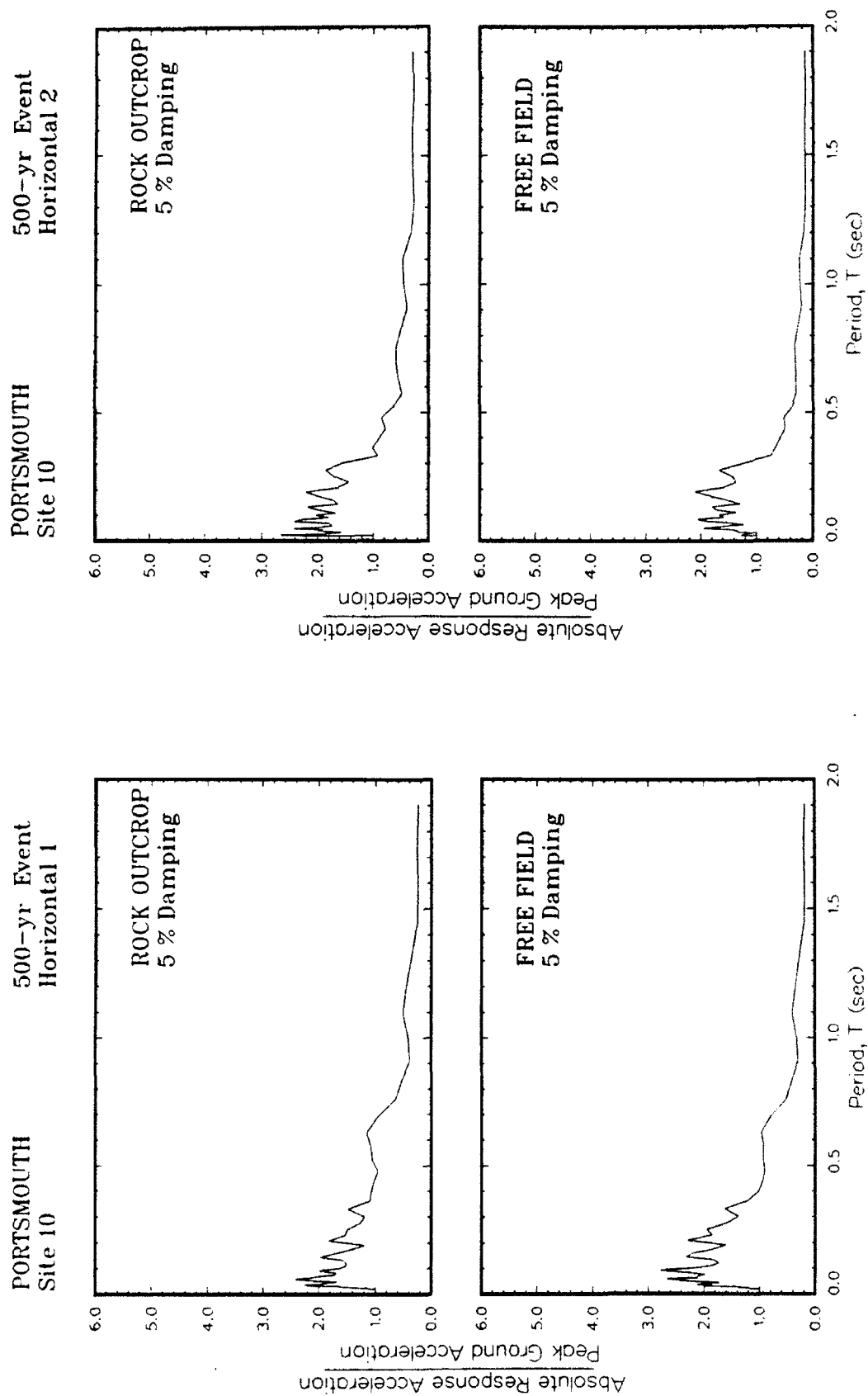


Figure G10. Ratio of amplification of absolute acceleration response spectra to peak acceleration at free field for Site 10

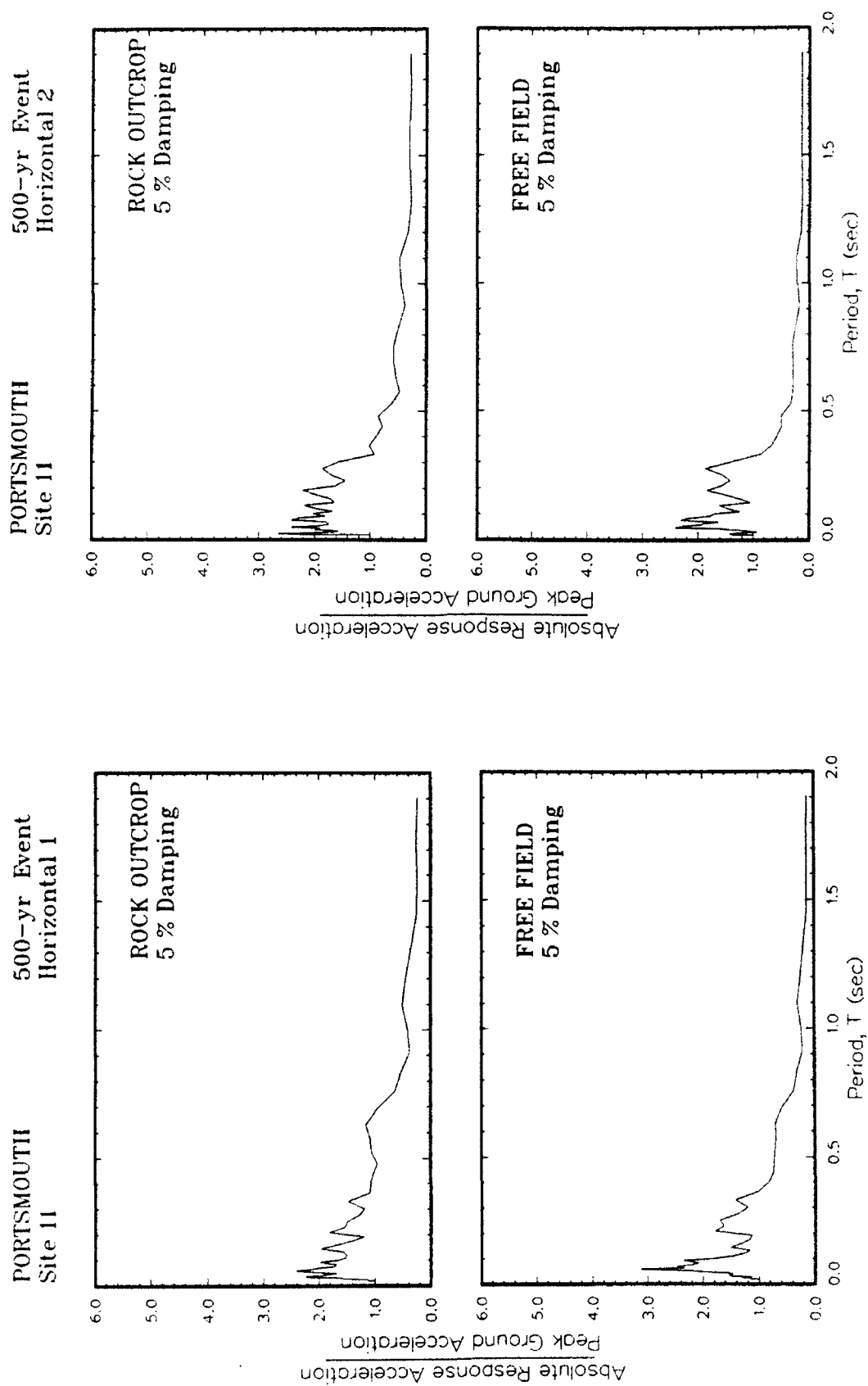


Figure G11. Ratio of amplification of absolute acceleration response spectra to peak acceleration at free field for Site 11

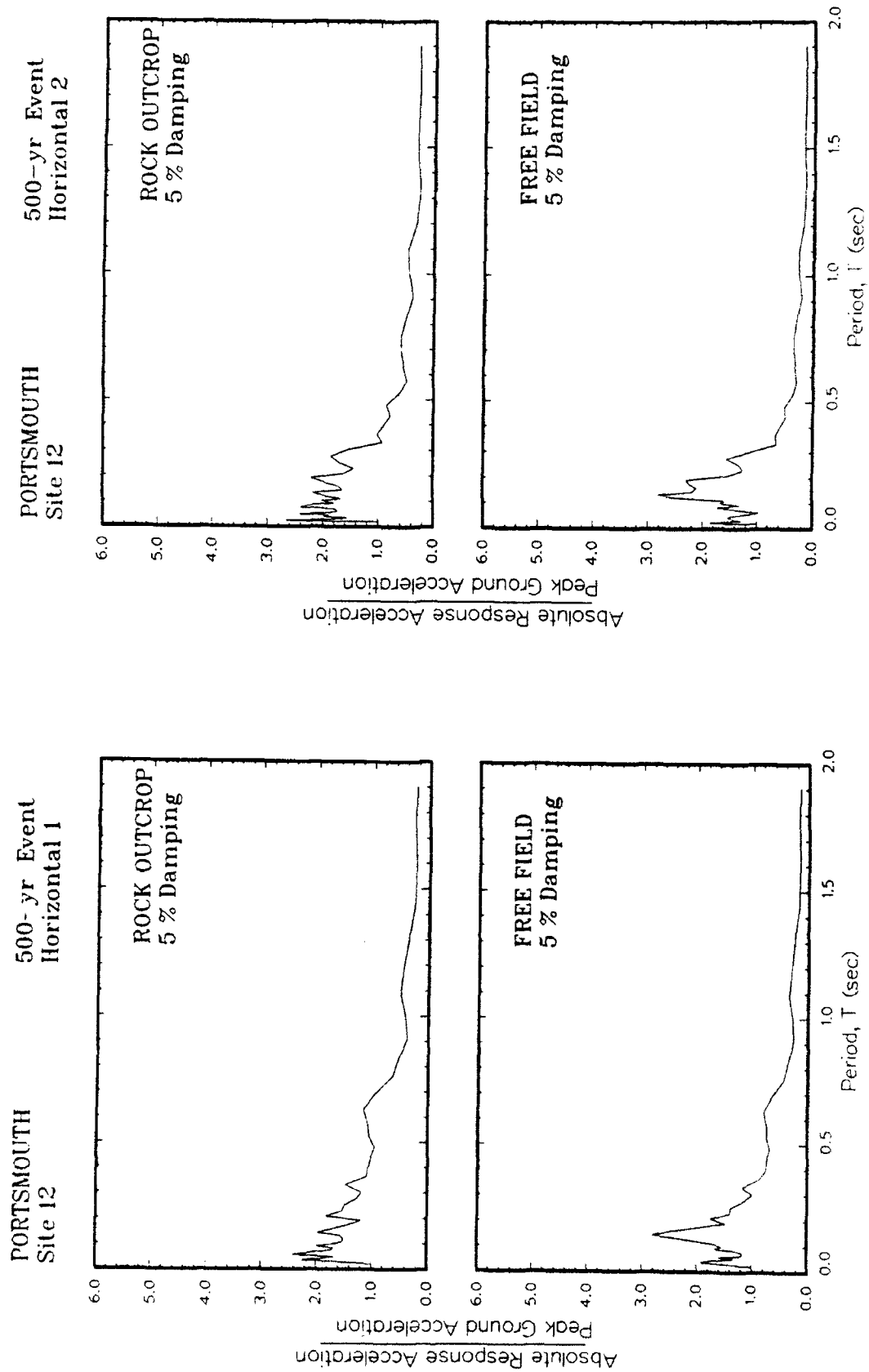


Figure G12. Ratio of amplification of absolute acceleration response spectra to peak acceleration at free field for Site 12

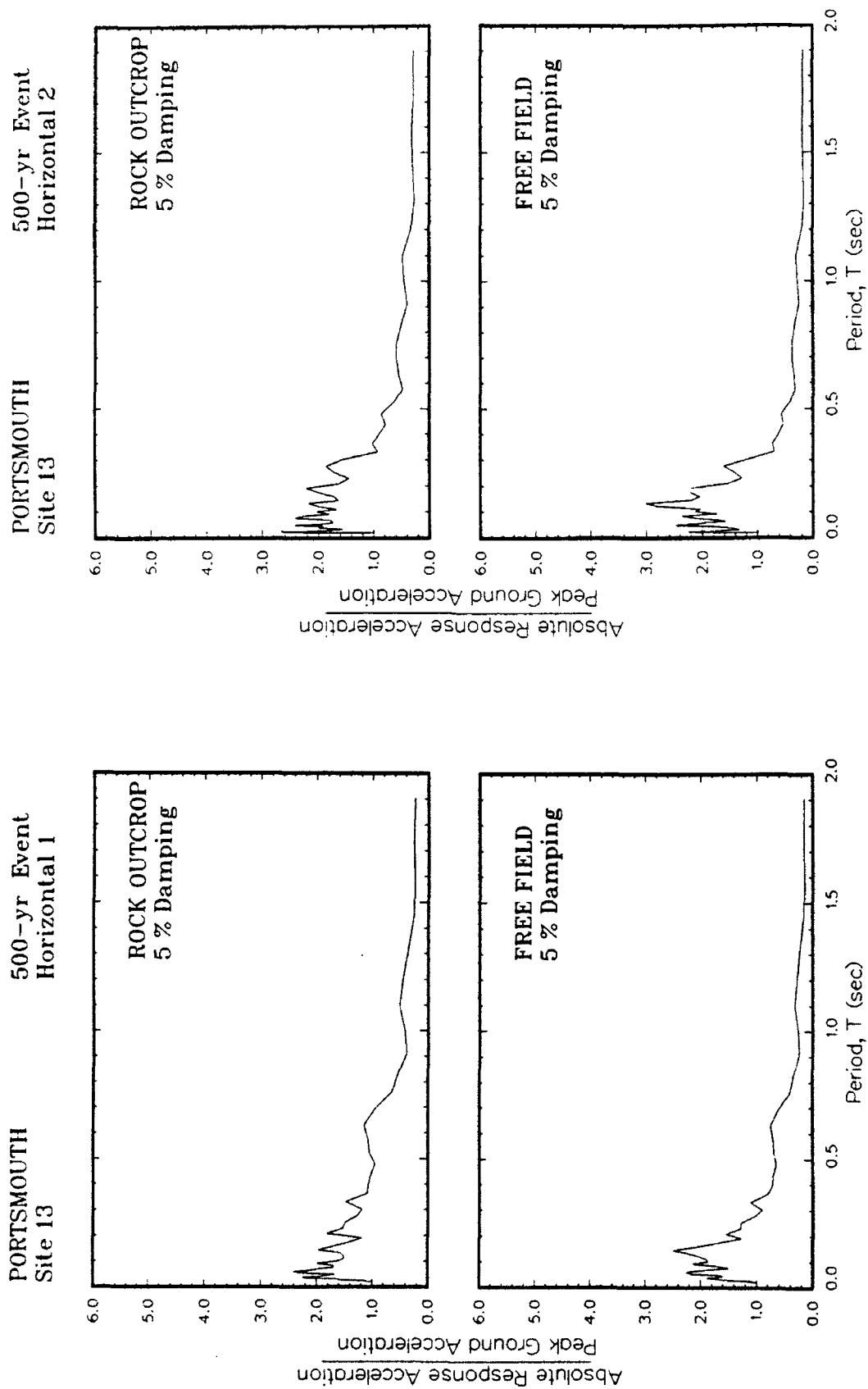


Figure G13. Ratio of amplification of absolute acceleration response spectra to peak acceleration at free field for Site 13

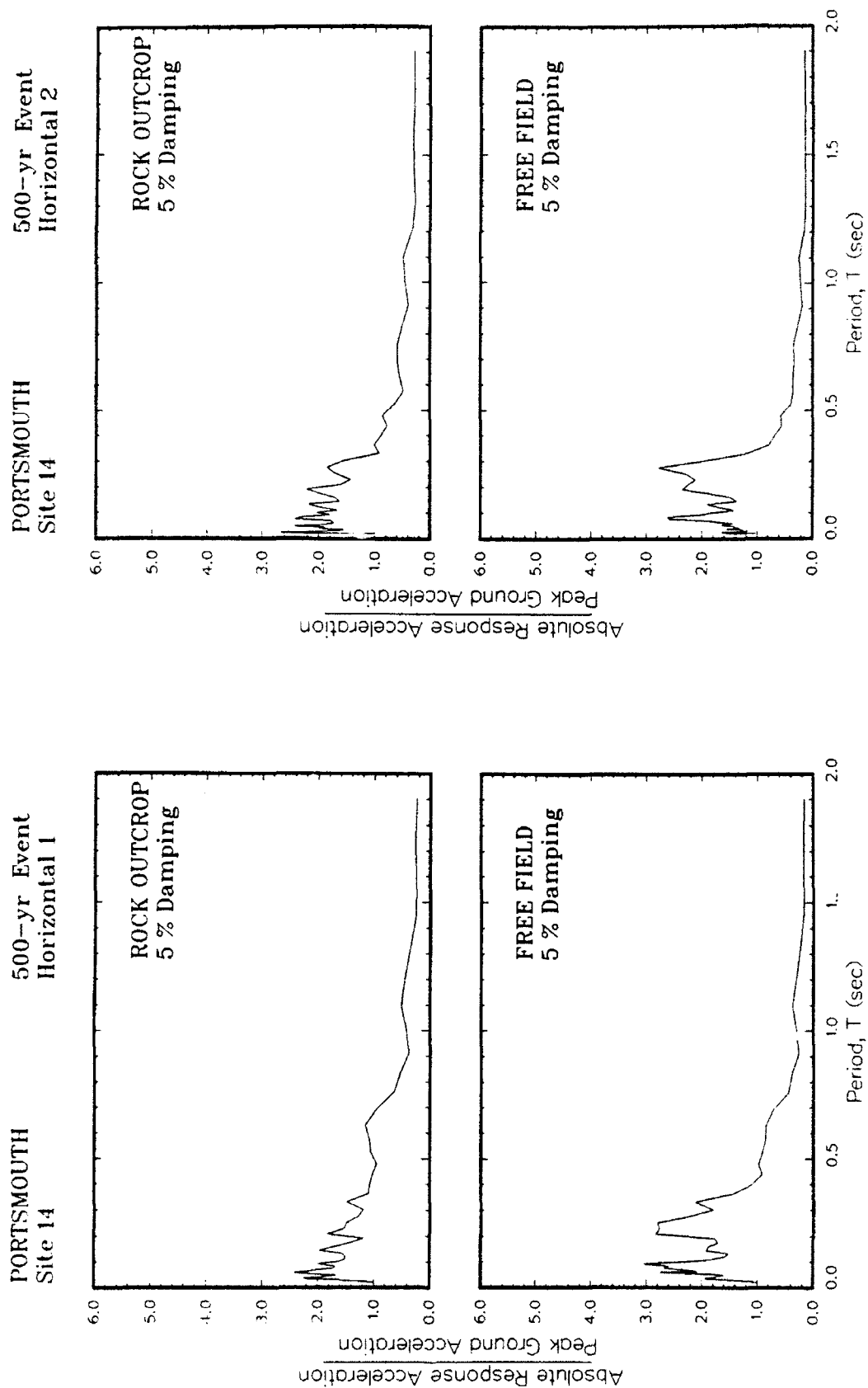


Figure G14. Ratio of amplification of absolute acceleration response spectra to peak acceleration at free field for Site 14

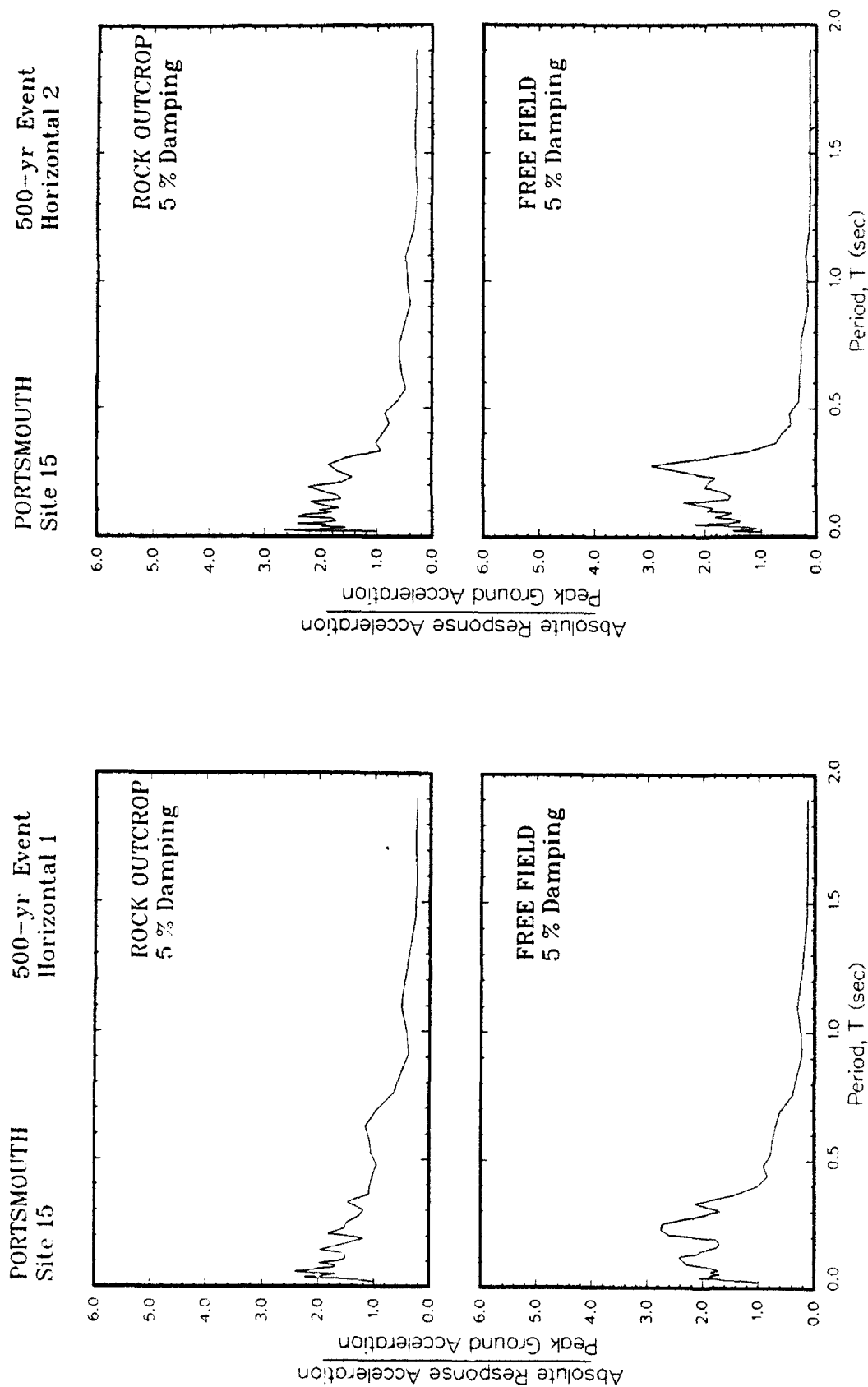


Figure G15. Ratio of amplification of absolute acceleration response spectra to peak acceleration at free field for Site 15

APPENDIX H: ACCELERATION-TIME RECORDS FOR 1000-YEAR EVENT

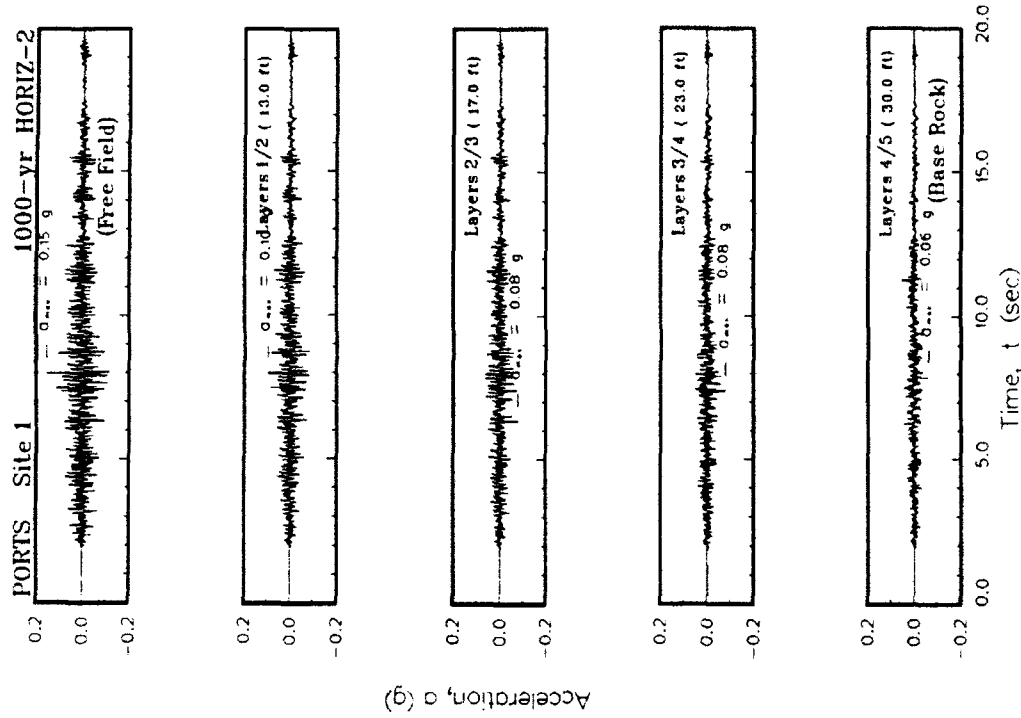
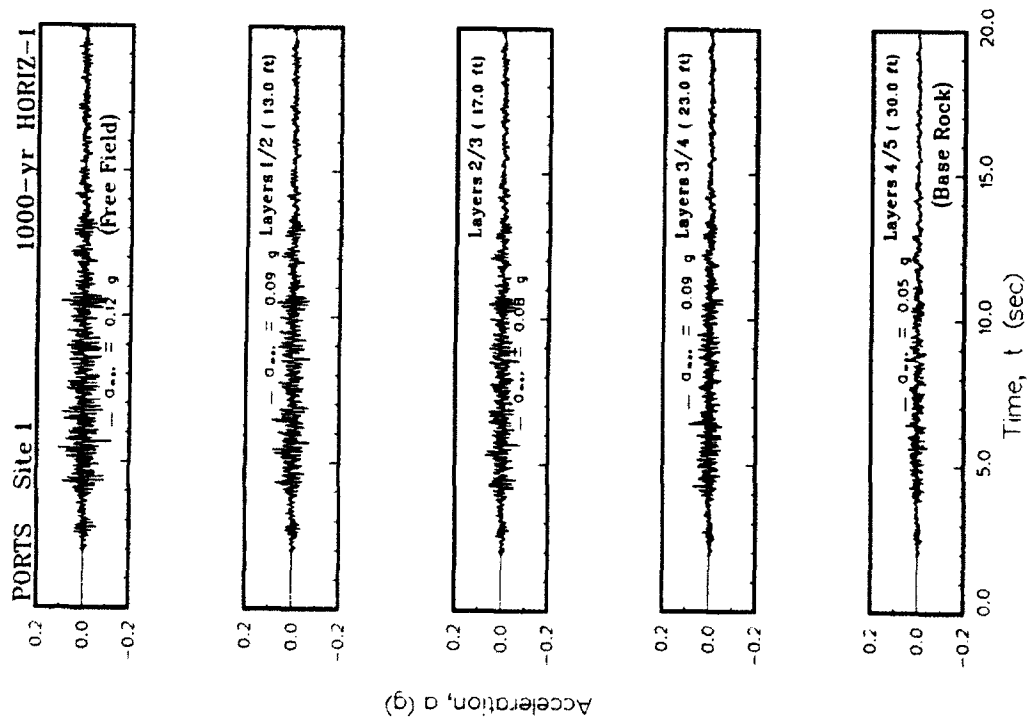


Figure H1. Variation of acceleration with time at the top of each layer for Site 1

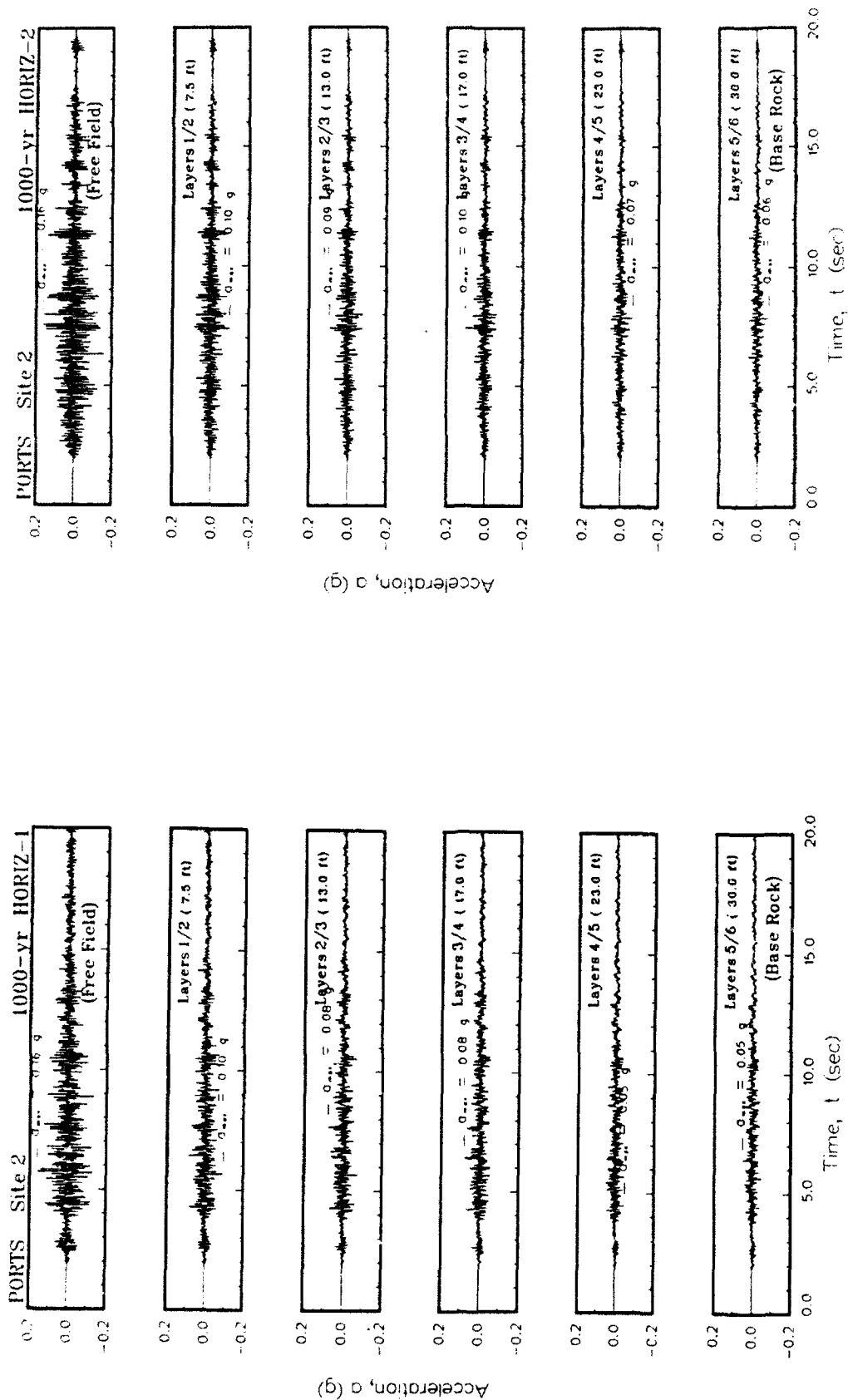


Figure H2. Variation of acceleration with time at the top of each layer for Site 2

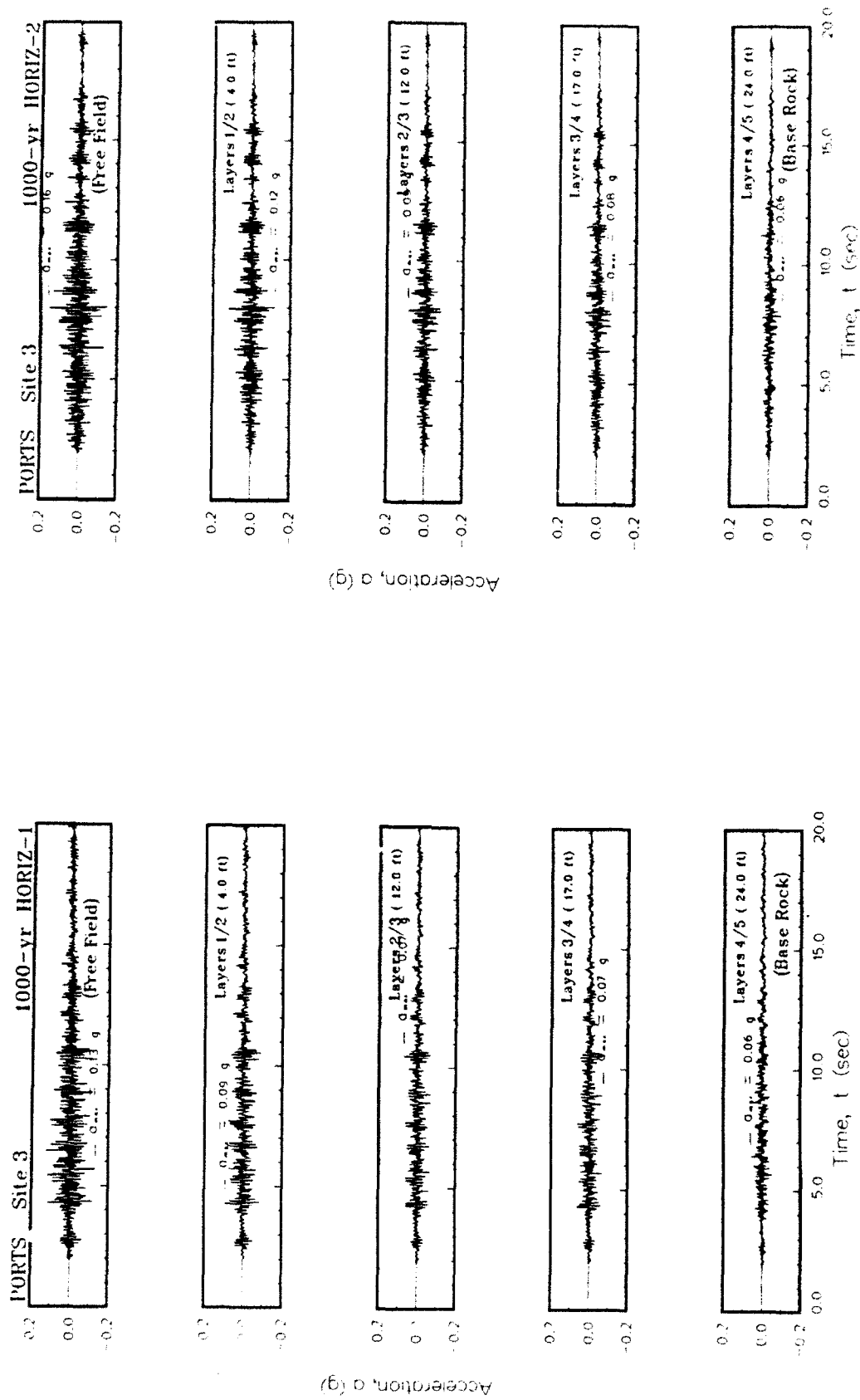


Figure H3. Variation of acceleration with time at the top of each layer for Site 3

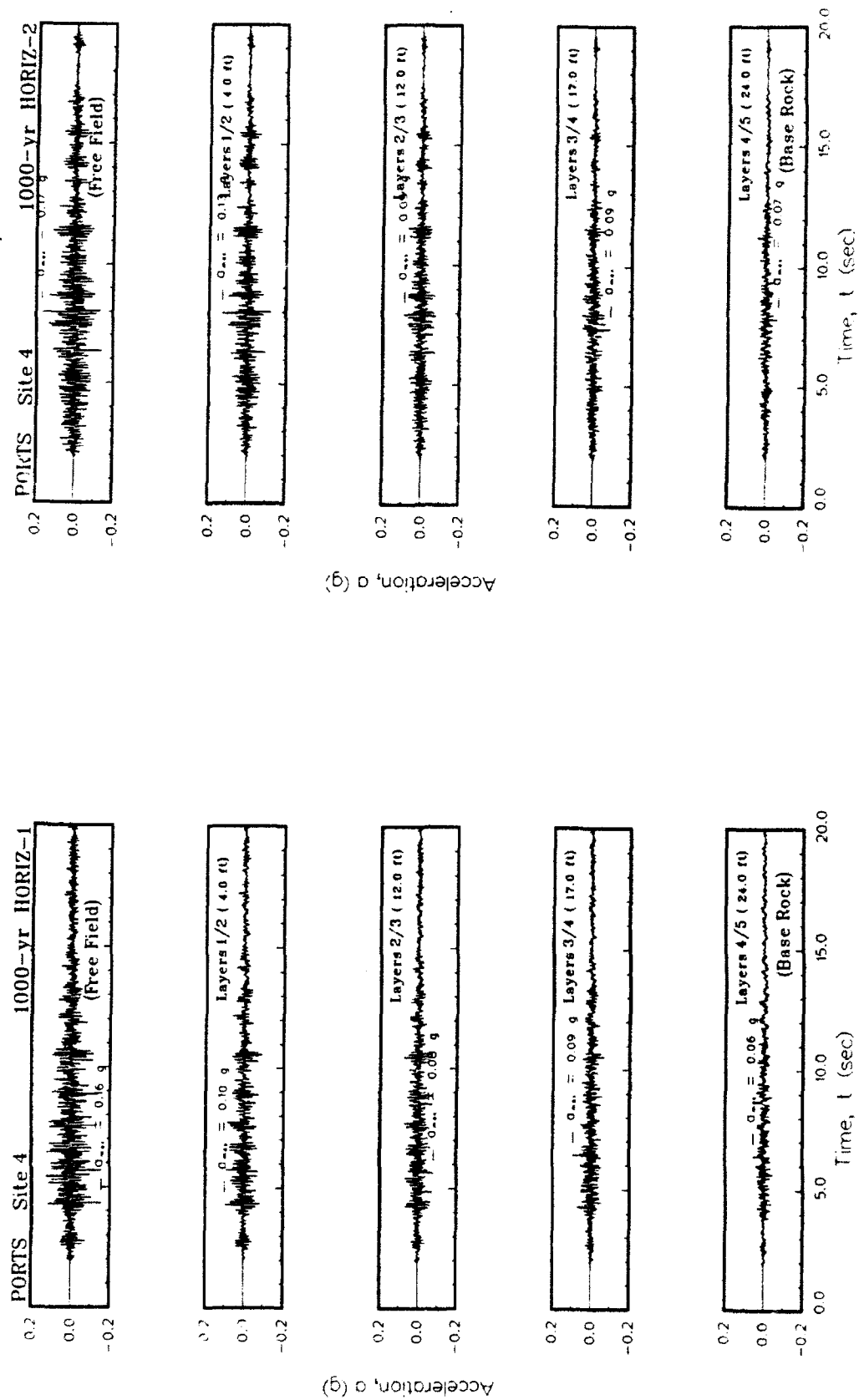


Figure H4. Variation of acceleration with time at the top of each layer for Site 4

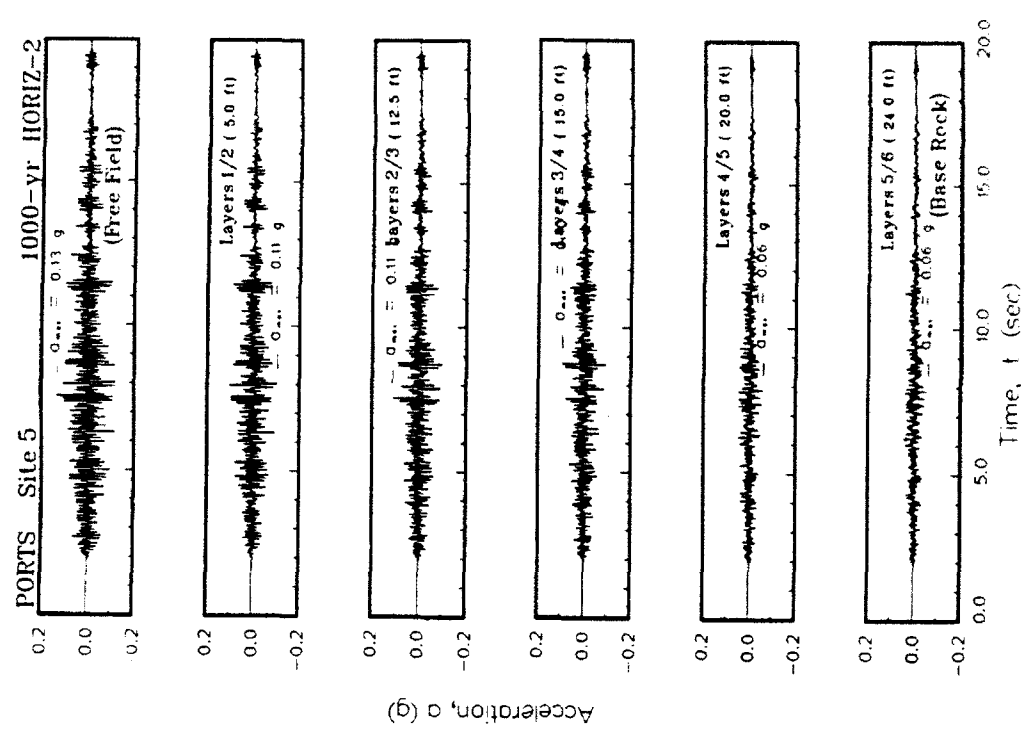
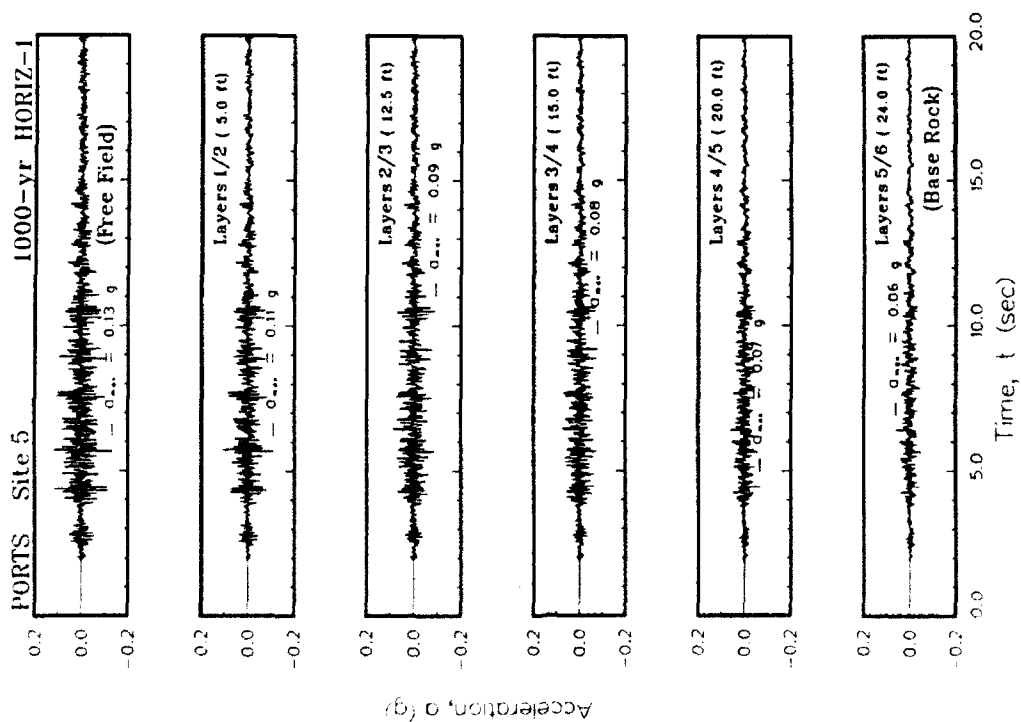


Figure H5. Variation of acceleration with time at the top of each layer for Site 5

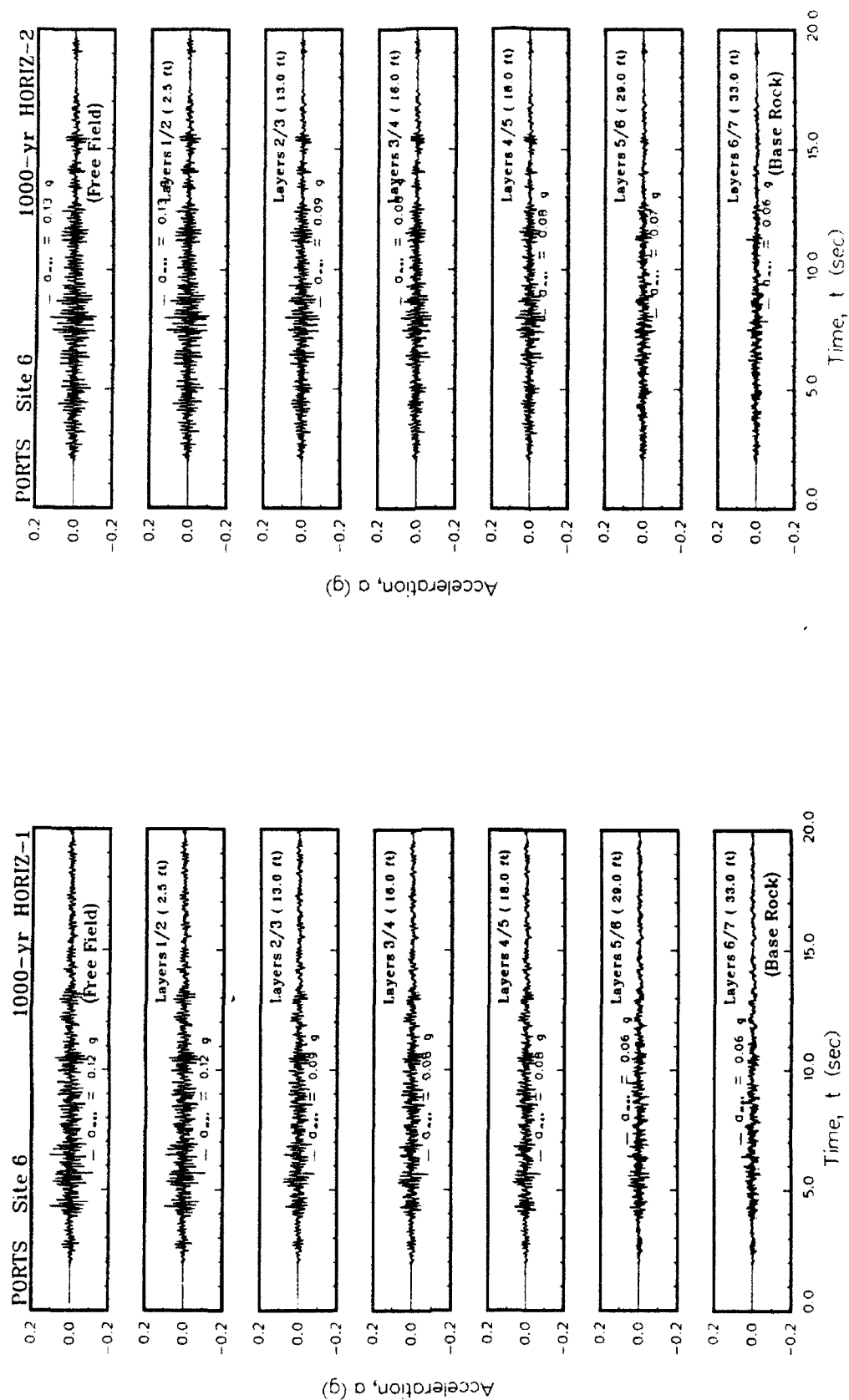


Figure H6. Variation of acceleration with time at the top of each layer for Site 6

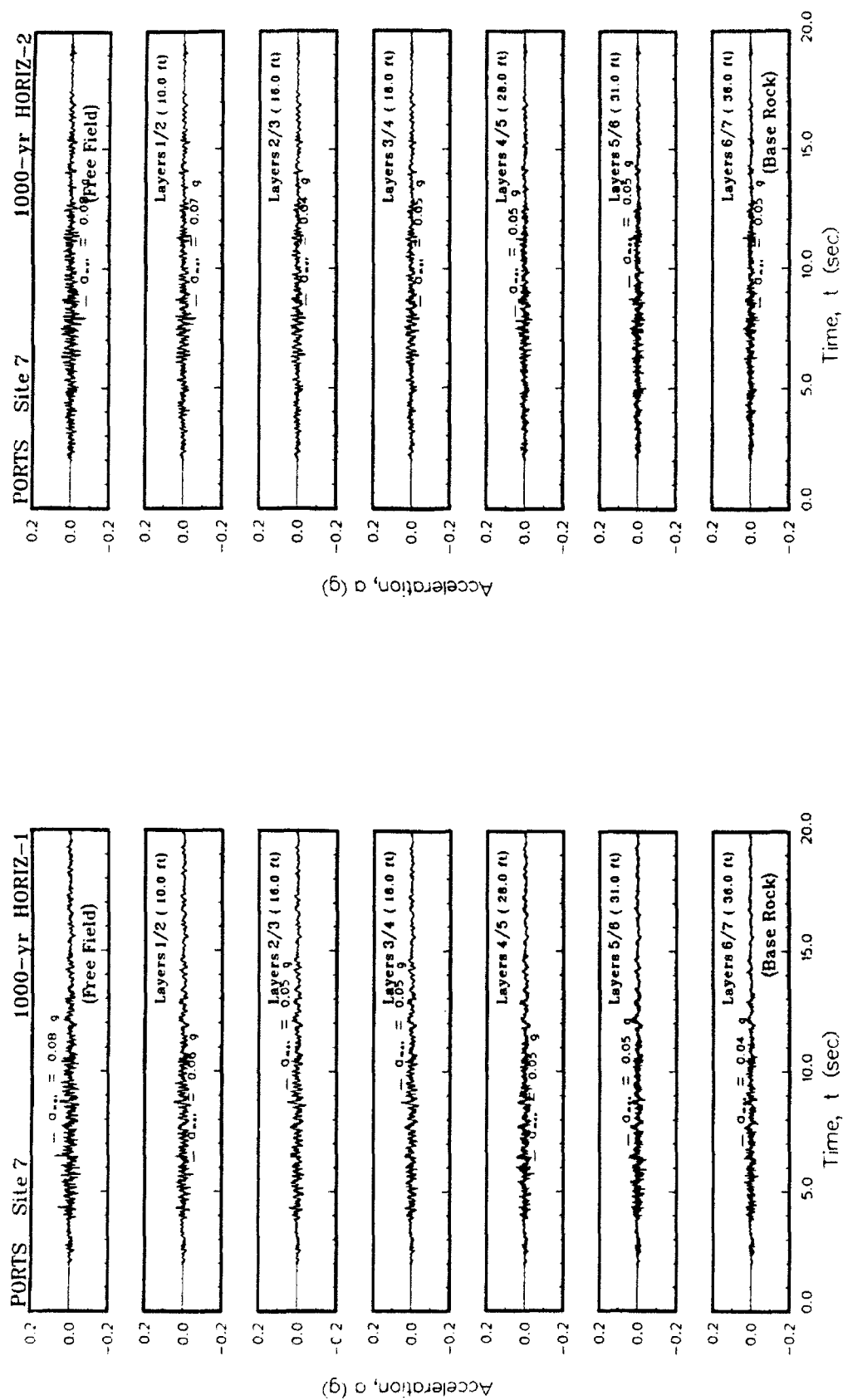


Figure H7. Variation of acceleration with time at the top of each layer for Site 7

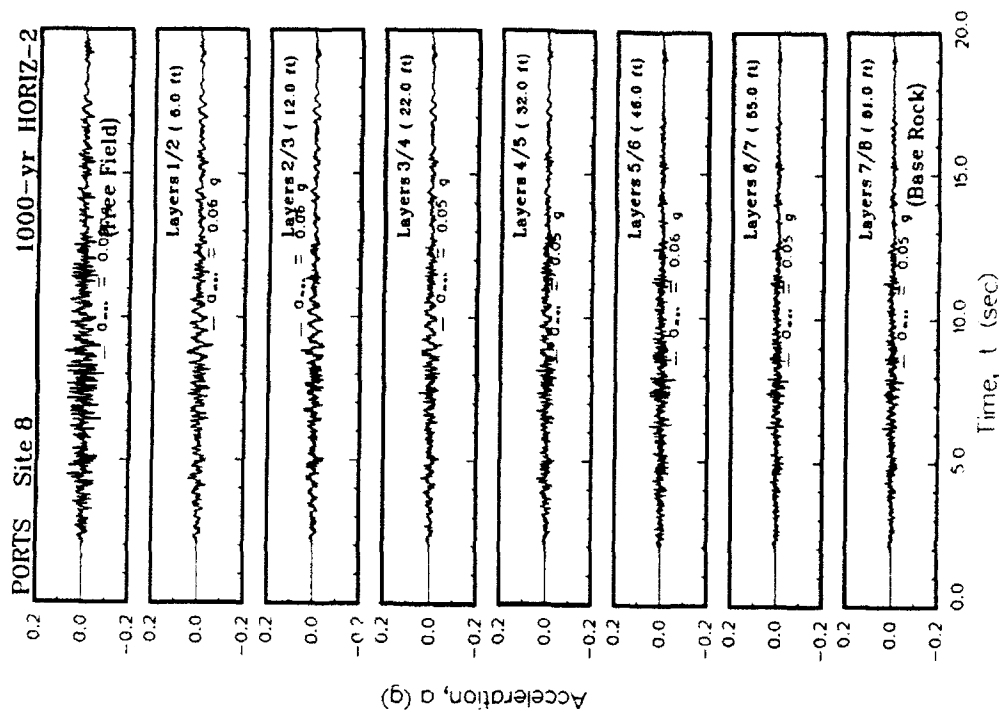
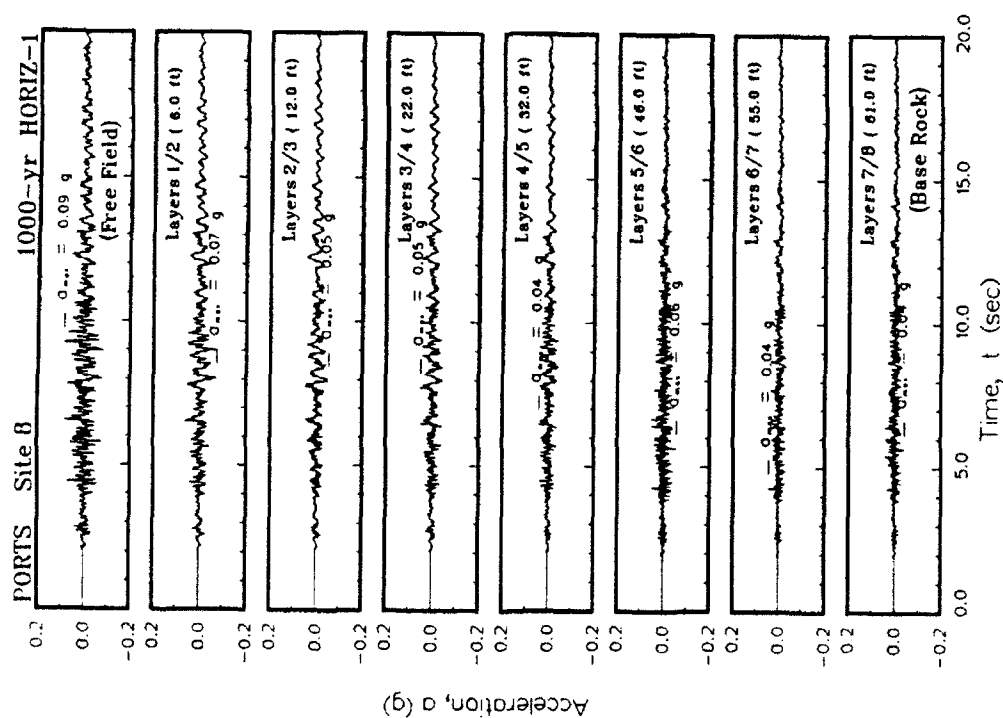


Figure H8. Variation of acceleration with time at the top of each layer for Site 8

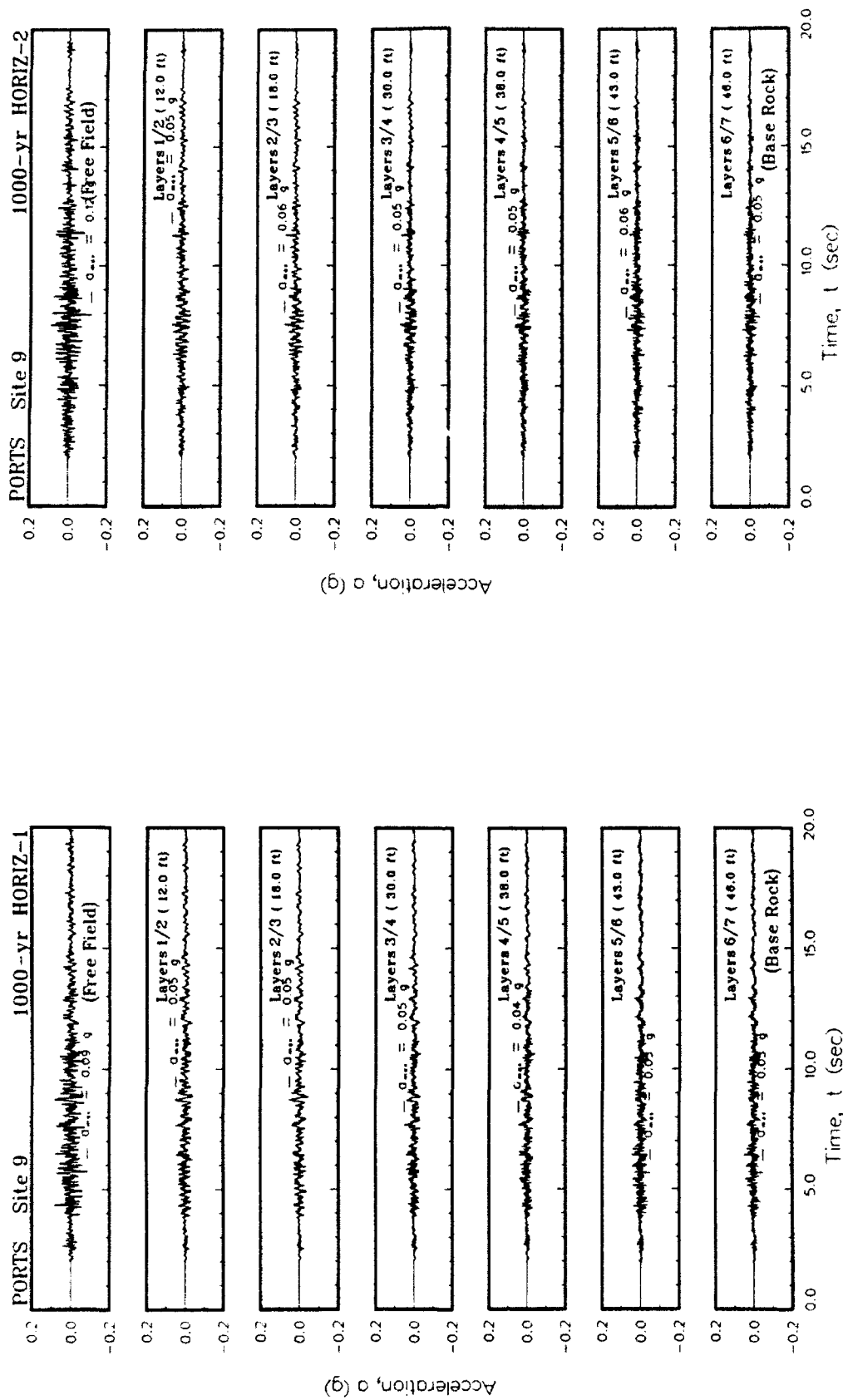


Figure H9. Variation of acceleration with time at the top of each layer for Site 9

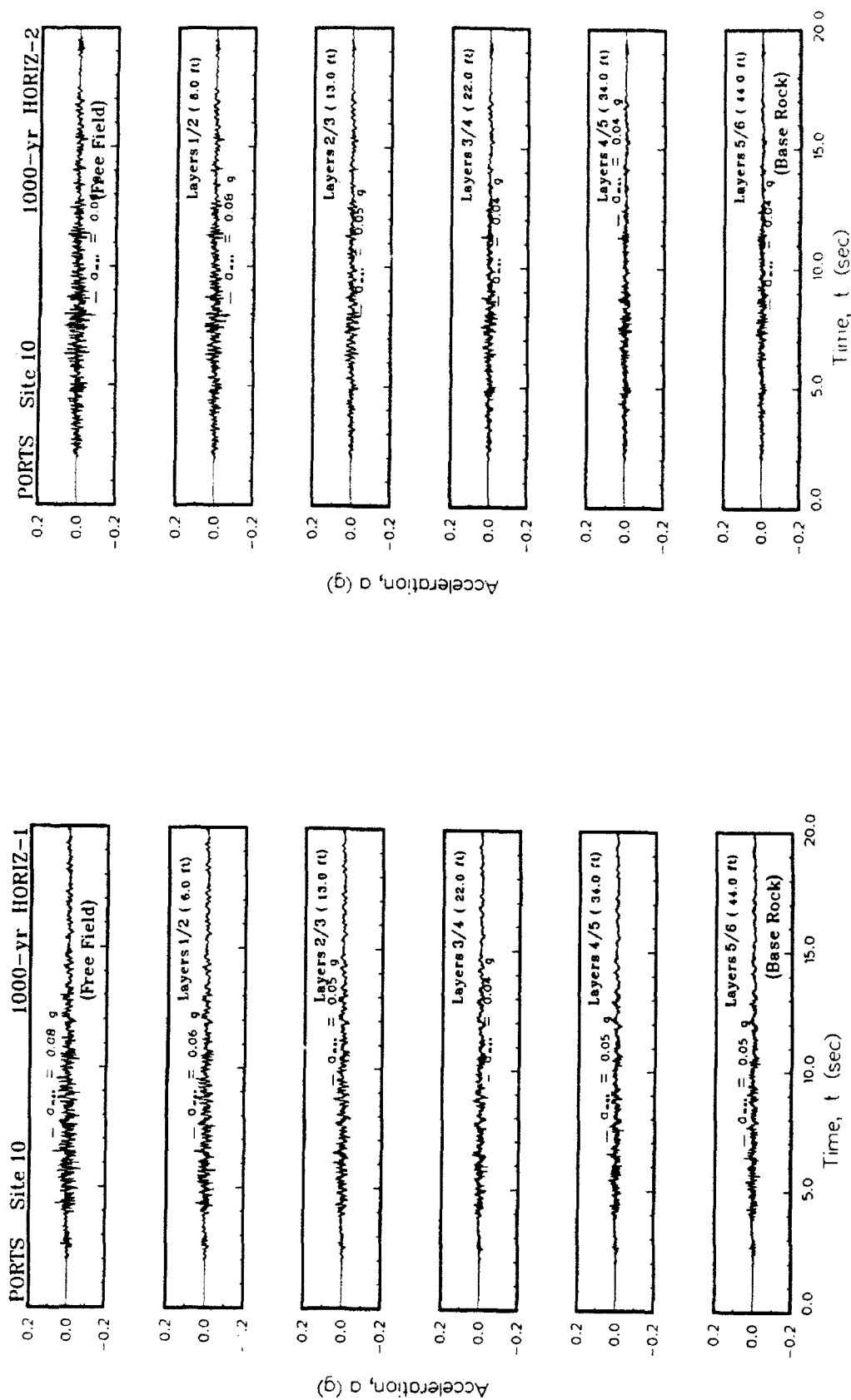


Figure H10. Variation of acceleration with time at the top of each layer for Site 10

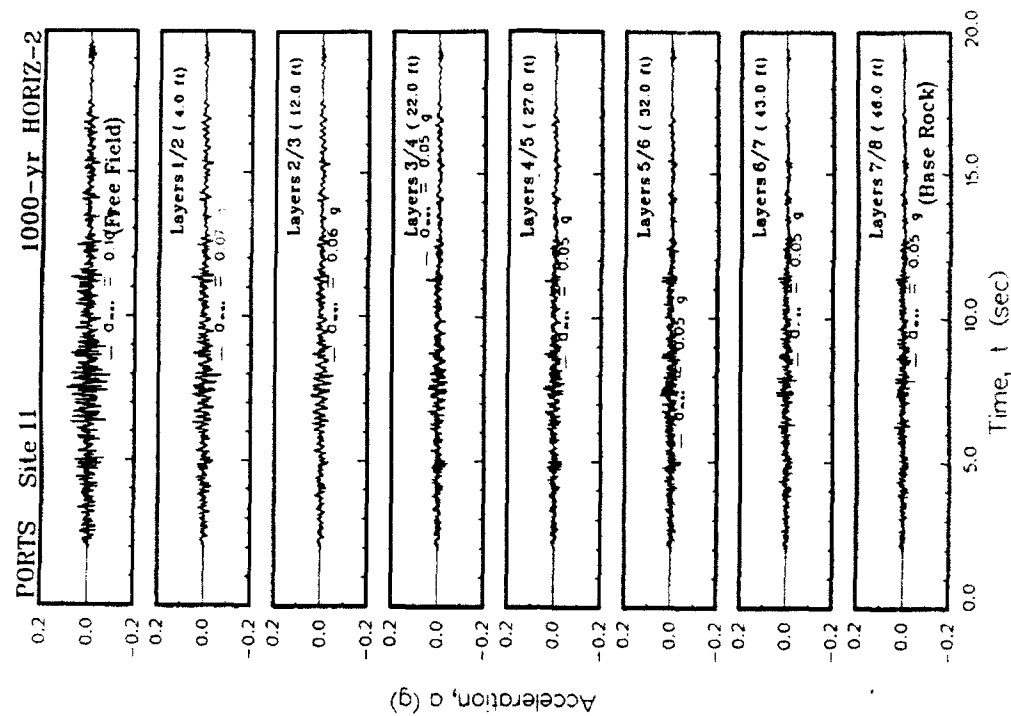
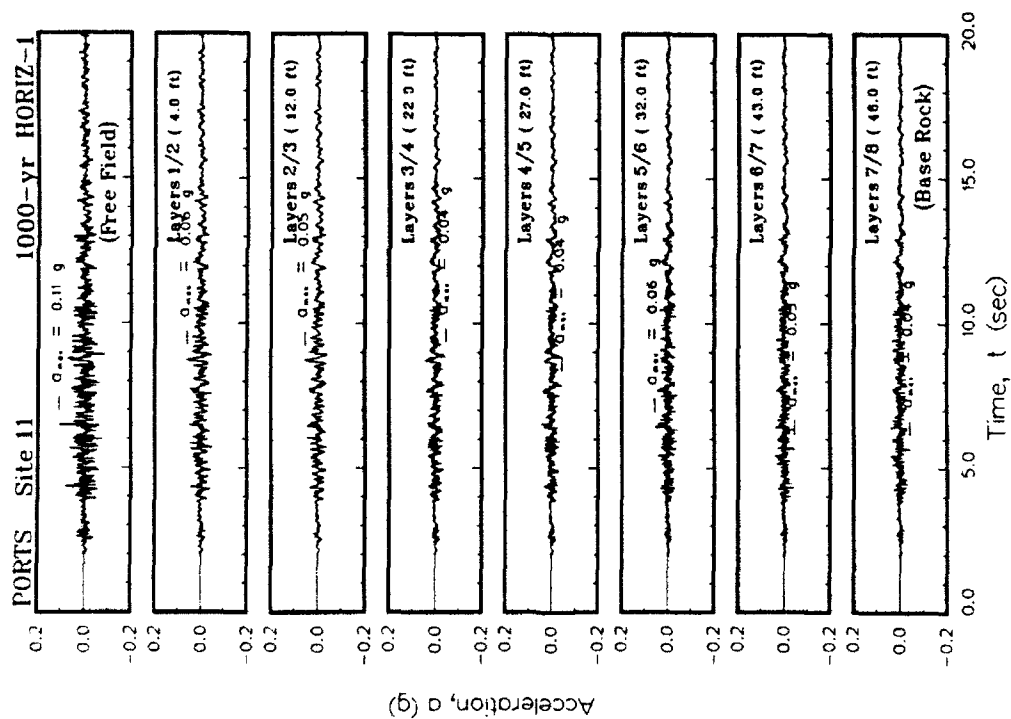


Figure H11. Variation of acceleration with time at the top of each layer for Site 11

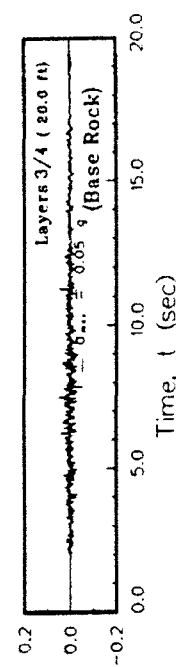
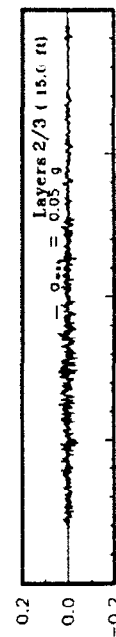
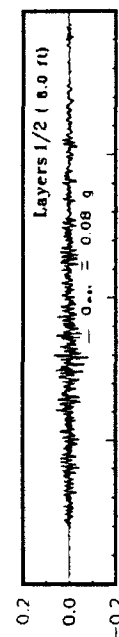
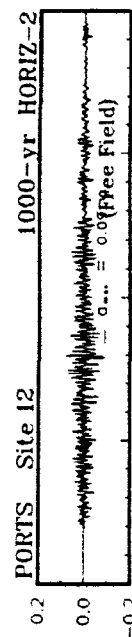
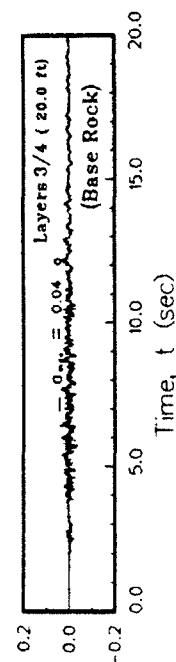
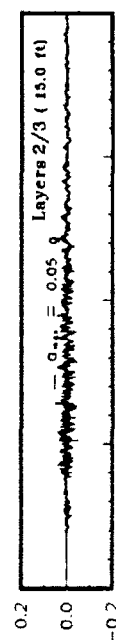
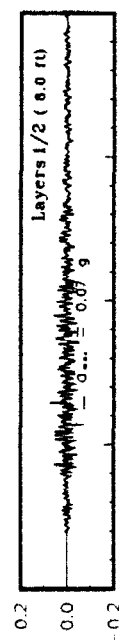
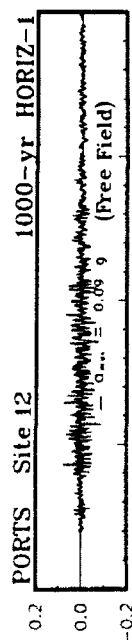


Figure H12. Variation of acceleration with time at the top of each layer for Site 12

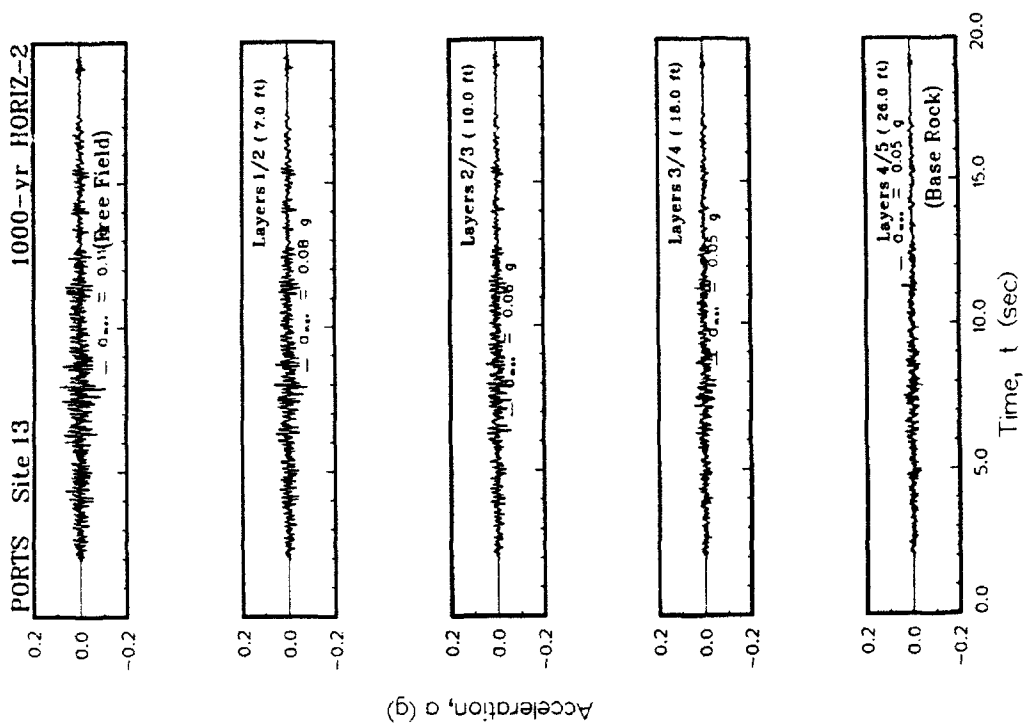
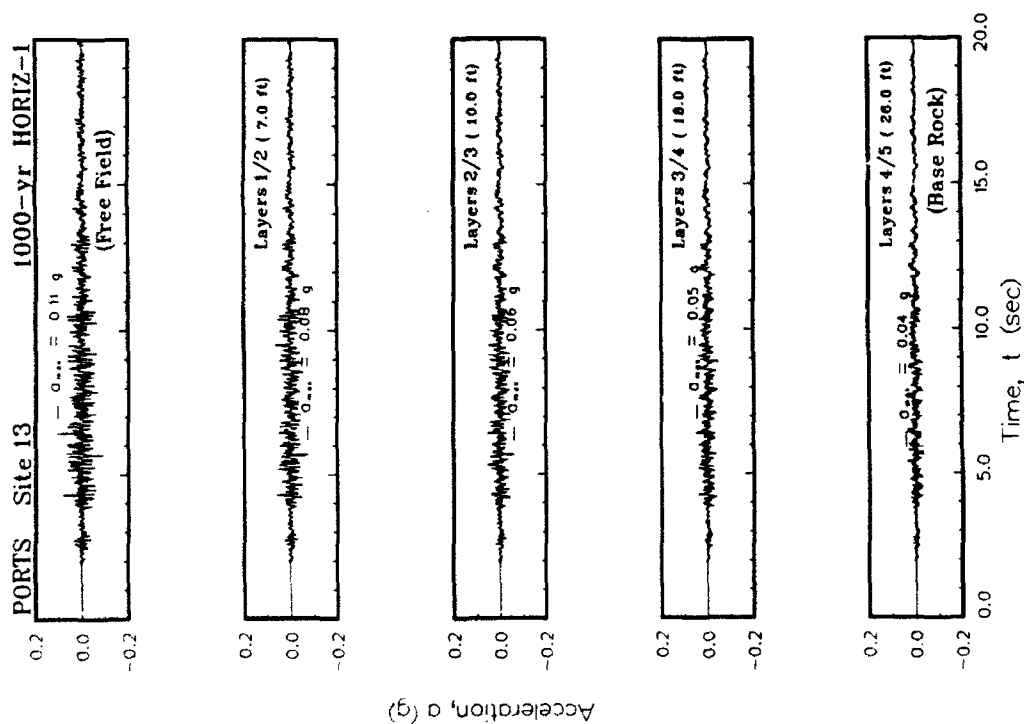


Figure H13. Variation of acceleration with time at the top of each layer for Site 13

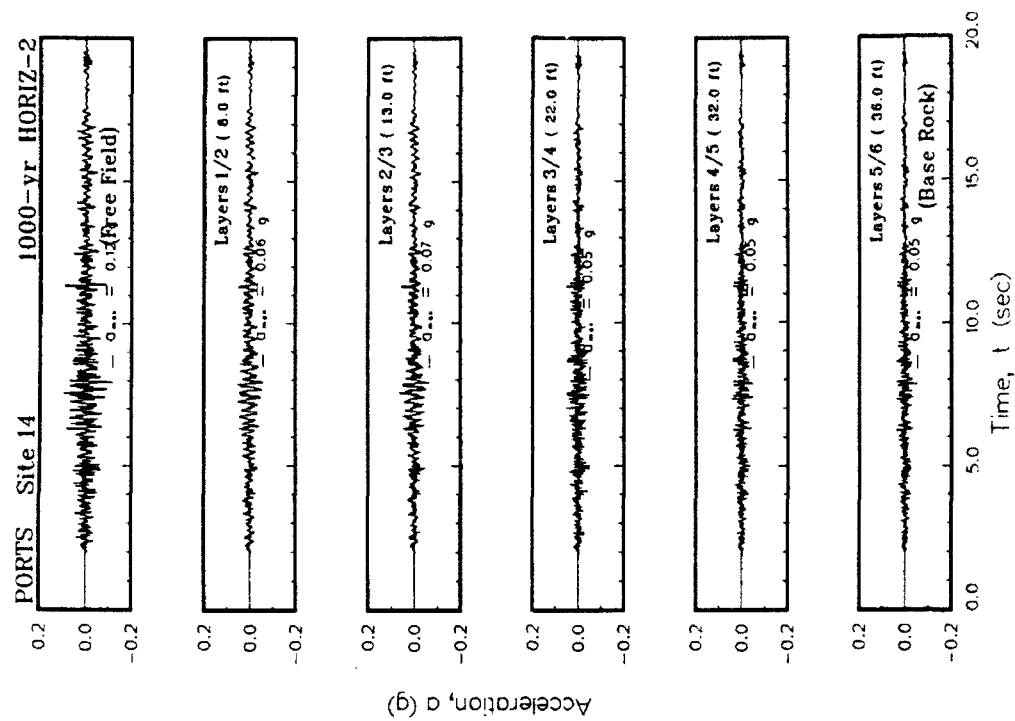
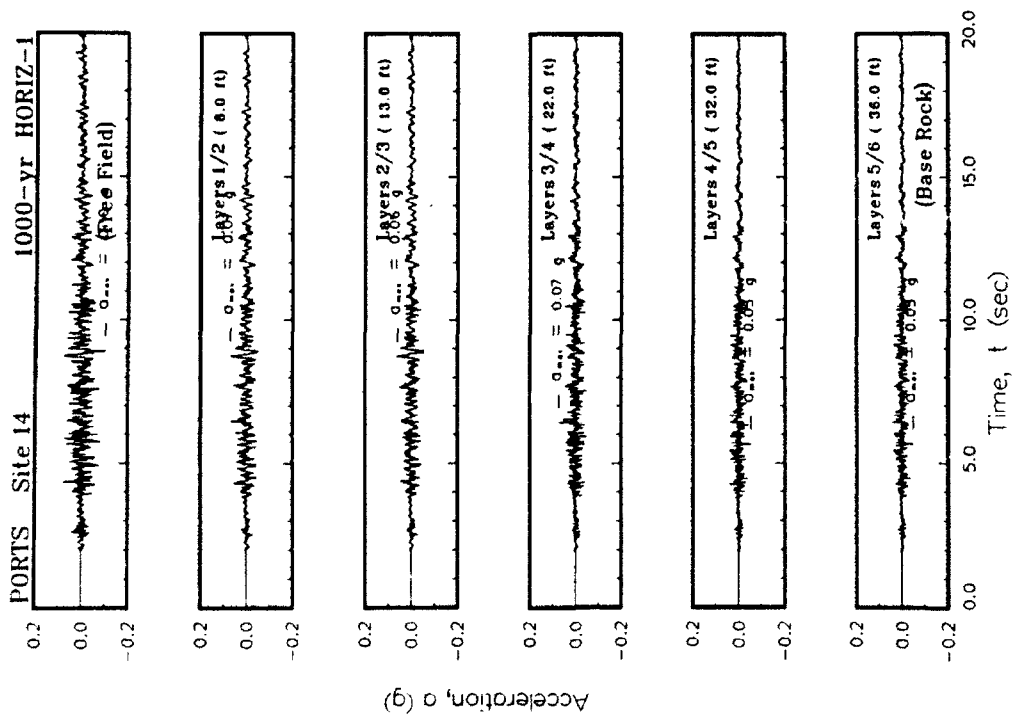


Figure H14. Variation of acceleration with time at the top of each layer for Site 14

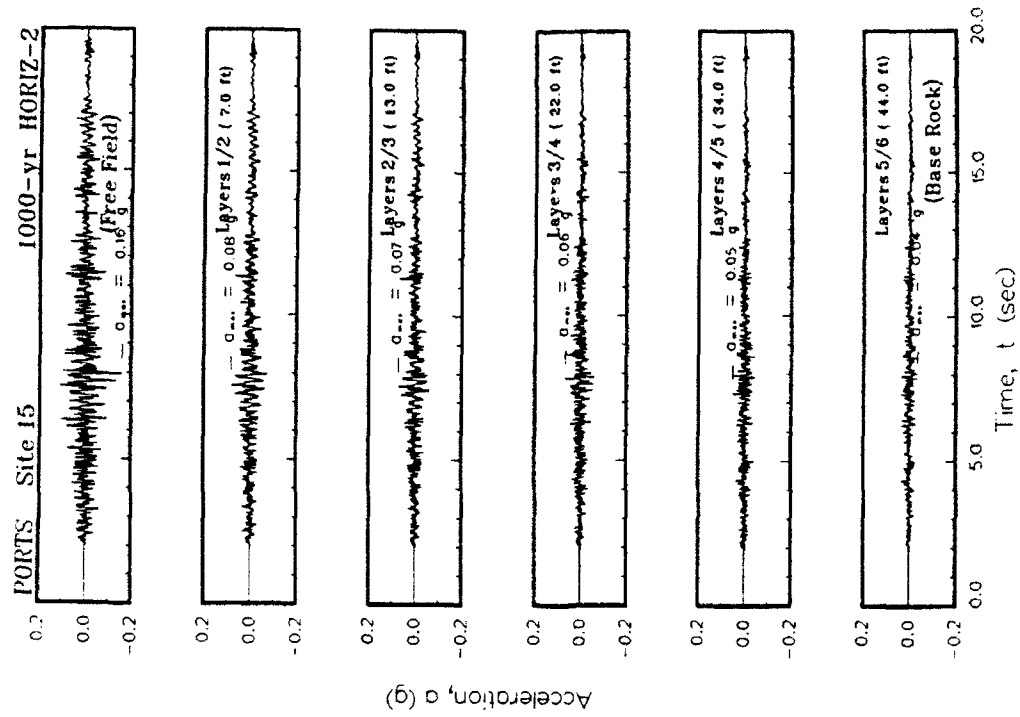
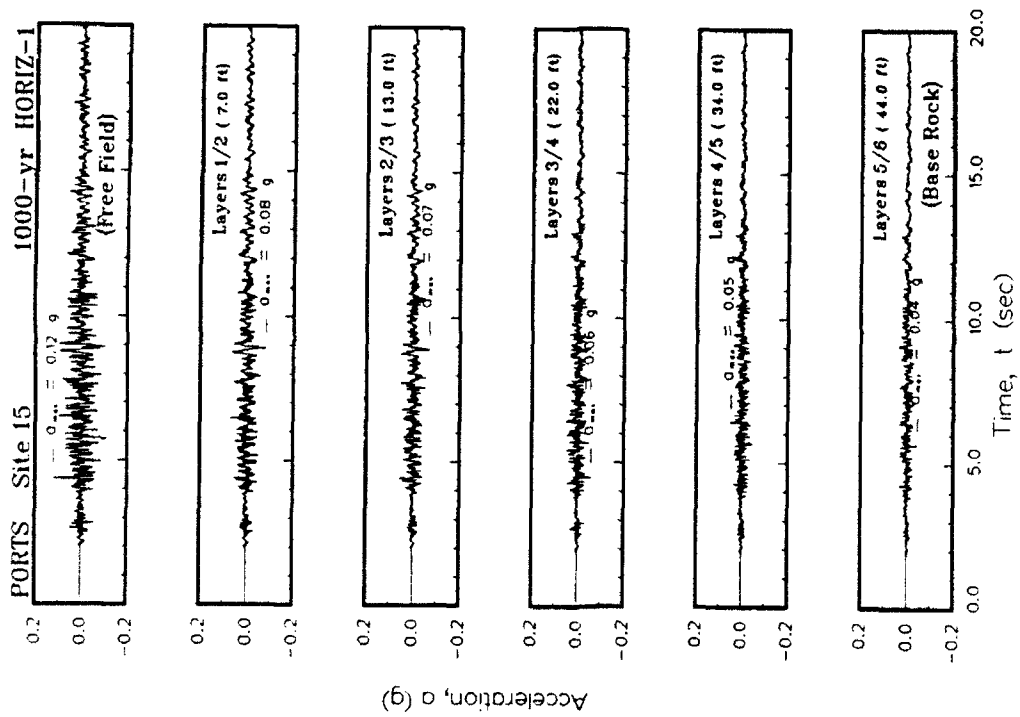
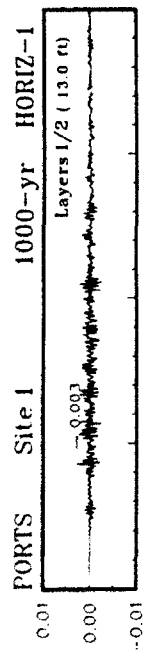
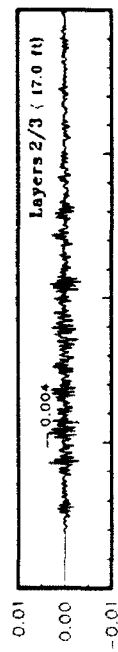


Figure H15. Variation of acceleration with time at the top of each layer for Site 15

APPENDIX I: SHEAR STRAINS FOR 1000-YEAR EVENT



Effective Shear Strain (percent)



Effective Shear Strain (percent)

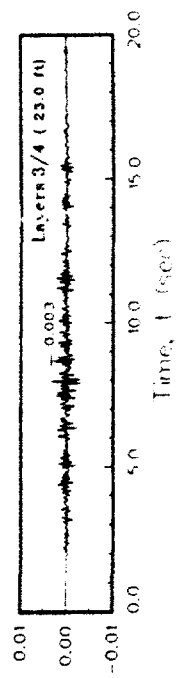
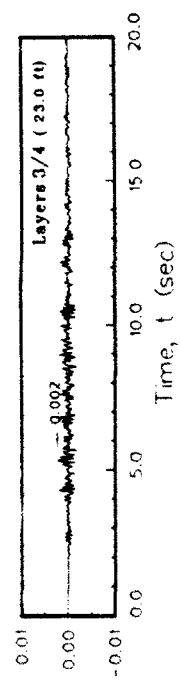
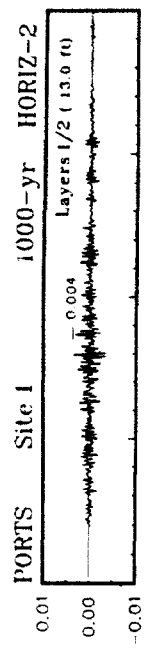
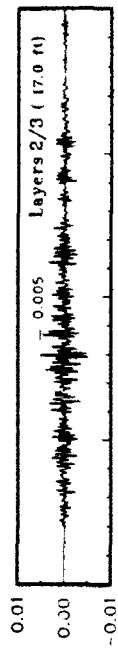


Figure 11. Variation of shear strain with time at contacts between layers for Site 1

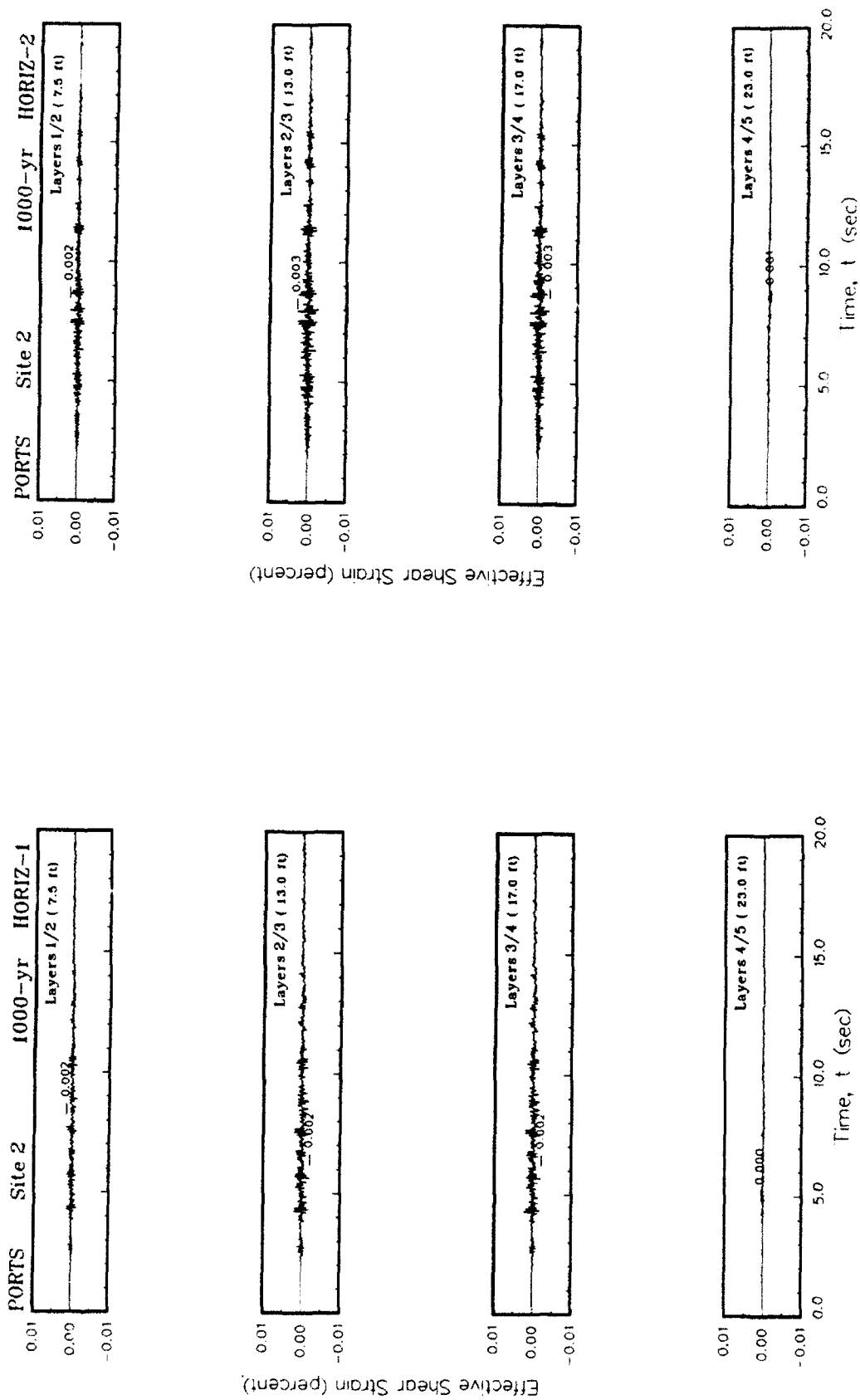
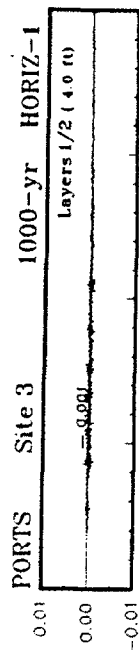
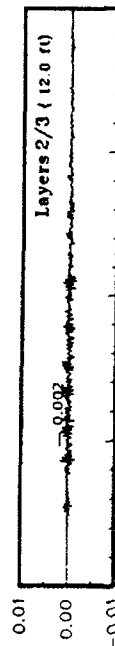


Figure 12. Variation of shear strain with time at contacts between layers for Site 2



Effective Shear Strain (percent)



Effective Shear Strain (percent)

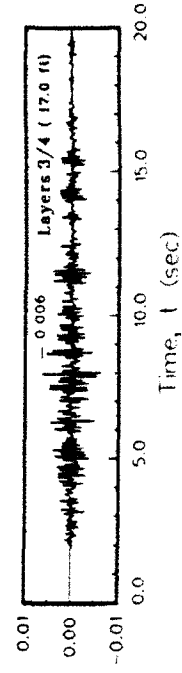
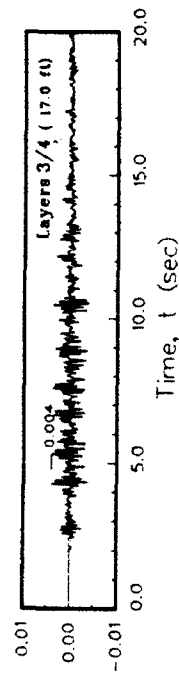
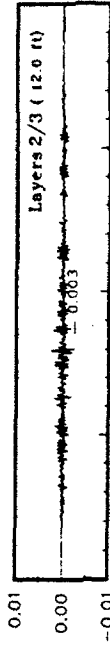


Figure I3. Variation of shear strain with time at contacts between layers for Site 3

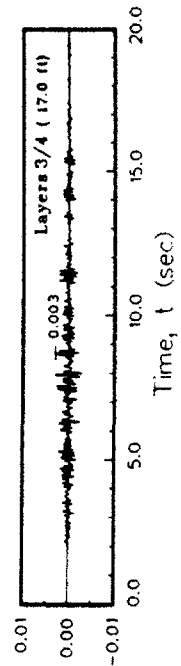
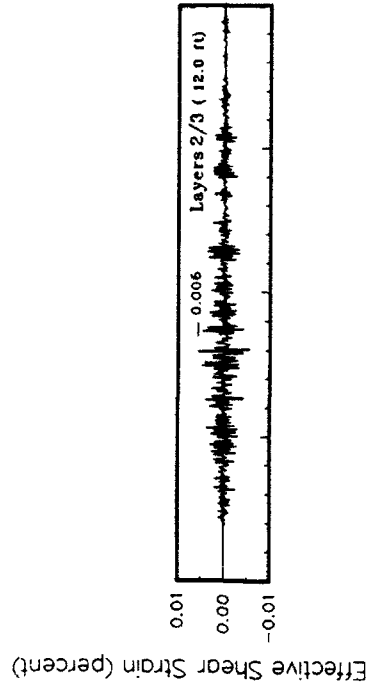
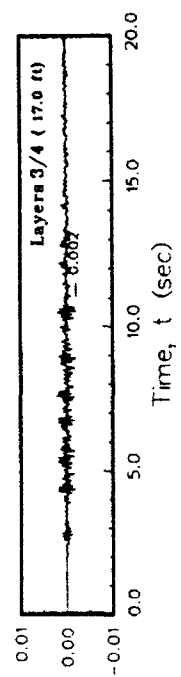
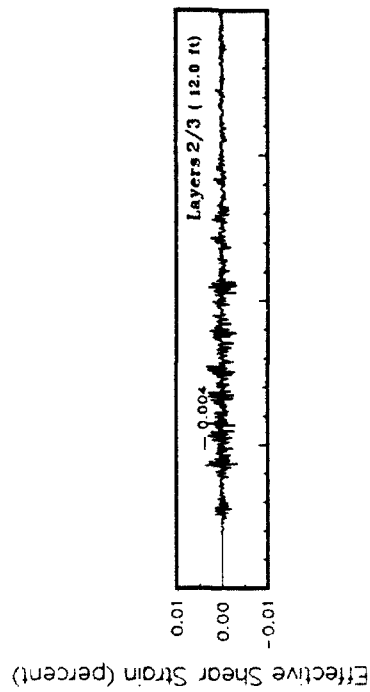
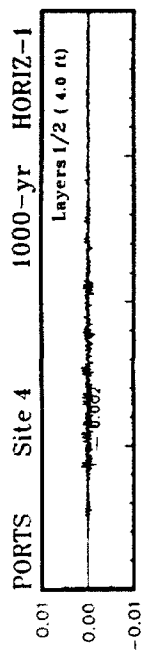


Figure I4. Variation of shear strain with time at contacts between layers for Site 4

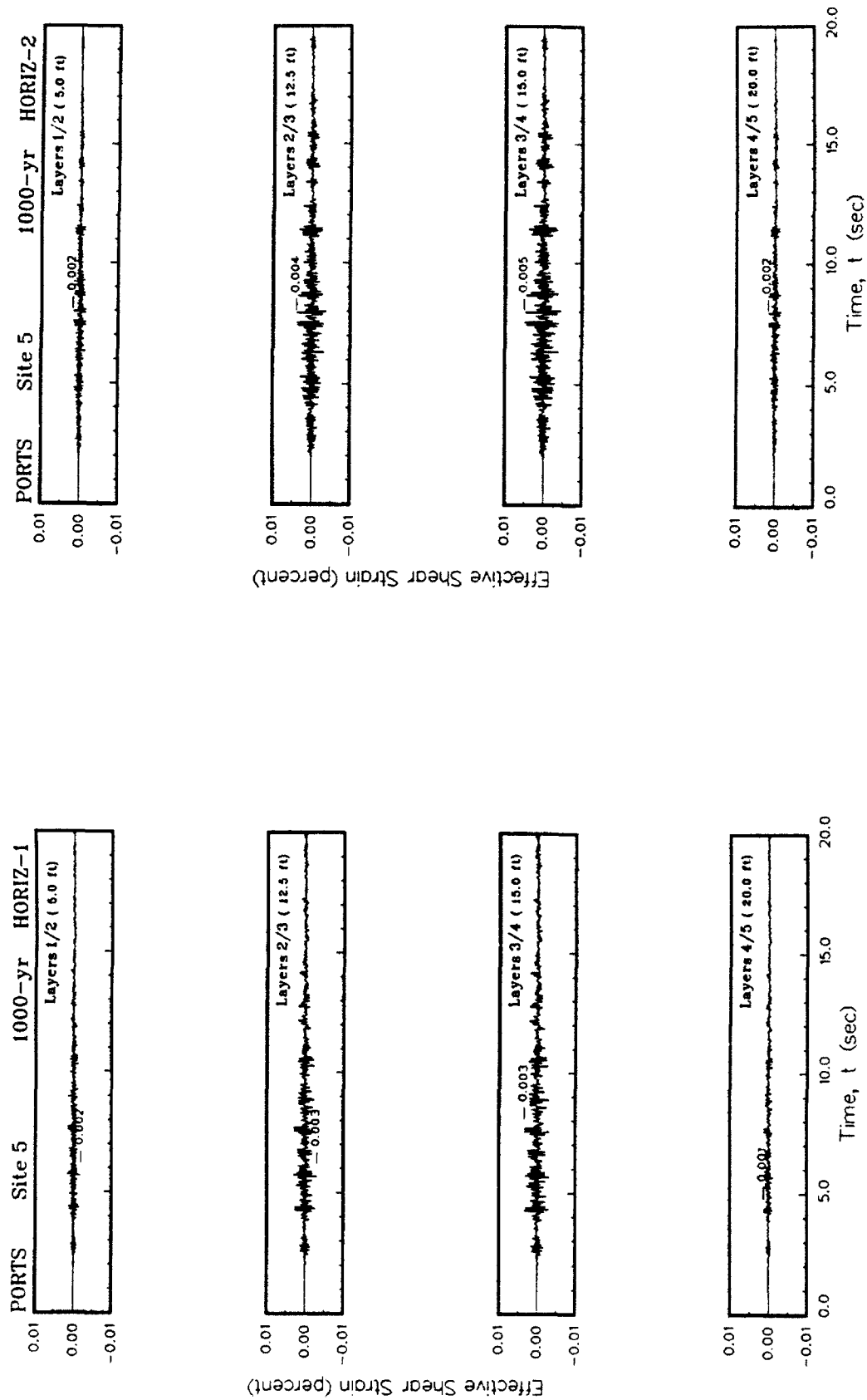


Figure I5. Variation of shear strain with time at contacts between layers for Site 5

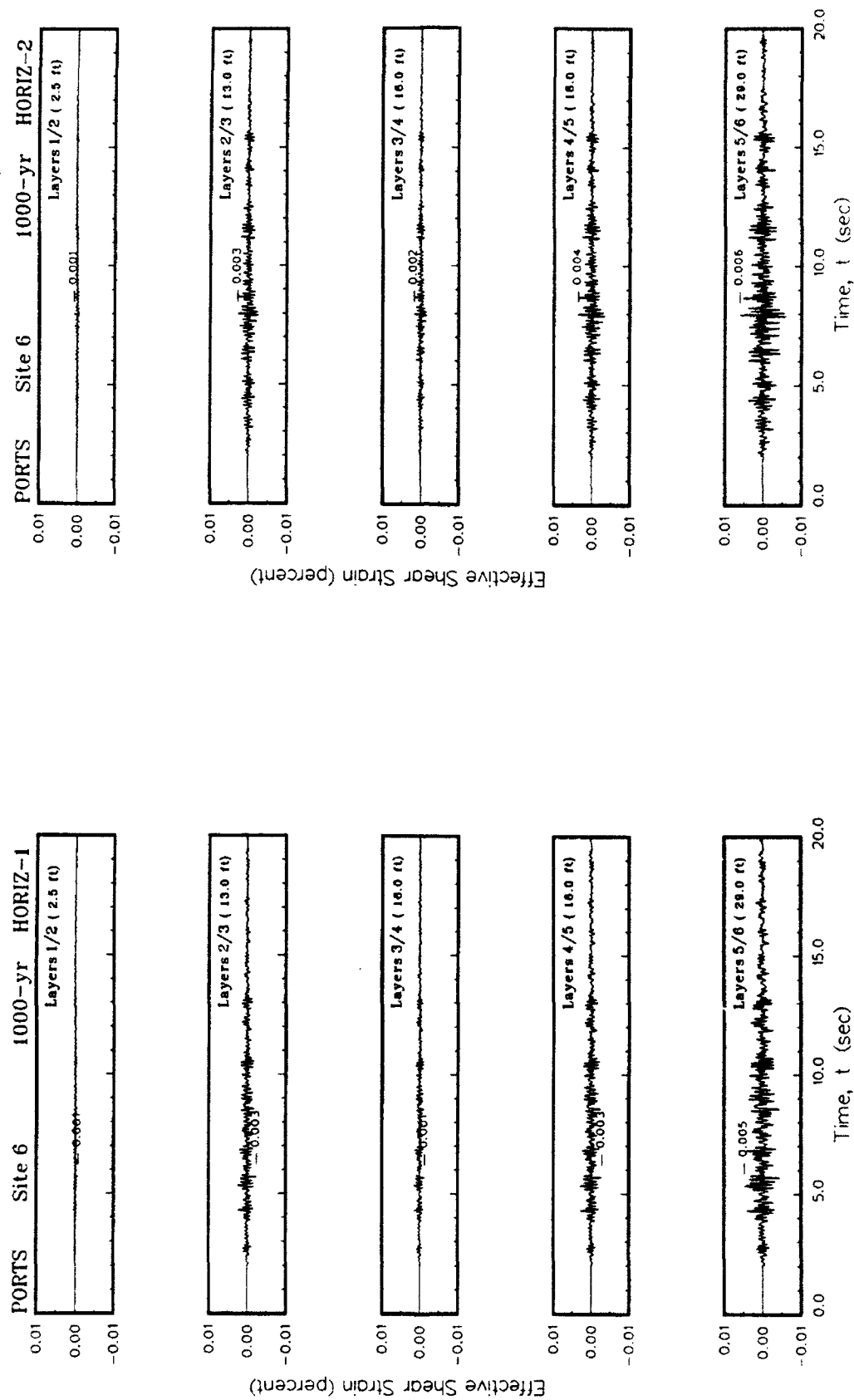


Figure 16. Variation of shear strain with time at contacts between layers for Site 6

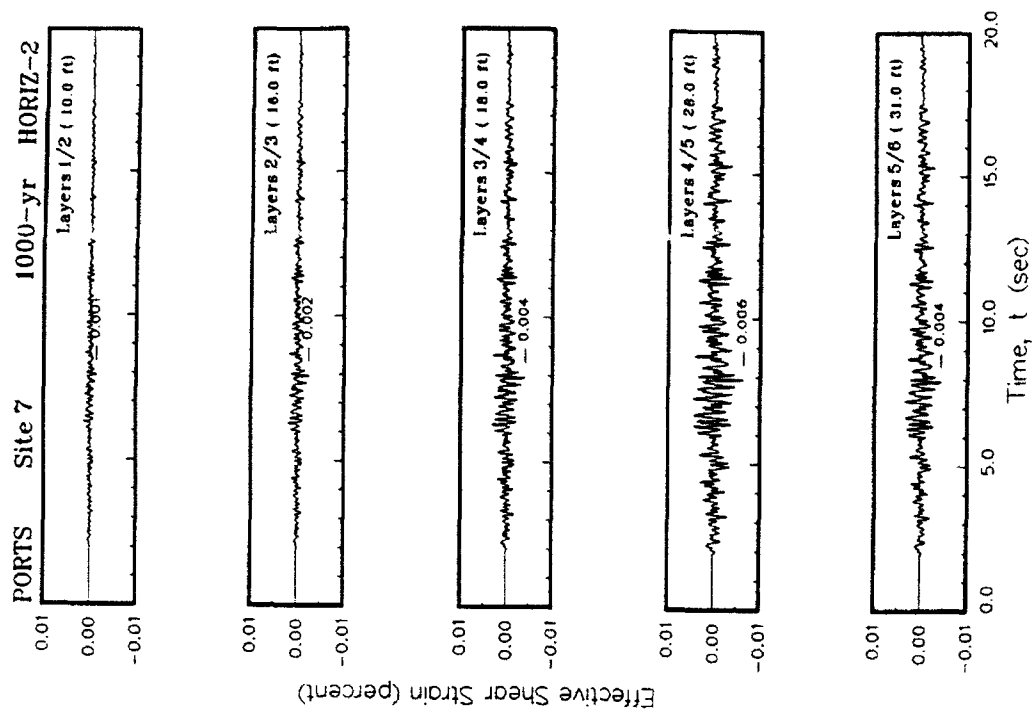
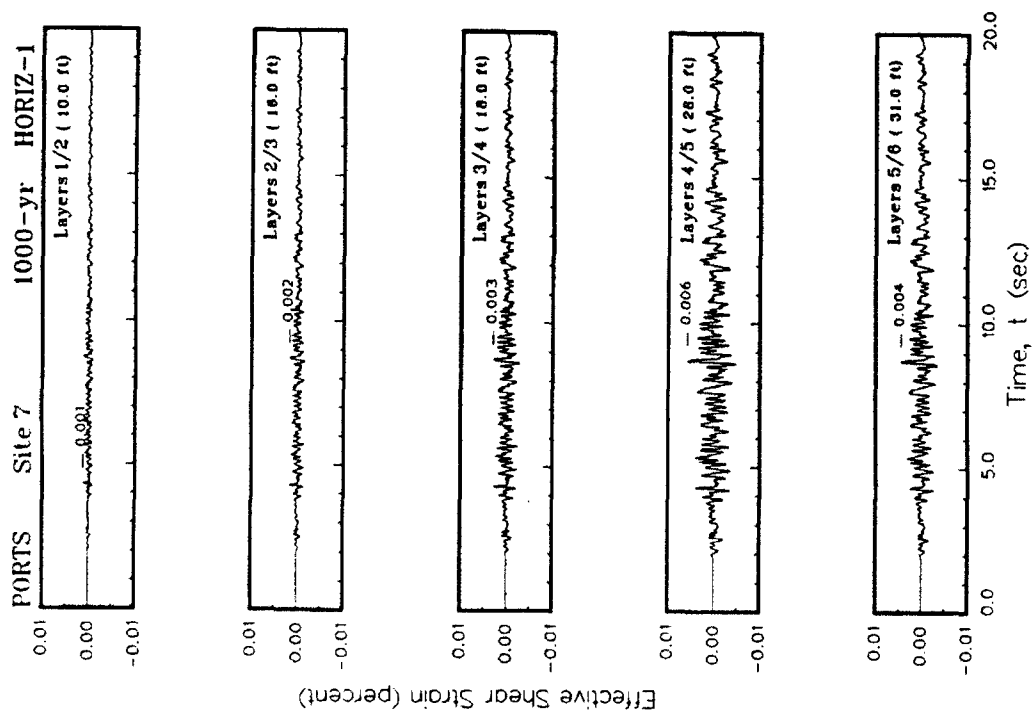


Figure I7. Variation of shear strain with time at contacts between layers for Site 7

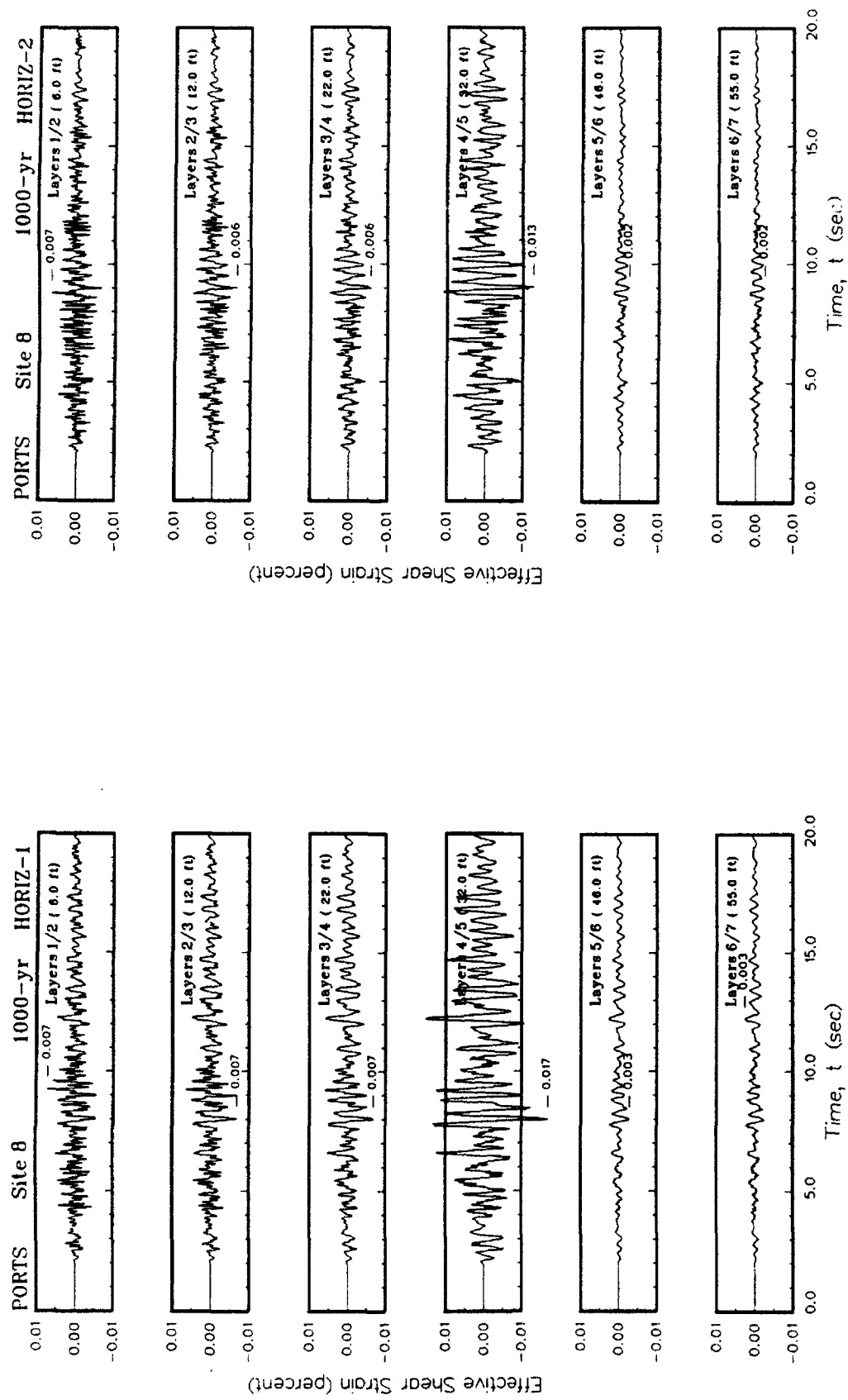


Figure 18. Variation of shear strain with time at contacts between layers for Site 8

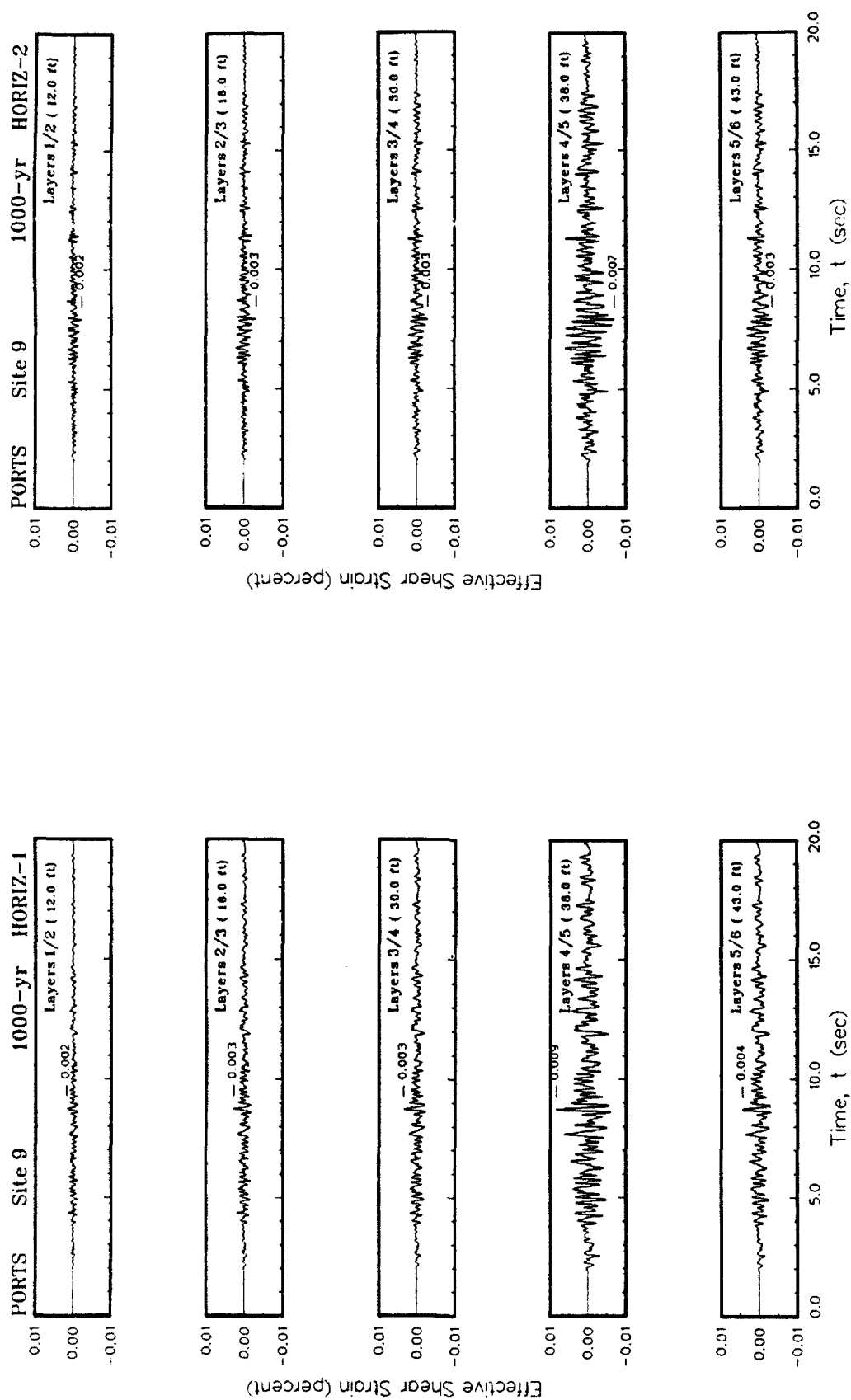


Figure 19. Variation of shear strain with time at contacts between layers for Site 9

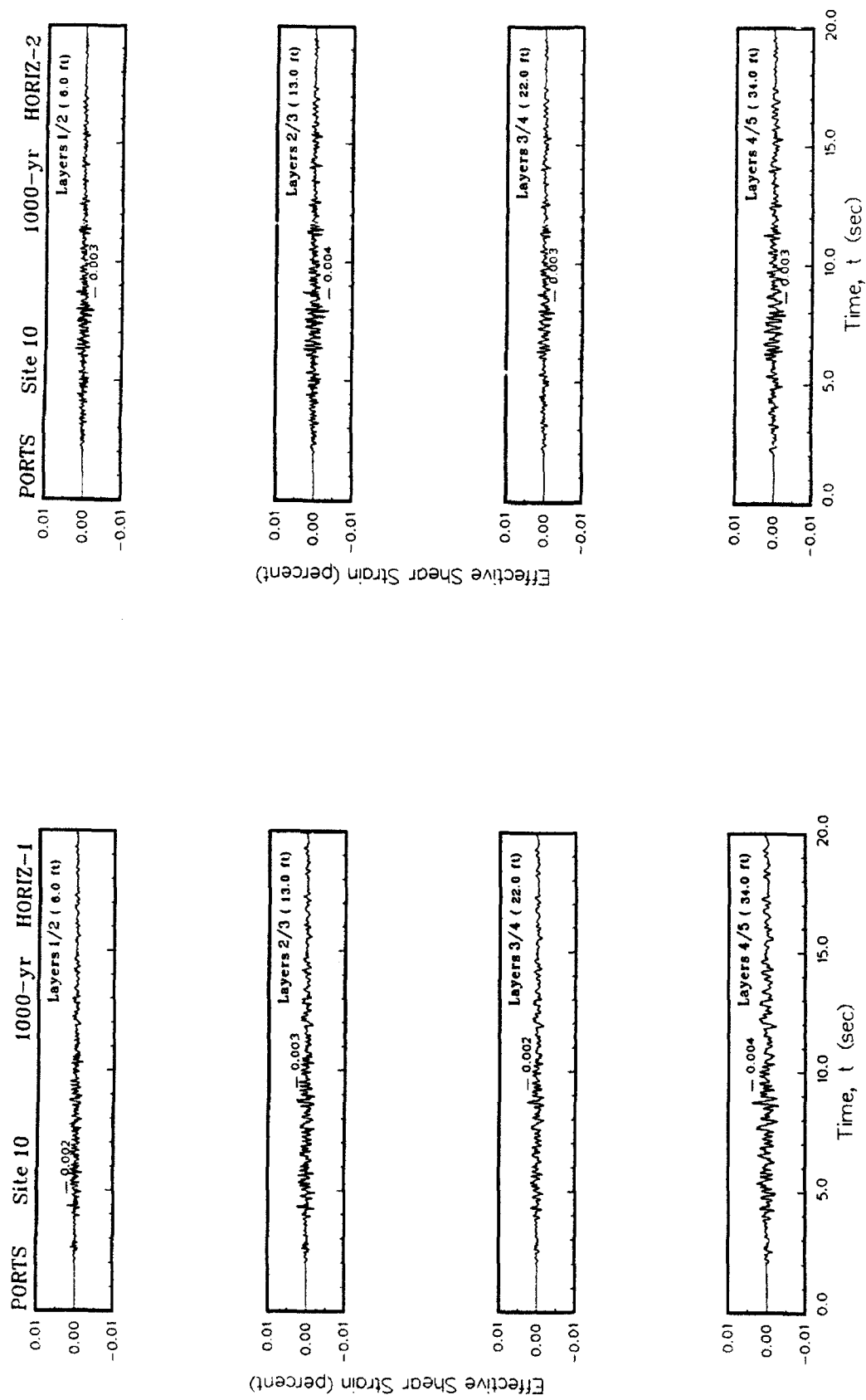


Figure 110. Variation of shear strain with time at contacts between layers for Site 10

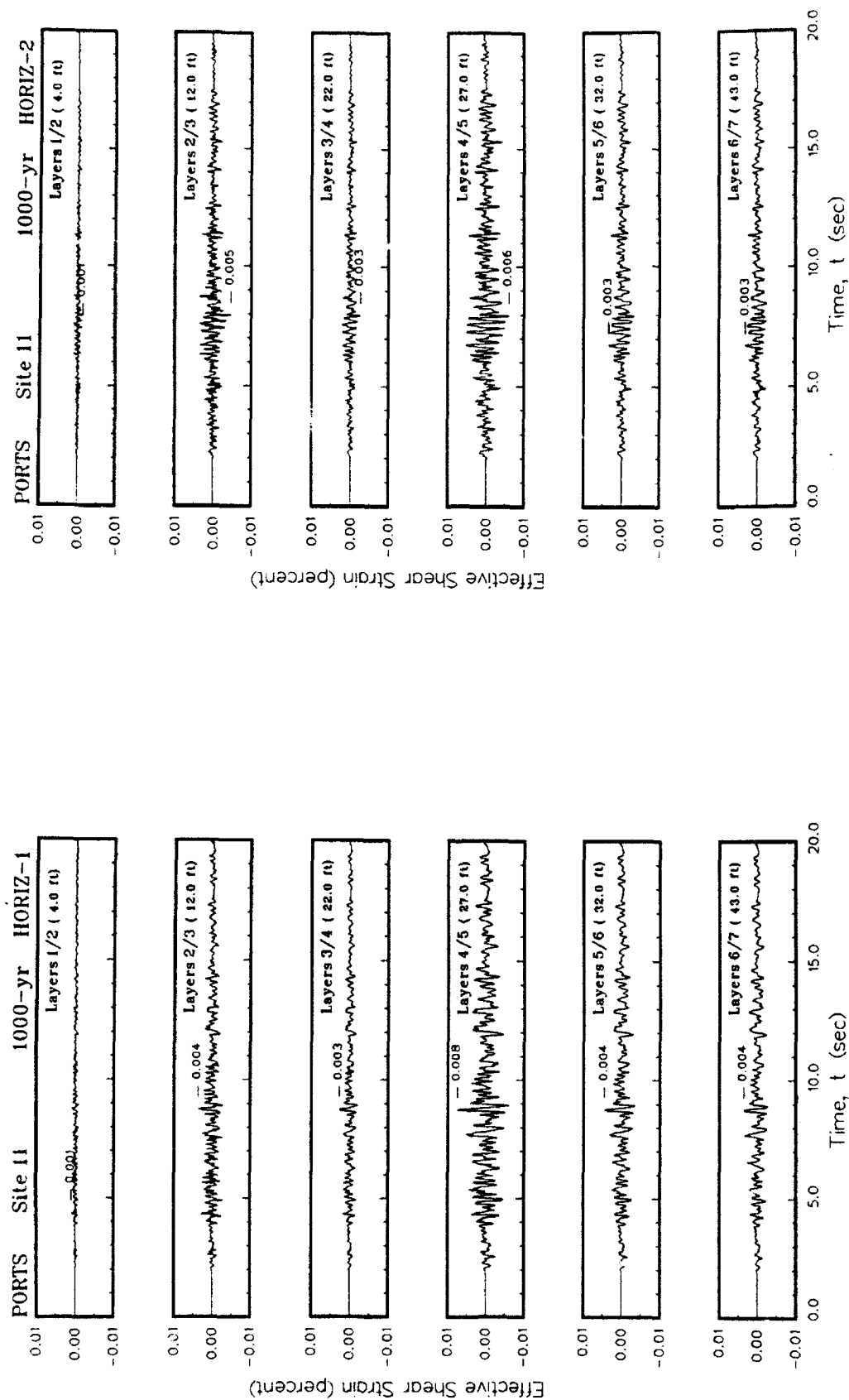
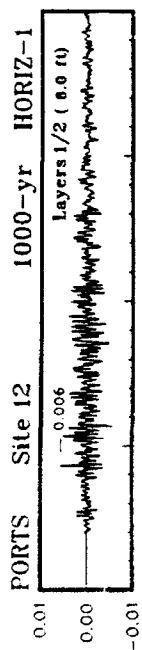
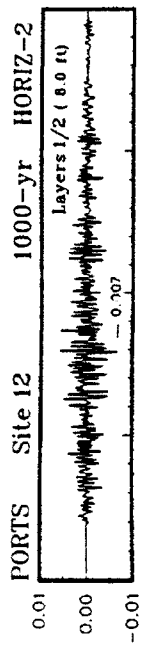


Figure I11. Variation of shear strain with time at contacts between layers for Site I1



Effective Shear Strain (percent)



Effective Shear Strain (percent)

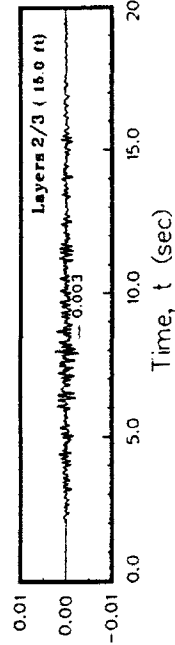
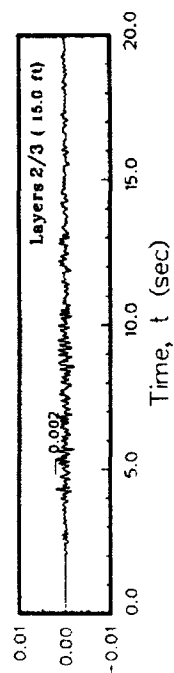
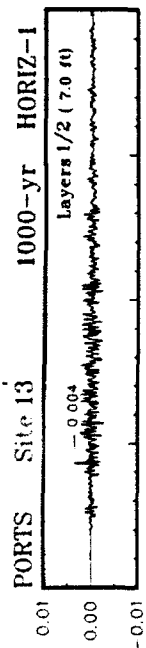


Figure I12. Variation of shear strain with time at contacts between layers for Site 12



Effective Shear Strain (percent)



Effective Shear Strain (percent)

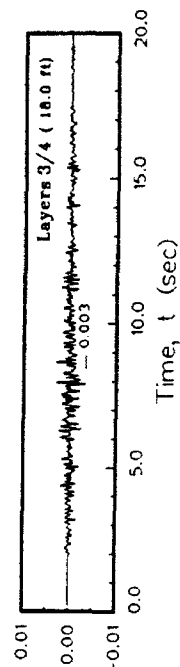
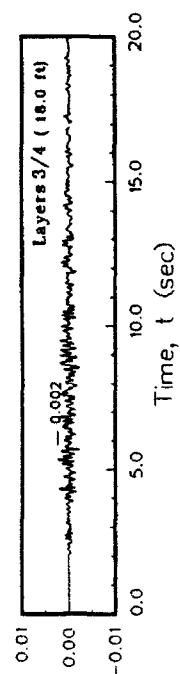
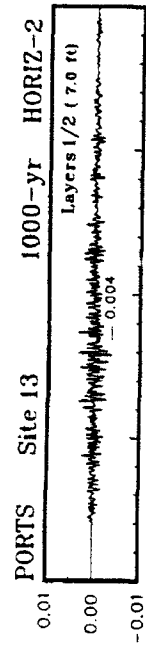
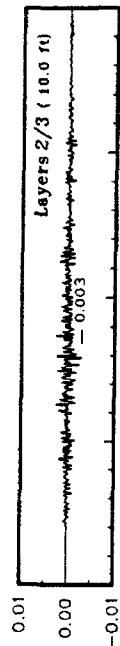


Figure I13. Variation of shear strain with time at contacts between layers for Site 13

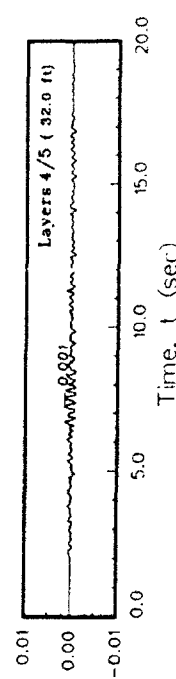
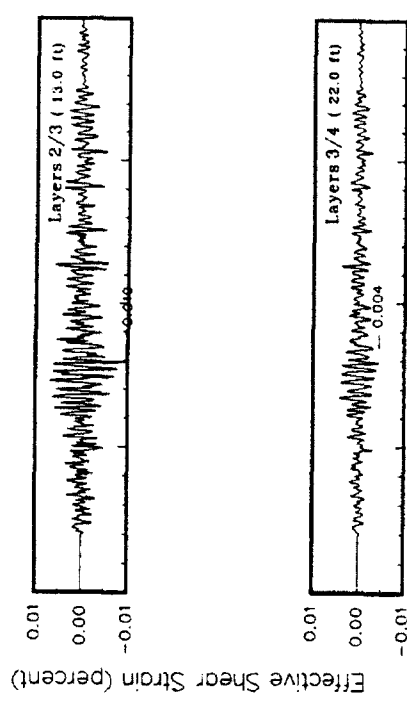
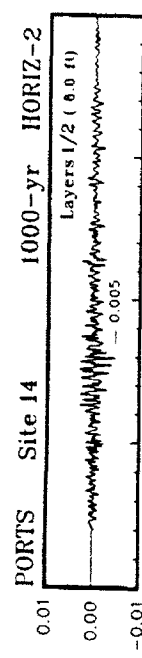
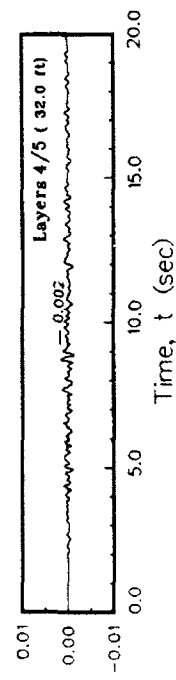
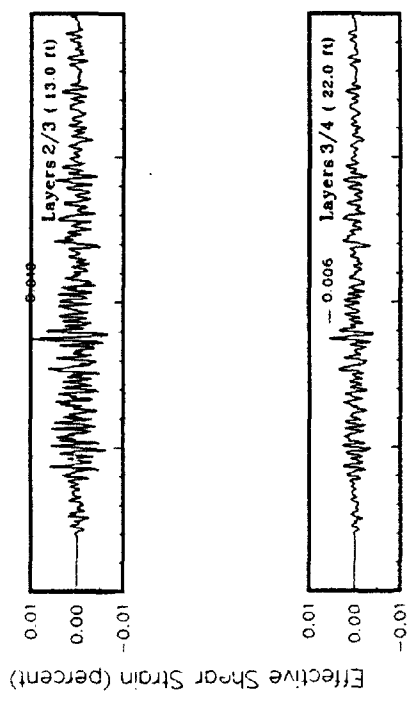
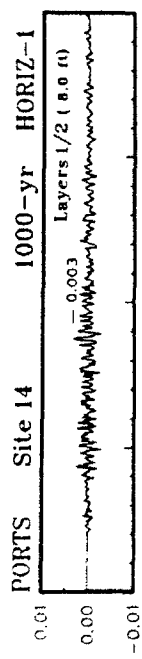


Figure I14. Variation of shear strain with time at contacts between layers for Site 14

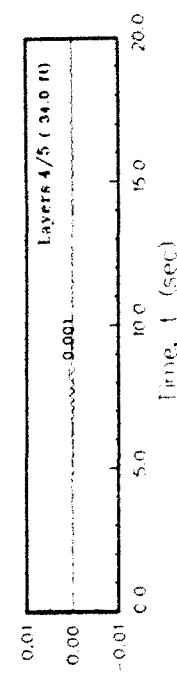
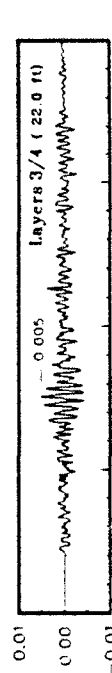
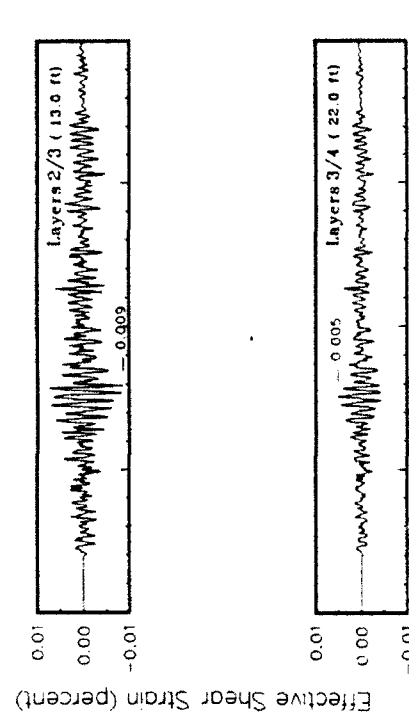
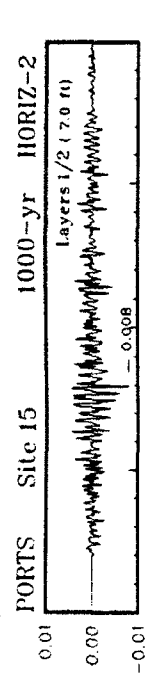
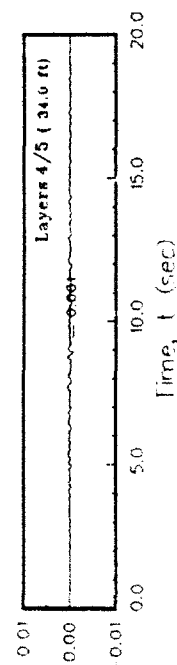
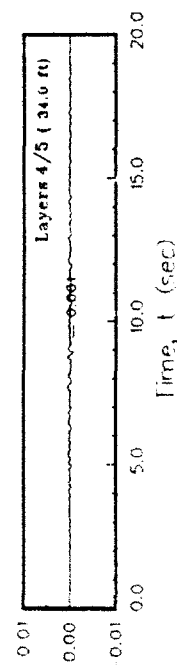
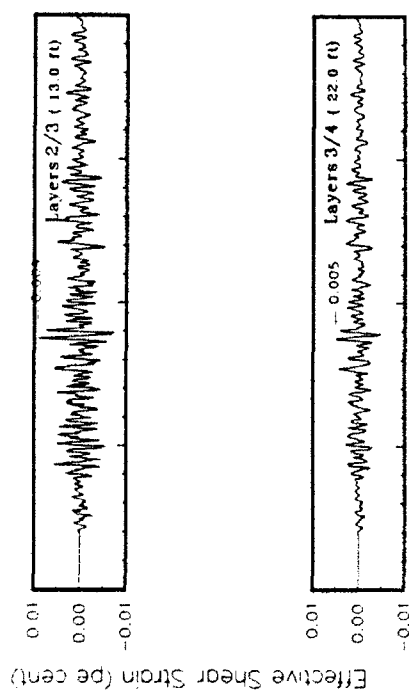
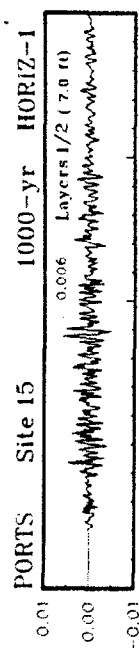


Figure I15. Variation of shear strain with time at contacts between layers for Site 15

APPENDIX J: TRIPARTITE RESPONSE SPECTRA FOR 1000-YEAR EVENT

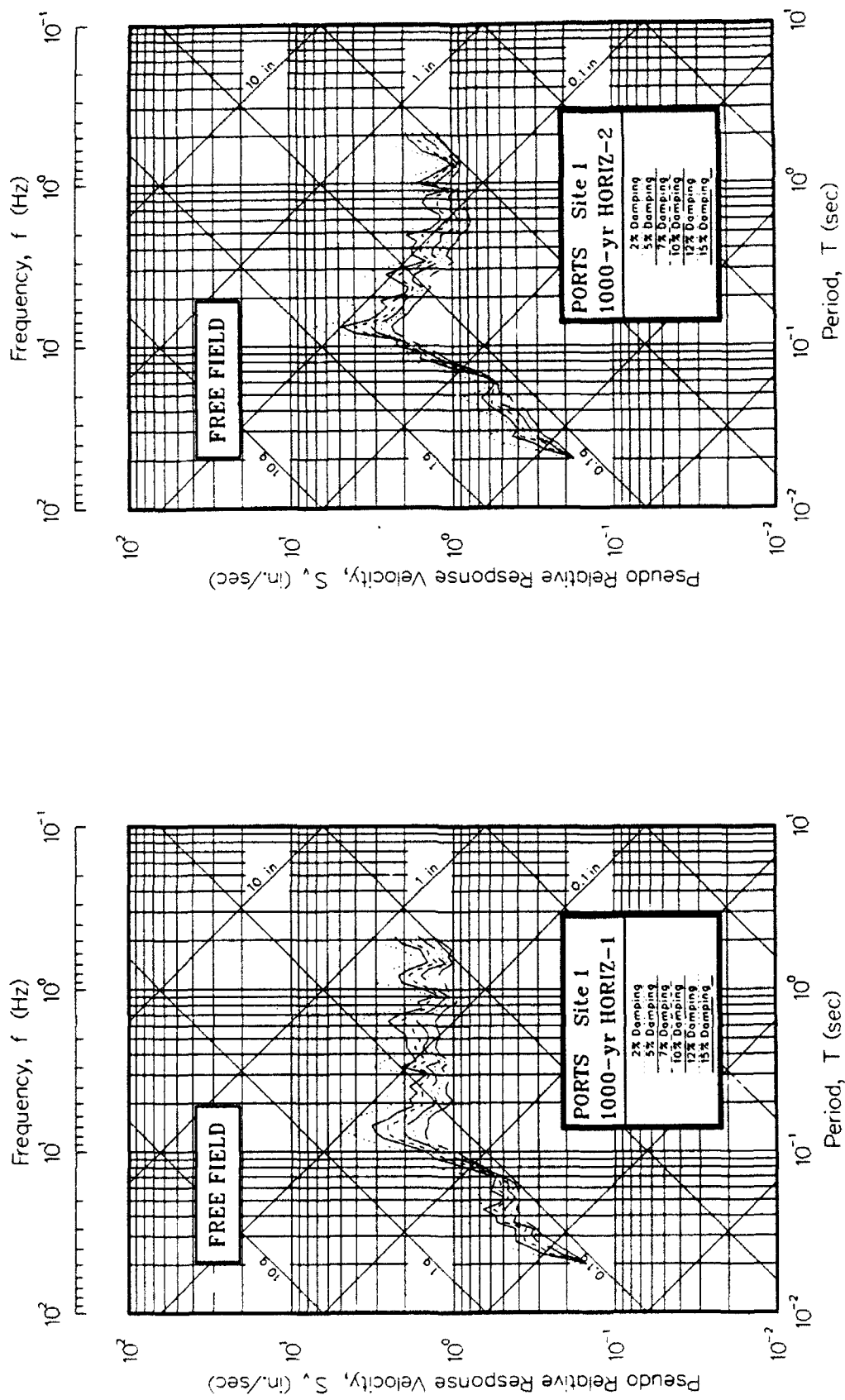


Figure J1. Psuedo-relative velocity spectra in tripartite form at free field for Site 1

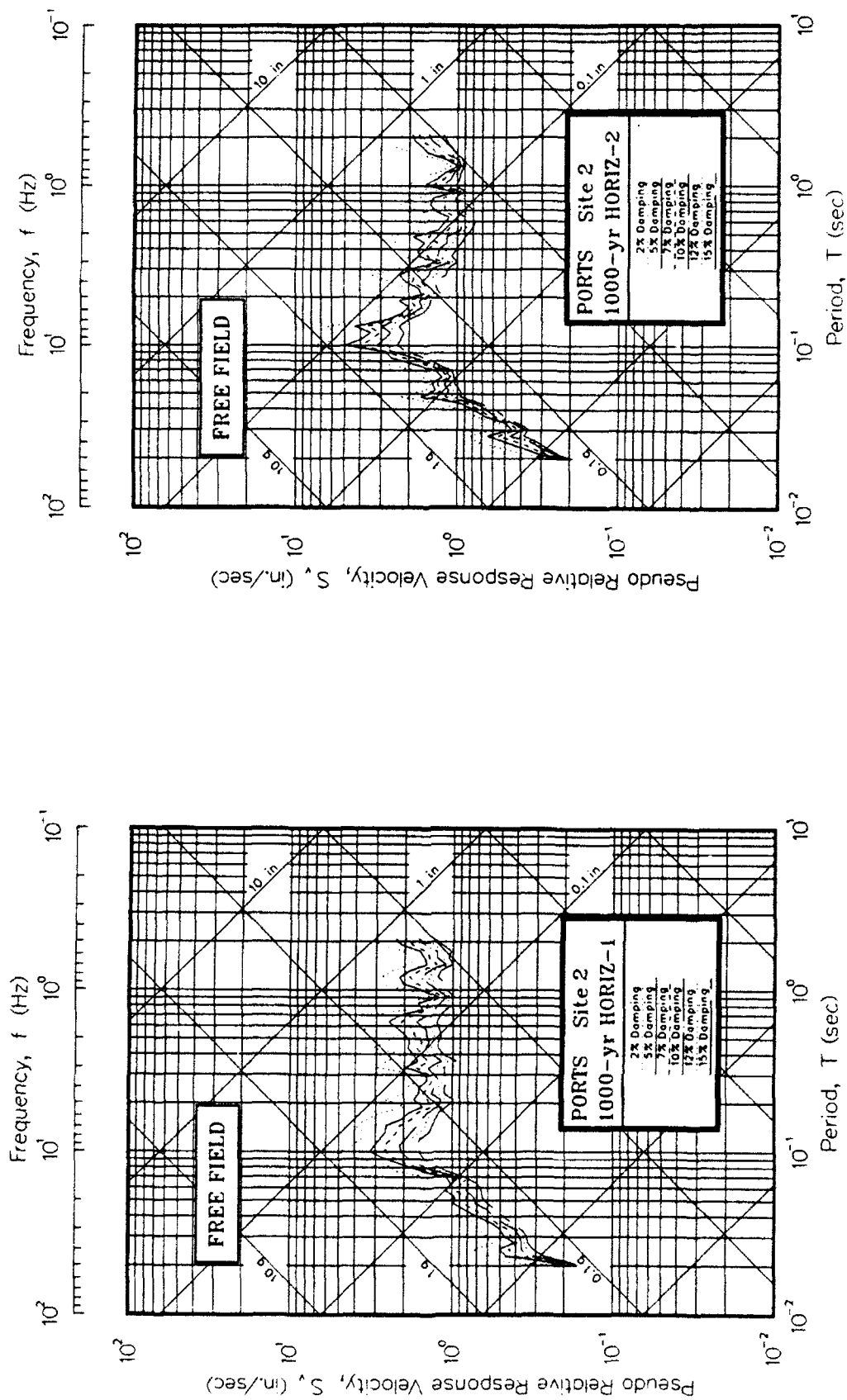


Figure J2. Psuedo-relative velocity spectra in tripartite form at free field for Site 2

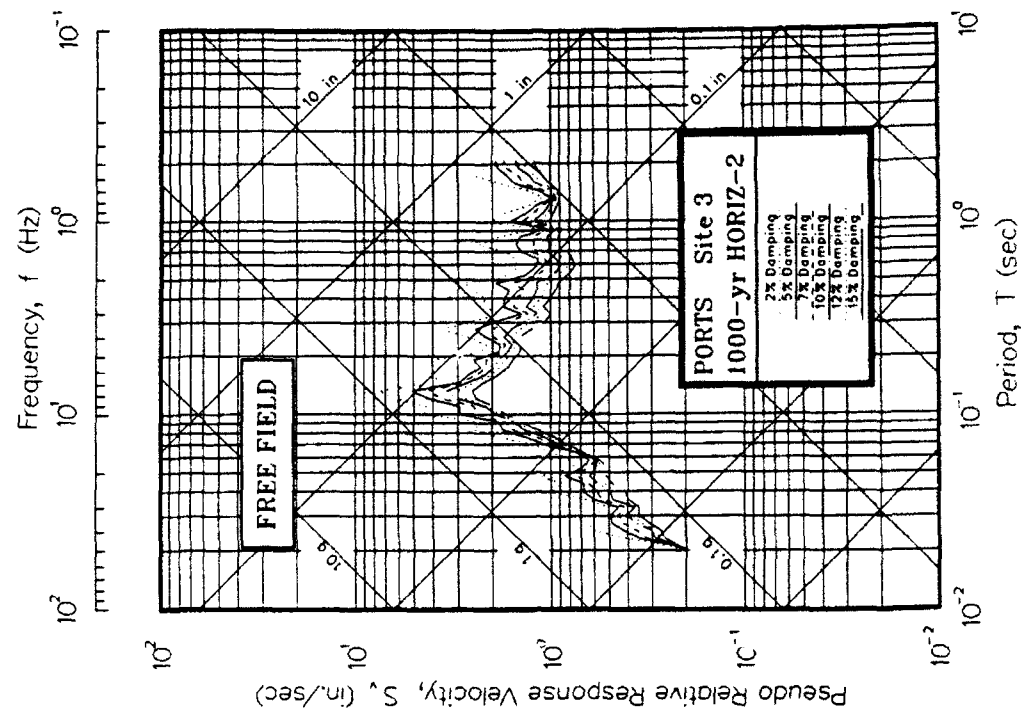
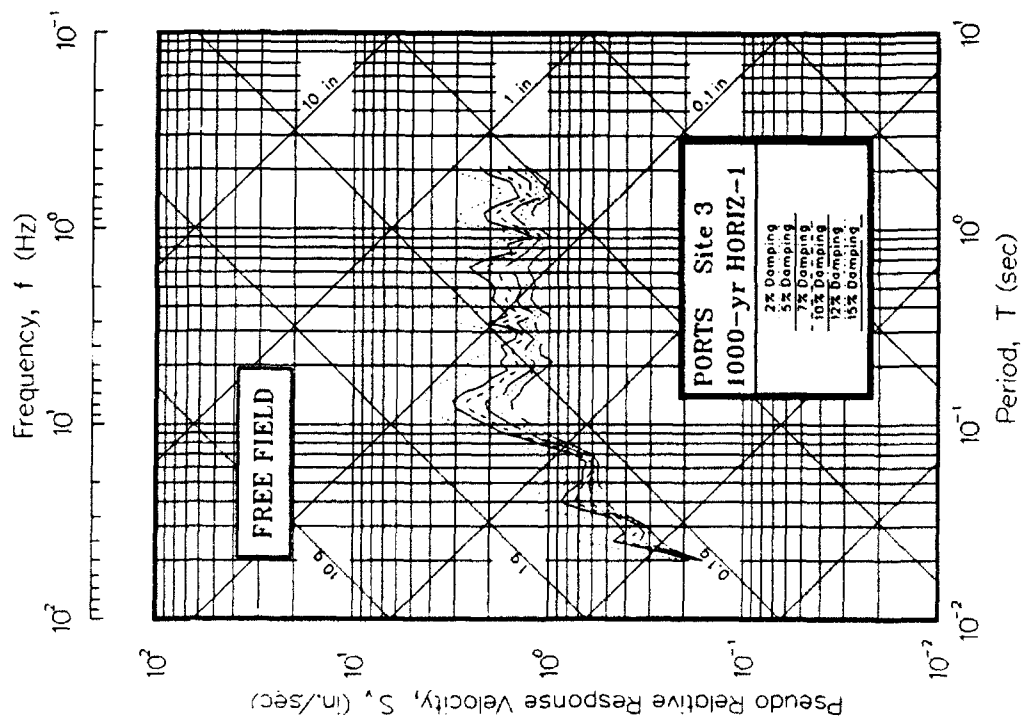


Figure J3. Psuedo-relative velocity spectra in tripartite form at free field for Site 3

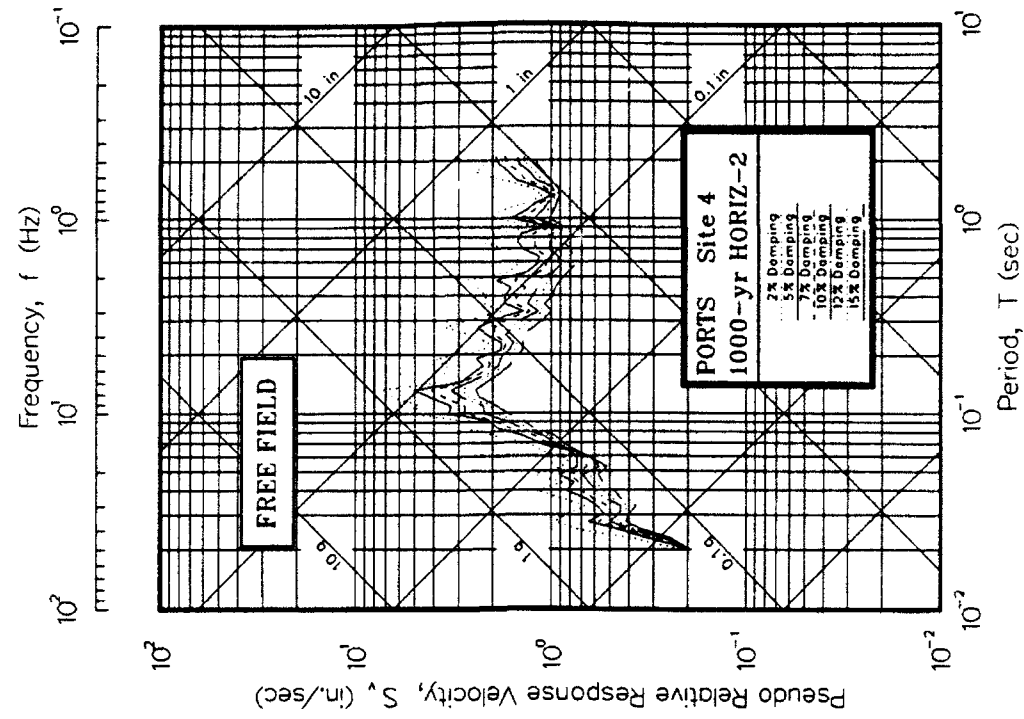
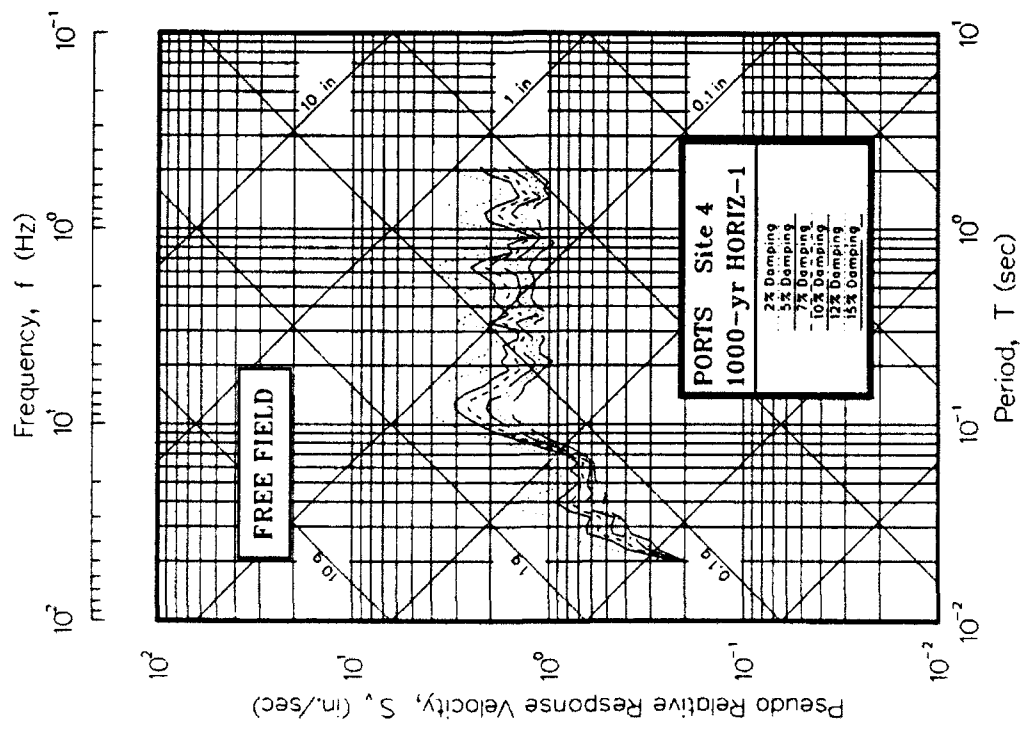


Figure J4. Pseudo-relative velocity spectra in tripartite form at free field for Site 4

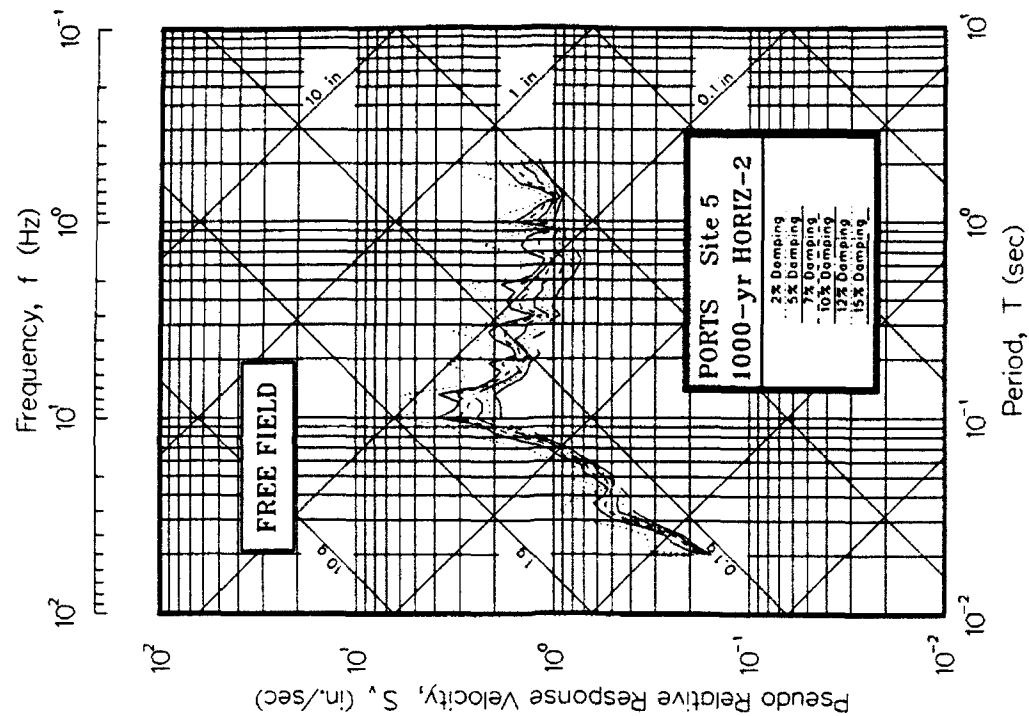
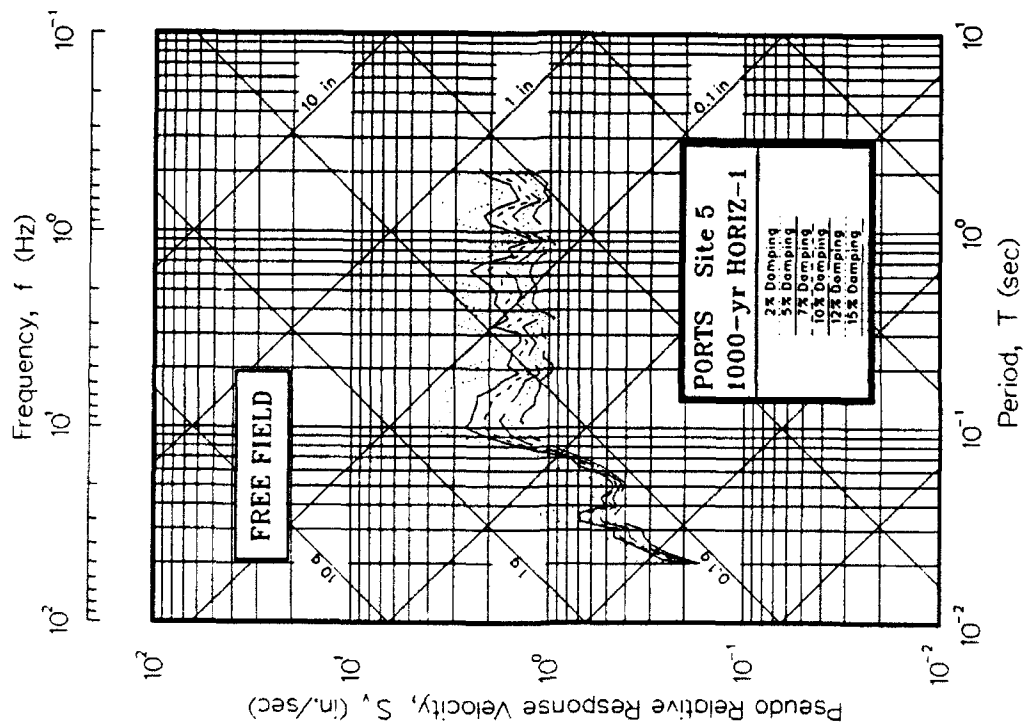


Figure J5. Psuedo-relative velocity spectra in tripartite form at free field for Site 5

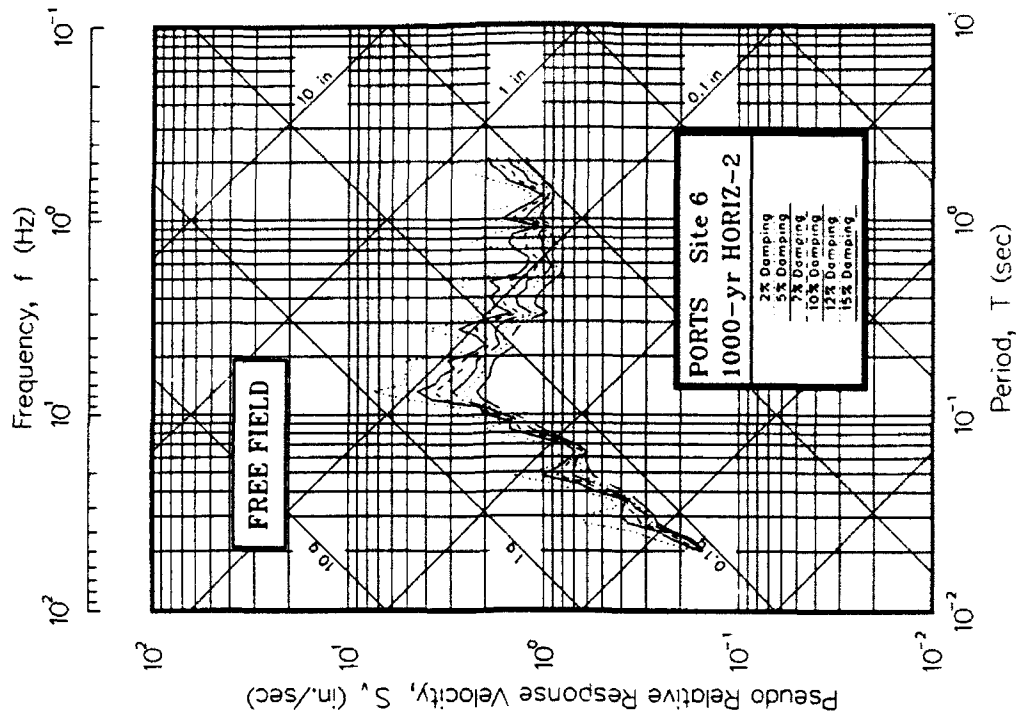
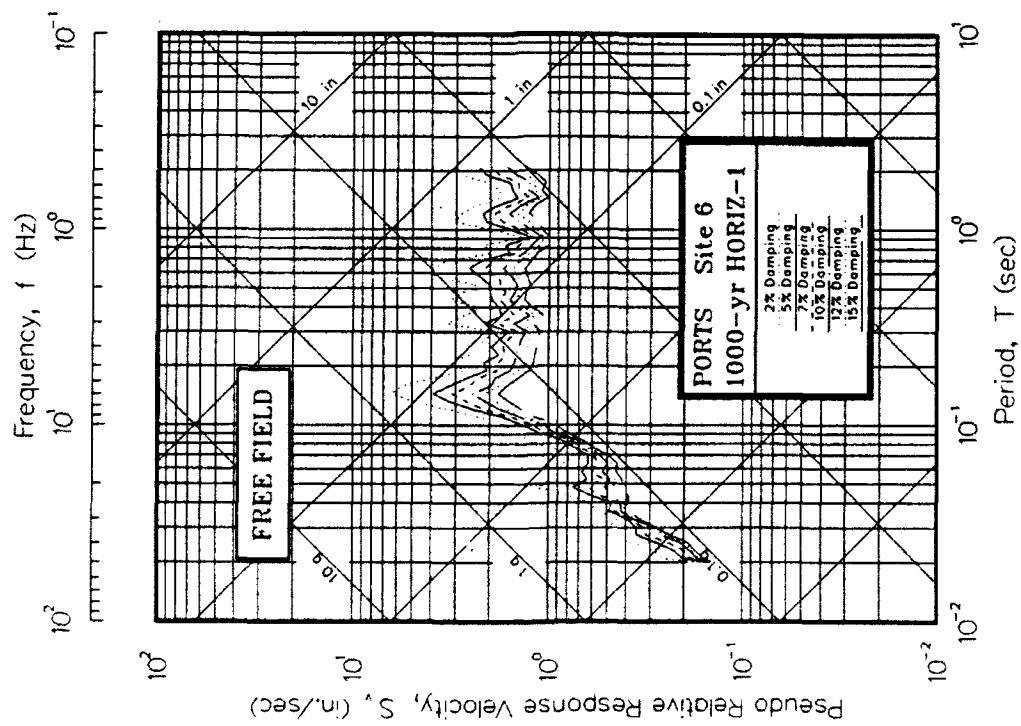


Figure J6. Pseudo-relative velocity spectra in tripartite form at free field for Site 6

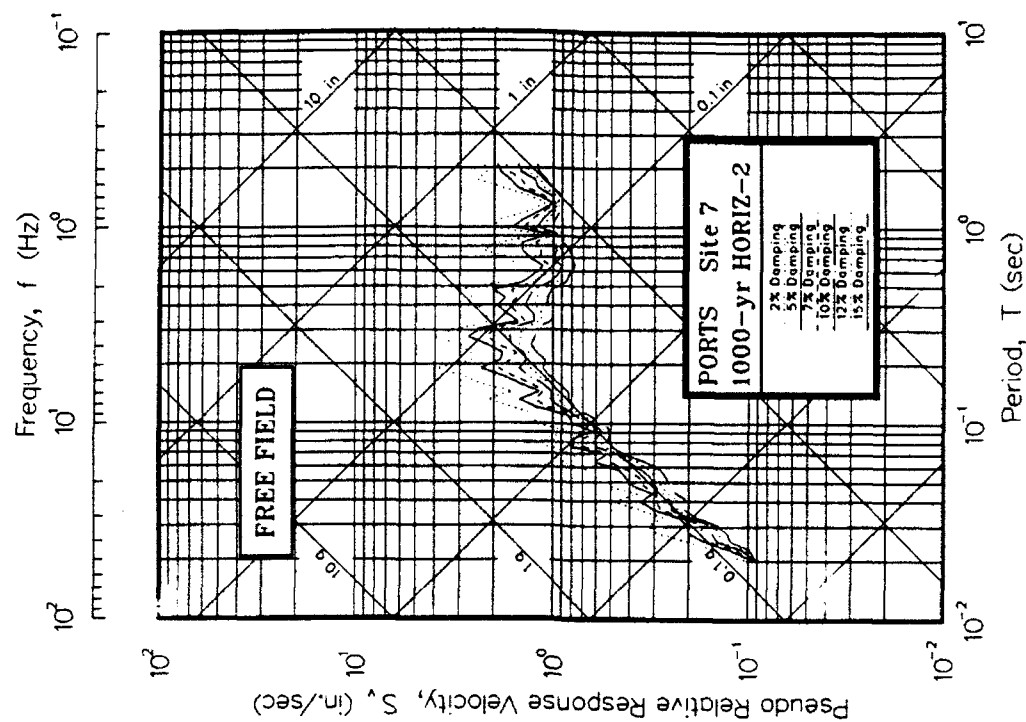
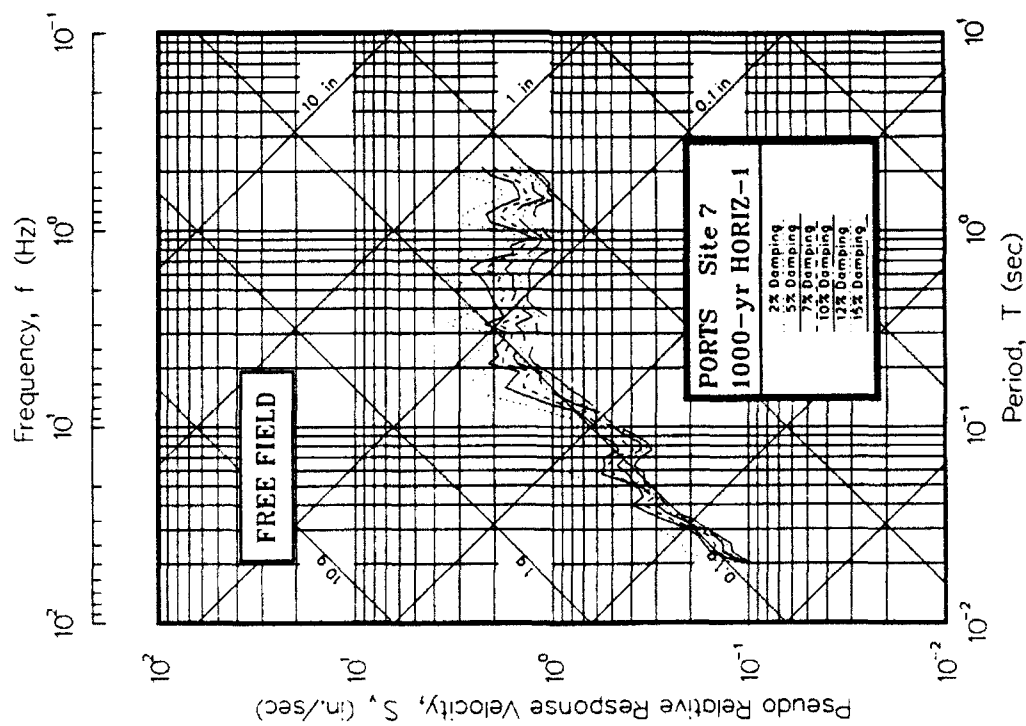


Figure J7. Psuedo-relative velocity spectra in tripartite form at free field for Site 7

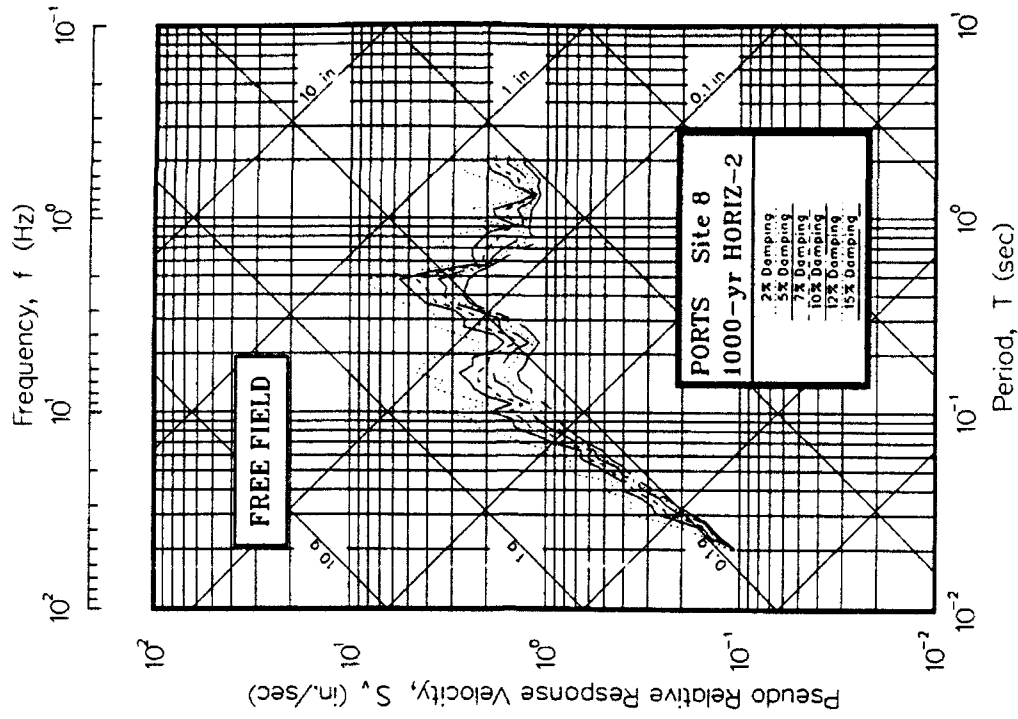
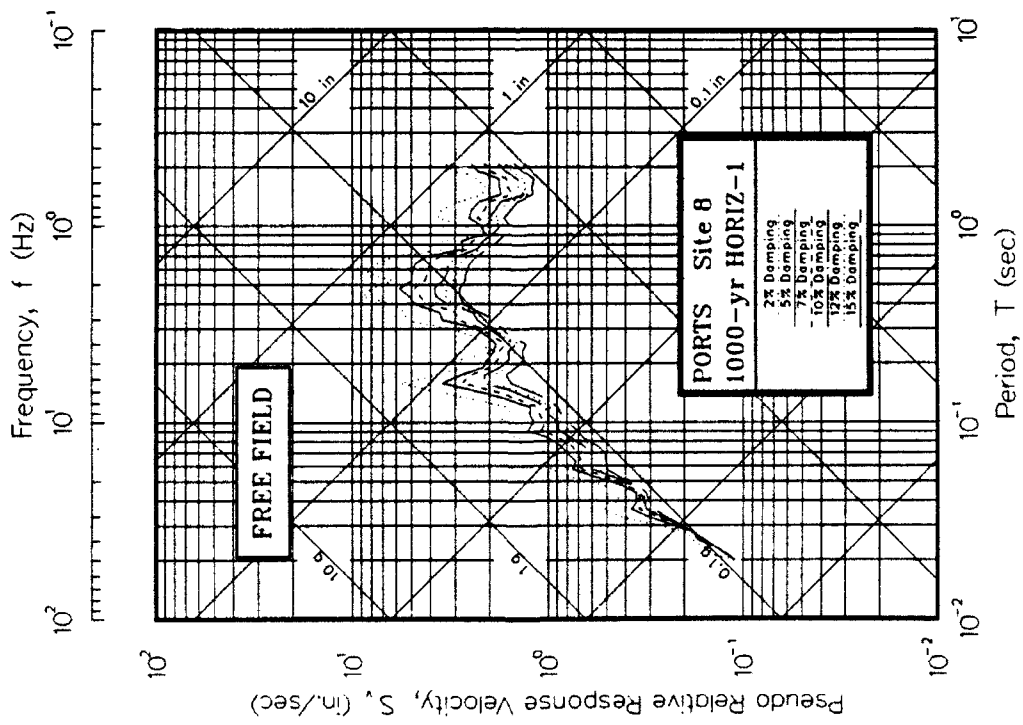


Figure J8. Psuedo-relative velocity spectra in tripartite form at free field for Site 8

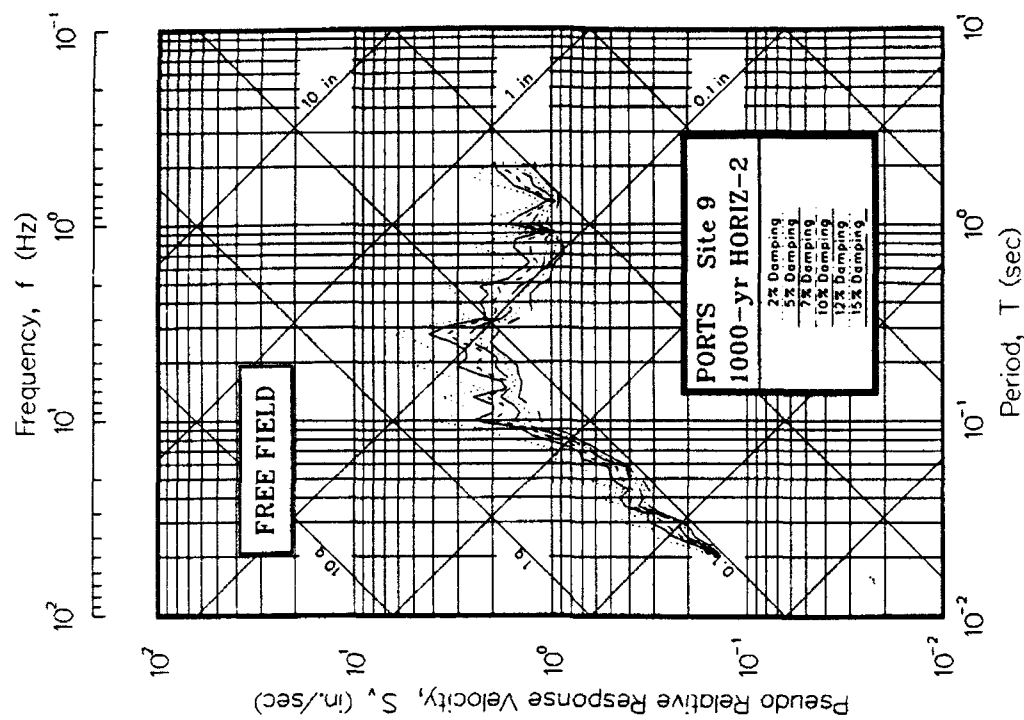
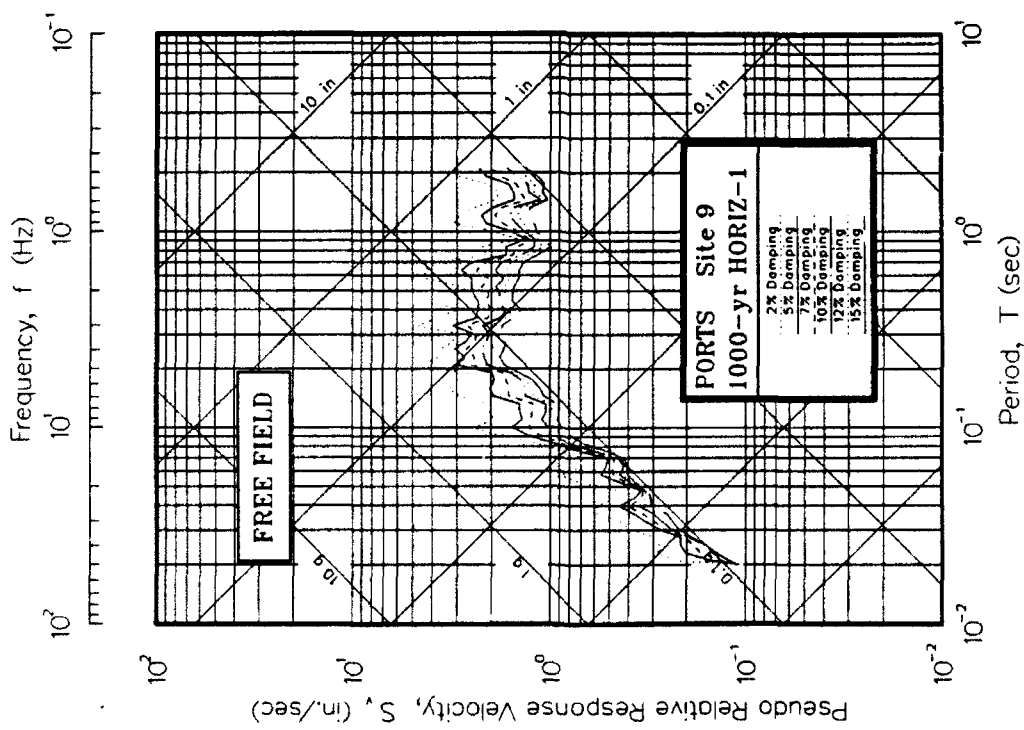


Figure J9. Psuedo-relative velocity spectra in tripartite form at free field for Site 9

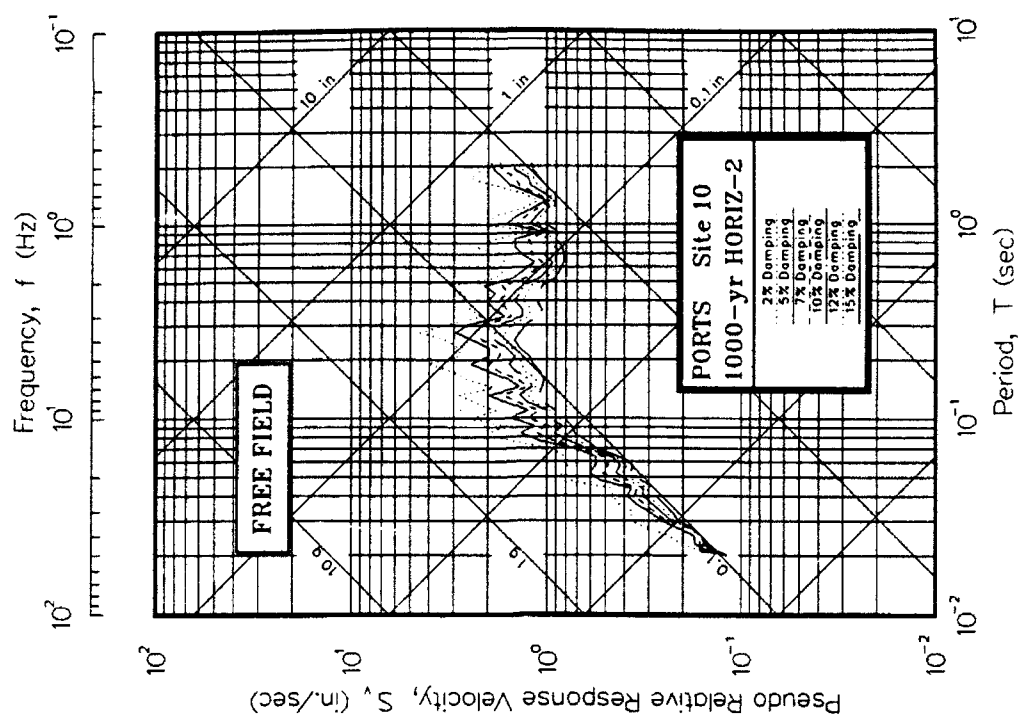
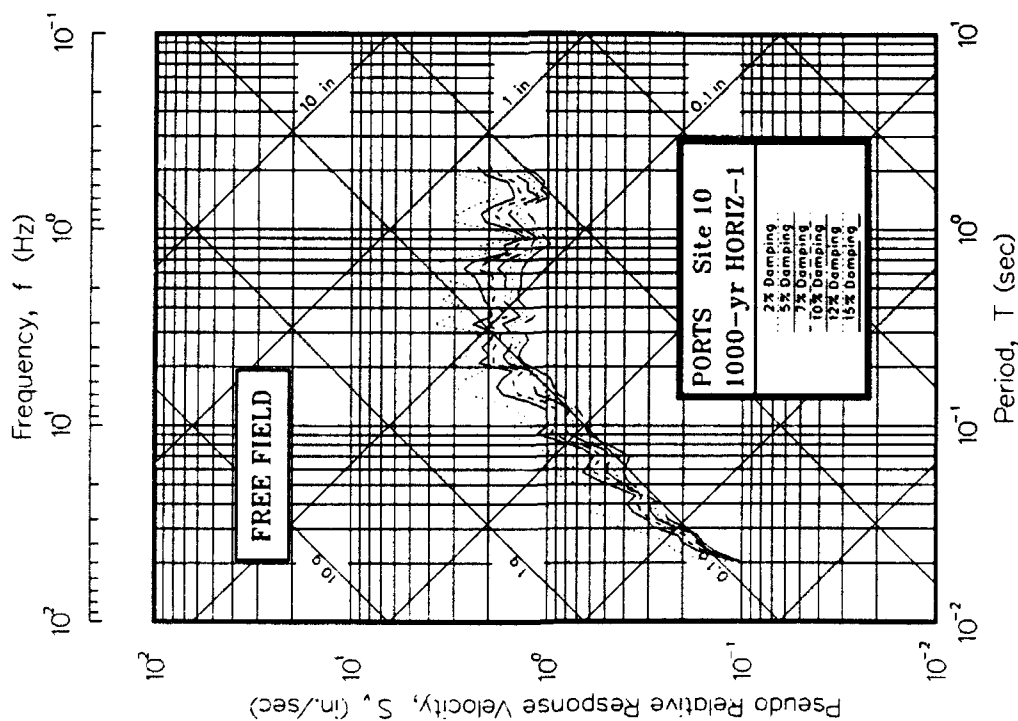


Figure J10. Psuedo-relative velocity spectra in tripartite form at free field for Site 10

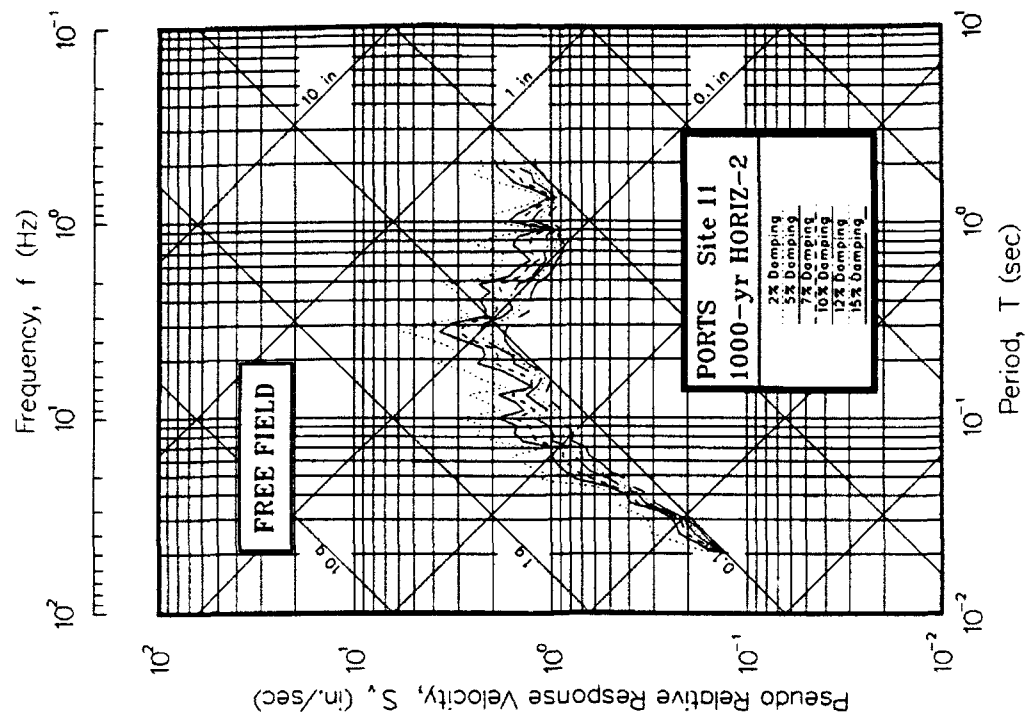
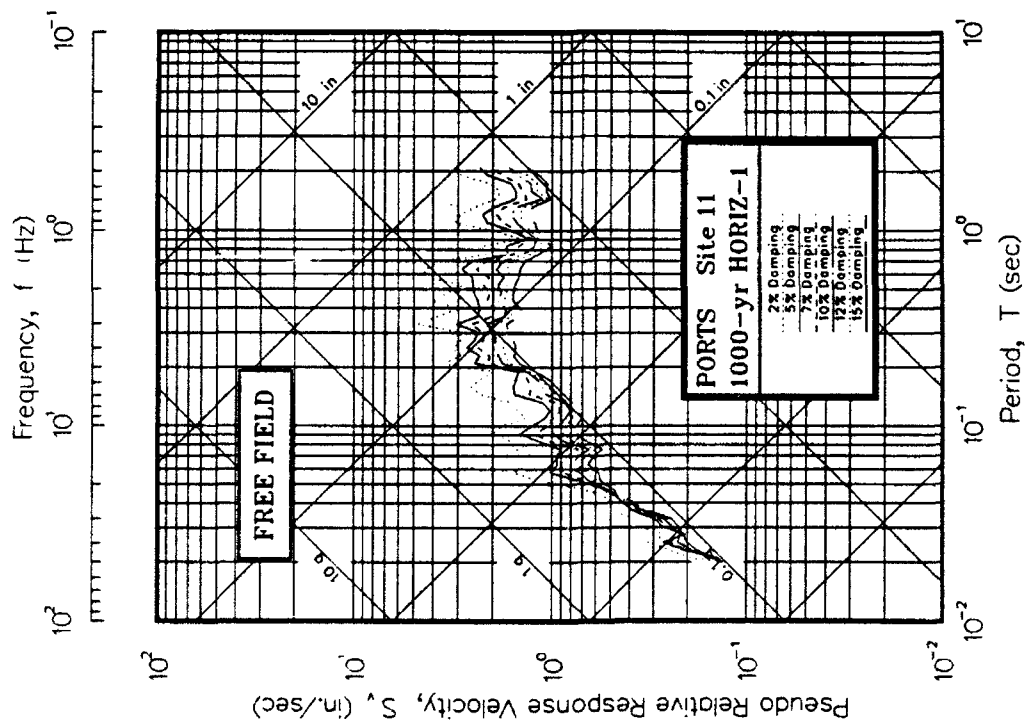


Figure J11. Psuedo-relative velocity spectra in tripartite form at free field for Site 11

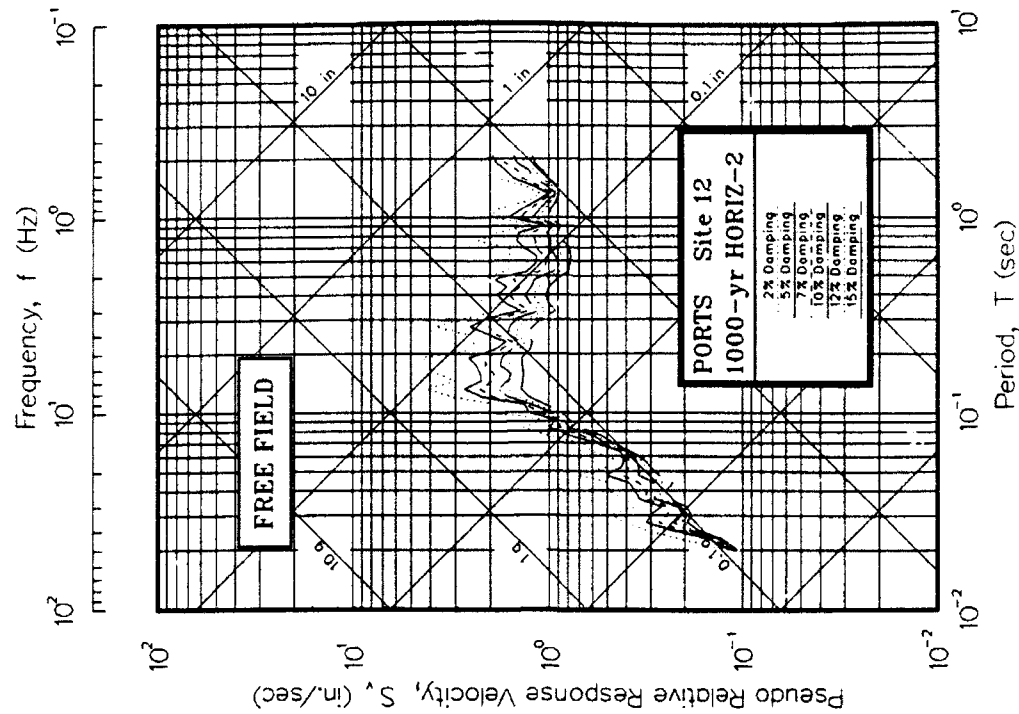
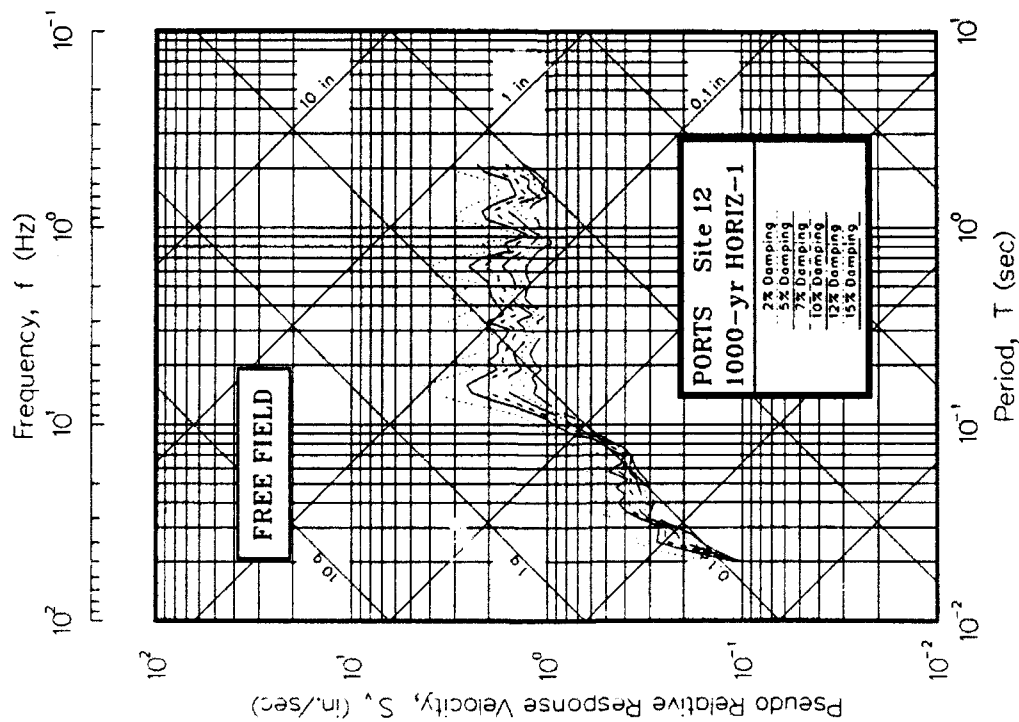


Figure J12. Psuedo-relative velocity spectra in tripartite form at free field for Site 12

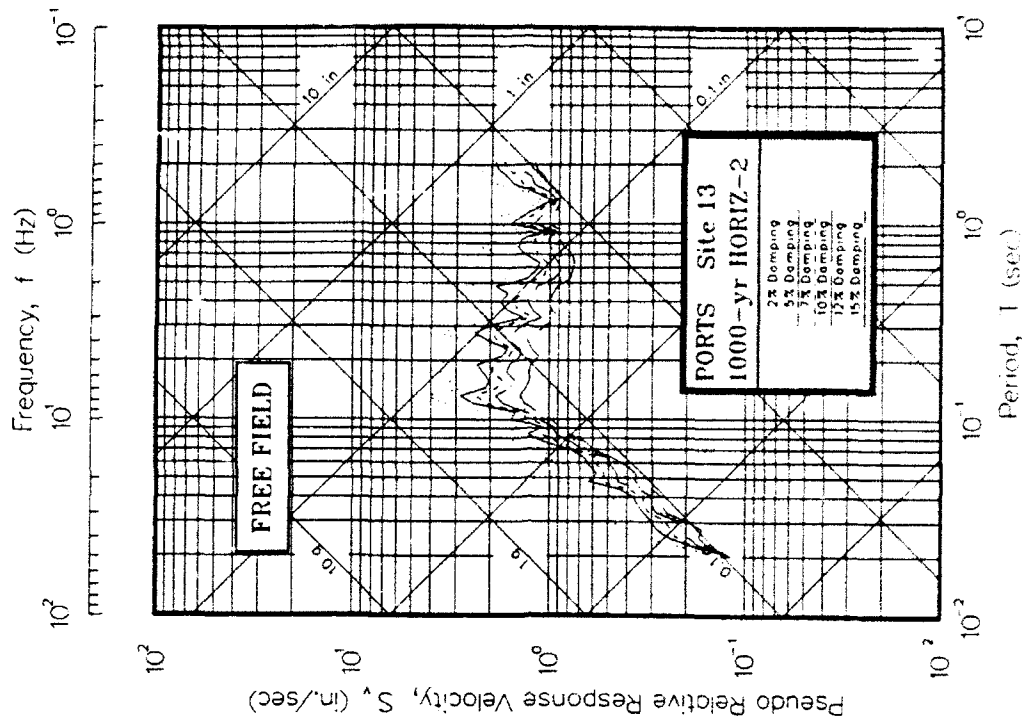
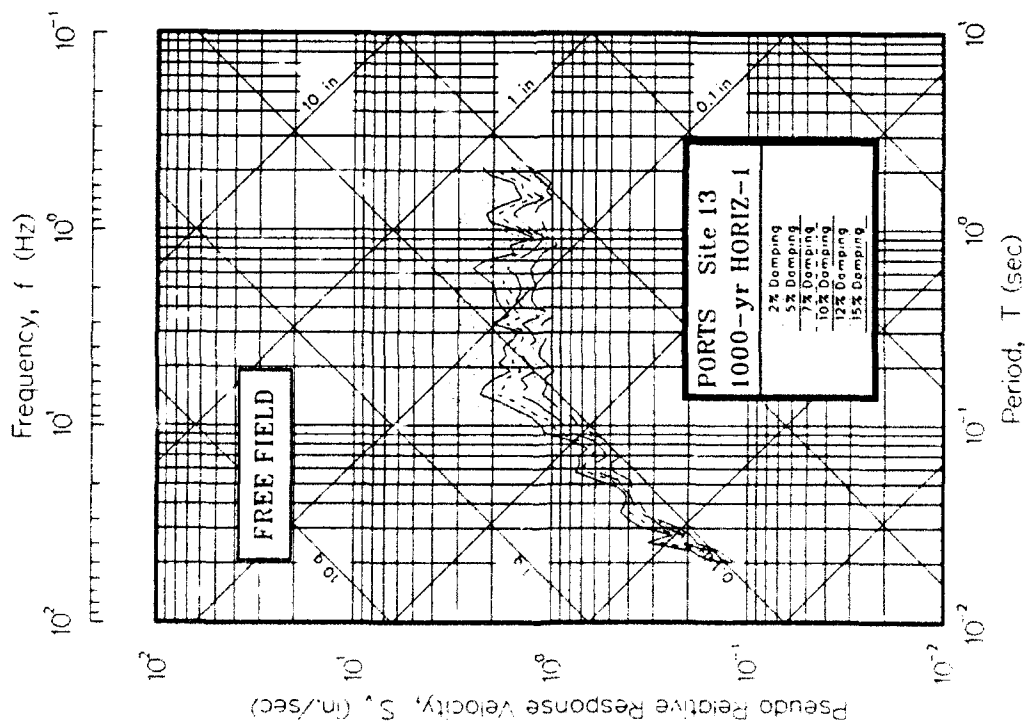


Figure J13. Pseudo-relative velocity spectra in tripartite form at free field for Site 13

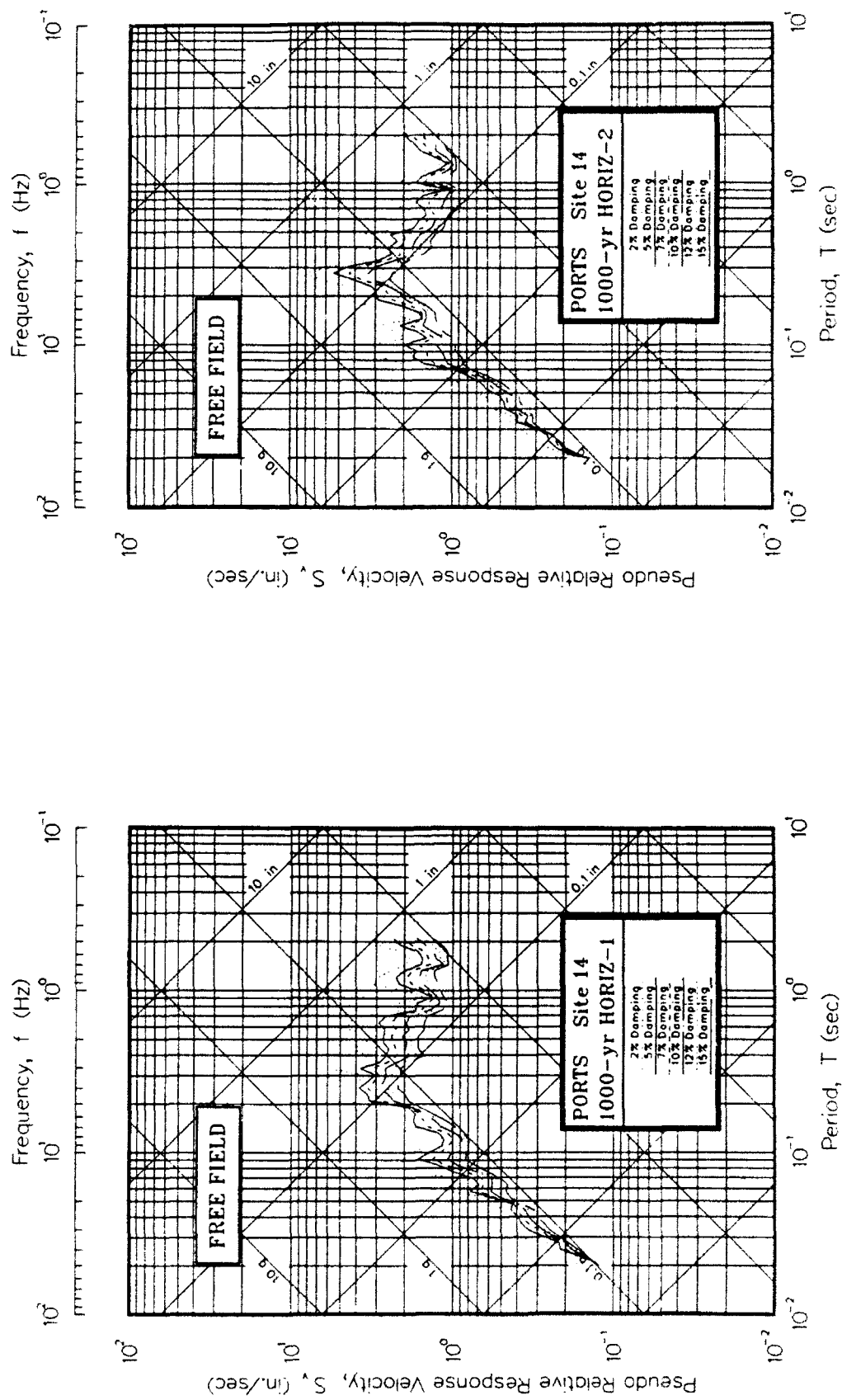


Figure J14. Psuedo-relative velocity spectra in tripartite form at free field for Site 14

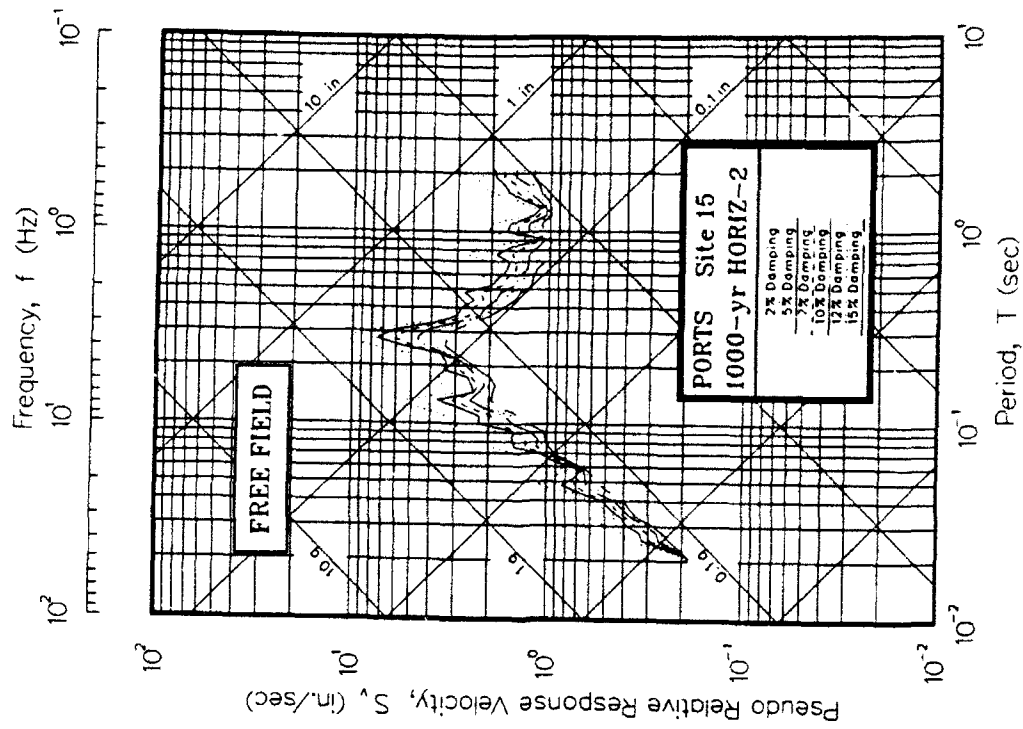
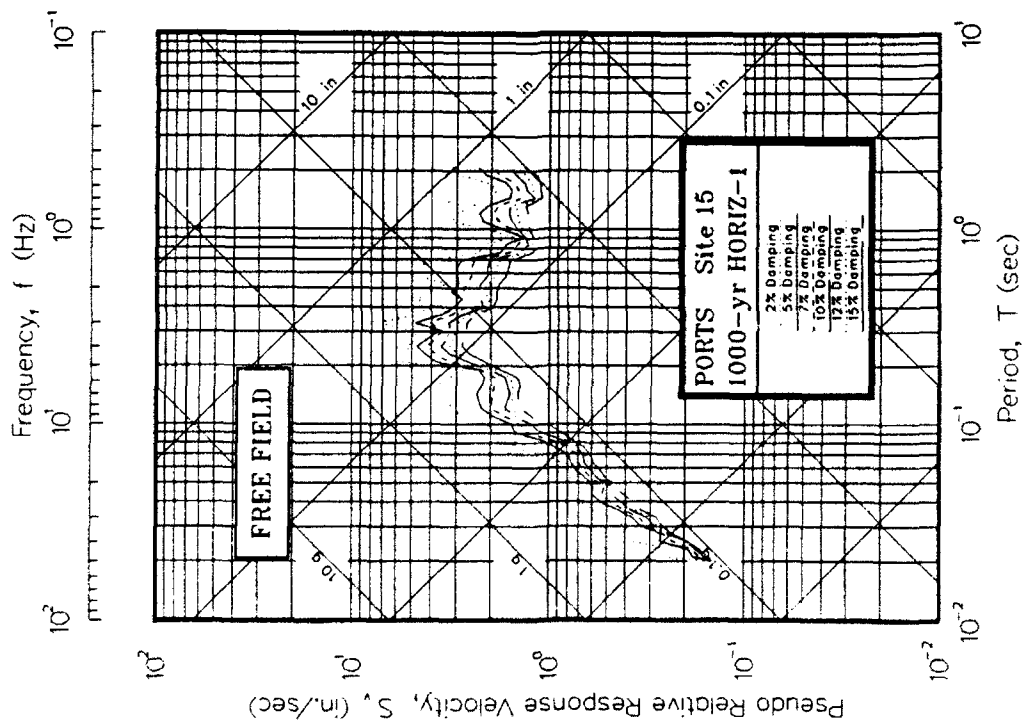


Figure J15. Psuedo-relative velocity spectra in tripartite form at free field for Site 15

APPENDIX K: ACCELERATION SPECTRA FOR 1000-YEAR EVENT

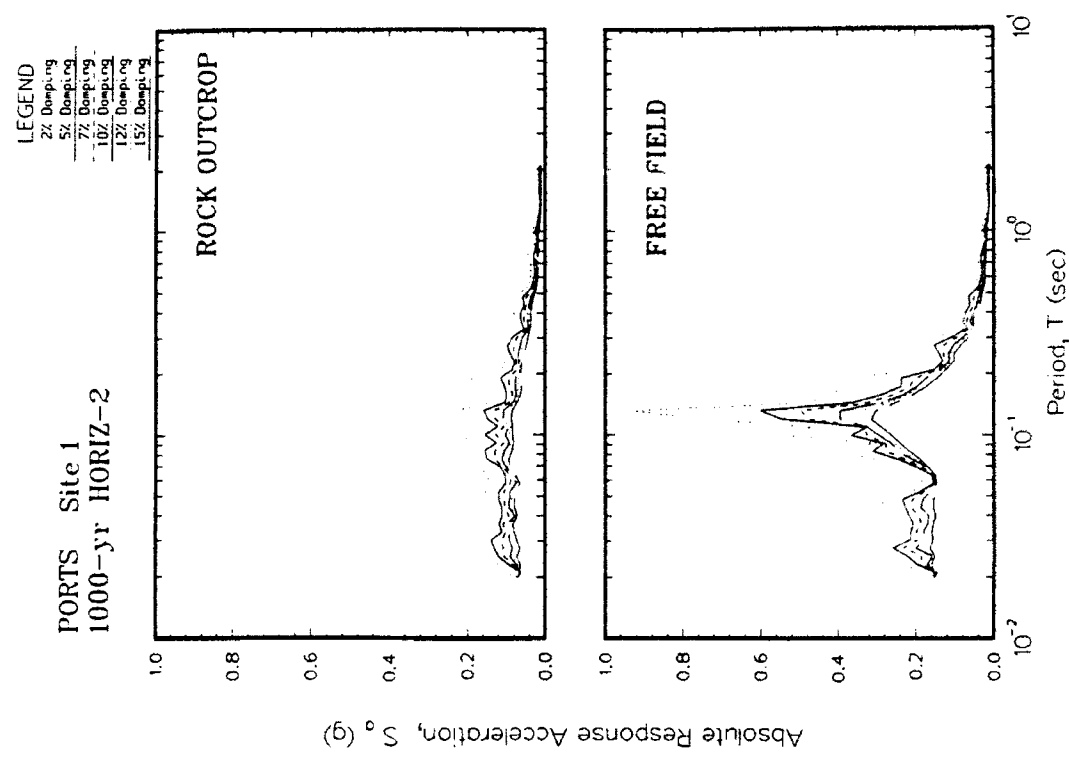
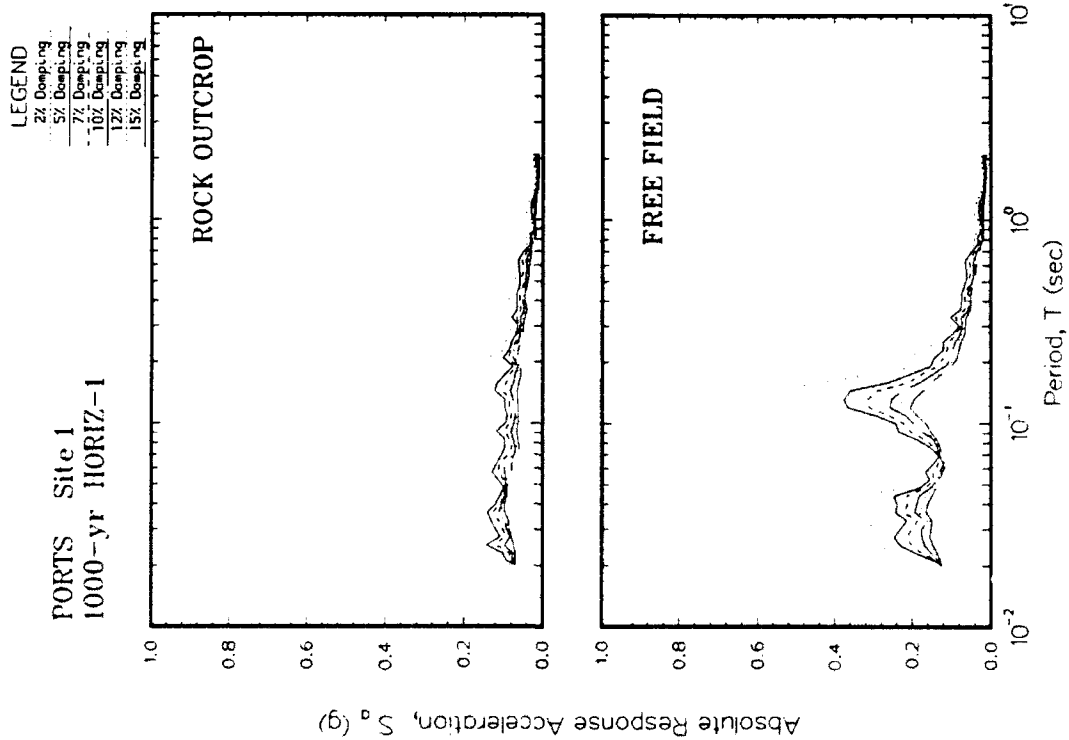


Figure K1. Absolute acceleration response spectra at free field for Site 1

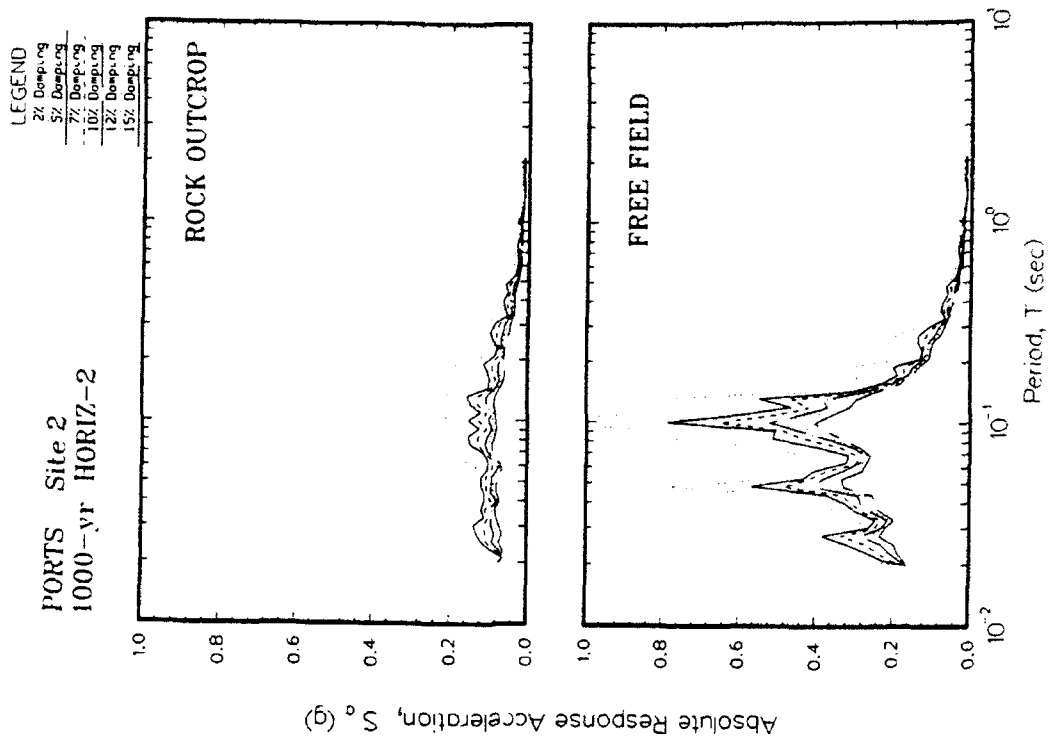
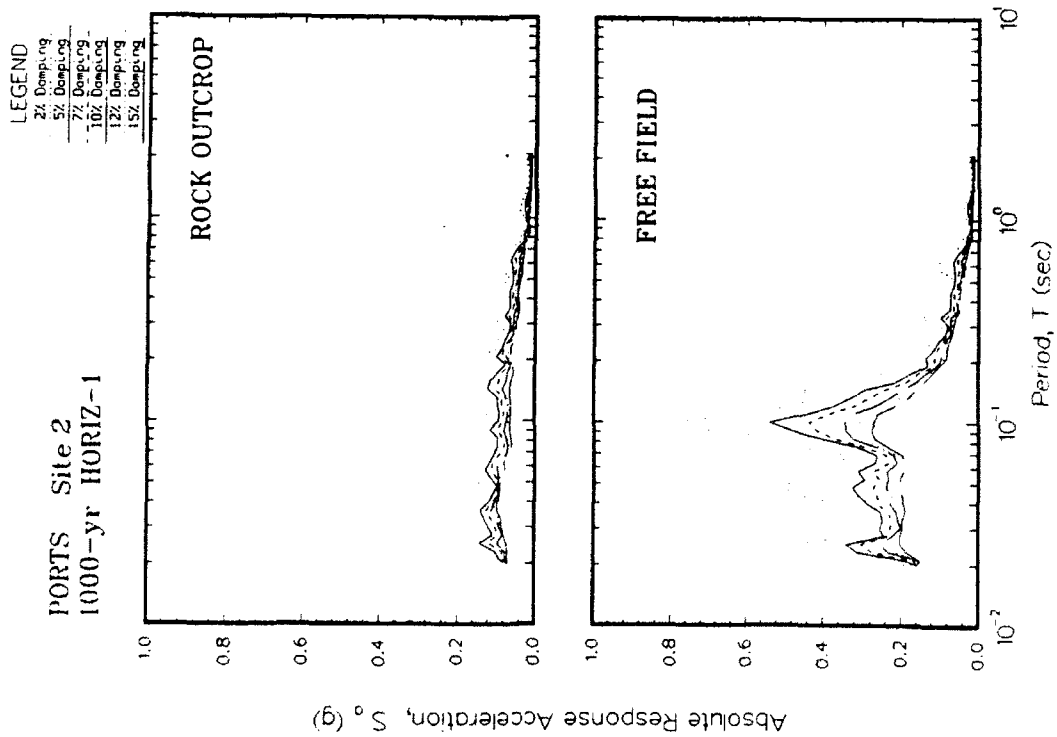


Figure K2. Absolute acceleration response spectra at free field for Site 2

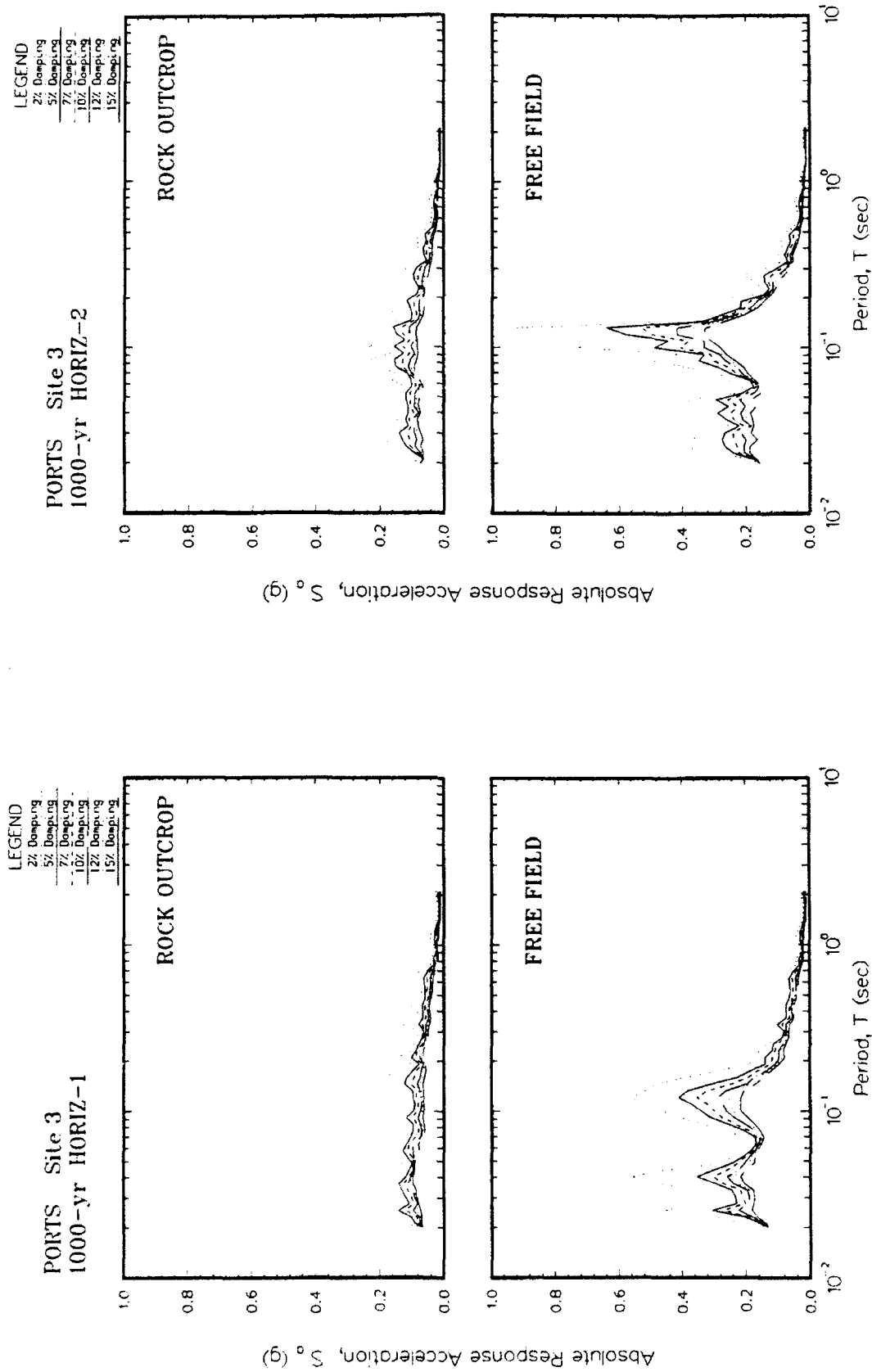


Figure K3. Absolute acceleration response spectra at free field for Site 3

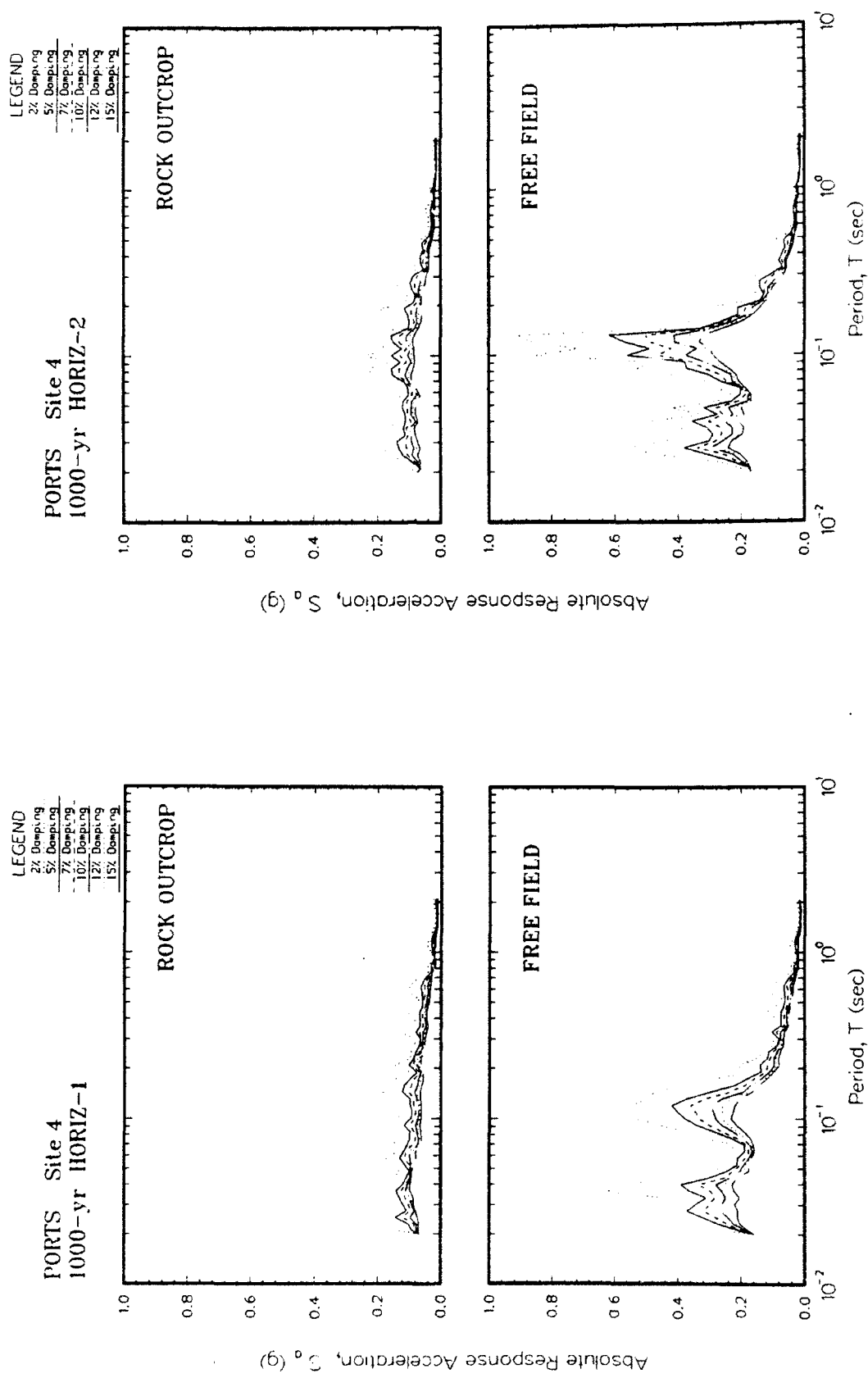


Figure K4. Absolute acceleration response spectra at free field for Site 4

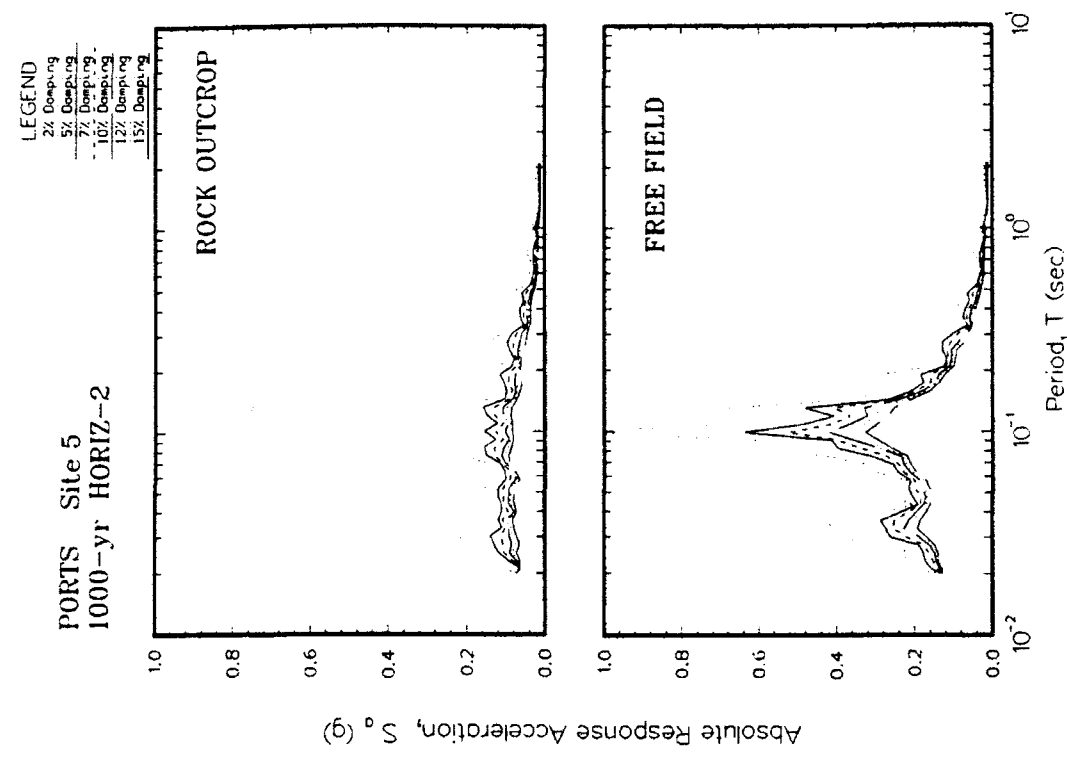
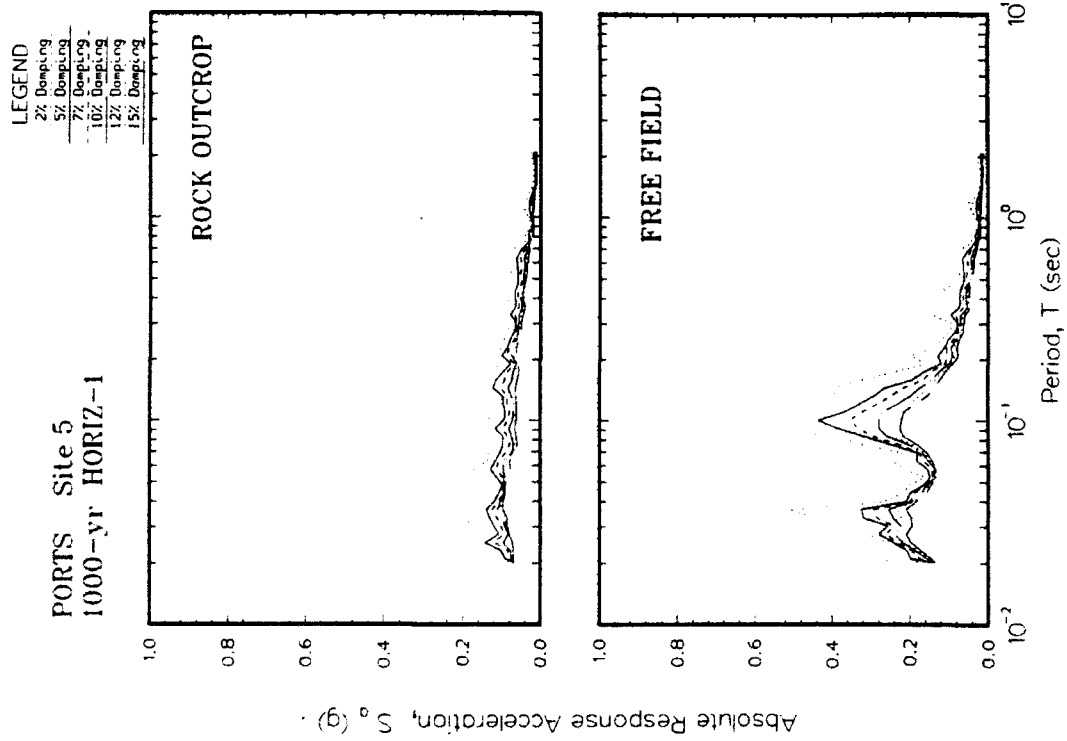


Figure K5. Absolute acceleration response spectra at free field for Site 5

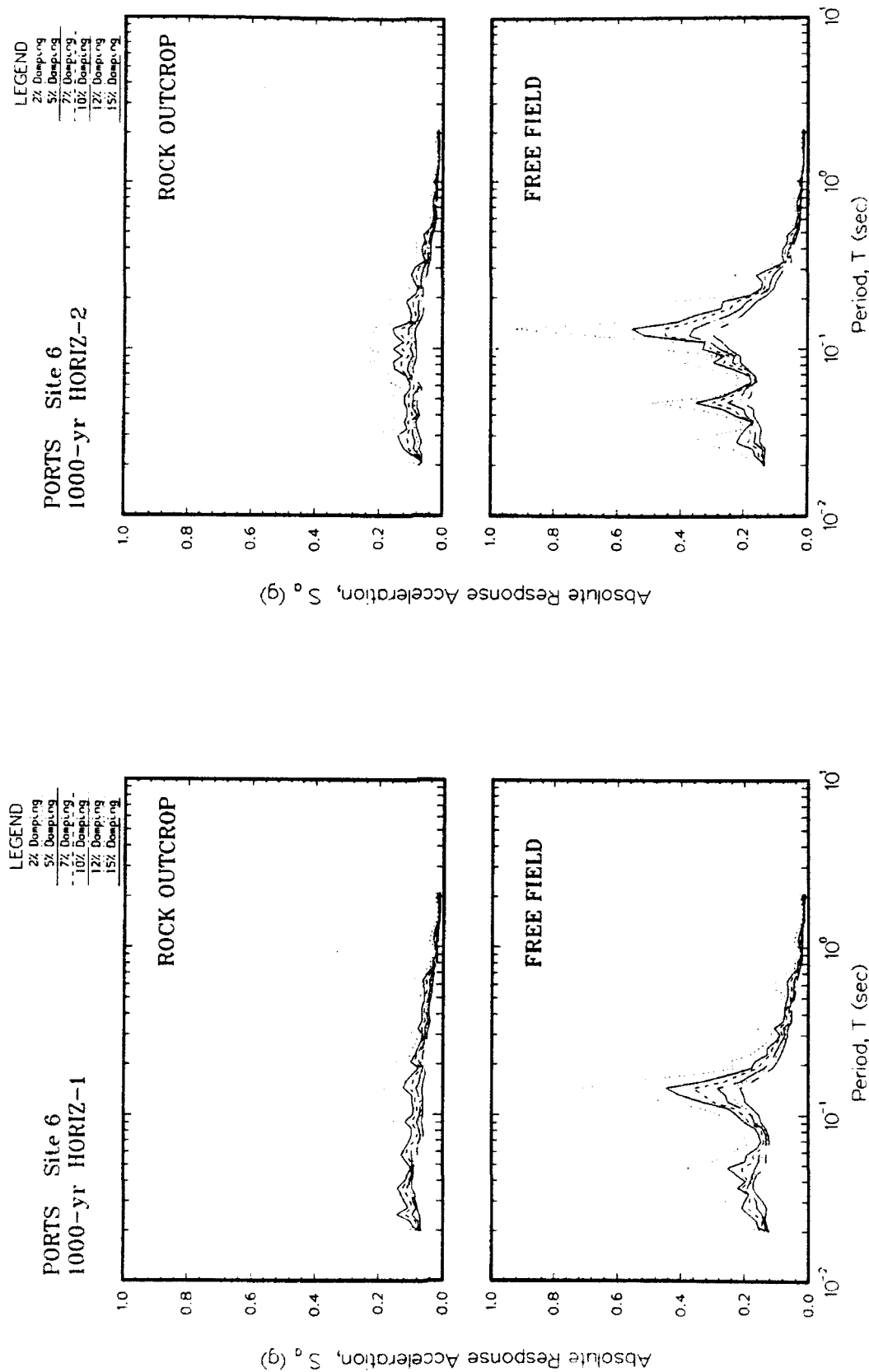


Figure K6. Absolute acceleration response spectra at free field for Site 6

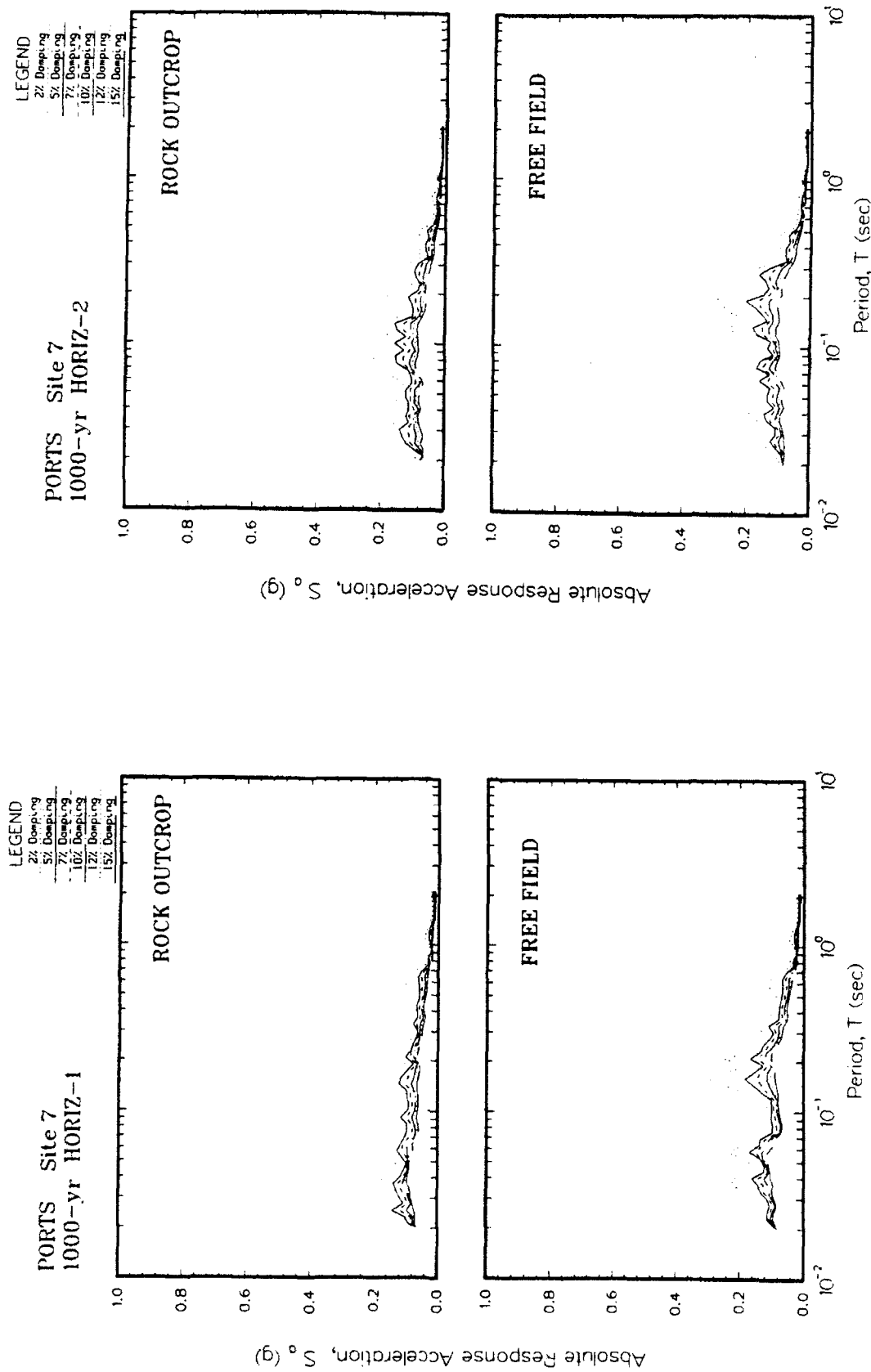


Figure K7. Absolute acceleration response spectra at free field for Site 7

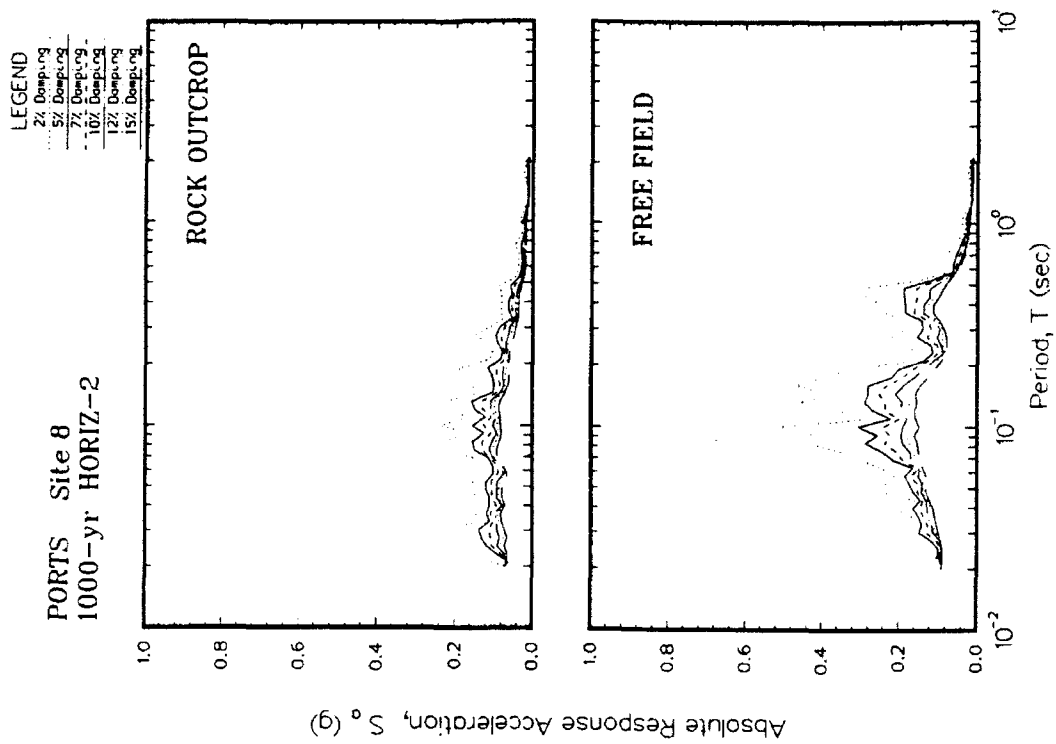
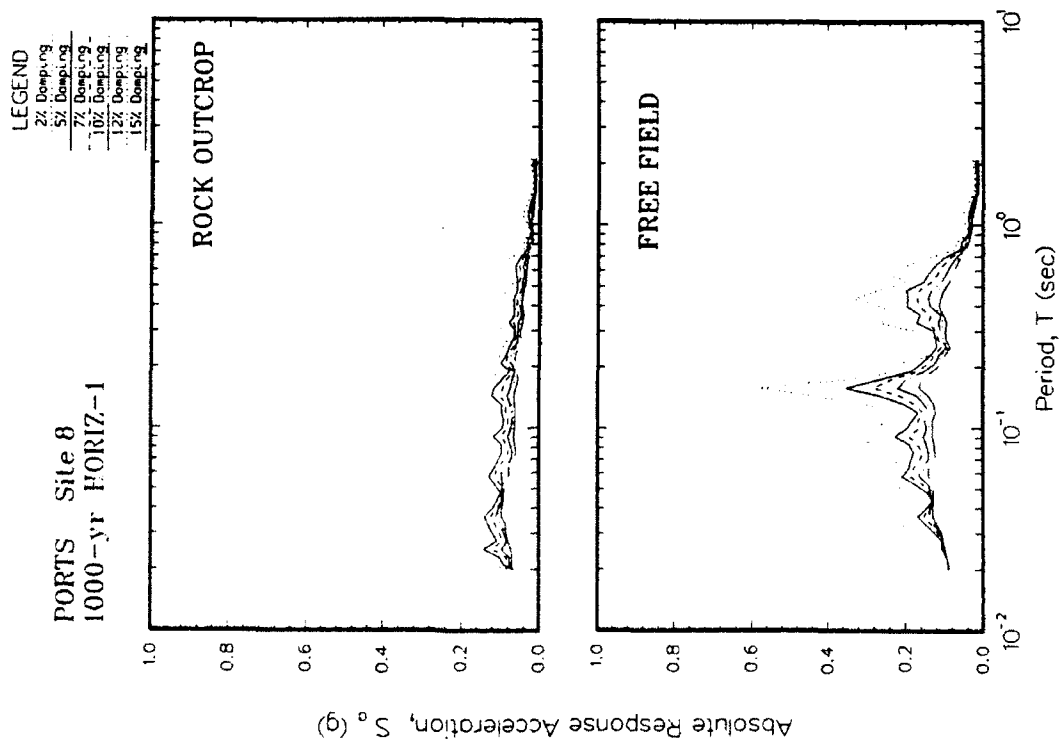


Figure K8. Absolute acceleration response spectra at free field for Site 8

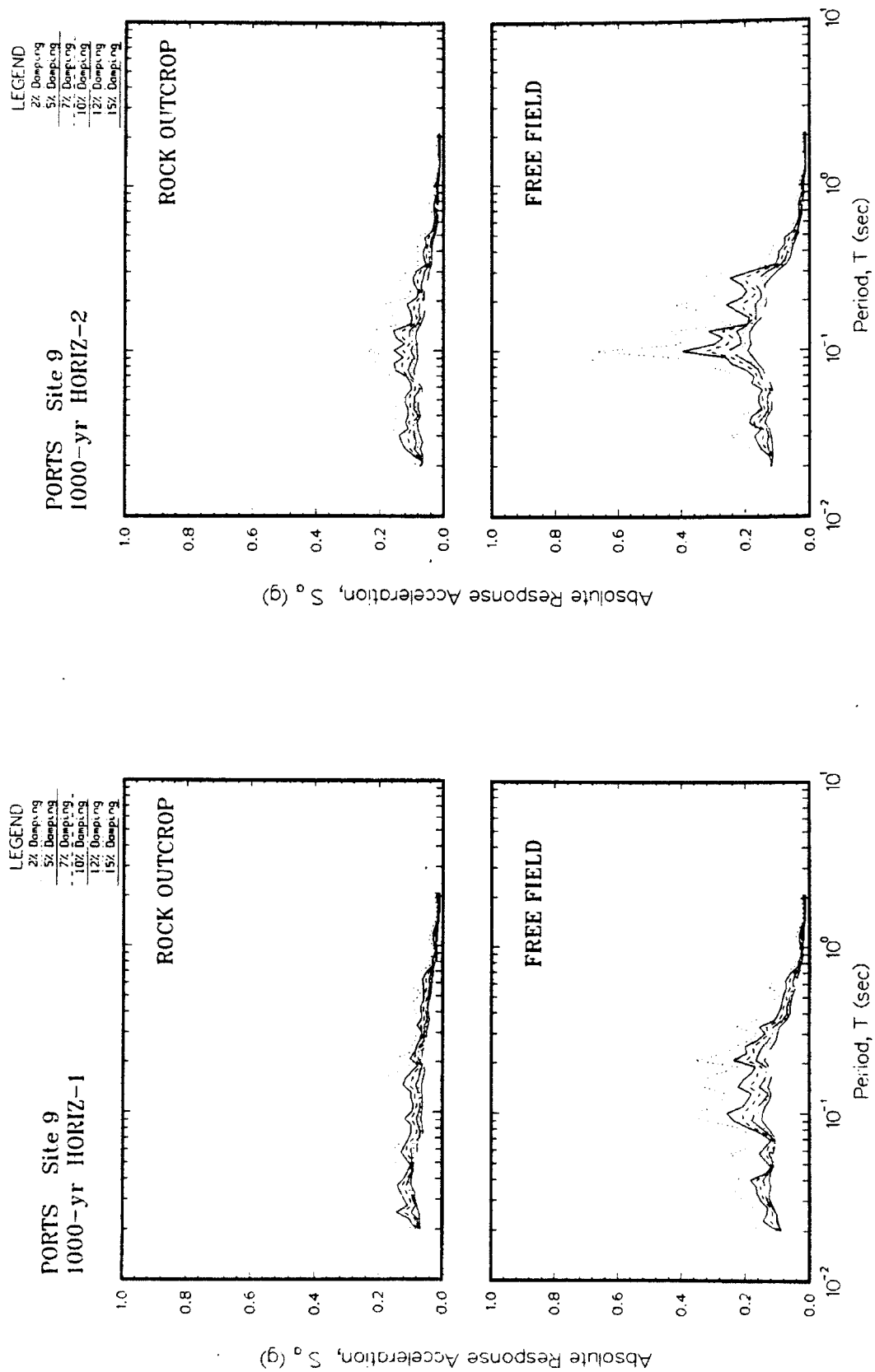


Figure K9. Absolute acceleration response spectra at free field for Site 9

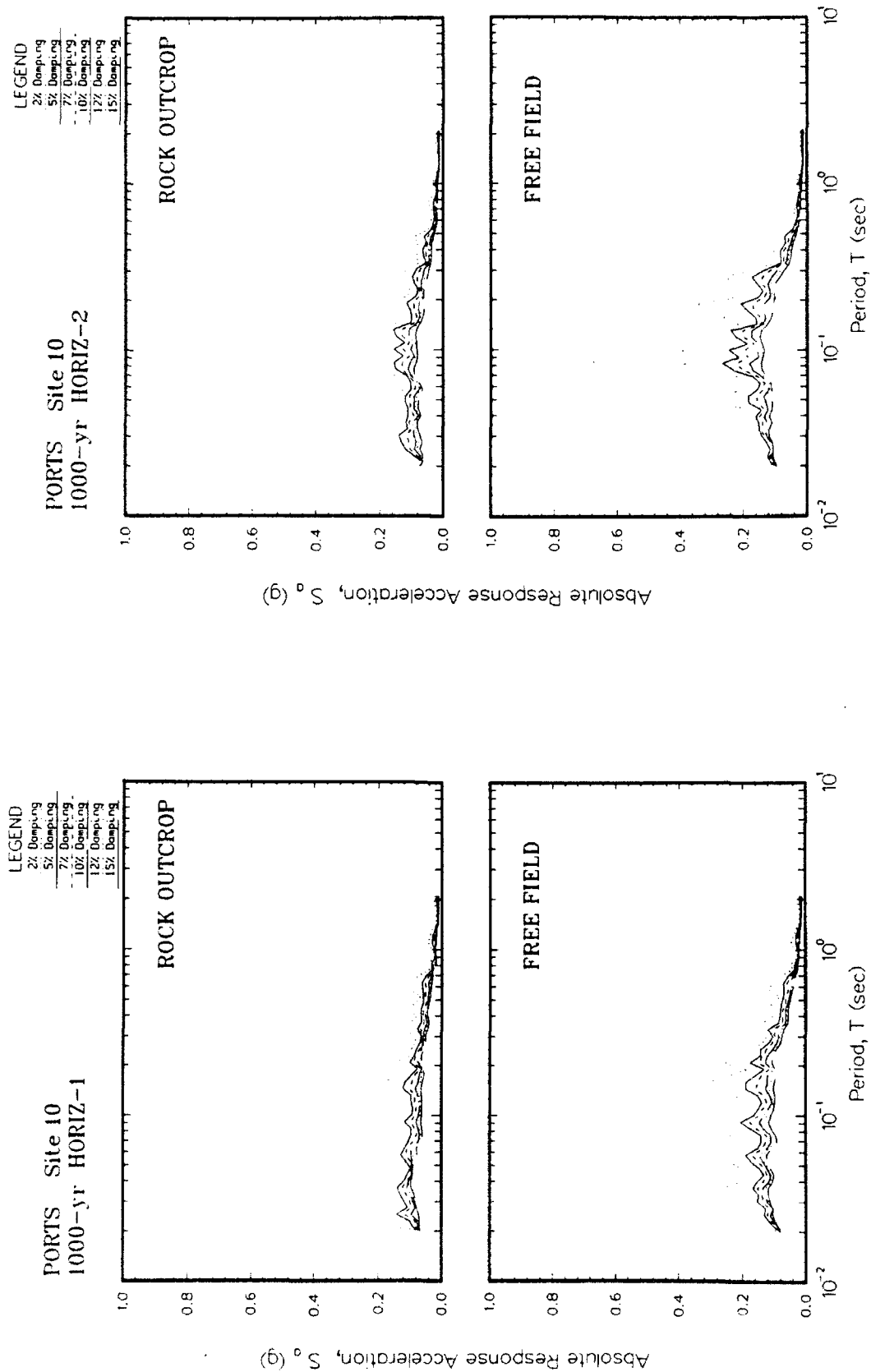


Figure K10. Absolute acceleration response spectra at free field for Site 10

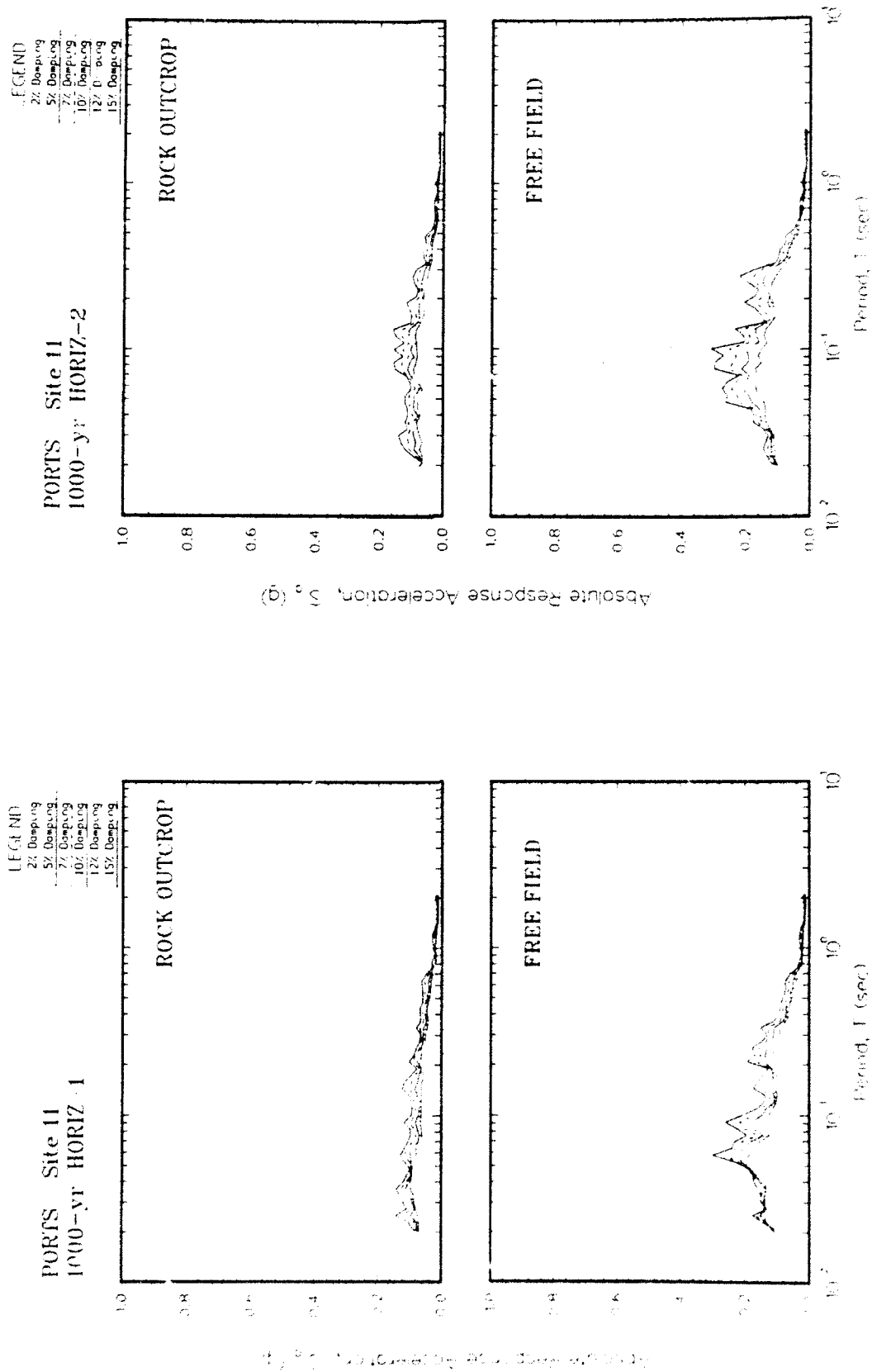
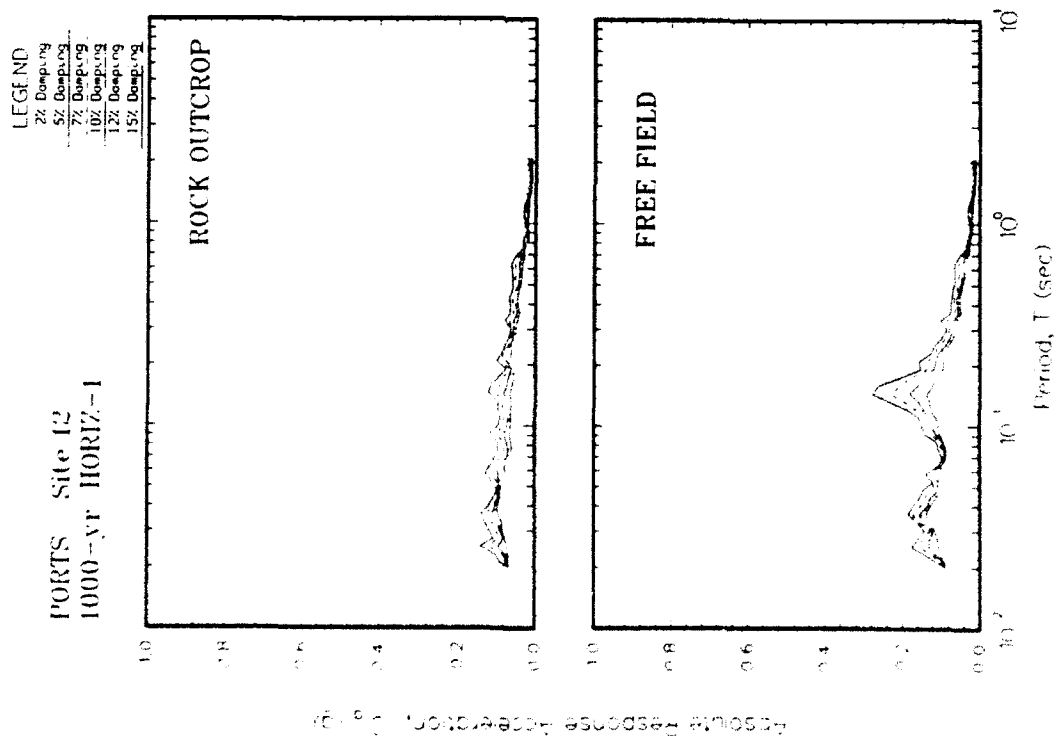


Figure K11. Absolute acceleration response spectra at free field for Site 11



K13

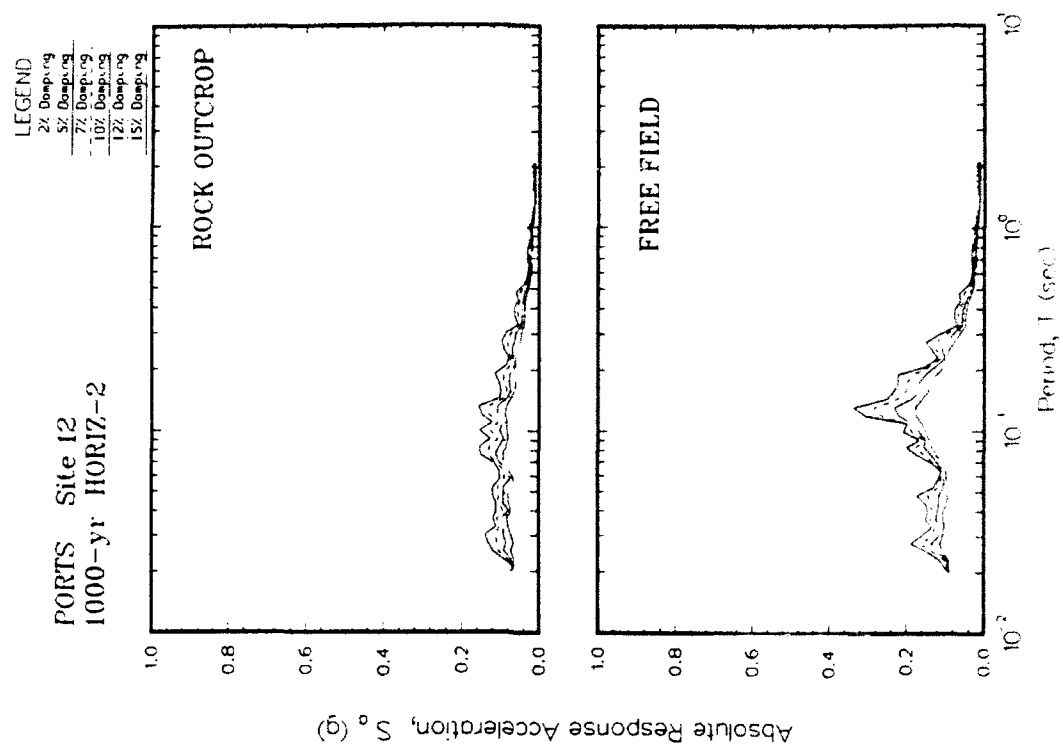


Figure K12. Absolute acceleration response spectra at free field for Site 12

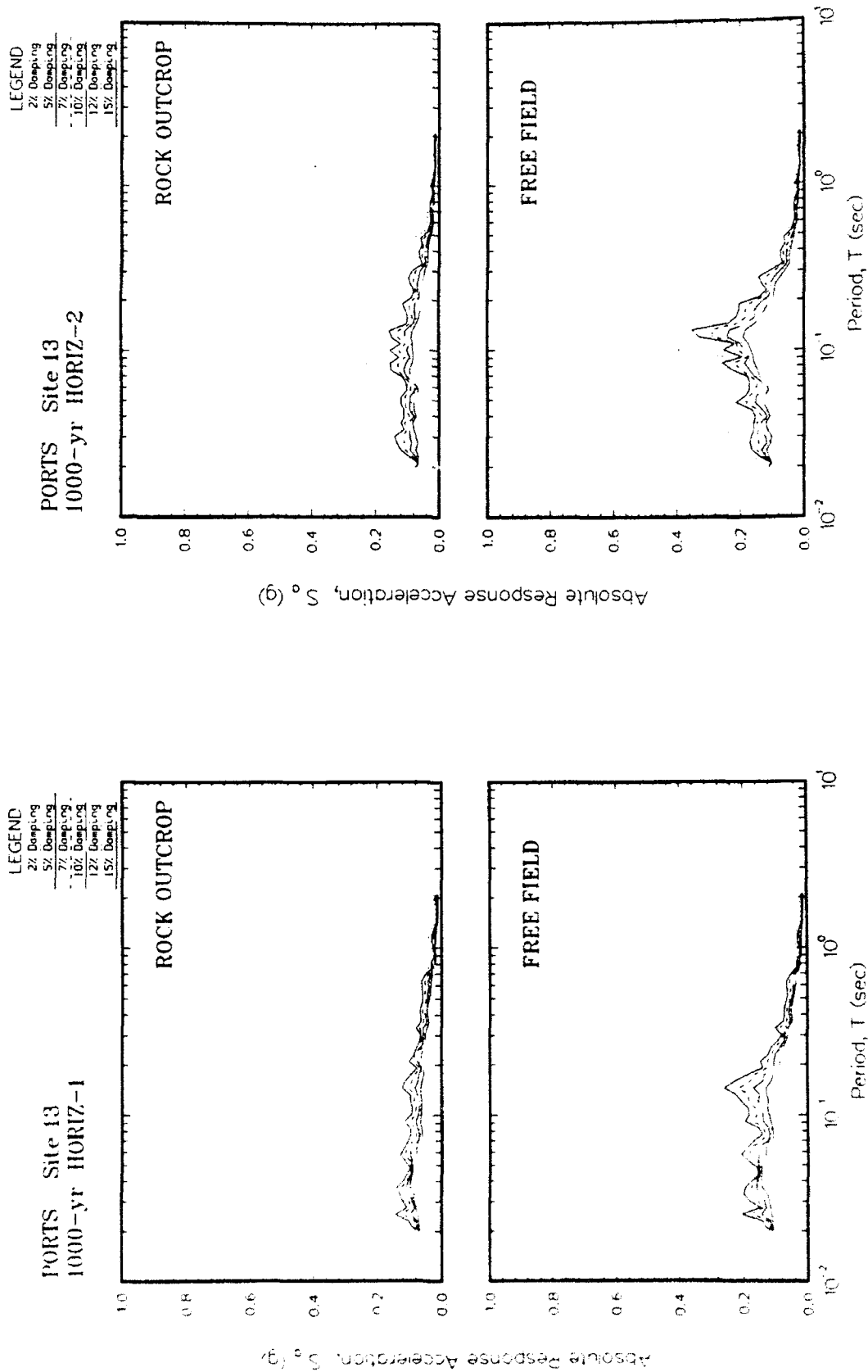


Figure K13. Absolute acceleration response spectra at free field for Site 13

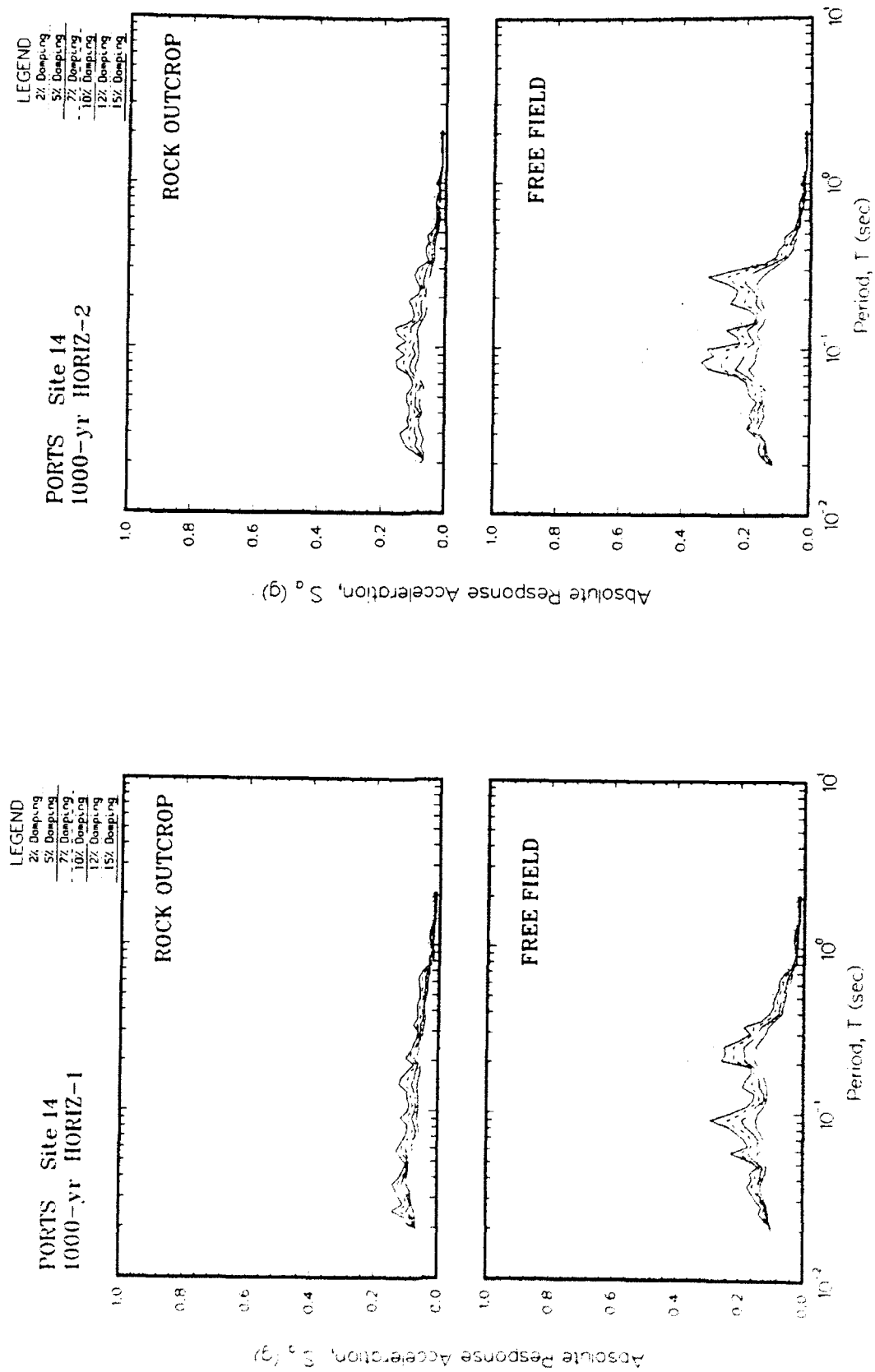


Figure K14. Absolute acceleration response spectra at free field for Site 14

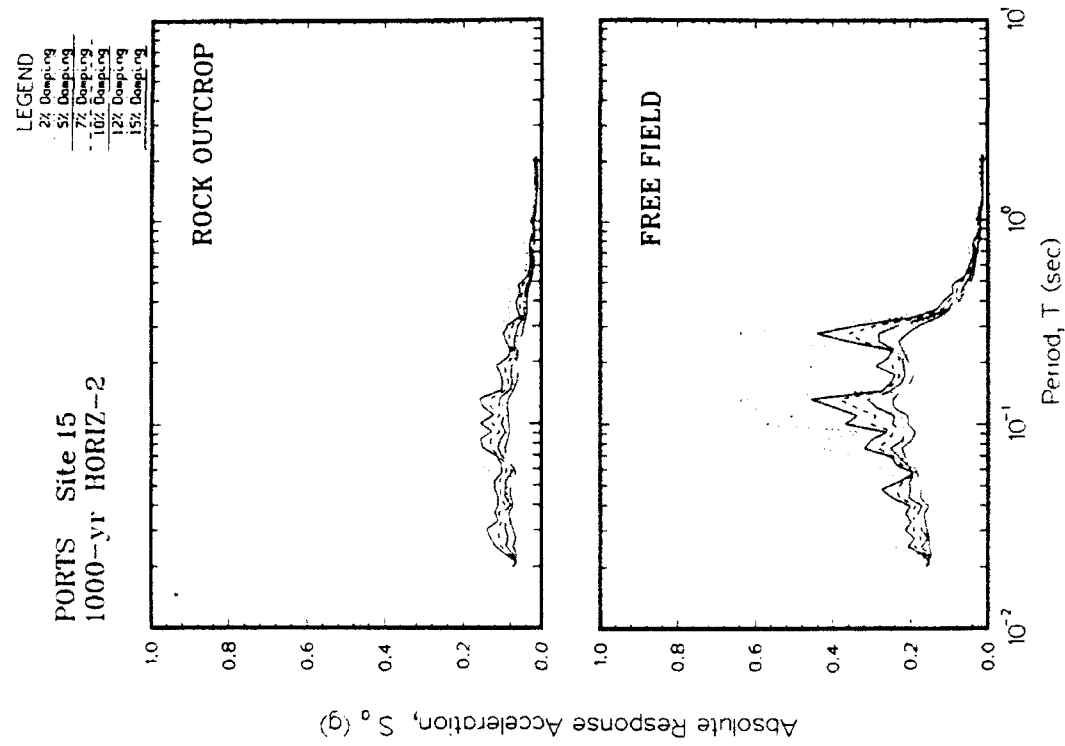
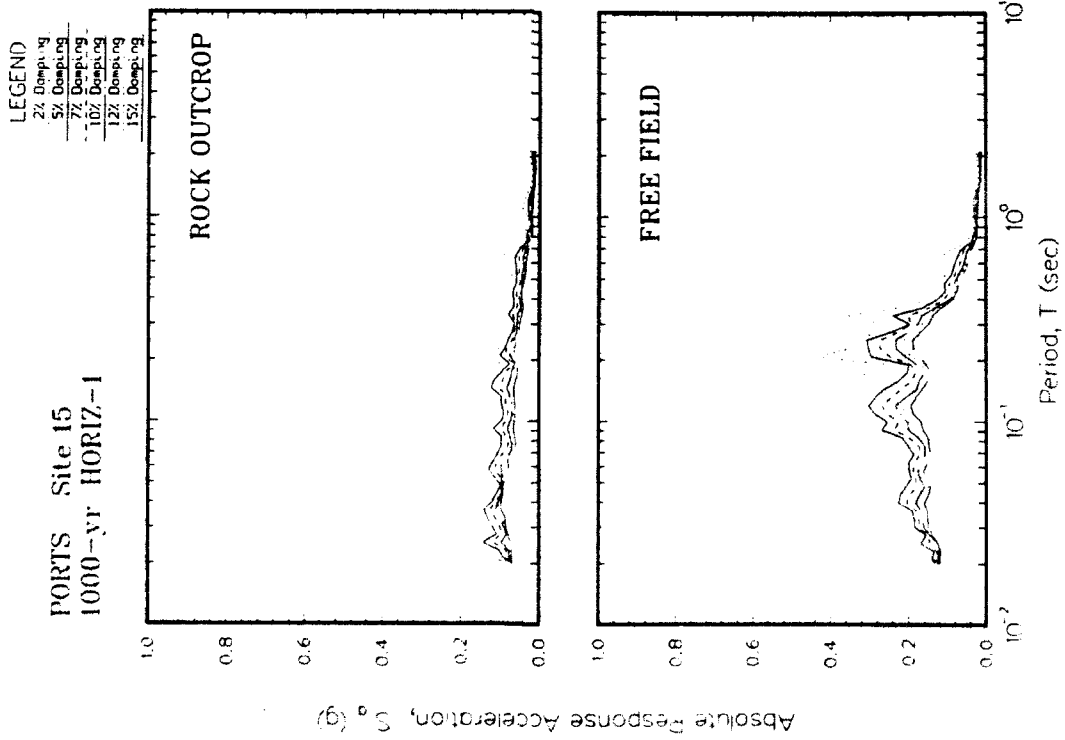


Figure K15. Absolute acceleration response spectra at free field for Site 15

APPENDIX L: RATIO OF ACCELERATION SPECTRA FOR 1000-YEAR EVENT .

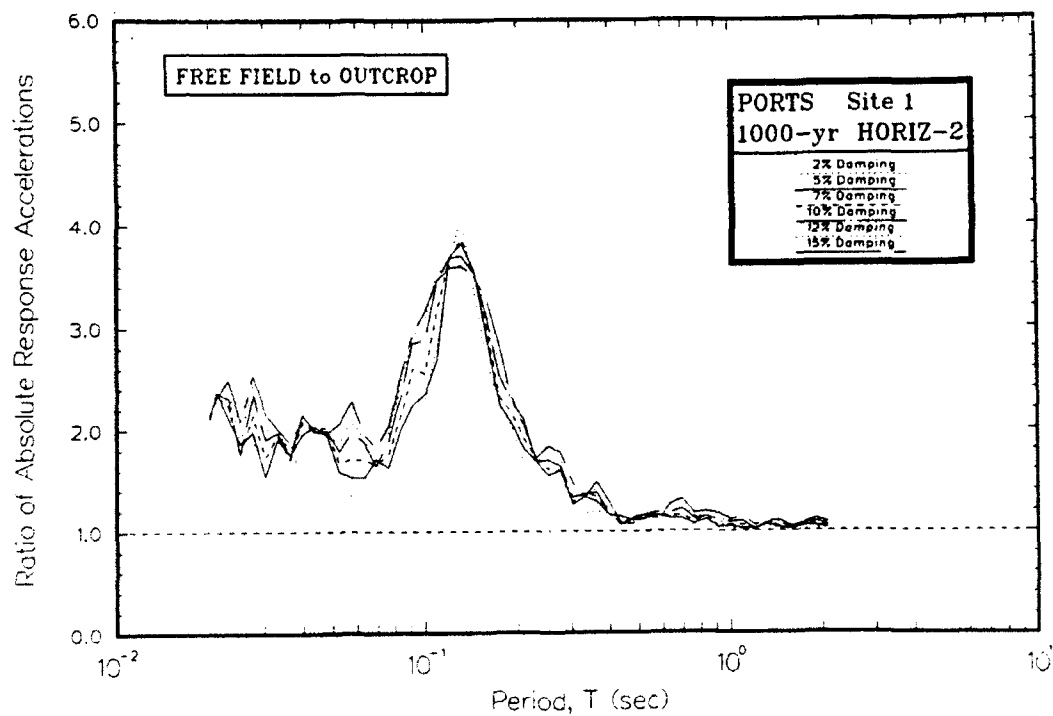
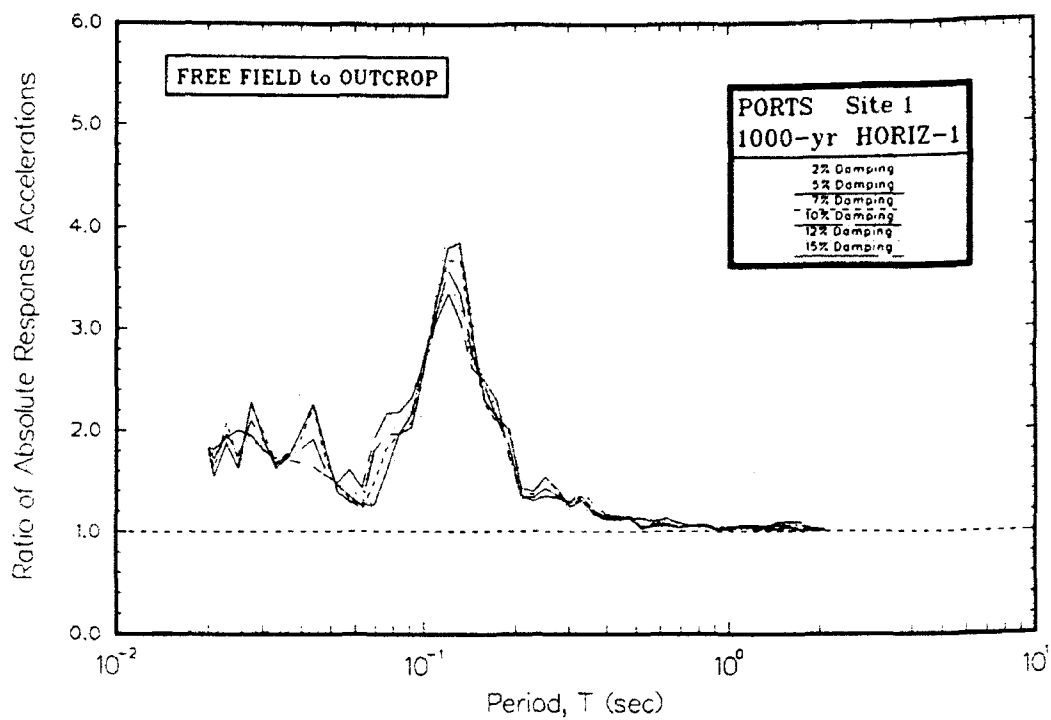


Figure L1. Ratio of absolute acceleration response spectra at free field to rock for Site 1

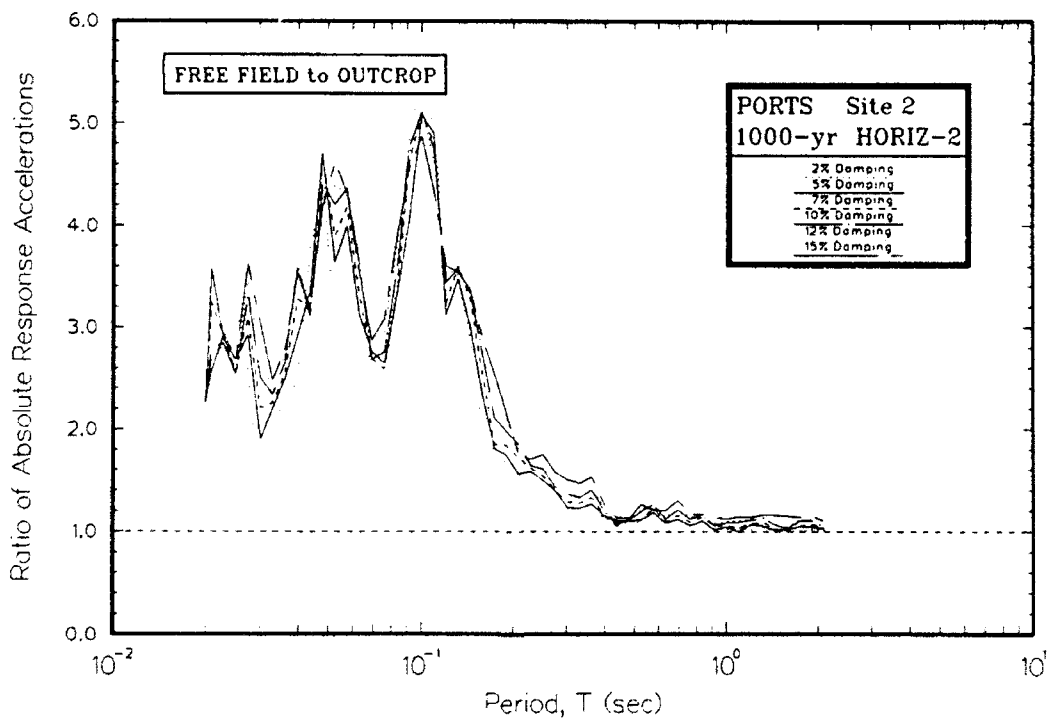
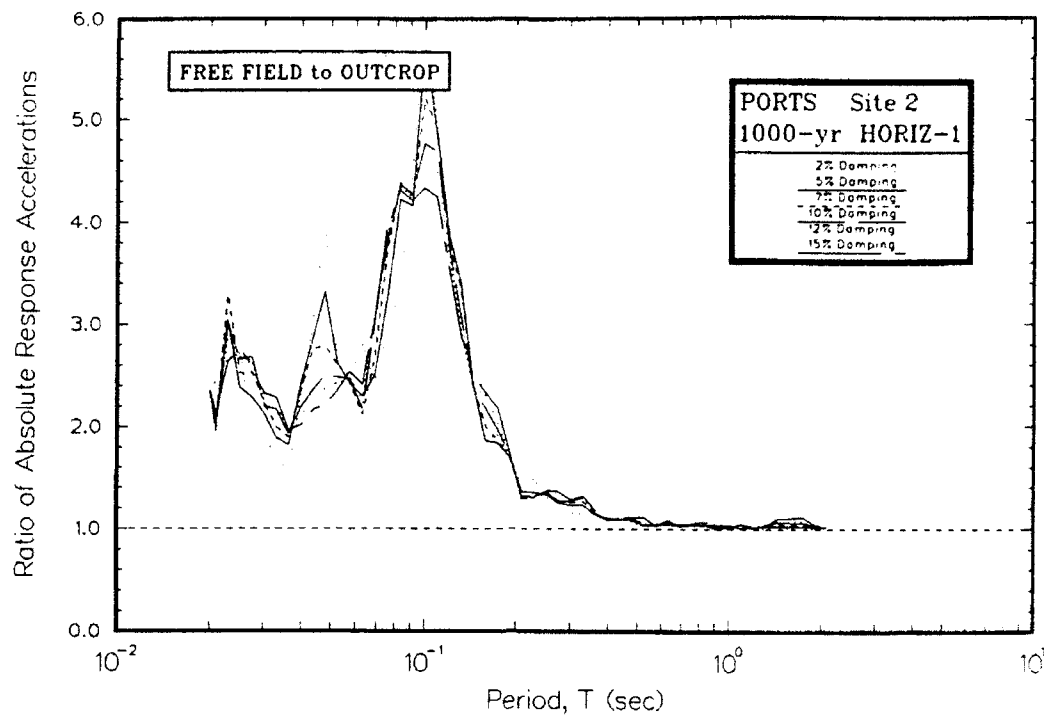


Figure L2. Ratio of absolute acceleration response spectra at free field to rock for Site 2

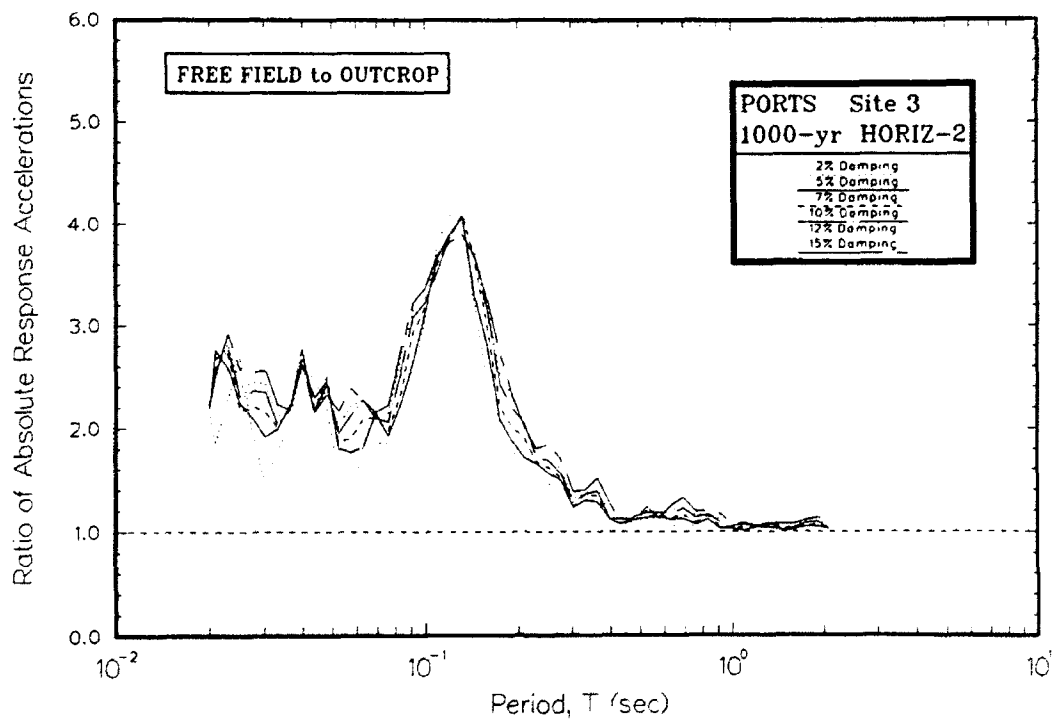
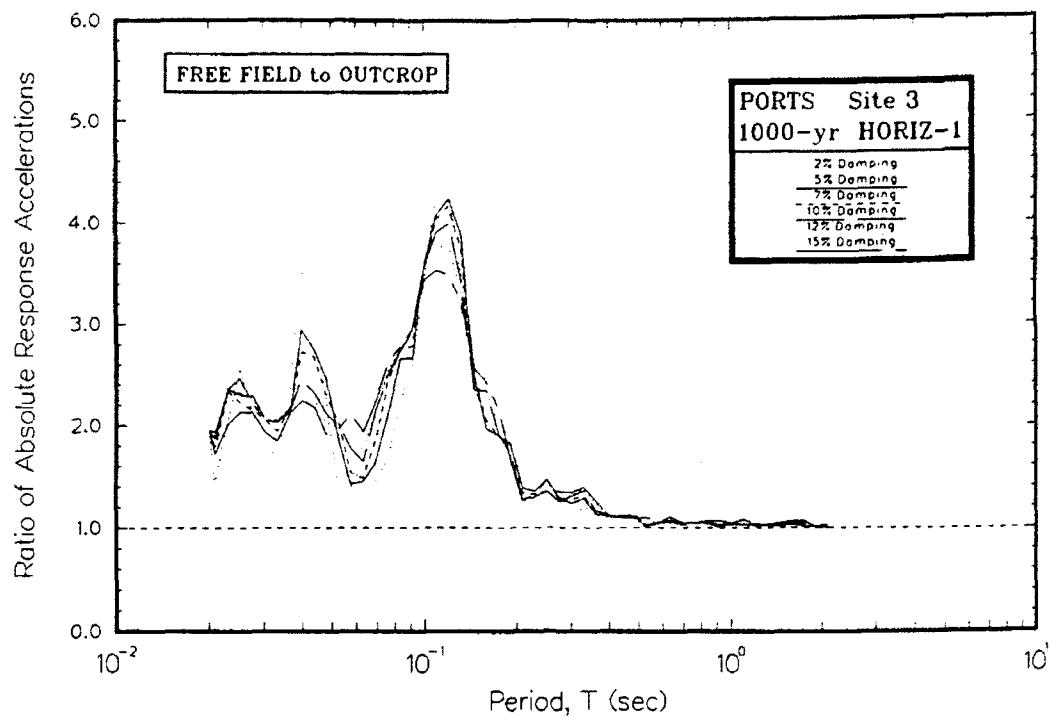


Figure L3. Ratio of absolute acceleration response spectra at free field to rock for Site 3

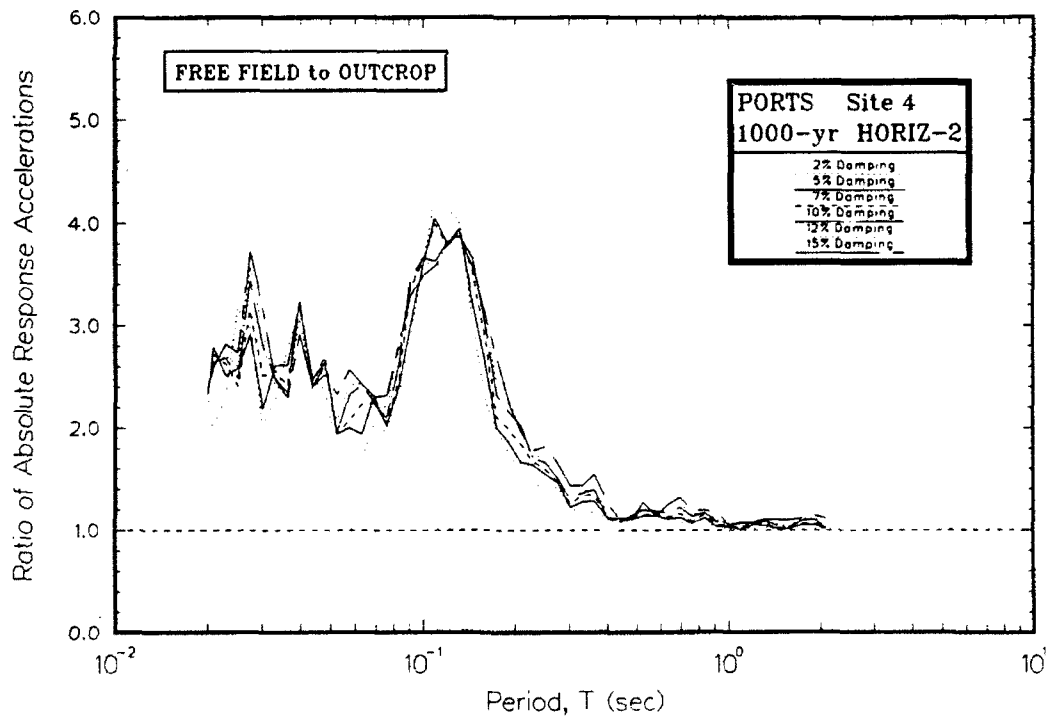
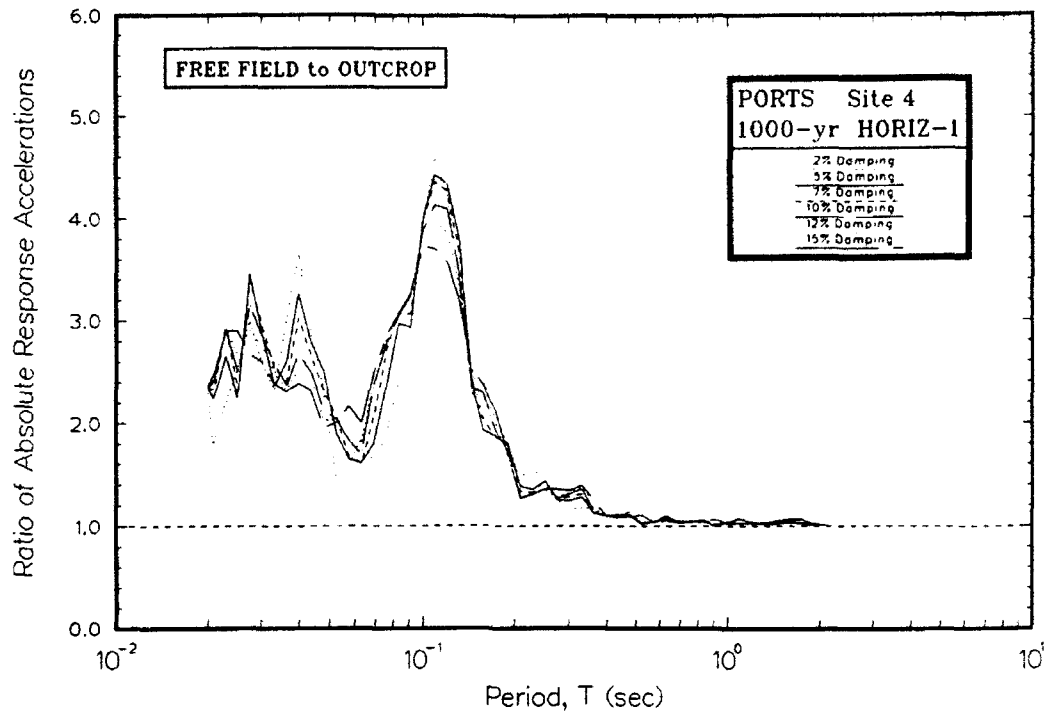


Figure L4. Ratio of absolute acceleration response spectra at free field to rock for Site 4

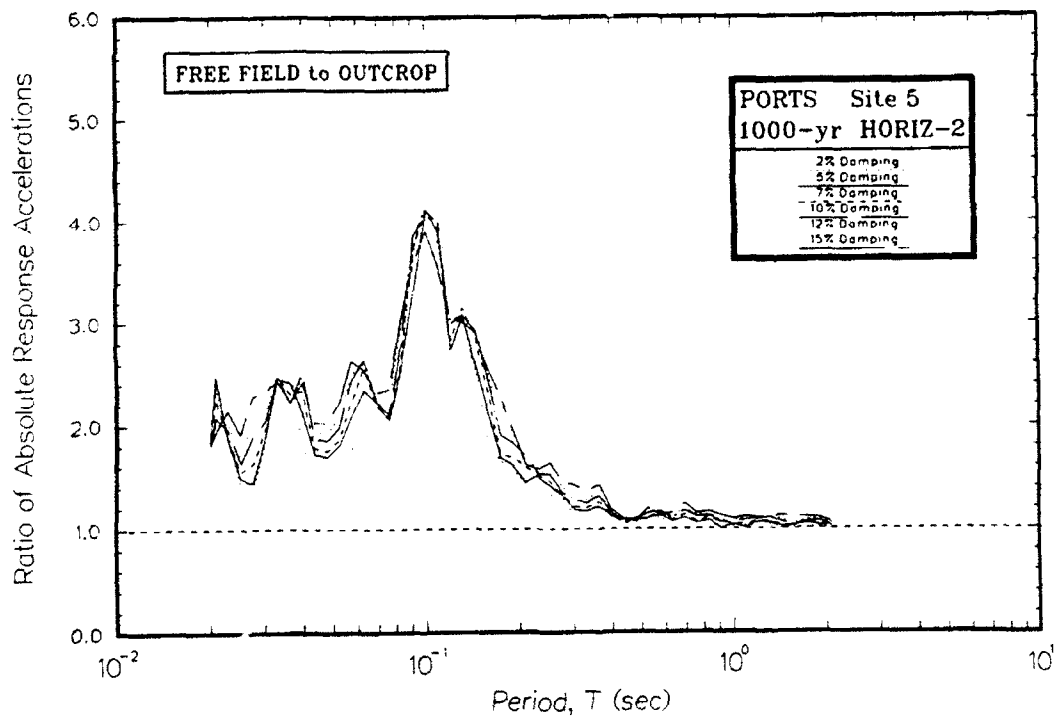
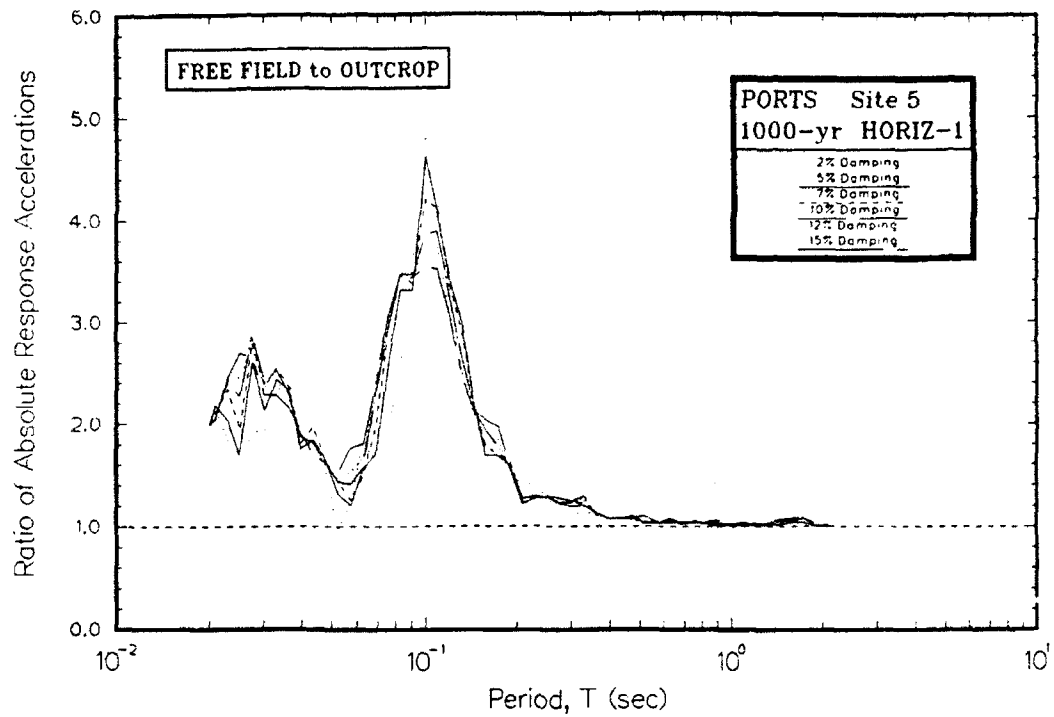
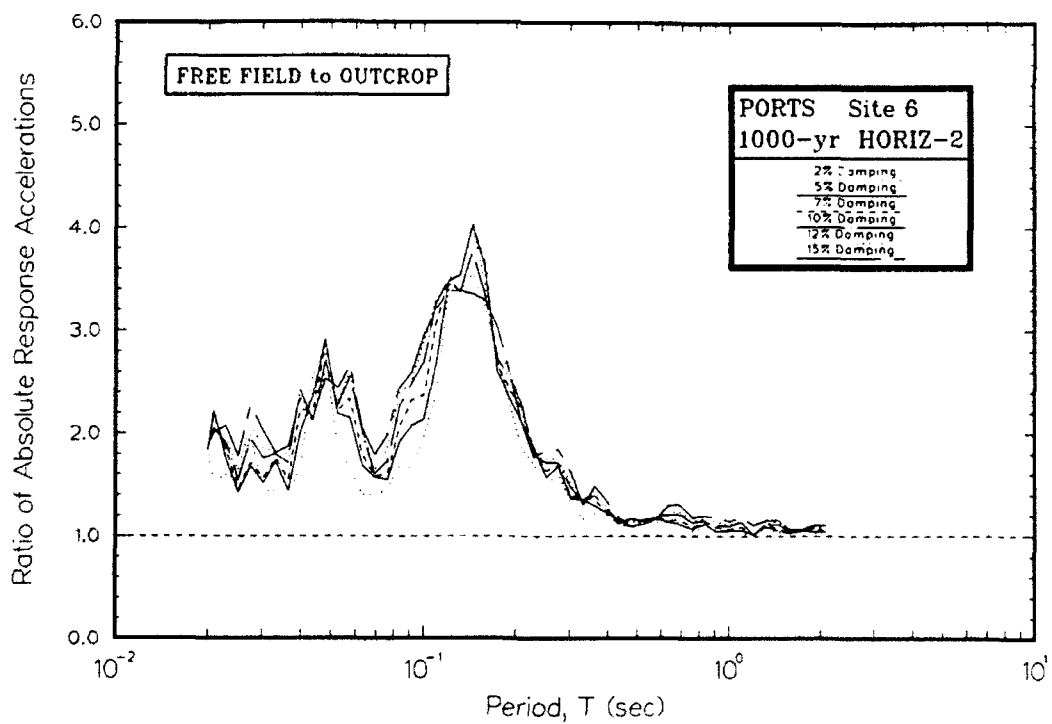
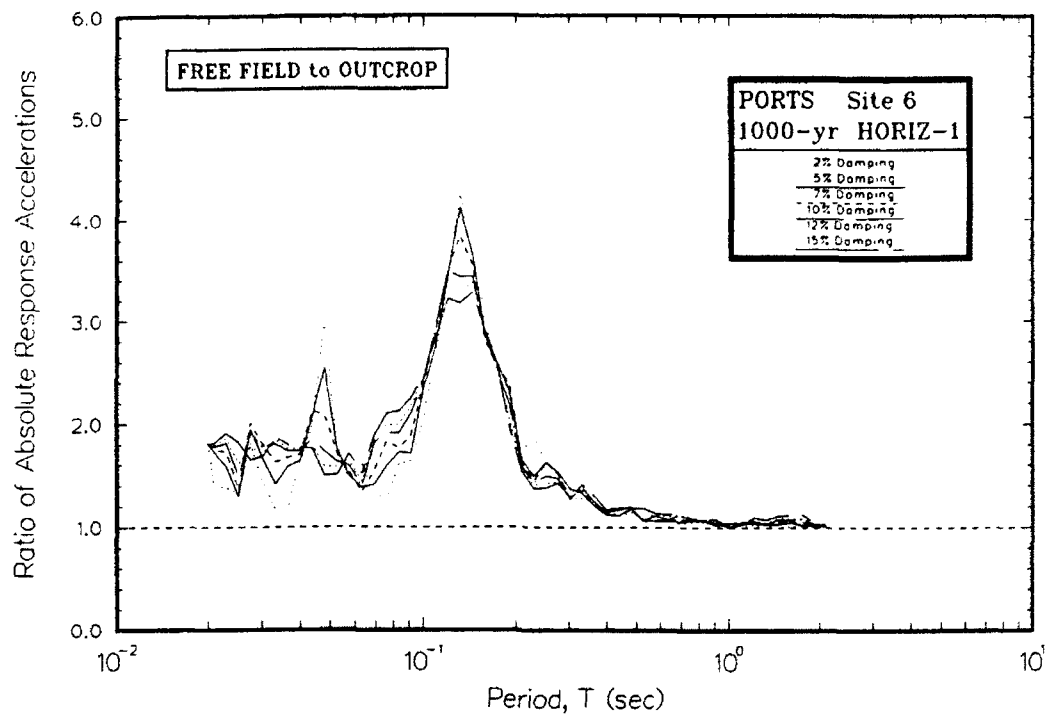


Figure L5. Ratio of absolute acceleration response spectra at free field to rock for Site 5



**Figure L6. Ratio of absolute acceleration response spectra
at free field to rock for Site 6**

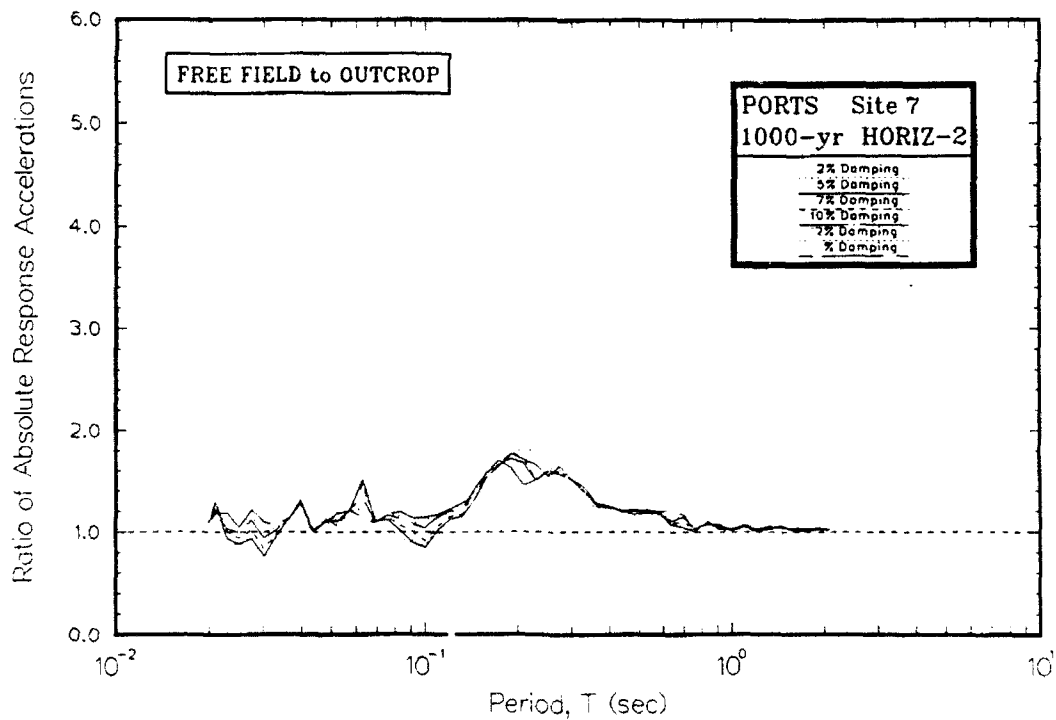
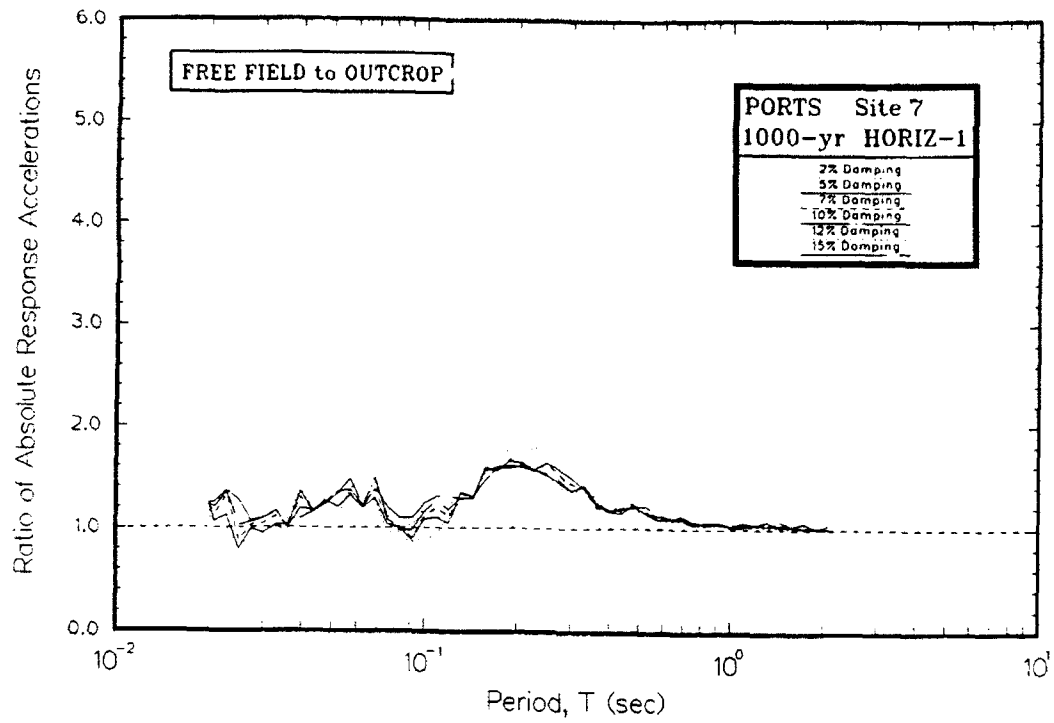


Figure L7. Ratio of absolute acceleration response spectra at free field to rock for Site 7

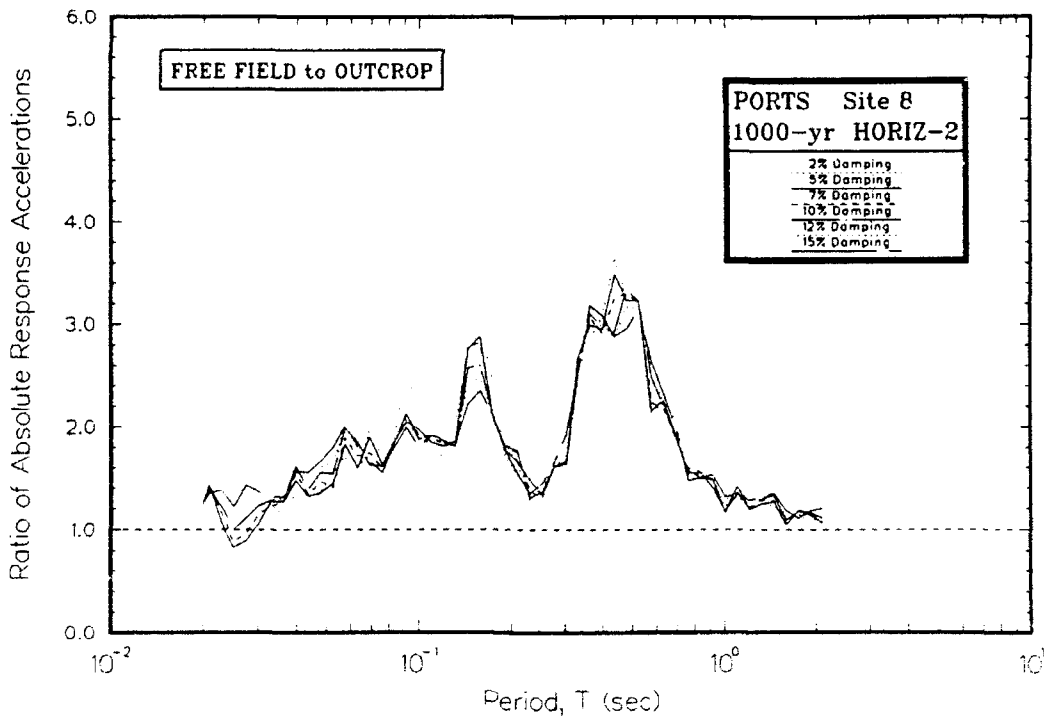
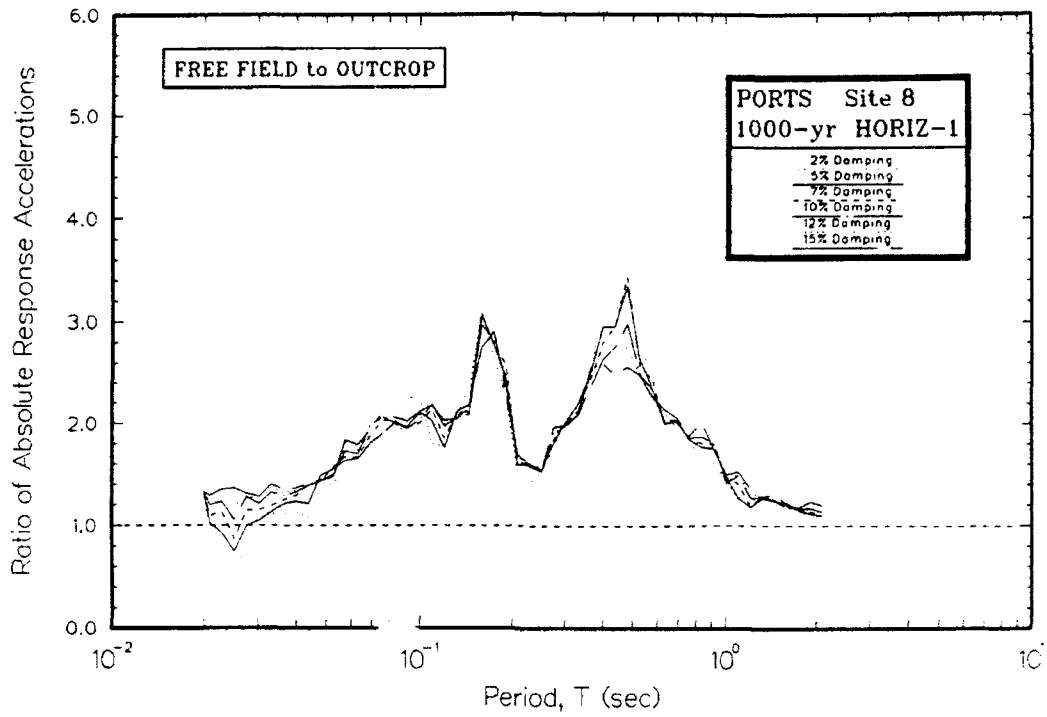


Figure L8. Ratio of absolute acceleration response spectra at free field to rock for Site 8

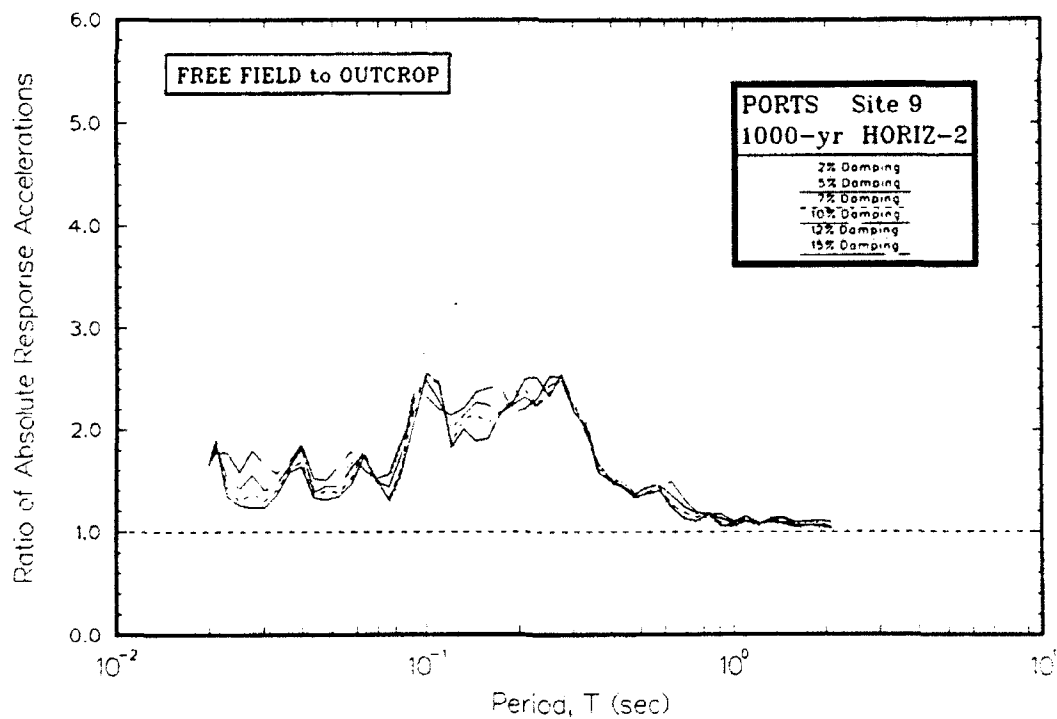
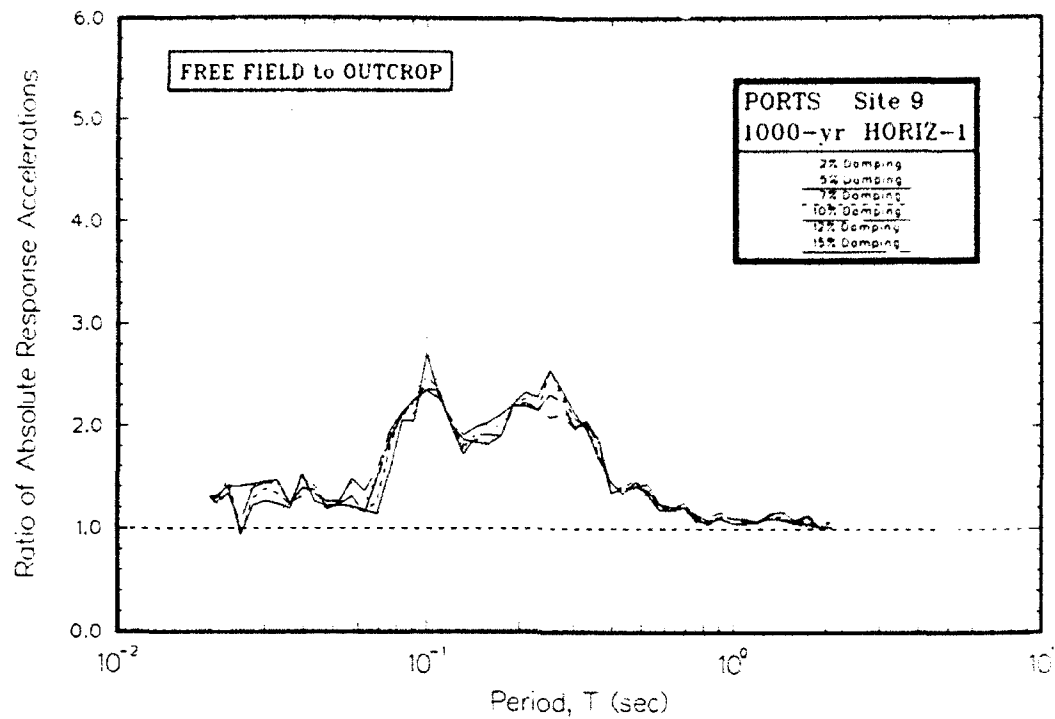


Figure L9. Ratio of absolute acceleration response spectra at free field to rock for Site 9

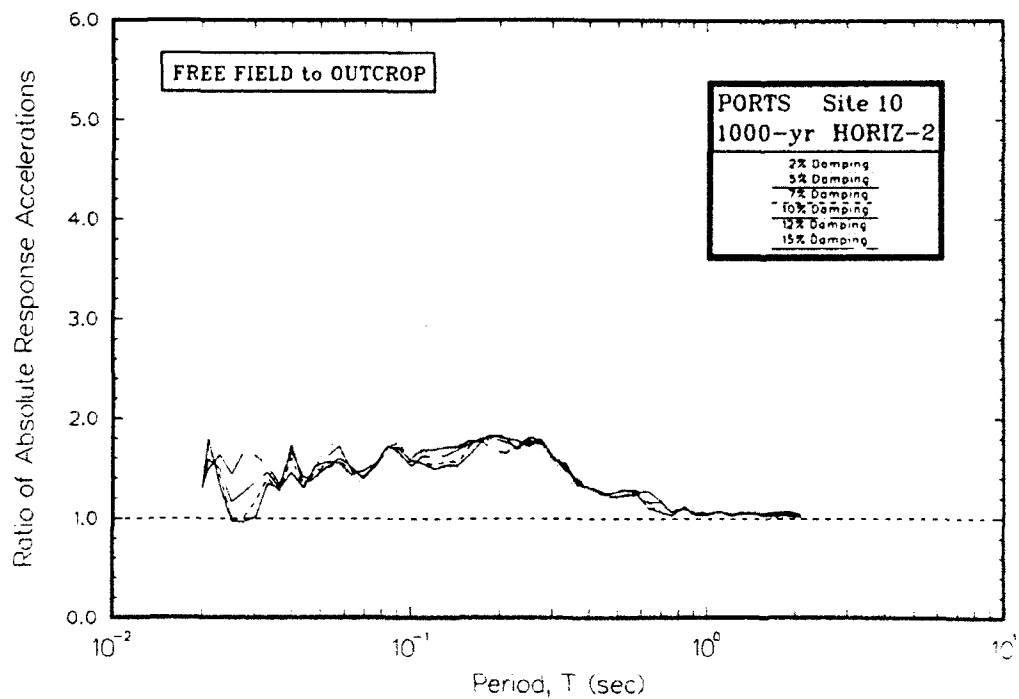
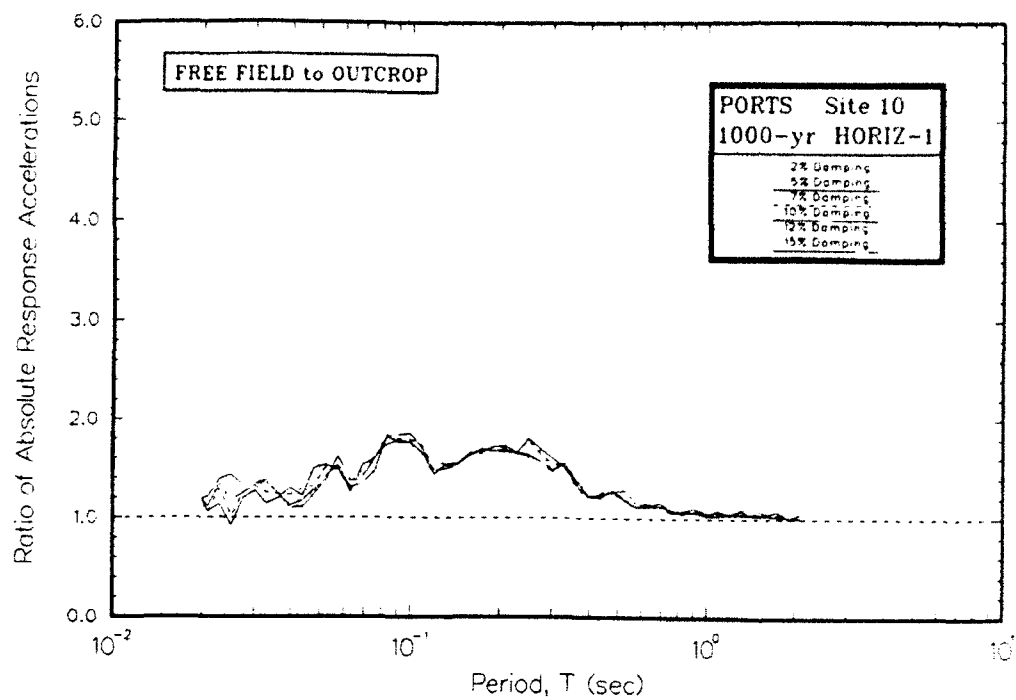


Figure L10. Ratio of absolute acceleration response spectra at free field to rock for Site 10

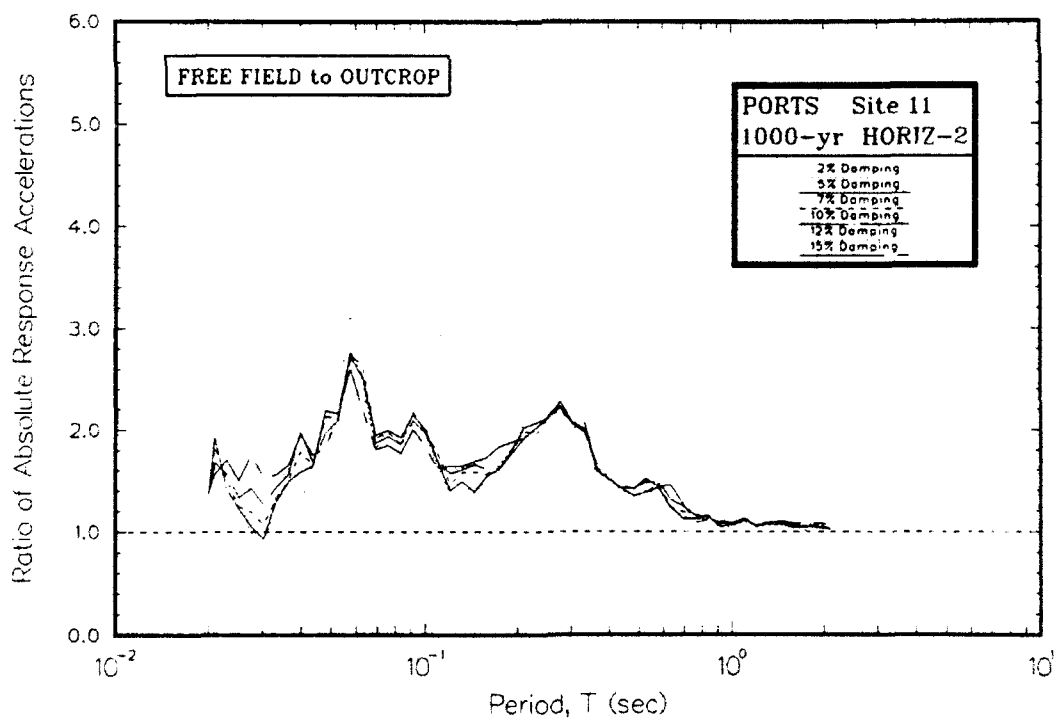
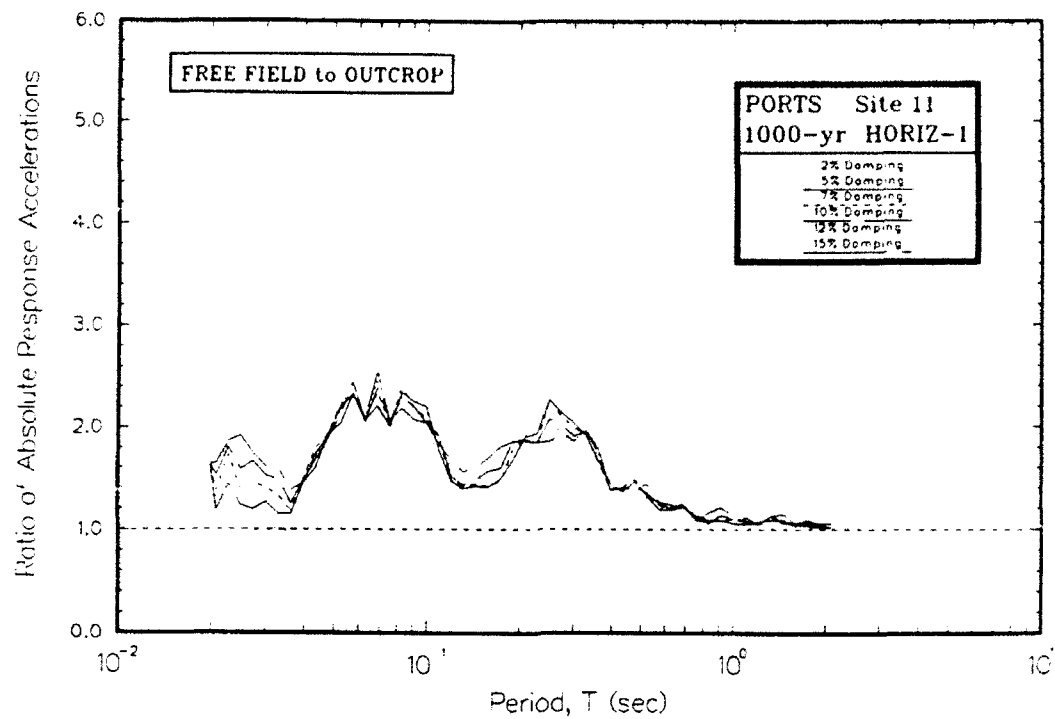


figure L11. Ratio of absolute acceleration response spectra at free field to rock for Site 11

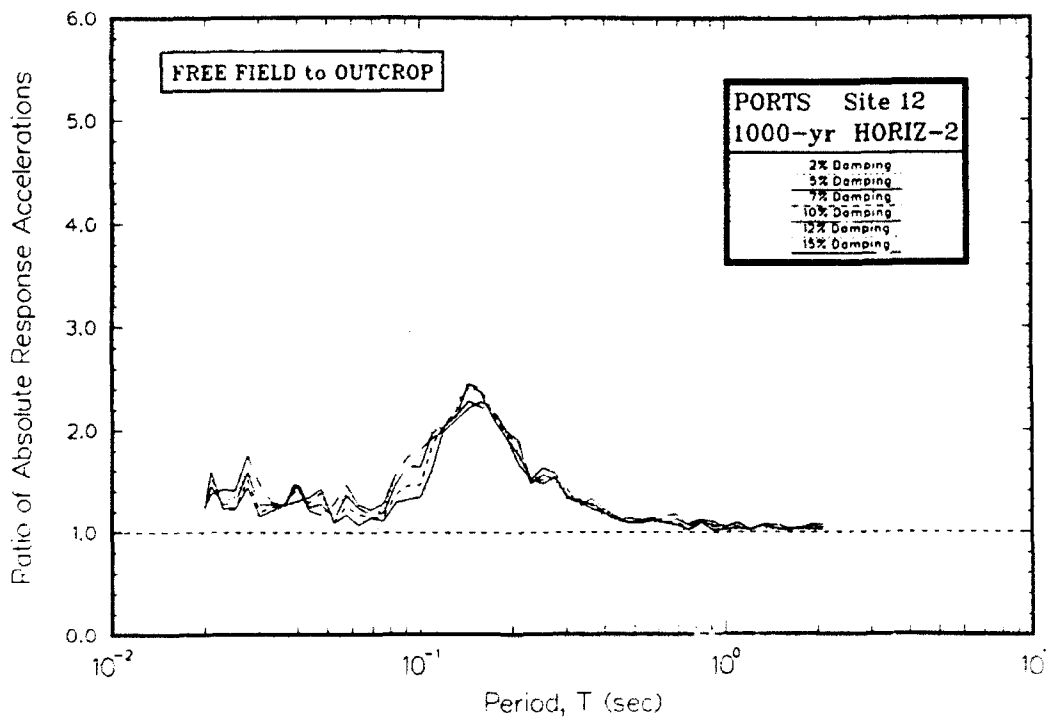
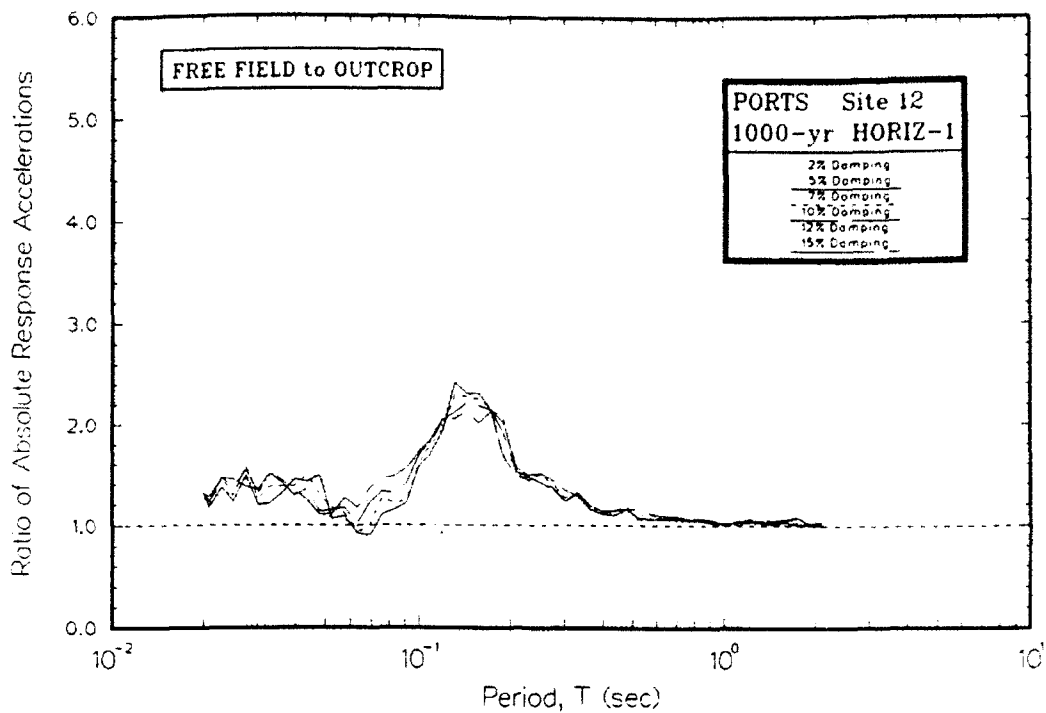


Figure L12. Ratio of absolute acceleration response spectra at free field to rock for Site 12

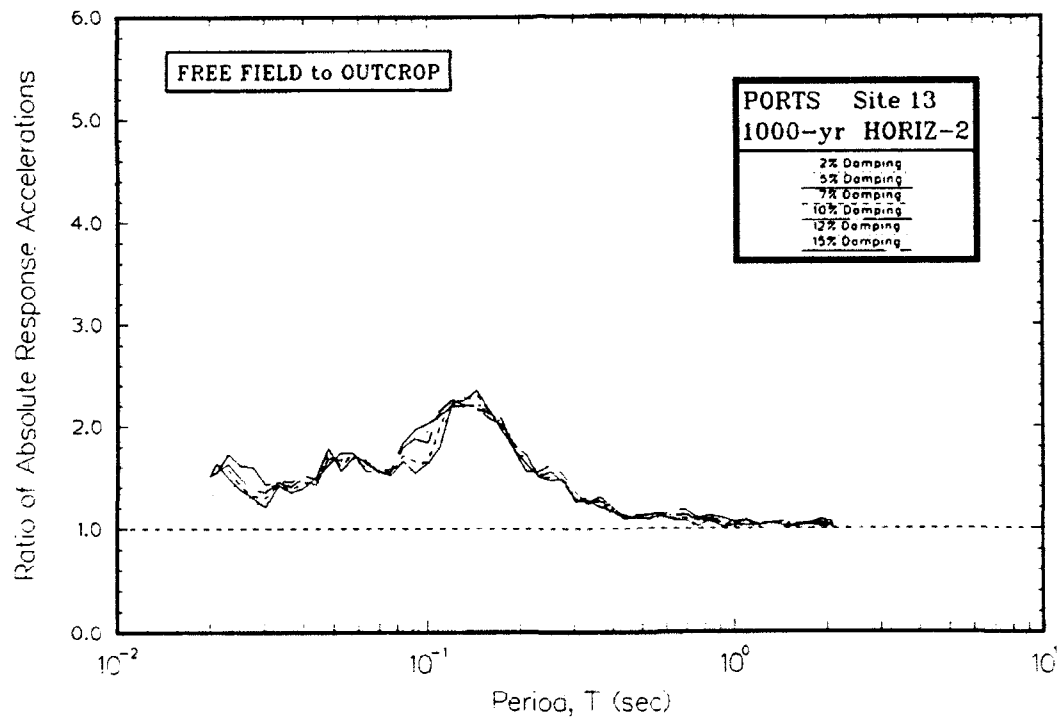
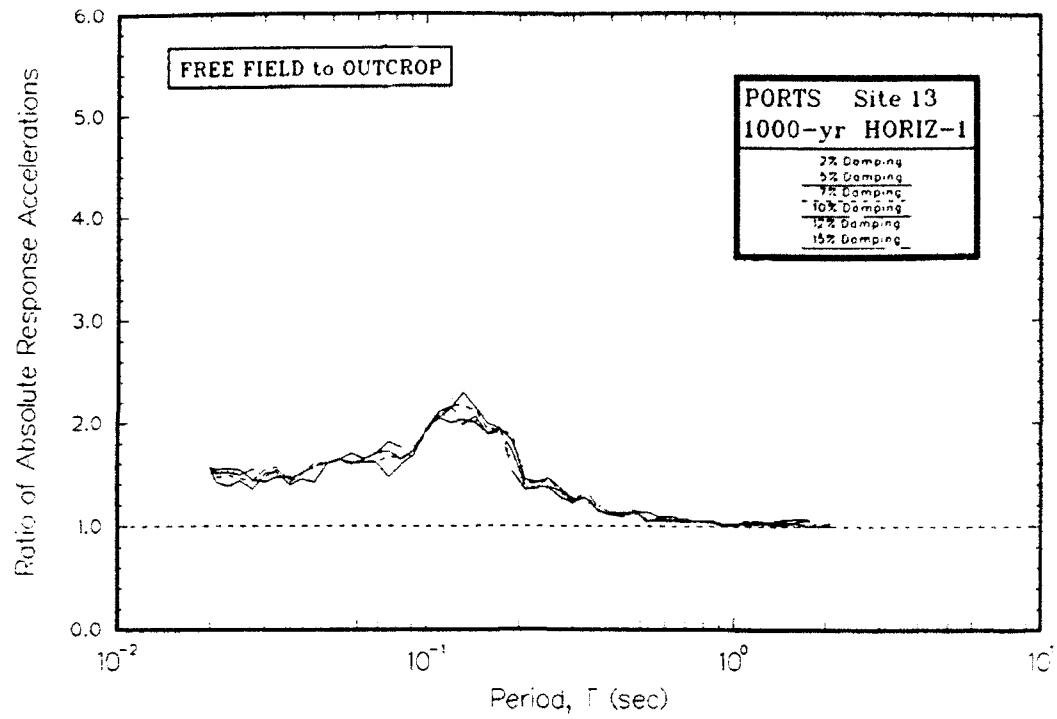


Figure L13. Ratio of absolute acceleration response spectra at free field to rock for Site 13

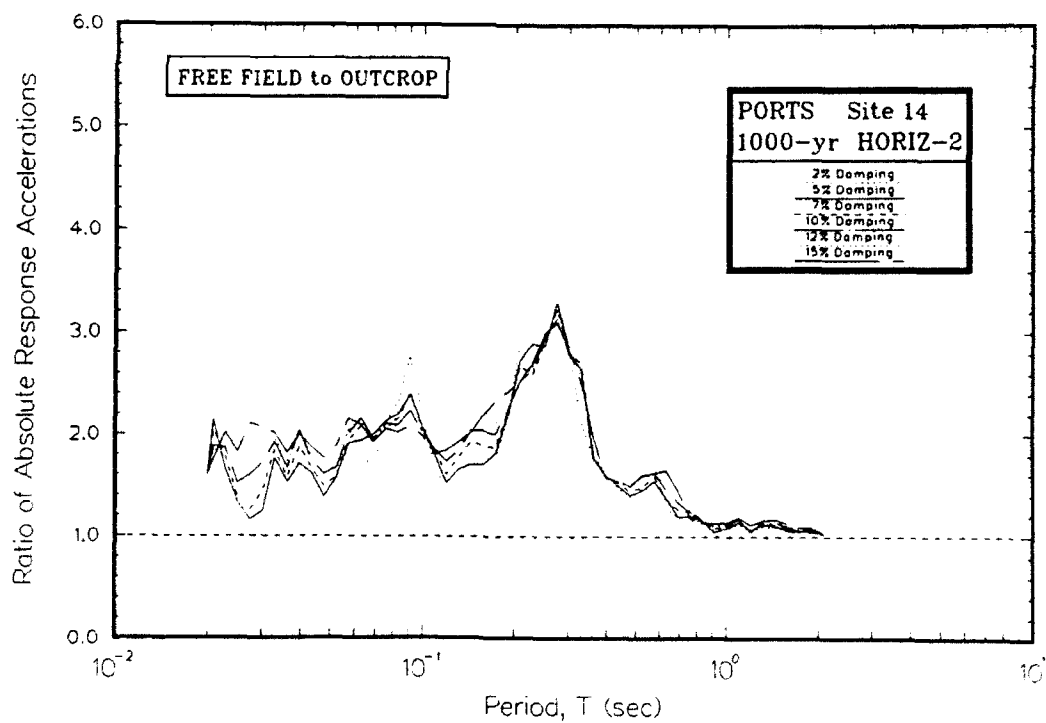
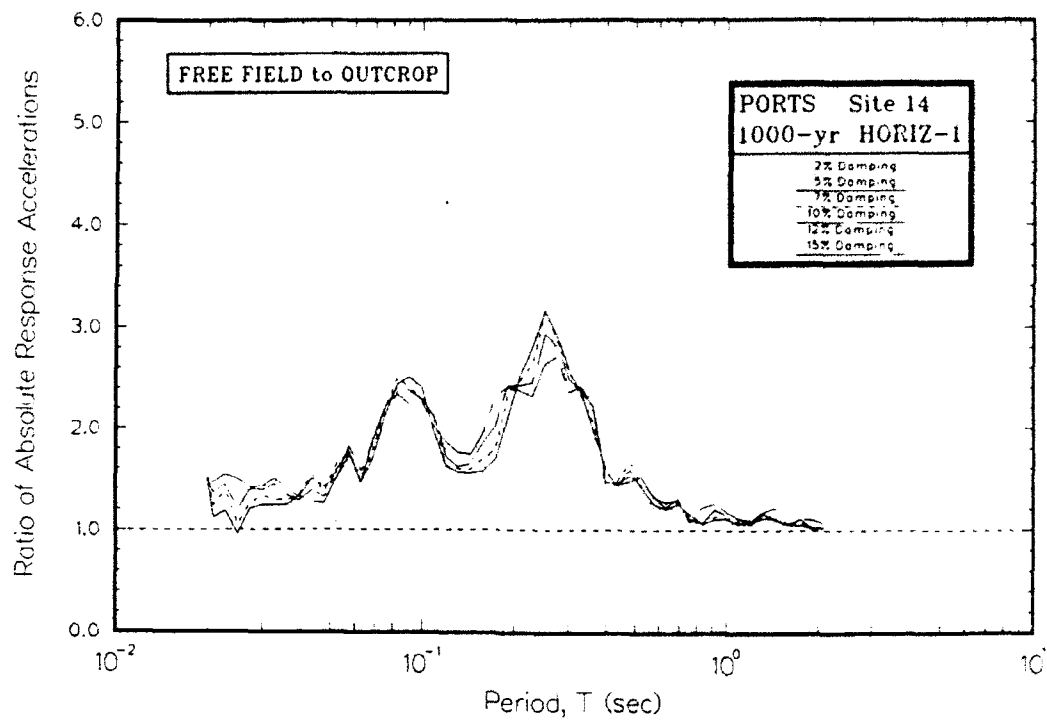


Figure L14. Ratio of absolute acceleration response spectra at free field to rock for Site 14

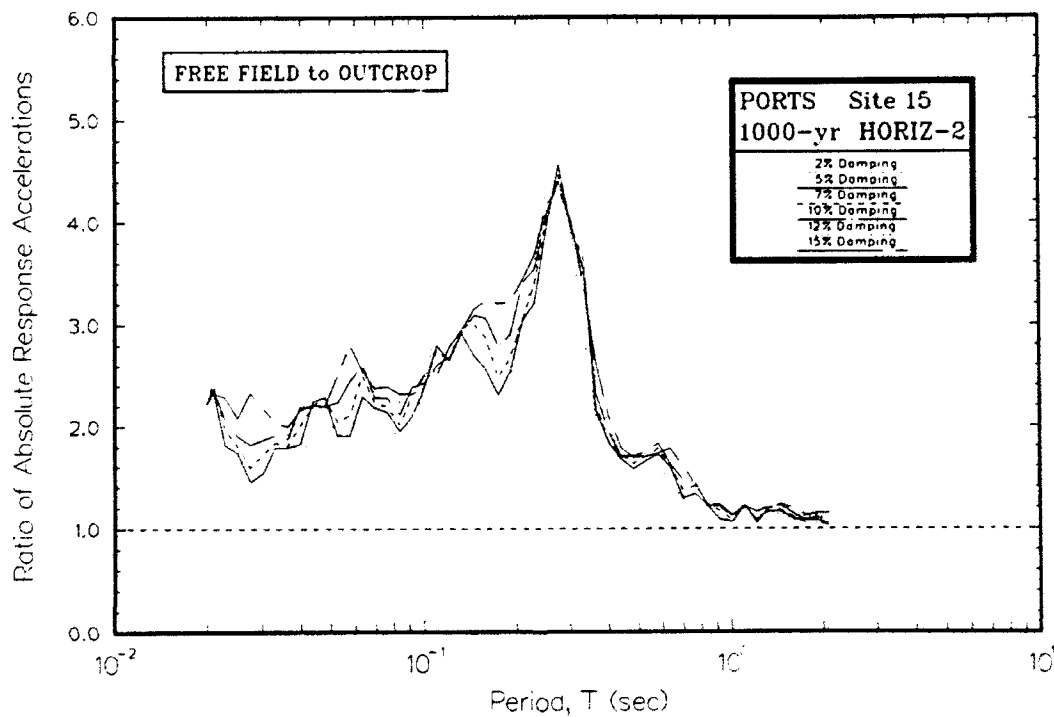
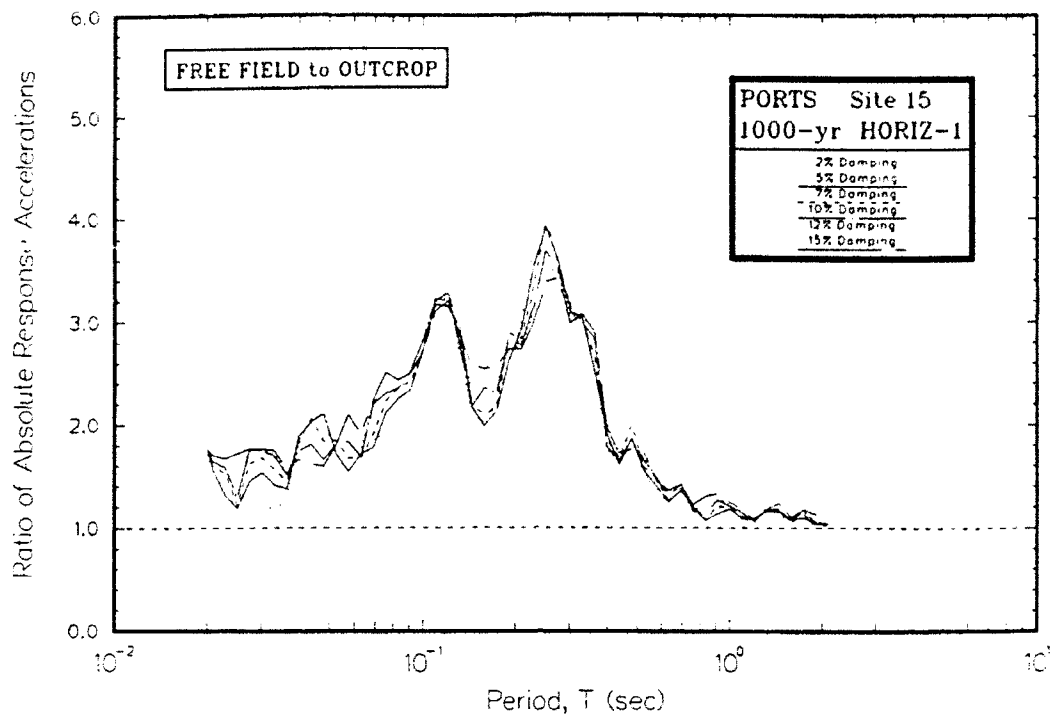


Figure L15. Ratio of absolute acceleration response spectra at free field to rock for Site 15

APPENDIX M: AMPLIFICATION RATIOS FOR 1000-YEAR EVENT

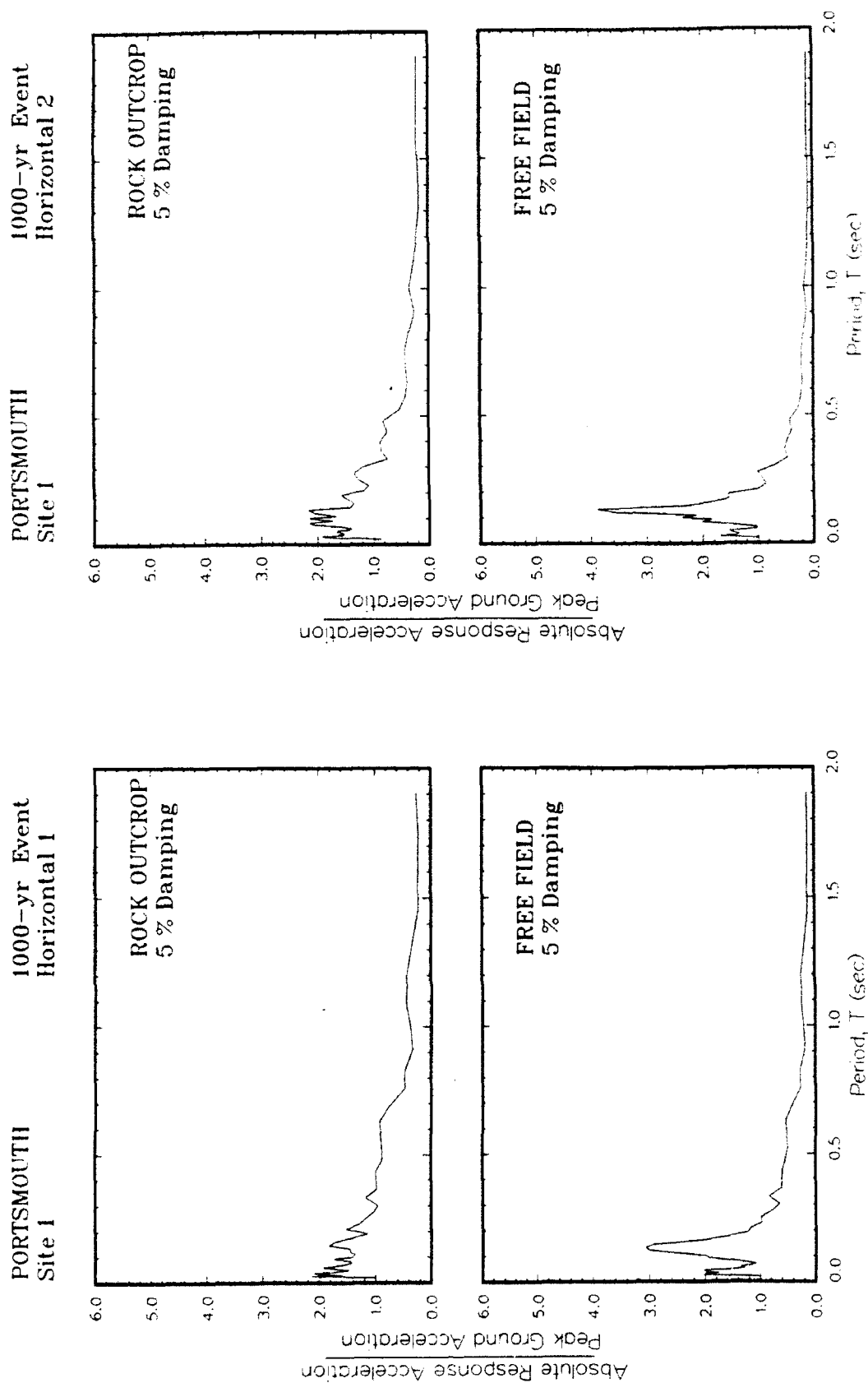


Figure M1. Ratio of amplification of absolute acceleration response spectra to peak acceleration at free field for Site 1

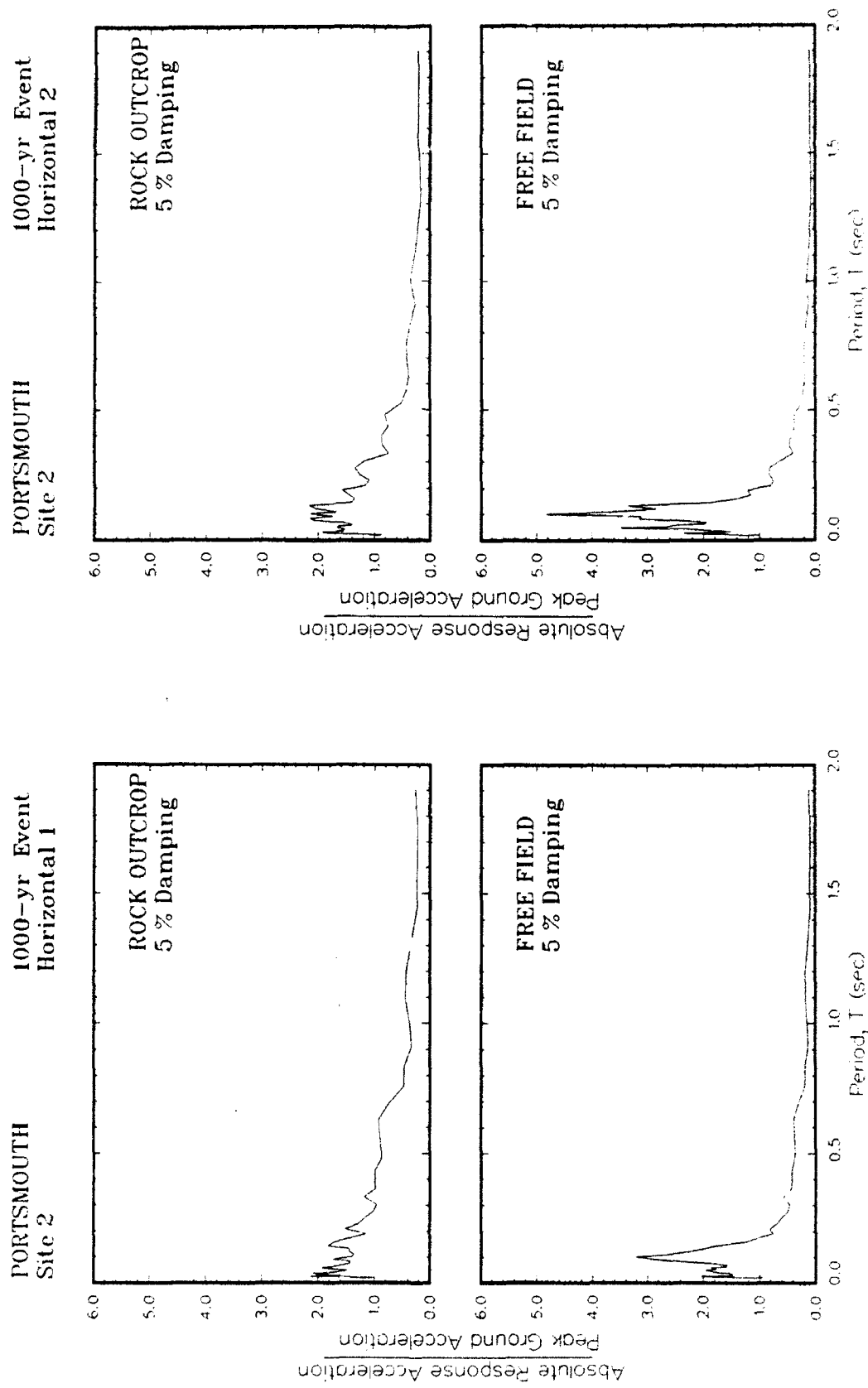


Figure M2. Ratio of amplification of absolute acceleration response spectra to peak acceleration at free field for Site 2

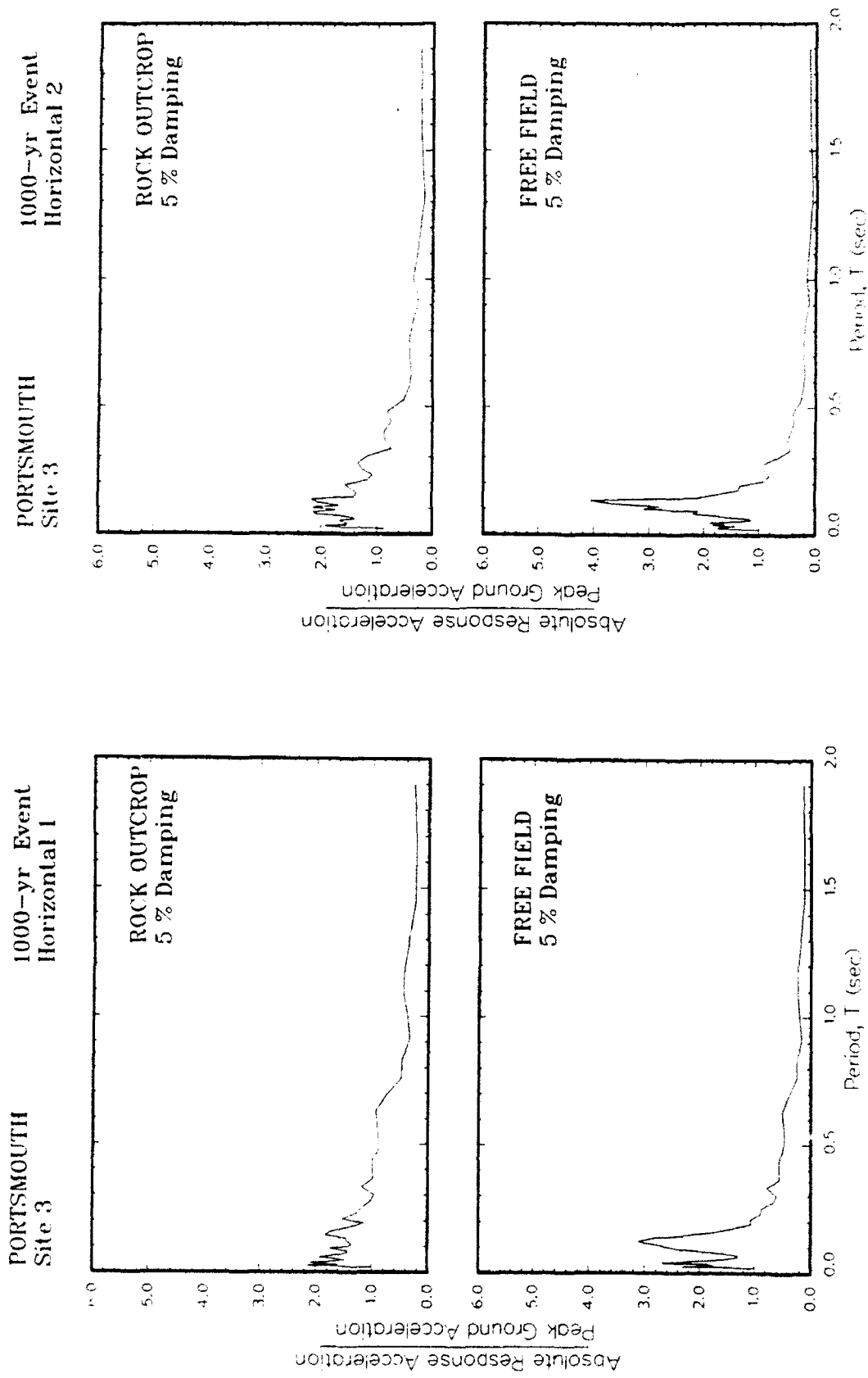


Figure M3. Ratio of amplification of absolute acceleration response spectra to peak acceleration at free field for Site 3

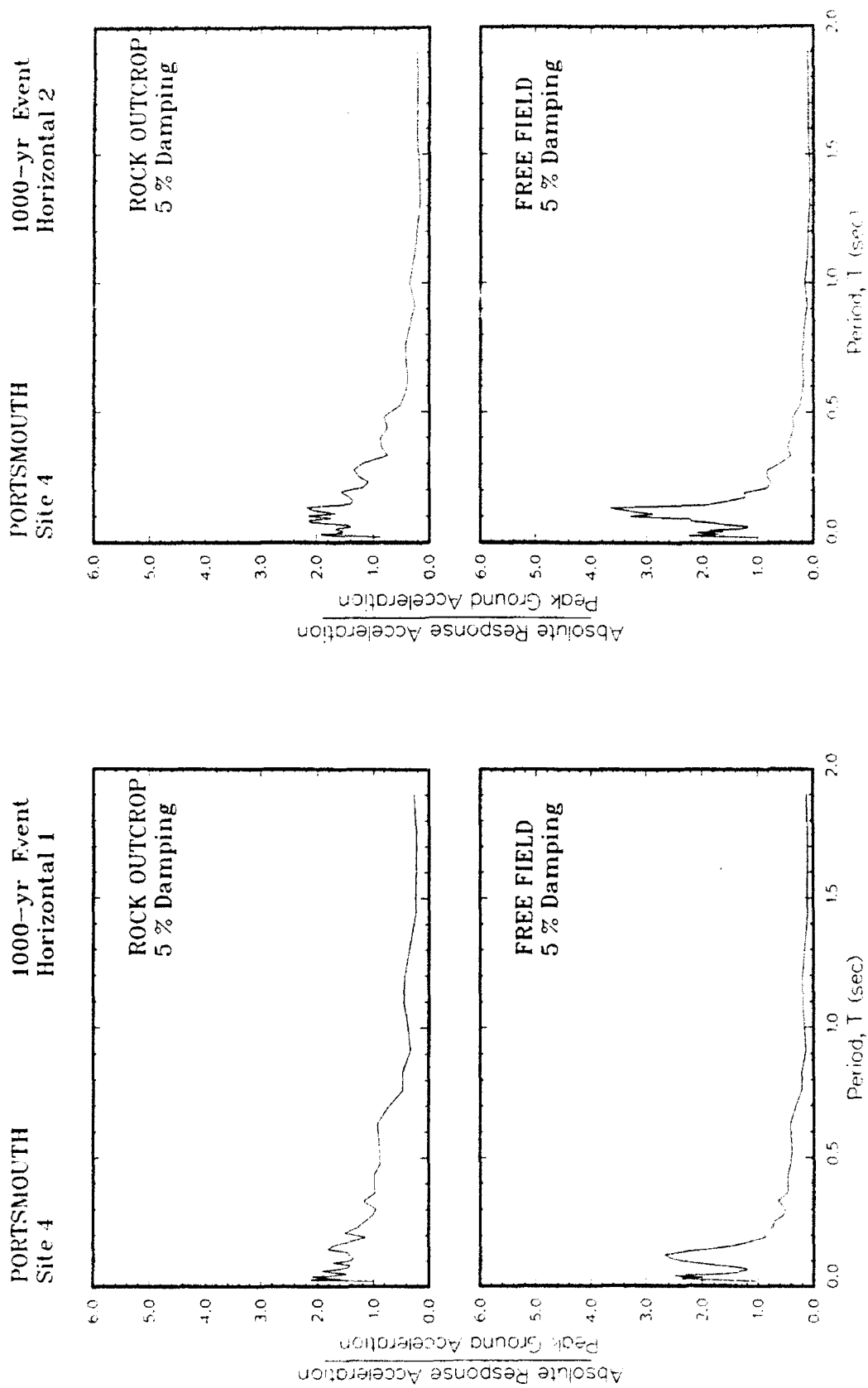


Figure M4. Ratio of amplification of absolute acceleration response spectra to peak acceleration at free field for Site 4

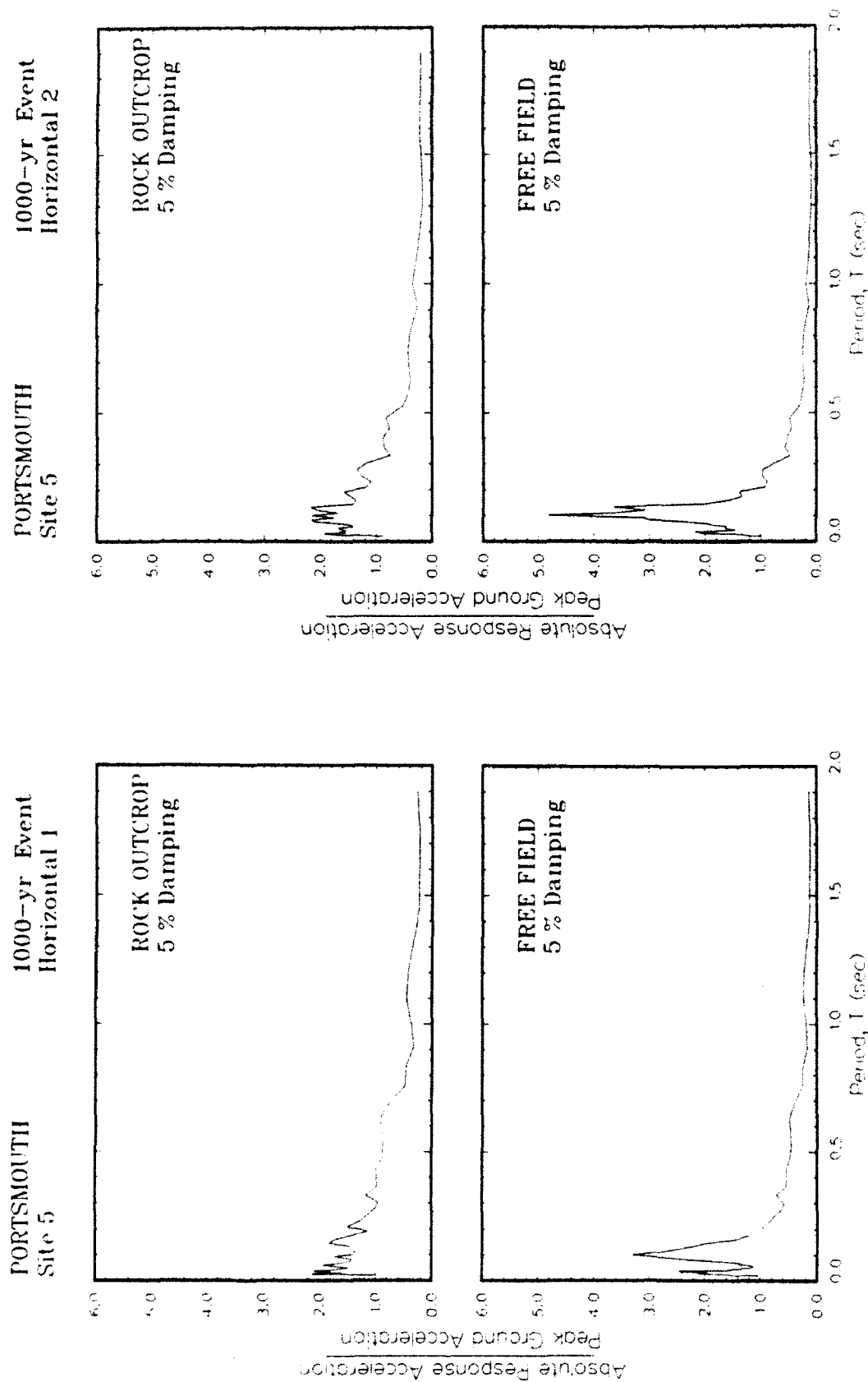


Figure M5. Ratio of amplification of absolute acceleration response spectra to peak acceleration at free field for Site 5

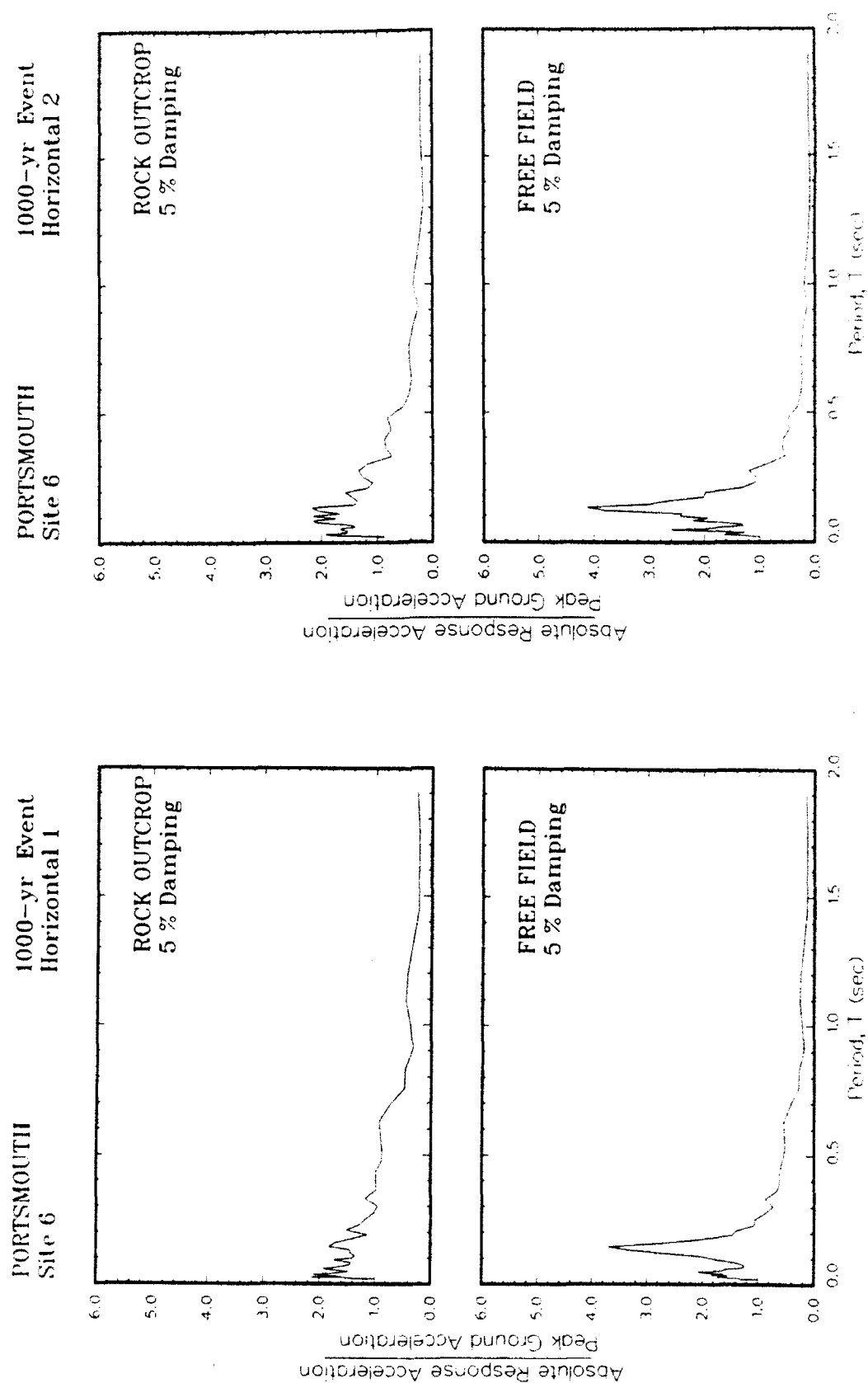


Figure M6. Ratio of amplification of absolute acceleration response spectra to peak acceleration at free field for Site 6

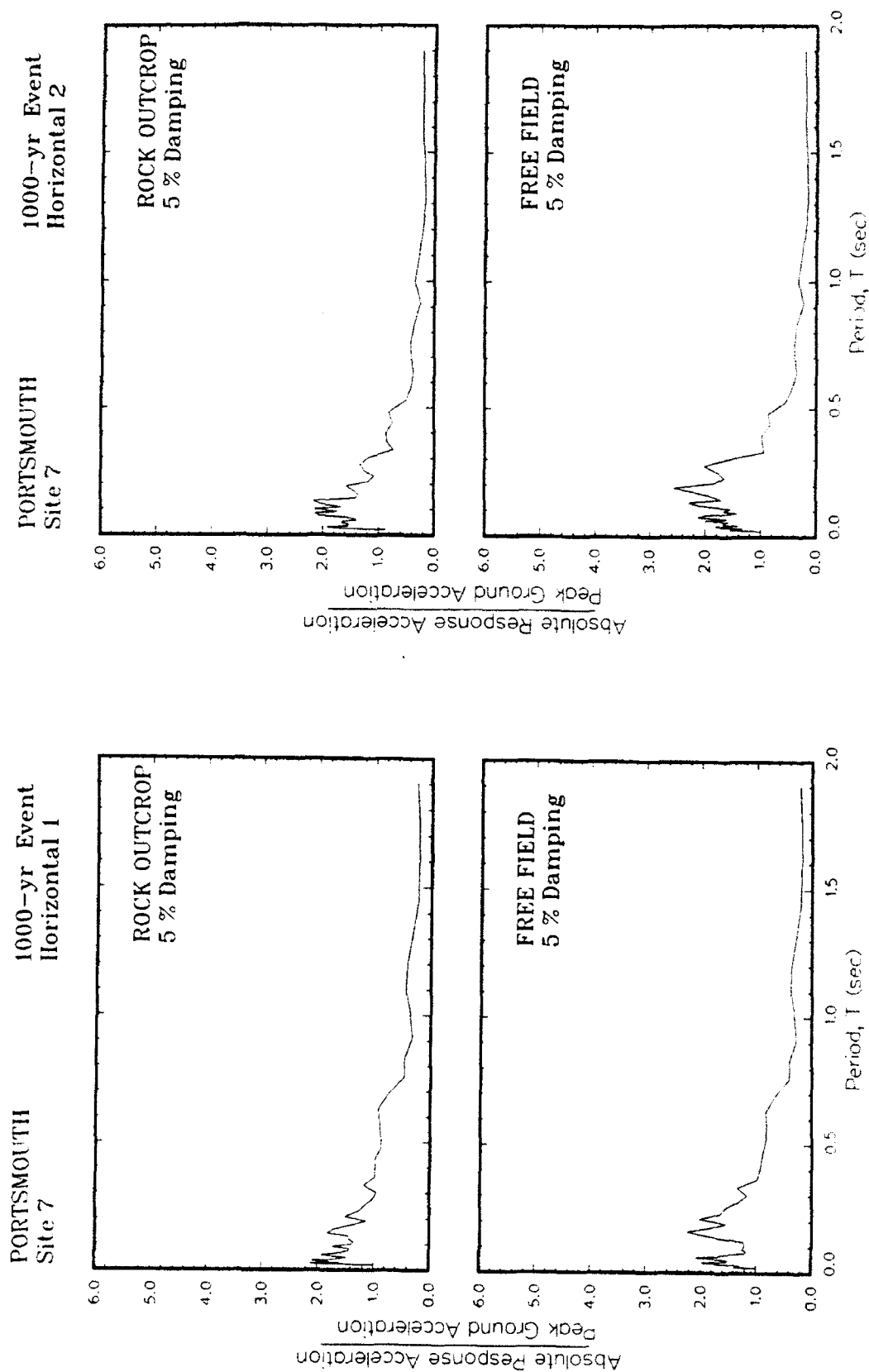


Figure M7. Ratio of amplification of absolute acceleration response spectra to peak acceleration at free field for Site 7

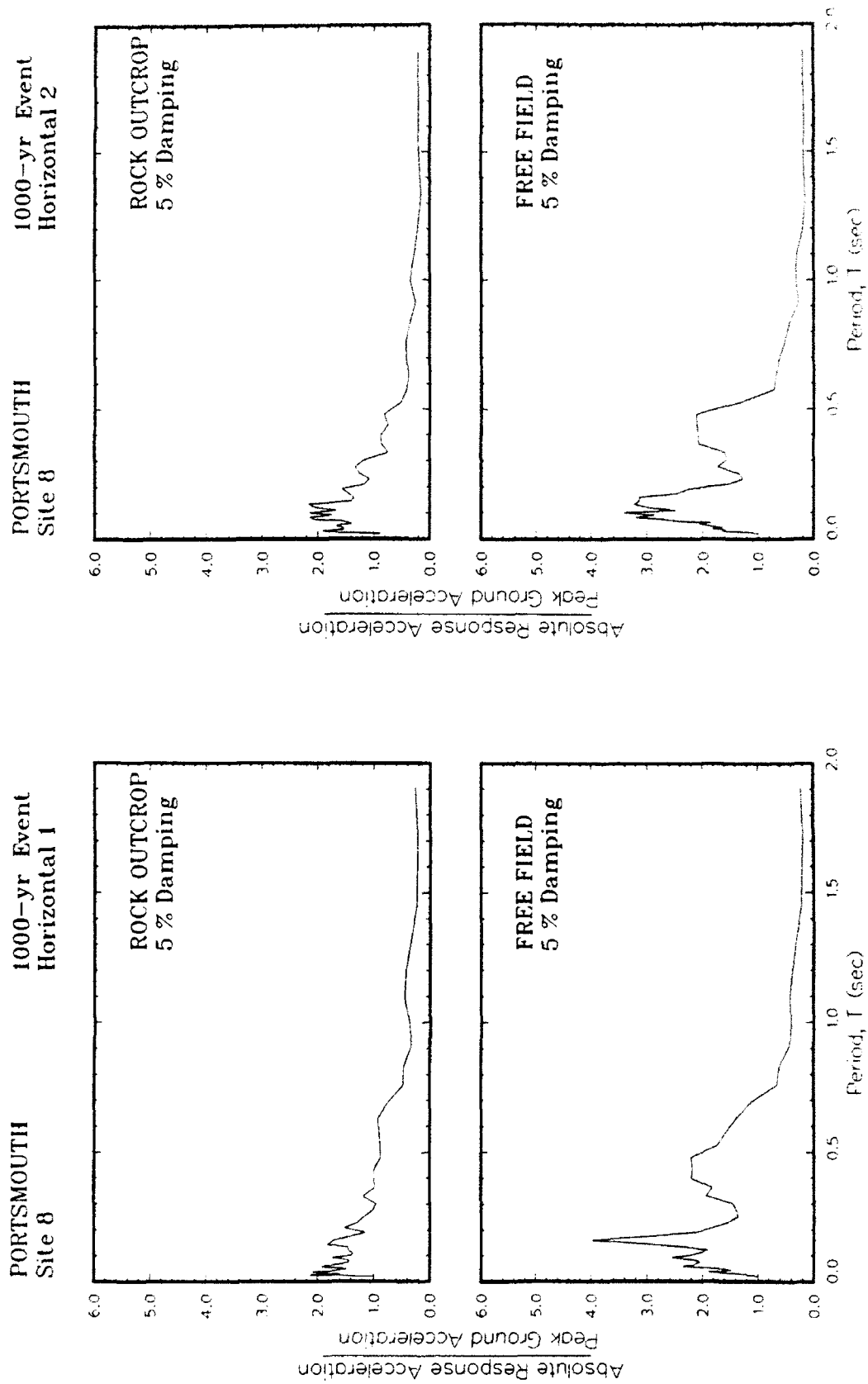


Figure M8. Ratio of amplification of absolute acceleration response spectra to peak acceleration at free field for Site 8

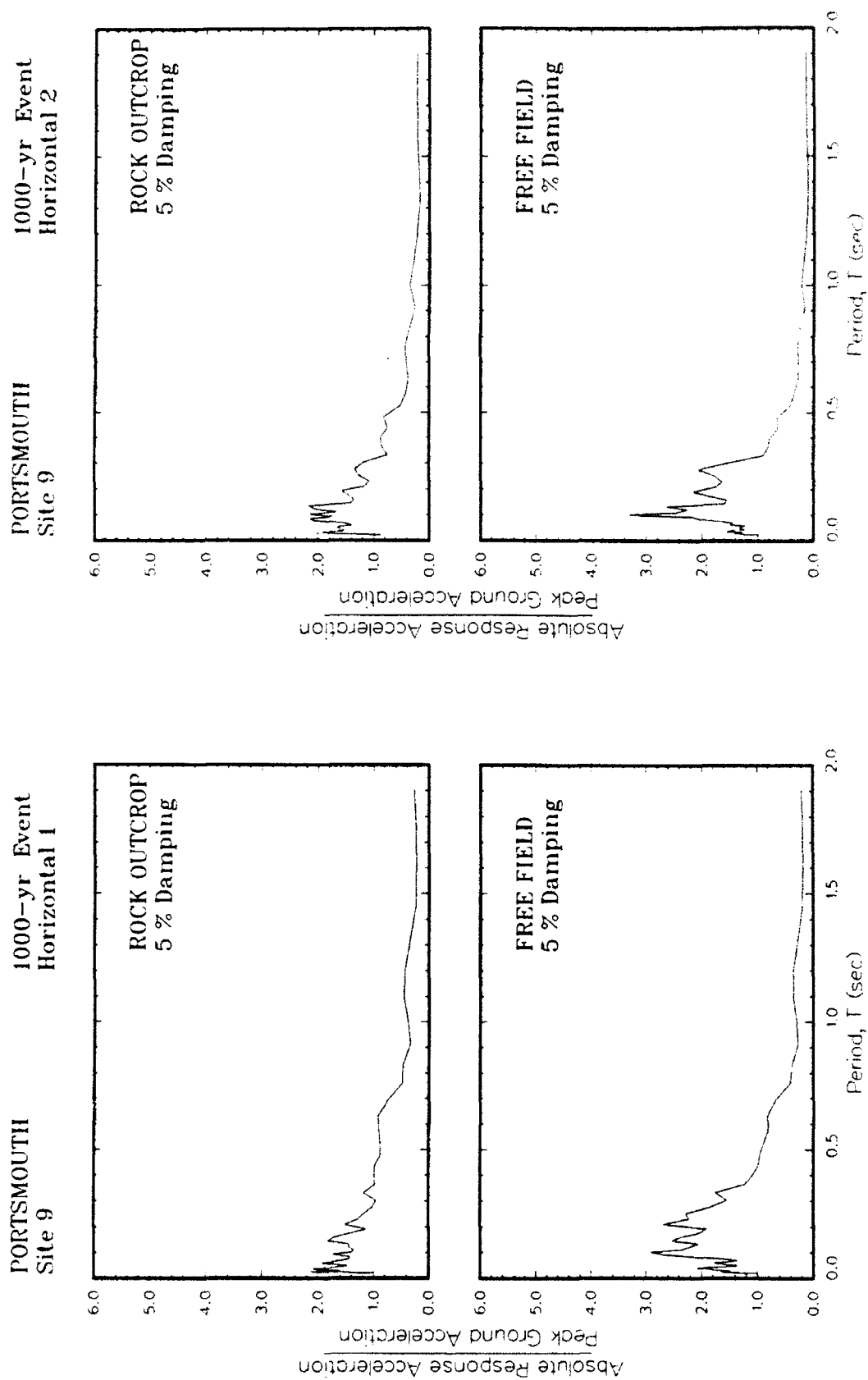


Figure M9. Ratio of amplification of absolute acceleration response spectra to peak acceleration at free field for Site 9

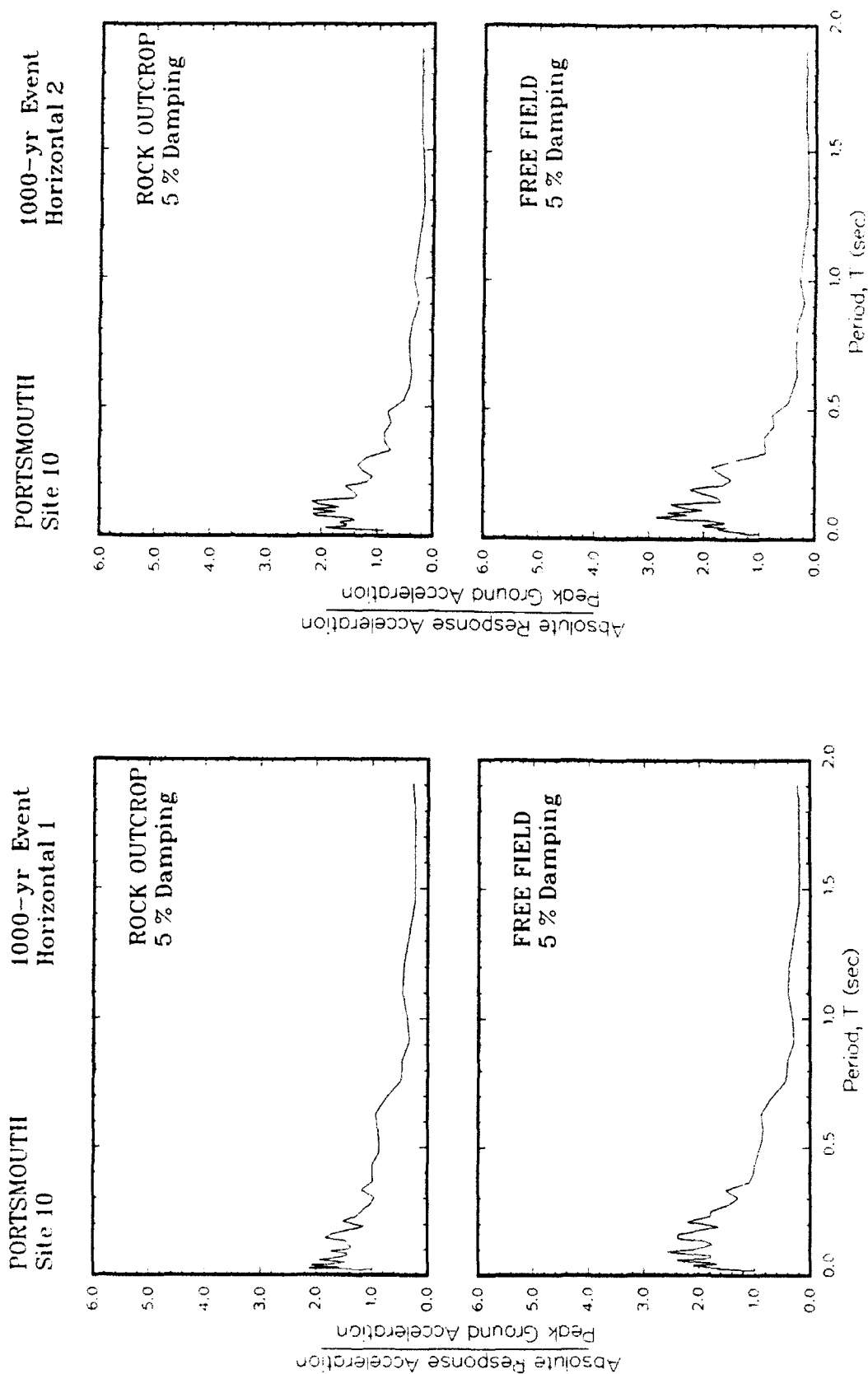


Figure M10. Ratio of amplification of absolute acceleration response spectra to peak acceleration at free field for Site 10

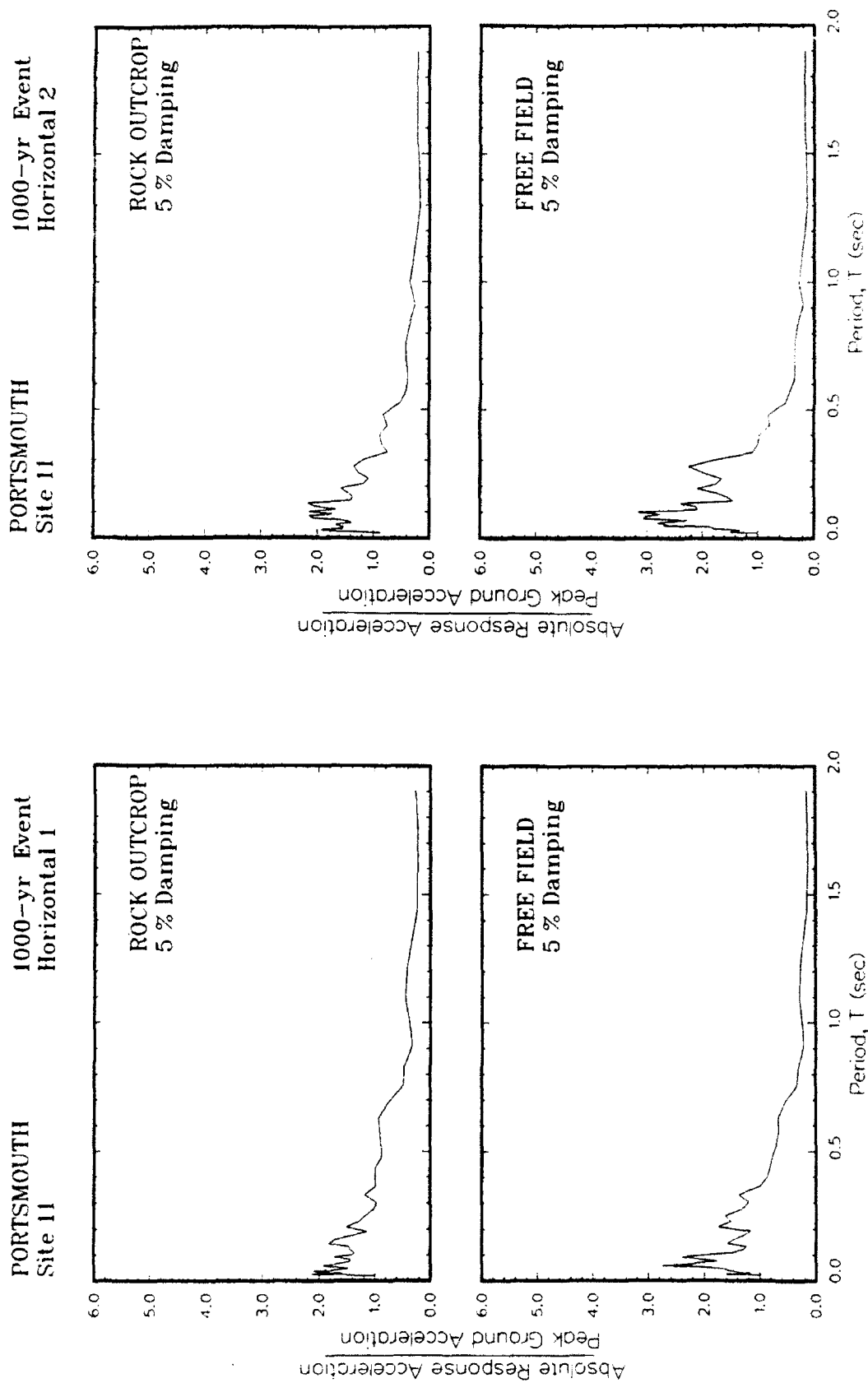


Figure M11. Ratio of amplification of absolute acceleration response spectra to peak acceleration at free field for Site 11

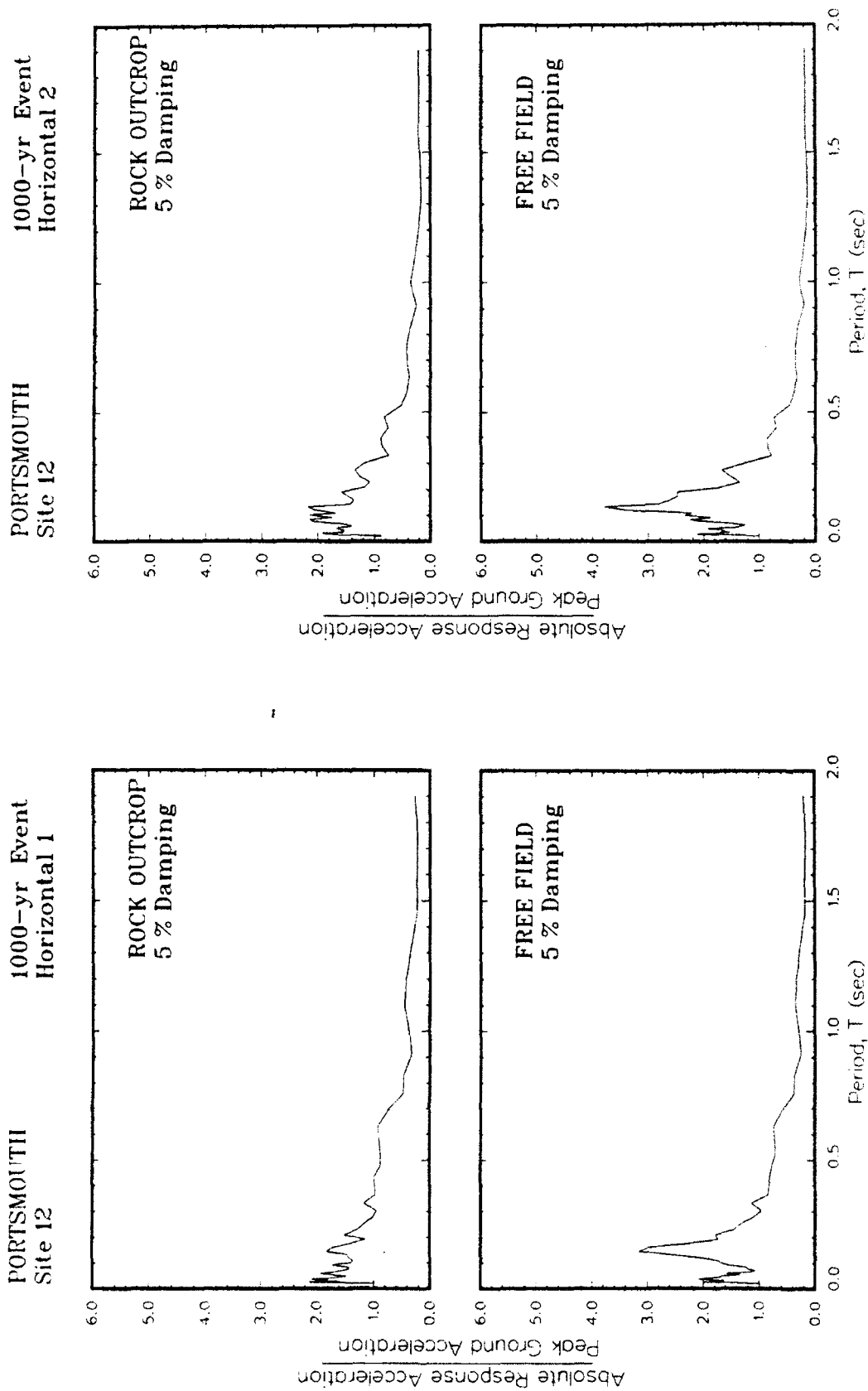


Figure M12. Ratio of amplification of absolute acceleration response spectra to peak acceleration at free field for Site 12

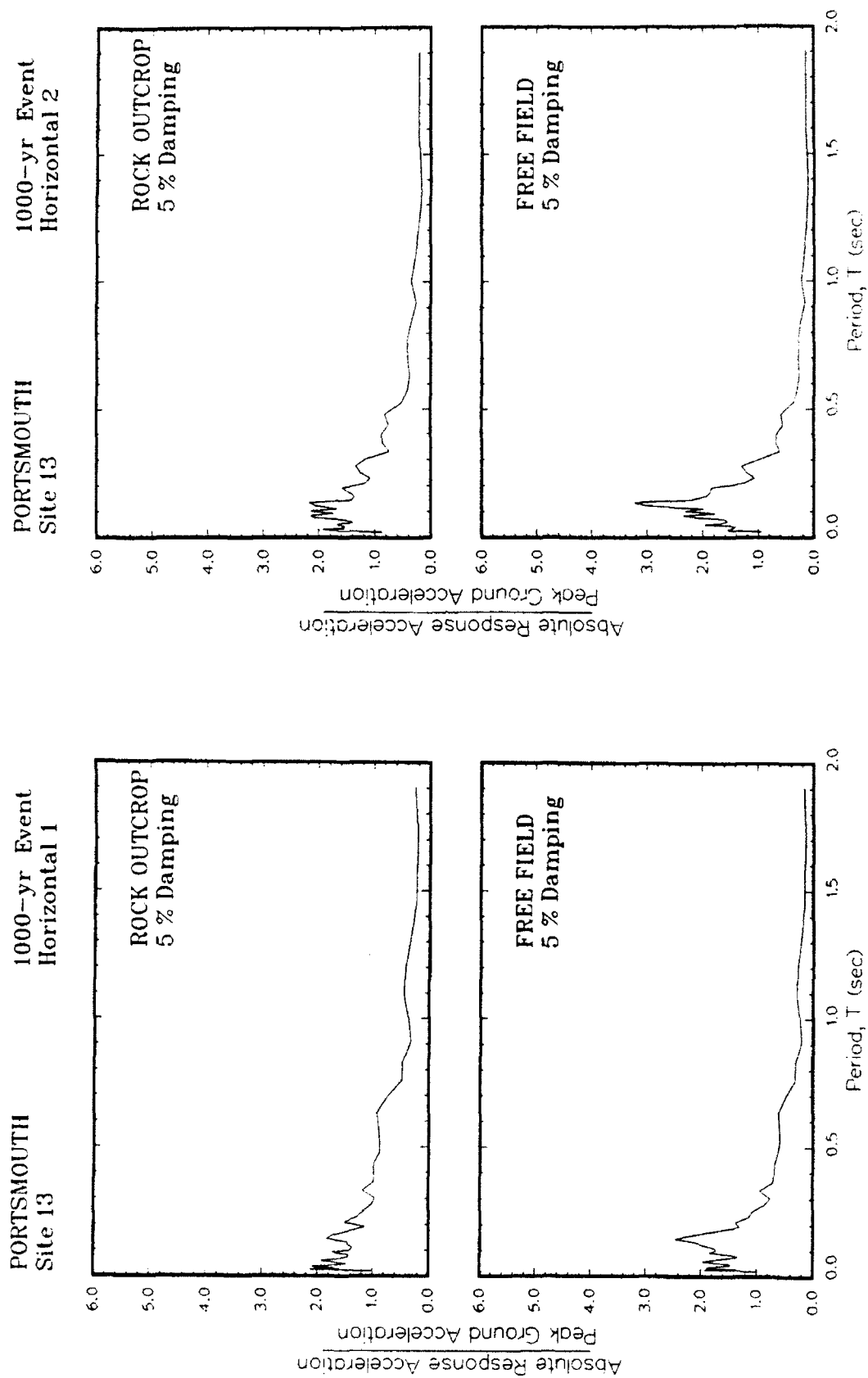


Figure M13. Ratio of amplification of absolute acceleration response spectra to peak acceleration at free field for Site 13

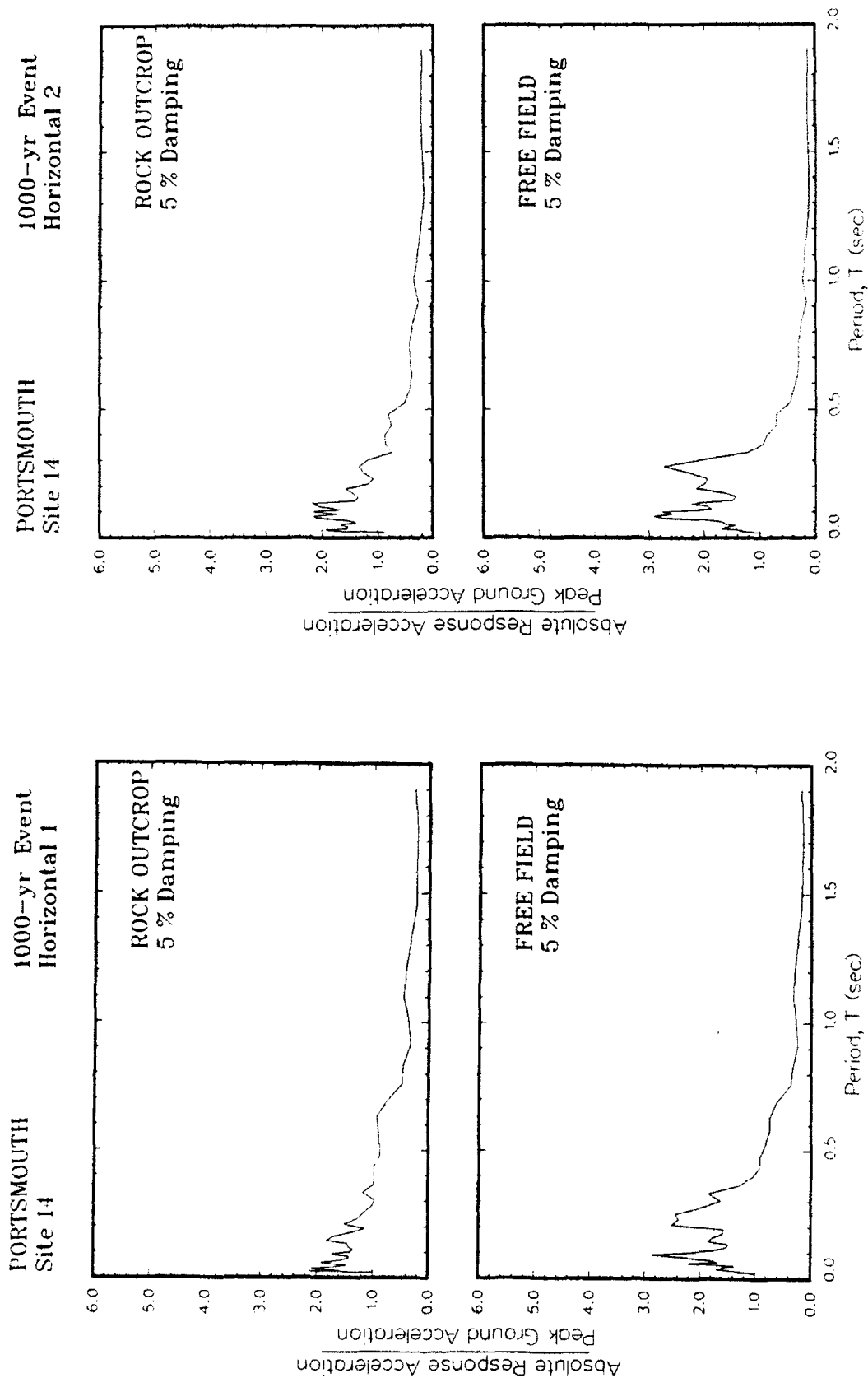


Figure M14. Ratio of amplification of absolute acceleration response spectra to peak acceleration at free field for Site 14

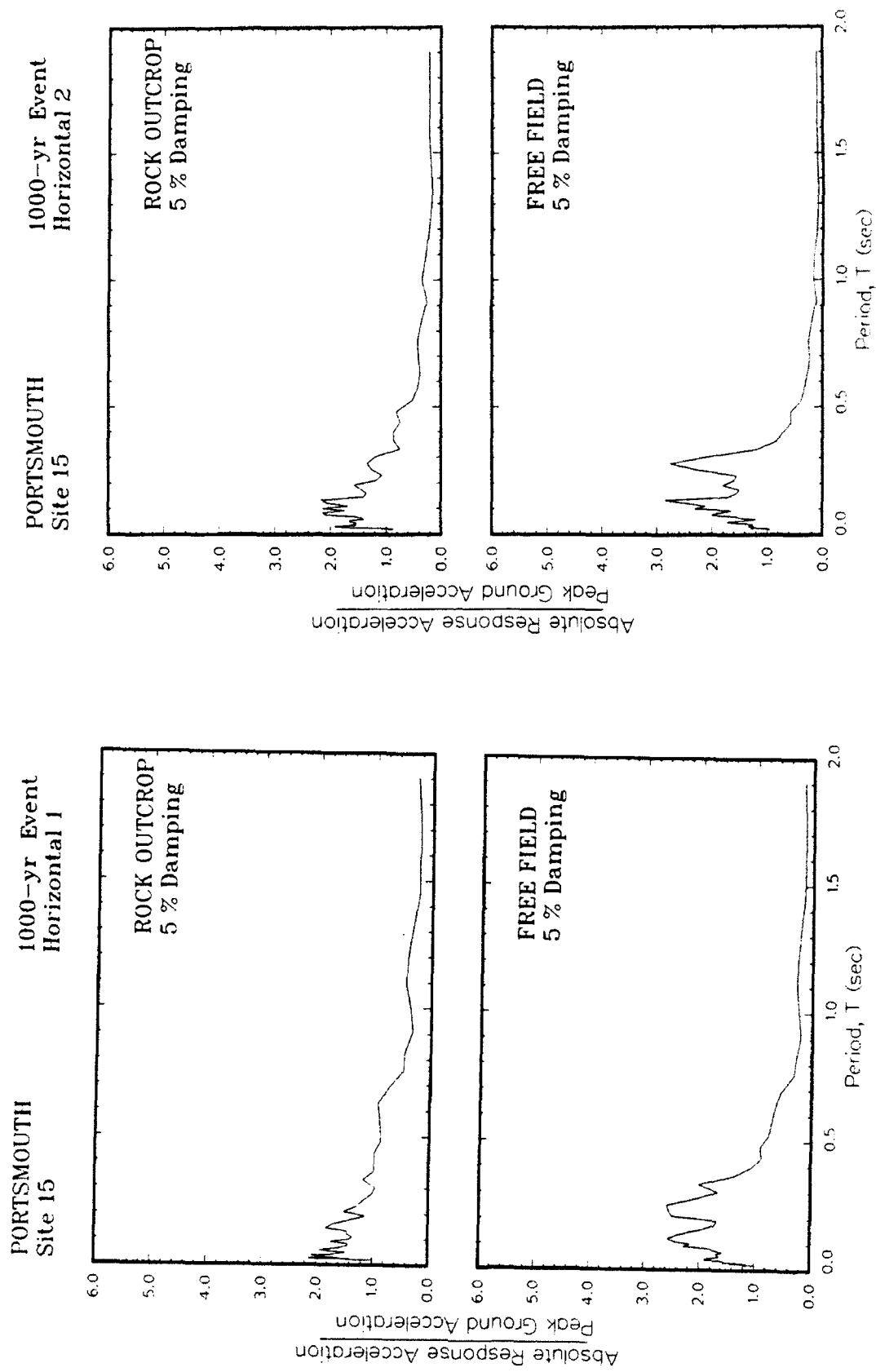


Figure M15. Ratio of amplification of absolute acceleration response spectra to peak acceleration at free field for Site 15

APPENDIX N: ACCELERATION-TIME RECORDS FOR 5000-YEAR EVENT

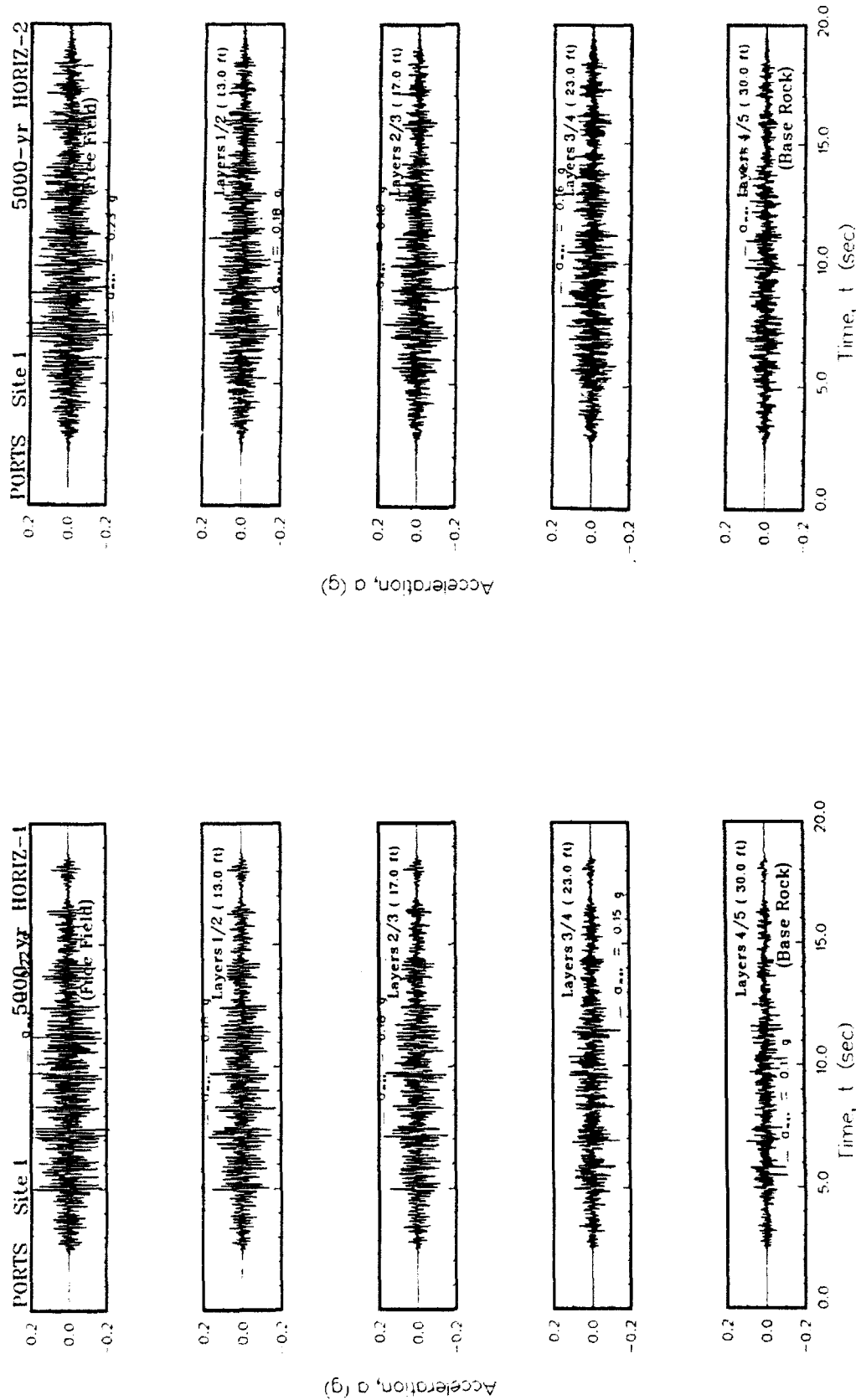


Figure N1. Variation of acceleration with time at the top of each layer for Site 1

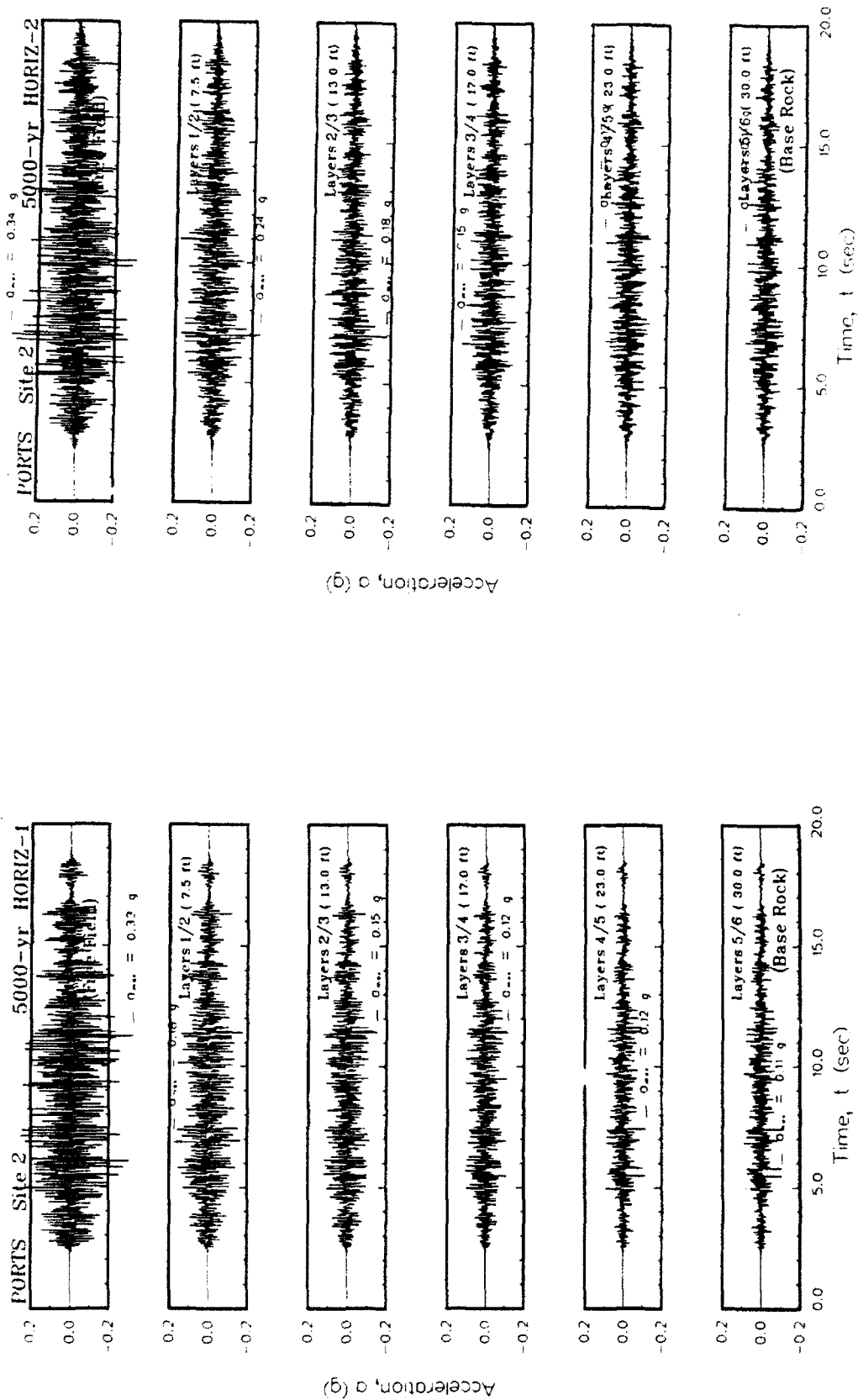


Figure N2. Variation of acceleration with time at the top of each layer for Site 2

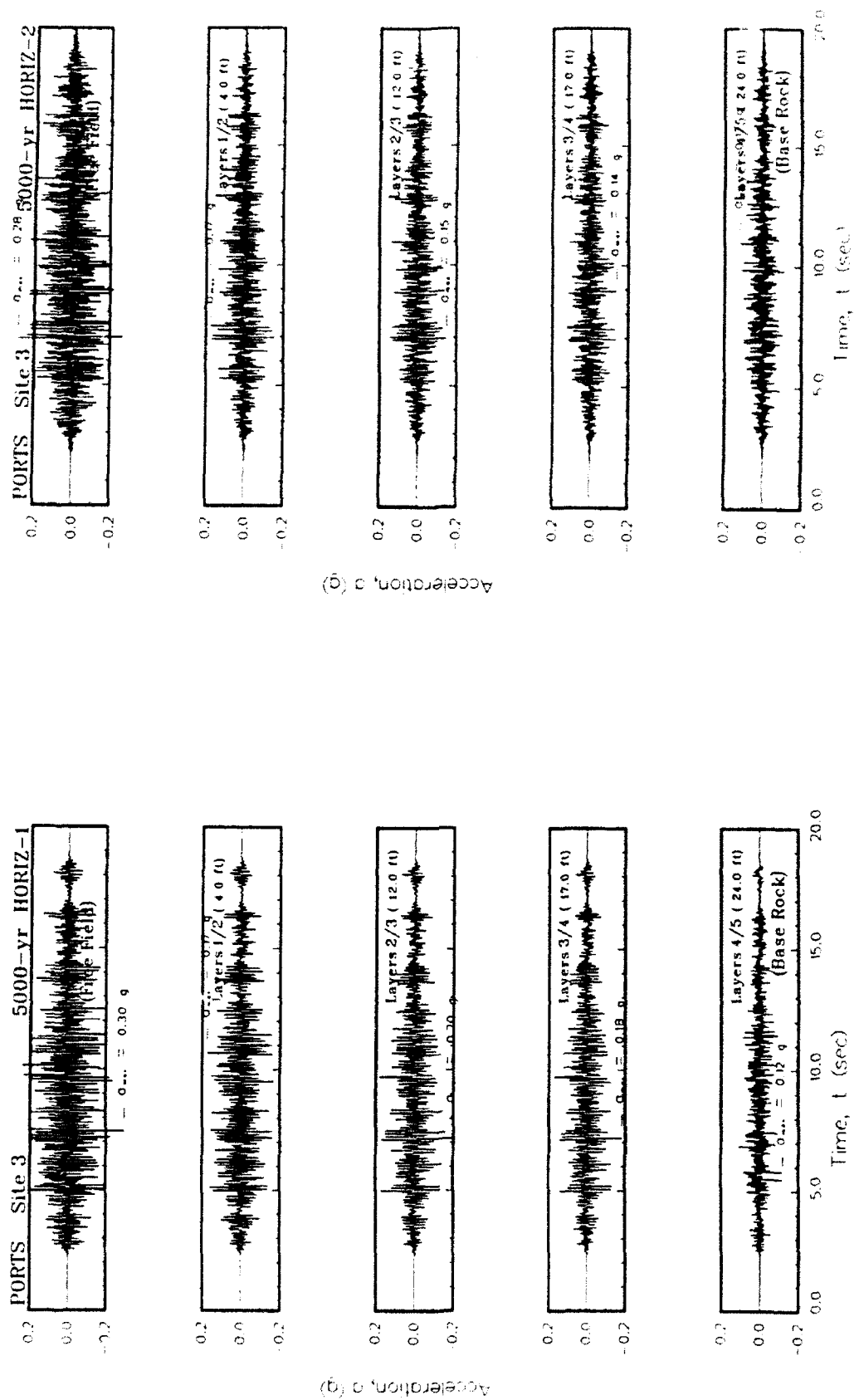


Figure N3. Variation of acceleration with time at the top of each layer for Site 3

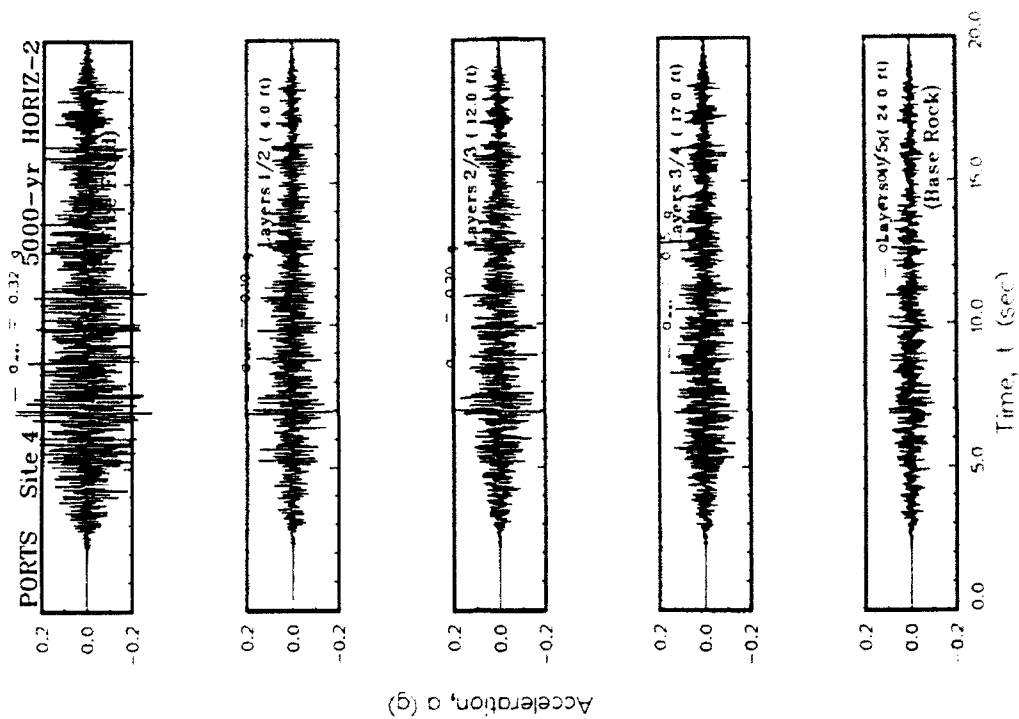
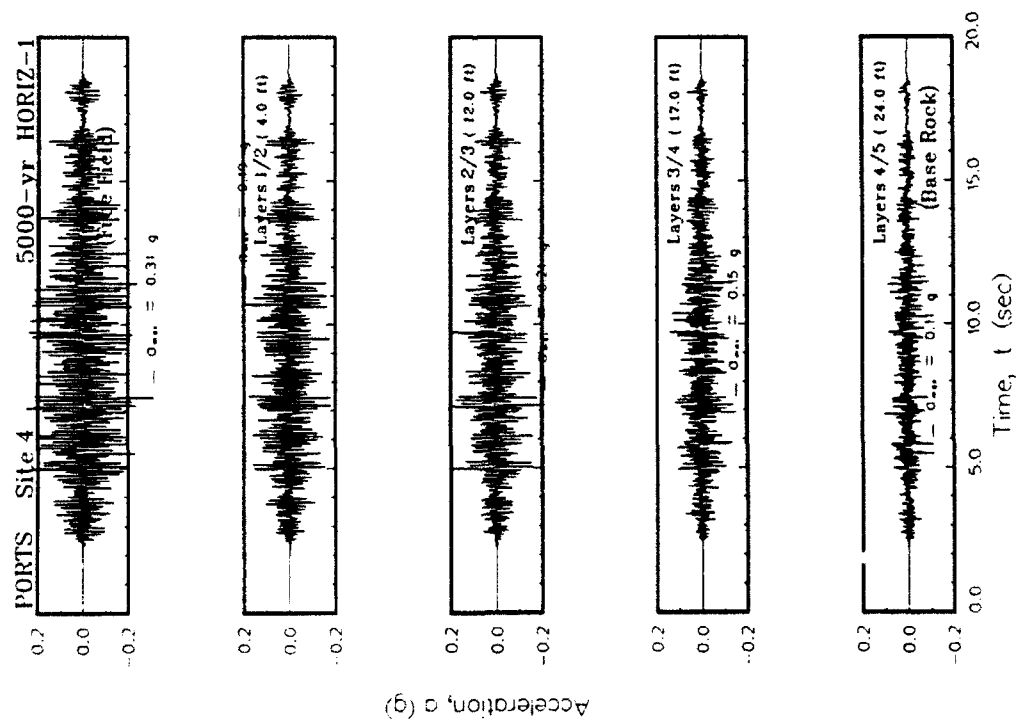


Figure N4. Variation of acceleration with time at the top of each layer for Site 4

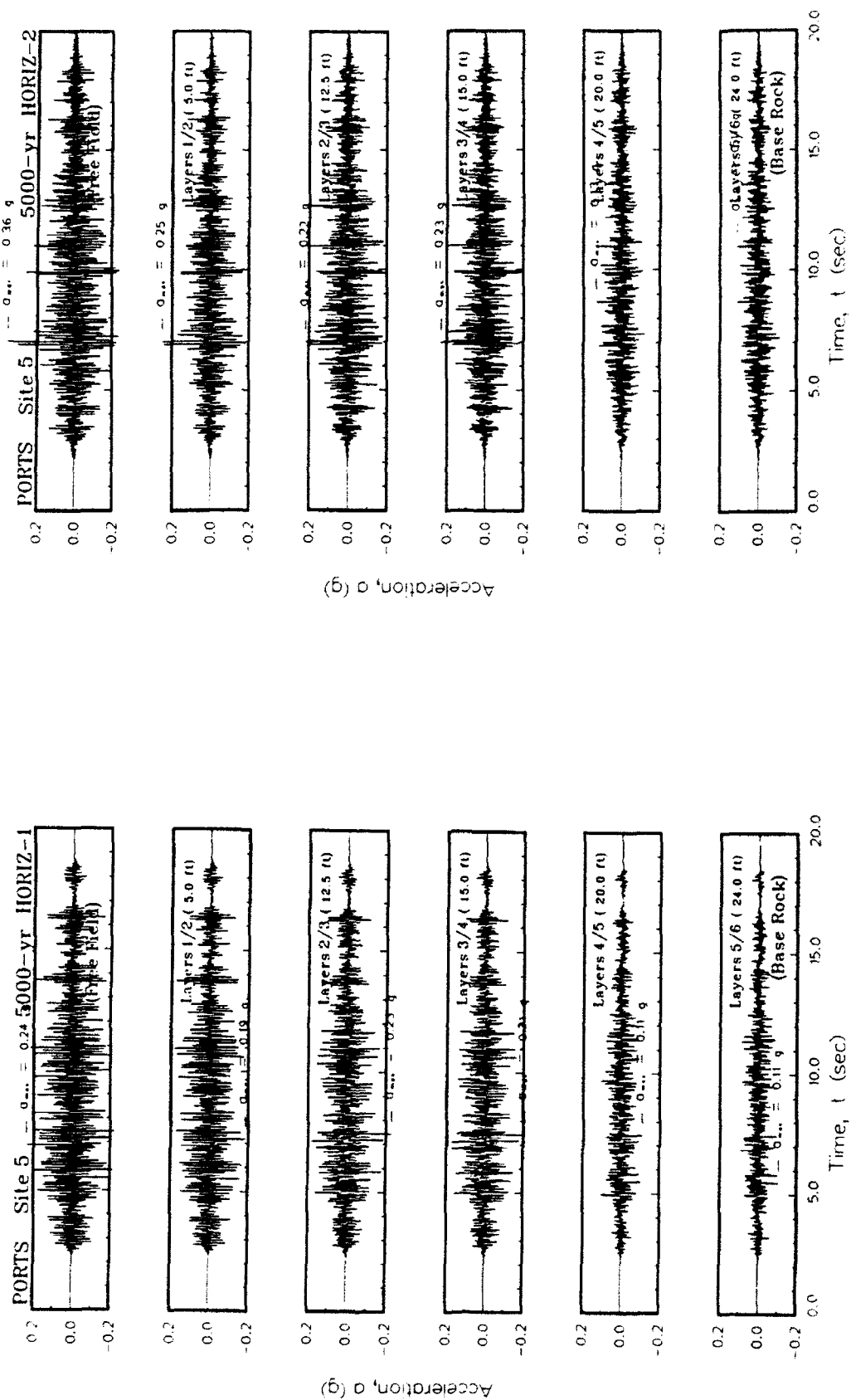


Figure N5. Variation of acceleration with time at the top of each layer for Site 5

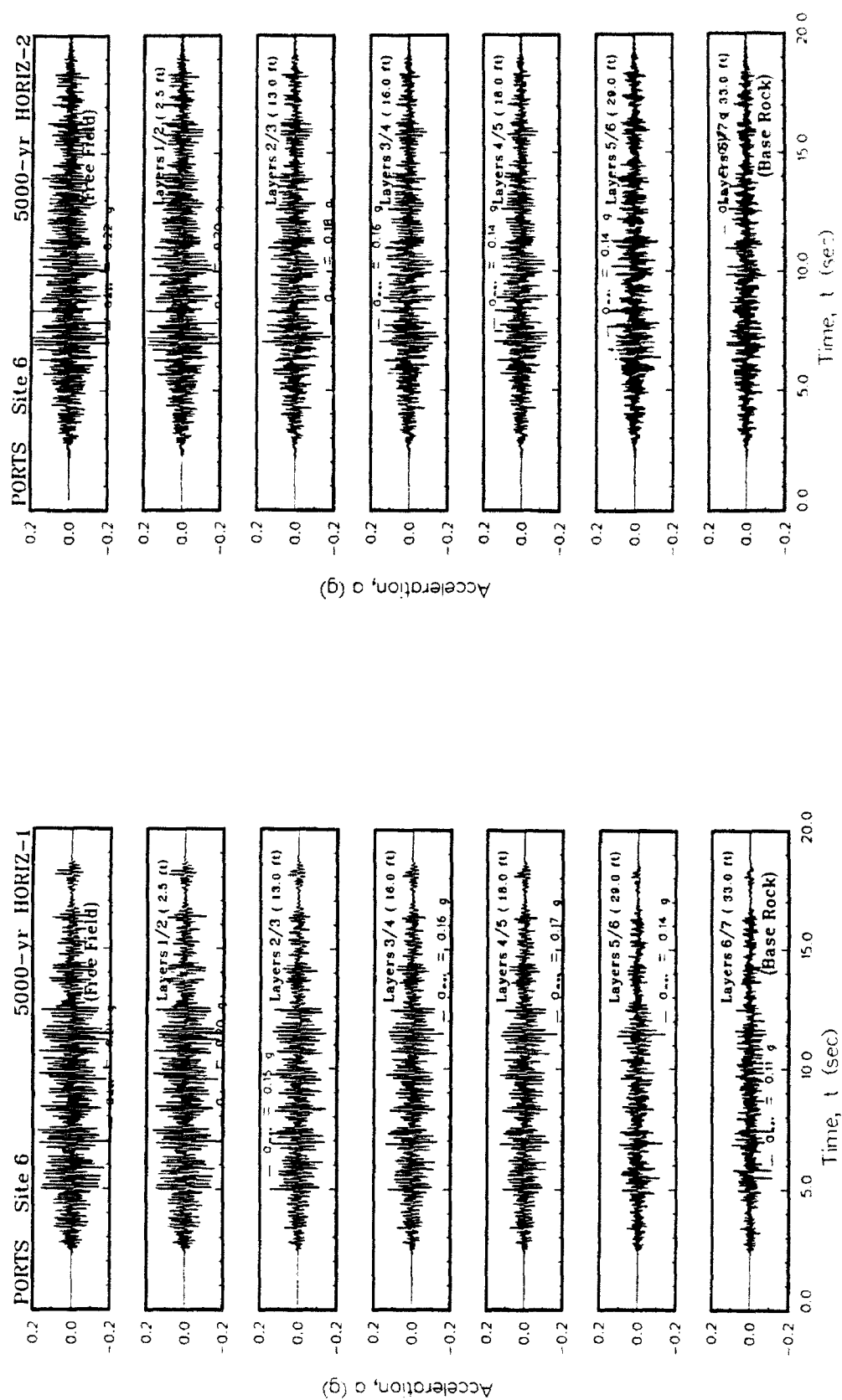


Figure N6. Variation of acceleration with time at the top of each layer for Site 6

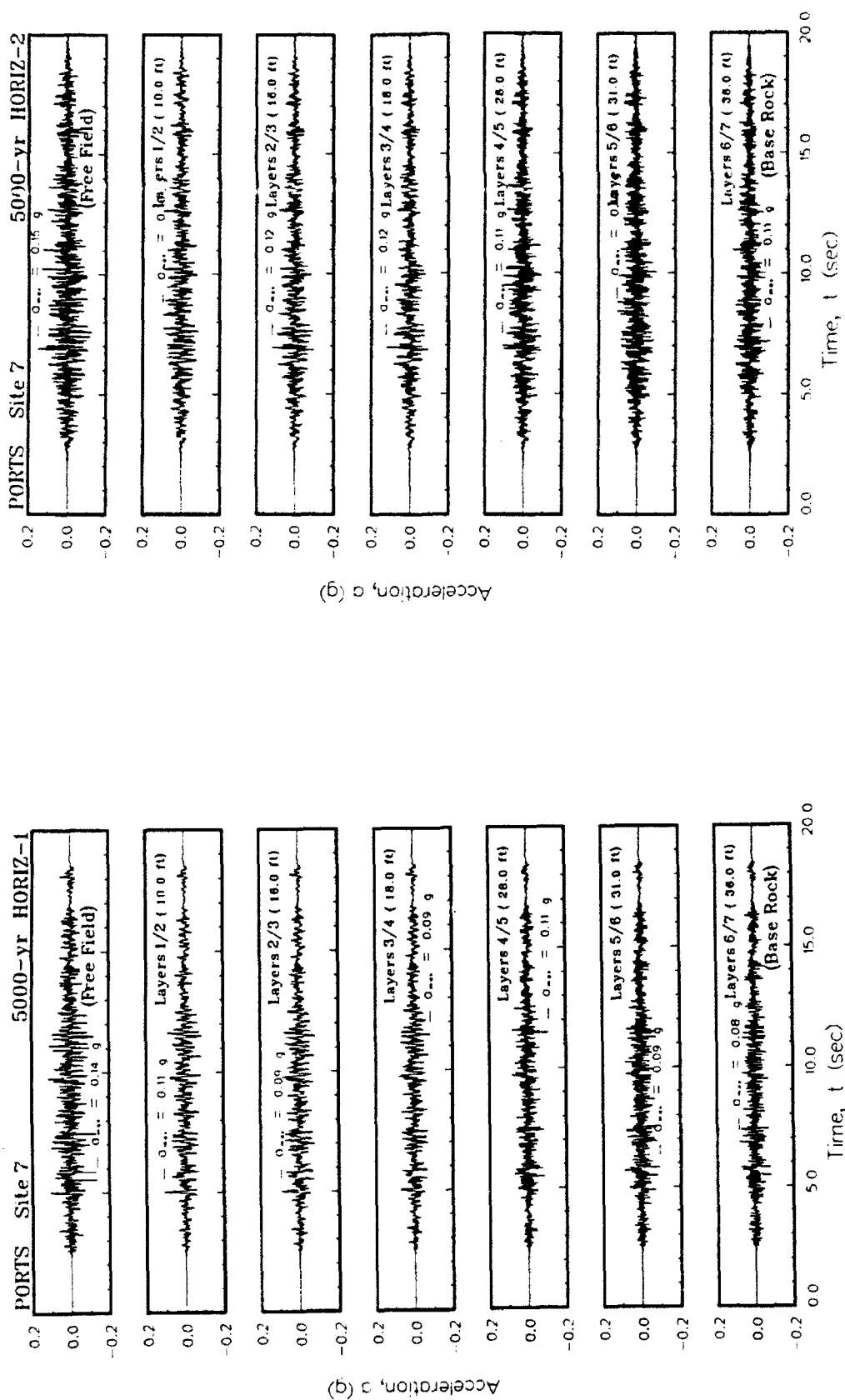


Figure N7. Variation of acceleration with time at the top of each layer for Site 7

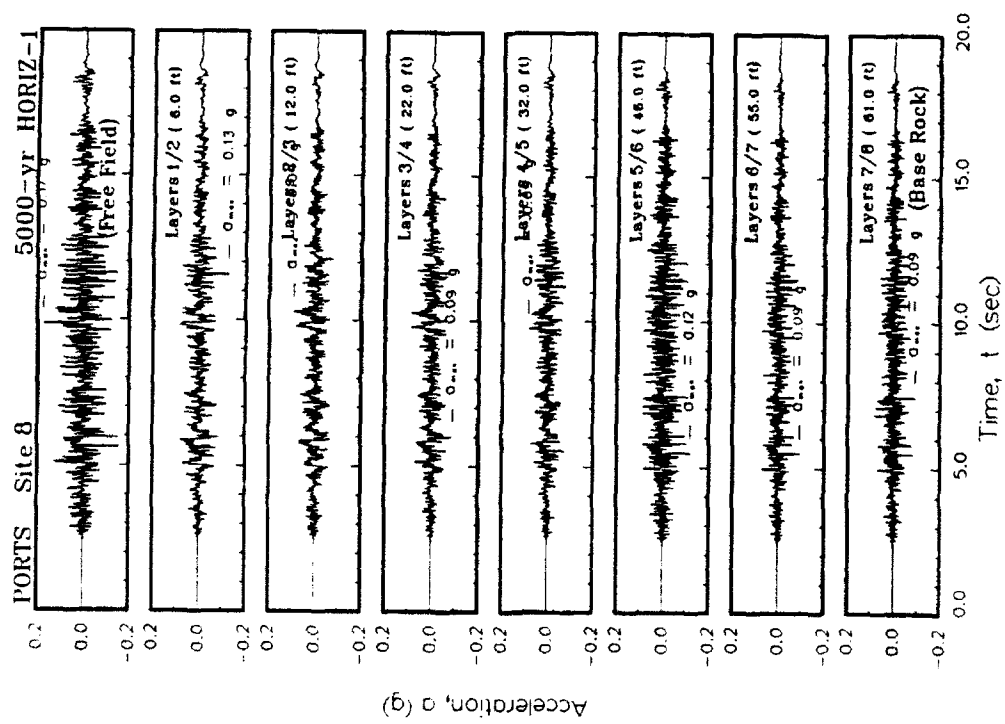
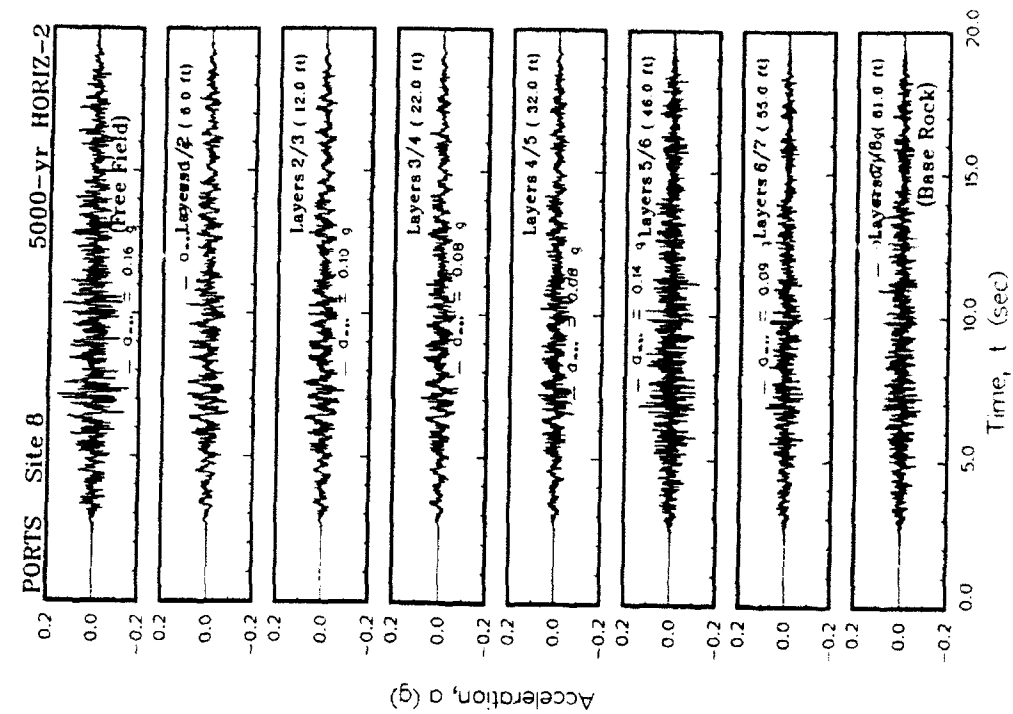


Figure N8. Variation of acceleration with time at the top of each layer for Site 8

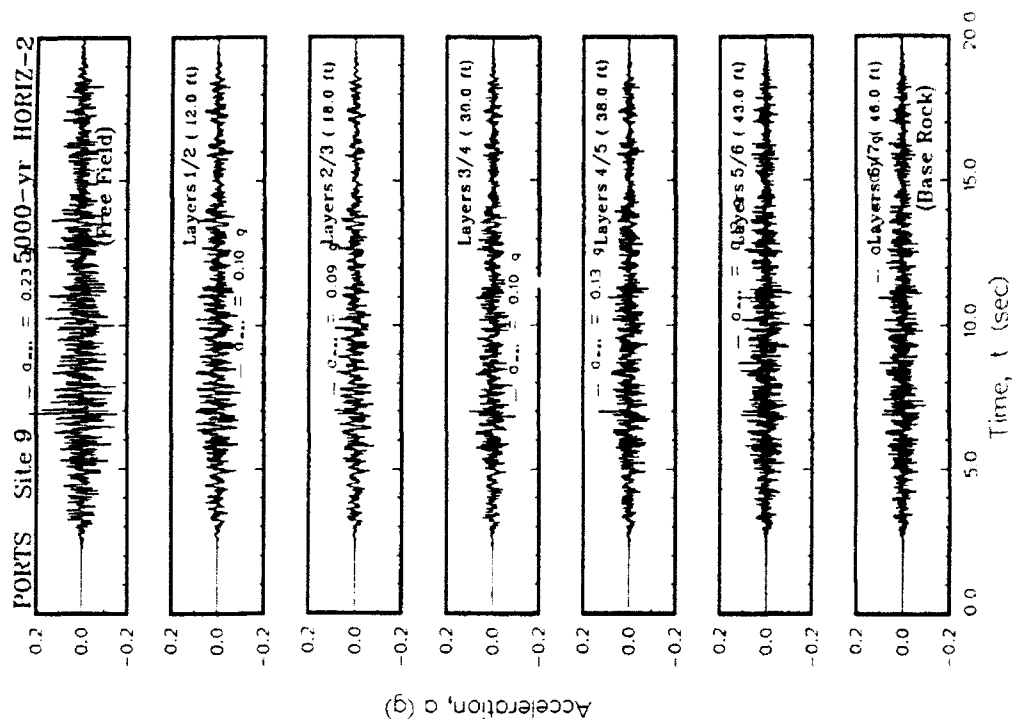
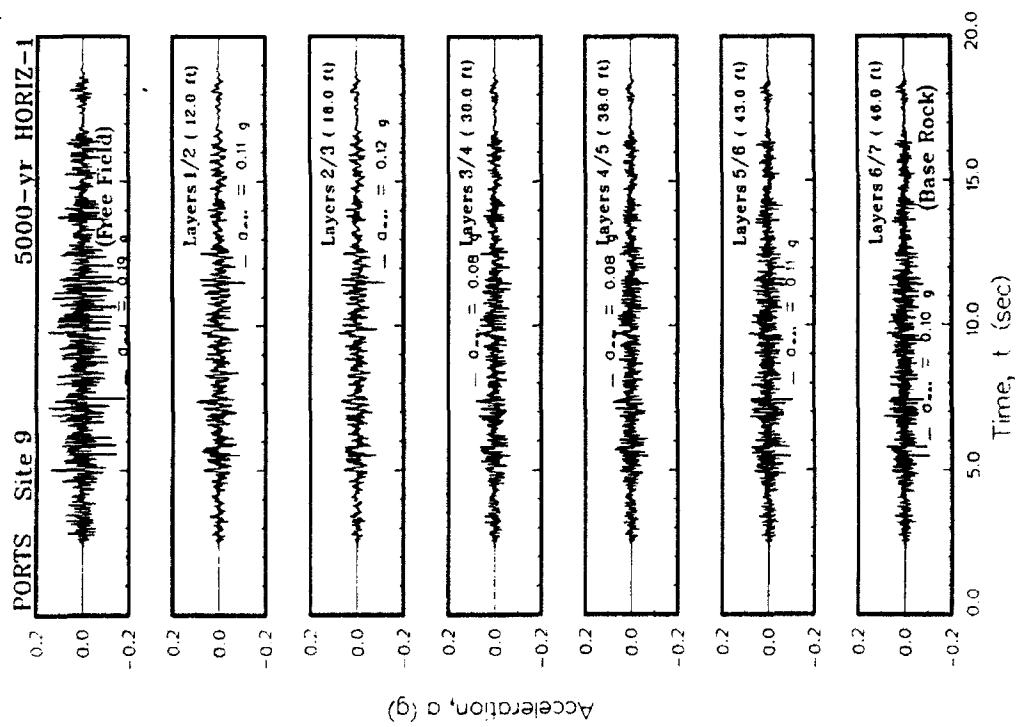


Figure N9. Variation of acceleration with time at the top of each layer for Site 9

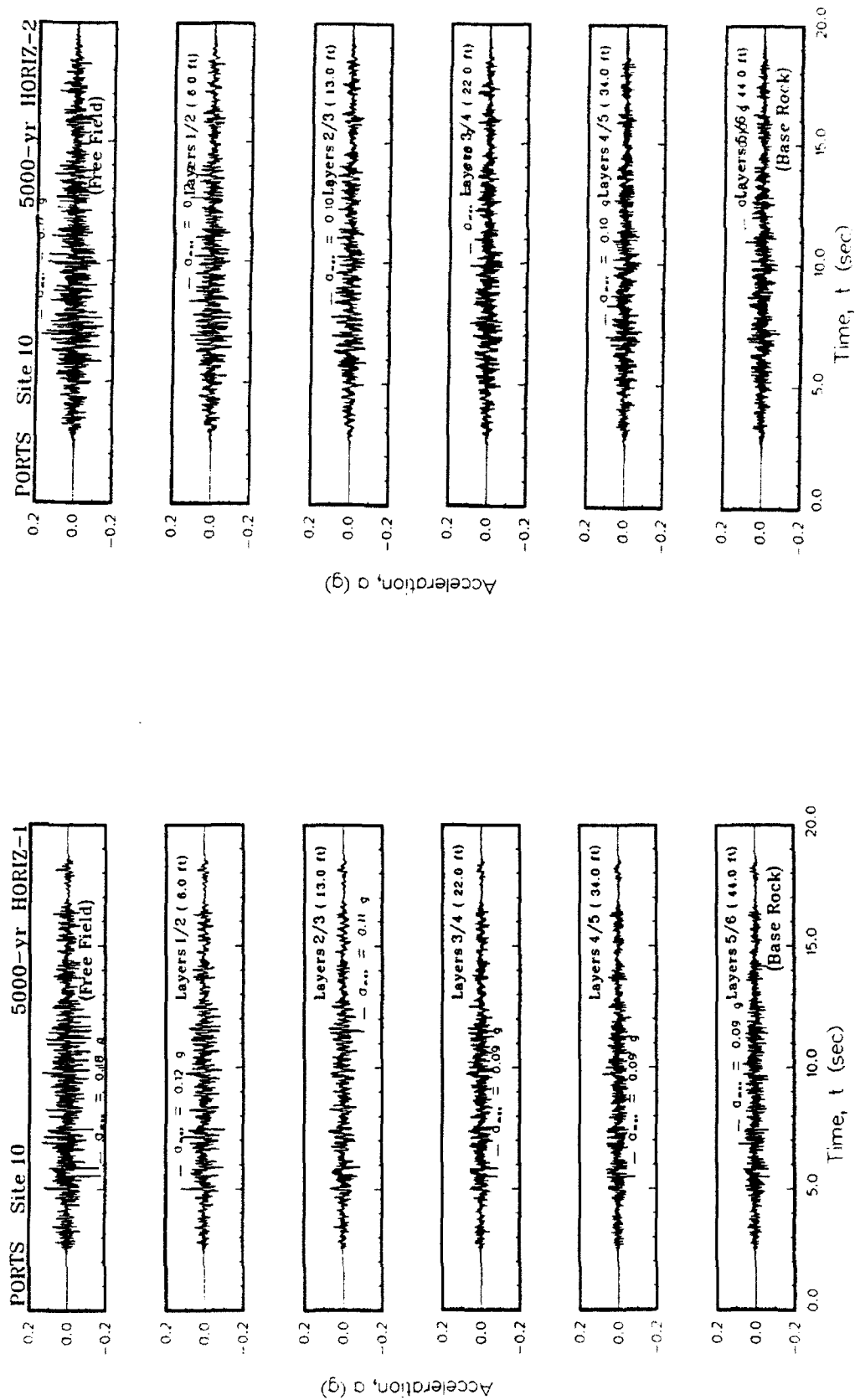


Figure N10. Variation of acceleration with time at the top of each layer for Site 10

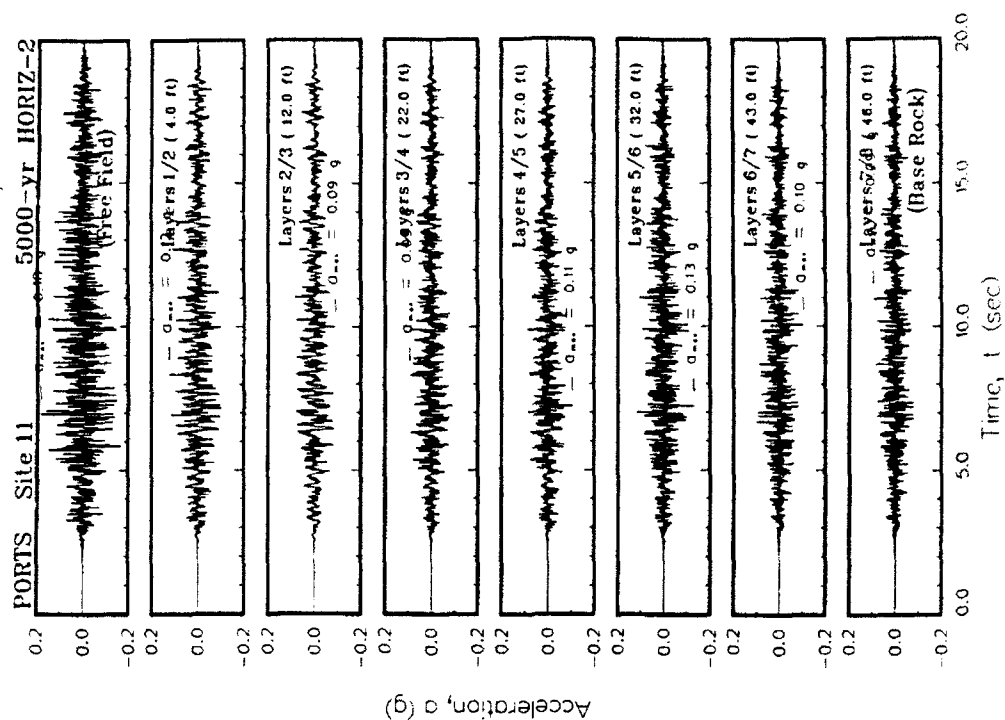
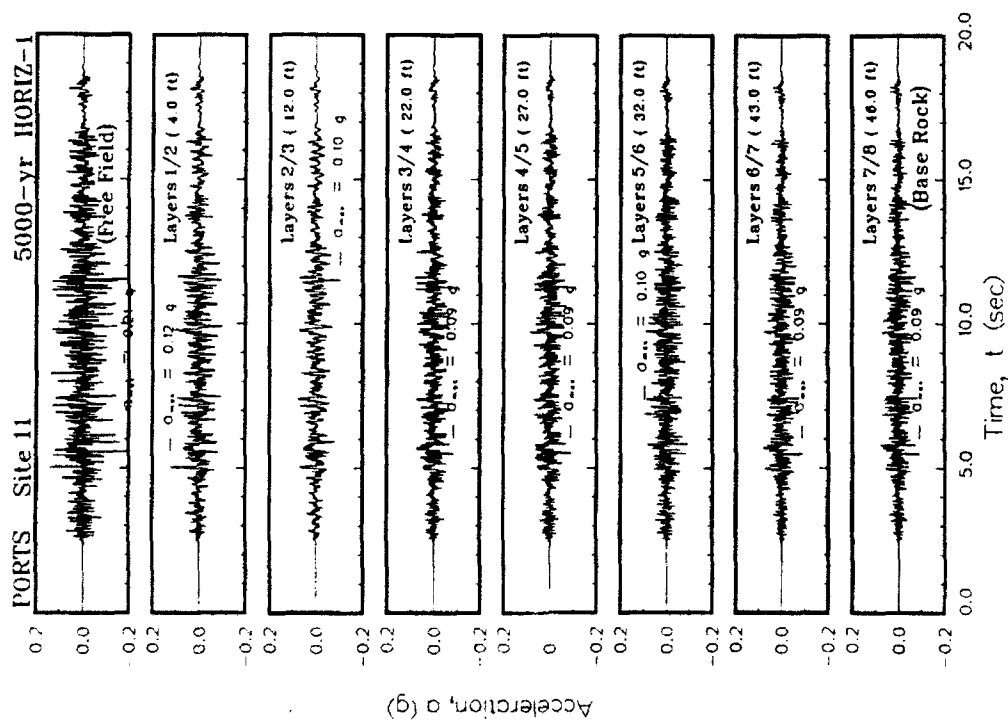


Figure N11. Variation of acceleration with time at the top of each layer for Site 11

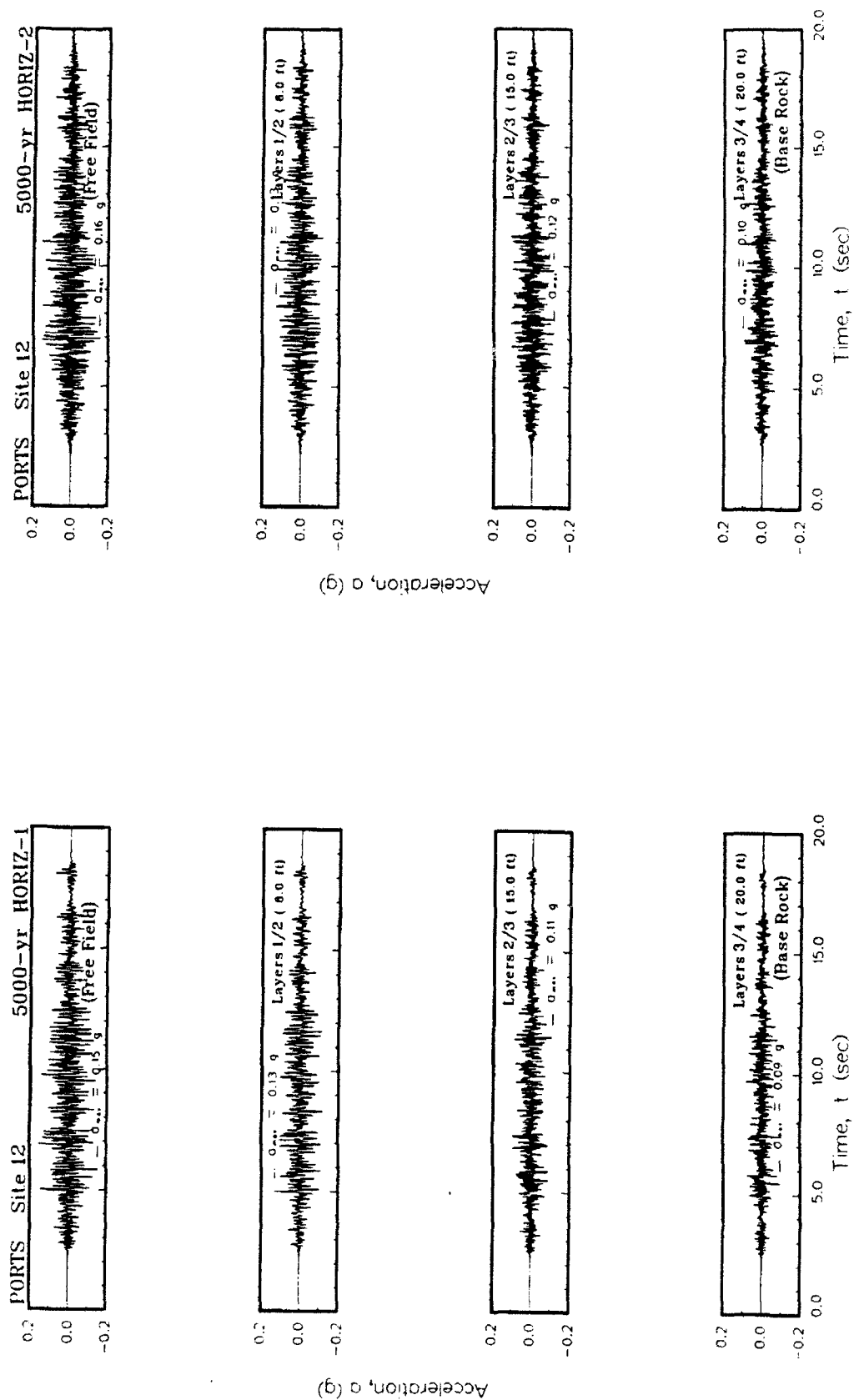


Figure N12. Variation of acceleration with time at the top of each layer for Site 12

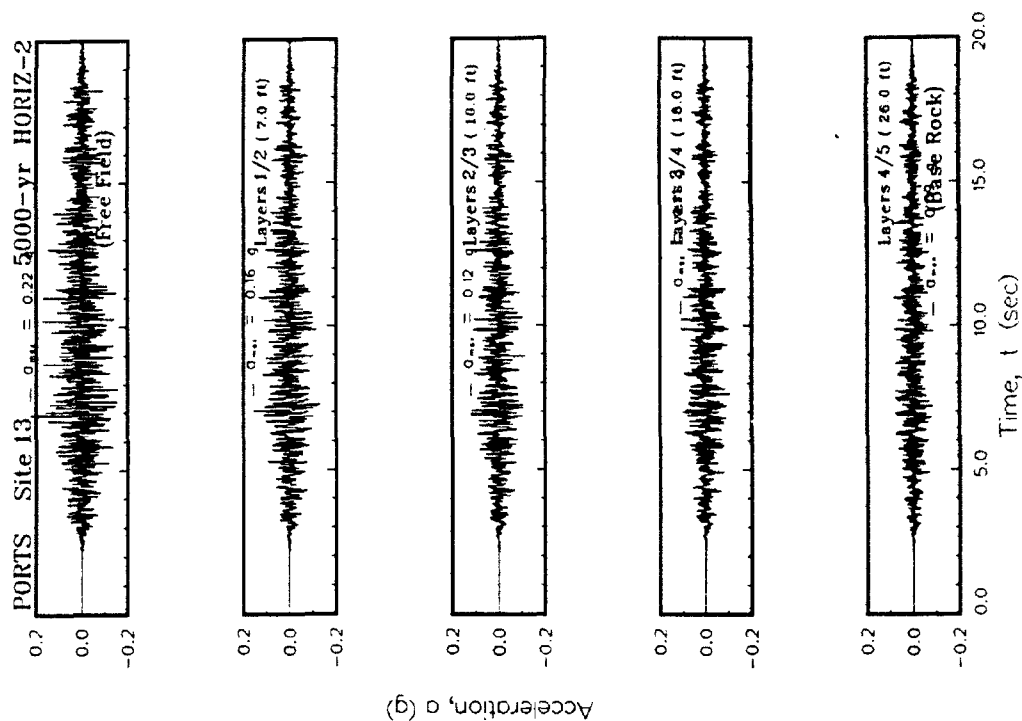
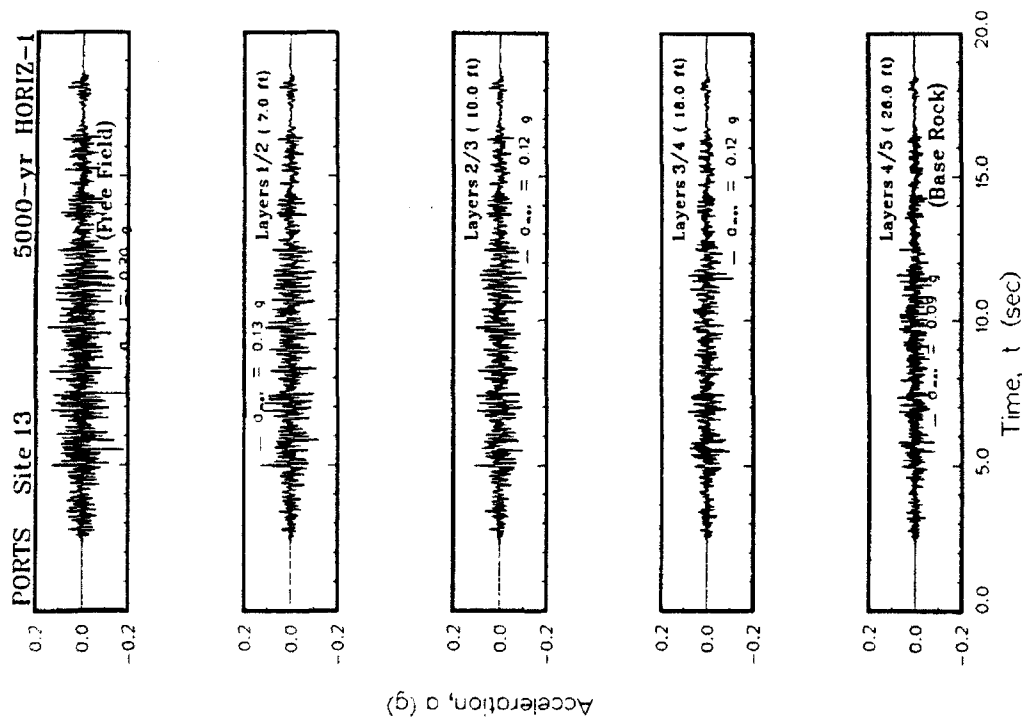


Figure N13. Variation of acceleration with time at the top of each layer for Site 13

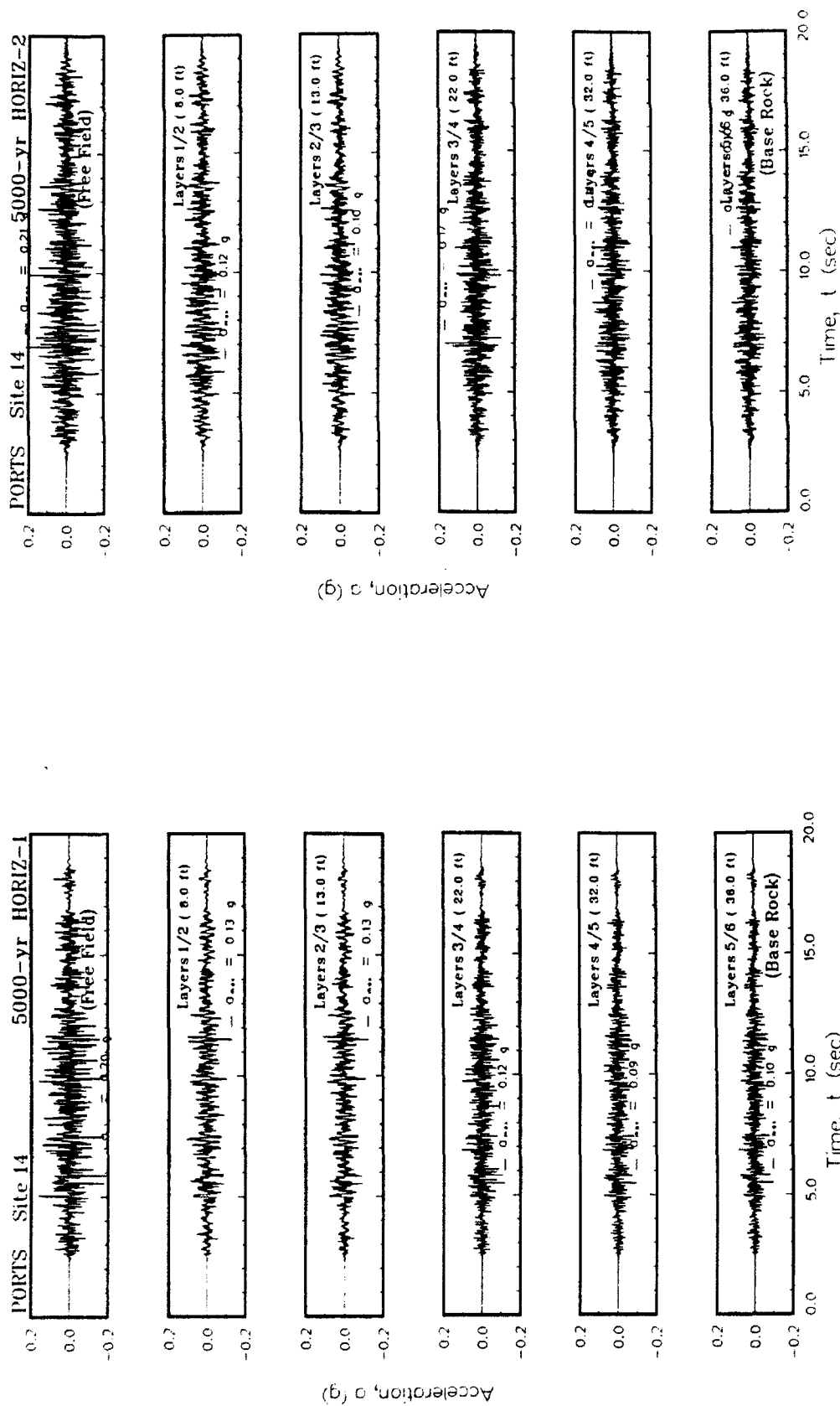


Figure N14. Variation of acceleration with time at the top of each layer for Site 14

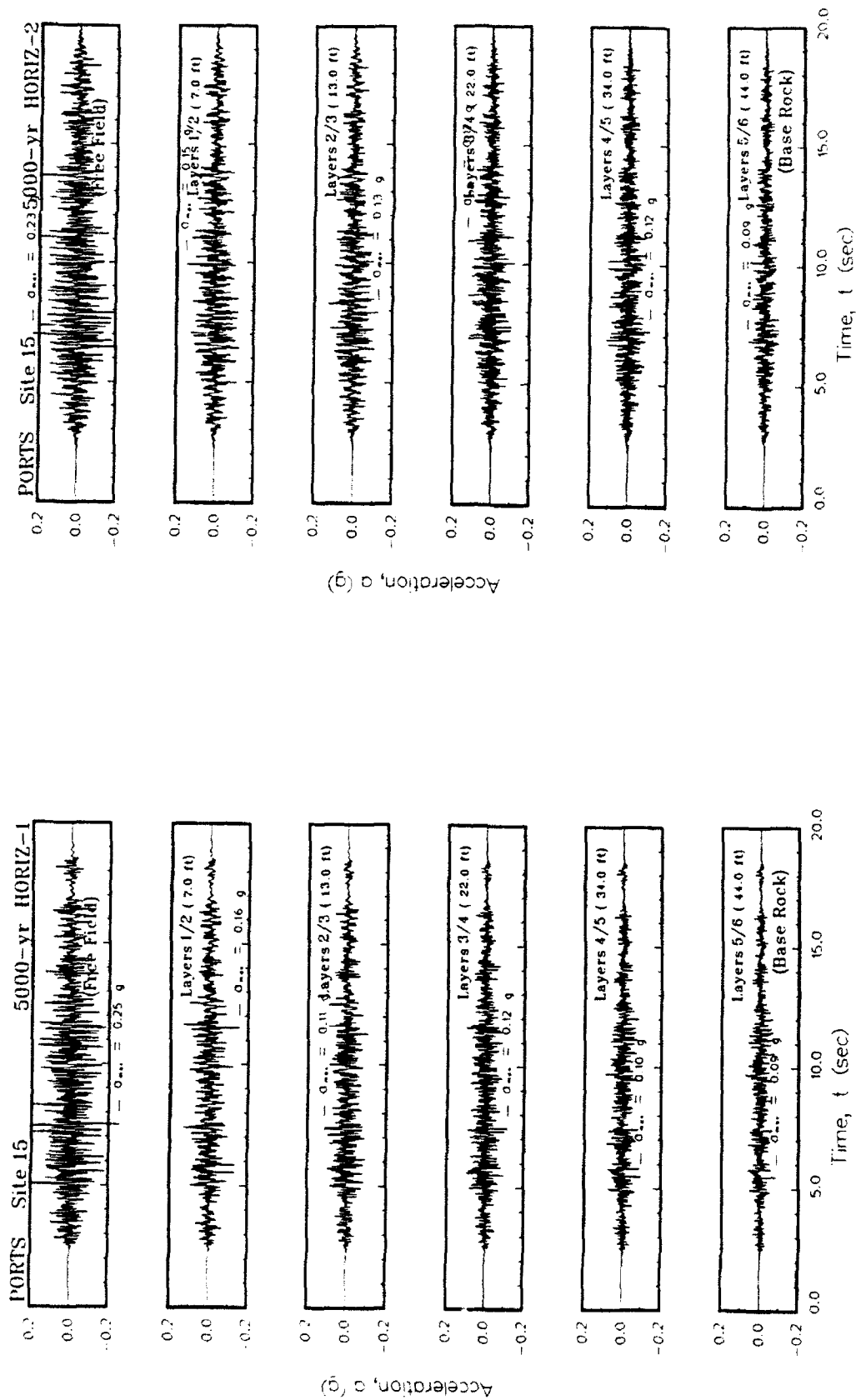
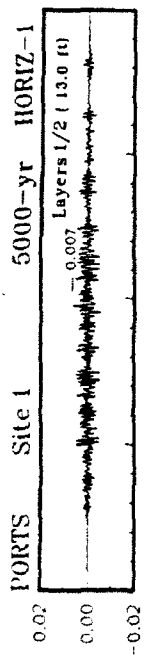
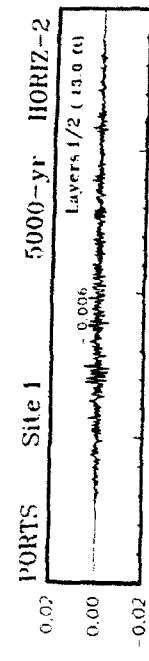
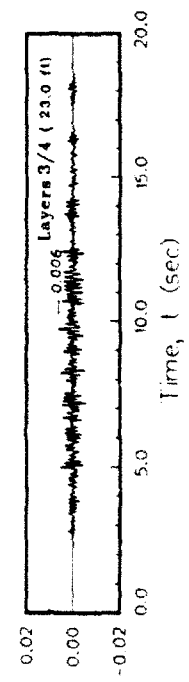
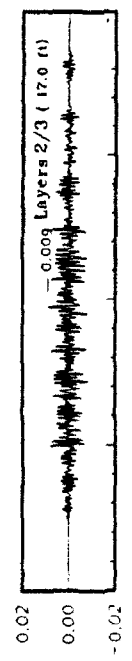


Figure N15. Variation of acceleration with time at the top of each layer for Site 15

APPENDIX O: SHEAR STRAINS FOR 5000-YEAR EVENT



Effective Shear Strain (percent)



Effective Shear Strain (percent)

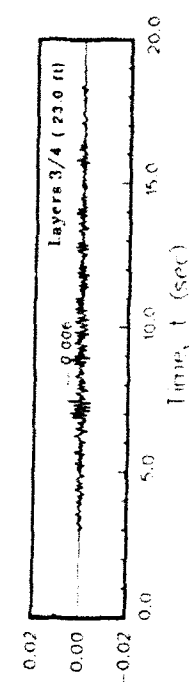
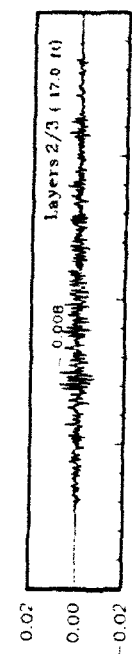


Figure 01. Variation of shear strain with time at contacts between layers for Site 1

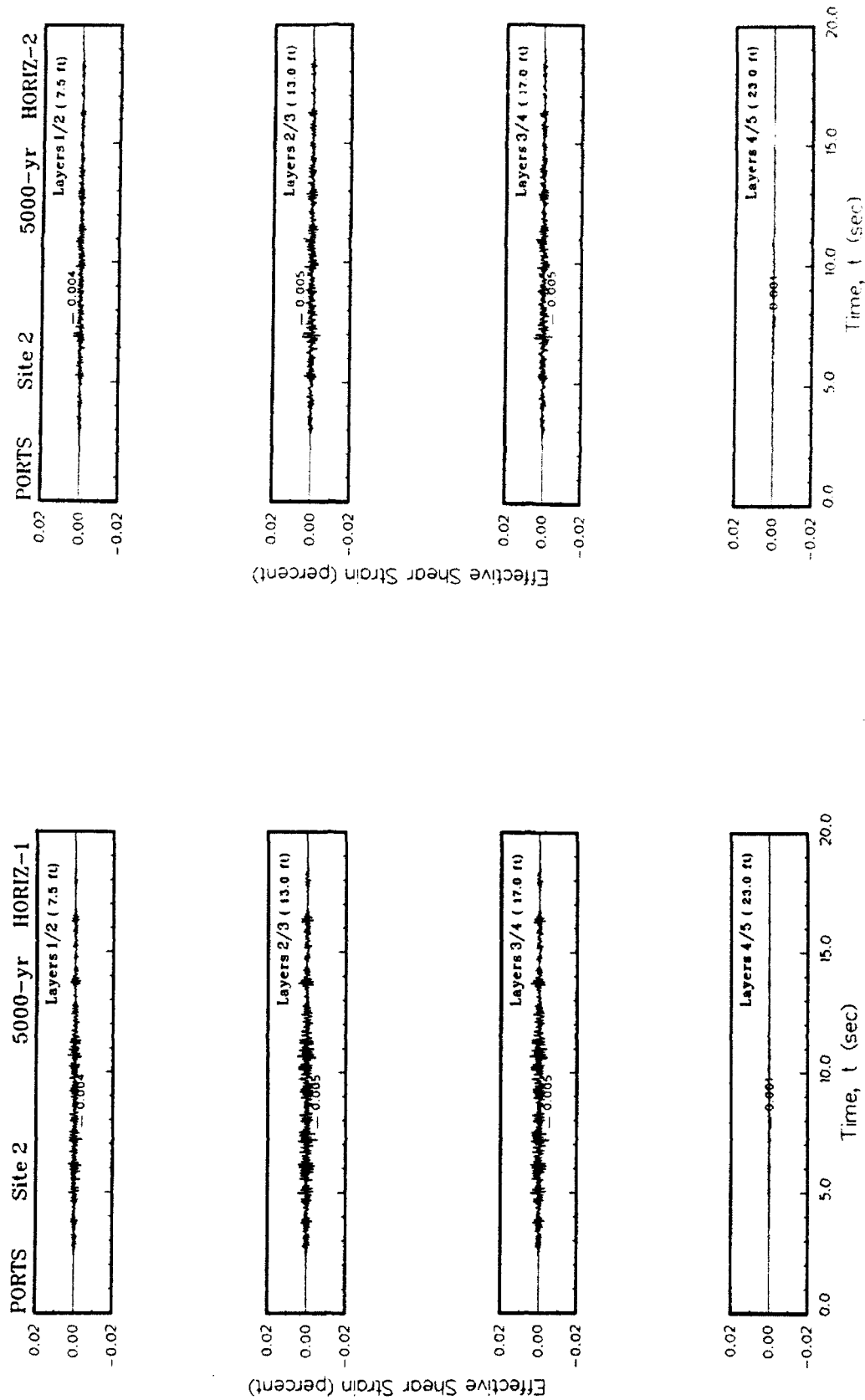


Figure 02. Variation of shear strain with time at contacts between layers for Site 2

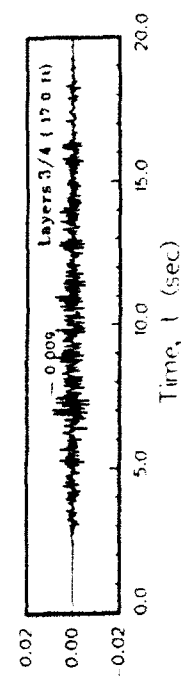
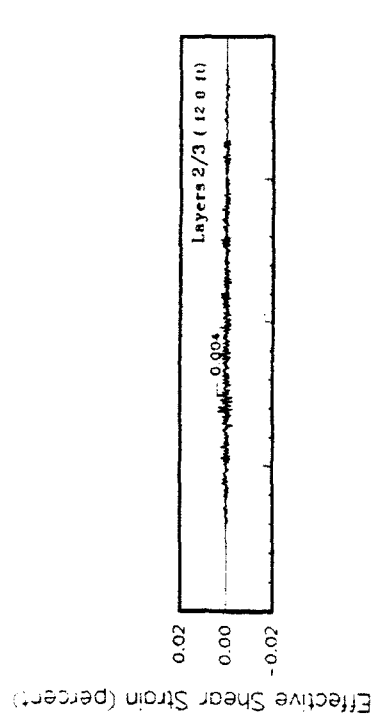
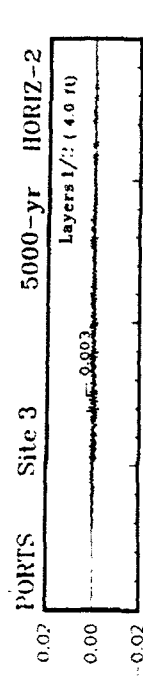
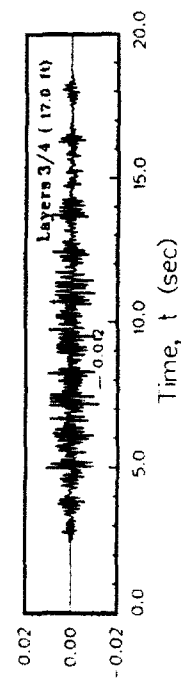
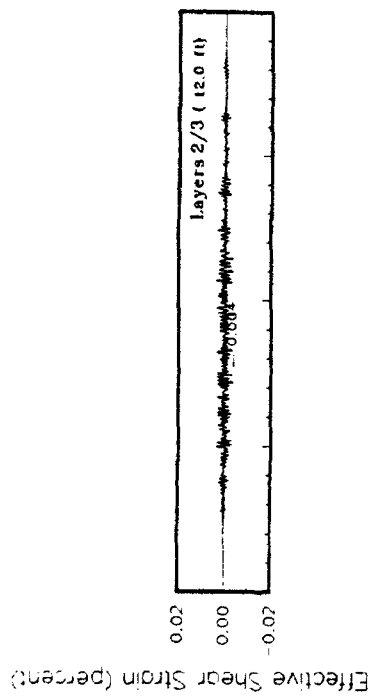
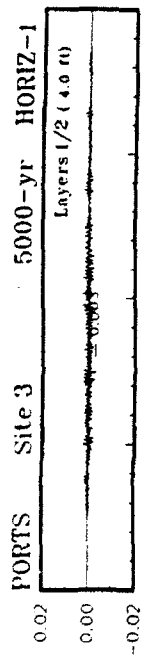
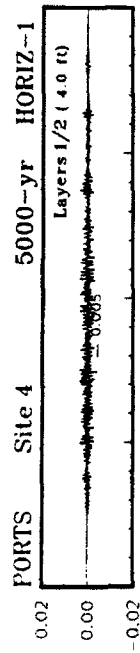


Figure O3. Variation of shear strain with time at contacts between layers for Site 3



Effective Shear Strain (percent)



Effective Shear Strain (percent)

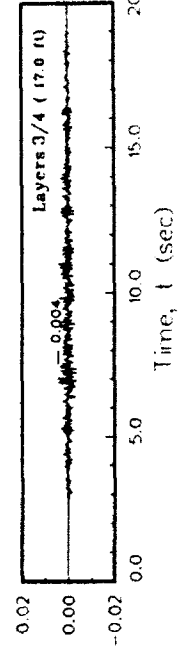
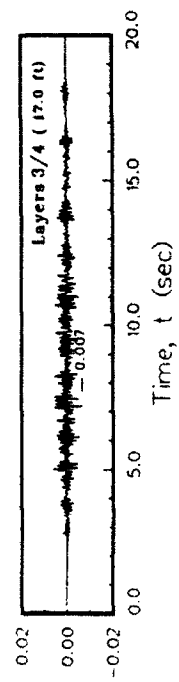
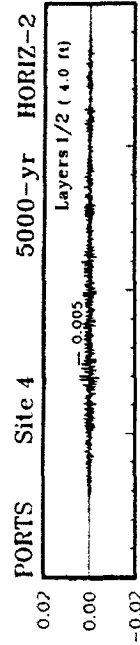
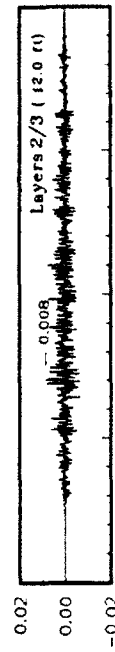


Figure 04. Variation of shear strain with time at contacts between layers for Site 4

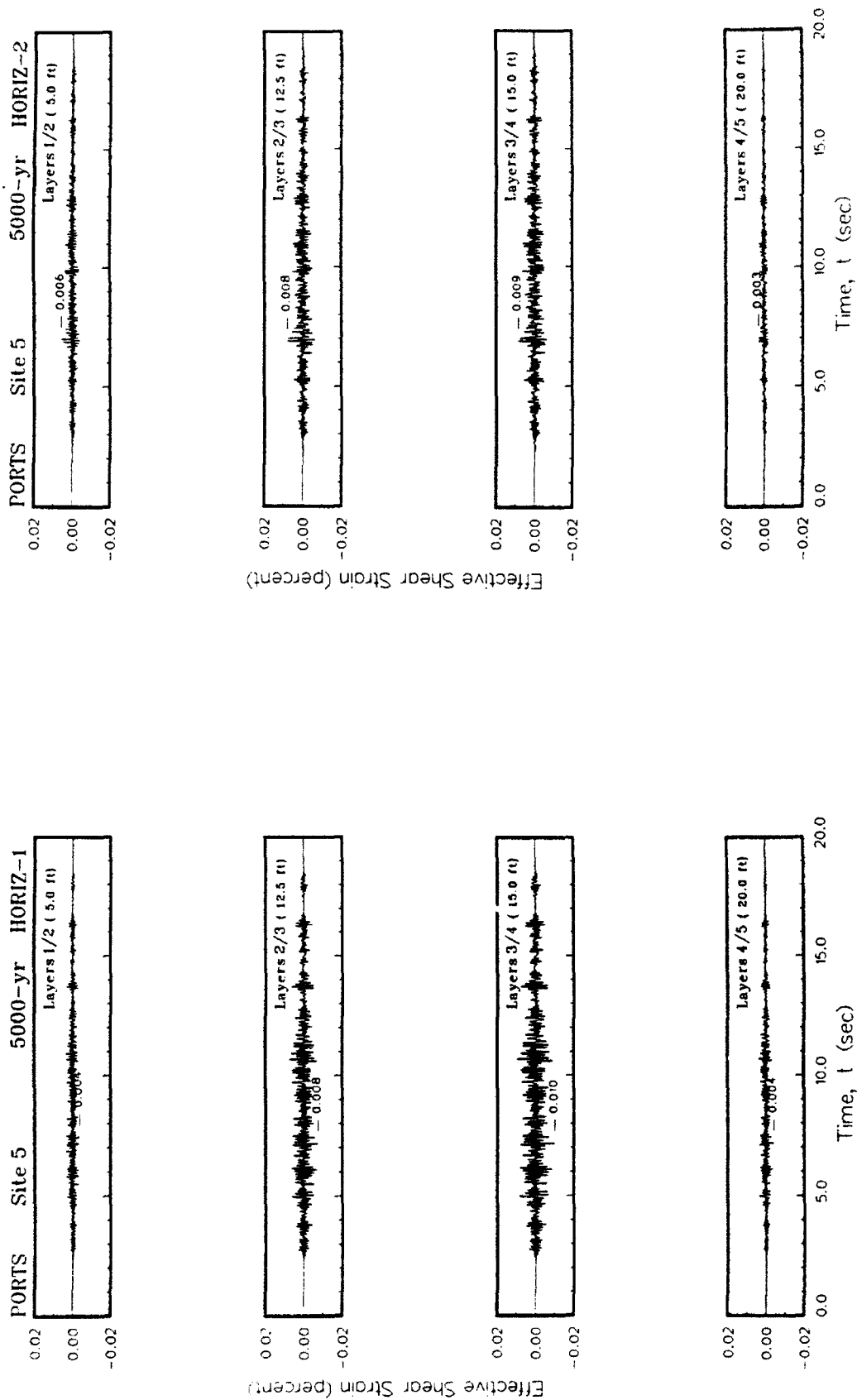


Figure O5. Variation of shear strain with time at contacts between layers for Site 5

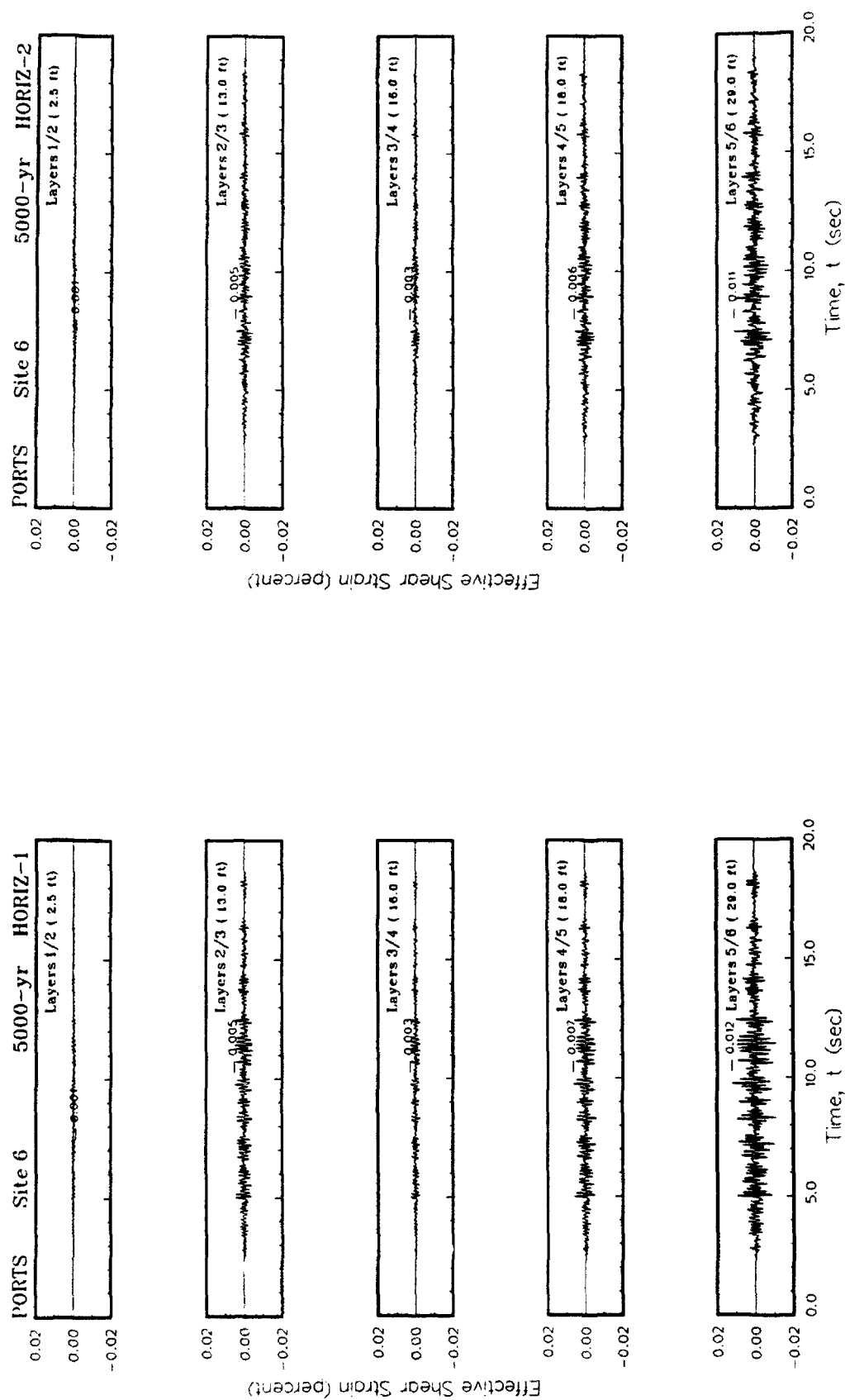


Figure 06. Variation of shear strain with time at contacts between layers for Site 6

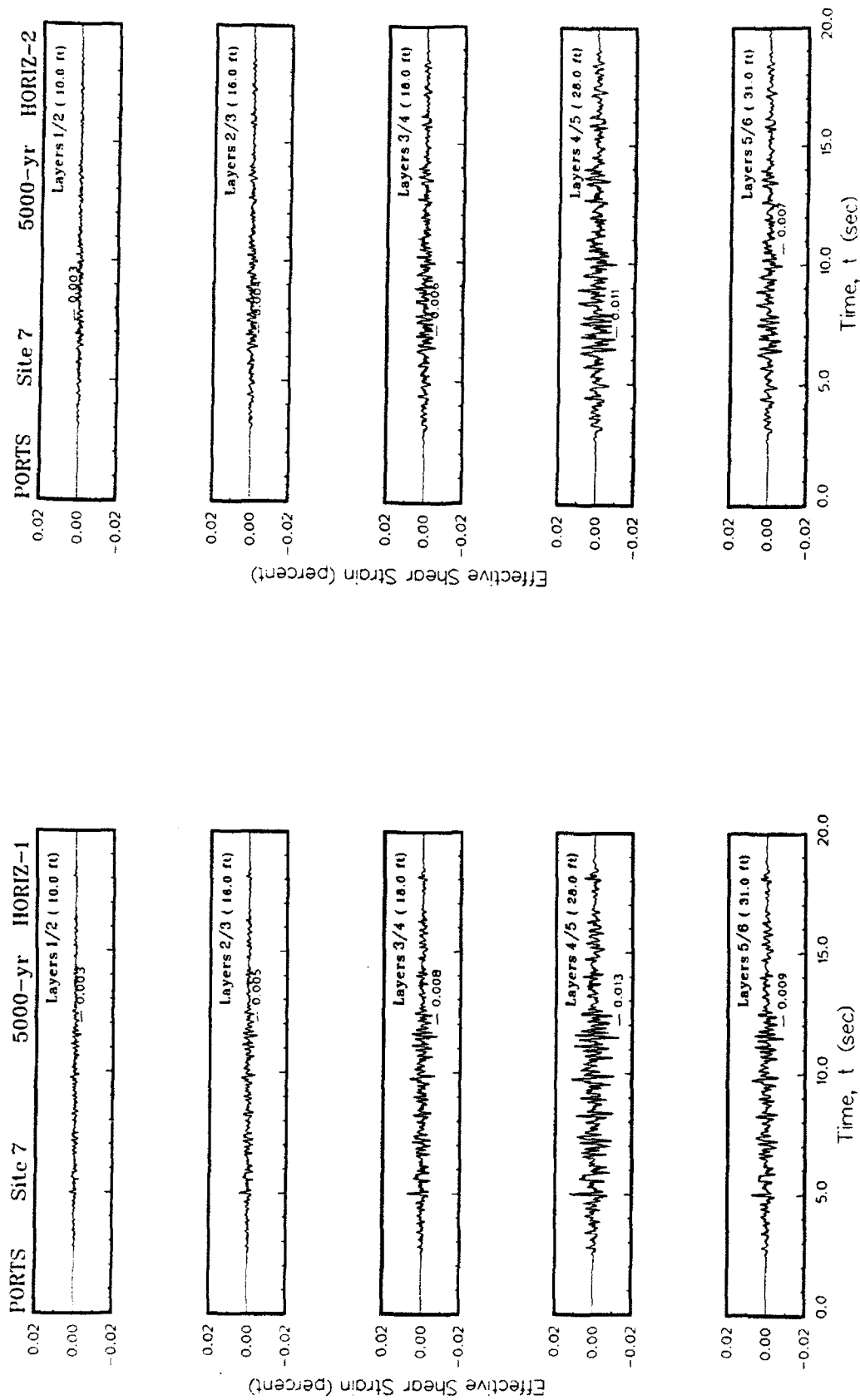


Figure O7. Variation of shear strain with time at contacts between layers for Site 7

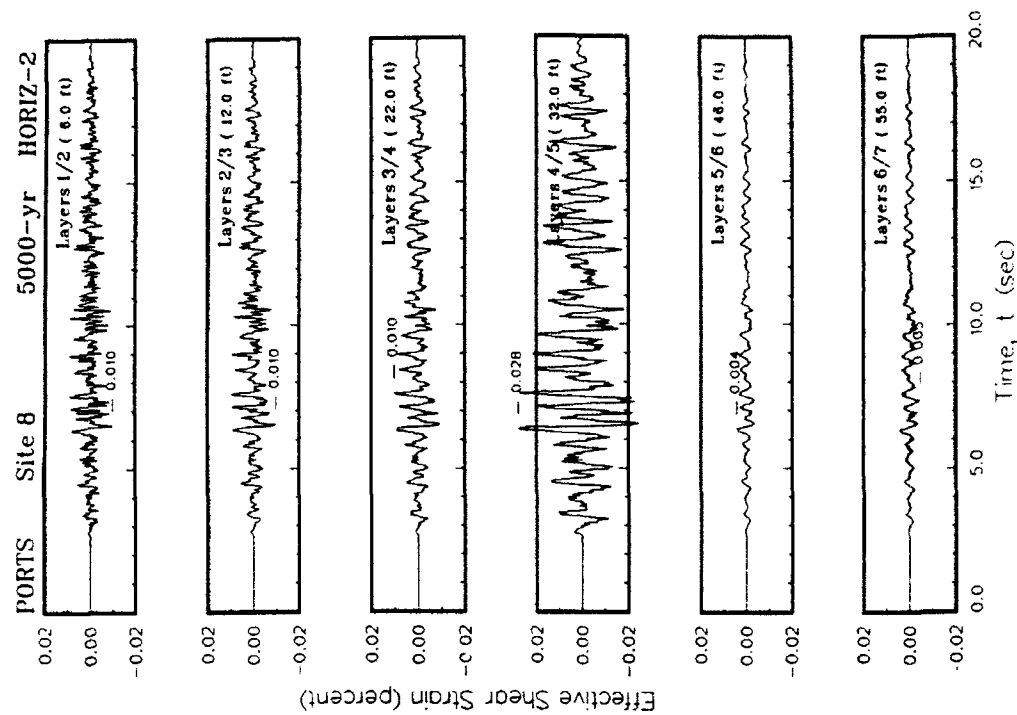
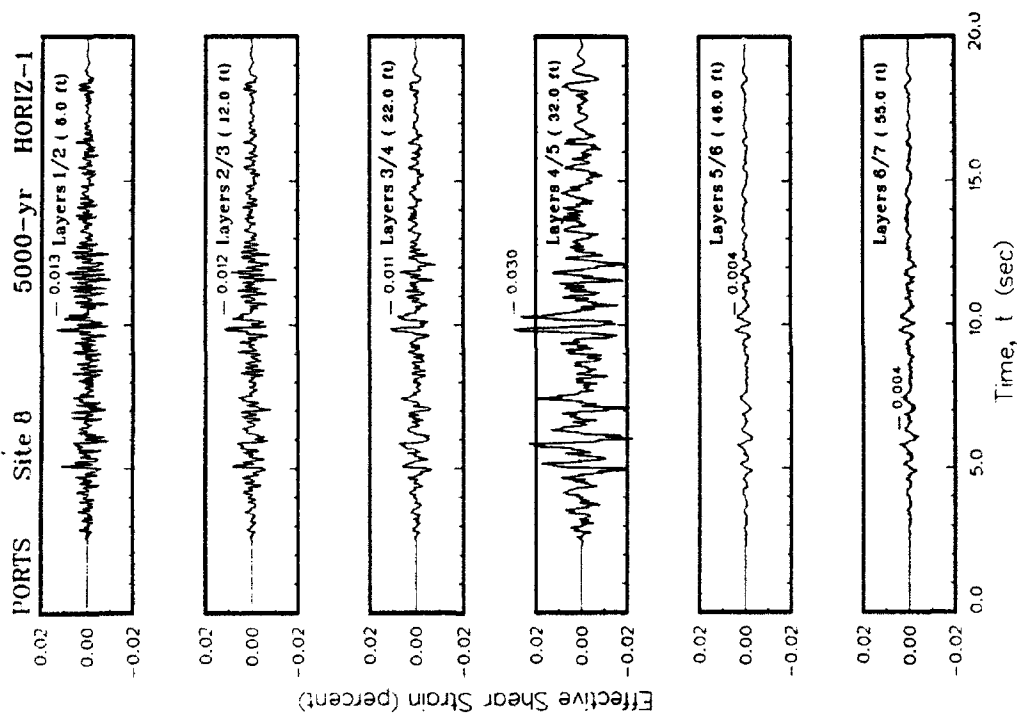


Figure O8. Variation of shear strain with time at contacts between layers for Site 8

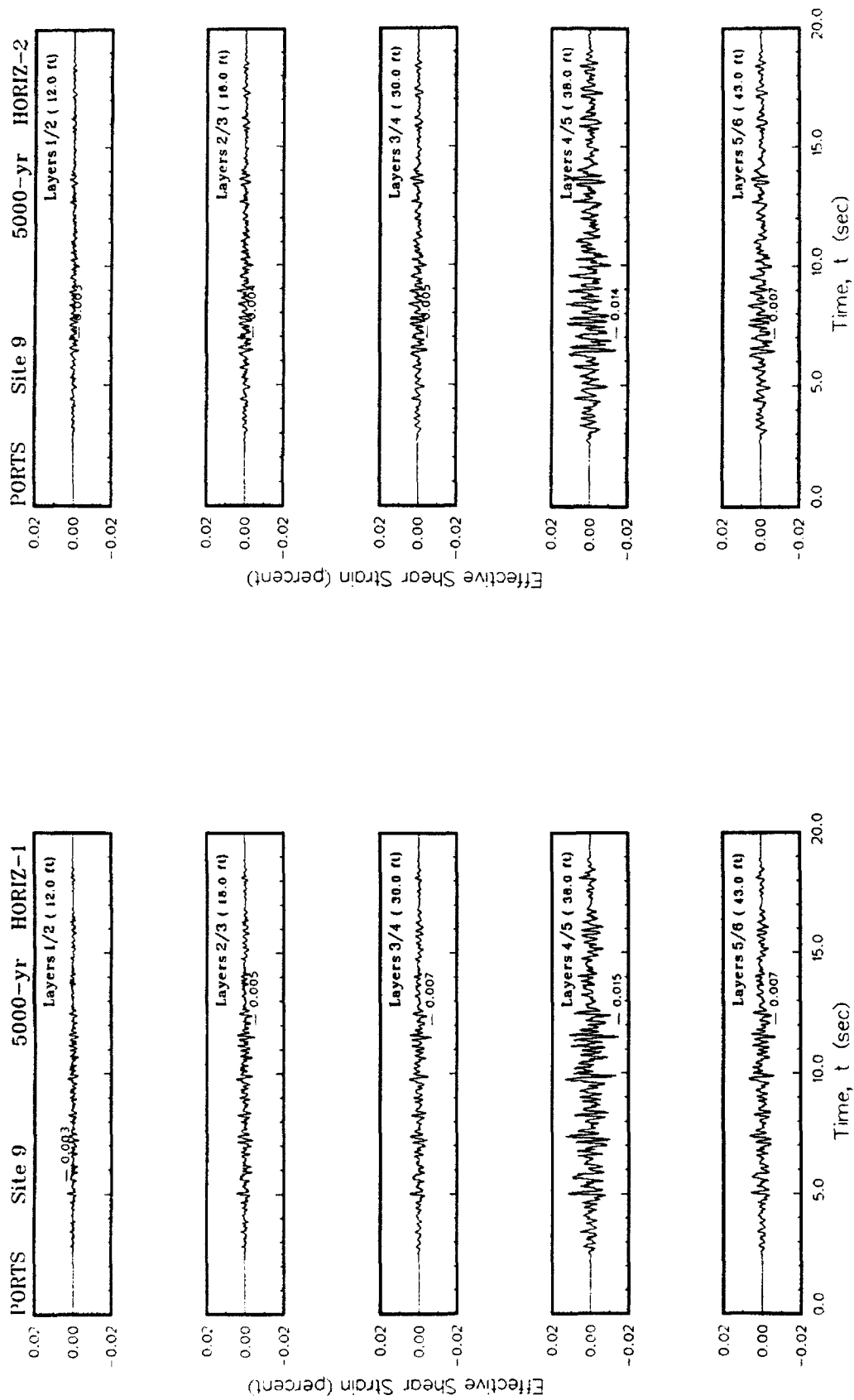


Figure 09. Variation of shear strain with time at contacts between layers for Site 9

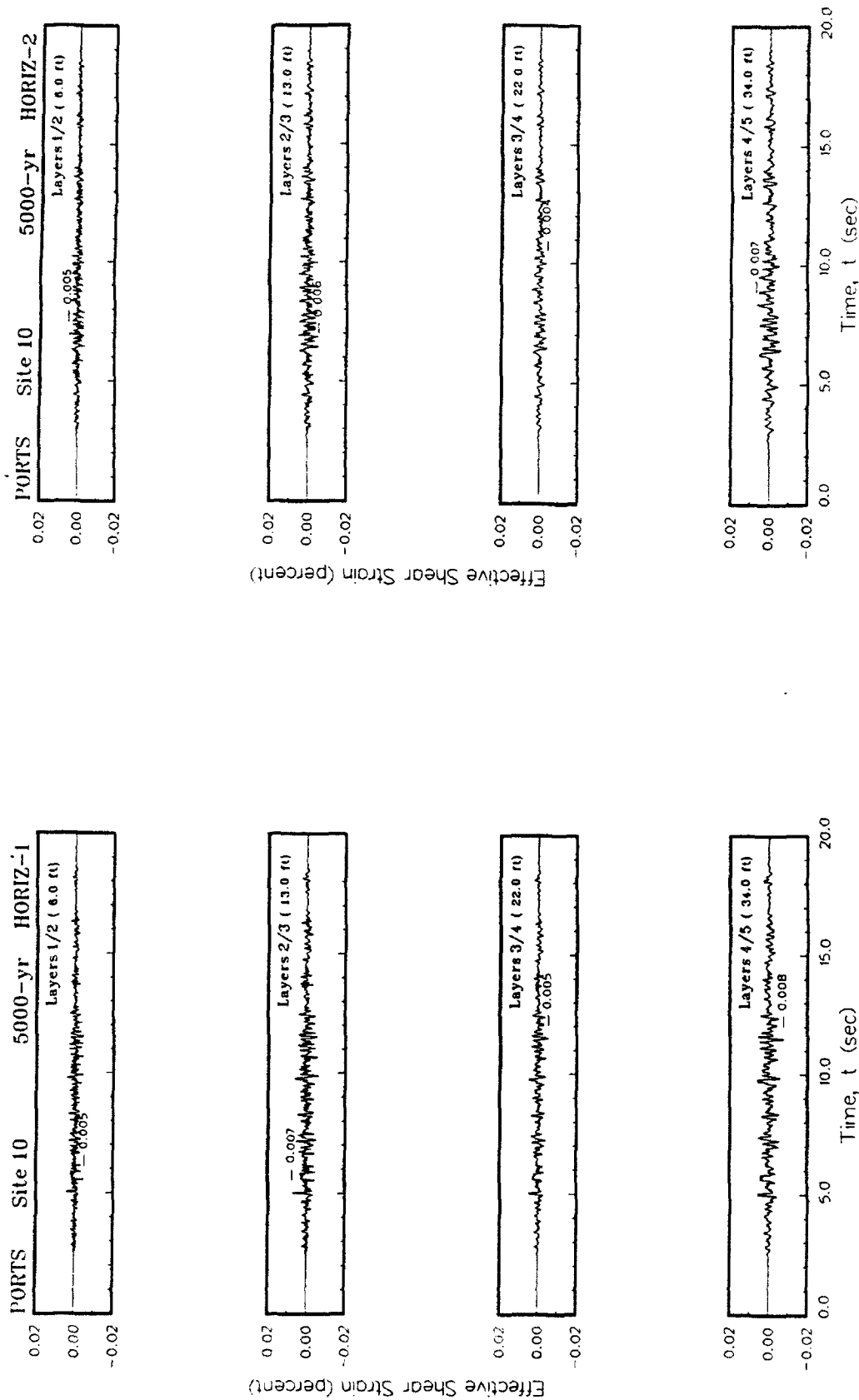


Figure O10. Variation of shear strain with time at contacts between layers for Site 10

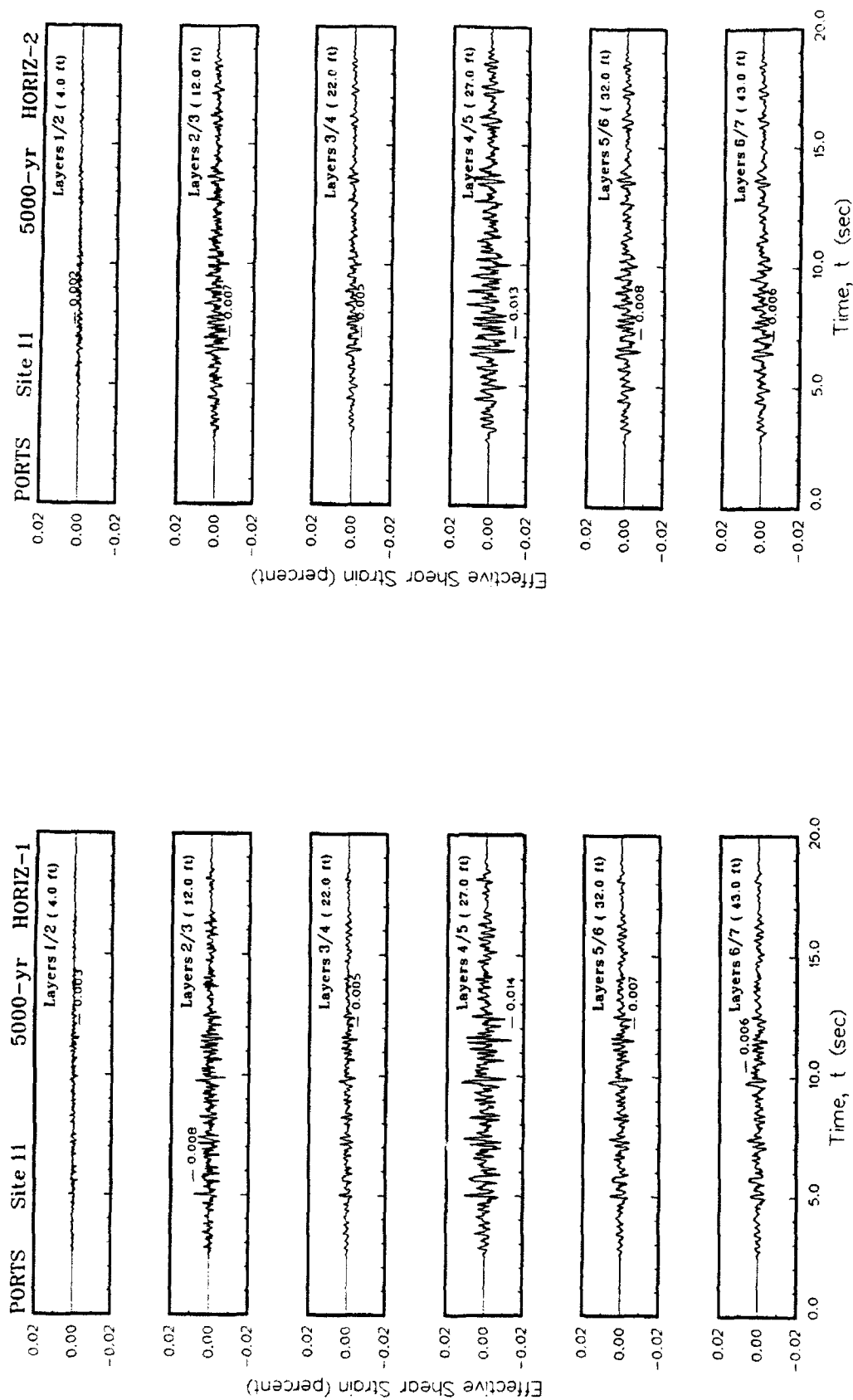
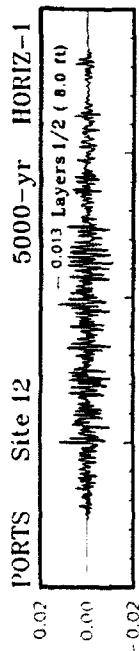
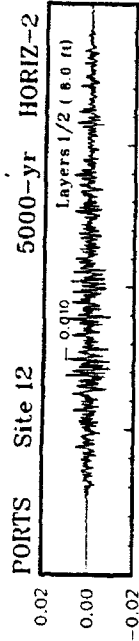


Figure O11. Variation of shear strain with time at contacts between layers for Site 11



Effective Shear Strain (percent)



Effective Shear Strain (percent)

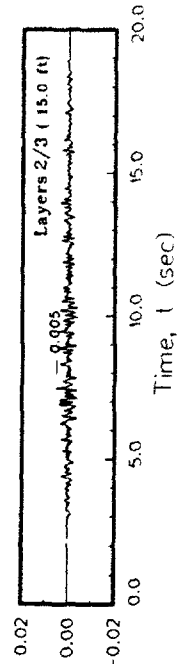
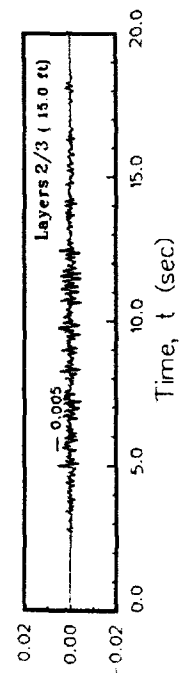
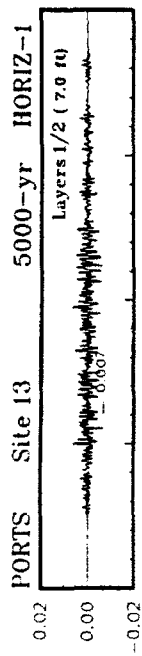
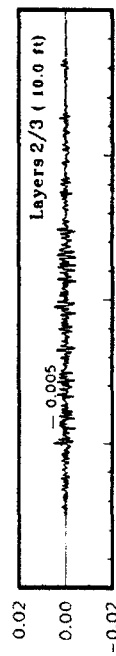


Figure 012. Variation of shear strain with time at contacts between layers for Site 12



Effective Shear Strain (percent)



Effective Shear Strain (percent)

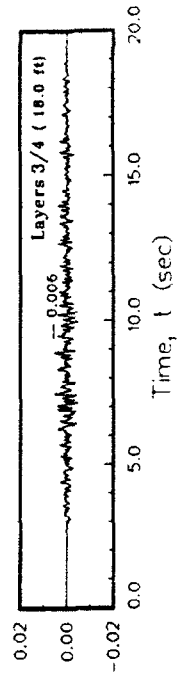
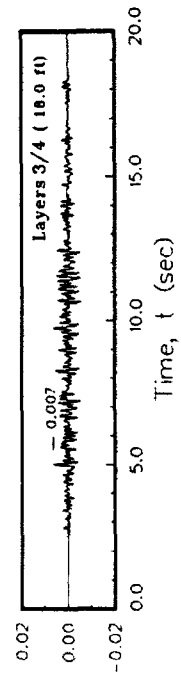
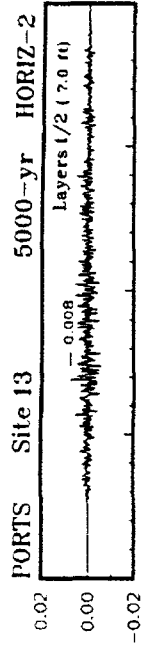
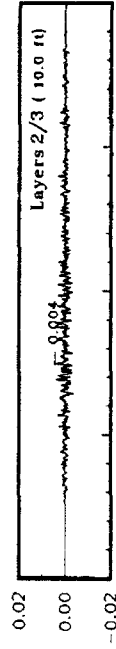


Figure 013. Variation of shear strain with time at contacts between layers for Site 13

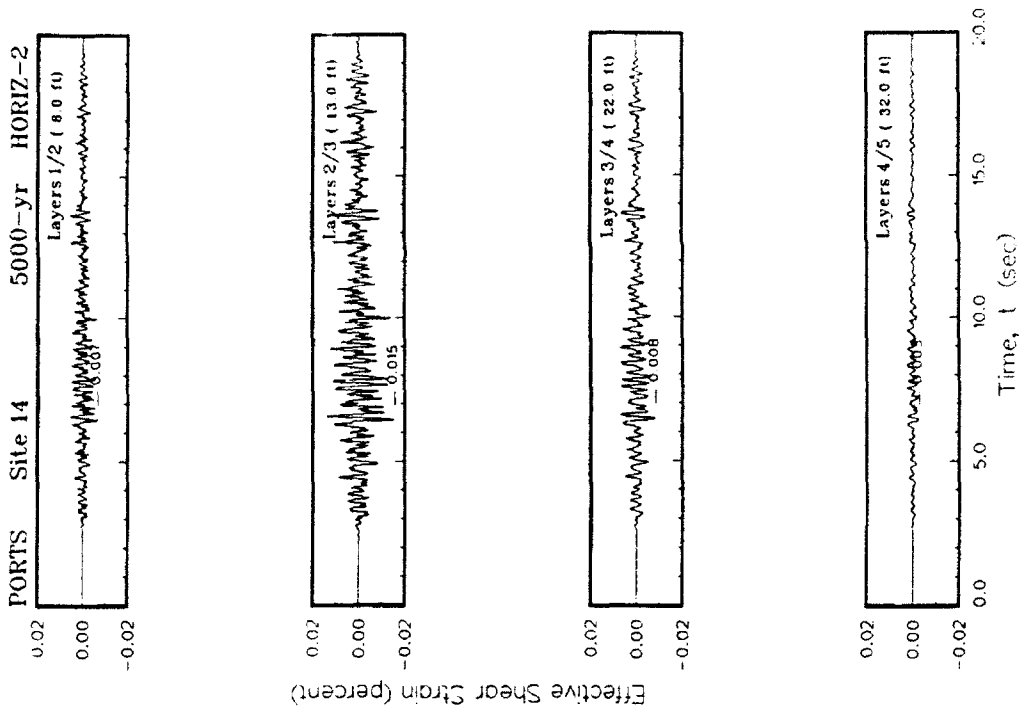
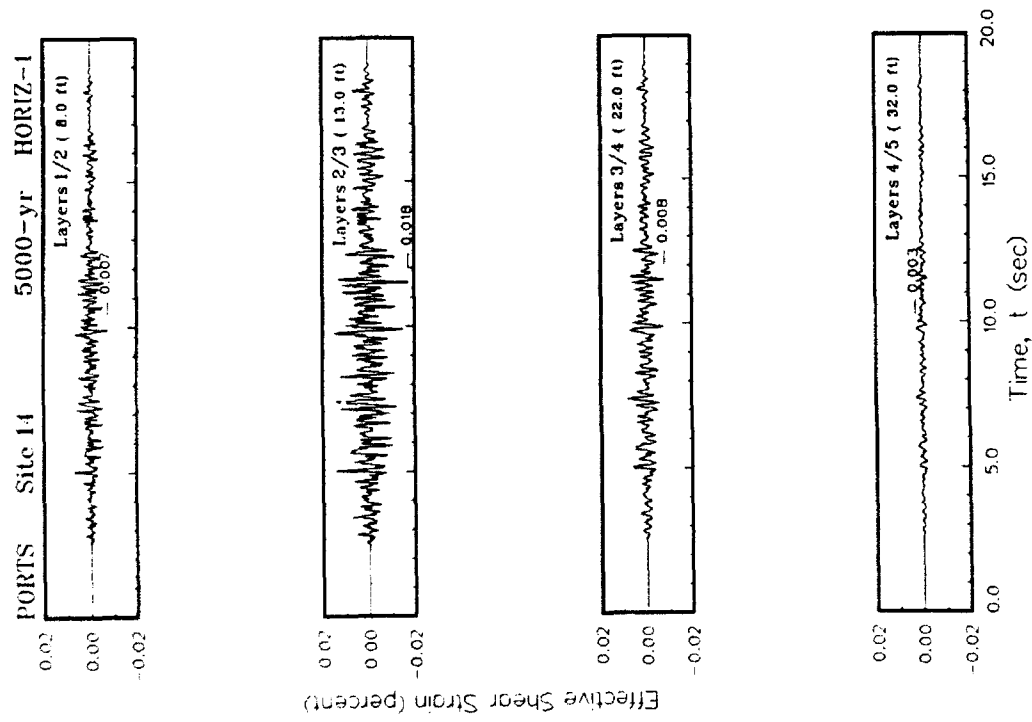


Figure O14. Variation of shear strain with time at contacts between layers for Site 14

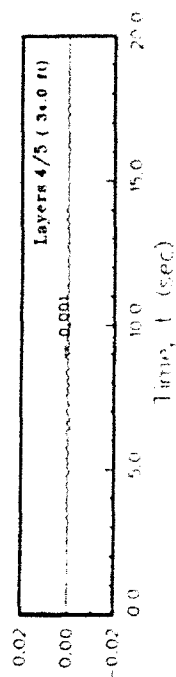
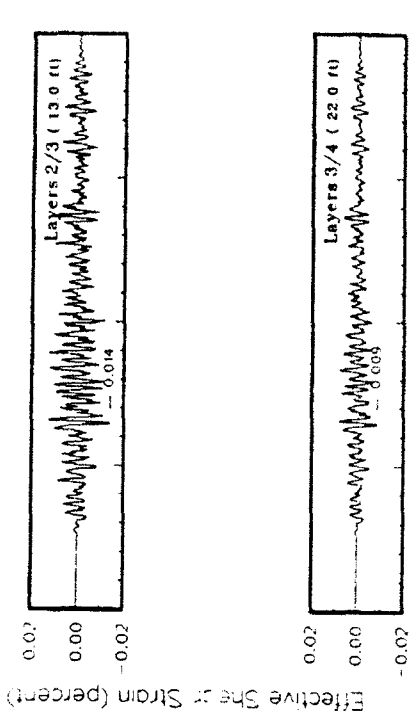
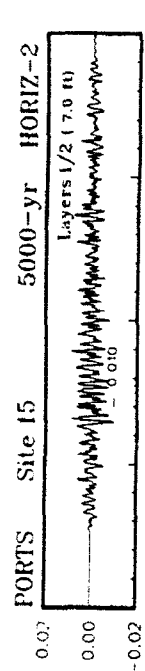
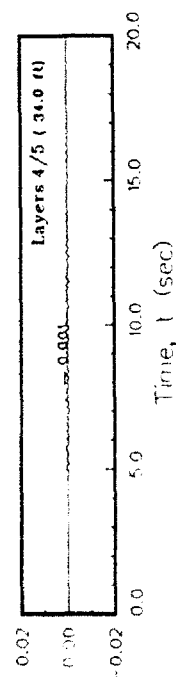
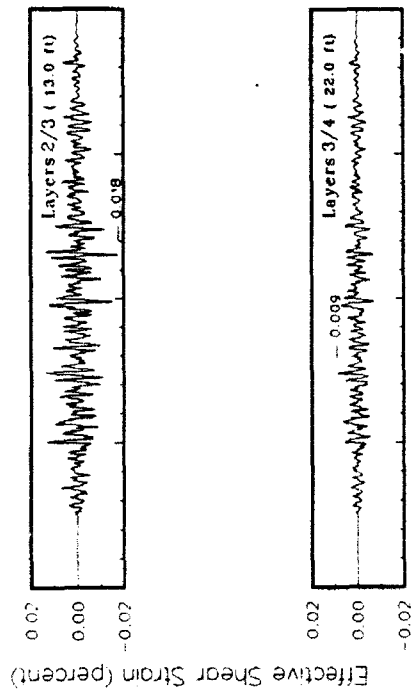
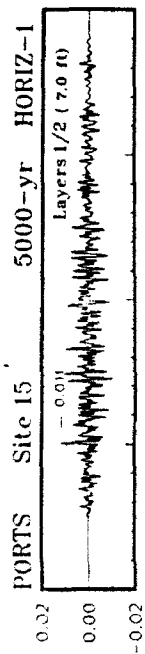


Figure O15. Variation of shear strain with time at contacts between layers for Site 15

APPENDIX P: TRIPARTITE RESPONSE SPECTRA FOR 5000-YEAR EVENT

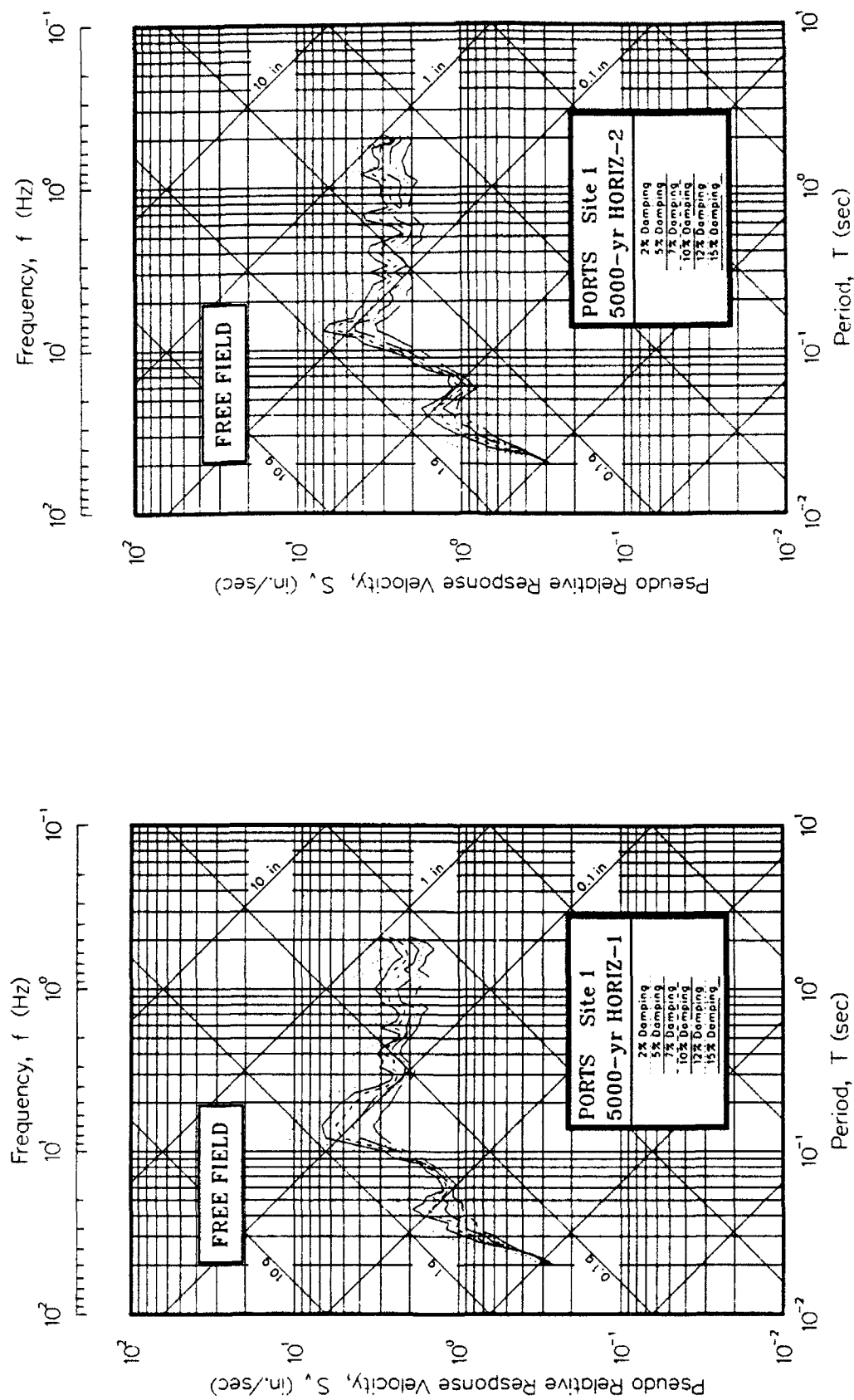


Figure P1. Pseudo-relative velocity spectra in tripartite form at free field for Site 1

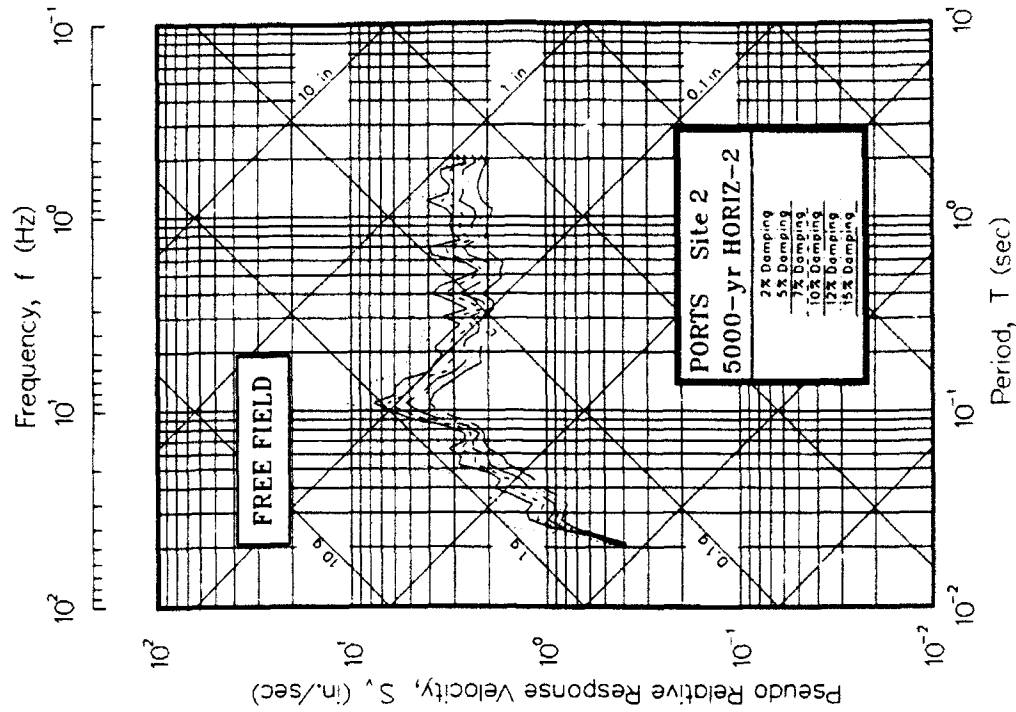
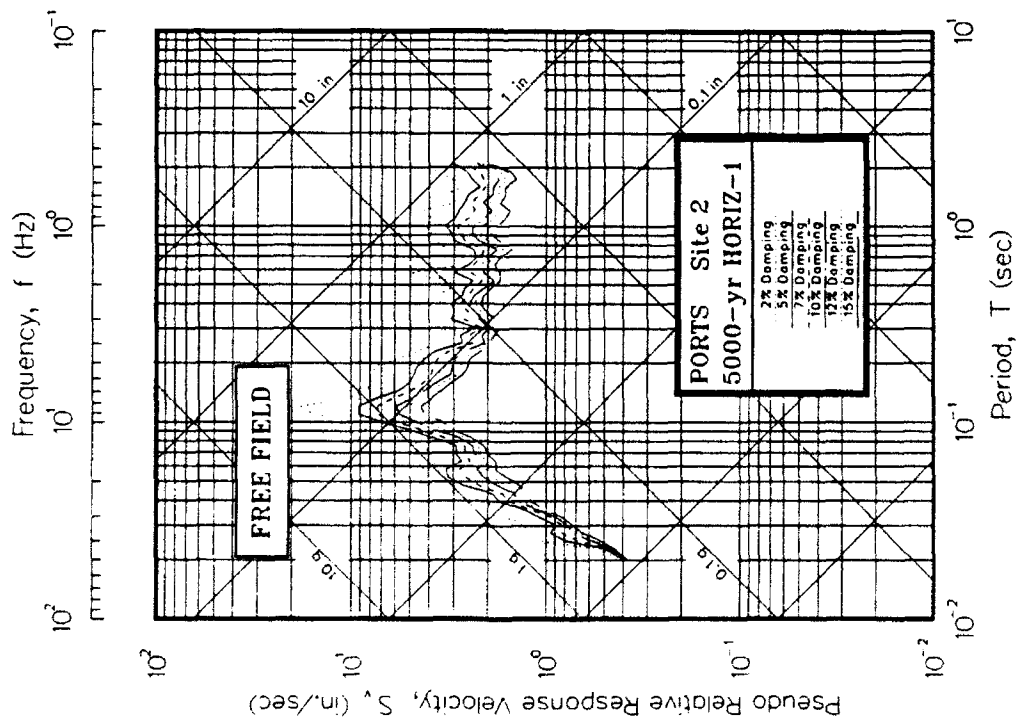


Figure P2. Psuedo-relative velocity spectra in tripartite form at free field for Site 2

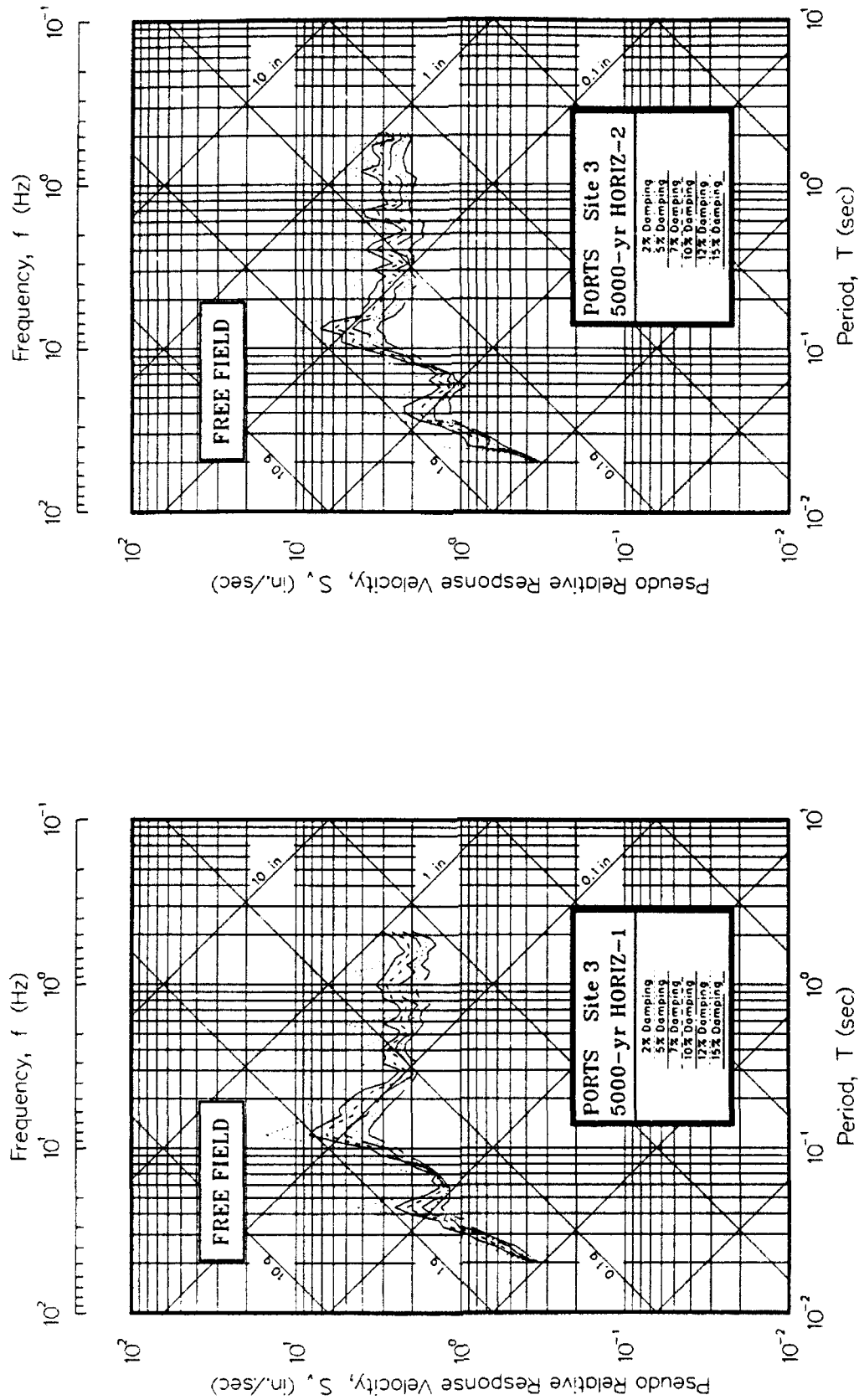


Figure P3. Psuedo-relative velocity spectra in tripartite form at free field for Site 3

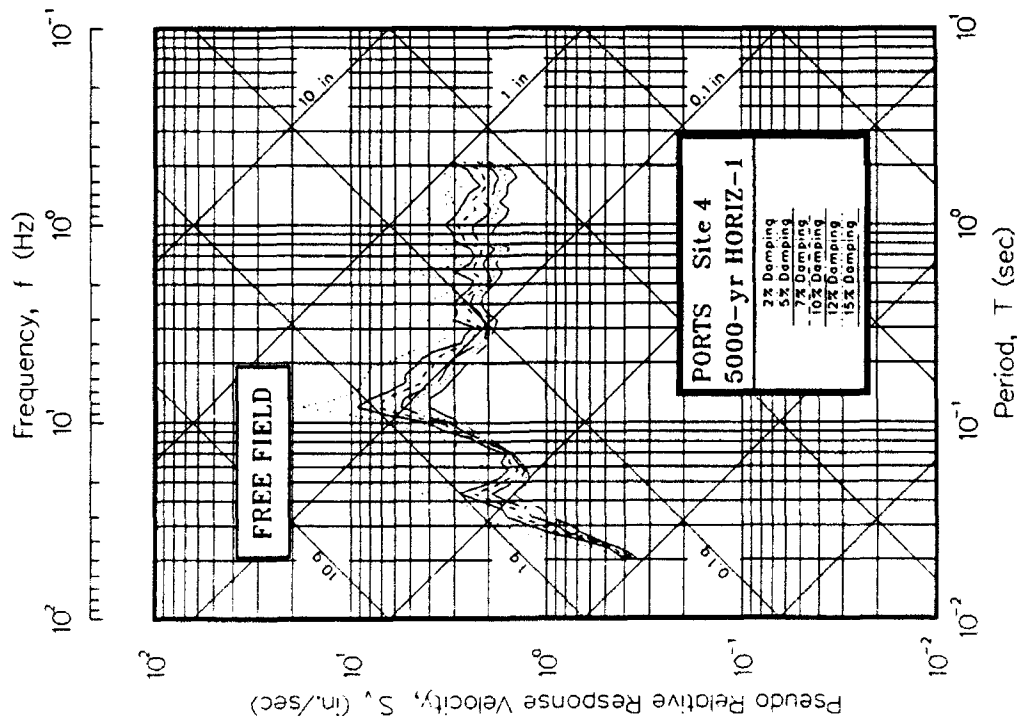
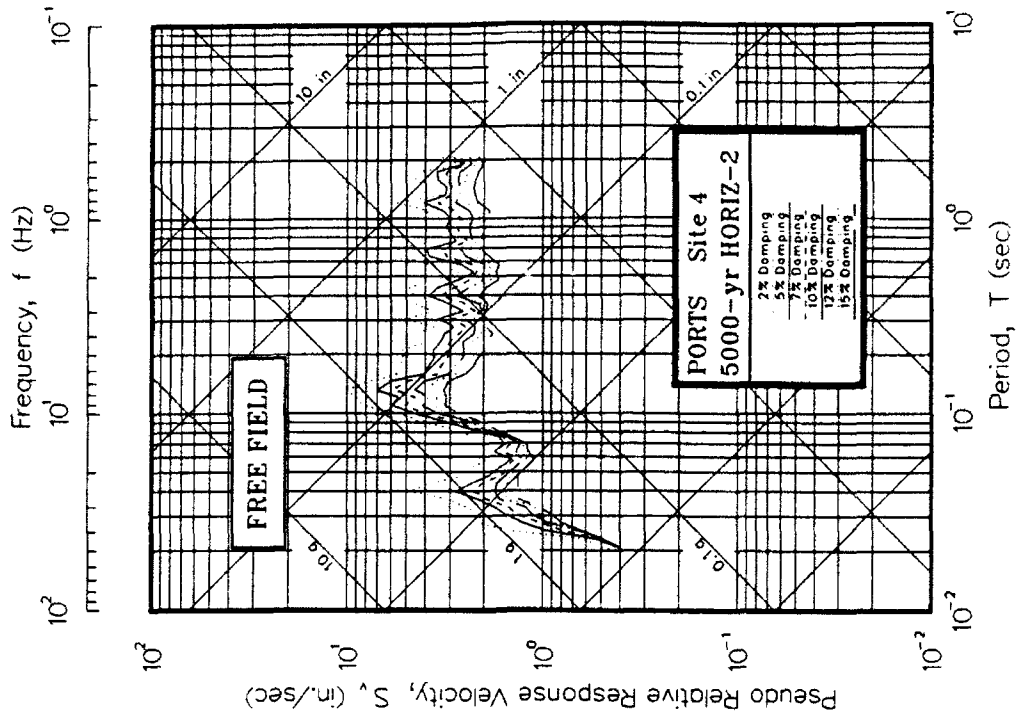


Figure P4. Psuedo-relative velocity spectra in tripartite form at free field for Site 4

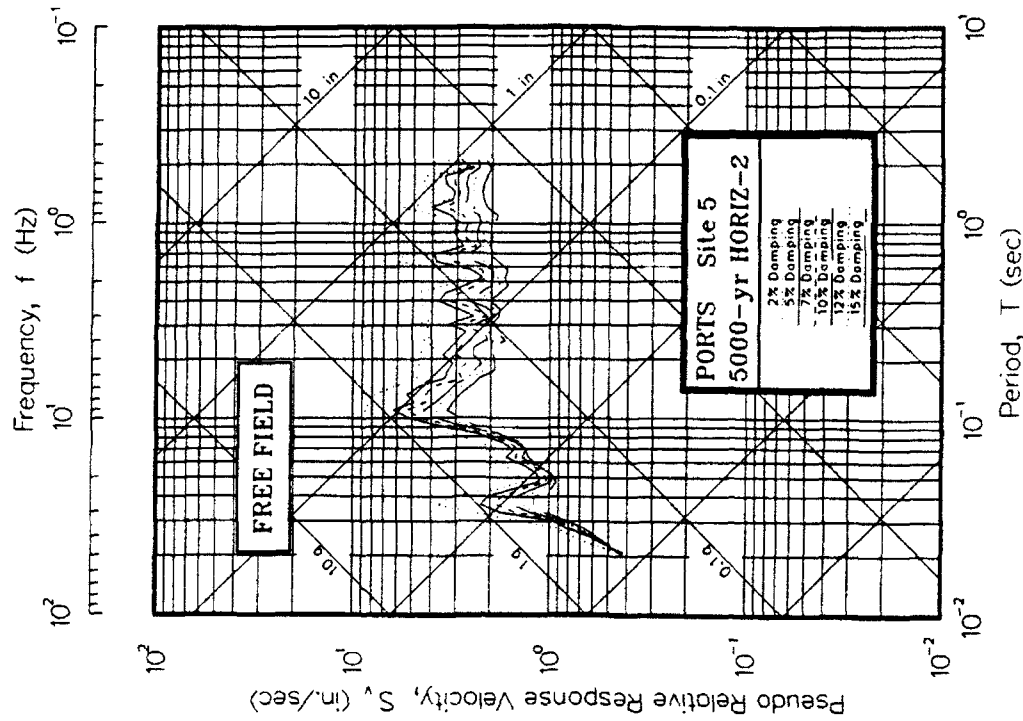
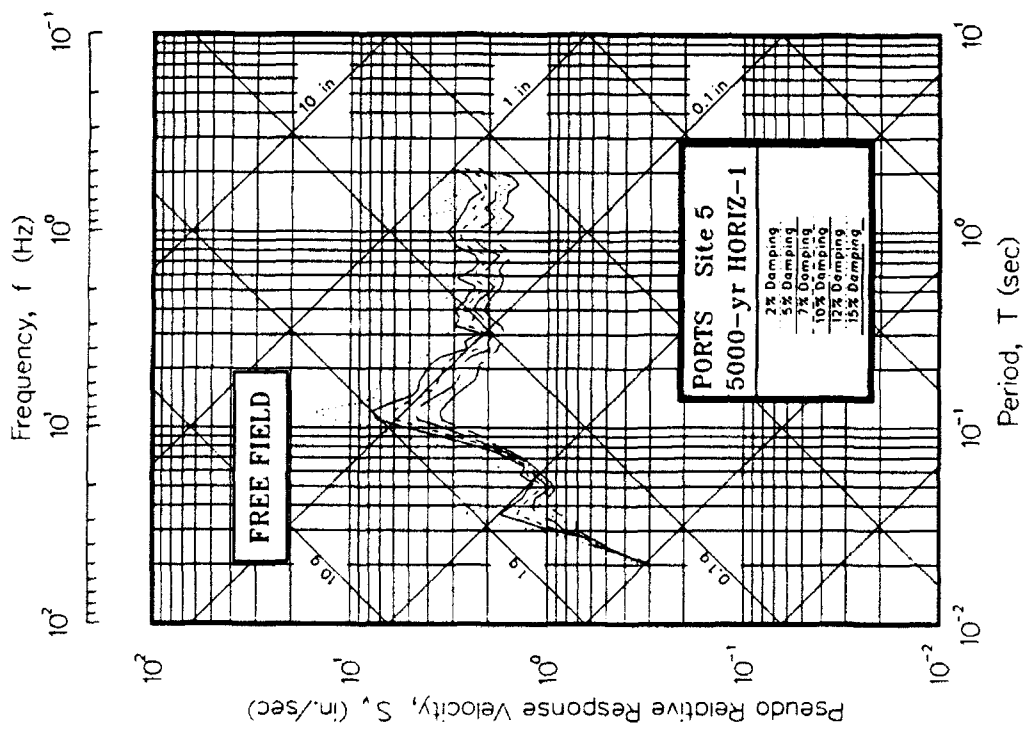


Figure P5. Psuedo-relative velocity spectra in tripartite form at free field for Site 5

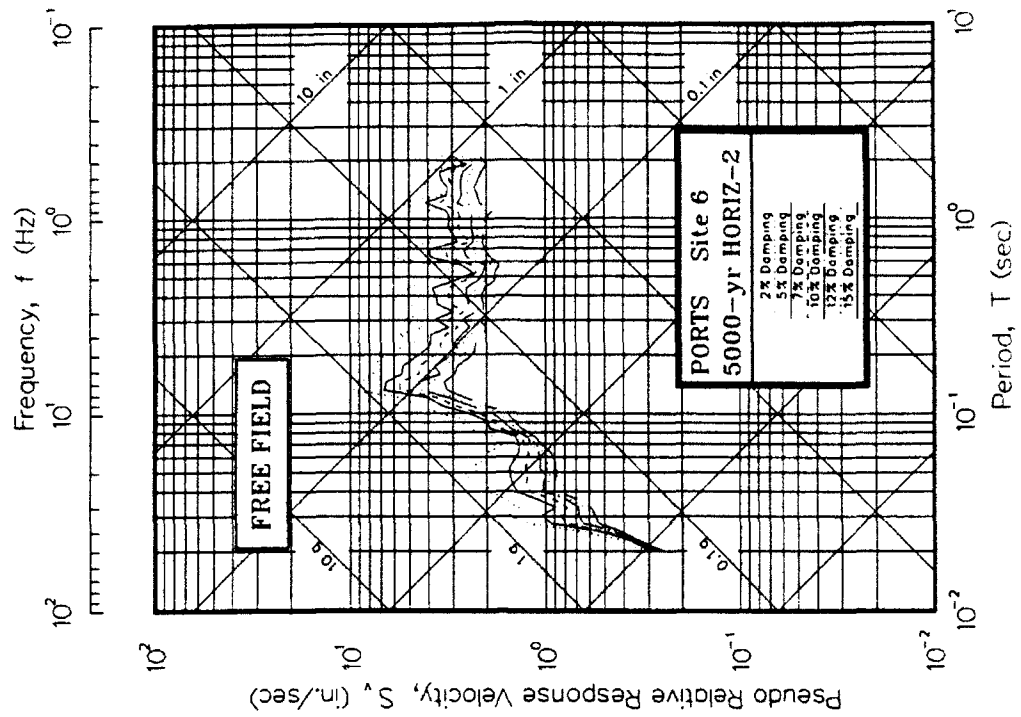
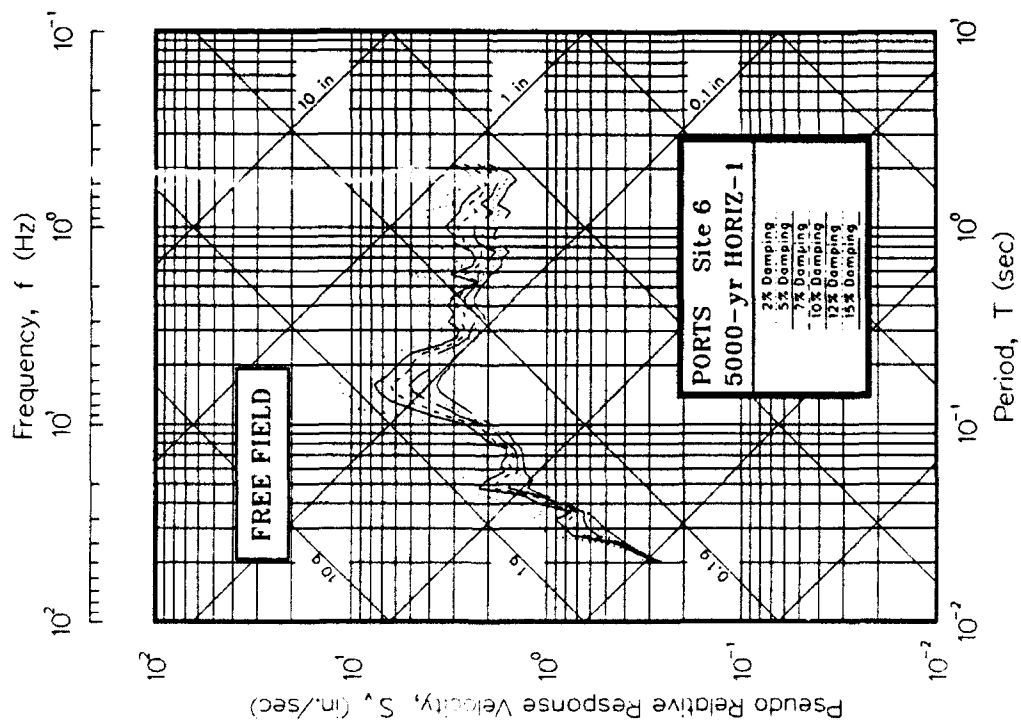


Figure P6. Psuedo-relative velocity spectra in tripartite form at free field for Site 6

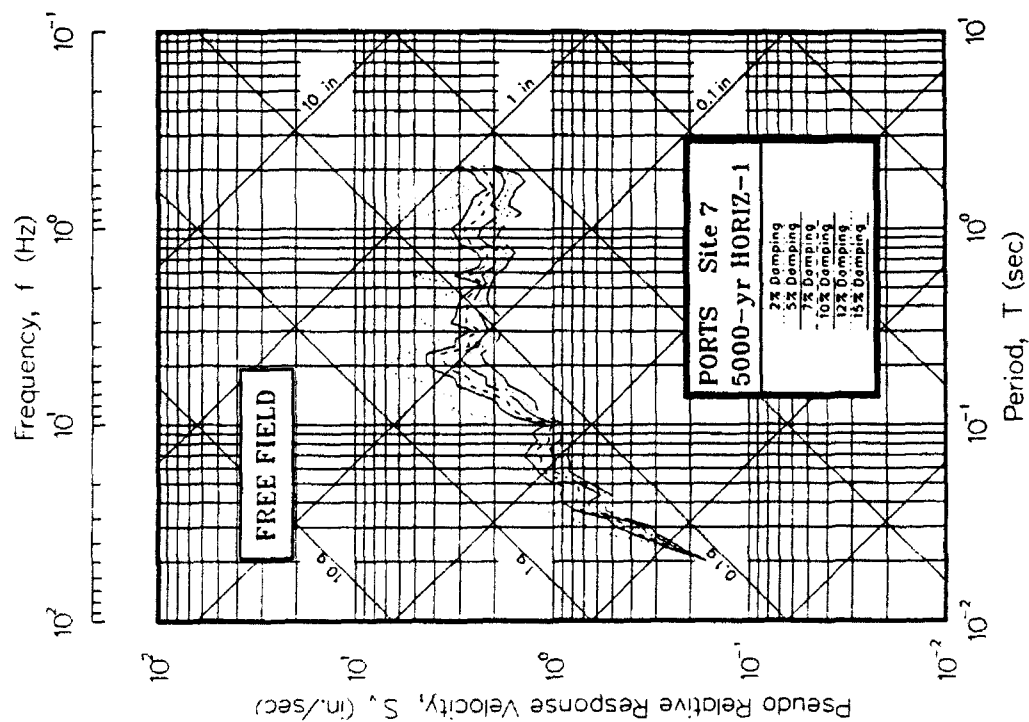
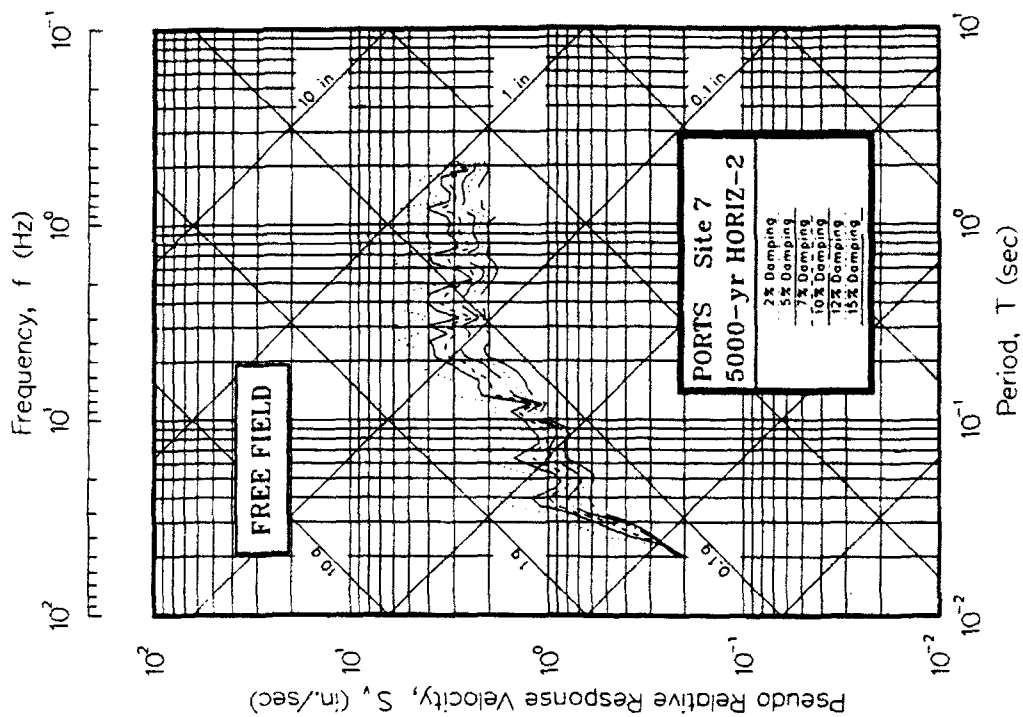


Figure P7. Psuedo-relative velocity spectra in tripartite form at free field for Site 7

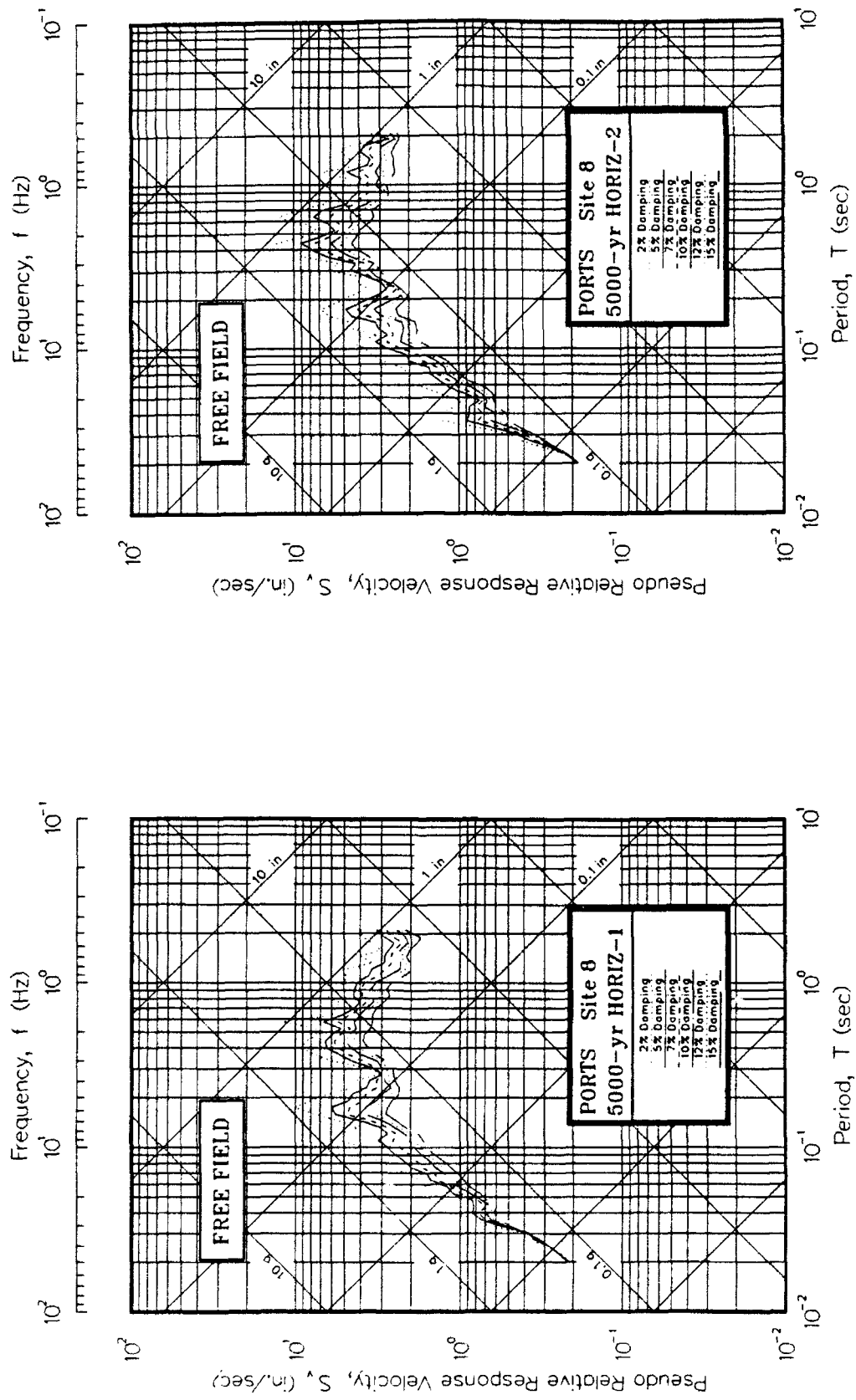


Figure P8. Psuedo-relative velocity spectra in tripartite form at free field for Site 8

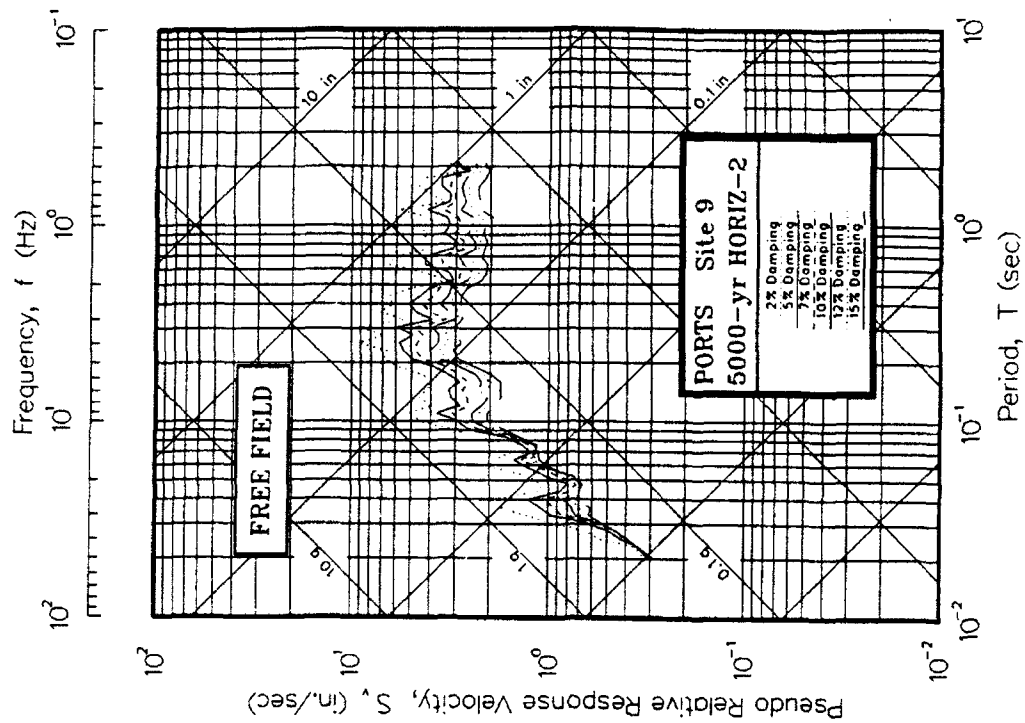
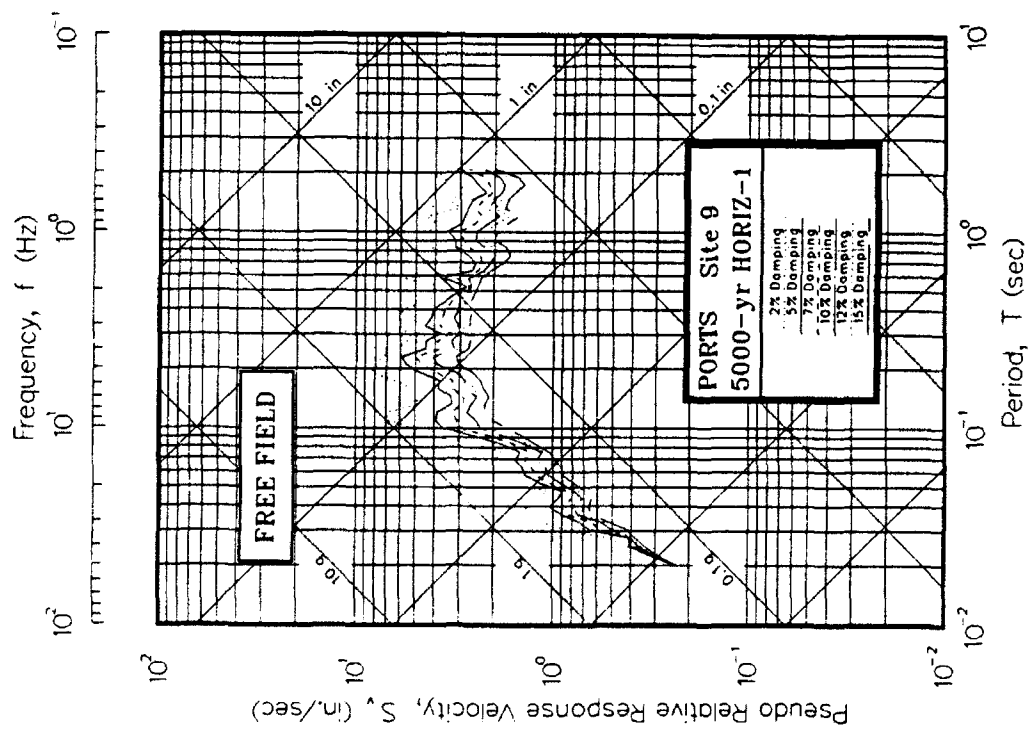


Figure P9. Psuedo-relative velocity spectra in tripartite form at free field for Site 9

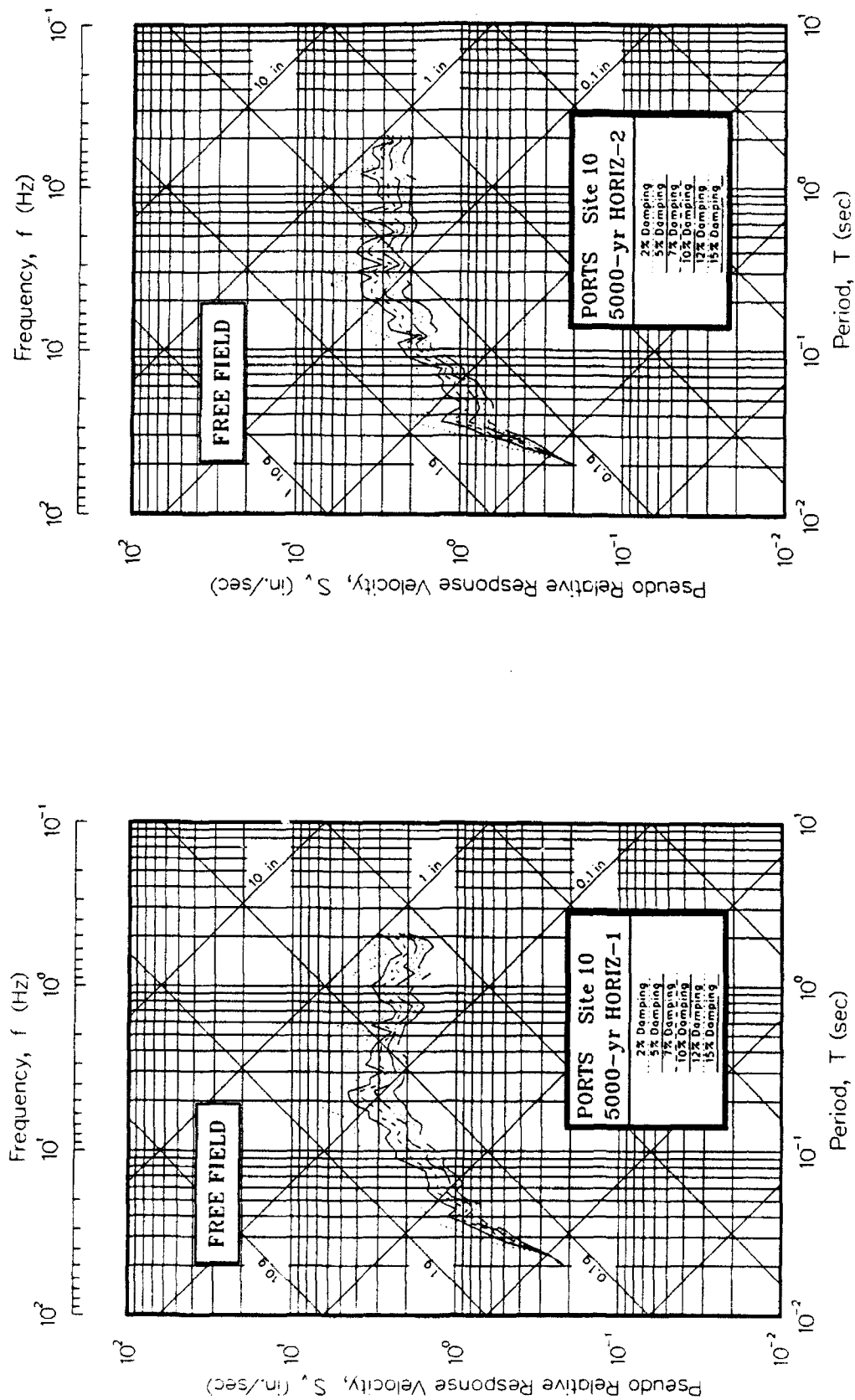


Figure P10. Psuedo-relative velocity spectra in tripartite form at free field for Site 10

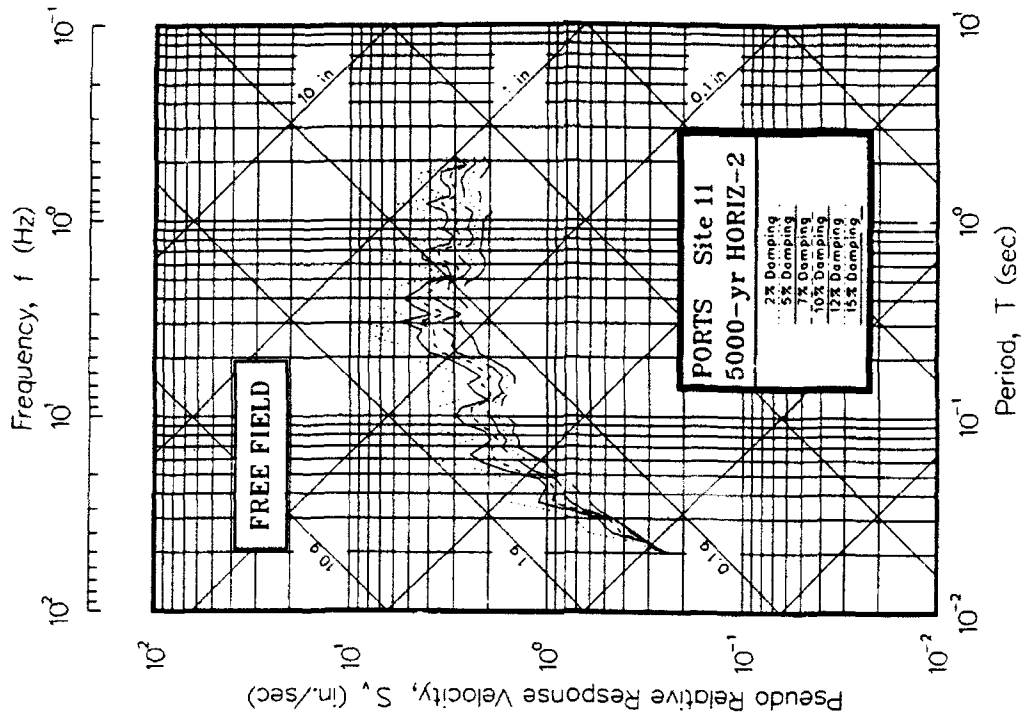
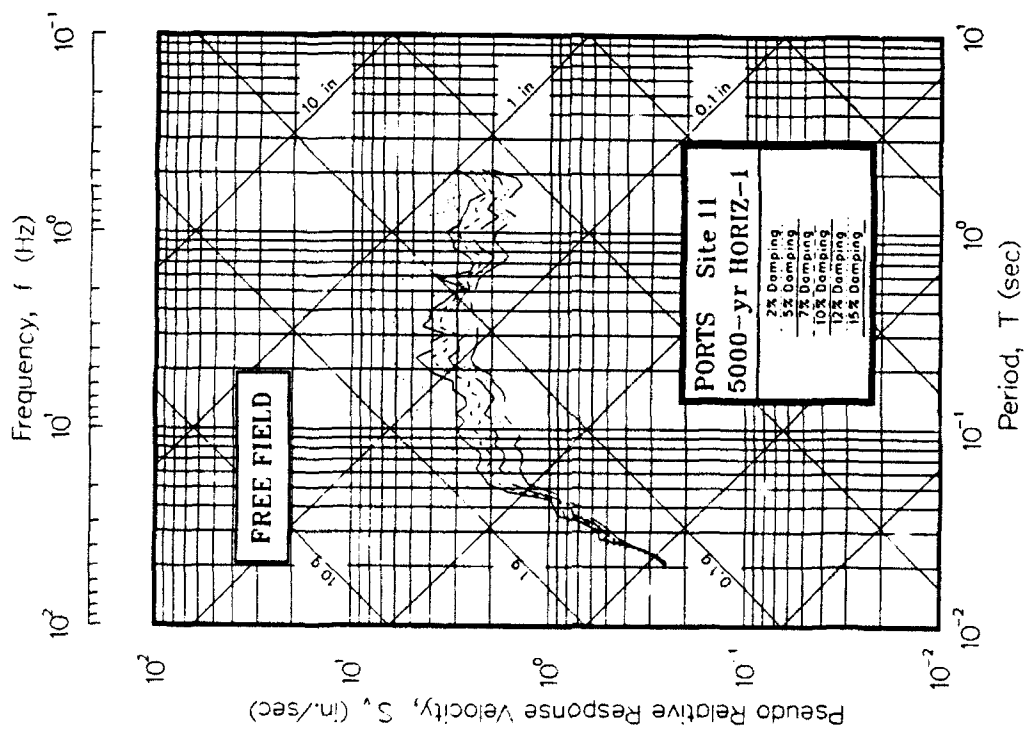


Figure P11. Psuedo-relative velocity spectra in tripartite form at free field for Site 11

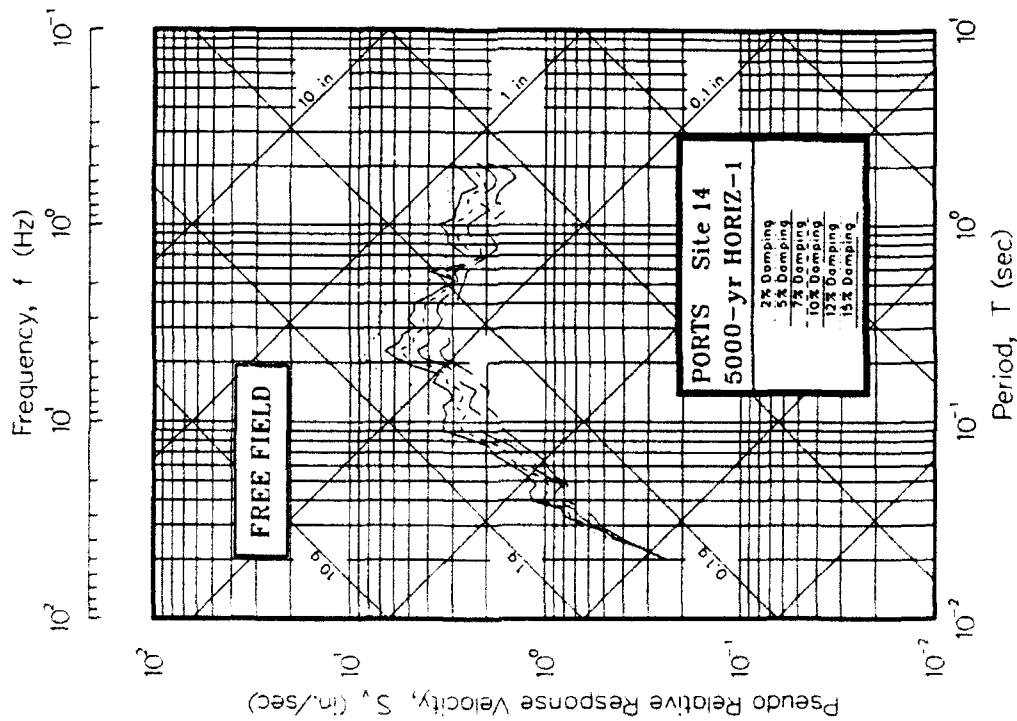
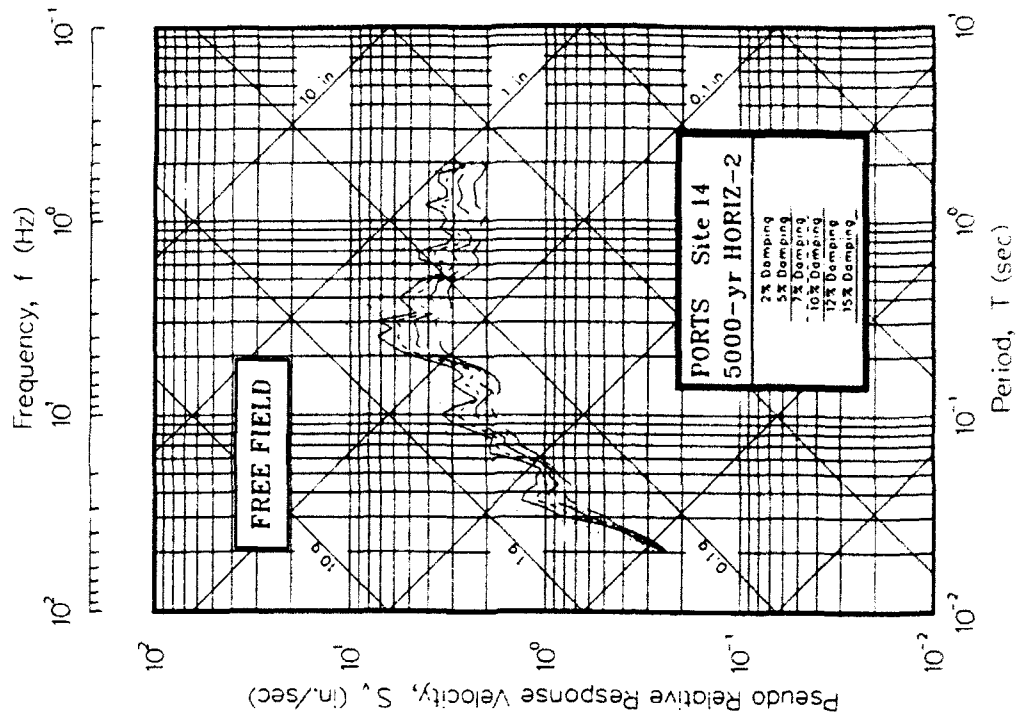


Figure P14. Psuedo-relative velocity spectra in tripartite form at free field for Site 14

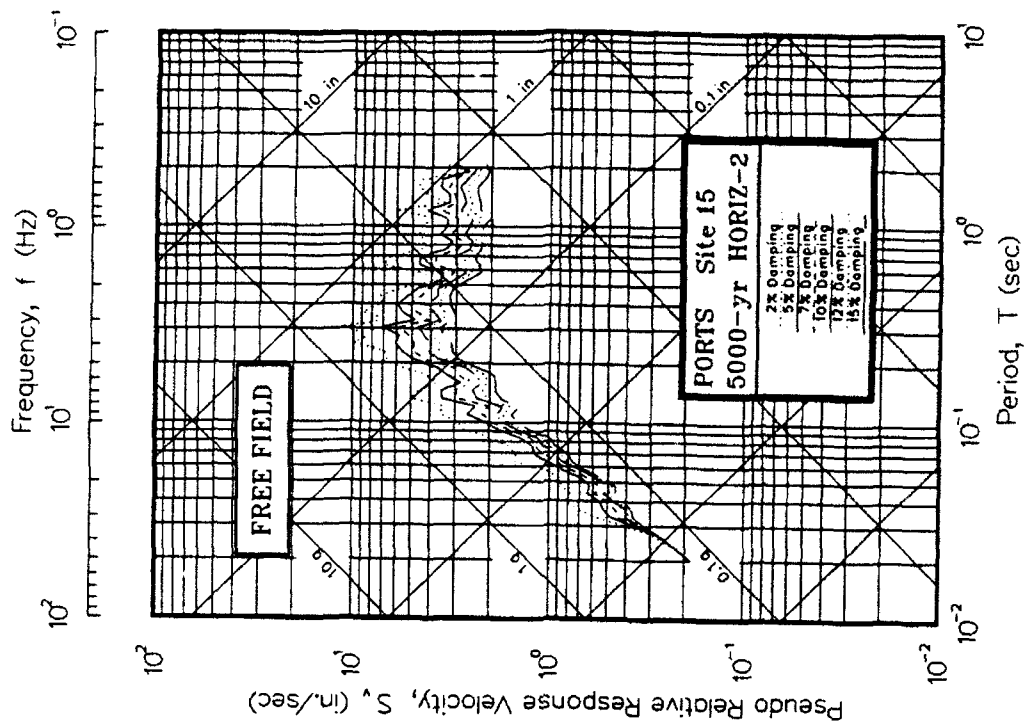
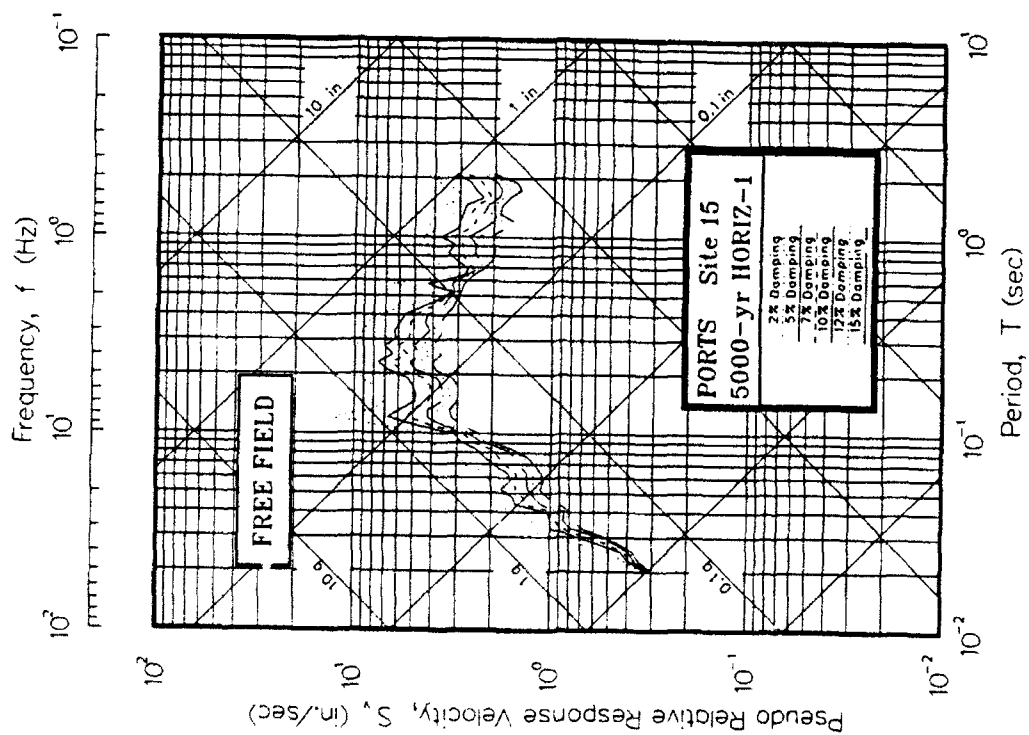


Figure P15. Psuedo-relative velocity spectra in tripartite form at free field for Site 15

APPENDIX Q: ACCELERATION SPECTRA FOR 5000-YEAR EVENT

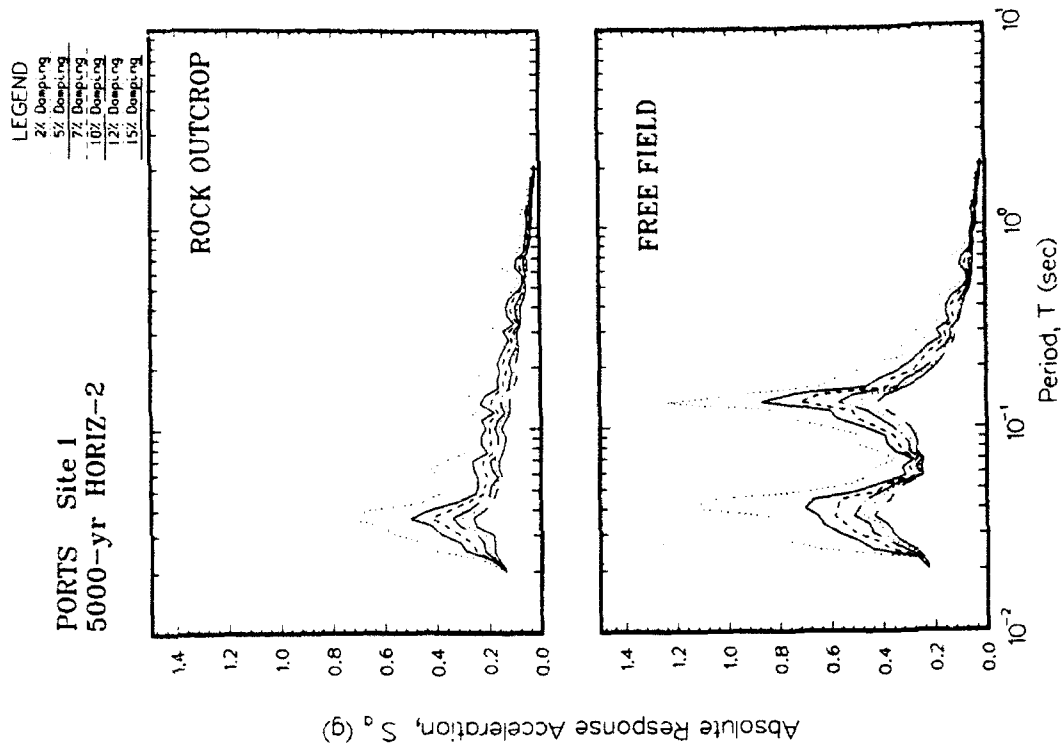
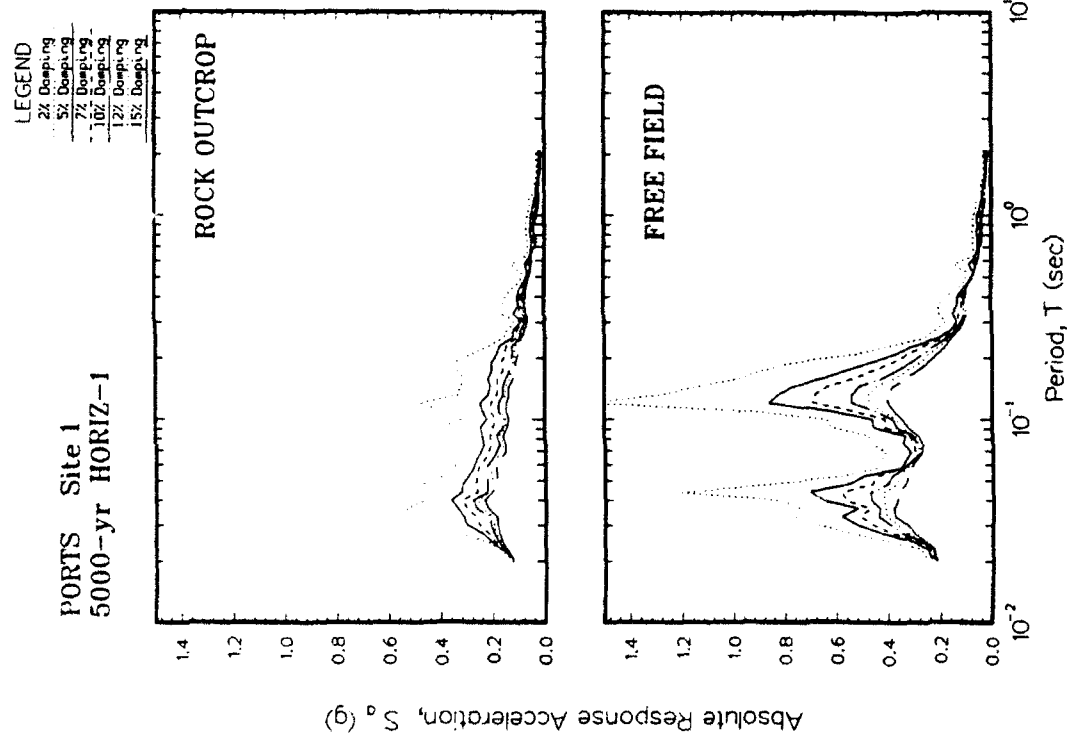


Figure Q1. Absolute acceleration response spectra at free field for Site 1

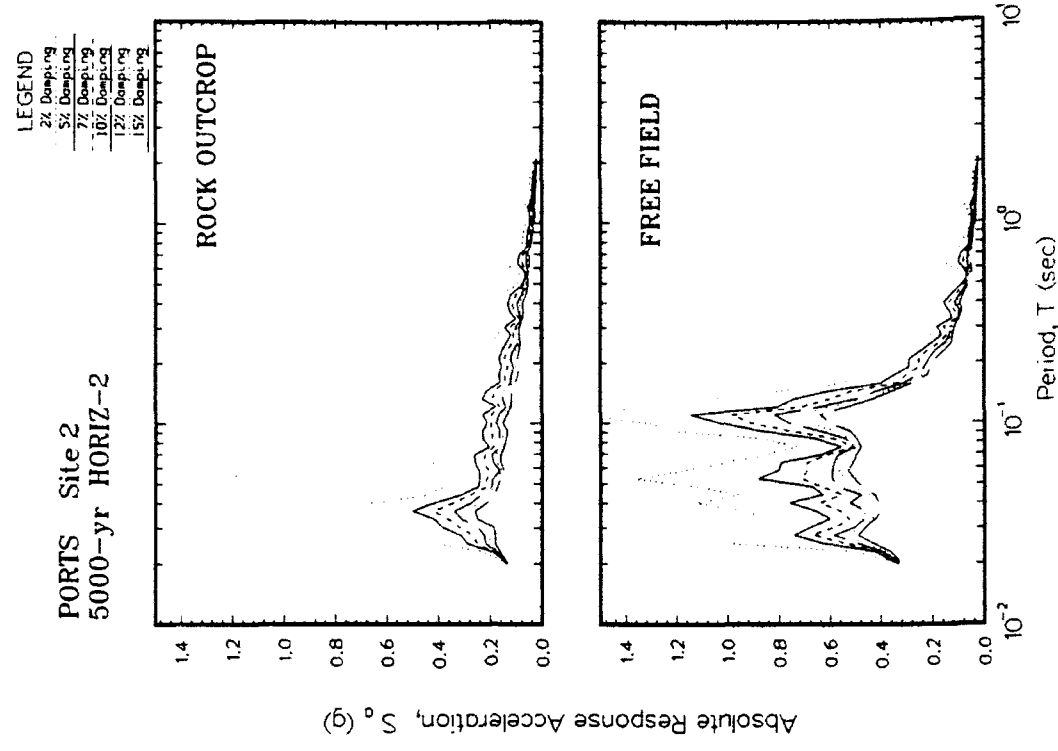
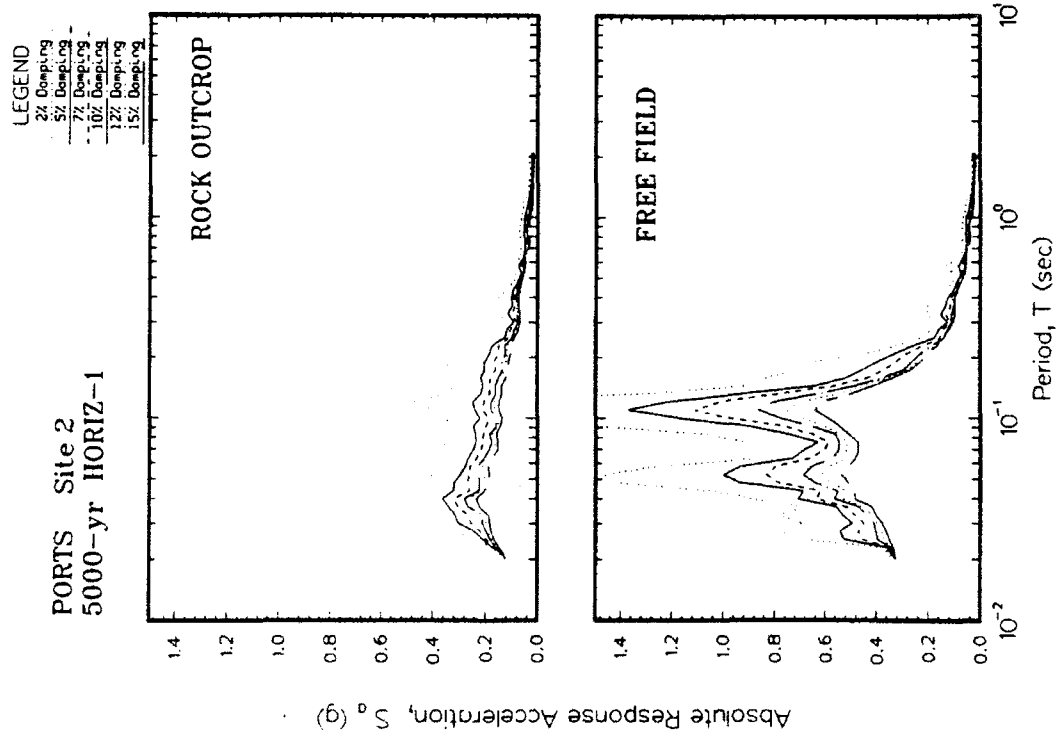


Figure Q2. Absolute acceleration response spectra at free field for Site 2

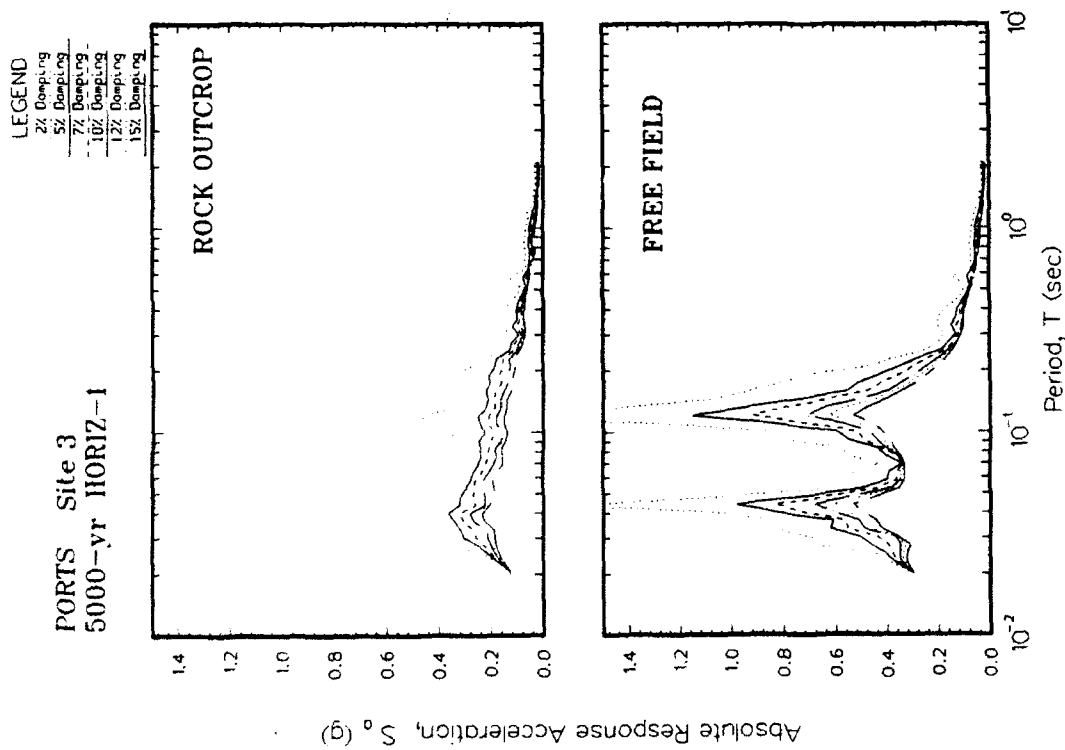
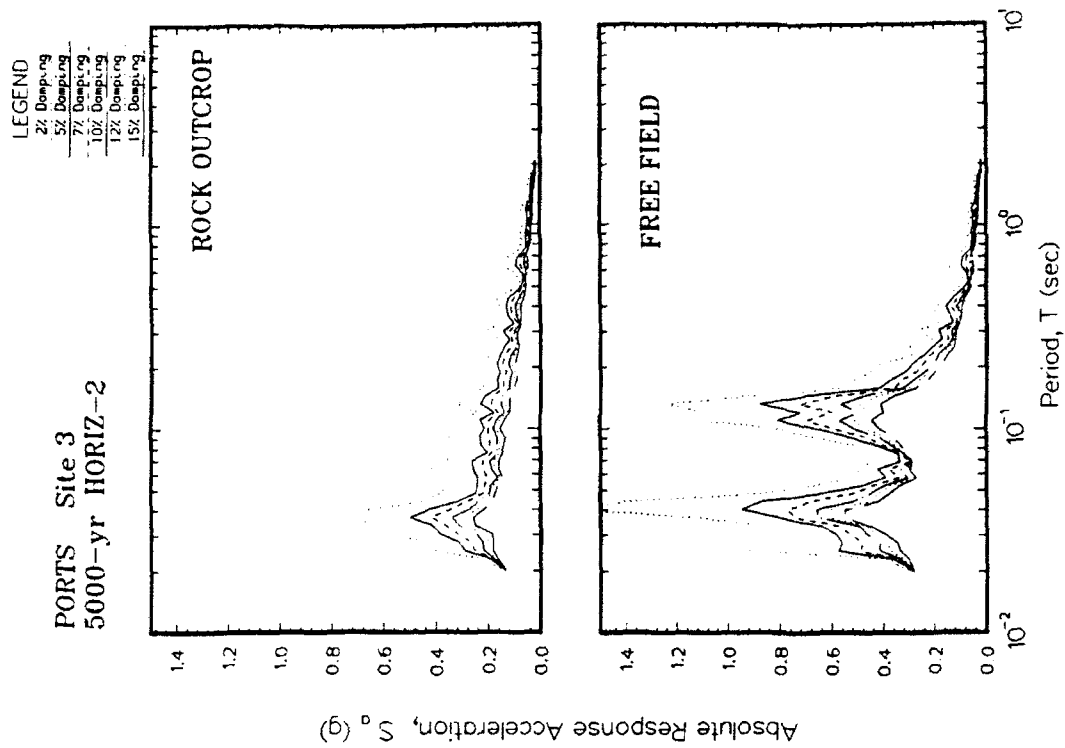


Figure Q3. Absolute acceleration response spectra at free field for Site 3

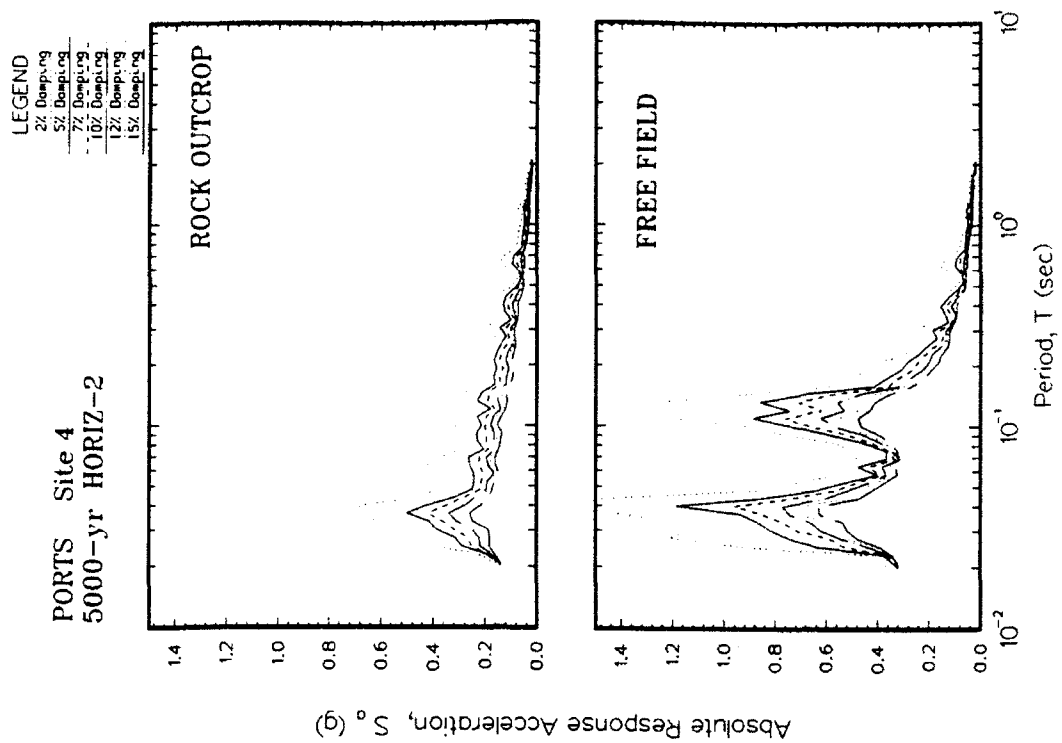
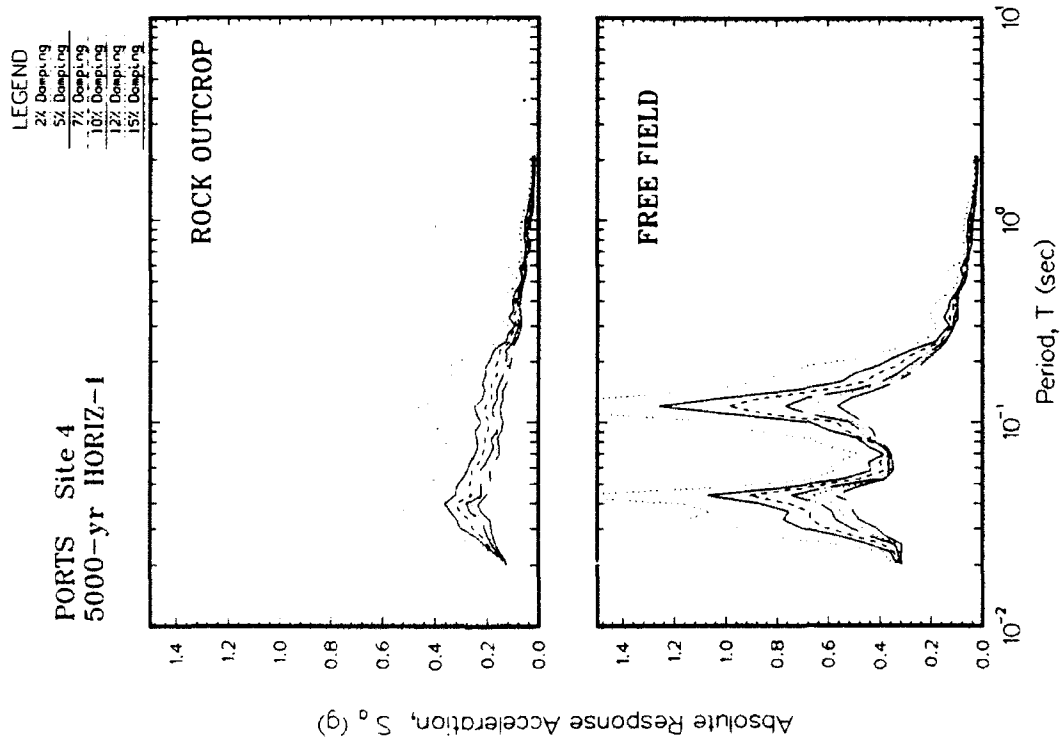


Figure Q4. Absolute acceleration response spectra at free field for Site 4

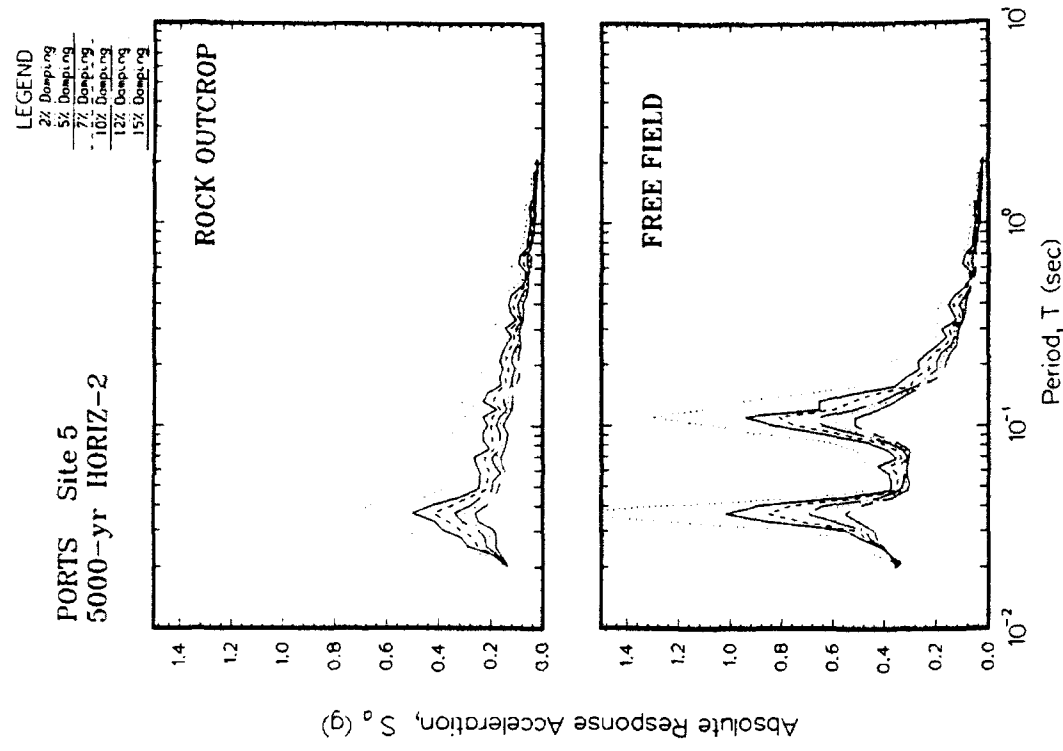
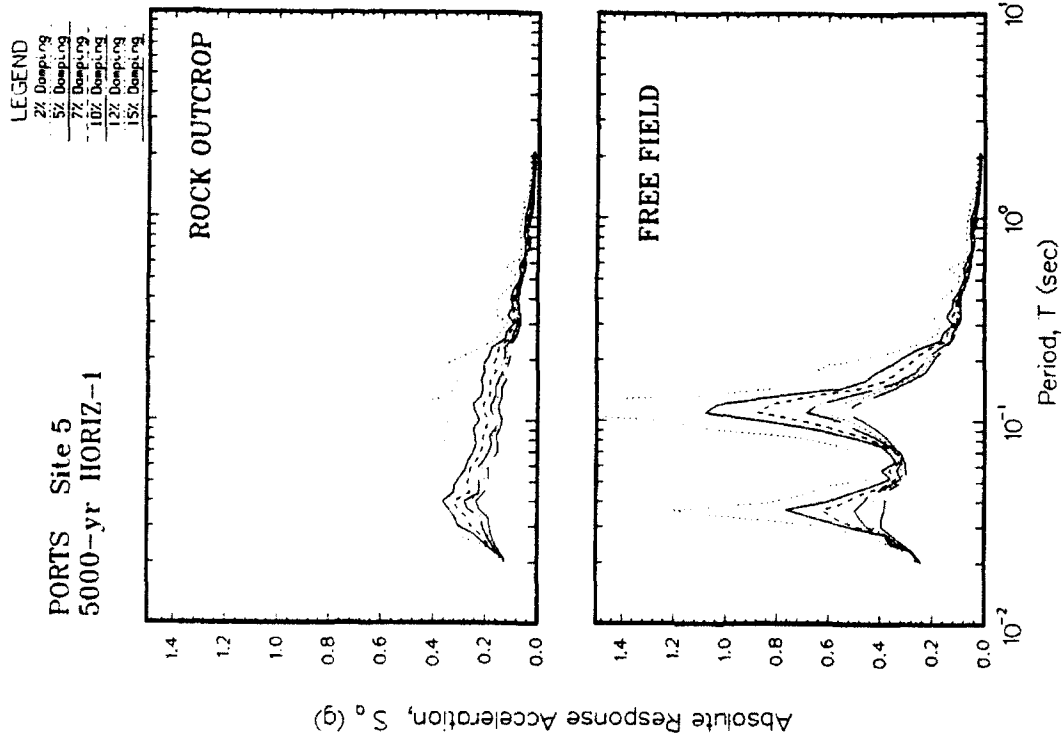


Figure Q5. Absolute acceleration response spectra at free field for Site 5

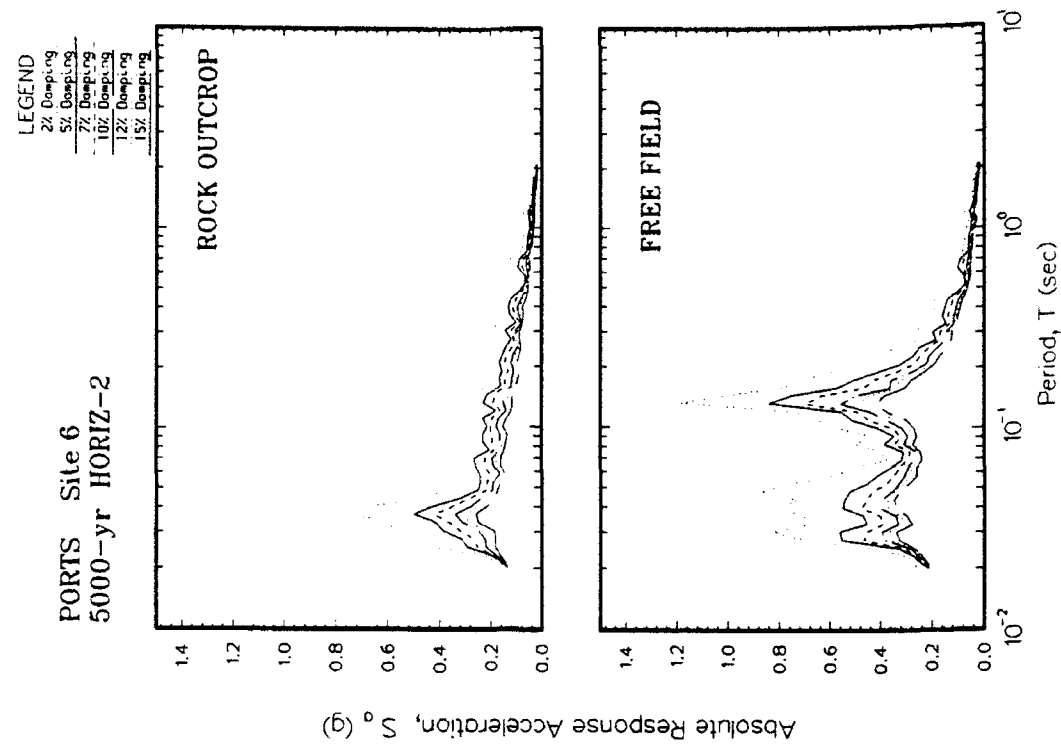
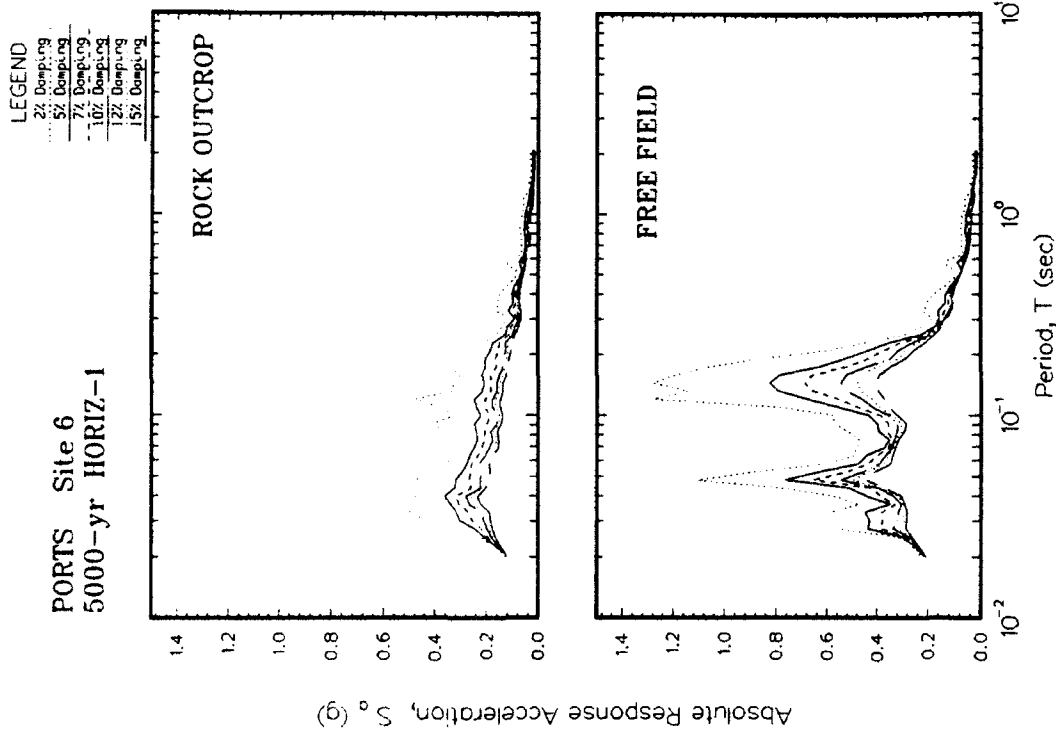


Figure Q6. Absolute acceleration response spectra at free field for Site 6

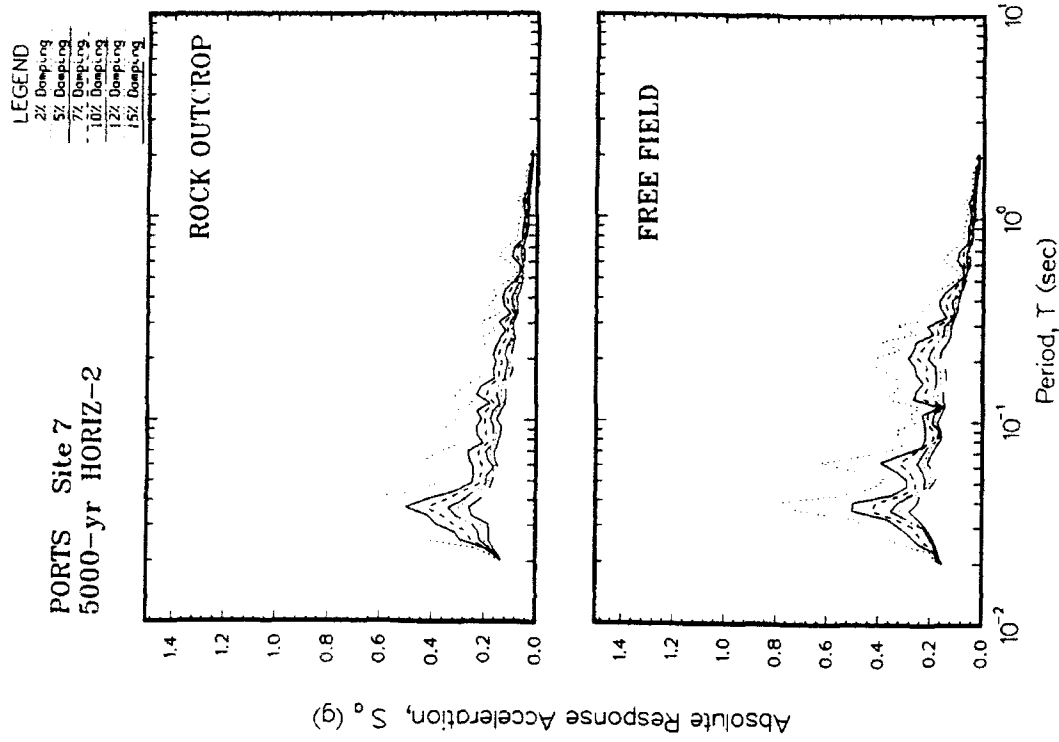
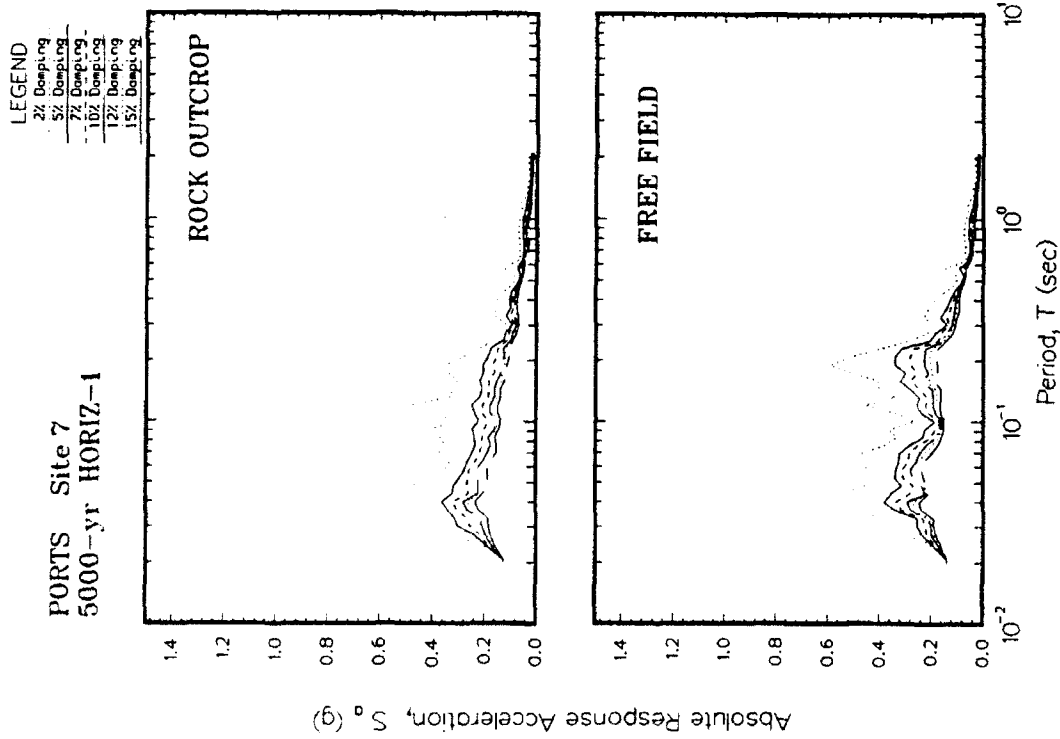


Figure Q7. Absolute acceleration response spectra at free field for Site 7

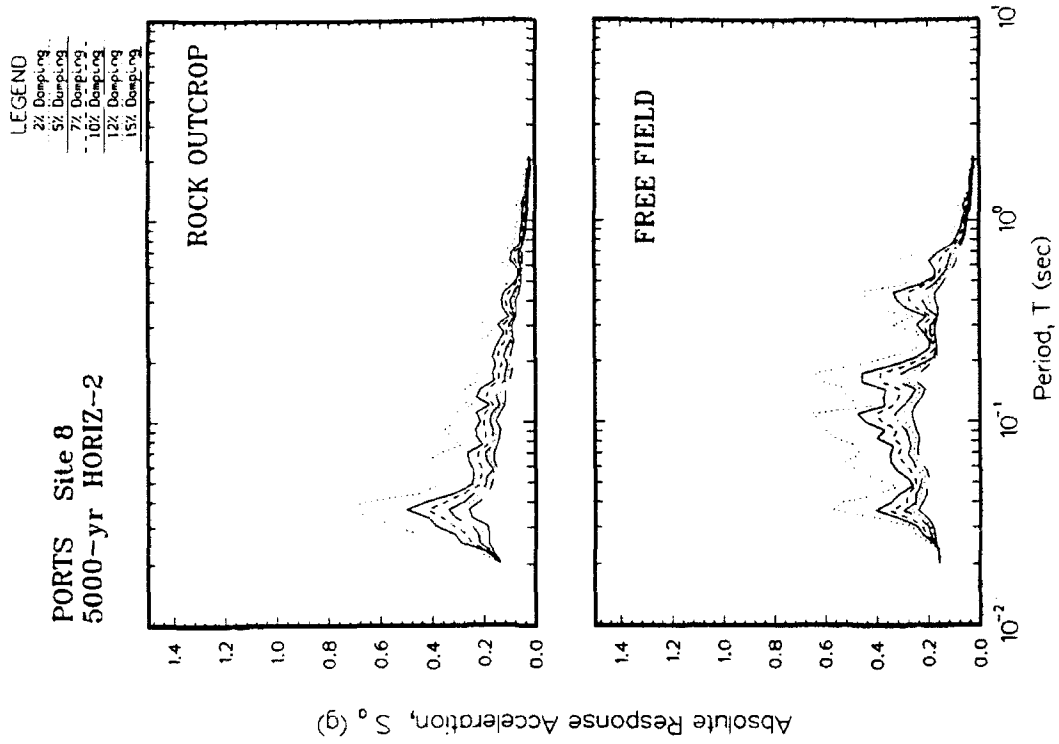
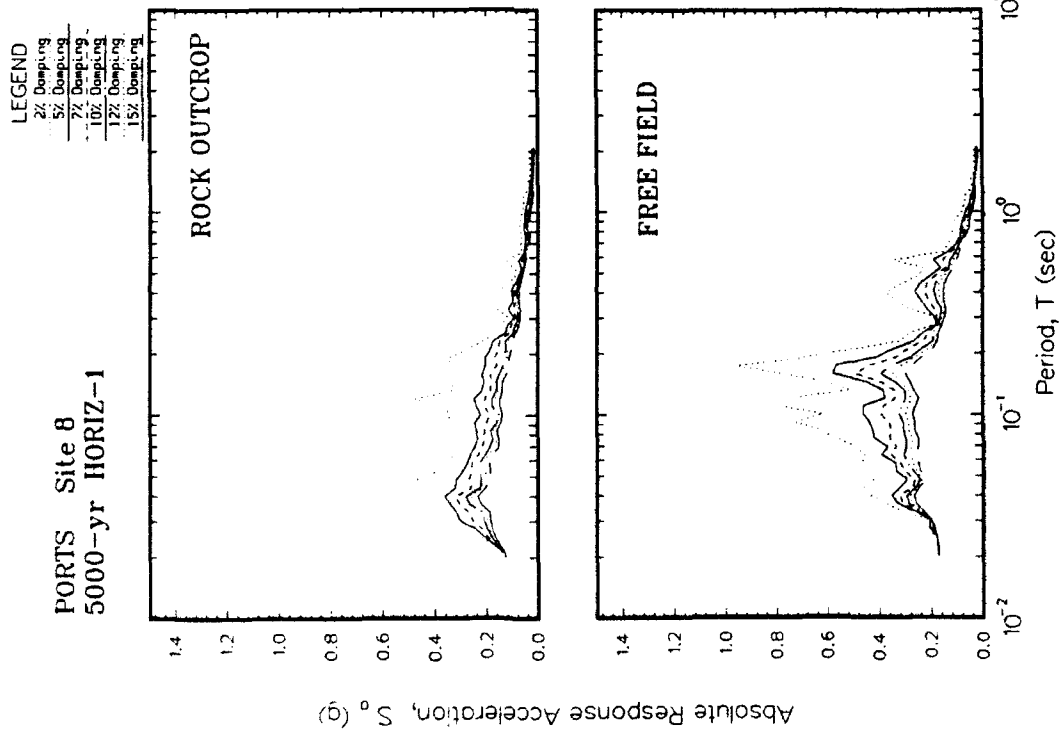


Figure Q8. Absolute acceleration response spectra at free field for Site 8

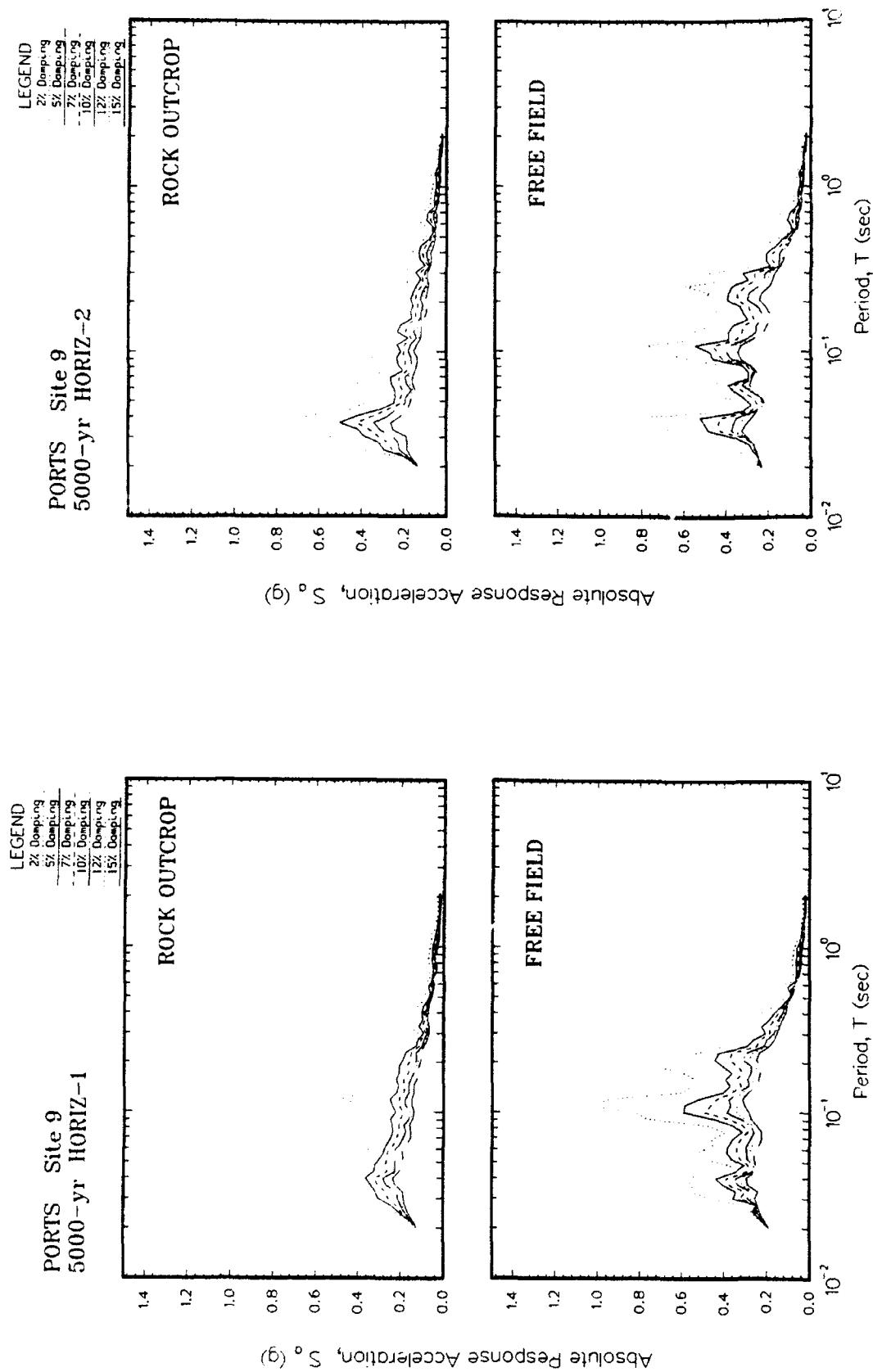


Figure Q9. Absolute acceleration response spectra at free field for Site 9

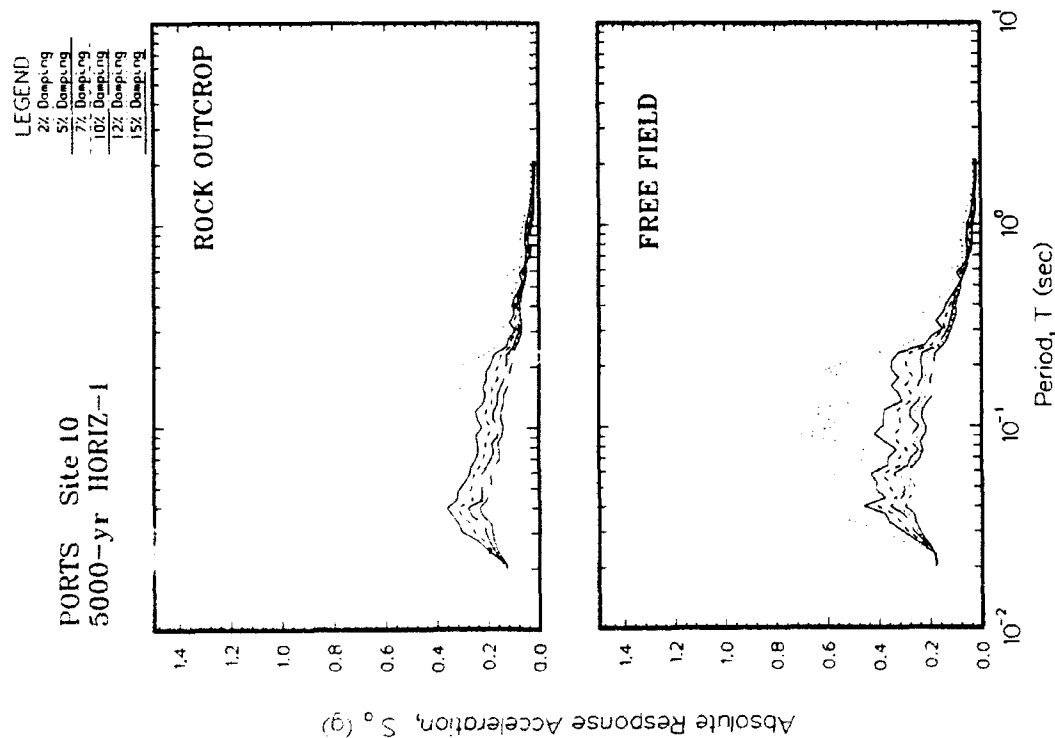
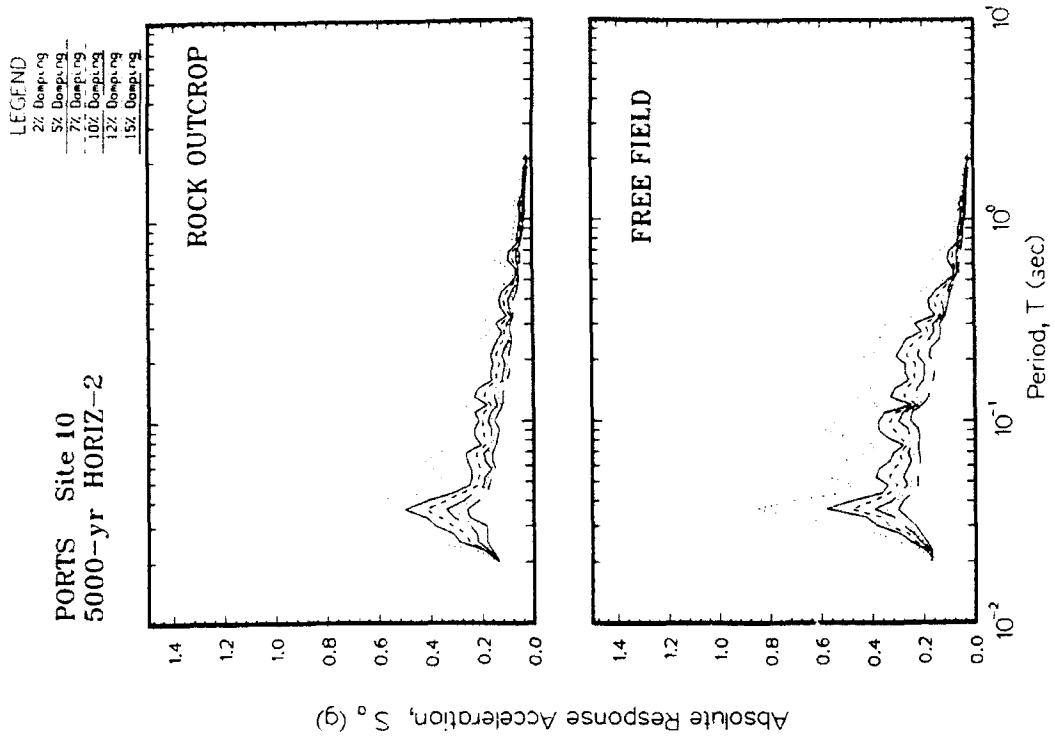


Figure Q10. Absolute acceleration response spectra at free field for Site 10

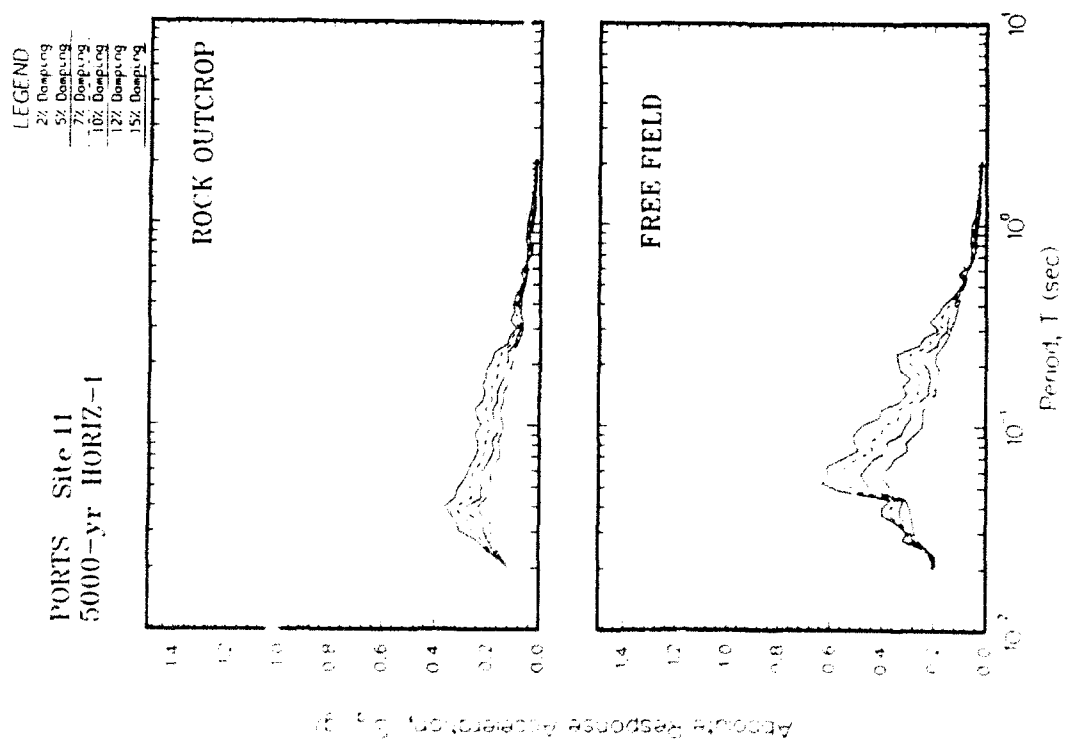
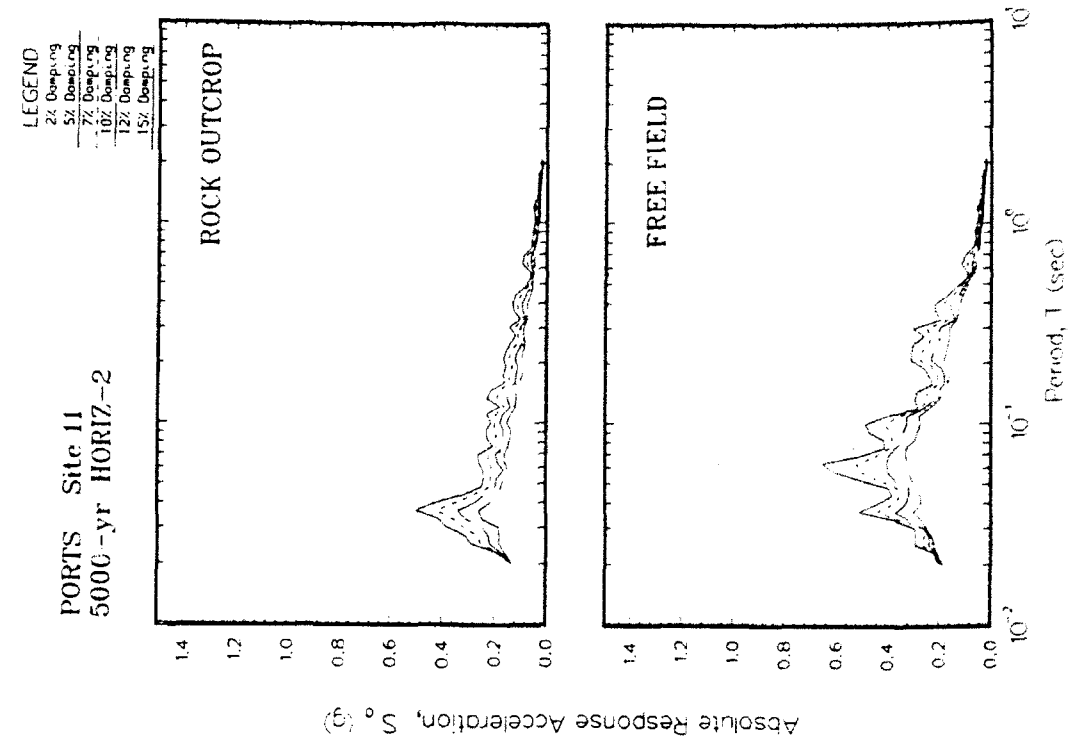


Figure Q11. Absolute acceleration response spectra at free field for Site 11

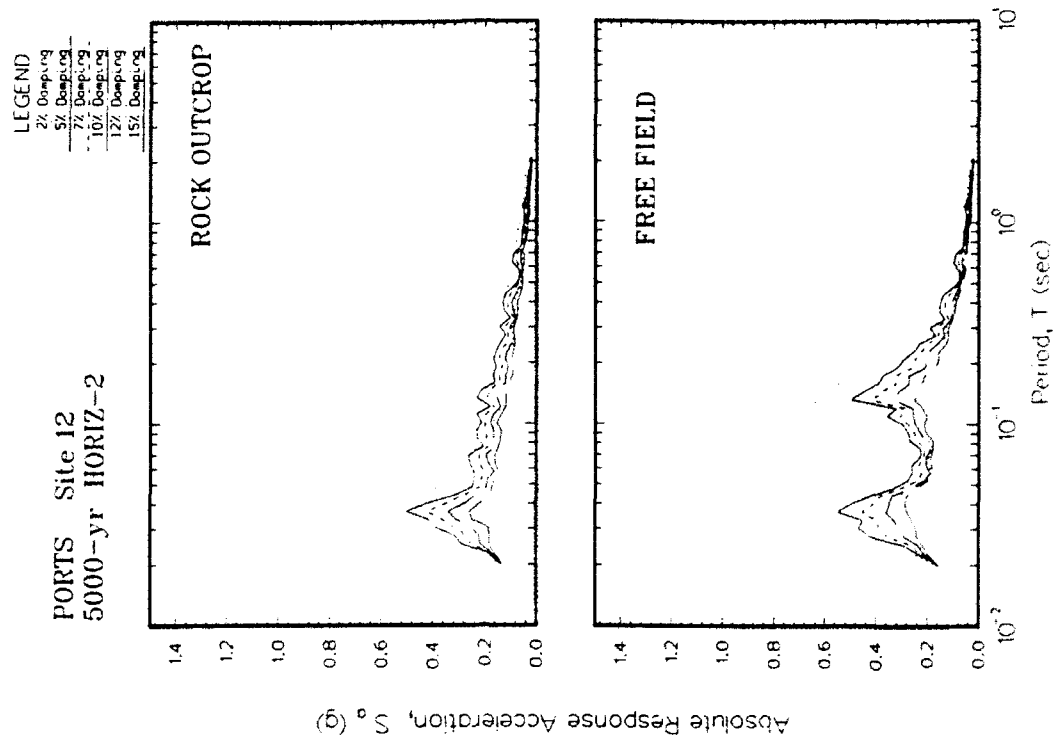
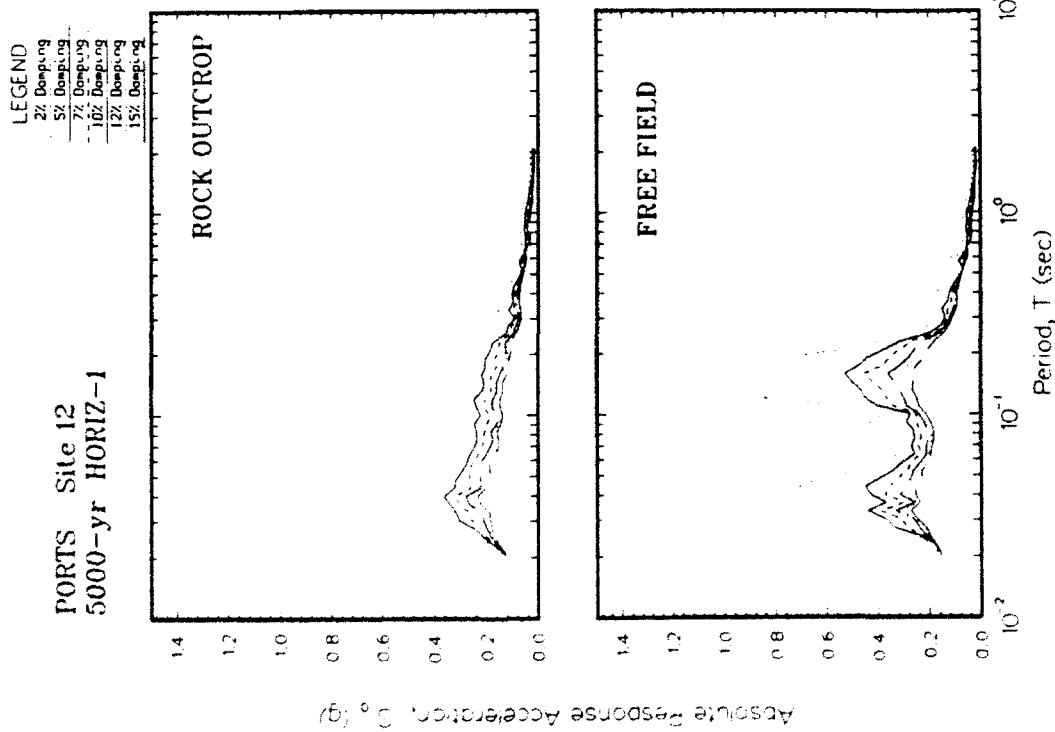


Figure Q12. Absolute acceleration response spectra at free field for Site 12

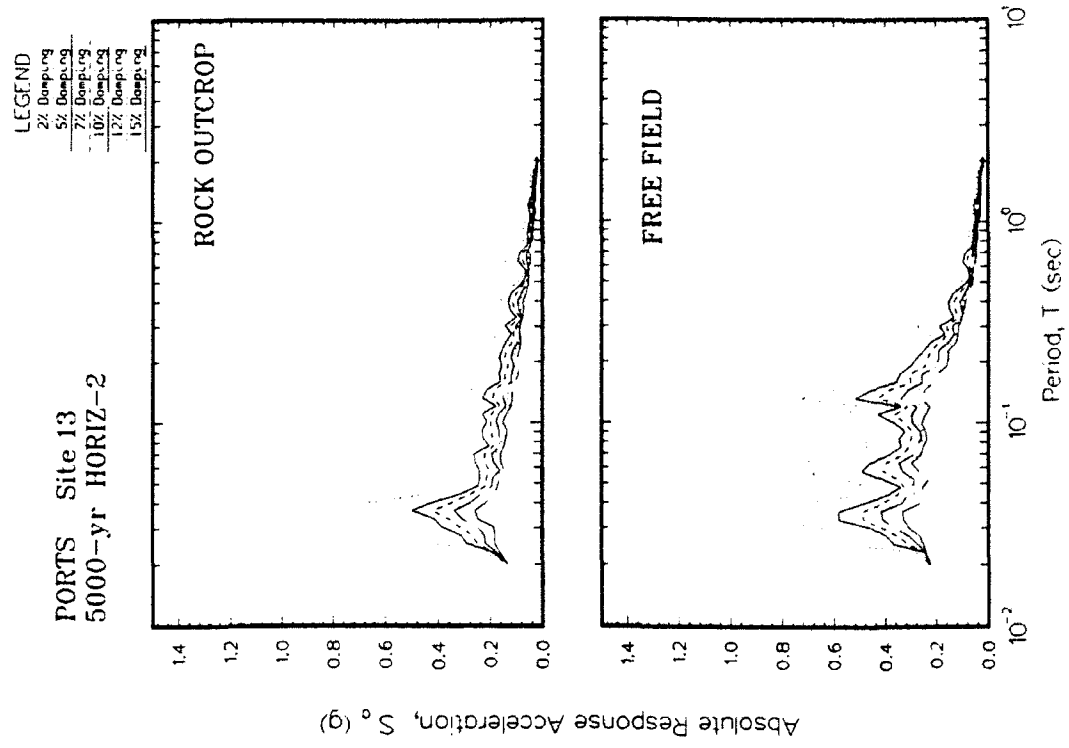
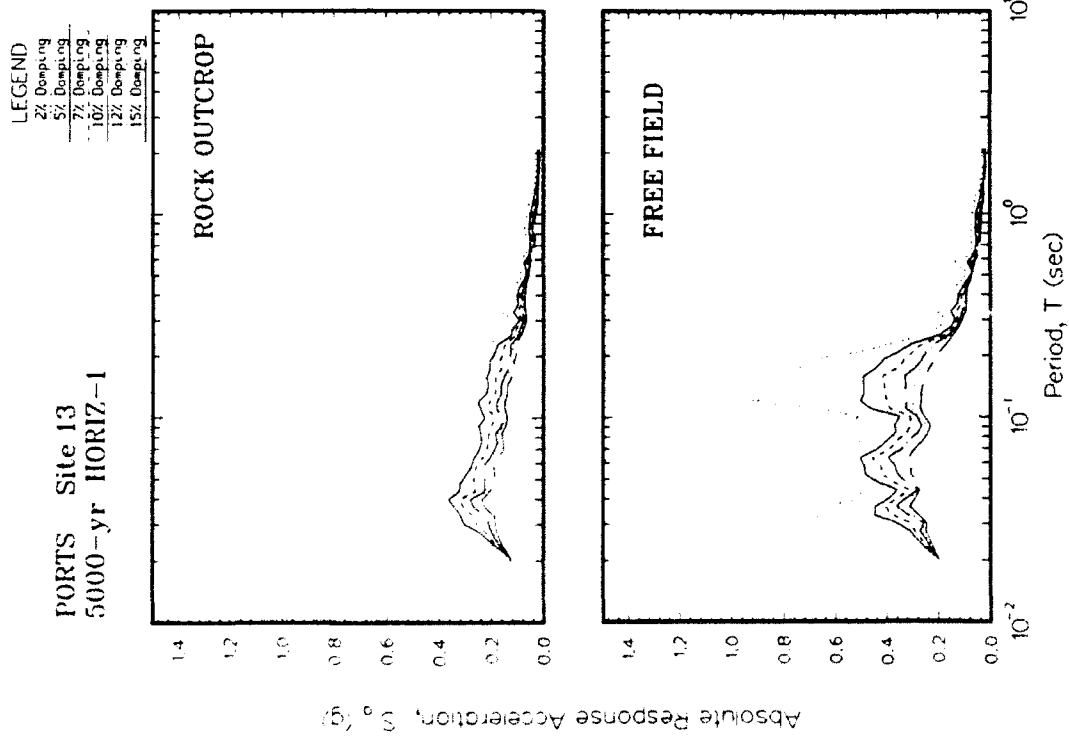


Figure Q13. Absolute acceleration response spectra at free field for Site 13

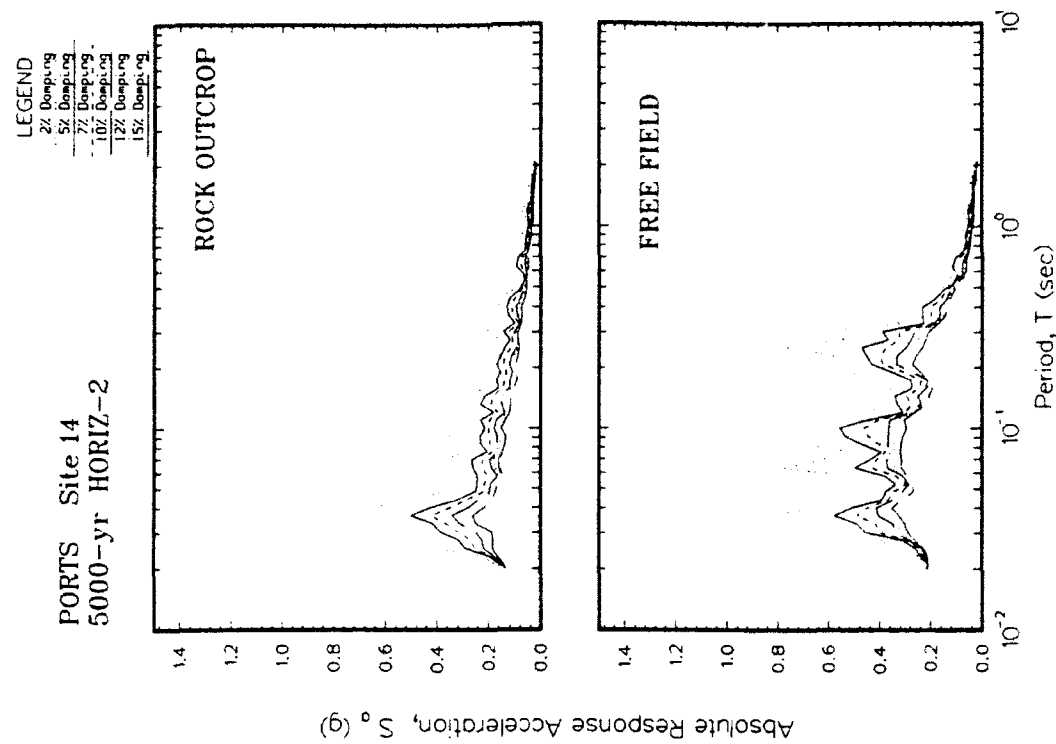
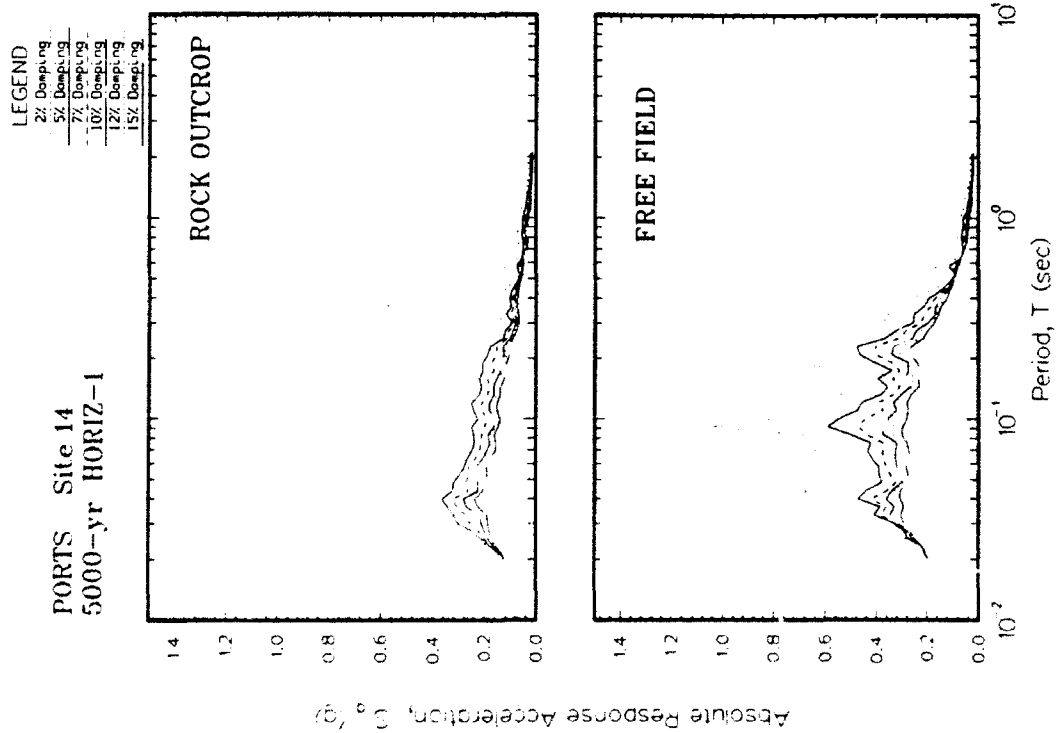


Figure Q14. Absolute acceleration response spectra at free field for Site 14

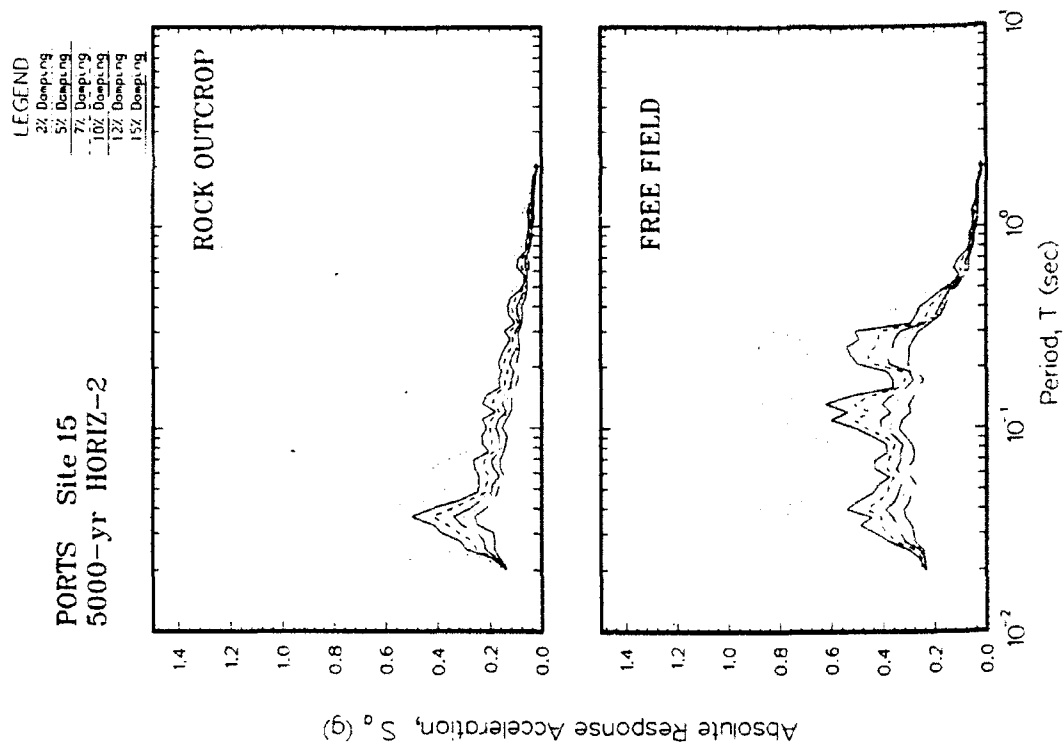
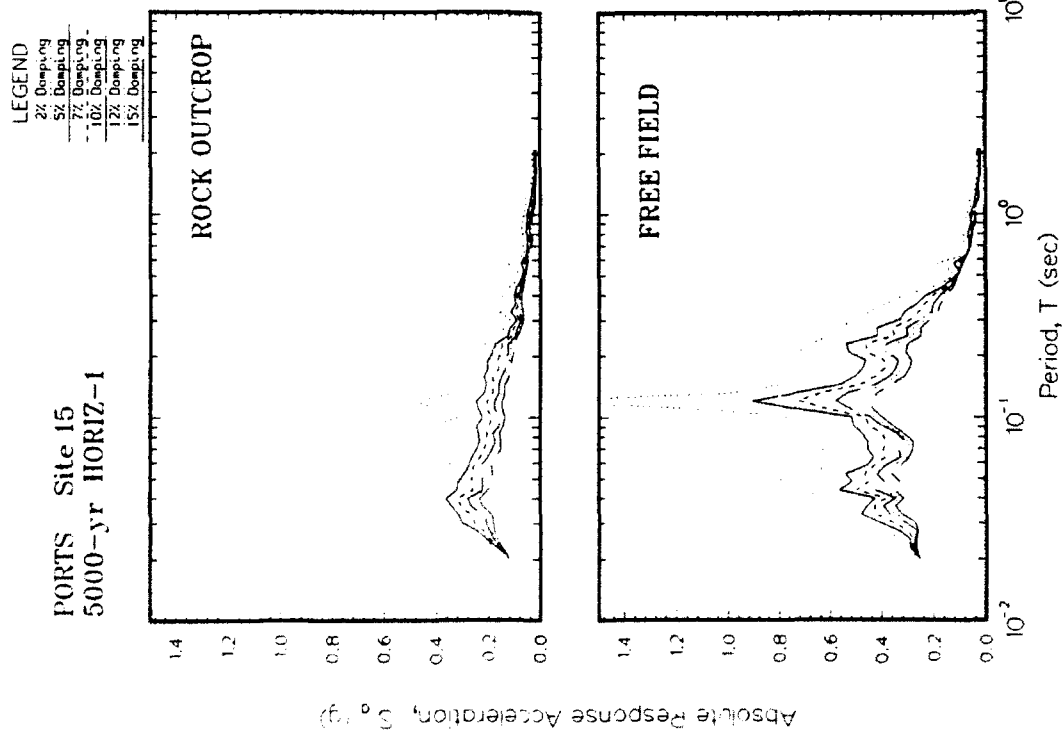


Figure Q15. Absolute acceleration response spectra at free field for Site 15

APPENDIX R: RATIO OF ACCELERATION SPECTRA FOR 5000-YEAR EVENT

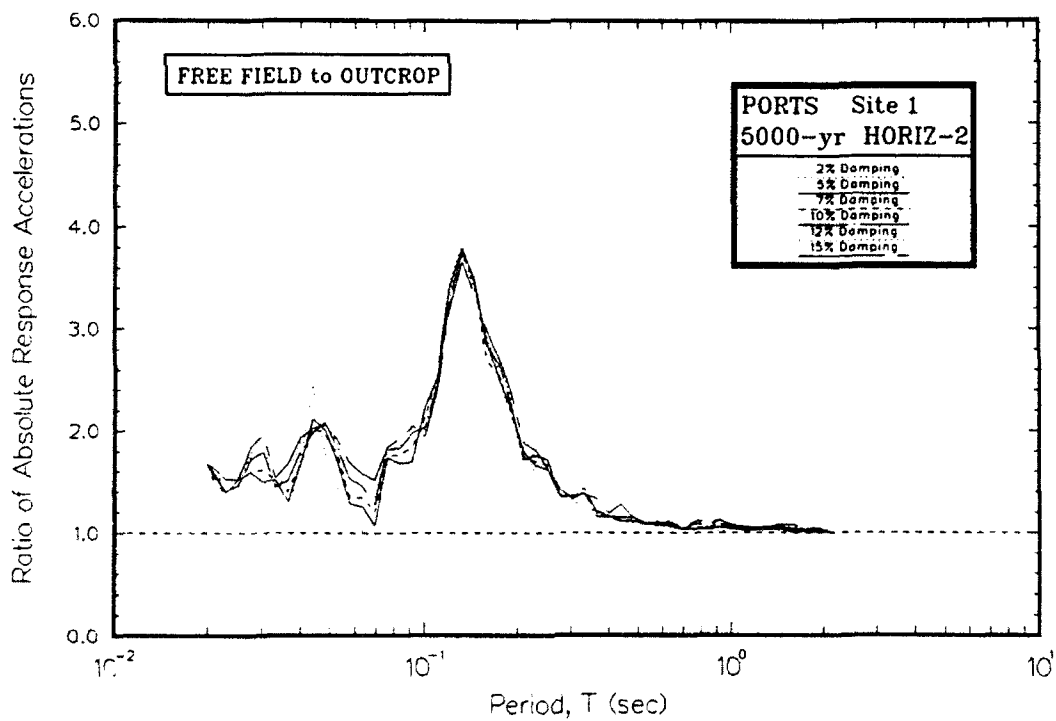
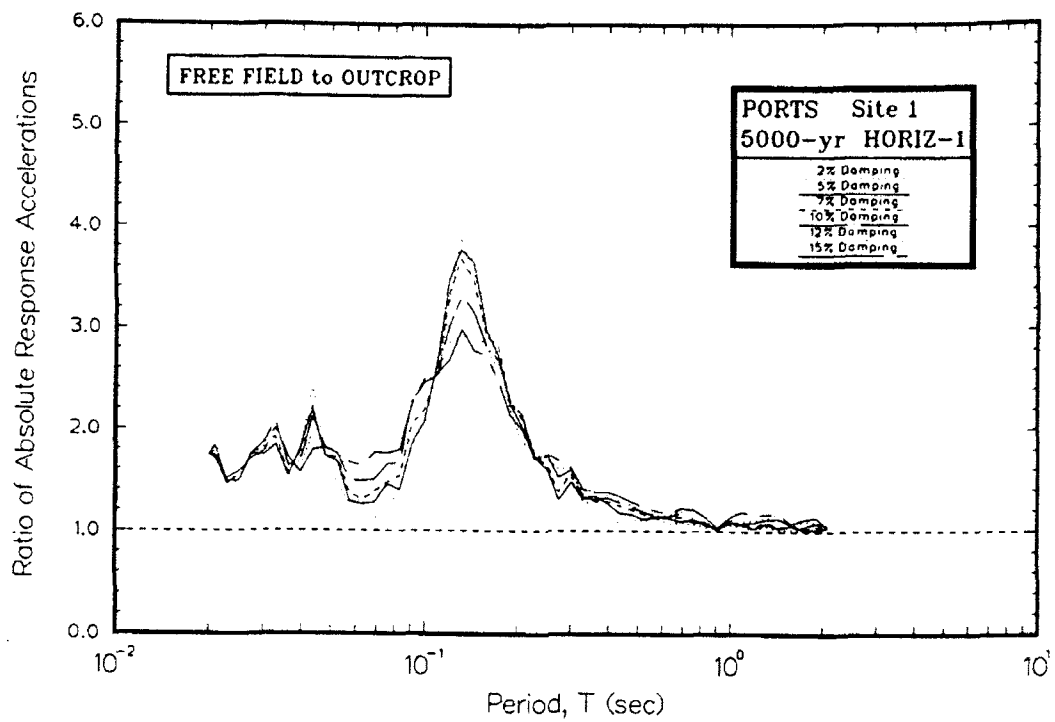


Figure R1. Ratio of absolute acceleration response spectra at free field to rock for Site 1

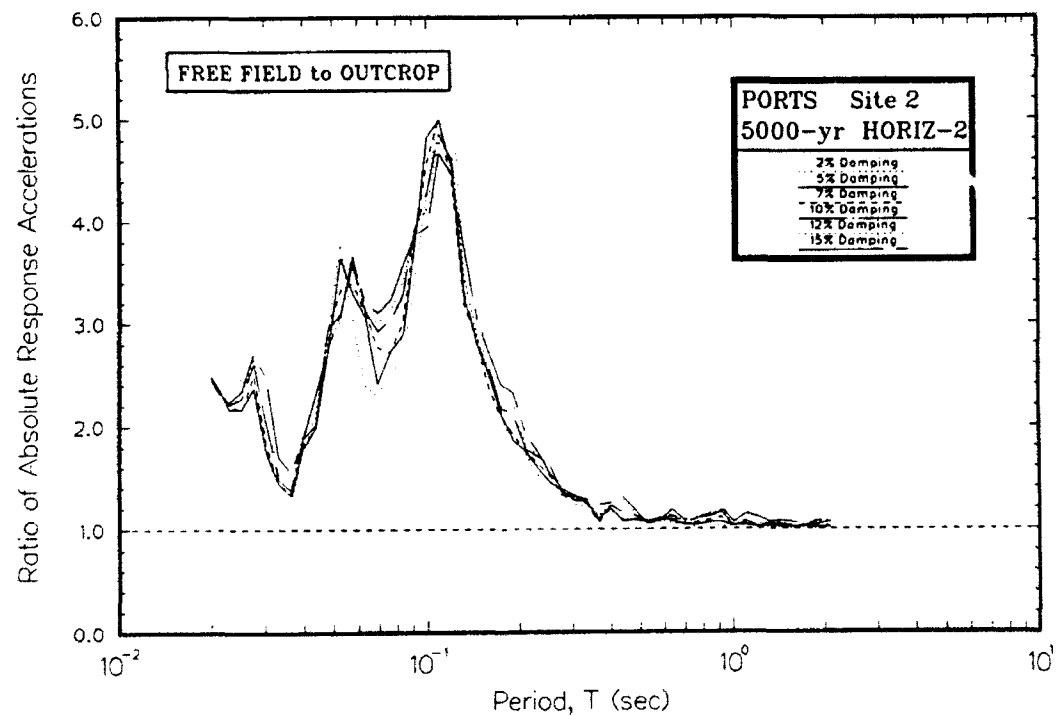
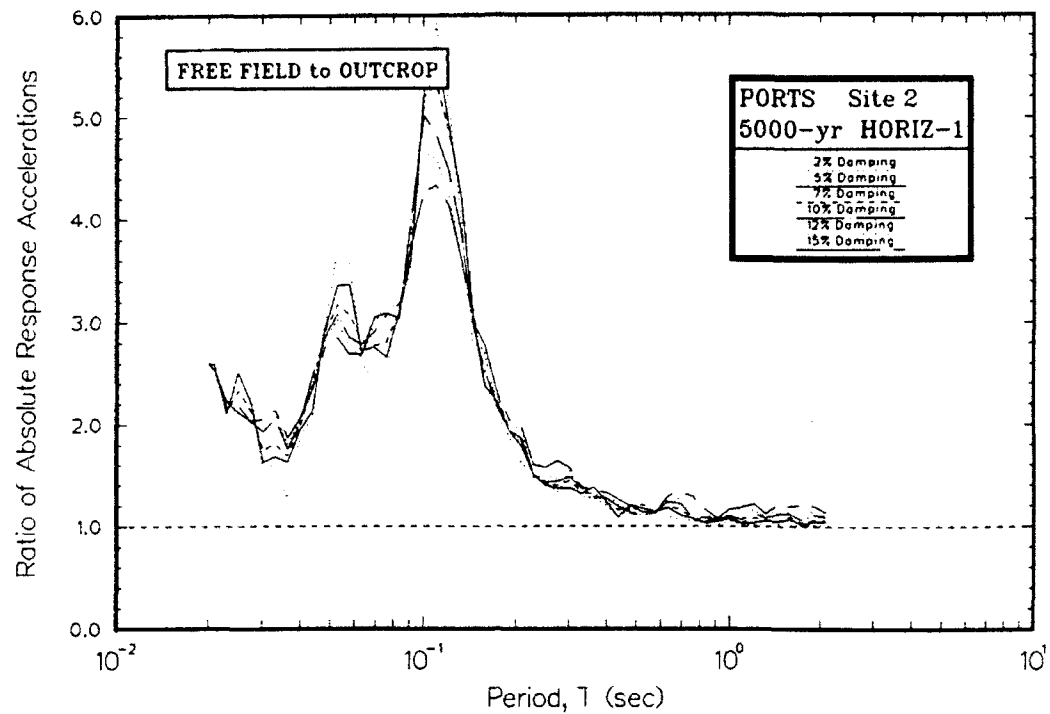


Figure R2. Ratio of absolute acceleration response spectra at free field to rock for Site 2

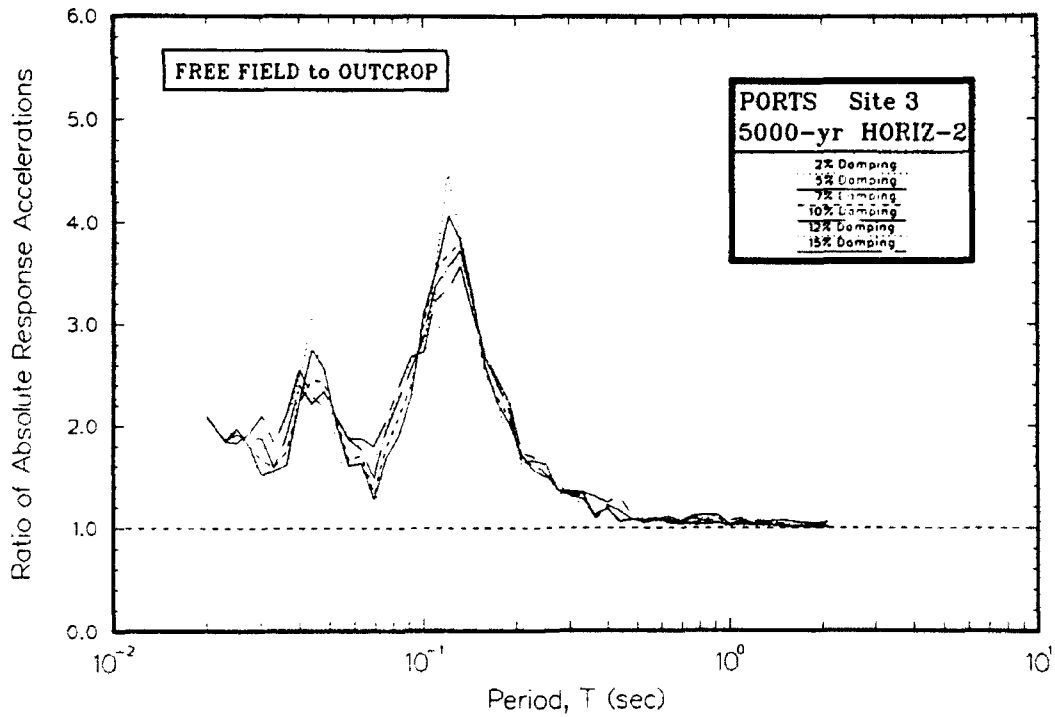
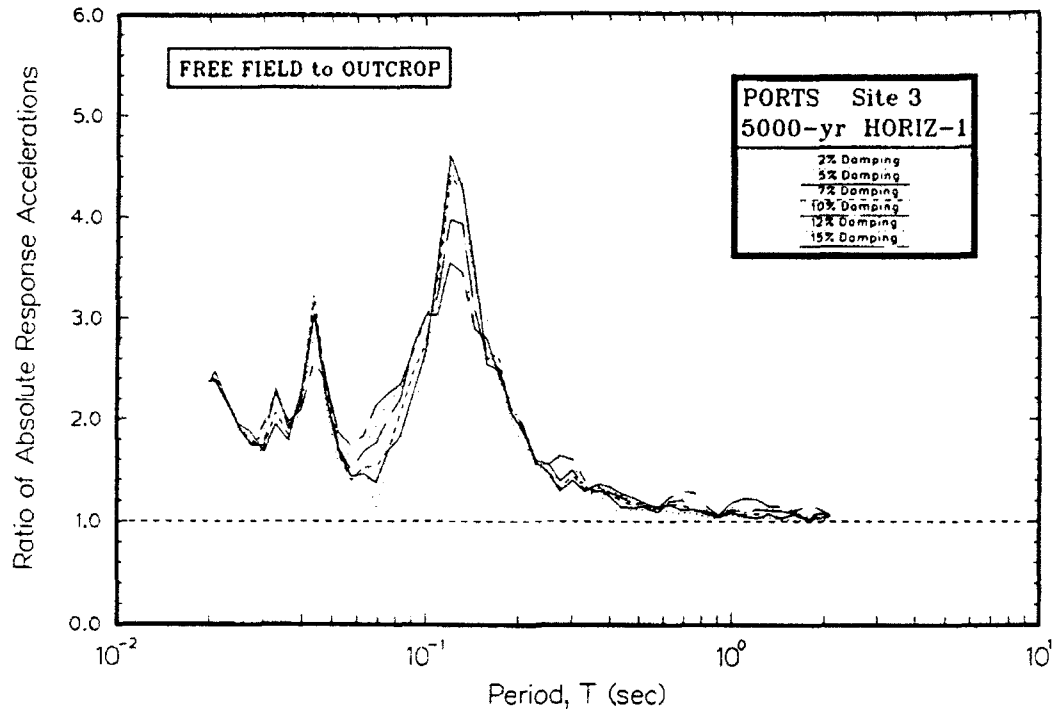


Figure R3. Ratio of absolute acceleration response spectra at free field to rock for Site 3

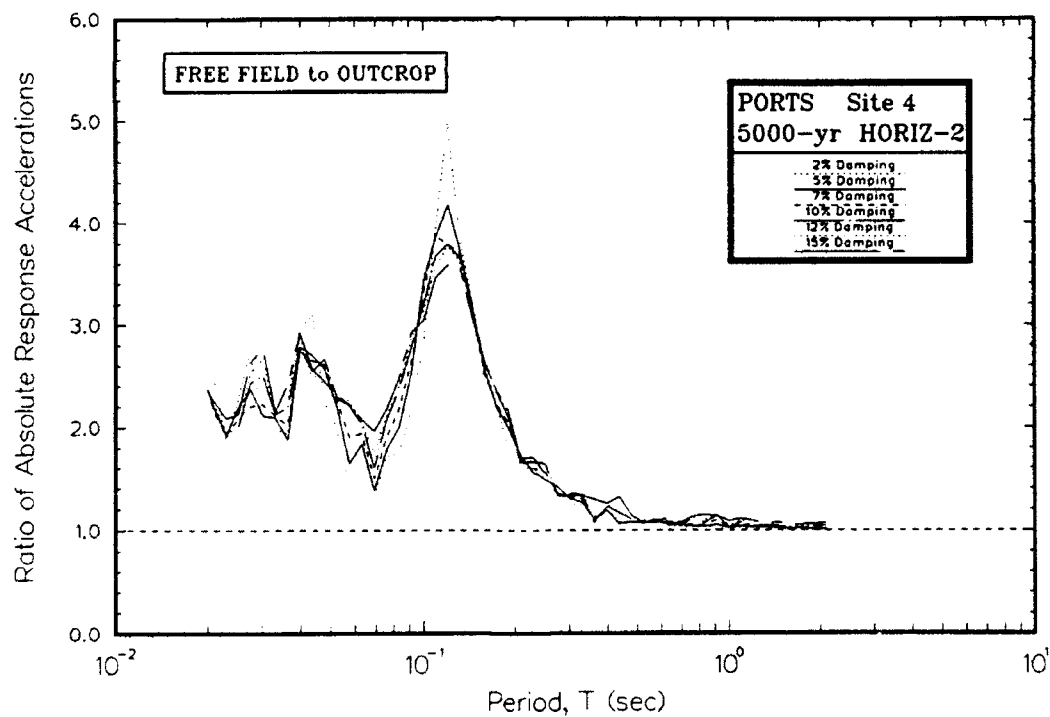
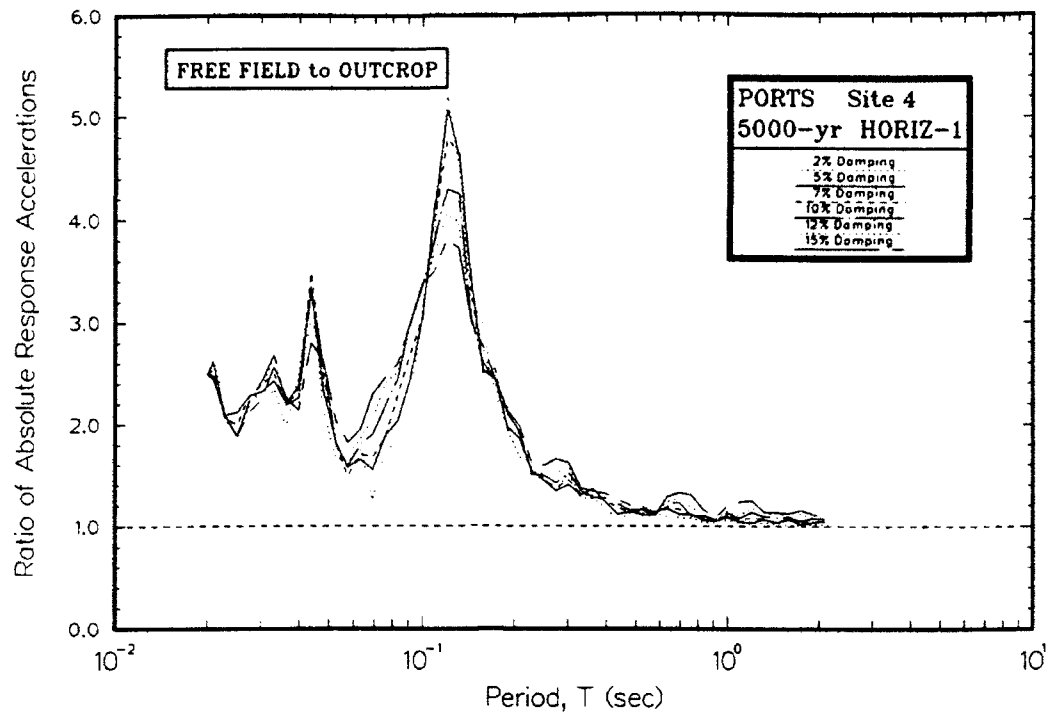


Figure R4. Ratio of absolute acceleration response spectra at free field to rock for Site 4

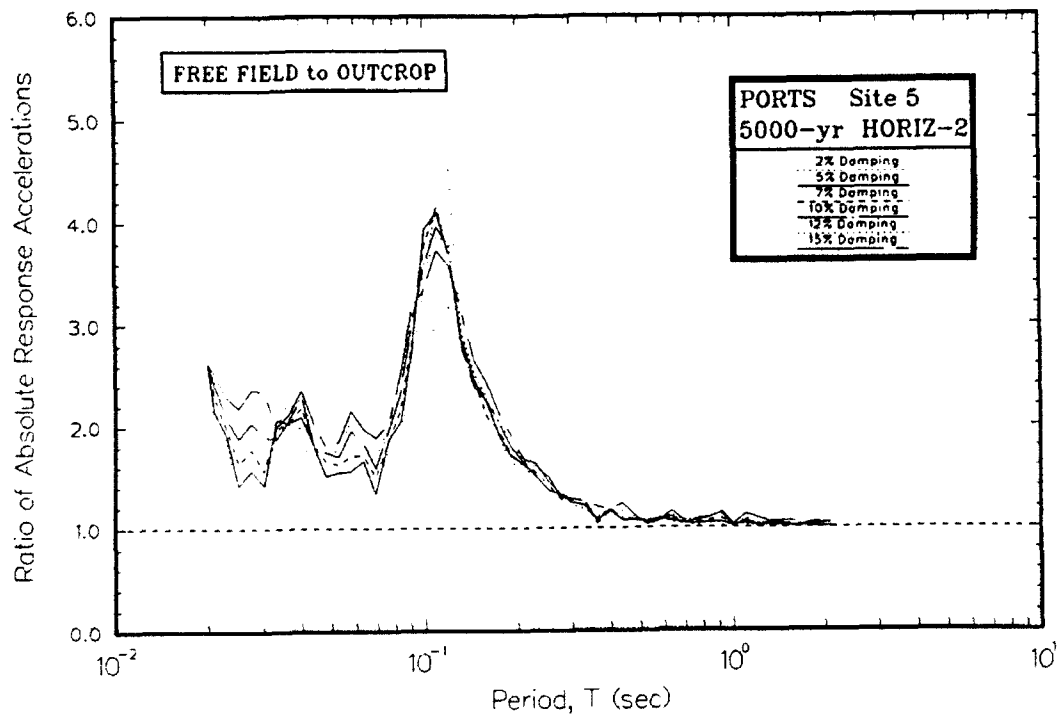
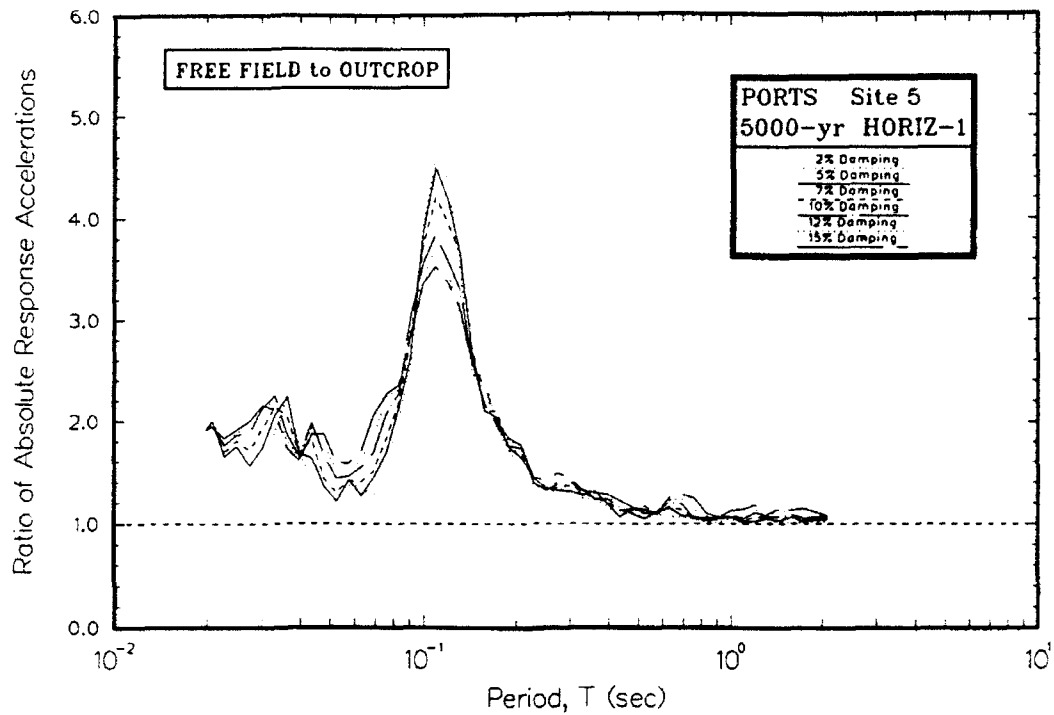


Figure R5. Ratio of absolute acceleration response spectra at free field to rock for Site 5

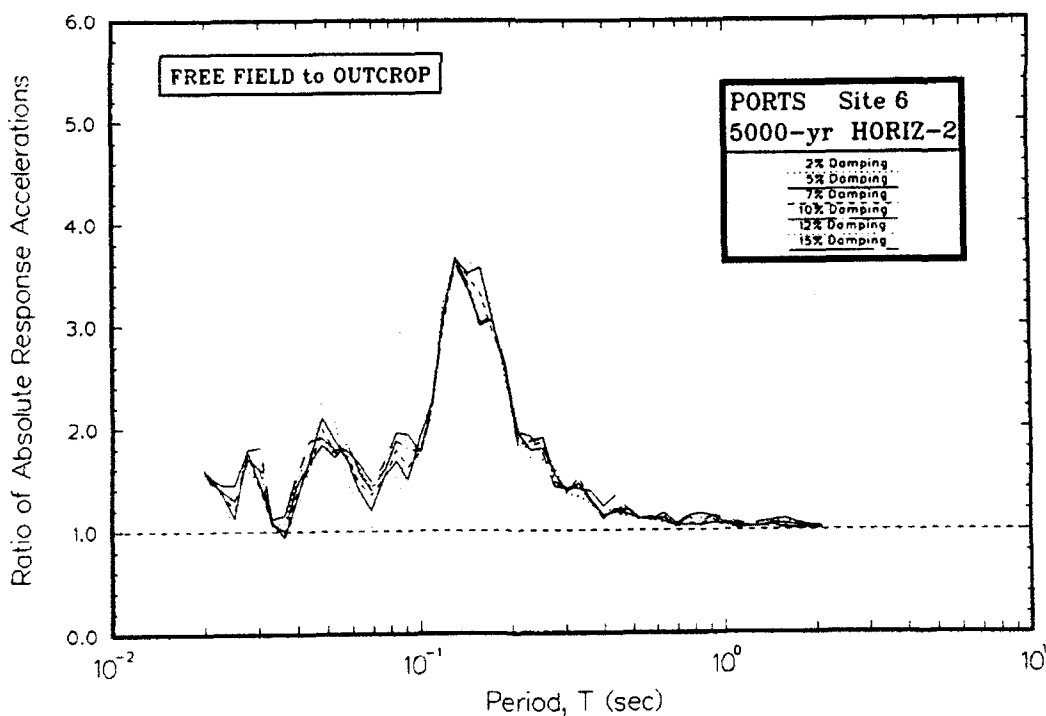
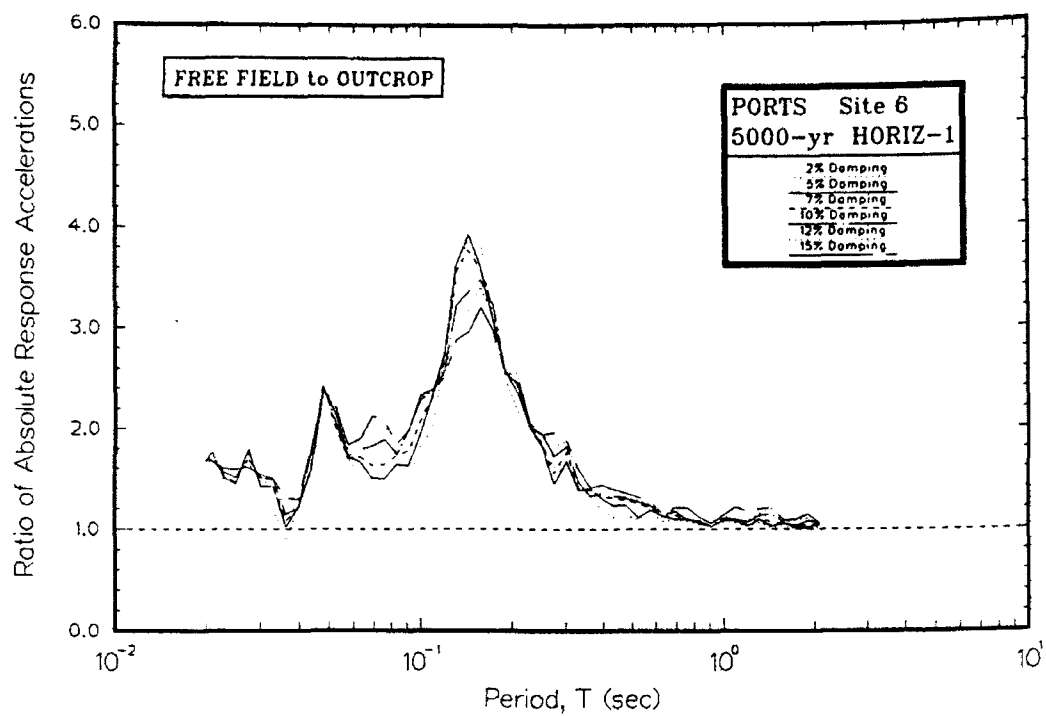


Figure R6. Ratio of absolute acceleration response spectra at free field to rock for Site 6

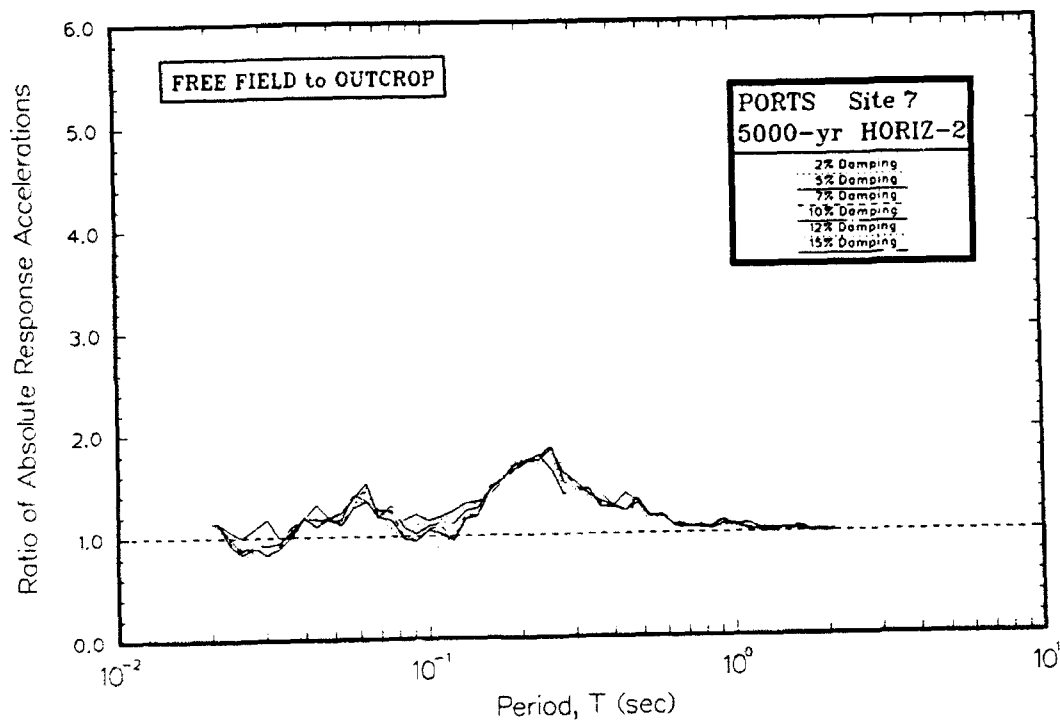
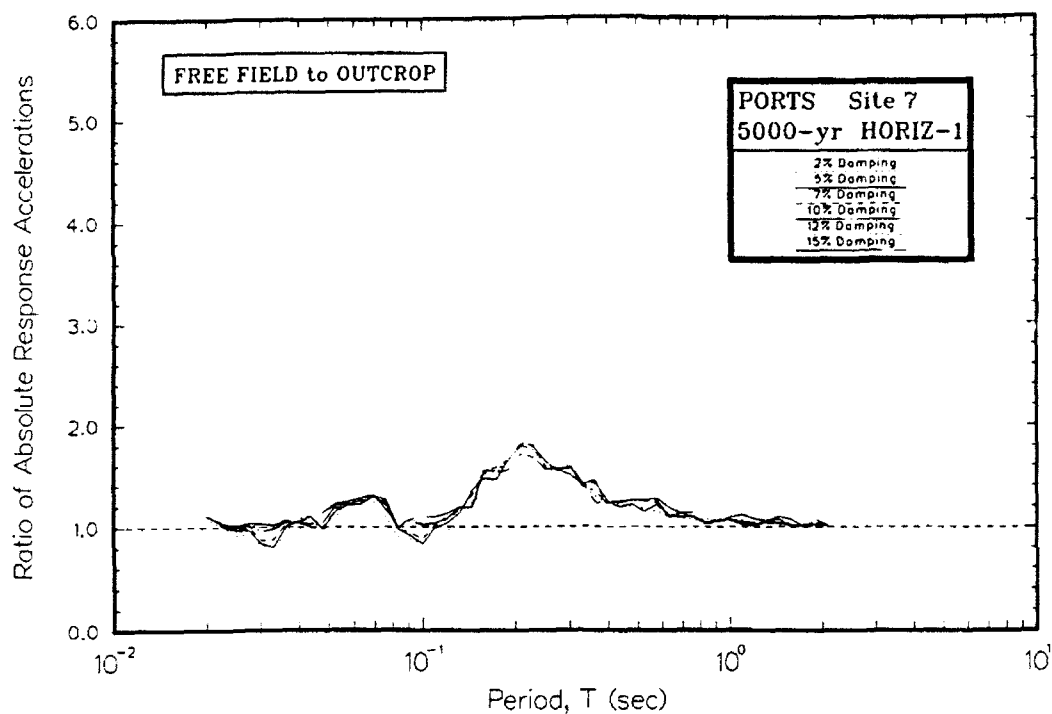


Figure R7. Ratio of absolute acceleration response spectra at free field to rock for Site 7

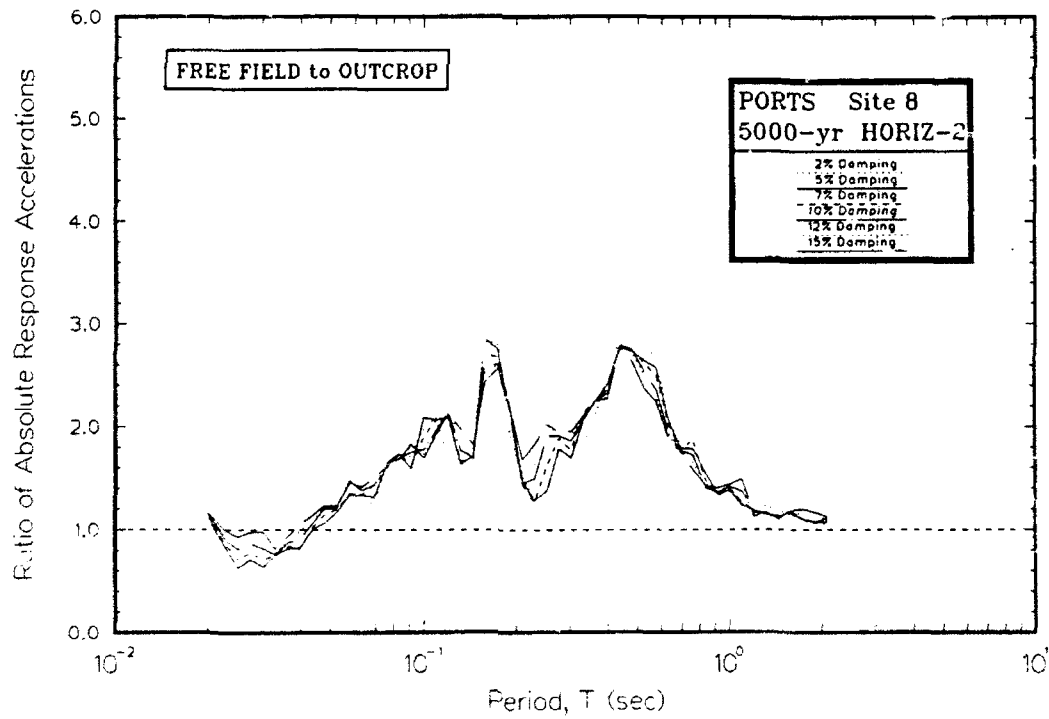
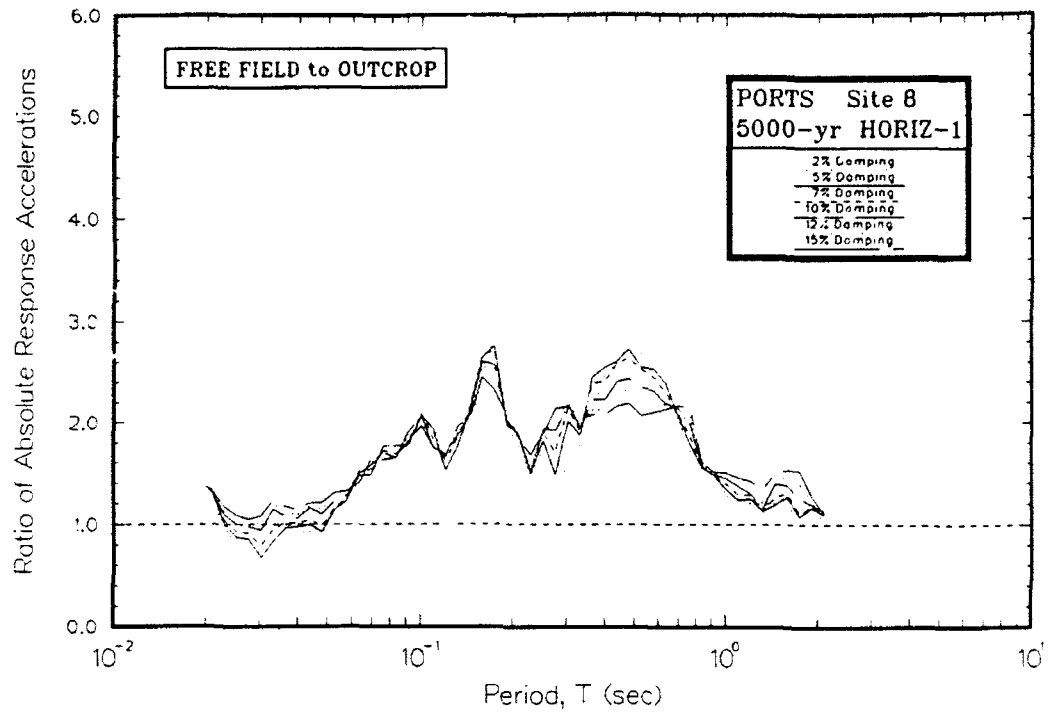


Figure R8. Ratio of absolute acceleration response spectra at free field to rock for Site 8

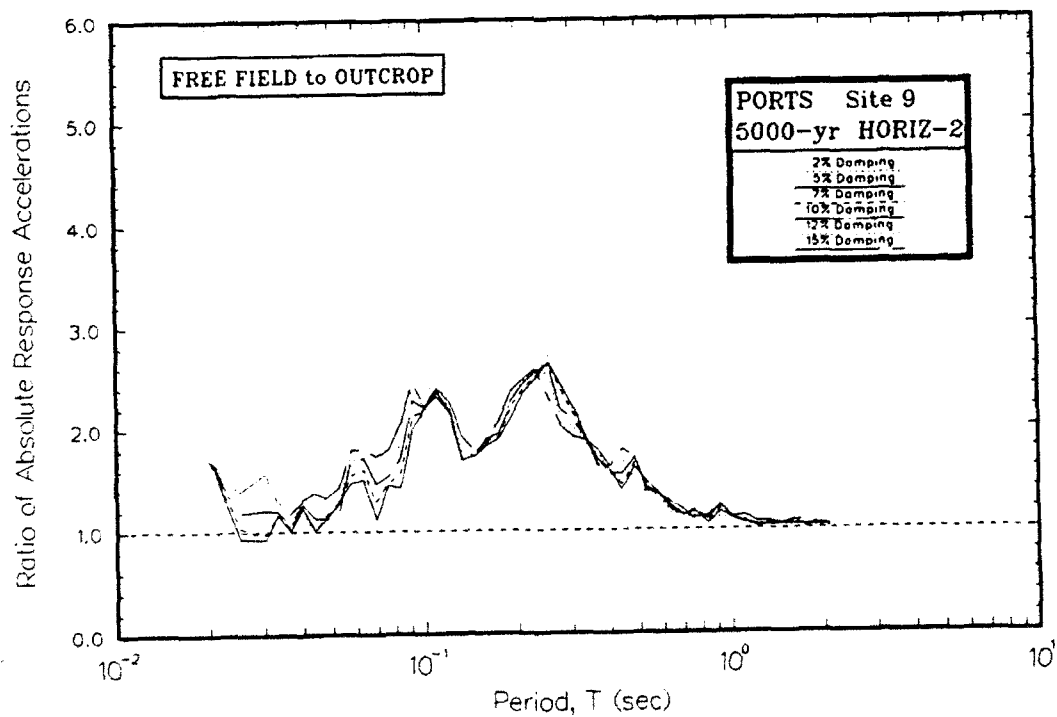
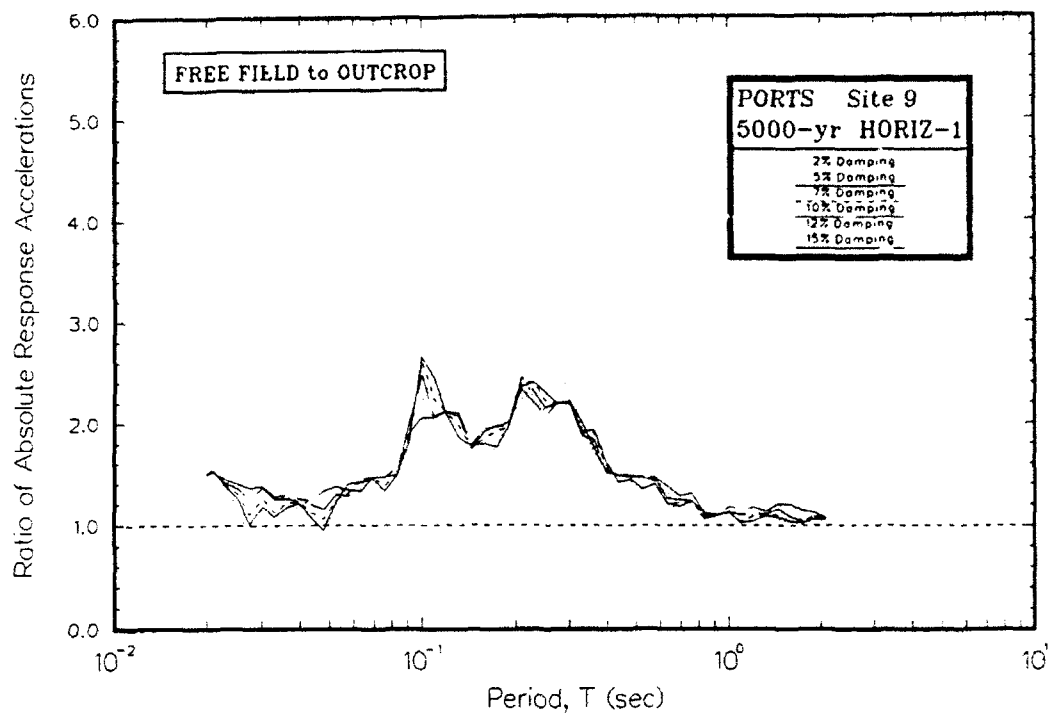


Figure R9. Ratio of absolute acceleration response spectra at free field to rock for Site 9

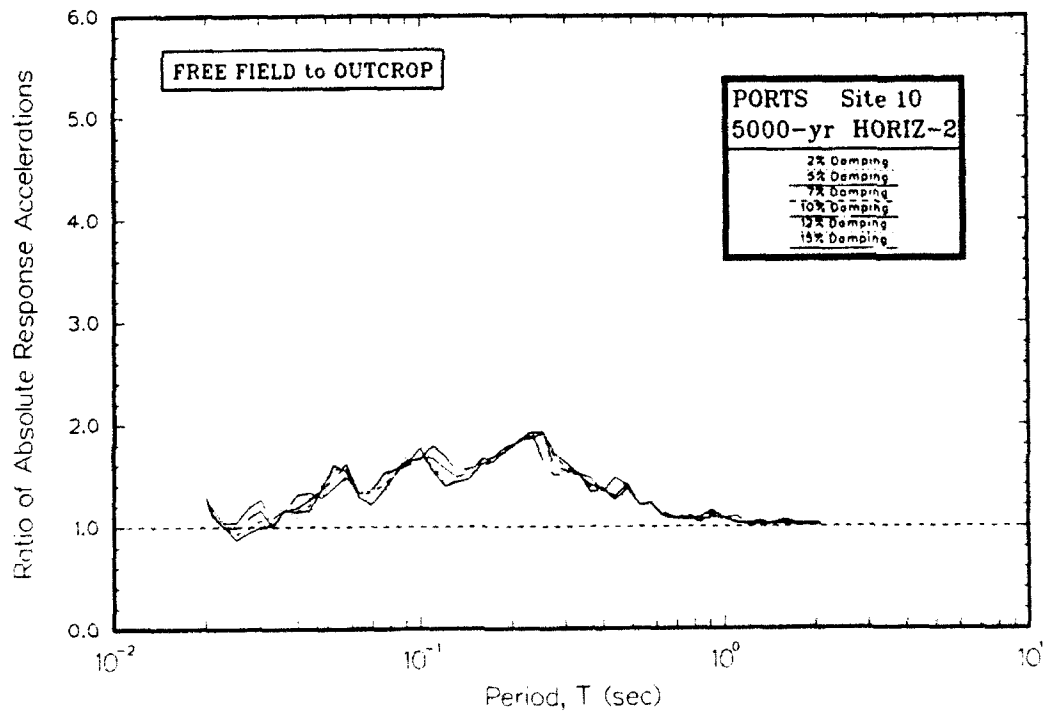
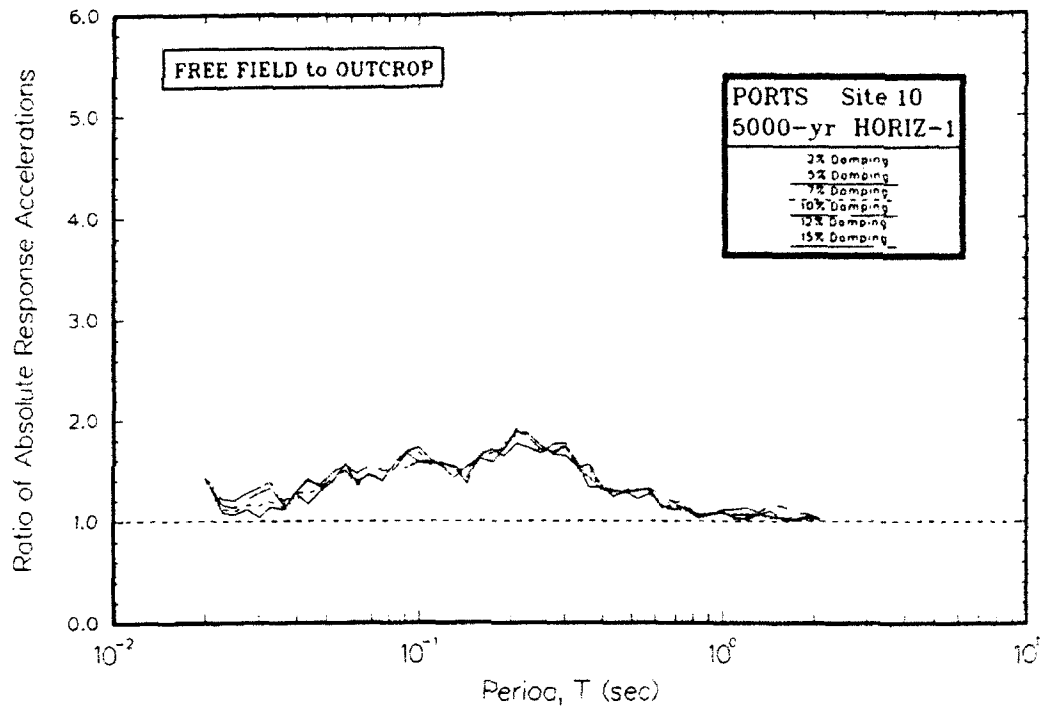


Figure R10. Ratio of absolute acceleration response spectra at free field to rock for Site 10

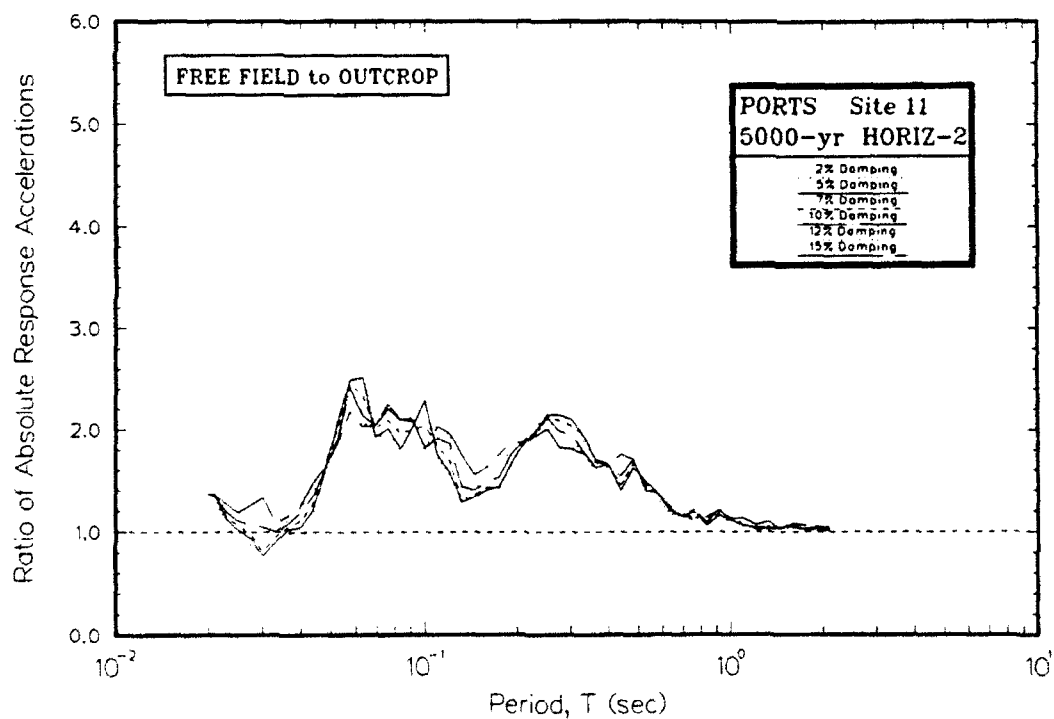
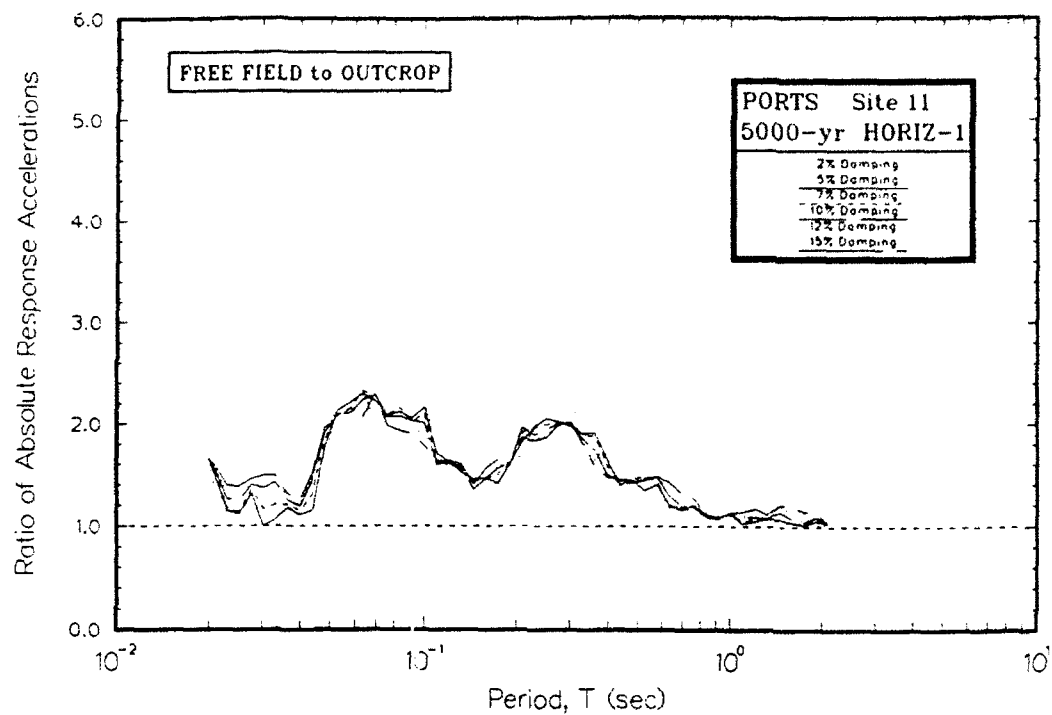


Figure R11. Ratio of absolute acceleration response spectra at free field to rock for Site 11

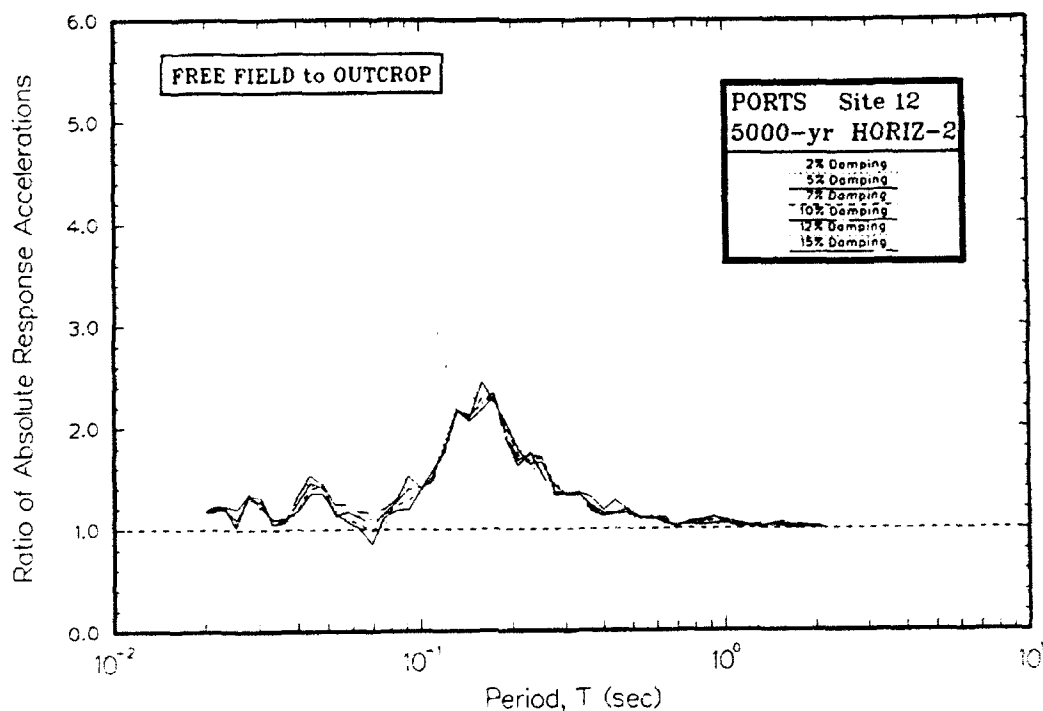
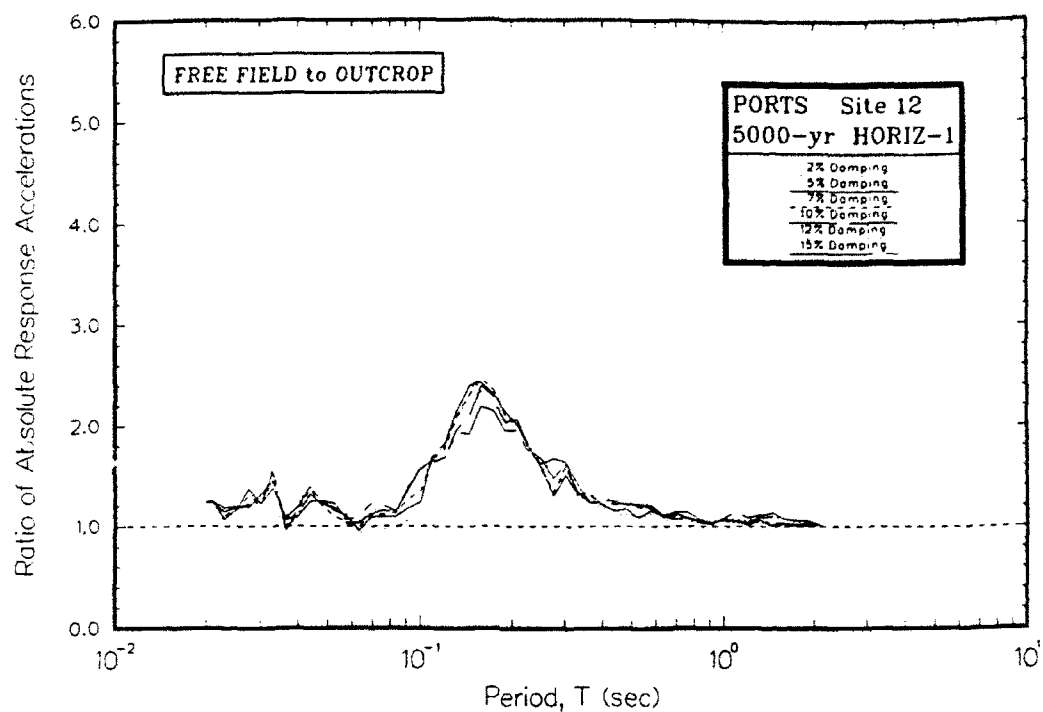


Figure R12. Ratio of absolute acceleration response spectra at free field to rock for Site 12

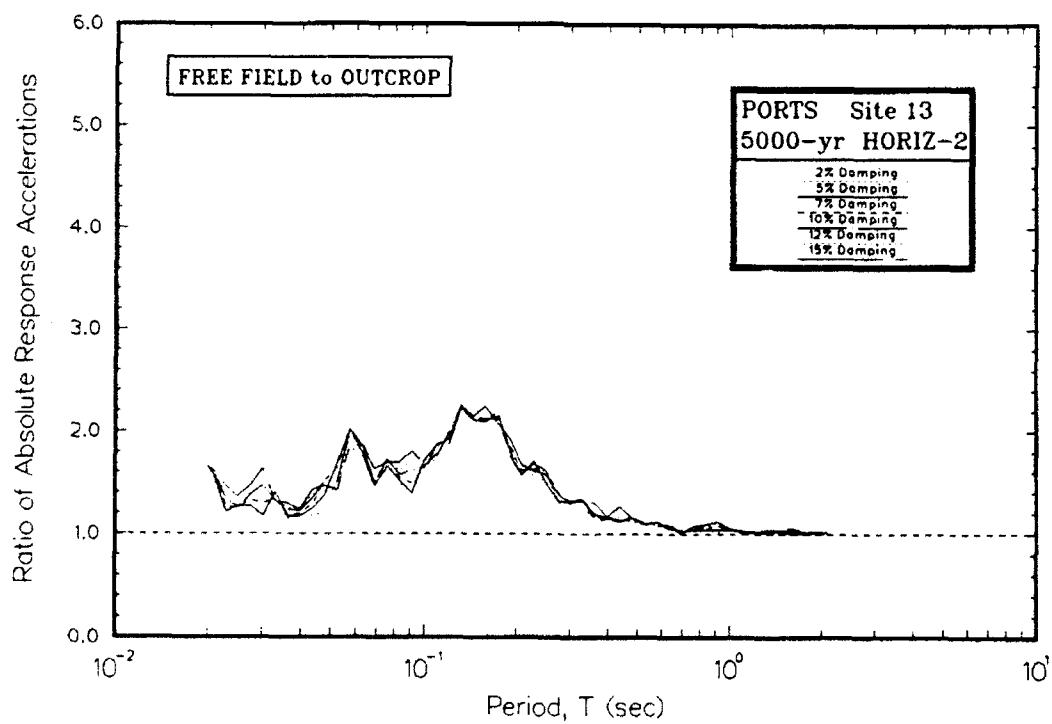
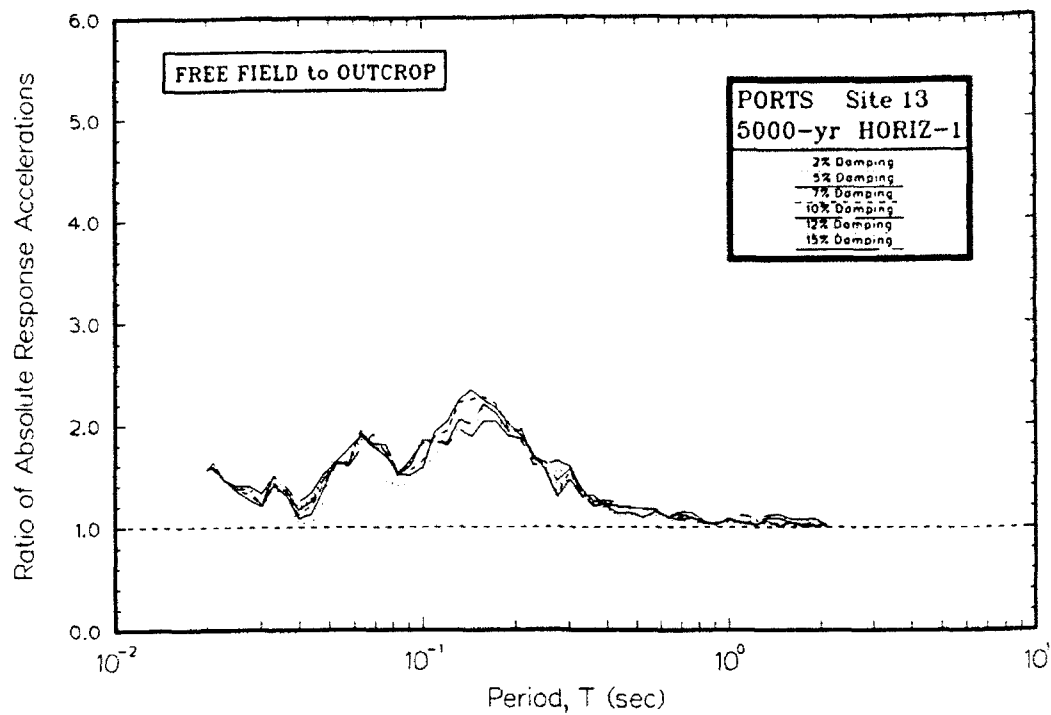


Figure R13. Ratio of absolute acceleration response spectra at free field to rock for Site 13

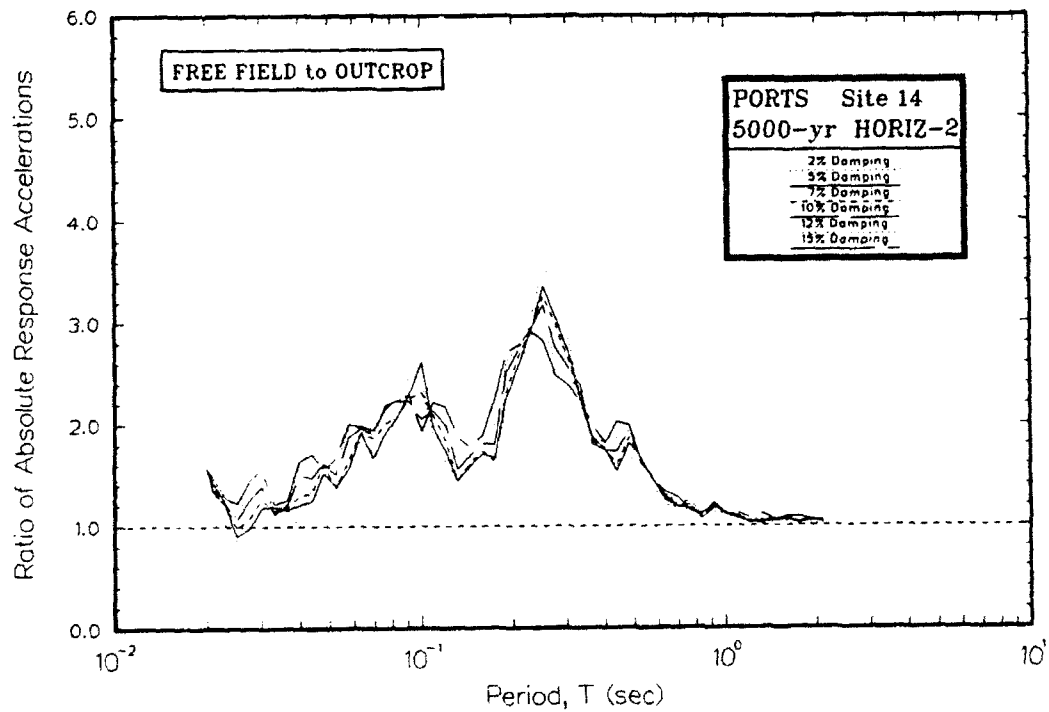
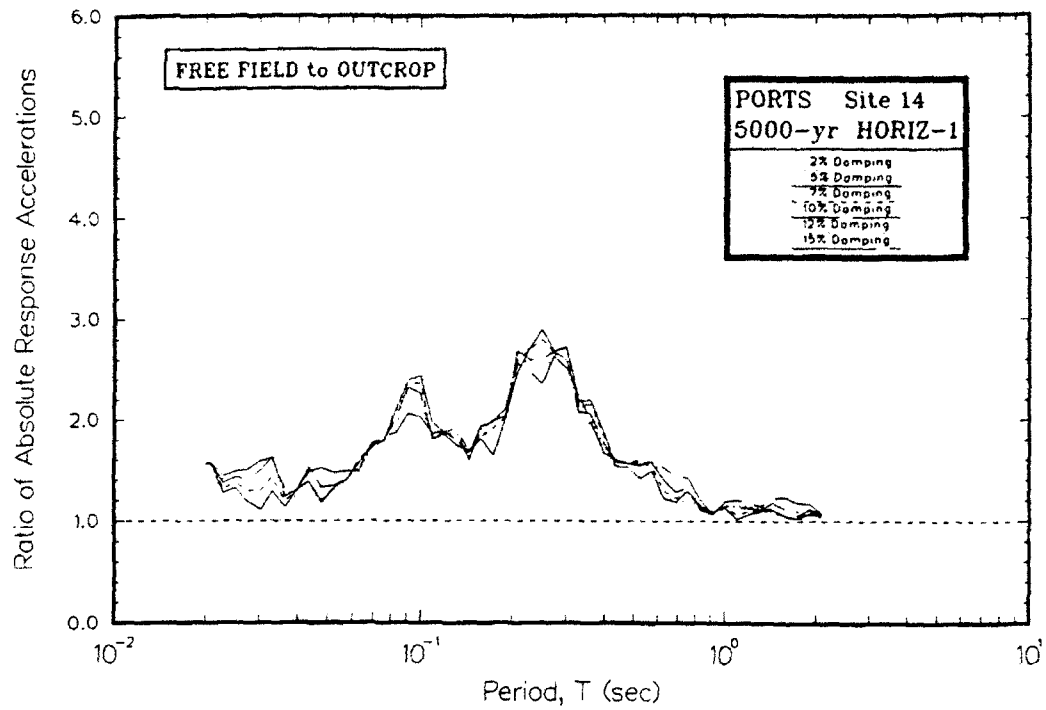


Figure R14. Ratio of absolute acceleration response spectra at free field to rock for Site 14

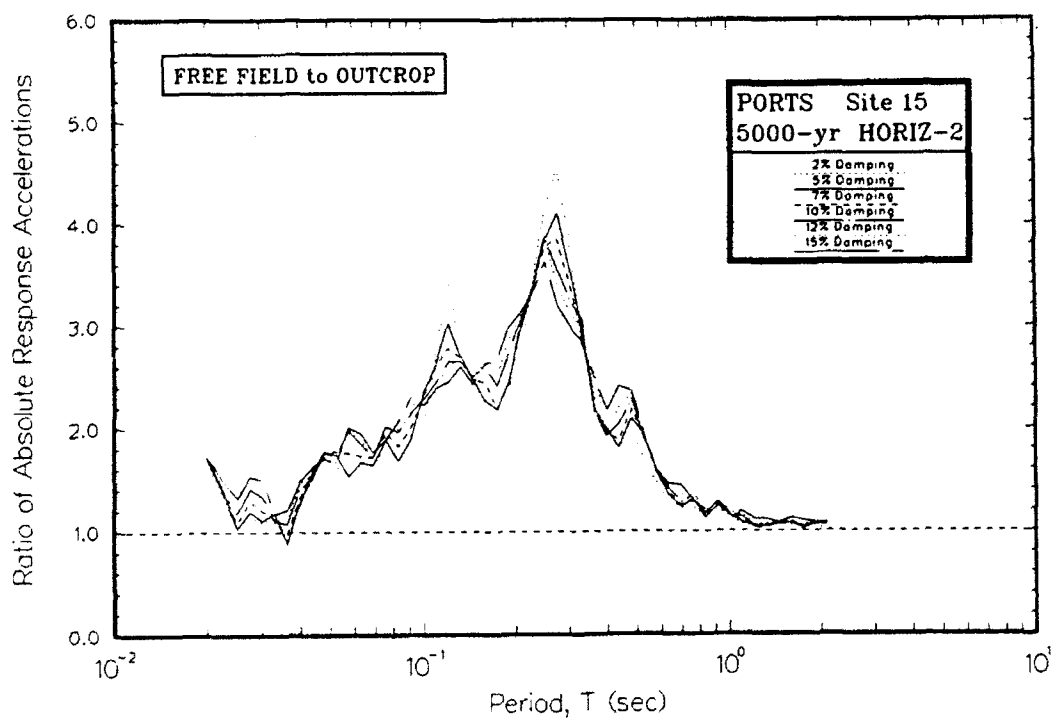
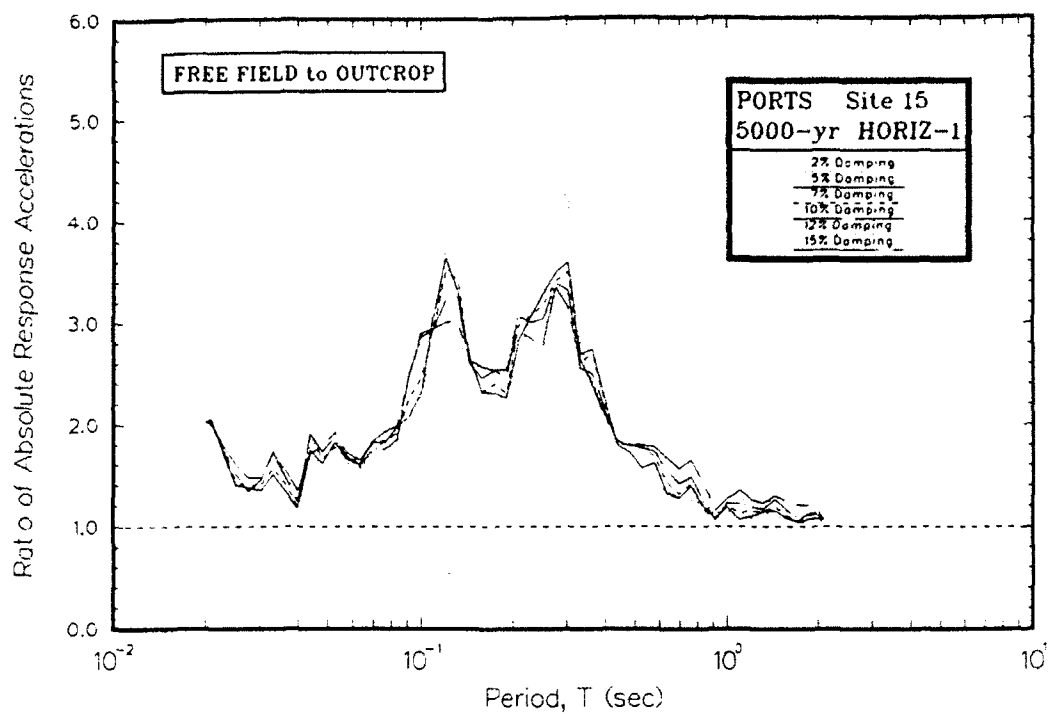


Figure R15. Ratio of absolute acceleration response spectra at free field to rock for Site 15

APPENDIX S: AMPLIFICATION RATIOS FOR 5000-YEAR EVENT

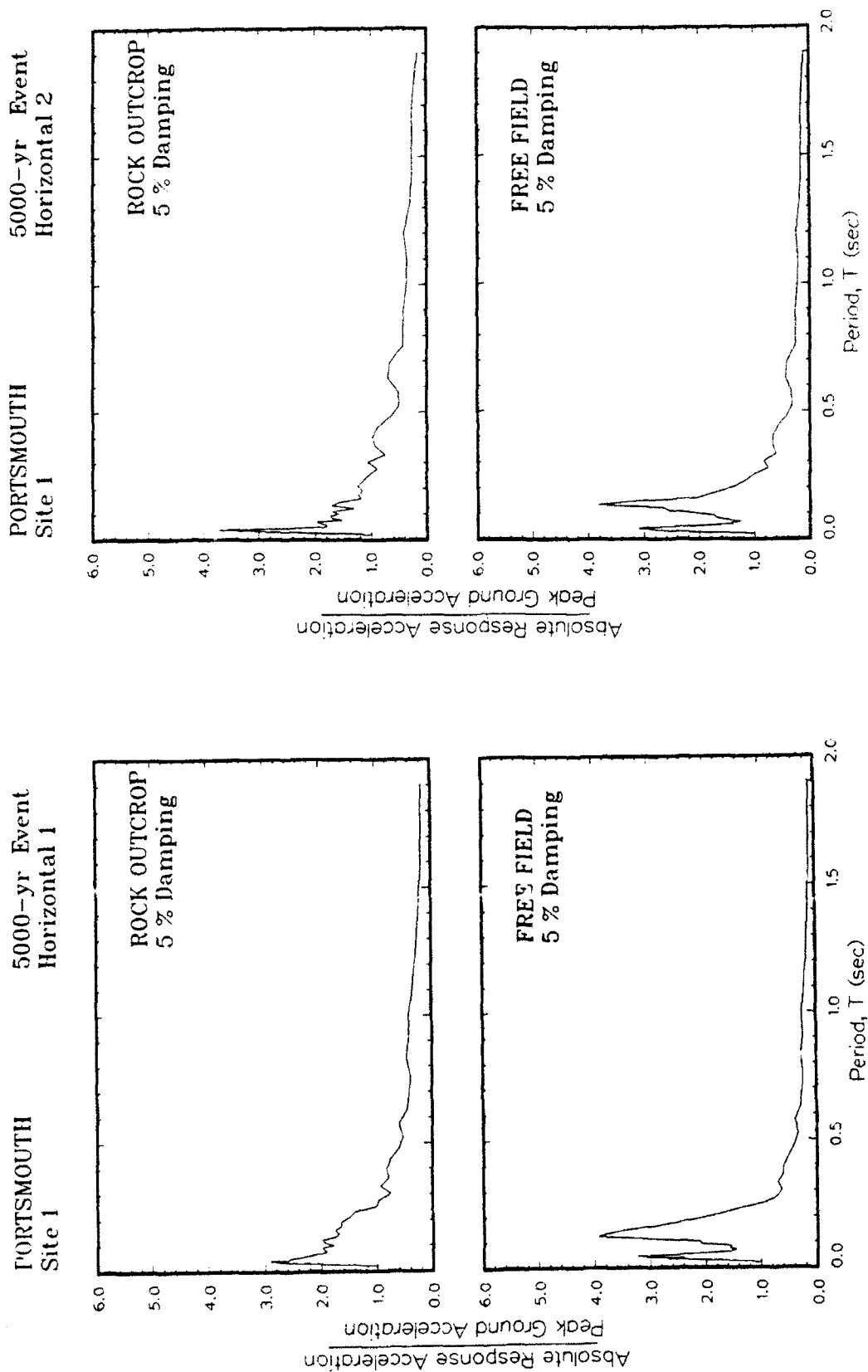


Figure S1. Ratio of amplification of absolute acceleration response spectra to peak acceleration at free field for Site 1

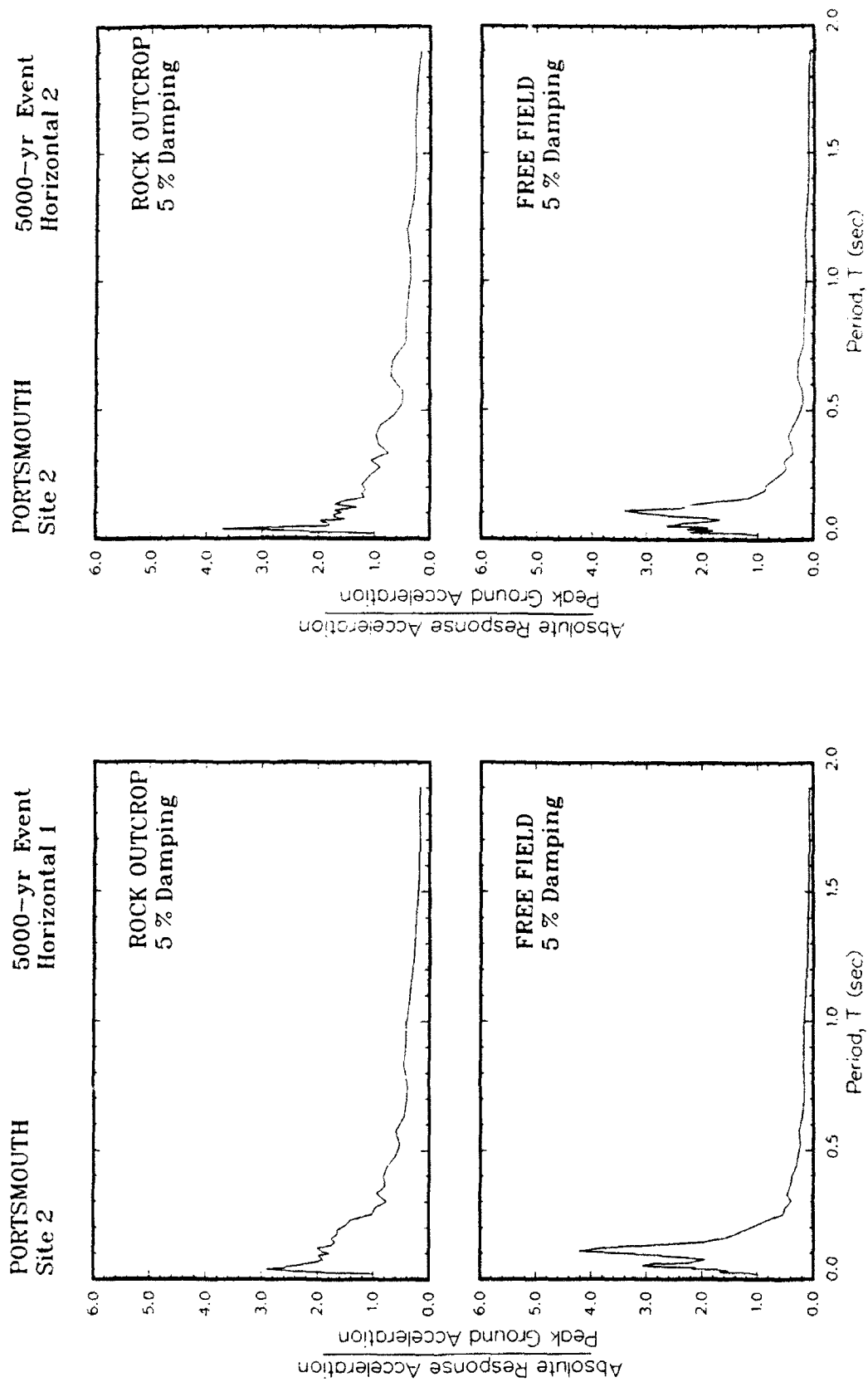


Figure S2. Ratio of amplification of absolute acceleration response spectra to peak acceleration at free field for Site 2

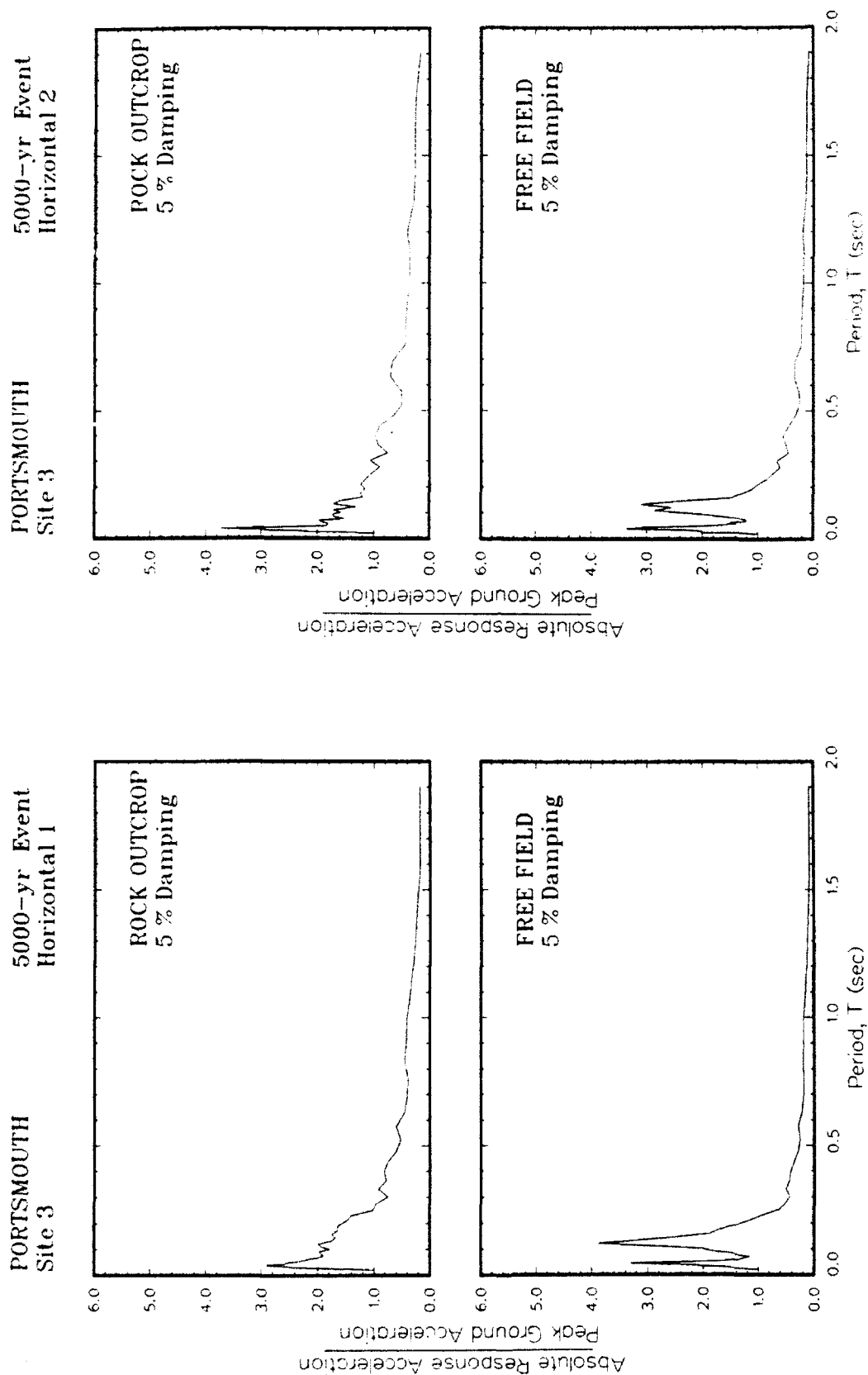


Figure S3. Ratio of amplification of absolute acceleration response spectra to peak acceleration at free field for Site 3

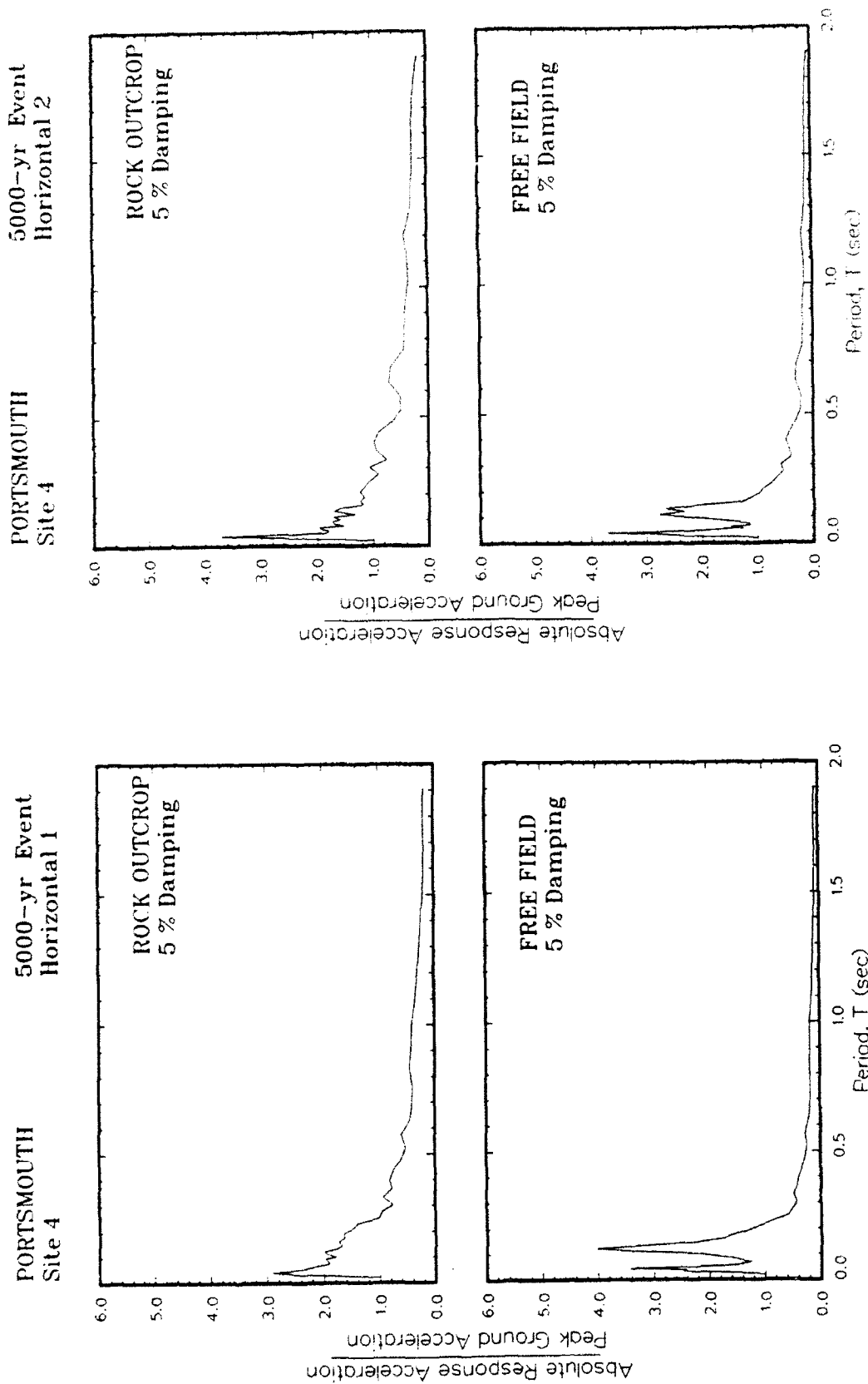


Figure S4. Ratio of amplification of absolute acceleration response spectra to peak acceleration at free field for Site 4

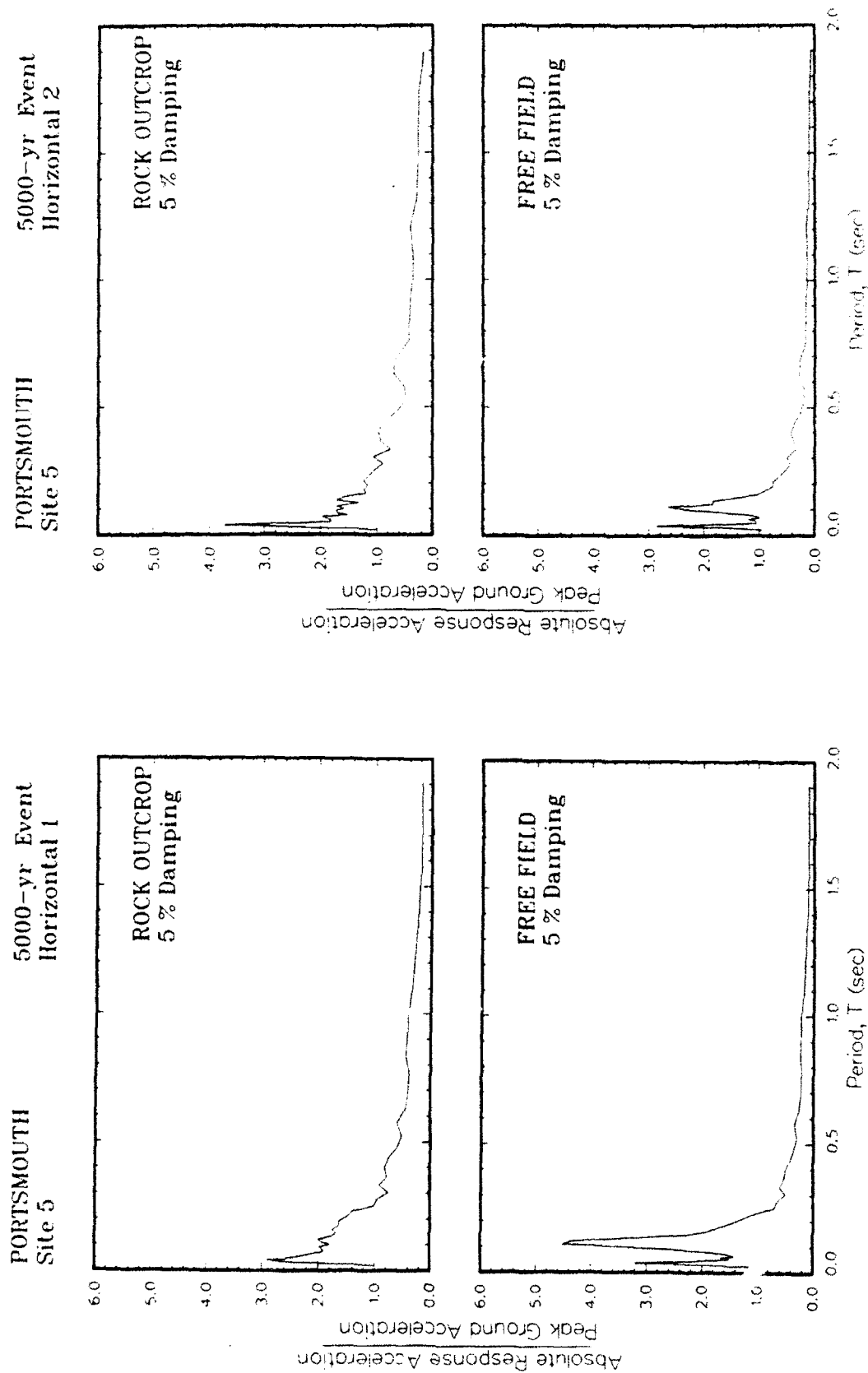


Figure S5. Ratio of amplification of absolute acceleration response spectra to peak acceleration at free field for Site 5

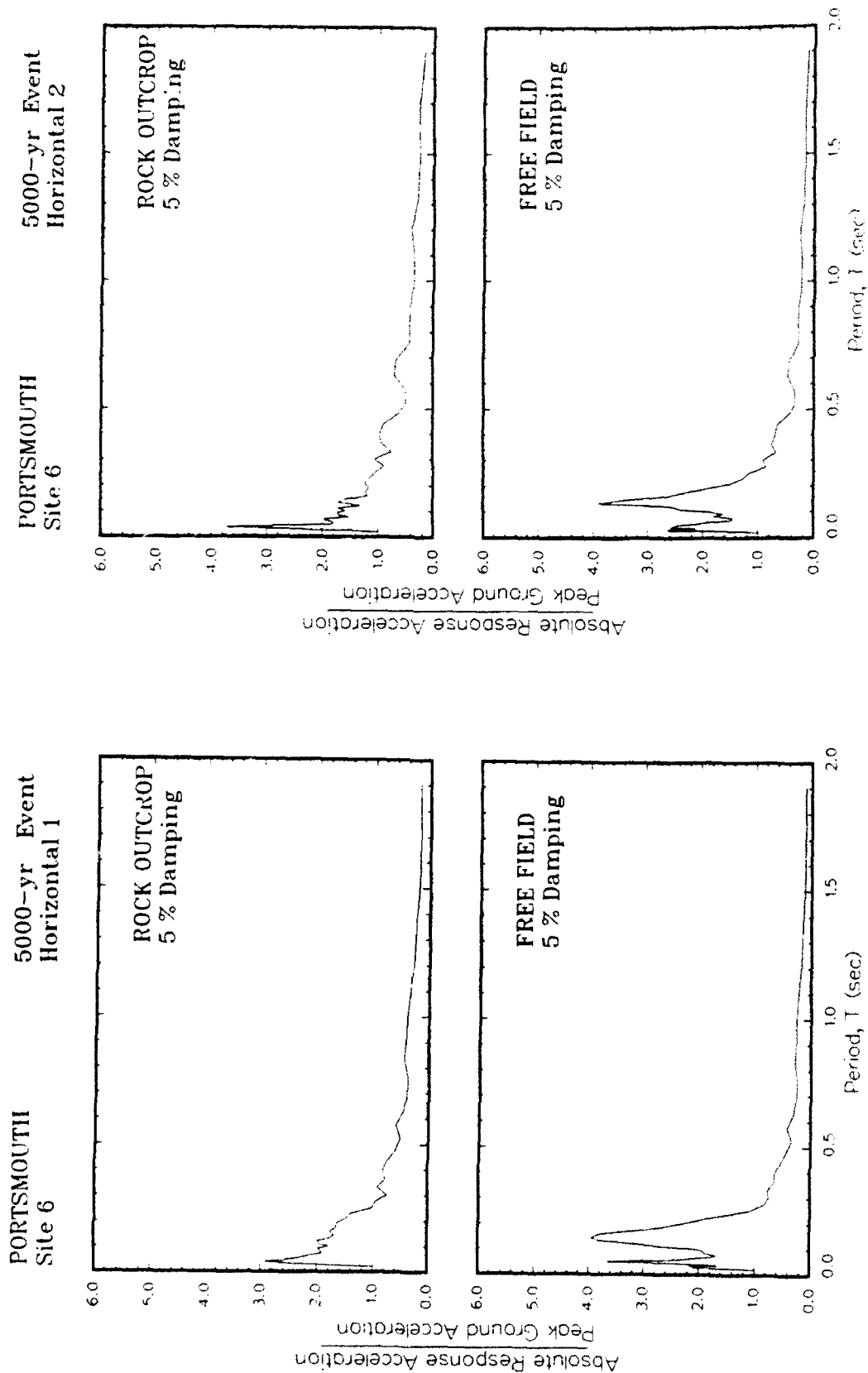


Figure S6. Ratio of amplification of absolute acceleration response spectra to peak acceleration at free field for Site 6

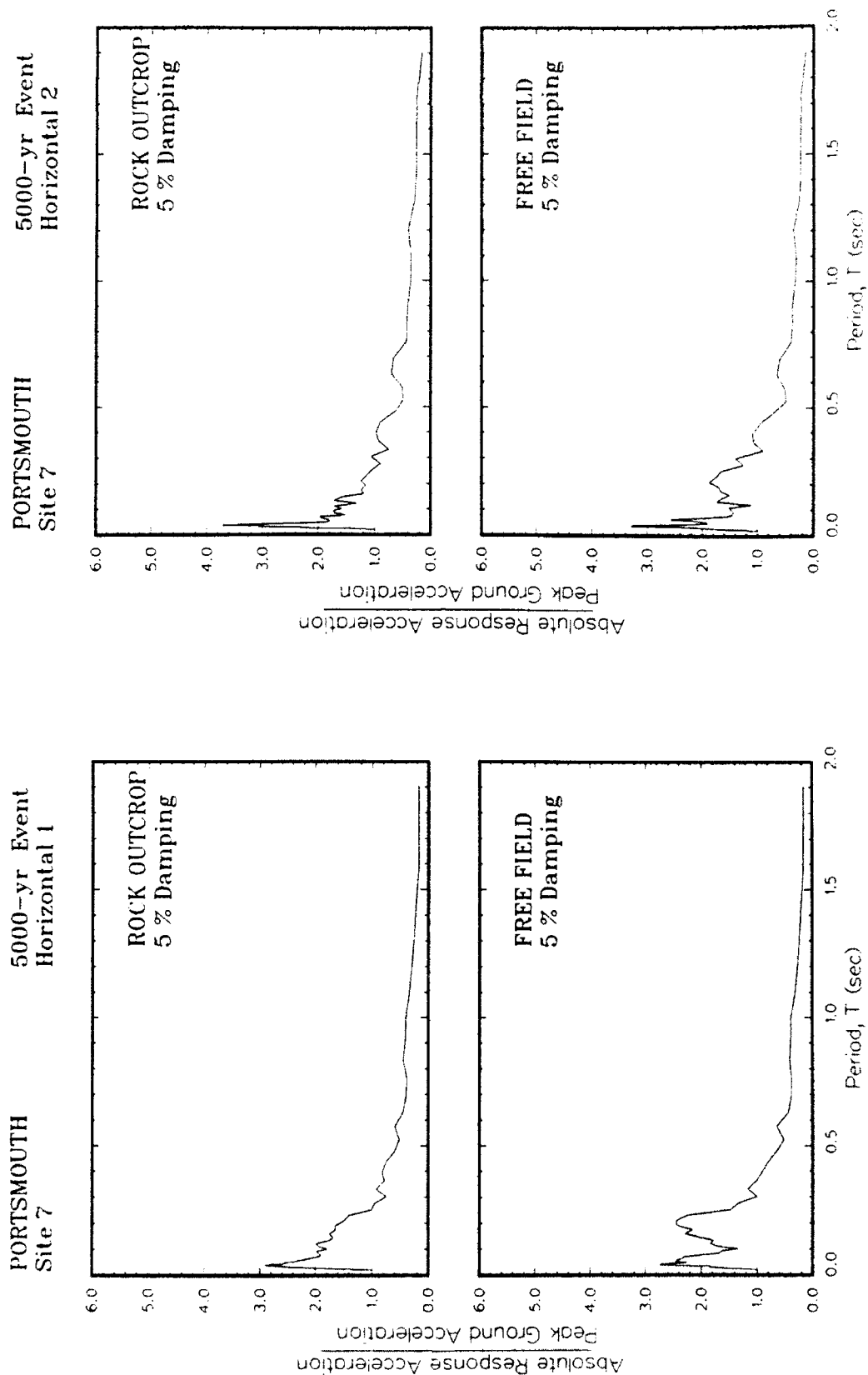


Figure S7. Ratio of amplification of absolute acceleration response spectra to peak acceleration at free field for Site 7

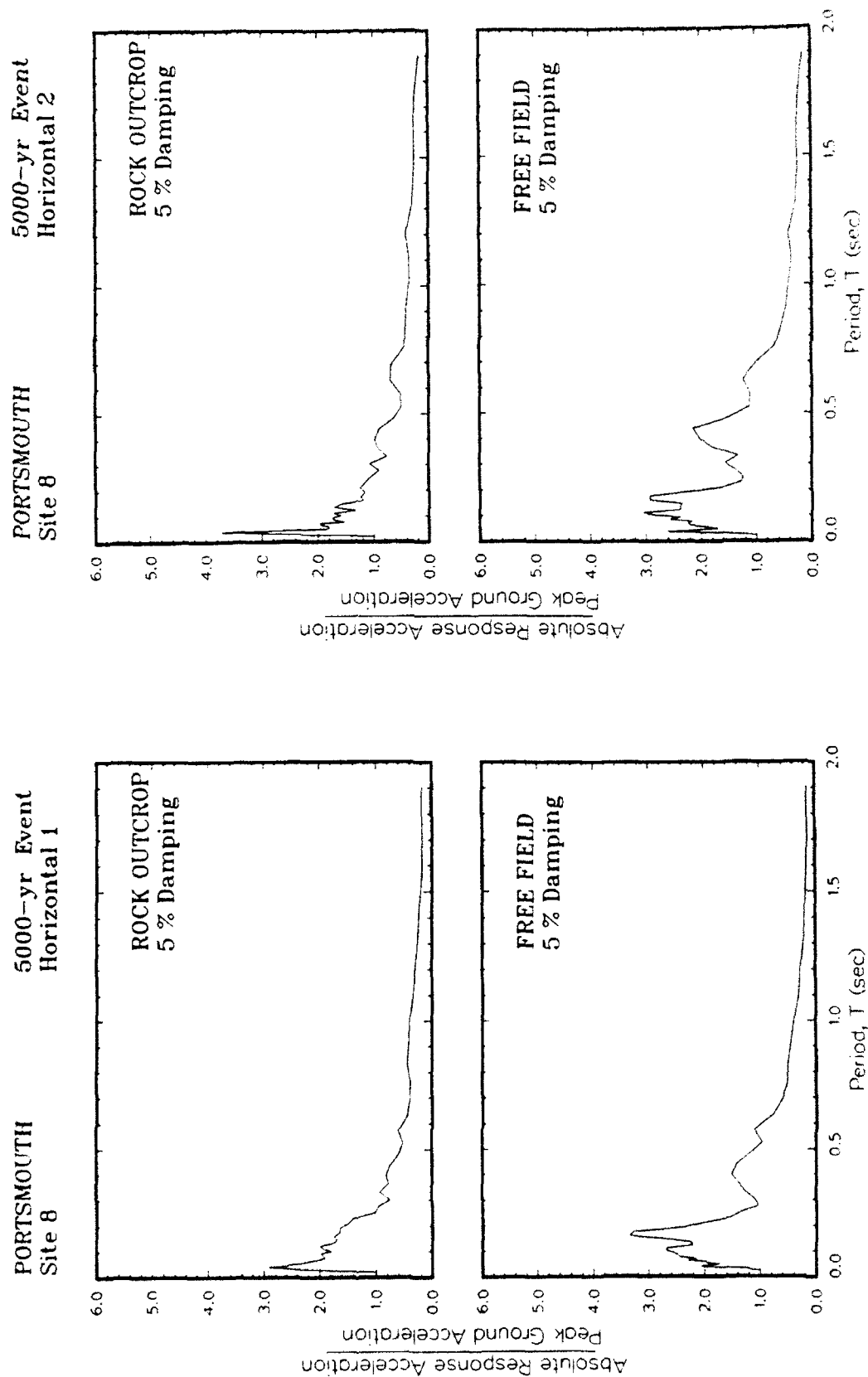


Figure S8. Ratio of amplification of absolute acceleration response spectra to peak acceleration at free field for Site 8

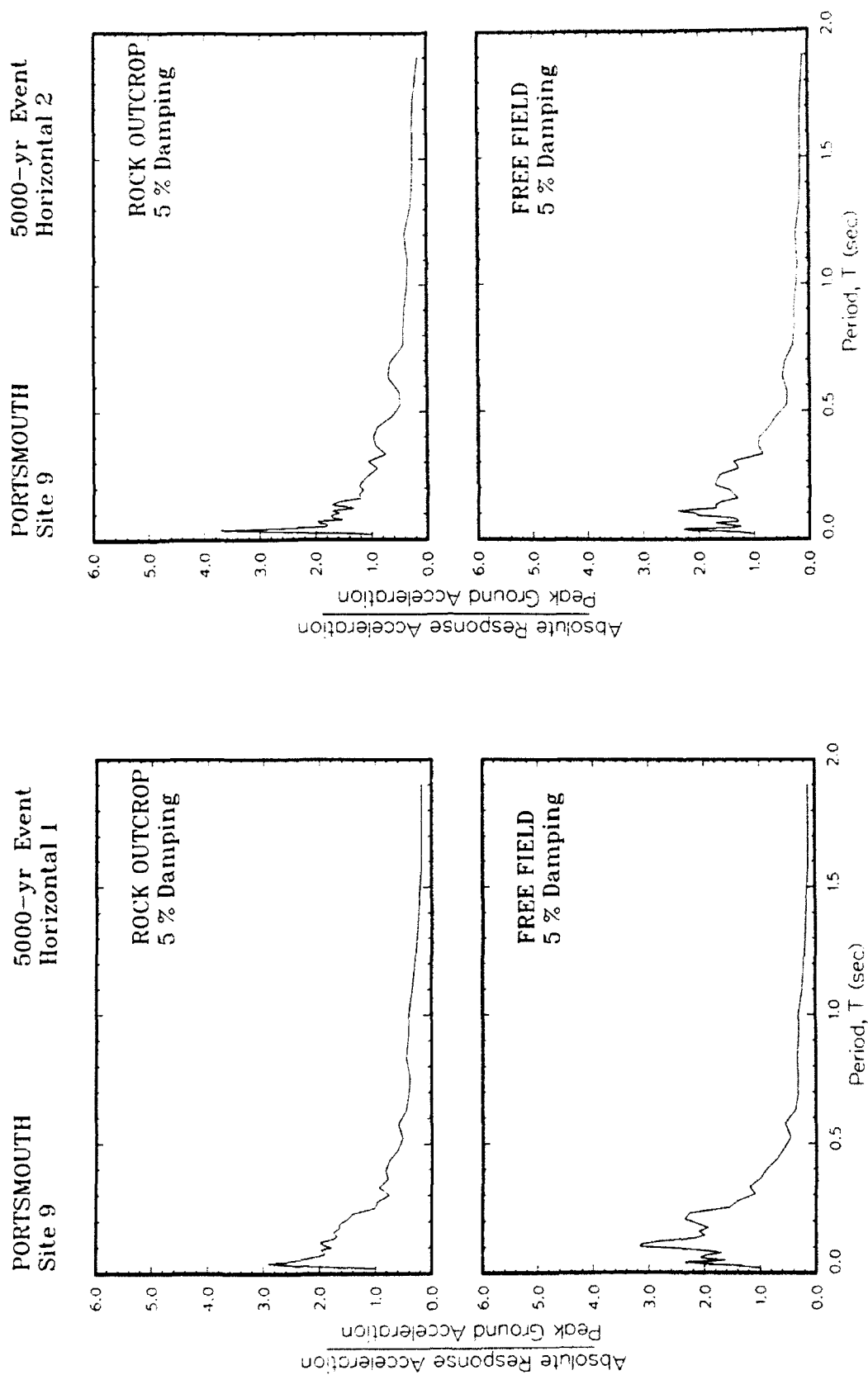


Figure S9. Ratio of amplification of absolute acceleration response spectra to peak acceleration at free field for Site 9

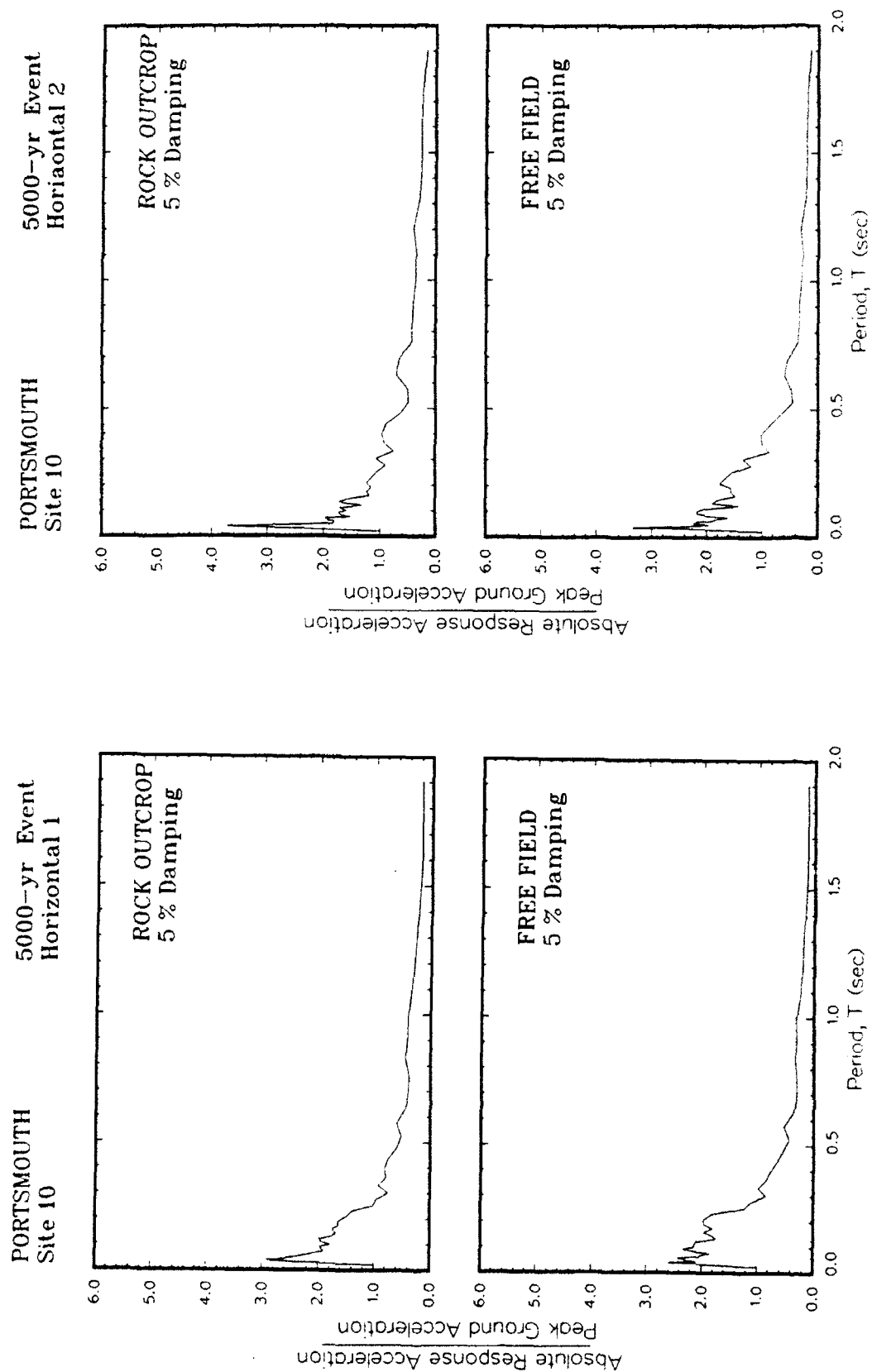


Figure S10. Ratio of amplification of absolute acceleration response spectra to peak acceleration at free field for Site 10

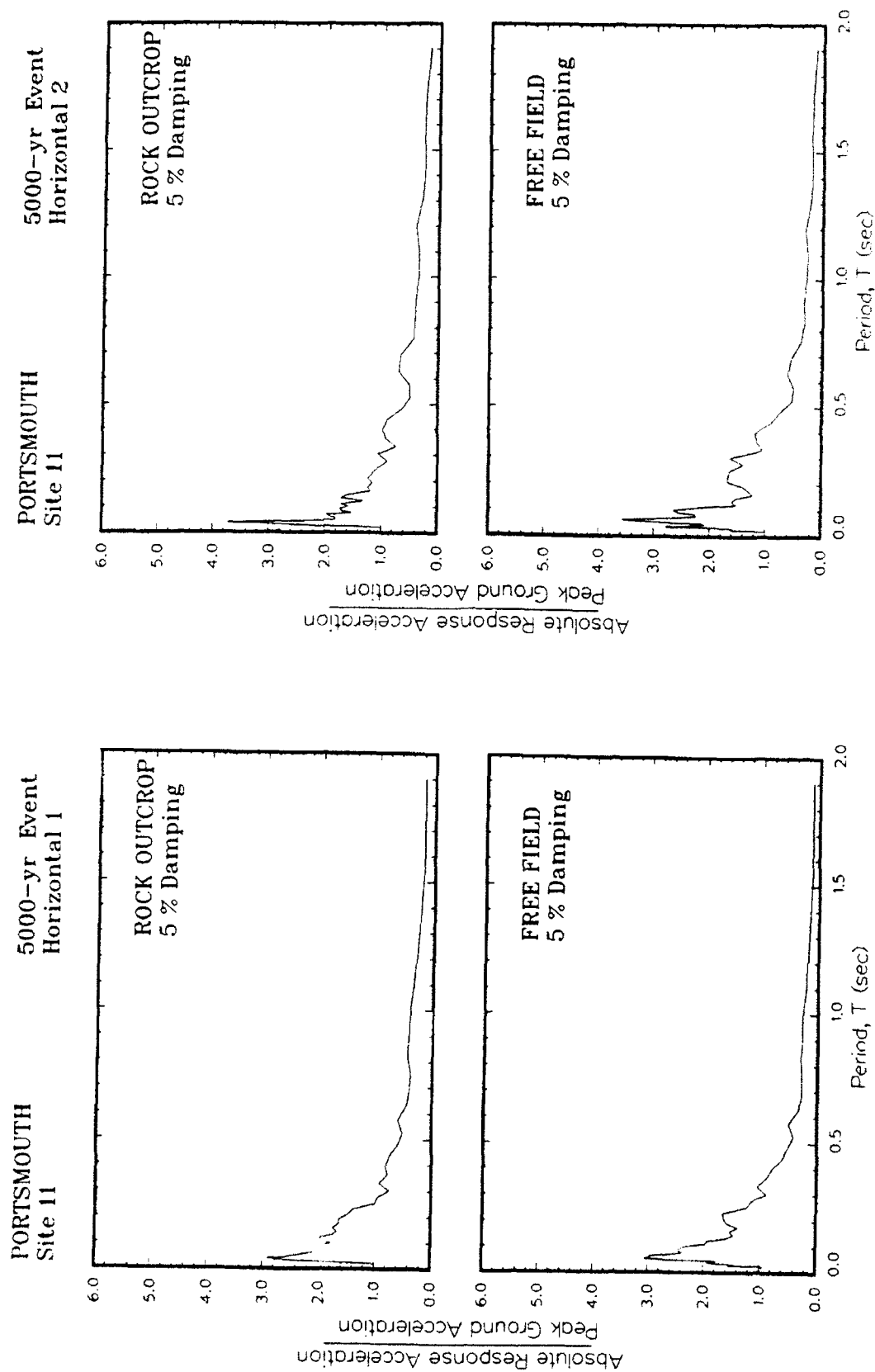


Figure S11. Ratio of amplification of absolute acceleration response spectra to peak acceleration at free field for Site 11

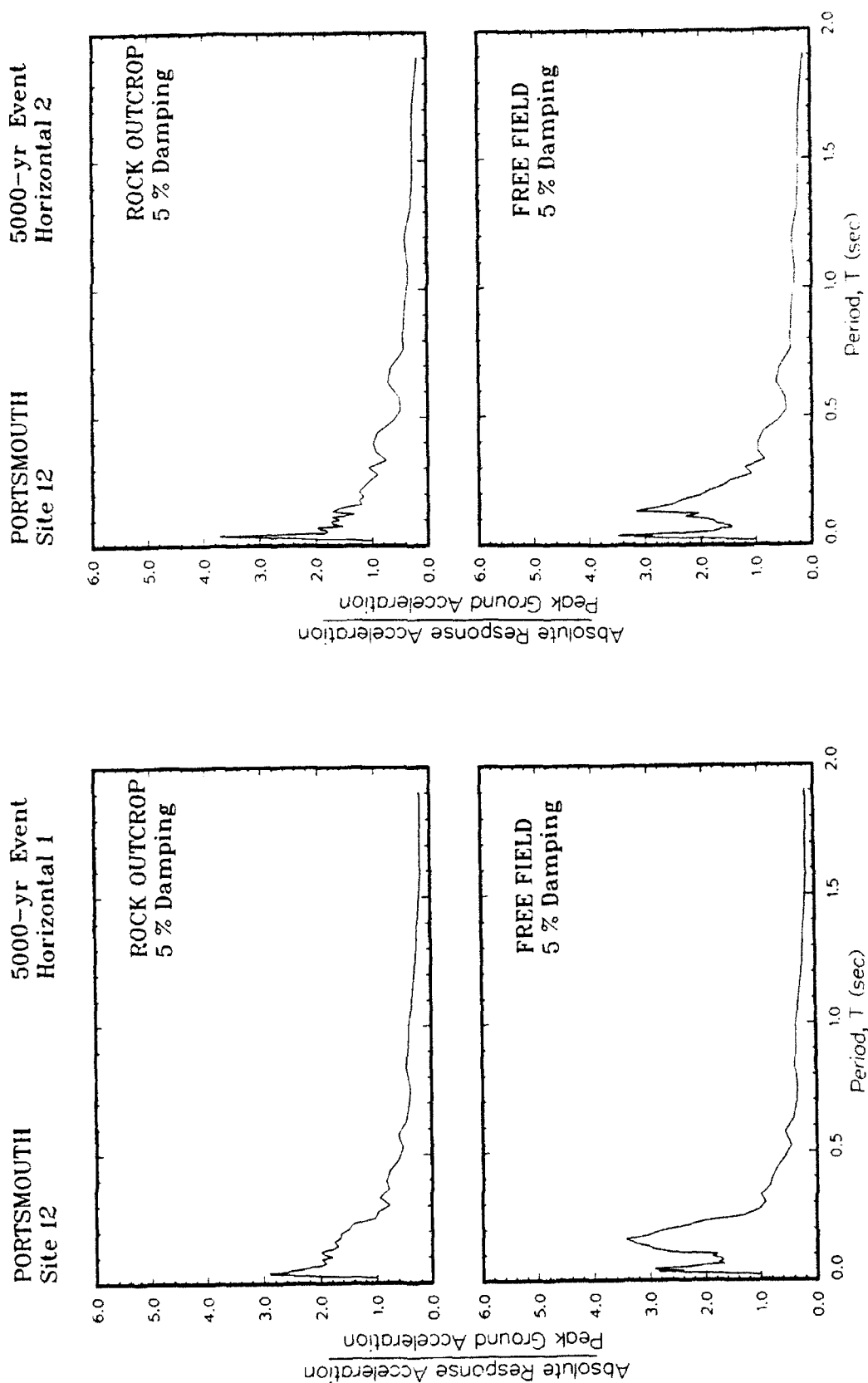


Figure S12. Ratio of amplification of absolute acceleration response spectra to peak acceleration at free field for Site 12

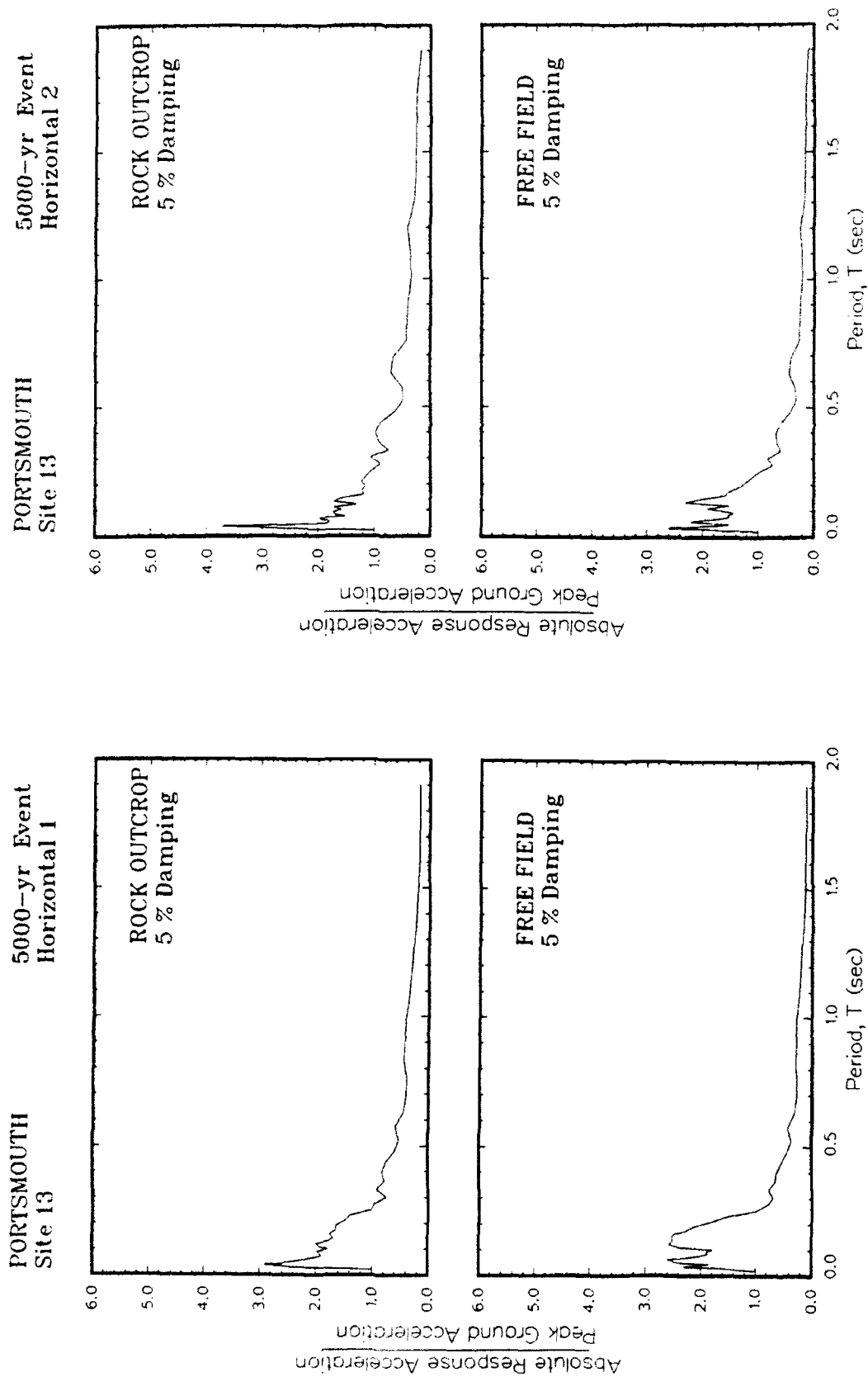


Figure S13. Ratio of amplification of absolute acceleration response spectra to peak acceleration at free field for Site 13

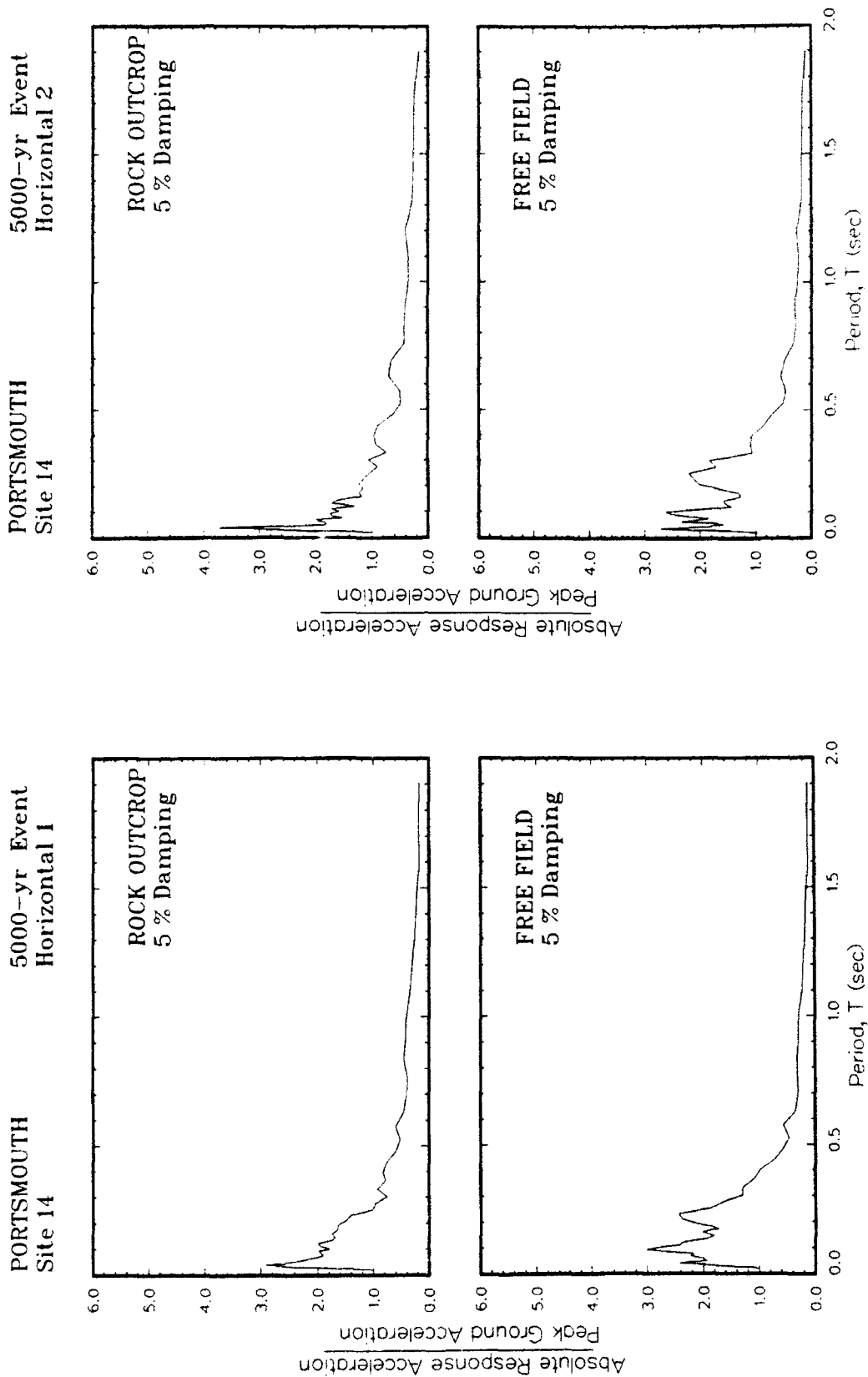


Figure S14. Ratio of amplification of absolute acceleration response spectra to peak acceleration at free field for Site 14

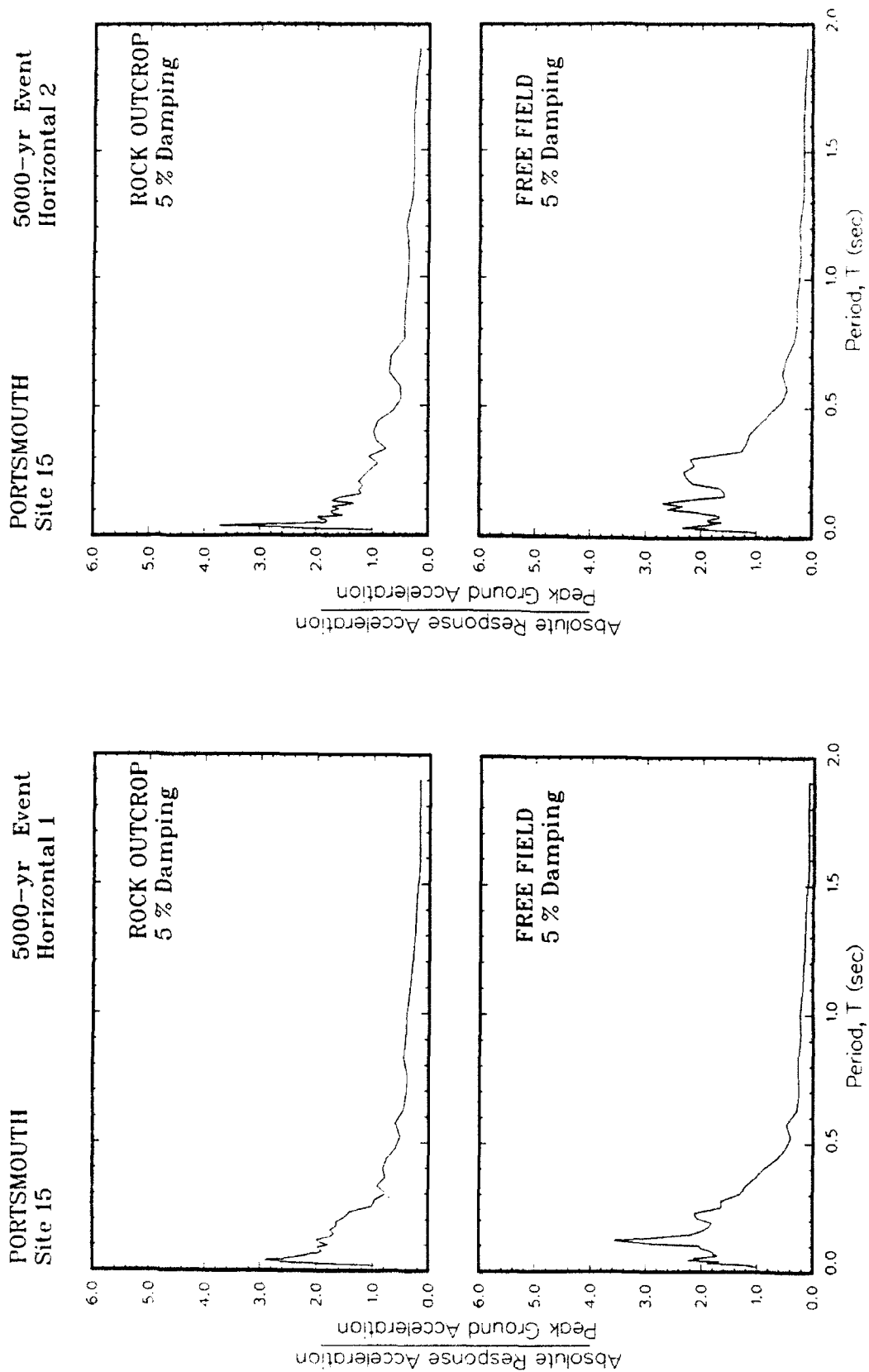


Figure S15. Ratio of amplification of absolute acceleration response spectra to peak acceleration at free field for Site 15

REPORT DOCUMENTATION PAGE			Form Approved OMB No. 0704-0188	
<small>Public reporting burden for this collection of information is estimated to average 1 hour per response, including the time for reviewing instructions, searching existing data sources, gathering and maintaining the data needed, and completing and reviewing the collection of information. Send comments regarding this burden estimate or any other aspect of this collection of information, including suggestions for reducing this burden, to Washington Headquarters Services, Directorate for Information Operations and Reports, 1215 Jefferson Davis Highway, Suite 1204, Arlington, VA 22202-4302, and to the Office of Management and Budget, Paperwork Reduction Project (0704-0188), Washington, DC 20503</small>				
1. AGENCY USE ONLY (Leave blank)	2. REPORT DATE August 1993	3. REPORT TYPE AND DATES COVERED Final report		
4. TITLE AND SUBTITLE Site-Specific Earthquake Response Analysis for Portsmouth Gaseous Diffusion Plant, Portsmouth, Ohio			5. FUNDING NUMBERS IAG No. DE-AI05-910R21971	
6. AUTHOR(S) David W. Sykora and Jennifer J. Davis				
7. PERFORMING ORGANIZATION NAME(S) AND ADDRESS(ES) U.S. Army Engineer Waterways Experiment Station, Geotechnical Laboratory, 3909 Halls Ferry Road, Vicksburg, MS 39180-6199			8. PERFORMING ORGANIZATION REPORT NUMBER Miscellaneous Paper GL-93-13	
9. SPONSORING/MONITORING AGENCY NAME(S) AND ADDRESS(ES) U.S. Department of Energy, Oak Ridge Operations, Oak Ridge, TN 37831-8650			10. SPONSORING/MONITORING AGENCY REPORT NUMBER	
11. SUPPLEMENTARY NOTES This report is available from the National Technical Information Service, 5285 Port Royal Road, Springfield, VA 22161.				
12a. DISTRIBUTION/AVAILABILITY STATEMENT Approved for public release; distribution is unlimited			12b. DISTRIBUTION CODE	
13. ABSTRACT (Maximum 200 words) A site response analysis has been conducted for the DOE Portsmouth Gaseous Diffusion Plant (PGDP) located south of Portsmouth. Synthetic earthquake records corresponding to three return periods were provided. Geotechnical and seismic geophysical data were collected from previous investigations conducted for the proposed plant additions and used to create fifteen individual soil columns and one average column. The soils primarily consist of lacustrine deposits of silt and clay overlying alluvial deposits. Fifteen soil columns were created with a range of total soil thickness from 20 to 61 ft and all material types represented. The shear wave velocities for soil range from 280 fps near the ground surface to 2545 fps but generally are between 500 and 1100 fps. The results of 1-D calculations using <i>SHAKE</i> indicate that ground motions will be amplified at site periods between 0.02 and 2 sec. Natural site periods range from 0.1 to 0.3 sec. The peak free field accelerations are 0.12, 0.17, and 0.36 g for the 500-, 1000-, and 5000-year events, respectively. A sensitivity analysis of various inputs was also conducted.				
14. SUBJECT TERMS Earthquake engineering Site response Soil amplification Vibration Wave propagation			15. NUMBER OF PAGES 409	
			16. PRICE CODE	
17. SECURITY CLASSIFICATION OF REPORT Unclassified	18. SECURITY CLASSIFICATION OF THIS PAGE Unclassified	19. SECURITY CLASSIFICATION OF ABSTRACT	20. LIMITATION OF ABSTRACT	